# 구두발표논문 초록

■ SESSION: D [DG1]
10월 23일(목), 12:30 - 14:00
장 소: 201호

**D-01(초) Direct Transmission Detection of Tunable Mechanical Resonance in an Individual Carbon Nanofiber Relay** ERIKSSON Anders, LEE SangWook[1], SOURAB Abdelrahim A., ISACSSON Andreas[2], KAUNISTO Risto[3], KINARET Jari M.[2], CAMPBELL Eleanor E. B.[4](*Gothenburg University, Department of Physics, Gothenburg, Sweden. [1]Knkuk University, Department of Physics. [2]Department of Applied Physics, Chalmers UniVersity of Technology, Gothenburg, Sweden. [3]Nokia Research Center, Nokia Group, Helsinki, Finland. [4]Edinburgh University, Department of Chemistry, Edinburgh, Scotland.*) A direct on-chip transmission measurement of the resonance frequency of an individual singly clamped carbon nanofiber relay is reported. The experimental results are in good agreement with a small signal model and show the expected tuning of the resonance frequency with changing bias voltage.

**D-02 Quantum Interference in Radial Heterostructure Nanowires** 정 민경, 이 준성, 송 윤, 김 영헌, 이 상돈, 김 남, 김 진희, 최 만수[1], 박 정희[2], 이 효영[3](*한국표준과학연구원. [1]고려대학교, 물리학과. [2]고려대학교, 화학과. [3]한국전자통신연구원.*) Core/shell heterostructure nanowires are one of the most interesting mesoscopic systems potentially suitable for the study of quantum interference phenomena. Here, we report on experimental observations of both the Aharonov-Bohm ($h/e$) and the Altshuler-Aronov-Spivak ($h/2e$) oscillations in radial core/shell ($In_2O_3/InO_x$) heterostructure nanowires. For a long channel device with a length-to-width ratio of about 33, the magnetoresistance curves at low temperatures exhibited a crossover from low-field $h/2e$ oscillation to high-field $h/e$ oscillation. The relationship between the oscillation period and the core width was investigated for freestanding or substrate-supported devices, and indicated that the current flows dominantly through the core/shell interface.

**D-03 Coherent Lattice Vibrations in Small Diameter Single-Wall Carbon Nanotubes** 안 재금, 임 용식, 이 기주[1], J. Kono[2](*건국대, 신소재과학부 전자정보. [1]충남대, 물리학과. [2]Rice U.*) We report the generation and the detection of coherent lattice vibrations in micelle-suspended CoMoCAT single-walled carbon nanotubes (SWNTs) corresponding to the radial-breathing mode (RBM) using ultrashort laser pulses. We performed degenerate pump-probe measurements in a quartz cell with an optical path length of 1mm at room-temperature using ~ 50 fs pulses from a mode-locked Ti:Sapphire laser with a bandwidth of ~ 35nm and a tuning range from 710 nm to 840 nm in 5-nm step. In stark contrast to HipCo SWNTs, coherent lattice vibrations of CoMoCAT SWNTs show several RBMs resonantly excited by the $E_{11}$ optical transition as well as the $E_{22}$ optical transition. The RBMs excited by the $E_{22}$ transition are similar to those of HipCo SWNTs showing peaks at 266 $cm^{-1}$ (11,0), 266 $cm^{-1}$, 257 $cm^{-1}$ (9,4), 245 $cm^{-1}$ (8,6), 238 $cm^{-1}$ (12,1), 226 $cm^{-1}$ (10,5), and 215 $cm^{-1}$ (14,0). Meanwhile, the RBMs excited by the $E_{11}$ transition show high vibration modes with peak positions at 309 $cm^{-1}$ (6,5), 329 $cm^{-1}$ (7,3), and 372 $cm^{-1}$ (5,4). This indicates that *(n-m)* mod 3 = +1 nanotubes have stronger signals than *(n-m)* mod 3 = -1 for the first optical transition, $E_{11}$, in an individual semiconducting SWNT. We will discuss about the excitation energy dependence of measured RBMs showing ultrafast band gap oscillations and compare the difference between CoMoCAT SWNTs and HipCo SWNTs.

**D-04 Revival of Electron Coherence in a Finite-Length Quantum Wire** KIM Jaeuk, LEE Woo-Ram, LEE Hyun-Woo[1], SIM Heung-Sun(*KAIST, 물리학과. [1]POSTECH, 물리학과.*) We study the spatial decay of electron coherence due to electron-electron interaction in a finite-length disorder-free quantum wire. Based on the Luttinger liquid theory, we demonstrate that the coherence length characterizing the exponential decay of the coherence varies from region to region, and that the coherence can even revive after the decay. This counterintuitive behavior, which is in clear contrast to the conventional exponential decay with single coherence length, is due to the fractionalization of an electron and the finite-size-induced recombination of the fractions.

**D-05 Comparative Studies of The Electronic Properties of Bulk and Nanowire Vanadium Dioxide by Ab Initio Density Functional Calculations** KIET HoangAnh Tuan, VU Ong Phuong[1], KANG Dae Joon(*성균관대학교 물리학과. [1]성균관대학교 재료공학과.*) Single crystalline nanowires, for example, provide a truly one dimensional system with vastly different boundary conditions when compared with bulk material. Vanadium dioxide ($VO_2$) and its MIT transition at $T_{bulk} = 68^0C$ continues to receive great interest not only due to its applications but also because understanding this material gives us insight into the fundamental physics behind strongly correlated materials. Since we have already successfully synthesized single crystal $VO_2$ nanowires [Sohn J. I. *et al.*, *Nano Lett*. 7, 1570-1574 (2007)], we have the unique opportunity to take advantage of a realistic experimental basis to which we can compare our theoretical results. In this presentation, we will report the comparative studies of the electronic properties of bulk and nanowire vanadium dioxide of rutile phase which were determined by density functional theory calculations. The following topics will be covered: 1) band structure 2) charge density of bulk and nanowire $VO_2$ will be discussed. We will also review the diameter dependence of the $VO_2$ nanowire on the electronic properties. The results provide an understanding of the electronic properties of the vanadium dioxide nanowire.

■ SESSION: D [DG2]
10월 23일(목), 12:30 - 14:15
장 소: 206호

**D-06 Magnetic properties of heavy fermioni system**

**$Ce_{1-x}Gd_xCoSi_3$** HONG J. B., LIM J. H., KWON Y. S.(*Department of Physics, Sungkyunkwan university.*) Magnetic properties of heavy fermion system $Ce_{1-x}Gd_xCoSi_3$ ($0 \le x \le 1$) have been investigated by specific heat and electrical resistivity measurements. The specific heat shows an antiferromagnetism at 9 K for $GdCoSi_3$ ($x$ = 1.0). With increasing Ce concentration, $T_N$ decreases and suppressed at $x$ = 0.1. For $x$ = 0.1, $C/T$ diverges and the linear temperature dependence in the electrical resistivity is observed even it goes down to 0.6 K. This divergence in $C/T$ and the linear temperature dependence in electrical resistivity at $x$ = 0.1 are similar to behaviors in another heavy fermion system $CeNi_{1-x}Co_xGe_2$. These features deviate from the Landau fermi liquid model. We will report the magnetic properties of heavy fermion system $Ce_{1-x}Gd_xCoSi_3$ in the meeting.

**D-07** **The electric-field induced gap state in Cr doped $SrZrO_3$ films** OH S.-J., PARK W.G., CHO S.(*Department of physics and astronomy, Seoul National University.*) In order to make clear the electro-forming process in resistance random access memory (RRAM), the electronic structures of Cr:$SrZrO_3$ films epitaxially grown by Pulsed Laser Deposition (PLD) were investigated by using X-ray PhotoElectron Spectroscopies(PES) and X-ray Absorption Spectroscopy (XAS). After electro-forming process, new states were found below the conduction band minimum. Those states possibly induced by the applied electric field were accompanied with changes in Cr valency and enlargement in crystal field of oxygen octahedral. We suggest that Cr can act as a controlled valence material to make mixture of $Cr^{III}$ and $Cr^{IV}$ while oxygen ions underneath top electrode were rearranged by Joule heating during the electro-forming process.

**D-08** **LASER ARPES studies on Sr2RuO4** 김 철, 박 승룡, 임 춘식, 송 동준, 김 용관, 최 성균, 정 원식, 고 윤영, 김 창영 (*연세대학교 물리 및 응용물리 사업단.*) LASER ARPES was performed on Sr2RuO4. We could confirm the bulk sensitivity of LASER ARPES. With the bulk sensitivity, we could see a nice match between the calculated Fermi surface and the Fermi surface from LASER ARPES without aging process. We extracted lifetime from fitting the lineshape and compared with lifetimes which appeared in publish papers. Sub meV resoution data from LASER ARPES gives us more information about Sr2RuO4.

**D-09** **삼각형 격자 구조를 지닌 $Pr_5Ni_2Si_3$의 자기적 특성** 이 경은, 이 찬익, 권 용성(*성균관대학교 물리학과.*) $Pr_5Ni_2Si_3$는 $Ce_2NiSi$형의 육방정계 결정구조를 지니고 있으며, Pr 이온은 삼각형 격자구조를 이루고 있어 기학학적인 frustration계에 속하는 흥미로운 계이다. $Pr_5Ni_2Si_3$의 frustration을 연구하기 위하여, 다양한 자기장 하에서의 자기 감수율, 자화율, 전기비저항 그리고 비열을 측정하였다. M(T ) 측정에서 $T_{C1}$=50K과 $T_{C2}$=66K에서 강자성체가 나타나고, 반강자성적 상호작용에 의한 자화의 감소가 $T_N^*$=25K 근처에서 나타난다. $T_N^*$는 자기장의 세기가 세질수록 저온으로 이동한다. 전기비저항 측정 결과 $T_{C1}$강자성체로의 전이에 의해 산란이 적어져 전기비저항이 급속히 감소한다. 한편 $T_{C2}$에서 강자성체로의 전이가 보임에도 불구하고 금속 비금속 전이가 관측되었고 $H$>2T에서 사라진다. 30K 근처에서 온도가 감소함에 따라서 전기비저항이 증가하는데, 이는 single impurity Kondo 모델로서 이해할 수가 있다. 또한 5K 이하에서 전기비저항이 $H$=0~9T에서 다시 증가한다. 이와 같은 온도에서 비열 $C$가 증가한다. 이 비열의 증가가 $H$=8T까지 자기장에 관계없이 관측되었다. 이는 Kondo 효과에 의해 덜 차폐된 자기 모멘트의 frustration에 의해 일어나는 spin liquid 현상으로 이해된다.

**D-10** **Quantitative determination of the enhanced magnetoelectric coupling in $BiFeO_3$-$CoFe_2O_4$ nanostructures** OH Yoon Seok, KIM Hyeong-Jin, CRANE Steven P.[1], LEE Seongsu[2], RAMESH R.[1], CHEONG S-W.[2], KIM Kee Hoon(*Department of Physics and Astronomy, Seoul National University. [1]Department of Materials Science and Engineering, University of California, Berkeley. [2]Rutgers Center for Emergent Materials, Department of Physics and Astronomy, Rutgers University.*) With growing interest worldwide toward utilizing multiferroic materials for novel memory and sensor devices, there have been various efforts to synthesize multiferroic thin films with large magnetoelectric coupling. Toward this direction, for example, a $BiFeO_3$-$CoFe_2O_4$ nanostructure, in which nanopillars of $CoFe_2O_4$ are embedded in a host matrix film of $BiFeO_3$, has been reported as a promising approach to improve the magnetoelectric coupling via enhancement of the strain coupling between the two components. In spite of the expected strongly enhanced magnetoelectric coupling in this nanopillar structure, quantitative magnetoelectric susceptibility (MES) value is not yet available because it is difficult to measure a reduced magnetoelectric voltage signal in the thin film form due to its small electrode size and thickness. In this work, we report the quantitative MES data for a $BiFeO_3$-$CoFe_2O_4$ nanostructure film (300 nm thick), a $BiFeO_3$ thin film (250 nm thick), and a $BiFeO_3$ single crystal, respectively. Using the custom-made MES measurement system operating in cryogenic (down to 2 K) and high magnetic field ($H$) environments (up to 9 T), we find that the MES vs $H$ curve of the $BiFeO_3$-$CoFe_2O_4$ nanostructure shows an anti-symmetric shape with the dc $H$, as expected in magnetoelectric materials with large strain coupling. Moreover, the MES response becomes anisotropic with the change of $H$-directions. When $H$- and electric polarization directions are perpendicular, the MES of the nanostructure becomes as high as $1\times10^{-10}$ s/m at relatively low $H$=1.4 T, while those of the pure $BiFeO_3$ thin film and the single crystal show a quasi-linear increase up to 9 T. We further demonstrate that the maximum MES value of the nanostructure is larger by approximately one order of magnitude than that of a pure $BiFeO_3$ film, and by two orders of magnitude than that of a single crystal of $BiFeO_3$.

**D-11** **Comparative study of the electronic structures of $SrMO_3$ (M = Ti, V, Mn, Fe, and Co; M = Zr, Mo,Ru, and Rh) by O 1s x-ray absorption spectroscopy** NOH H-J, KIM B J[1], OH S-J[1], PARK J-H[2], LIN H-J[3], CHEN C T[3], LEE Y S[4], YAMAURA K[5], TAKAYAMA-MUROMACHI E[5](*전남대학교 물리학과. [1]서울대학교 물리학과. [2]포항공과대학교 물리학과. [3]NSRRC. [4]숭실*

*대학교 물리학과. [5]Advanced Nano Materials Laboratory, National Institute ofr Materials Science.*) We obtained O 1s x-ray absorption spectra of perovskite $SrMO_3$ (M =Zr, Mo, Ru, and Rh) to investigate general trends of the electronic structures of the partially filled 4*d* compounds in comparison with 3*d* ones (M = Ti, V, Mn, Fe, and Co). The parameter values for the crystal electric field, 10Dq, and hybridization strength, $V_{pd}$, are estimated from the configuration interaction cluster model calculation withfull ionic multiplets (CICM), showing a systematic change with the increase of the delectron number. The calculated spectra of the 4*d* compounds from the CICM showgood agreement with the measured spectra in the $t_{2g}$ region, but give a considerabledeviation in the $e_g$ region, implying orbital dependent correlation effects.

**D-12** **PE hysteresis loops measurement in perovskite rare-earth manganites with the double-wave method** CHAI Yisheng, YANG Yongsoo, PARK J. B., MANIVANNAN N, WANG lijuan[1], FENG shaomin[1], JIN changqing[1], KIM keehoon(*Department of Physics and Astronomy, Seoul National University. [1]Institute of Physics, Chinese Academy of Sciences, Beijing 100190.*) Recently, in order to reliably characterize the ferroelectricity in ferro- or antiferro-electric materials, a new technique called the double-wave method was developed to examine only the hysteretic components in the *PE*-loop (*P*: polarization, *E*: electric field) [1]. While rather complex circuits and DAQ board have been used in the original report [1], in this work, we have realized the double-wave method with only a function generator and a conventional Sawyer–Tower circuit. To prove the validity of the simplified double-wave method, we have investigated the *PE* hysteresis loop of the orthorhombic rare-earth manganite $RMnO_3$ (*R*=Tm, Yb, Ho) synthesized under high pressure. Large remnant polarization values are observed in $RMnO_3$ with high electric poling voltage, and is comparable to that observed in the *P*(*T*) curve at the same temperatures. Therefore, our results prove that there exists large ferroelectric polarization in this system [2,3]. We investigate the systematic rare earth ion-dependent remnant polarization and discuss the results based on the exchange striction in the E-type spin structure. Moreover, the influence of d*E*/dt on the shape of the *PE* loop is also investigated. Our preliminary results suggest that a high d*E*/dt is required to obtain a fine hysteresis loop under a high electric field.
[1] Mamoru Fukunaga and Yukio Noda, J. Phys. Soc. Jpn. 77, 064706 (2008). [2] Ivan A. Sergienko, Cengiz Sen and Elbio Dagotto, Phys. Rev. Lett., 97, 227204 (2006). [3] Makoto Tachibana, *et al*. Phys. Rev. B, 75, 144425 (2007).

■ SESSION: D [DG3]
10월 23일(목), 12:30 - 14:00
장 소: 207호

**D-13** **First-Principles Study of Local p(2×2) Structures on Si(100) Surface** KIM Min-Kook, CHOI Hyoung Joon (*Department of Physics and IPAP, Yonsei University.*) We study structural defects inducing local p(2×2) structures in c(4×2)-reconstructed Si(100) surface, using an *ab-initio* pseudopotential density functional method. The local density approximation to the density functional theory is used and electronic wavefunctions are expanded with pseudo-atomic orbitals. Our calculations show that the defects increase the total energy of the system but they are energetically stable with energy barrier. STM images for occupied and unoccupied states are simulated to investigate the surface electronic structures. Effects of electron doping and external electric field on the defects are also studied.
* This work was supported by the KRF (KRF-2007-314-C00075) and by the KOSEF Grant No. R01-2007-000-20922-0. Computational resources have been provided by KISTI Supercomputing Center (KSC-2008-S02-0004).

**D-14** **Negative Differential Resistance in a Tip-induced Quantum Well Potential on Si(001) Surface** LYO In-Whan, CHO Doohee, JUNG Woojin(*Yonsei University, Department of physics.*) We report on the zero-dimensional quantum well states on a Si(100) surface, the outcome of local band-bending induced by the electric field between the STM tip and the surface. Scanning tunneling spectroscopy data of the bulk band gap region exhibit a multitude of the negative differential resistance (NDR) peaks, strongly indicating the existence of the atom-like high density states. Each NDR peak corresponds to an energy level of the quantum well state because the tunneling current is enhanced when the localized tip state is in resonance with the quantum well state. It is also found that under higher tunneling current, the NDR's shift to the higher binding energy, in agreement with the behavior of the quantum well under the external electric field provided by the STM tip. The role of the quantum well states in the creation of bisolitons by fast field switching conditions will be discussed.

**D-15** **First-principles Study of the YSZ (001) Surfaces** YANG Jae Won(*포항공과대학교, 물리학과.*) First principles calculations have been performed on the structural and electronic properties of bulk yttria-stabilized zirconia (YSZ) and YSZ (001) surfaces. The thermodynamic stability of the different configurations of YSZ (001) surface are also analyzed, taking into account the influence of the chemical environment as a function of the relative richness in Y and O. The experimental results, segregation of yttria at the surface and grain boundary, are compared with the thermodynamic stability diagram of this calculation. We conclude that, at high Y chemical potential, Y surface is more stable then Zr and O surface.

**D-16** **Controlling the ground state of atomic wires by electron doping** MORIKAWA Harumo, KANG Se Hun, BYUN Jung Hoon, JUNG Won Yong, HWANG Chan Cuk[1], YEOM Han Woong[2](*1. Institute of physics and Applied physics and Center for Atomic Wires and Layers, Yonsei Universtity. [1]2. Pohang Accelerator Laboratory. [2]1. Institute of physics and Applied physics and*

*Center for Atomic Wires and Layers, Yonsei Universtity.*) Controlling the property of atomic scale structures is important because they are the most fundamental basis for the atomic scale devices. One of such strategies is electron/hole doping to modify the band filling and thus the Fermi surface, which is in charge of the most of the physical property. A well known challenge was done in the old study by Shirakawa and co-workers who successfully produced the high conductivity in the linear conjugated polymers by making mid-gap states[1]. Various atomically well-defined structures are known on solid surfaces. However, few studies have been done successfully to modify their electronic structures[2,3]. In this study, we control the electronic structure of the In/Si(111)-4x1 atomic wire array by Na deposition. This surface, in its pristine form, has a well-nested Fermi surface in a x2 periodicity, and transits from the metallic 4x1 to the insulating 8x2 phase at low temperature. The deposition of a small amount (<0.01 monolayer) of Na lowers the transition temperature drastically. Angle-resolved photoemission reveals that the Na-deposited surface keeps metallic even at well below the transition temperature. The surface state bands have a larger electron filling than 4x1, which increases monotonically with the Na coverage. This is a typical electron doping behavior. The doped electrons enlarge the nesting vector slightly from the commensurate x2 nesting condition. Surprisingly, they spread non-locally and two-dimensionally, in spite of the strong anisotropy of the system, as shown by scanning tunneling microscopy. The doped domain shows a weak doubled periodicity, and similar spectrum in the In-4*d* core level to 4x1. The above results would imply that Na induces the metallic 4x2 phase which was theoretically suggested to have a close electronic structure to 4x1 [4]. On the other hand, the high sensitivity of the 8x2 transition against the nesting vector strongly indicates that the 8x2 transition is driven purely by the Fermi surface nesting, not a theoretically suggested order-disorder transition[4,5].

* References [1] H. Shirakawa *et al.,* J. Chem. Soc. Chem. Commun. 578 (1977). [2] J. N. Crain *et al.*, PRB 72, 045312 (2005) [3] W. H. Choi *et al.,* PRL 100, 126801 (2008). [4] J.-H. Cho *et al.*, PRB 71, 081310 (2005). [5] C. Gonzalez *et al.*, PRL 96, 136101(2006).

**D-17** **Novel Energy Transfer Mechanism in Creation of Bisolitons on Si(001) Surfaces** JUNG WOOJIN, CHO DOOHEE, LYO In-Whan(*Institute of Physics and Applied Physics.*) We developed single carrier spectroscopy and controllable arbitrary waveform to study solitons made up of phase kinks that resulting from the creation of local Si(100)-p(2×2) structure in the ground state of Si(100)-c(4×2). The programmed bias pulses to Si surface and the yield related to respective pulses shows that the solitons were not induced by the direct excitation caused by tunneling electrons but the decay of quantum well state, produced by abrupt field switching. When the sample bias suddenly changes from positive to opposite, electrons near the quantum well move to compensate the non-equilibrium charge distribution and fill the quantum well. The decay of the quantum well provides excess energy to induce structural transition, the lifetime of the quantum well can be deduced from the soliton creation yield. The lifetime was increased with the bias and was on the order of a few hundred *n*sec. Such a fine control of bias pulse can be used to make artificial nano structure like 1 dimensional chain or laterally linked bisolitons.

**D-18** **Giant Kink in the Electron Dispersion of a Lead Monolayer on Stepped Si(111)** KIM Keun Su, YEOM Han Woong(*Institute of Physics and Applied Physics and Center for Atomic Wires and Layers, Yonsei University, Seoul 120-749, Korea.*) Physical properties of condensed matters are largely governed by many-body interactions between electrons or between electrons and collective excitations. Kinks in the dispersion of electrons are indicative of such interactions as typically observed in relation to collective excitations of lattice vibrations, phonons [1]. However, recent spectroscopic studies discovered unusual “giant kinks” at energies much higher than phonons on various high-Tc superconductors and graphene sparking debates on their origin and possible relation with exotic properties of these materials [2-5]. Despite diverse interpretations in terms of various collective excitations or electron-electron interactions, the underlying mechanism remains elusive due partly to the complexity in the materials themselves.In this presentation, we report a photoelectron spectroscopy result showing a consistent giant kink in a markedly simpler system, a lead monolayer supported on a semiconducting substrate with a week nanostripe corrugation [6]. In this system, the magnetic and plasmonic degrees of freedom are not allowed and well out of the energy range, respectively, excluding unambiguously a few possible interpretations except for a purely electronic mechanism proposed very recently [7]. Indeed, the characteristics of the kink are well explained quantitatively by the electronic kink theory [7] attributing the giant kink to a generic feature of Fermi liquid with electron correlation.

* References [1] A. Damascelli *et al.*, *Rev. Mod. Phys.* 75, 473 (2003). [2] J. Graf *et al.*, *Phys. Rev. Lett.* 98, 067004 (2007). [3] B. P. Xie *et al.*, *Phys. Rev. Lett.* 98, 147001 (2007). [4] T. Valla *et al.*, *Phys. Rev. Lett*. 98, 167003 (2007). [5] A. Bostwick *et al., Nature Physics* 3, 36 (2007). [6] K. S. Kim *et al.*, *Phys. Rev. Lett*. 99, 196804 (2007). [7] K. Byczuk *et al.*, *Nature Physics* 3, 168 (2007)

■ SESSION: D [DG4]
10월 23일(목), 12:30 - 14:00
장 소: 401호

**D-19(초)** **우리나라 자기공명 실험의 지난 50 년을 되돌아보다** 조 성호(*고려대학교 물리학과.*) 2008년은 우리나라에서 최초로 핵자기공명 신호를 관찰한지 50 년이 되는 해이다. 당시 서울대학교 물리학과 4 학년의 연구실험에서 4인 공동으로 250 kg 전자석과 고주파 발진부 및 수신부를 직접 제작하여 물 속에 있는 수소(H) 원자핵의 공명신호를 측정하여 양성자의 자기모멘트를 구했던 것이다. 이 실험은 1960년대 초 서울대학교에서 1.5 MeV

싸이클로트론 가속기의 건조로 이어지고, 또한 연세대학교의 베타선 분석기 제작에도 관련되었다. 1970년대 고려대학교에 핵자기공명과 핵사중극 공명장치가 각각 자체적으로 꾸며졌고, 또한 미국 Varian 사의 WL-112 NMR Spectrometer 가 도입되었다. 이는 국내 최초의 고성능 고체 핵자기공명 장치였다. 1980년대 한국기초과학 지원연구소에 도이치 Bruker 사의 X-밴드와 Q-밴드 EMR Spectrometer 가 비치됨으로서 국내 자기공명 실험연구의 기틀이 잡혀졌다. 우리나라 자기공명 연구의 발자취를 주로 발표자의 활동과 실험장치 측면에서 핵자기공명, 핵사중극공명, 및 전자자기공명 분야로 나누어 연대순으로 되돌아보고자 한다.

**D-20** **Magnetic Properties of Metal-dsDNAs** LEE Chang Hoon, KWON Young-Wan[1], JIN Jung-Il[1], KOH Eui-Kwan[2] (*Dept. of Polymer Sciences &Engineering, Chosun University.* [1]*Dept. of Chemistry, Korea University.* [2]*KBSI, Seoul Branch.*) Here, we presented magnetic properties obtained from various metal-dsDNAs (M-DNAs) in dry state. Interestingly, the magnetic properties were found to be enchanced as the metal elements doped were decreased. In order to explain these unconventional behaviors, it is considered a helical charge transport through the M-DNAs, which might be severely purtervebd in the high-doping but not in the low-doping levels of metal ions.

**D-21** **CoFe/Pt 다층박막의 자기구역경계선의 roughning exponent 분석.** 이 강수, 이 창원[1], 조 영진[1], 서 순애[1], 최 석봉(*서울대학교, 물리 천문학부.* [1]*삼성 종합기술원.*) 경계면의 형성은 많은 요인에 의해 영향을 받게 된다. 그럼에도 불구하고 경계의 형태는 기본적인 법칙 몇 가지에 의해 결정된다고 많은 과학자들은 믿고 있다. 경계면의 형태가 무엇에 의해 영향을 받는지, 어떻게 영향을 받는지 알고 형태를 우리가 원하는 데로 조정할 수 있다면 많은 산업에 응용될 수 있는데, 이는 자기구역경계선도 마찬가지이다. 이에 본 연구는 PMA 성질을 나타내는 CoFe/Pt 다층박막의 roughening exponent 와 이에 영향을 주는 요인들을 분석하고 실험하였다. MOKE 현미경을 이용해 자기구역의 경계면을 시각화하였고, 컴퓨터 프로그램을 통한 이미지 작업을 통해 분석을 하였다.

**D-22** **Characterization of magnetic interface roughness and magnetic domain structure in a magnetic multilayer using soft x-ray resonant magnetic scattering** 이 동렬, 박 지희[1], CHOI Yongseong[2], FREELAND John W.[2], JIANG J. S.[2](*숭실대, 물리학과.* [1]*포항공대, 물리학과.* [2]*Argonne National Laboratory, USA.*) We present a soft x-ray resonant magnetic scattering(XRMS) study of in-field magnetic structures in a Gd/Fe multilayer where Gd and Fe layers couple antiferromagnetically at their interfaces. We have measured the XRMS intensities in the transverse diffuse scattering geometry, where the sample angle is varied with the detector angle fixed, to characterize the lateral morphologies of structural and magnetic interface roughnesses. Since the sum and difference of the diffuse scattered intensities for opposite photon helicities of circular polarized incident x-rays are related to the height-height cross correlation functions of the structural-structural and structural-magnetic rough interfaces, respectively,[1] the sum and difference intensities have been measured to separately characterize structurally and magnetically rough interface morphologies.We have also measured the hysteresis loop of the XRMS intensities while the applied field cycling at various sample angles, yielding different lateral components of the momentum transfer q_parallel, to investigate the evolution of the magnetic domain structures under the applied field. While the loops measured at specular positions (q_parallel = 0) show a typical magnetic hysteresis loop we have observed markedly unusual shapes at off-specular positions with nonzero q_parallel values. This unusual off-specular loop has been also observed for the annealed CoFe film but not been explained in detail.[2] Here we have observed that such an unusual loop appears strongly at low q_parallels and becomes same as the specular loop as q_parallel increases. Furthermore, when we have measured the sum and difference of the XRMS hysteresis loops for opposite photon helicities in a similar manner to the diffuse scattering related to the height-height correlation function, we have found that while the sum loops show different shapes with different q_parallel positions the shapes of the difference loops are same regardless of q_parallel. This implies that there exist magnetic domains as well as magnetic roughness because the magnetic domain scattering manifest itself only in the sum intensities[1] .

*[1] D. R. Lee et al., Phys. Rev. B68, 224410 (2003). [2] E. Negusse et al., Appl. Phys. Lett. 90, 092502 (2007).

**D-23** **Magnetic Methods for Determining the Monodispersity of Ferrofluids** YOON Sunghyun(*군산대학교 물리학과.*) Methods of determining the particle size and its distribution of nanoparticle ferrofluid through magnetic measurements were described. For these measurements, a water-based magnetite ferrofluid was prepared by the chemical coprecipitation method. Direct morphological study using TEM showed that nominal radius of the particles was 6 nm with some distribution width. The DC magnetization curve at room temperature was shown to be superparamagnetic, in good aggreement with a theoretical curve calculated for a particle size distribution with an averaged radius of 5.45 nm, and the distribution width 3.8 nm. The frequency dependence of the complex susceptibility $\chi(\omega)=\chi'-i\chi''$ of the ferrofluid was measured by the slit-toroid technique. The sample exhibited frequency response due to Neel's rotational relaxation, from which estimate was made of particle size. Effects of inter-particl interaction was examined through the dilution experiments. The observed relaxation was well explained by a superposition of single particle process for a ferrofluid with some degree of size distribution. All the particle sizes and distributions were obtained by introducing an improved model distribution function. Introducing a revised lognormal distribution, a good fit to the experimental data was obtained. Neel type relaxation was a dominant mechanism in the ferrofluid examined. While the ac susceptibility measurement yielded more sharp distribution than the DC magnetization measurement did, it gave an averaged radius roughly consistent with both the electron microscopy and the DC method. The ac method was found to be more sensitive to the variation of hydrodynamic volume or the inter-particle interaction

in the ferrofluids.

■ SESSION: D [DG5]
10월 23일(목), 16:30 - 18:30
장 소: 201호

**D-24** **Nonequilibrium Dephasing in an Electronic Mach-Zehnder Interferometer** 윤 석찬, 이 현우[1], 심 흥선(*KAIST, 물리학과. [1]Postech, 물리학과.*) We study nonequilibrium dephasing in an electronic Mach-Zehnder interferometer. We demonstrate that the shot noise at the beam splitter of the interferometer generates an ensemble of nonequilibrium electron density configurations and that electron interactions induce configuration-specific phase shifts of an interfering electron. The resulting dephasing exhibits two characteristic features, a lobe pattern in the visibility and phase jumps of pi, in good agreement with experimental data.

**D-25** **Studies of Quantum-Hall Edge States in Graphene** 기 동근, 정 동찬, 조 상현, 이 후종(*포항공과대학교, 물리학과.*) Since 1980's, the quantum Hall effect (QHE) in two-dimensional systems has been studied intensively and still provides many interesting topics of studies. One of the most stimulating features of the QHE is the formation of edge states, where the current (the edge current) can flow along the edges of a two-dimensional system only in a clockwise or counterclockwise direction, depending on the direction of a perpendicular magnetic field, without dissipation. By taking the advantages of this edge-current state, a solid-state version of the beam splitter was successfully made and the electronic Mach-Zehnder interferometer was also established in a GaAs/AlGaAs heterostructure [1]. In a graphene sheet, a sheet of mono-layer graphite, the type of charge carriers can be changed by simply applying an appropriate gate voltage, where the direction of the edge current can be altered for a fixed perpendicular magnetic field in the same sample. In consequence, depending on the position of the electrical ground and the gate voltage, the two-terminal conductance of a graphene sheet can be either finite or zero. In this work, we measured the quantum Hall effect in a monolayer graphene sheet and proved the directionality of the edge current by simply changing the gate voltage and the measurement configuration. In addition, the possible formation of a beam-splitter for Dirac fermions in graphene will be suggested and discussed.
* [1] Y. Ji, Y. Chung, D. Sprinzak, M. Heiblum, D. Mahalu, and H. Shtrikman, Nature 422, 415 (2003).

**D-26** **Inelastic scattering in a monolayer graphene sheet probed by weak-localization measurements** JEONG Dongchan, KI Dong-Keun, CHOI Jae-Hyun, PARK Kee-Su[1], LEE Hu-Jong (*Department of Physics, Pohang University of Science and Technology. [1]Department of Physics, Pusan National University.*) Charge carriers in a graphene sheet, a single layer of graphite, exhibit much distinctive characteristics to those in other two-dimensional electronic systems because of their chiral nature. In this report, we focus on the observation of weak localization in a graphene sheet exfoliated from a piece of natural graphite and nano-patterned into a 1-μm-wide Hall-bar geometry. In weak localization studies, both conventional weak localization and anti-weak localization have been reported. Anti-weak localization is known to be caused by the chirality-conserving elastic scattering. However, much stronger chiral-symmetry-breaking elastic intervalley scattering in our graphene sheet restores the conventional weak localization, which is governed by the inelastic scattering. For quantitative analysis, we used weak-localization-included conductivity equation theoretically proposed in terms of three parameters ($L_\phi$, $L_i$, $L_*$). The resulting carrier-density and temperature dependence of the phase coherence length ($L_\phi$) reveal that the electron-electron interaction including a direct Coulomb interaction is the main inelastic scattering factor while electron-hole puddles enhance the inelastic scattering near the Dirac point.

**D-27** **Shot Noise Properties in a GaAs Small Quantum Dot** 김 영상, 서 요한, 전 한경, 정 희준(*한양대학교 응용물리학과.*) This experiment provides a low-frequency shot noise properties of tunneling current performed in a GaAs quantum dot with a small number of confined electrons. The shot noise of current evaluates the temporal correlations between charge transfer events through a conductor. Fano factor described as the shot noise deviation from the Possonian value has proven to be a powerful tool to study transport in mesoscopic conductors. The elastic and inelastic cotunneling transports are evaluated by the conductance measurement and Fano factor analysis extracted from the noise measurement for the inside and the outside of Coulomb diamond region. Consequently, we demonstrate the variation of Fano factor based on our experimental results and explain the related physical phenomena in detail.
* This work was supported by the Korea Research Foundation Grant funded by the Korean Government (MOEHRD) (KRF-2006-331-C00120).

**D-28** **Tailoring Electronic Structures of Carbon Nanotubes by Solvent with Electron Donating and Withdrawing Groups** KIM Soo Min, SHIN Hyeon-Jin[1], KIM Ki Kang[2], YOON Seon-Mi[1], KIM Sung Jin[3], PARK Hyun Ki[3], CHOI Jae-Young[1], LEE Young Hee[4](*Sungkyunkwan Advanced Institute of Nanotechnology, Sungkyunkwan University. [1]Samsung Advanced Institute of Technology. [2]Department of Physics, Sungkyunkwan University. [3]Department of Physics, Sungkyunkwan University. [4]Department of Physics, Sungkyunkwan Advanced Institute of Nanotechnology, Sungkyunkwan University.*) Various electron donating and withdrawing groups in aromatic and aliphatic backbones of solvent have been introduced to tailor the electronic structures of single-walled carbon nanotubes (SWCNTs). In case of solvent with a withdrawing group, electrons were extracted mainly from metallic SWCNTs, whereas small charge transfer was also observed in semiconducting SWCNTs. On the other hand, in case of solvent with a donating group, electrons

were donated to both metallic and semiconducting SWCNTs. This effect was less prominent in solvent with an aliphatic backbone than that with an aromatic backbone. The strong correlation between the sheet resistance and electronic structures of nanotubes is further discussed in conjunction with a modulation of Schottky barrier height.

**D-29** **Evalution of semiconducting/metallic ratio of single-walled carbon nanotubes with purification process.** 민 경인, 정 현[1], 김 기강[2], 최 수봉[3], 노 희석[4], 이 영희[2], 오 명규[5], 변 지수[5], 김 종수[5], 정 문석[5](*고등광기술연구소/전북대학교, 물리학과. [1]고등광기술연구소/전북대학교, 반도체기술학과. [2]성균관대학교, 물리학과. [3]서울대학교, 물리학과. [4]전북대학교, 물리학과. [5]고등광기술연구소.*) Arc-discharge로 합성된 single-walled carbon nanotubes(SWCNTs) pristine 시료와 열처리, 산처리를 통하여 정제한 시료들의 semiconducting/metallic 구성 비율을 UV-VIS-NIR absorption spectroscopy를 이용하여 계산하였으며 이 결과를 570~620 사이에서 파장변조가 가능한 dye laser와 700~900 nm 사이에서 파장변조가 가능한 cw-Ti:sapphire 레이저를 이용한 파장변조 공명라만산란 방법으로 검증하였다. Absorption spectroscopy 분석결과 1, 1.3, 1.8 eV에서 E11S, E22S, E11M 전이가 관측되었으며, 산처리등의 정제과정을 통하여 semiconducting SWCNTs의 구성 비율이 감소됨이 계산을 통해서 발견되었으며, 파장변조 공명라만산란실험에서도 정제과정에 따라 semiconducting SWCNTs의 peak가 사라지는 현상을 동일하게 관측하였다.

**D-30** **Dihydrogen Binding on Ca-inserted Porphyrin for Hydrogen Storage** HONG Suklyun, RYOU Junga, KIM Gunn[1](*Department of Physics and Institute of Fundamental Physics, Sejong University, Seoul 143-747. [1]BK21 Physics Research Division and Department of Physics, Sungkyunkwan University, Suwon 440-746.*) We have studied hydrogen binding on metal-inserted porphyrin using ab initio pseudopotential calculations. A Ca atom is inserted in the central $N_4$ cavity of porphyrin. By increasing the number of hydrogen molecules, we investigate dihydrogen binding on Ca-inserted porphyrin for hydrogen storage. Up to six hydrogen molecules are attached to the Ca atom. For LDA calculations, we find that the binding energy of $H_2$ molecules to the Ca atom is 0.25 eV/$H_2$ up to four hydrogen molecules. When the fifth or sixth $H_2$ molecule is adsorbed on the Ca atom, the molecule is physisorbed to the Ca atom. Up to six molecules, the $H_2$ binding energy is reduced to about 0.2 eV/$H_2$. Examining the projected density of states, we study orbital hybridization between the Ca atom and hydrogen molecules. Finally, the possibility of Ca-inserted porphyrin as a hydrogen storage material is discussed.

**D-31** **Origin and mechanism of size effects in organic nanocrystals** RIM Min Ho, SEO Jung In[1], LEE Yoon Sup[1], LEE Kwang-Sup[2], YOON Choon Sup(*Department of Physics, KAIST. [1]Department of Chemistry &School of Molecular Science (BK21), KAIST. [2]Department of Advanced materials, Hannam University, Daejeon 306-791, Korea.*) The origin and mechanism of the size effect in organic nanocrystals remain unexplained. The absorption spectra for different particle sizes of 3-methyl-4-methoxy-4'-nitrostilbene (MMONS) nanocrystals are characterized by two distinct types of absorption peak, one at around 375 nm and the other at around 475 nm. Using optical absorption spectra and density functional theory calculations as a basis, we report that the size effects in MMONS nanocrystals are governed largely by excitonic intramolecular charge transfer for particles smaller than about 14 nm and by excitonic intermolecular charge transfer through the hydrogen bond networks and π-π stackings for particles larger than about 14 nm. These size effects differ fundamentally from the quantum confinement effect that occurs in inorganic metal and semiconductor nanoparticles.

■ SESSION: D [DG6]
10월 23일(목), 16:30 - 18:15
장 소: 206호

**D-32** **Evidence for strong correlation between spin and charge dynamics in $La_2Cu_{1-x}Li_xO_4$** 박 은성, 박 두선[1], SARRAO J. L.[2], THOMPSON J. D.[2](*성균관대학교 물리학과. [1]성균관대학교 물리학과, Los Alamos National Laboratory. [2]Los Alamos National Laboratory.*) 리튬(Li)을 도핑(doping)한 $La_2CuO_4$에 대하여 유전상수와 교류 자화율을 온도에따라 측정하였다. 전이 온도가 진동수에따라서 변하는 전하글라스(charge glass) 및 스핀글라스(spin glass) 현상이 나타났으며, 이 두 현상이 밀접하게 연관되어 있음을 보이는 결과를 얻어냈다. 이 물질에서 스핀글라스온도가 전하글라스온도보다 높게 나타났는데 이는 온도가 낮아짐에 따라 스핀의 자유도(degree of freedom)가 먼저 얼어붙고 뒤이어 전하의 자유도가 얼어붙도록 영향을 주는 것으로 보여진다. 교류자기장의 진동수에 대한 유사한 반응은 스핀글라스와 전하글라스의 기작(mechanism)이 상호간에 강하게 연관되어있음을 암시한다.

**D-33** **Pseudo-gap in electron doped cuprates: Spin fluctuation origin and close relation with superconducting gap** 박 승룡, 송 동준, 임 춘식, 김 철, 최 성균, 김 용관, 정 원식, 고 윤영, 최 규진, 김 재훈, 김 창영, EISAKI Hiroshi[1](*연세대학교, 물리학과. [1]Japan, AIST.*) Pseudo gap in electron doped cuprates was discovered in angle-resolved photoemission (ARPES) and optical spectroscopy experiments. Recently, it was found that the locus of superconducting (SG) and pseudo gap (PG) maxima coincide in the momentum space. Therefore, any knowledge on what causes PG in electron doped cuprates may give us a hint on the origin of the high temperature superconductivity. Researchers have tried to resolve the issue in terms of long range anti-ferromagnetism model or strong correlation model such as Hubbard model. However, it was recently found that PG still exists even in optimal doped cuprates where long range AF order does not exist. In addition, it is unlikely that strong correlation model is a suitable model optimal doped regime. A natural candidate for the cause of PG could be spin fluctuation. However, there has not been any careful calculation based on the spin fluctuation model, at least to our best

knowledge. Recently, entire dynamic spin susceptibility of electron doped cuprate was obtained by using inelastic neutron scattering. Therefore, one could use electron-spin coupling which is proportional to the dynamic spin susceptibility and calculate the spectral function based on the electron-spin fluctuation coupling model. In this presentation, we first show calculated ARPES spectral function based on electron-spin fluctuation coupling model with the magnetic susceptibility as the input. We could identify the origin of PG as electron-spin fluctuation from this simulation, and we also could extract a rough value for the electron-spin fluctuation coupling strength g in electron doped cuprates by comparison between experimental data and simulation results. Experimentally, temperature dependent ARPES spectral function taken between 10K and 280K shows that PG is continually filled up but still exists even in 280K. This also supports the electron-spin fluctuation coupling model. Anomalous temperature dependent Hall coefficients may be due to this temperature dependent spectral weight evolution. We found that SC transition temperature is inversely proportional to the spectral weight of PG near Fermi energy by ARPES data of NCCO, SCCO, ECCO and GCCO. Based on the electron-spin fluctuation coupling model, we discuss the SC origin of electron doped cuprates.

**D-34** **Negligible effect of the eddy current to produce dendritic flux jumps in $MgB_2$ thin films** LEE Jae-Yeap, PARK Jae-Hyun, LEE Hu-Jong, LEE Sung-Ik[1], JOHANSEN T. H.[2], CHOI Eun-Mi[3], CHO Jae-Hum[4], CHO Young-Hun[4](*Department of Physics, Pohang University of Science and Technology.* [1]*Department of Physics, Sogang University.* [2]*Department of Physics, University of Oslo.* [3]*BK21 Division and Department of Physics, Sungkyunkwan University.* [4]*Quantum Material Research Team, Korea Basic Science Institute.*) It is well accepted that the dendritic avalanche (enhanced flux noise) in $MgB_2$ or in several other thin films is caused by thermo-magnetic instability. Previous studies show that placing a metallic layer on an $MgB_2$ film suppresses such instability. However, the effect of an eddy current in the metallic layer driven by the fast movement of vortices on this dendritic avalanche remains to be further examined. To distinguish these two effects, we intentionally insert a PMMA layer as an insulating layer between an $MgB_2$ thin film and a gold matallic layer, which blocks the heat diffusion between the two layers. With this insulating layer, flux noise still appears in the magnetic hysteresis loop. From this observation, we conclude that the eddy current produces a minor effect while the thermo-magnetic instability is the main cause of the enhanced flux noise.

**D-35** **First-principles study on structural properties of Iron-based superconducting compounds** PARK Se Young, MOON Chang-Youn, CHOI Hyoung Joon(*Department of Physics and IPAP, Yonsei University.*) The new family of high temperature superconductivity in doped Iron-based compounds has been drawing lots of interest. Starting from electron-doped LaOFeAs, there is a variety of compounds such as LiFeAs and $BaFe_2As_2$ which commonly have the same Fe-As layered structure. We calculate the structural and magnetic properties of LaOFeAs, LiFeAs and $BaFe_2As_2$ in non-magnetic (NM) phase as well as in stripe type antiferromagnetic (AF) phase by total-energy minimization and compare our results with experiments. In addition, we calculate the atomic structure and the magnetic moment of hypothetical compounds LaOFeSb, LiFeSb and $BaFe_2Sb_2$ in NM and AF phases. By comparing our calculated results, we find that substituting As with Sb increases lattice constants and Fe-Pn (Pn = As, Sb) distances with enhanced magnetic moments.

* This work was supported by the KRF (KRF-2007-314-C00075) and by the KOSEF Grant No. R01-2007-000-20922-0. Computational resources have been provided by KISTI Supercomputing Center (KSC-2008-S02-0004).

**D-36** **Scale free behavior in one dimensional superconducting vortex systems with variable range hopping** 조 영권, 김 기홍(*아주대 에너지시스템학부.*) We study one dimensional superconducting vortex systems with the variable range hopping effect due to the distribution of columnar defects of different sizes. In this model, the columnar defects are inhomogeneous pinning centers such that the vortex pinned at one defect does not prefer to hop to the nearest neighbor site. We derive the preferential hopping term in terms of the defect binding energy and the distance between two defects. Through the growth and preferential linking process, we construct the bosonic scale free network and compare it with the periodic, quasiperiodic and random cases. In our model, the defect structure determines the fitness distribution and the number of links at each site. We find the eigenvalue spectrum and analyze the physical quantities such as the inverse participation ratio and the superfluid density. In addition, we examine the influence of a tilted external magnetic field to the scale free behavior of vortex systems by considering the imaginary vector potential in bosonic systems.

**D-37** **Depinning Mechanism of Josephson Vortex Chains in Stacked High-$T_c$-superconductor Josephson Junctions** 이 길호, 진 용덕, 이 후종(*포항공과대학교 물리학과.*) We studied the depinning mechanism of Josephson vortices in $Bi_2Sr_2CaCu_2O_{8+x}$ (Bi-2212) high-$T_c$ superconducting single crystals with atomically layered structure. Current-voltage characteristics of a stack of Bi-2212 intrinsic Josephson junctions were measured in a crystal in-plane magnetic field up to 6.5 T. With increasing magnetic fields the quasiparticle branches are continuously suppressed. Raising magnetic field above 2.0 T vortex-flow branches start to appear in the low-bias regime. Each branch is characterized by a maximum current, above which a jump takes place to a next higher-voltage branch. This switching may correspond to a depinning of Josephson vortex chain in each junction because flowing vortex chain will give extra voltage along the c-axis. In this respect, vortex-flow branches are expected to provide valuable information on the Josephson vortex flow dynamics and the collective pinning interaction between Josephson vortices and the pinning elements

such as pancake vortices.To study the depinning mechanism of vortex chain we measured depinning current distribution (DCD) 10000 times at each temperature from 10 K down to 300 mK. Current was biased with a battery-powered current source to reduce any external electrical noise and the electrical measurement leads were carefully filtered by RC low-pass filters and pi filters. The DCD becomes narrower as lowering temperature. Below the crossover temperature $T_c$ of ~3 K, the width of the DCD becomes saturated and temperature independent. Above $T_c$, the thermal activation from the pinning potential due to thermal fluctuation plays a major role in the switching events. Below $T_c$, however, a temperature-independent depinning mechanism such as quantum depinning out of the pinning potential is supposed to become dominant. Raising magnetic field introduces more Josephson vortices and tilting angle controls the number of pancake vortices so we can manipulate the interaction between Josephson vortices and pancake vortices. We will discuss on the magnetic-field and the tilted-angle dependence of DCD measured in the separated experiment in the temperature range of 4.3 K to 65 K.

**D-38** **Josephson Vortex Dynamics In Stacked High-$T_c$-Superconductor Josephson Junctions** JIN Yong-Duk, LEE Gil-Ho, LEE Hu-Jong(*포항공과대학교, 물리학과.*) Densely stacked intrinsic Josephson junctions (IJJs) formed in a high-$T_c$ superconducting materials such as $Bi_2Sr_2CaCuO_{8+\delta}$ (Bi2212), with their self-oscillating feature and the large superconducting gap, can be used for an application to a promising electromagnetic wave source in a terahertz range. To realize efficient terahertz emission from the stacked junctions, it is essential to make the entire junctions behave coherently. One of the schemes to achieve a coherent state over the junctions is to exploit the collective Josephson vortex motion by applying a high enough in-plane magnetic field to form a Josephson vortex lattice. The possibility of terahertz emission by employing collective Josephson vortex motion has been confirmed experimentally by Bae, Lee, and Choi. To optimize the terahertz emission condition precise characterization of the Josephson vortex state and its dynamic characteristics is required. We prepared Bi2212 stacks, each with a finite number of IJJs sandwiched between two gold layers without a basal part, to precisely characterize the Josephson vortex dynamics without the interference of Josephson vortices in the basal part. In tunneling current-voltage characteristics along the *c* axis in various magnetic field strength, field angles, and temperatures, we observed an additional branch structure, so-called Josephson vortex flow branches (JVFBs), along with the usual quasiparticle branches. Investigation of dependence of JVFBs on field strength and field angle revealed that JVFBs originate from non-collective pinning and depinning of Josephson vortices in each layer. In addition, comparison of our results with the observation of terahertz emission by Bae, Lee, and Choi leads to a conclusion that the Josephson vortices form an oblique-rectangular lattice with a specific phase difference $2\pi/n$ between adjacent layers, where $n$ is the number of junctions with moving Jospehson vortices.



■ SESSION: D [DS1]
10월 23일(목), 16:30 - 18:10
장 소: 401호

**DS-01(초)** **Multiple Conditioned MuSR Techniques Using Pulsed Muons at the RIKEN-RAL Muon Facility** WATANABE Isao(*RIKEN Nishina Center.*) Muon-Spin-Relaxation/Rotation/Resonance (MuSR) techniques at the RIKEN-RAL Muon Facility in the UK are introduced. The Nishina Center for Accelerator-Based Science of RIKEN (The Institute of Physical and Chemical Research) has constructed the RIKEN-RAL Muon Facility at the Rutherford-Appleton Laboratory (RAL) in the UK. The world-wide strongest pulsed muon beam is available for material sciences at the RIKEN-RAL Muon Facility in the wide range of the muon momentum from 27 to 120 MeV/c [1]. Conventional MuSR techniques are available in the temperature range from 20 mK to 500 K and in the field range from zero to 4 kG. Lots of MuSR studies on magnetic materials, superconductors, heavy fermions, organic magnets/superconductors and other related functional materials have been carried out in collaboration with universities and instates in the world. Recently, novel multiple conditioned MuSR techniques using Laser applications, high-pressure applications [2], ultrasonic-wave applications and radio-frequency applications have been established to offer new experimental tools to material scientists. These experimental conditions for MuSR are available only at the RIKEN-RAL Muon Facility in the world. Parameters of each experimental condition are; Laser(25 Hz) Nd:YAG, 400 – 1600 mJ, 355 – 1064 nm, EX OPO: 430 – 2500 nm: Light(25Hz) ~ 40 W, Flush Ramp (white light): High Pressure gas pressurized (He), up to 6.4 kbar: Ultrasonic Wave ~ 10 MHz, up to 30 W: Radio Frequency 20 – 60 MHz, up to 250 W. In my talk, I would like to introduce the RIKEN-RAL Muon Facility itself and explain what is MuSR and how do we carry out MuSR experiments. I would also like to introduce the novel multiple conditioned MuSR techniques mentioned above, and how to apply to RIKEN to use the RIKEN-RAL Muon Facility.
[1] K. Nagamine *et al.*, Hyperfine Interact. 87 (1994) 1091. [2] I. Watanabe, *et al.*, Physica B (in press).

**DS-02(초)** **Magnetic Spectroscopy at EPU6 Beamline** KIM J.-Y.(*Pohang Accelerator Laboratory.*) 방사광을 이용하여 자성 물질을 연구하는 자성분광학 분야는 1990년대 이후, 3세대 방사광 가속기가 등장하고 광원의 획기적인 성능향상이 이루어진 다음에야 비약적인 발전이 시작되었는데, 그 이유는 자성물질을 연구하기 위해서는 광원의 편광을 자유롭게 조절할 수 있어야 한다는 조건과 더불어, 빛과 자기 모멘트 사이의 상호작용이 빛과 전하간의 상호 작용보다 훨씬 작아서 고휘도의 광원이 필수적이었기 때문이다. 이렇게 짧은 역사와 함께 그 실험방법과 해석의 난해함 등으로 인해 자성분광학 분야는 지금까지도 여러 가지의 방법론이 제안되고 검증되는 과정이 계속되고 있으며, 그 중에서 방법론이 비교적 잘 정립되어 널리 이용되고 있는 실험 방법으로는 x-선 자기원형편광 이색성(x-ray Magnetic Circular Dichroism, XMCD)실

험, 편광별 x-선 흡수(polarization dependent x-ray absorption spectrum)실험, 스핀분해 광전자 분광법(Spin-resolved photoemission, SRPES) 등이 있다. 이중에서 XMCD는 조사되는 원형 편광 x-선의 나선 방향과 시료내의 자기 모멘트의 자화 방향의 차이에 따라서 x-선 흡수율에 차이가 생기는 현상을 측정하는 것으로, 시료가 여러 가지 원소의 화합물이거나 구조물일 경우 각각의 원소에 대한 자성을 분리해서 측정하는 것이 가능하며, 스핀 자기 모멘트와 오비탈 자기 모멘트를 따로따로 분리해 낼 수 있어서 결정구조 및 표면, 계면과 자기 이방성 간의 관계를 규명하는데 유용하다. 한편 최근 들어서는 연 x-선 자기 공명 산란(soft x-ray resonant magnetic scattering, SXRMS) 실험이 전 세계의 여러 빔라인에서 경쟁적으로 시도되기 시작하였는데, 이것은 soft x-ray 영역(400 eV ~ 2000 eV)에 자성물질의 대부분을 이루는 3*d* 전이원소와 4*f* 희토류 원소의 가장 중요한 흡수선이 모두 존재할 뿐만 아니라, 또한 그 파장의 크기가 망간화합물 및 다강체의 스핀 및 오비탈 정렬의 주기와 유사하여, 고체 내에서의 자기 모멘트의 정렬을 좀 더 직접적으로 측정하는 것이 가능하기 때문이다. 또한, 자성 다층 박막이나, 나노 점 배열 같은 초격자 인공구조물의 경우에도 그 격자 크기가 연 x-선의 파장과 일치하기 때문에 이러한 분야에서도 SXRMS를 이용한 연구의 중요성이 점차 부각되고 있다. 이 발표에서는 포항 방사광 가속기의 자성 분광학 실험장치로 건설된 EPU6 빔라인 및 이를 이용한 나노입자, 다강체, 희박 자성반도체 및 자성나노박에 대한 최근 연구결과들을 소개하고자 한다.

**DS-03(초)** **Status of Three Neutron Spectrometer Projects at HANARO** SO J.-Y., CHOI Y. N., PARK J. M. Sungil(*Korea Atomic Energy Research Institute, Neutron Science Division.*) The High-flux Advanced Neutron Application Reactor (HANARO) is a 30 MW world-class research reactor well-suited for neutron scattering research. Neutrons excel at studying atomic and molecular dynamics on the order of meV's and the reactor produces high flux neutron beams to perform leading edge research. Through the Cold Neutron Research Facility project and as part of the Atomic Energy Technology Development Program, 3 neutron spectrometers - a cold neutron triple-axis spectrometer, a disk-chopper time-of-flight spectrometer and a thermal triple-axis spectrometer - are being built at HANARO. In this presentation, we discuss how these instruments work and what are the implications to the condensed matter physics community in Korea and the neighboring countries.

■ SESSION: D [DG7]
10월 24일(금), 09:00 - 10:45
장 소: 201호

**D-39** **Diameter modulation of single-walled carbon nanotubes via heat-driven diffusion and evaporation of catalytic nanoparticles** W. Song, C. Jeon, W. C. Choi, Y. T. Kwon, Y. S. Kim, D. S. Jung, S. W. Jang, C.-Y. Park(*BK21 Physics Research Division and Center for Nanotubes and Nanostructured Composites (CNNC), Sungkyunkwan University, Suwon 440-746, Republic of Korea.*) It is widely recognized that single-walled carbon nanotubes (SWNTs) have emerged as alternative materials for next-generation electronics owing to extraordinary electrical properties associated with one-dimensional nature [1]. The electronic properties of SWNT depend on their geometrical structure. Controlling SWNT diameter is thus considered as an ultimate goal for application of SWNTs-based nanoelectronics. It is well known that the correlation between catalyst size and SWNT diameter [2]. Accordingly, tailoring catalytic nanoparticles is one of the flagship factors to obtain nanoengineered SWNTs. Here, we present a novel process that takes advantage of diffusion and evaporation characteristics of Fe catalytic nanoparticles by annealing-time modulation resulting in growth of nanoengineered SWNTs with extremely narrow diameter distribution. The characterization of SWNTs was performed by resonant Raman spectroscopy with excitation wavelength of 514 nm (2.41 eV) and 633 nm (1.96 eV) and scanning electron microscopy, and transmission electron microscopy (TEM). In addition, we systematically study the heat-driven diffusion and evaporation mechanisms of catalytic nanoparticles in order to elucidate the SWNTs with extremely narrow diameter distribution and diameter shrinking process, which investigated by X-ray photoelectron spectroscopy with a monochromatic Al Kα radiation, secondary ion mass spectroscopy and TEM.

* Reference [1] R. Saito, G. Dresselhaus, M. S. Dresselhaus, Physical Properties of Carbon Nanotubes Imperial College, London (1998). [2] Ali Javey, Hongjie Dai, J. AM. CHEM. SOC., 127, 11942-11943 (2005).

**D-40** **Development of Spin-Coatable Indium doped Zinc Oxide Nanostructures using an Electron Beam** SHAHID Muhammad, RHEN Danielle[1], YANG Hyoungwoo[1], KANG Dae Joon[1](*성균관대학교 성균나노과학기술원. [1]성균관대학교 물리학과.*) Electron beam lithography is a patterning technique using an electron beam to pattern material (called a resist). It by-passes the conventional method of sputtering and lift-off and achieves nanoscale resolution. In this work spin-coatable IZO resist was prepared by chemically reacting zinc naphthenate with indium nitrate. The films were patterned with an electron beam writer and exhibited sensitivity and contrast of ~6.15mC $cm^{-2}$ and 2.7, respectively. The electron beam exposed region became insoluble in toluene, thus yielding negative patterns. IZO films were characterized after annealing treatment with X-ray Diffraction (XRD), atomic force microscopy (AFM), Raman and UV-vis spectroscopy. We also present the effect of indium concentration on the transport properties of IZO nanostructures patterned by electron beam lithography.

**D-41** **Optical gain and Time resolved spectroscopy of CdSe Quantum Dot** 김 상민, 홍 경수[1], 양 호순(*부산대학교 물리학과. [1]한국기초과학지원연구원 부산센터.*) 나노 크기의 반도체 결정 물질의 경우 양자 구속 효과와 표면 효과에 의해서 특이한 광학적 성질을 가지고 있다. 특히 화학적 콜로이드 방법으로 만든 CdSe 양자점의 경우 균일한 크기의 양자

점을 얻을 수 있는 장점이 있으며 광학적 이득(optical gain)이 높아 광학 재료로 이용 될 수 있다. 그렇지만 양자점의 표면이 불안정성 하기 때문에 표면 상태에 따라 광학적 성질이 어떻게 변하게 되는가는 중요하다. 일반적으로 표면 상태의 좋게 하기 위해 CdSe 양자점보다 에너지 밴드갭이 더 큰 ZnS를 이용하여 core/shell 형태의 CdSe/ZnS양자점이 많이 사용된다. 그리고 양자점의 경우 포논 병목화 (phonon bottleneck) 효과로 에너지 사이의 전이가 억제 될 것으로 예측되었으나 표면 잡힘이나 Auger 재결합과 같은 비복사 천이의 증가로 인해 매우 빠른 감소 과정을 보이는 것으로 알려져 있으며 특히 표면 상태에 따라 감소 정도가 틀리게 될 것이다. 본 연구에서는 양자점 표면의 유기물에 의해서 다양한 양자 효율을 가지는 CdSe 양자점과 CdSe/ZnS 양자점을 콜로이드 방법으로 합성하였다. 그리고 VSLM (Variable stripe length method) 방법을 이용하여 광학적 이득을 측정 하였다. 그리고 오실로스코프를 이용한 Time resolved spectroscopy 실험을 통하여 양자점 표면에 따른 decay time을 비교하였다. 특히 낮은 양자효율을 가지는 CdSe 양자점의 경우 slow energy decay process가 나타남을 확인할 수 있었다.

**D-42** **Exchange Bias Effects In $Fe_3O_4/\gamma$-$Fe_2O_3$ Core/Shell Nanoparticles** S. Angappane, HWANG Yosun, AN Kwangjin[1], HYEON T.[1], PARK J.-G.(*BK21 Physics Division, Department of Physics, Sungkyungkwan University, Suwon-440 746, Korea. [1]National Creative Research Initiative Center for Oxide Nanocrystalline Materials and School of Chemical and Biological Engineering, Seoul National University, Seoul-151 744, Korea.*) Exchange bias effects in monodisperse and core/shell structured $Fe_3O_4/\gamma$-$Fe_2O_3$ nanoparticles, synthesized by thermal decomposition iron oleate complex, are studied for the first time in this work. The narrow size distribution and the well defined core/shell structure of these nanoparticles are very well established by transmission electron microscope (TEM) and X-ray magnetic circular dichroism (XMCD) studies. In these core/shell $Fe_3O_4/\gamma$-$Fe_2O_3$ nanoparticles, the interface exchange anisotropy, in addition to the surface anisotropy, is found to dominate the effective magnetic anisotropy, calculated from the blocking temperature ($T_B$). A phenomenological model including the interface exchange anisotropy parameter is found to convincingly fit the effective magnetic anisotropy data. Unlike the exchange bias effects in conventional ferromagnetic (FM)/antiferromagnetic (AFM) systems, the ferrimagnetic/ferrimagnetic interface of the core/shell structure gives exchange bias effects in our $Fe_3O_4/\gamma$-$Fe_2O_3$ nanoparticles below $T_B$. In this core-shell structured nanoparticles, a spin glass state in the $\gamma$-$Fe_2O_3$ shell might play the role of AFM layer to bring about the exchange bias effect. However the possibility of the uncompensated spins of $\gamma$-$Fe_2O_3$ at the interface, coupling ferromagnetically with the $Fe_3O_4$ core to give the exchange bias effect, cannot be entirely ruled out. It is plausible that the competition between the FM and AFM coupling of spins at the interface of $Fe_3O_4/\gamma$-$Fe_2O_3$ core/shell layers could be attributed to the observed positive exchange bias in this system down to about 0.2 $T_B$.

**D-43** **Growth Mechanism of Macro-scale aligned Carbon Nanotubes by Oxygen-assisted Microwave Plasma Chemical Vapor Deposition** Y. S. Kim, W. Song, S. Y. Lee, W. C. Choi, C.-Y. Park*(*BK21 Physics Research Division and Center for Nanotubes and Nanostructured Composites (CNNC),Sungkyunkwan University, Suwon 440-746, Korea.*) Carbon nanotubes (CNTs) have shown multi-faceted promise for diverse applications due to their extraordinary electrical and physical properties [1]. Intense research has been carried out to synthesize the long aligned CNTs for applications in electronics, biosensor, and many other areas.[2, 3] Macro-scale aligned arrays of thin-multiwalled carbon nanotube (thin-MWCNT) on layered Si substrates have been synthesized by oxygen-assisted microwave plasma chemical vapor deposition (MPCVD). Our group succeeded to grow vertically aligned MWCNT up to 4-mm long. And the CNTs were weak adhesion which allowed to be peeled off easily from the substrate. We systematically investigated that the CNTs were grown by variation in $O_2$ gas flow rate and growth time. This results show that the growth of macro-scale aligned CNTs can be achieved with $O_2$ healing gas. Furthermore, we were able to synthesize the CNTs with outstanding growth rate comparable with that of conventional thermal CVD (TCVD) technique. Scanning electron microscope(SEM), energy-dispersive spectroscopy(EDS), x-ray photoelectron spectroscopy (XPS), and Raman spectroscopy were used to analyze the CNT morphology, composition and growth mechanism. Intense research will be carried out to fabricate the yarn using CNTs grown by MPCVD for applications in electronics, biosensor, carbon nanotube yarns and many other areas.

* Reference [1] R. Saito, G. Dresselhaus, M. S. Dresselhaus, *Physical Properties of Carbon Nanotubes* Imperial College, London (1998). [2] Kenji Hata *et al.*, Science, 306, 1362 (2004) [3] Guofang Zhong *et al.*, J. Phys. Chem. B, 111, 1907 (2007)

* E-mail: kimys1216@skku.edu

**D-44** **Characterization and Electrical Properties of Cu, CuO and $Cu_2O$ Thin Films and Nanostructures from Quasi-Chemical Synthesis** RHEN danielle, SHAHID Muhammad[1], KULYK Nadia[2], CHUNG Chan-Hwa[2], KANG Dae Joon(*성균관대학교 물리학과. [1]성균관대학교 성균나노과학기술원. [2]성균관대학교 화학공학과.*) Either as interconnects in circuitry, as a photo-active material appropriate for solar cell applications or as a base for superconductors, copper (Cu) and copper oxides ($Cu_2O$ and CuO) are attractive materials. We seek to understand the behavior of these materials in the nano regime (thin films and nanostructures) in order to gain insight into the range of properties and functionalities available as the world begins to focus on smaller dimensions and quantum effects. In order to study this family consistently we chose a single precursor material that could be modified to suit our needs, i.e. synthesized as Cu, $Cu_2O$ or CuO. Using Cu naphthenate as a precursor films were spin-coated on quartz substrates and annealed at various temperatures in different atmospheric conditions, the results of which allowed us to determine the phase diagram of this material. From here we could see that all three materials could be realized inexpensively from the same

precursor. The precursor was analyzed prior to annealing by thermogravitational analysis (TGA). Annealed films were characterized by X-ray Diffraction (XRD), Raman Spectroscopy, Scanning Electron Microscopy (SEM), Photoluminescence (PL), and 4-terminal electrical measurements. Nanostructures were formed by electron beam lithography followed by the appropriate annealing conditions and their electrical transport was investigated. The degradation temperature of the precursor was determined by TGA. XRD and Raman revealed FCC, BC-monoclinic and cubic structures of Cu, CuO and $Cu_2O$, respectively. From SEM we approximated the grain size while PL and 4-terminal studies allowed us to investigate the band gap formation, resistivity and functionality of the materials, respectively. This frugal and simple method allowed us to understand the properties of this family of materials at the nanoscale. Furthermore the materials were of a high quality; Cu functionality, for example, was demonstrated in Cu self-catalysis for electroless Cu deposition on insulating substrates as well as in other applications.

**D-45** **Fabrication of CNT-emitters on Ag paste film and their field emission properties** KWON Young Taek, LEE Seung Youb, SONG Wooseok, KIM Yoo Seok, CHOI W. C., PARK Chong-Yun(*BK 21 Physics Research Division and Center for Nanotubes and Nanostructured Composites (CNNC) Sungkyunkwan University, Suwon 440-746, Korea.*) Carbon nanotubes (CNTs) have a great potential as a field and thermionic emitters due to their excellent electrical and mechanical characteristics. We have investigated field emission properties of the sprayed carbon nanotube (CNT) emitters on Ag paste film used as a binding material between CNTs and glass substrate. Ag paste was coated on glass substrate. The CNTs solution was thin-MWCNTs suspended 1,2-dichloroethane (DCE). Then, the dispersed CNTs solution was sprayed on the prepared substrates and the samples were annealed by thermal and microwave treatment for good adhesion between CNTs and glass. The structural properties of the aligned CNTs were characterized by scanning electron microscopy (SEM). The field-emission properties were measured using a conventional diode structure with 250μm anode-cathode gap in a high-vacuum system.

■ SESSION: D [DG8]
10월 24일(금), 09:00 - 10:00
장 소: 206호

**D-46** **Theoretical Analysis on Magnetovolume Instabilities of Bulk Iron** YANG Heok, LEE Eok Kyun, LEE Young Joo[1] (*KAIST, Department of Chemistry. [1]RIST, New Material &Components Research Division.*) We have studied mechanical stability and magnetic properties for the bcc and fcc structures of bulk iron using the first-principle density-functional theory. Because of the well-known failure of LSDA in the prediction the bcc ground state of the bulk iron, we used the generalized gradient approximation (GGA) for the exchange-correlation functional. We investigate ferromagnetic (FM), nonmagnetic (NM), antiferromagnetic (AFM) and paramagnetic spin configuration. For the antiferromagnetic structure, we studied two different structures to represent complex spin state. First one is alternating layers of up and down spin. The other one is consists of double layers with same spin orientation. In order to study paramagnetic state, we have used the super cell in which half of atoms are set to spin-up, and the other half spin down. We call it as paramagnetic state because its spin state is similar to thermally excited paramagnetic spin state.

**D-47** **Electronic Transport in Fe/MnAs/Fe Structures** KIM KYUNG YEON, CHOI HYOUNG JOON(*Department of Physics and IPAP, Yonsei University.*) We have performed first-principles calculations of electronic structures and tunneling magnetoresistance of Fe/MnAs/Fe structures, which are junctions of two semi-infinite metals and a half-metal placed between them. The electronic structures are described by the Kohn-Sham density functional theory, with local spin density approximation, norm-conserving semicore pseudopotentials, and pseudo-atomic orbital basis set. The tunneling magnetoresistance is obtained by using a scattering-state method, considering different configurations of the magnetization.
* This work was supported by the KRF (KRF-2007-314-C00075) and by the KOSEF Grant No. R01-2007-000-20922-0. Computational resources have been provided by KISTI Supercomputing Center (KSC-2008-S02-0004).

**D-48** **Magnetic Properties of (Ga,Mn)As Quantum Wells for Various Mn-doping Profiles** 김 혜정, 이 경수(*부산대학교, 물리학과.*) We investigated spin-resolved subband structures and spontaneous magnetizations for several different doping profiles of magnetic ions in diluted magnetic semiconductor (DMS) (Ga,Mn)As quantum wells. The subband structures are obtained self-consistently by solving coupled Schrödinger and Poisson equation. Coupling effects among heavy-hole, light-hole, and split-off bands are included in the calculation. We observe that, by selectively doping Mn ions in the quantum well, the coupling of magnetic ions and band carriers can be varied and, hence, the ferromagnetic behavior (such as degree of spin polarization, spontaneous magnetization, or Curie temperature) of the system can be tuned. For selective Mn doping case, spin-polarization and magnetization can be significantly enhanced. Results of six-band and two-band calculations will be compared. Additional modulation doping of acceptors (in the barriers) does not necessarily improve the magnetic behavior.

**D-49** **A First-principles Study on Structural Stability and Magnetism of FeSe** GUL Rahman, KIM In Gee(*POSTECH, GIFT.*) α-PbO-type $FeSe_{1-x}$ compound was studied extensively for its magnetic properties by Zhen *et al.*, [1] who concluded from observed hysteresis the ferromagnetic state in the nonstoichiometric

phase, but the nonmagnetic state in the stoichiometric phase. Their XRD and SEM also showed that the films transited from α to β (NiAs-type) phase depending on growth temperature. Very recently, it is also observed that α $FeSe_{1-x}$ is a superconductor with $T_c$ of 8 K [2]. Subsequently, $T_c$ has been raised rapidly up to 27 K at pressure $P$ = 1.48 GPa [3]. So it is very important to study the structural properties of FeSe in various crystallographic environments. We have investigated the magnetic and structural properties of FeSe in terms of first-principles calculations by using the all-electron full-potential linearized augmented plane wave (FLAPW) method as embodied in the QMD-FLAPW package [4] within the local density approximation (LDA). The calculations are carried out for three different types of crystal structures i.e. α-PbO, NiAs, and CsCl. We found that among these structures, stoichmetric α-PbO-type FeSe is more stable than NiAs and CsCl structures. We also found that α -PbO-tye FeSe is nonmagnetic, which is in agreement with experimental observations [1]. On the othre hand, the stable α -PbO-tye FeSe is nonmagnetic, but the metastable CsCl-type FeSe is ferromagnetic. Refs.)

[1] X.J. Wu *et al.*, J. Appl. Phys. 103, 113501 (2008). [2] F.-C. Hsu *et al.*, arXiv:0807.2369 (2008). [3] Y. Mizuguchi *et al.*, arXiv:0807.4315 (2008). [4] E. Wimmer *et al.*, Phys. Rev B 24, 864 (1981).

■ SESSION: D [DG9]
10월 24일(금), 09:00 - 10:15
장 소: 207호

**D-50** **Fusion step-specific switching of complexin function in neuronal SNARE-mediated membrane fusion** 윤 태영 (*KAIST, 물리학과 및 바이오 융합 연구소*) $Ca^{2+}$-triggered, synchronized synaptic vesicle fusion underlies inter-neuronal communication. Complexin is a major binding partner of the SNARE complex, the core fusion machinery at the presynapse. The physiological data on complexin, however, have been at odds with each other, making delineation of its molecular function difficult. Here we report on direct observation of two-faceted functions of complexin using the single-vesicle fluorescence fusion assay and electron paramagnetic resonance. We show that complexin I has two opposing effects on *trans*-SNARE assembly: Inhibition of SNARE complex formation and stabilization of assembled SNARE complexes. Remarkably, SNARE-mediated fusion is markedly stimulated by complexin, and further accelerated by two orders of magnitude in response to an externally applied $Ca^{2+}$ wave. We suggest that SNARE complexes, complexins, and phospholipids collectively form a complex substrate for $Ca^{2+}$ and $Ca^{2+}$-sensing fusion effectors in the neurotransmitter release.

**D-51** **Self-Assembled Nanotube Growth under the Reduced Tension** PARK Hyunjoo, KIM Mahnwon(*KAIST, Physics Dept.*) Self-assembled nanotube-Microtubule is a major cytoskeleton which supports the cell structure under the thermally fluctuating membrane. This fiber is the stiffest component with several mm order of persistence length, $l_p$, and involves with cell division using dynamic instability in length. Here, we presents the elastic deformation of lipids membrane by nanotube growth and classifies the final morphology as Φ, dumbbell, lemon, cherry and etc. This evolution of vesicle shape is affected by various ligands (hydrophobic small molecules and cosurfactant) which alter the mechanical properties of both nano-rods and membrane. The hydro phobic molecule taxol binds to the membrane and reduces the tension. In experiments, we develop the model system of a living cell using PEG containing giant unilamellar vesicle and quantify the membrane tension using micropipette aspiration.

**D-52** **Z-DNA Dynamics Probed via Single-Molecule FRET** 배 상수, 김 도연[1], 김 경규[1], 김 양균[2], 홍 성철(*서울대학교, 물리천문학부. [1]성균관대학교, 의과대학. [2]성균관대학교, 화학과.*) *Z-DNA*, the non-canonical DNA conformation with left helicity, has been speculated as an important regulatory factor in gene regulation. Since its first discovery in 1972, people have pondered how Z-DNA, which is thermodynamically much less stable than the normal right-handed DNA structure, can be formed in the cell. Currently three factors which help Z-DNA formation are identified: high salt, binding to Z-DNA forming proteins, and negative supercoiling, but detailed mechanisms of Z-DNA formation due to those factors still need to be elucidated. In this study we developed single-molecule FRET (Fluorescence Resonance Energy Transfer) assays to address the questions. A variety of DNA duplexes containing CG repeats were prepared so that Z-form and B-form could be distinguished via FRET, and the conformational transitions between B-form and Z-form was studied in real time at varying salt and protein concentrations. As a result, we could observe 1) the different dynamics of salt-induced and protein-induced B-Z transitions, 2) base-flipping at B-Z junction, 3) the effect of B-Z junction on Z-DNA formation and so on.

**D-53** **Development Of a Novel Single-molecule Alternating Laser Excitation Three-color FRET Technique For Conformation Determination Of Dynamic Immobilized Molecules.** 이 상화, 홍 성철(*서울대학교, 물리천문학부.*) Conventional single-molecule fluorescence resonance energy transfer (FRET) technique, which uses one donor and one acceptor as FRET probes, has been widely used to study conformational dynamics of biological molecules and intermolecular interactions. As biological systems become complex, however, the capability to monitor the correlated motion of more than three parts has been required. To address the problem, we previously developed single-molecule three-color FRET using Cy3, Cy5, and Cy5.5, but the huge spectral overlap between Cy5 and Cy5.5 emission prevented us from performing clear data interpretation. Furthermore, spatial configuration of three fluorophores could not be uniquely determined. To solve the problems, we developed a novel single-molecule three-color FRET technique. By replacing Cy5.5 with Cy7, we greatly reduced the cross-talk be-

tween detection channels, thus removing possible errors during data manipulation. By adopting Alternation Laser Excitation (ALEX) technique, we could determine all of three inter-dye distances in real time, thus unambiguously determining molecular conformation. The improved capabilities of our new setup were confirmed by the experiments with triply-labeled duplex DNA and the Holliday junctions.

**D-54** **Conformational stability of BWYV Pseudoknot studied via single-molecule FRET spectroscopy** YOON Jeongmin, KIM Yang-Gyun[1], HOHNG Sungchul(*Seoul National University, Department of Physics &Astronomy.* [1]*SungKyunkwan University, Department of Chemistry.*) The -1 programmed ribosomal frameshifting, a way of translation regulation used in a number of pathogenic viruses such as SARS and HIV, is known to be stimulated by the tensile stress generated by the downstream pseudoknot. However, the mechanism of pseudoknot unfolding, a critical step for the translation of downstream sequences, is not understood yet. To address the question, we developed single-molecule fluorescence resonance energy transfer (FRET) assay to study the conformational dynamics of the pseudoknot from beet western yellow virus. Our data clearly show that the pseudoknot is stabilized by metal ions, but the exact form of the pseudoknot seems to be determined by cation type. We also studied how the stability of pseudoknot depends on pH and mutations of specific bases.

■ SESSION: D [DF1]
10월 24일(금), 09:00 - 11:00
장 소: 401호

**DF-01(초)** **Features of the *s*π pairing state as a model for FeAs superconductors** CHOIA Han-Yong, LEE Nayoung, BANG Yunkyu[1], LEE Hyun Cheol[2], WON Hyekyung[3](*Department of Physics, SungKyunKwan University, Suwon 440-746.* [1]*Department of Physics, Chonnam Natinal University, Kwangju 500-757.* [2]*Department of Physics, Sogang University, Seoul 100-611.* [3]*Department of Physics, Hallym University, Chuncheon 200-702.*) The alluring prospect of opening a key window to understanding the mechanism of high temperature superconductivity has attracted fierce research activities in the FeAs superconductors. The first step towards this goal is to establish the pairing symmetry. Among the many ideas put forward, particularly appealing is the sign reversing pairing state suggested by Mazin and coworkers. It is the ground state of two band superconductivity where both pairing order parameters on the two bands have full gaps while acquiring the phase shift between them, which is referred to as the pairing state. It was noticed early on that there is this type of solution to a multi-band BCS gap equation and it is quite exciting that it seems to be actually realized in the newly found superconductors. A repulsive inter-band interaction is turned to induce pairing by generating the sign reversal between the two condensates. The state seems to be able to explain most of the experimental observations indicating the full gap behavior as well as a gapless behavior. We will present how the seemingly conflicting experimental observations may be understood in terms of the pairing state for the FeAs superconductors, including the tunneling spectroscopy, relaxation rate, neutron resonance, ARPES and others.

**DF-02(초)** **Possible pairing symmetries of the FeAs superconductors** BANG Yunkyu, CHOI Han-Yong[1], WON Hyekyung[2] (*Department of Physics, Chonnam Natinal University, Kwangju 500-757.* [1]*Department of Physics, SungKyunKwan University, Suwon 440-746.* [2]*Department of Physics, Hallym University, Chuncheon 200-702.*) With a theoretical analysis, we propose that the sign-changing s-wave gap is the most promising gap symmetry of these new high-$T_c$ superconductors [1]. Then, I will focus on the contradicting experimental observations in NMR and penetration depth measurements which indicate a superconducting state with lines of node and a fully opened gap, respectively. I will show an important role of resonant impurity scattering in the sign-changing s-wave gap and how to explain the experimental puzzles with it [2]. If time allows, I will discuss a possible common thread of pairing mechanism from the high-$T_c$ superconducting cupurates ($T_c$~100 K) , Fe-based superconductors ($T_c$~50 K), Pu-115 superconductors ($T_c$ ~ 20 K) and various heavy fermion superconductors ($T_c$<1 K).
[1] Yunkyu Bang, Han-Yong Choi, arXiv:0807.3912; Han-Yong Choi, Yunkyu Bang, arXiv:0807.4604 [2] Yunkyu Bang, Han-Yong Choi, arXiv:0808.0302; Yunkyu Bang, Han-Yong Choi, Hyekyung Won, arXiv:0808.3473

**DF-03(초)** **Magnetic and electric properties of single crystalline $EuFe_2As_2$** KIM J. Y., SUNG N. H., CHO B. K.(*School of Photonic Science and Technology, Dept. of Materials Science and Engineering, Gwangju Institute of Science and Technology (GIST), Gwangju 500-712.*) Recent discovery of superconductivity at $T_c$ » 50 K in iron-pnictide compound LaFeAsO has stimulated much interest in elucidating the mechanism of superconductivity as well as in searching for new superconducting materials. The iron-based layered oxypnictide $LaFeAsO_{1-x}F_x$ showed a superconducting transition temperature $T_c$=26 K [1]. The transition temperature was raised up to $T_c$=43 K when La was replaced by other rare-earth (R) elements with smaller ionic size, such as Ce, Pr, Nd, and Sm [2]. Besides, the transition temperature was found to be strongly correlated with the doping level of fluorine. Remarkably, the superconductivity was found to be in the vicinity of a spin-density-wave (SDW) instability, which indicates that the superconductivity was intimately related to the magnetic fluctuation. On the other hand, it was also found that the ternary iron arsenide $BaFe_2As_2$ with a tetragonal $ThCr_2Si_2$-type structure, which contains identical edge-sharing $Fe_2As_2$ tetrahedral layers as LaFeAsO, exhibits a similar SDW instability at 140 K. It is therefore suggested that $BaFe_2As_2$ could serve as a new parent compound for ternary iron arsenide superconductors. Indeed, the superconductivity with $T_c$=38 K was found in potassium(K)-doped $BaFe_2As_2$, which was suggested to be a hole-doped iron arsenide superconductor [3]. In this work, we report the fabrication of single crystals of $RFe_2As_2$, espe-

cially R = Sm and Eu, and the physical properties of the compounds. We found that $EuFe_2As_2$ exhibits two phase transitions at $T$=19 and 190 K in both temperature-dependent resistivity and magnetization measurements. A phase transition at $T$ = 190 K is likely due to SDW, which is similar to that of LaFeAsO, and a phase transition at $T$=19 K is due to antiferromagnetic ordering of $Eu^{2+}$ moments. We found also that there is a significant anisotropy in electric transport with the resistivity along the *c* axis, $r_{||}$, being larger than that perpendicular to the c-axis, r^, in a whole temperature range 2 K£$T$£300 K and $r_{||}/r^{\wedge}$=15 at $T$=300 K.

[1] H. Takahashi, K. Igawa, K. Arii, Y. Kamihara, M. Hirano, and H. Hosono, Nature (London) 453, 376 (2008). [2] X. H. Chen, T. Wu, G. Wu, R. H. Liu, H. Chen, and D. F. Fang, Nature (London) 453, 761 (2008); G. F. Chen, Z. Li, D. Wu, G. Li, W. Z. Hu, J. Dong, P. Zheng, J. L. Luo, and N. L. Wang, Phys. Rev. Lett. 100, 247002 (2008). [3] G. F. Chen, Z. Li, G. Li, W. Z. Hu, J. Dong, X. D. Zhang, P. Zheng, N. L. Wang, and J. L. Luo, arXiv:0806.1209.

**DF-04(초)** **High-pressure growing of superconducting single crystals of $SmFeAsO_{1-x}F_y$ and $SmFeAsO_{0.85}$** LEE Hyun-Sook, LEE Jae-Yeap, PARK Jae-Hyun, SUNG Nak-Heon[1], CHO B. K.[1], JUNG Chang-Uk[2], LEE Hu-Jong(*Department of Physics, Pohang University of Science and Technology, Pohang 790-784. [1]Center for Frontier Materials and Department of Materials Science and Engineering, GIST, Gwangju 500-712. [2]Department of Physics, Hankuk University of Foreign Studies, Yongin, Gyeonggi 449-791.*) Superconducting single crystals of $SmFeAsO_{1-x}F_y$ and $SmFeAsO_{0.85}$ were grown at a high pressure and a high temperature by using self-flux method. For the growth of single crystals starting materials of SmAs, FeAs, $Fe_2O_3$, Fe, and $SmF_3$ for $SmFeAsO_{1-x}F_y$ (SmAs, $Fe_2O_3$, and Fe for $SmFeAsO_{0.85}$) were mixed in the desired stoichiometry and ground thoroughly. The resulting mixture powders were pressed into a pellet, which in turn was placed inside a boron-nitride crucible and pressurized up to 3.3 GPa at room temperature by using a 14mm cubic-anvil press. The temperature was then ramped up to 1300-1500℃. The crucible was crushed and single crystals were recovered among polycrystalline product. Plate-shaped single crystals ranging of a few~200 micrometers in their lateral size were obtained. Optimum growth conditions were tuned by varying the maximum pressure, composition, reaction time, and heating/cooling rate. Polycrystalline states of both materials show the superconducting transition at temperature around 54 K. Usually crystals from each batch show somewhat lower transition temperature than the corresponding polycrystalline product. We will present results of characterization of single crystals, including the resistive transition, magnetoresistance, and structural analysis.

■ SESSION: D [DG10]
10월 24일(금), 11:00 - 12:30
장 소: 201호

**D-55** **Direct Observation of p-type gapped Graphene** PARK Ji-Hoon, JEON Cheolho, KIM Minkook, PARK Chong-Yun, AHN Joung Real(*Department of Physics, Sungkyunkwan University.*) Graphene, a monolayer graphite sheet, has many unique properties, which could be applied to electronics and nanodevices. Especially, gapped graphene is required in the development of graphene-based MOSFET device. Very recently, some research groups reported n-type epitaxial graphene. As the next step, we have tried to achieve p-type graphene, especially p-type gapped graphene, using tetrafluoro-tetracyanoquinodimethane(4F-TCNQ). In our experiments, we used gapped monolayer graphene grown epitaxially on 6H-SiC(0001) which was characterized by using angle-resolved photoemission spectroscopy with the photon energy of 40.8 eV in UHV after adsorption of 4F-TCNQ. Variation of energy band near the K-point of its surface Brillouin zone was measured. Angle-resolved photoemission spectroscopy spectra of 4F-TCNQ/graphene show that the Dirac point moves to lower binding energy by ~0.3eV and the gap at the Dirac point is slightly reduced. Detailed underlying mechanism will be presented.

**D-56** **Tailoring Characteristics of Graphite Oxides by Oxygen Treatment Time** JEONG Hae-Kyung, JIN Mei Hua[1], SO Kang Pyo[2], KIM Sung Jin[1], GENG Hong-Zhang[3], LIM Seong Chu[4], JEONG Mun Seok[5], LEE Young Hee[6](*Center for Nanotubes and Nanostructured Composites, Sungkyunkwan University. [1]Department of Physics, Sungkyunkwan University. [2]Sungkyunkwan Advanced Institute of Nanotechnology, Sungkyunkwan University. [3]BK21 Physics Devision, Center for Nanotubes and Nanostructured Composites, Sungkyunkwan Advanced Institute of Nanotechnology, Sungkyunkwan University. [4]Center for Nanotubes and Nanostructured Composites, Sungkyunkwan Advanced Institute of Nanotechnology, Sungkyunkwan University. [5]Advanced Photonics Research Institute, Gwangju Institute of Science and Technology. [6]Department of Physics, BK21 Physics Devision, Center for Nanotubes and Nanostructured Composites, Sungkyunkwan Advanced Institute of Nanotechnology, Sungkyunkwan University.*) We have synthesized graphite oxide with different oxidation times and characterized its physical and chemical properties. The degree of oxidation in graphite oxide was systematically controlled with oxidation times. We found that the expansion of interlayer distance was taken place by forming an intermediate precursor state, identified by x-ray diffraction. The compositional atomic ratio of O/C shows a strong coupling with (002) peak of graphite oxide phase of XRD, while atomic percentage of carbon was strongly correlated with (002) peak of the pristine graphite phase. An amount of functional groups of graphite oxides increases as oxidation time increases. Band gap of graphite oxides can be tuned by oxidation level in which band gap increases as oxidized and saturates to 2.3 eV after 6 hours of oxidation.

**D-57** **Possible Origin of Defect-Induced Magnetic Ordering in Carbon-Irradiated Graphite** LEE Hosik, MIYAMOTO Yoshiyuki, YU Jaejun[1](*NEC. [1]Seoul National University, Department of Physics and Astronomy.*) We investigated possible sources of defect-induced magnetic ordering in carbon-irradiated graphite from

first-principles calculations. Among the candidate structures with interstitial defect configurations, which could be generated during the carbon irradiation process, two meta stable configurations with finite magnetic moments were identified. They are coupled ferromagnetically to their neighboring defects, thereby being able to contribute to the observed macroscopic magnetic ordering. The ferromagnetic ordering driving forces will be explained by the RKKY interactions.

**D-58** **Synthesis and Luminescence Properties of $Dy^{3+}$: YAP Nanophosphors** 문 병기, GANJI Seeta RamaRaju, 박 진영, 정 홍채, 정 중현(*부경대학교, 물리학과.*) In order to development of high resolution optical display systems and lamps in day to day competitive life create a motivation for the research of high efficiency luminescence phosphors. It is well known that rare earth (RE) ions activated phosphors have found excellent luminescent materials because of their marked improvements in lumen output, color rending index, energy efficiency and greater radiation stability [1-3]. The RE ions are characterized by a partially filled 4f shell that is shielded by $5s^2$ and $5p^6$ electrons. The combination of $Y_2O_3$ and $Al_2O_3$ such as $Y_3Al_5O_{12}$ (YAG) and $YAlO_3$ (YAP) are well known as chemically stable and which are suitable hosts for the replacement of $RE^{3+}$ ($Ce^{3+}$, $Nd^{3+}$, $Er^{3+}$, $Eu^{3+}$, $Tb^{3+}$, $Sm^{3+}$ &$Dy^{3+}$) activators. Among these, Yttrium Aluminum Perovskite (YAP) is the important phosphor host materials with orthorhombic structure [4]. Furthermore $Dy^{3+}$ ions can show strong luminescence in variety of lattices and exhibits both blue ($^4F_{9/2}$à$^6H_{15/2}$) and yellow ($^4F_{9/2}$à$^6H_{13/2}$) emissions, which are necessary for the development of white light emission and is very useful in light emitting diodes(LEDs)[5]. In this context we have synthesize the $Dy^{3+}$: YAP phosphors by means of solvothermal process, because this process is one of the most prominent method to control the particle size in nanometers, morphology and distribution of phosphor particles with efficient luminescence properties.$Dy^{3+}$: YAP nanophosphors have been newly synthesized by means of solvothermal process. Very fine particles in nanometer range could be prepared by this method as evidenced by X-ray diffraction. XRD profiles confirm their orthorhombic nature, which are well correlated with the reported results. The luminescence studies on these compounds have been carried out from the measurement of their emission, excitation and lifetimes. $Dy^{3+}$: YAP nanophosphors exhibit the emission in blue ($^4F_{9/2}$à$^6H_{15/2}$) and yellow ($^4F_{9/2}$à$^6H_{13/2}$) regions. The Emission mechanism in these systems has also been elucidated by an energy level scheme. Furthermore, the yellow to blue intensity ratios of $Dy^{3+}$:YAP nanophosphors are almost equal to 1, which indicates that the emitted light approaches the CIE ideal white conditions. Such luminescent powders are expected to find potential applications such as white light emitting diodes.

1. Sang Do Han, S.P. Khatkar, V.B. Taxak, Dinesh Kumar and Jo-Yong Park, Combustion synthesis and luminescent properties of $Eu^{3+}$-doped $LnAlO_3$ (Ln = Y &Gd) phosphors, *Mater. Sci. Eng., B,127 (2006) 272-275*2. 2. Kai Zhang, Wenbin Hu, Yating Wu and Hezhou Liu, Photoluminescence investigations of $(Y_{1-x}Ln_x)_3Al_5O_{12}$:Ce ($Ln^{3+}$=$Gd^{3+}$, $La^{3+}$) nanophosphors. *Physica B 403 (2008) 1678-1681*3. 3. Junjie Wu and Bing Yan, Sol–gel composition of hybrid precursors to synthesize $RE_xGd_{1-x}AlO_3$:$Eu^{3+}$(RE = La, Y) phosphors, *J. Alloys Comp, 432 (2007) 293-297*4. 4. Geller S, Bala V.B. Crystallographic Studies of Perovskite like compounds. II Rare earth Aluminates, *Acta Cryst.* 9 (1956) 10195. 5. G. Seeta Rama Raju, S. Buddhudu, Emission analysis of Sm3+&Dy3+:MgLaLiSi2O7 powder phosphors, *Spectrochim. Acta, Part A 70 (2008) 601-605*

**D-59** **Synthesis and Luminescent Properties behavior of Nano and Bulk Phosphors by Solid-State Reaction and Planetary Ball Milling** 양 현경, 정 중현, 문 병기, 최 병춘(*부경대학교, 물리학과.*) In this research, a facile synthetic route for the preparation of nanocrystalline powder phosphors by planetary ball milling method is reported, the as-grown powders were found to be amorphous, which crystallized to the tetragonal phase without YAG and $GdVO_4$ by product after various temperature condition for 100 hours. The corresponding bulk YAG:$Eu^{3+}$ and $GdVO_4$:$Eu^{3+}$ were synthesized by high temperature solid-state reaction. The corresponding bulk YAG:$Eu^{3+}$ and $GdVO_4$:$Eu^{3+}$ were synthesized by high temperature solid-state reaction. All the products were systematically characterized by powder X-ray diffraction (XRD), infrared spectroscopy (IR), field emission-scanning electron microscopy (FE-SEM), transmission electron microscopy (TEM), photoluminescence (PL) and photoluminescent excitation spectra (PLE). The luminescence mechanism and the size dependence of their fluorescence properties are also discussed.

**D-60** **Luminescence behavior of $CaTiO_3$: $Pr^{3+}$ nanopowder phosphors by solvothermal method** 정 종원, 박 성욱, 문 병기, 정 중현(*부경대학교, 물리학과.*) The interest for $ABO_3$ materials is expanding very fast worldwide due to their large range of applications in several fields and especially in microelectronics. Great attention has been paid recently in the development of advanced displays for the multimedia application, which can replace some cathode-ray tubes (CRTs). Field emission display (FED) is one of the candidates for advanced flat panel application. Therefore the development of phosphors suitable for FED is urgently needed. $CaTiO_3$:$Pr^{3+}$ nanopowders were synthesized by using a solvothermal reaction. The crystallinity and photoluminescence of nanopowders were highly dependent on Li ion content. The doped concentration of Pr was various 0, 0.02, 0.04, 0.06, 0.08 and 1 mol, $Ca(AcAc)_3$, $Pr(AcAc)_3$, and Titanium butoxide were used as starting materials and they were dissolved in 2-PrOH.. Stoichiometric amounts of above solutions were mixed and the solution was initially heated at 250℃ in air and continuously stirred in a mixture for 10h. The samples were dried at 50℃ in air for 5h. The as-prepared samples were sintered temperature at 900℃ for 10h. Their crystalline structures, surface morphologies and phase transitions were investigated for the samples prepared at various annealing processes by using X-ray diffraction (XRD), scanning electron microscopy (SEM), photoluminescence

(PL) and cathodoluminescence (CL), respectively. The room temperature PL spectra of $CaTiO_3:Pr^{3+}$ nanophosphors showed red emission peak 613 nm. The bands at 613 result from the $^1D_2$à$^3H_4$ transition of the $Pr^{3+}$ ion. The PL intensity of $CaTiO_3:Pr^{3+}$ nanopowders had a macimum at $Li^+$ ion was 3 w%. The purpose of this study is to compare the luminescence characteristics of $CaTiO_3:Pr^{3+}$ phosphors which were synthesized at $Pr^{3+}$ ion concentration.

■ SESSION: D [DG11]
10월 24일(금), 11:00 - 12:45
장 소: 206호

**D-61** **Analysis of the Fermi Arc Observed by ARPES in High-Tc Superconductors** KIM Hyun-tak(*ETRI, MIT Device Team.*) Since the discovery of a high-*T*c superconductor in 1986, a consensus theory explaining high-*T*c superconductivity has not been developed. Several problems remain unsolved. Many scholars have believed that paring symmetry of high-*T*c superconductors is *d*-wave. They have issued the difference of Fermi surfaces between in the under-doped region and in the over-doped region. Particularly, they calls the Fermi surface, which is observed by angle resolved photo emission spectroscopy (ARPES) in the under-doped region, a Fermi arc with a part of Fermi surface. Furthermore, they have not understood identity of the Fermi arc and the large Fermi surface in the over-doped region because the d-wave superconductors have not the Fermi surface but four points at nodes without the superconducting true gap. Here, I show analysis on the Fermi arc in papers published within recent 2-3 years, on the basis of inhomogeneity of high-*T*c superconductors. The analysis concludes that the high-*T*c superconductor is s-wave.
(Reference: Physica C 460-462 (2007) 943)

**D-62** **Extraction of the pairing glue spectra from ARPES experiments for high $T_c$ Superconductor $Bi_2Sr_2CaCu_2O_{8+\delta}$.** YUN Jae Hyun, BOK Jin Mo, CHOI Han-Yong, KONDO Takeshi[1], KAMINSKI Adam[1], VARMA Chandra M.[2](*Department of Physics and Institute for Basic Sciende Research, SungKyunKwan University, Suwon 440-746, Korea. [1]Ames Laboratory and Department of Physics and Astronomy, Iowa State University, Ames, Iowa 50011 USA. [2]Physics Department, University of California, Riverside, California 92507, USA.*) We report the "pairing glue" spectra of high $T_c$ *d*-wave superconductor, $Bi_2Sr_2CaCu_2O_{8+\delta}$ (Bi2212) by analyzing the angle resolved photoemission spectroscopy (ARPES) experiments. This is an extension of the McMillan-Rowell-Galkin analysis of the tunneling conductance to the d-wave superconductors. A major difference is that there are two distinct glue functions for *d*-wave superconductors. Consequently, we need twice more experimental inputs to perform this analysis; the pairing function and self-energy. We first describe how to extract them from ARPES data. Then, using the obtained experimental inputs we invert the *d*-wave Eliashberg equation to extract the glue spectra. The results will be reported for several temperatures above and below $T_c$ and will be compared with other studies.

**D-63** **Tunneling spectroscopy in *sπ* pairing Superconductor/Ferromagnet Hybrid Structures** 이 나영, 최 한용(*성균관대학교, 물리 학과.*) We study the FeAs superconductors based on the model including an *sπ* pairing state of a two band superconductivity using the self-consistent Bogoliubov-de Gennes formalism. The *sπ* pairing state is an *s*-wave pairing state with an internal p phase, that is, nodeless gaps on each band but with the opposite signs. We calculated the local density of states (LDOS) of the π phase superconductor/normal metal bilayer[1]. We also investigate in detail the LDOS of superconductor/ferromagnet bilayers with the *sπ* state. In addition, the pairing amplitude of S/F bilayers with the *sπ* state is calculated. The spin dependence at the interface of between superconductor and ferromagnet is not considered. We discuss the zero bias conductance peak as observed in tunneling spectroscopy experiments on FeAs superconductors and the interplay between the internal and external p phases.
[1] Han-Yong Choi, Yunkyu Bang, arXiv: 0807.4604

**D-64** **Single crystal growth and superconducting properties of $Ba_{1-x}K_xFe_2As_2$** YONG Liu, KIM Hyeong-Jin Kim, OH Yoon Seok, KHIM Seung Hyun, KIM Jae Wook, NAM Dong Hak, STEWART G. R.[1], KIM Kee Hoon(*FPRD, Department of Physics and Astronomy, Seoul National University, Seoul 151-747, S. Korea. [1]Department of Physics, University of Florida, Gainesville, Florida 32611-8440, USA.*) We report the successful growth of the single crystals $Ba_{1-x}K_xFe_2As_2$ by the Sn flux method. The transport and magnetic measurements were performed in both H⊥c and H||c configurations to study the $H_{c2}$ anisotropy and to check the two-band signature in this system. The effect of the Sn flux on the transport and magnetic properties, in conjunction with its chemical etching characteristics, will be also discussed.

**D-65** **Properties of $YBa_2Cu_3O_{7-d}$ Thin Film Grown on a Nanocluster-Modified Substrate by PLD Method** YOO Jaeun, KO Rock-Kil[1], JUNG Yehyun, KWAK Kisung, LEE SangMoo, RHEE JonnKyu, AHN ChiWon[2], OH SangJun[3], YOUM Dojun, OH SangSoo[1](*Korea Advanced Institute of Science and Technology. [1]Korea Electrotechnology Research Institute. [2]Nantional Nano Fab Center. [3]National Fusion Research Center.*) Approximately 200 nm thick YBCO films were grown on nanocluster-modified $LaAlO_3$ substrates by pulsed laser deposition. Zr nanoclusters were deposited on the $LaAlO_3$ substrate using a nanocluster deposition system (Mantis Deposition Ltd. Nanosys 500). In the system, the size and density of nanoclusters were controlled by varying sputtering power, Ar/He mixed gas flow, and the length of the cooling zone. As the density was increased, the cluster size deposited was increased. The angle and field dependence of the critical current of the YBCO films grown on nanocluster-modified LAO substrates were compared with those on single crystals.

* This work was supported by the Korea Research Foundation Grant funded by the Korean Government (MOEHRD) (KRF-2007-313-C00201)

**D-66** **Strong Magnetic Polaron in Superconducting $alpha$–$FeSe_{1-x}$** LEE Kwan-Woo, PARDO Vardo[1], PICKETT Warren E.[2](*Department of Display and Semiconductor Physics, Korea University.* [1]*Departamento de Fisica Aplicada, Universidad de Santiago de Compostela, Spain.* [2]*Department of Physics, University of Califonia, Davis, USA.*) The discovery of superconductivity up to 55 K in the LaFeAsO class of compounds has caused great excitement, as happened in the high $T_c$ cuprates. In these novel compounds, competition between superconductivity and magnetism is very evident, and the assortment of observed phenomena is leading to a confusing picture of these new superconductors. In this presentation we address a very specific question that may help in elucidating the theoretical understanding of these materials. We focus on $FeSe_{1-x}$, superconducting at $x$~1/8 up to 27 K, in which Se vacancies are necessary for producting the high $T_c$ superconducting state. Our first principles calculations indicate that the vacancy forms an immobile strong magnetic polaron in nearly magnetic bulk FeSe and for the ordered $x$=1/8 alloy leads to a half metallic electronic structure. Additionally, from fixed spin moment calculations, we find evidence that the low energy excitations in $FeSe_{1-x}$ are antiparamagnon-like magnetic fluctuations with short correlation length.

**D-67** **Enhanced Spin Density Wave in LaOFeSb : First-principles Study** MOON Chang-Youn, PARK Se Young, CHOI Hyoung Joon(*Department of Physics and IPAP, Yonsei University.*) We predict atomic, electronic, and magnetic structures of a hypothetical compound LaOFeSb by first-principlesdensity-functionalcalculations. It is shown that LaOFeSb prefers a stripe-type antiferromagneticphase (i.e., spin density wave (SDW) phase) to the non-magnetic (NM) phase, with a larger Fe spin moment and greater SDW-NM energy difference than those of LaOFeAs. The SDW phase is found to favor the orthorhombic structure while the tetragonal structure is more stable in the NM phase. In the NM-phase LaOFeSb, the electronic bandwidth near the Fermi energy is reduced compared with LaOFeAs, indicating smaller orbital overlap between Fe *d* states and subsequently enhanced intra-atomic exchange coupling. The calculated Fermi surface in the NM phase consists of three hole and two electron sheets, and shows increased nesting between two hole and two electron sheets compared with LaOFeAs. Monotonous changes found in our calculated material properties of LaOFePn (Pn=P, As, and Sb), along with reported superconducting properties of doped LaOFeP and LaOFeAs, suggest that doped LaOFeSb may have a higher superconducting transition temperature.

* This work was supported by the KRF (KRF-2007-314-C00075) and by the KOSEF Grant No. R01-2007-000-20922-0. Computational resources have been provided by KISTI Supercomputing Center (KSC-2008-S02-0004).

■ SESSION: D [DG12]
10월 24일(금), 11:00 - 12:30
장 소: 207호

**D-68** **Modification of graphene using electron beam and nitrogen ion** 김 기정, 최 정헌[1], 이 한구[2], 이 한길[3], 정 민철, 신 현준, 강 태희, 김 봉수, 김 세훈[1](*포항가속기연구소.* [1]*KAIST, 화학과.* [2]*하이닉스.* [3]*숙명여자대학교, 화학과.*) Graphene, a single layer of carbon atoms, is the starting point for carbon-based materials and is widely used to describe properties of these materials. Furthermore, the physical properties of graphene layer can be controlled by doping metals and molecules, it is important to characterize surface property and electronic structure change on the graphene. But, there are difficulties that graphene surface is very stable, the molecules cannot be easily adsorbed on the graphene surface. So, many efforts has been done to functionalize the surface. Among them, we introduced the electron beam and ions to modify the graphene surface and its property changes were investigated. Graphene layer grown on 6H-SiC(0001) were irradiated with 1 MeV electron beam and 300 eV nitrogen ions. Surface property changes were studied using photoemission spectroscopy(PES), near edge X-ray adsorption spectroscopy(NEXAFS) and atomic force microscopy(AFM). The electron beam irradiation in ambient condition can induce controlled oxidation of the graphene layer without aqueous detergent treatments. N 1s core-level spectra show that three kinds of nitrogen species were existed on the nitrogen ion implanted graphene surface.

**D-69** **Interaction Mechanism Between 8-hydroxiquinolato-lithium (Liq) and Al: The Electrode Formation in Organic Light Emitting Devices (OLEDs).** 이 연진, 이 영미[1], 박 용섭[1], 김 정원 (*한국표준과학연구원, 나노측정센터.* [1]*경희대학교, 물리학과.*) The interaction between Liq molecule and Al was studied. When the Al is deposited on the pre-deposited Liq layer, gap state is formed in the energy gap of Liq molecule and N 1s and Li 1s core level new components. This indicates there are chemical interaction between Liq and Al. The gap state is identified with photoemission and density functional theory calculation. The detailed interaction mechanism will be presented.

**D-70** **Adsorption Structure of Pyrazine on Si(100): DFT Calculations** JUNG Sung Chul, KANG Myung Ho(*포스텍 물리학과.*) We have studied the adsorption of pyrazine ($C_4H_4N_2$) on the Si(100) surface using density-functional theory calculations. Our calculations demonstrate that the cross-row model, where $C_4H_4N_2$ connects two dimer rows by forming two N-Si bonds, is the energetically and microscopically sound structural model for the $C_4H_4N_2$/Si(100) surface. It is also shown that the cross-row structure favors a configuration in which molecules arrange in series along the row-perpendicular direction as observed in a recent scanning tunneling microscopy experiment. The N-Si bonding nature and the molecular aromaticity will be discussed based on the de-

tailed atomic-structure information.

**D-71** **Atomic and Electronic Structure of Lewis acid $AlCl_3$ molecule on Ge(001)** HONG Suklyun, SUNG Dongchul, RYOU Junga, JUNG Soon Jung[1], KIM Sehun[1](*Sejong University, Department of Physics. [1]KAIST, Department of Chemistry.*) The zwitterionic-like property of the dimer on the germanium (001) surface opens up possibilities of using nucleophilic and electrophilic attachment reactions. Up to now, most of the work done in this area only focus on the interaction between electrophilic down-Ge atom and Lewis base molecules such as ammonia, trimethylamine, and pyridine on Ge(001). So, it is necessary to understand the interaction between nucleophilic up-Ge atom and Lewis acid molecules. Aluminum trichloride ($AlCl_3$) is a Lewis acid that forms donor-acceptor complexes with electron-rich molecules. We have performed density functional theory calculations for $AlCl_3$ adsorbed on Ge(001) in order to investigate its atomic and electronic structure. The various adsorption sites were observed in the scanning tunneling microscopy (STM) images. By comparison of the experimental STM images with the simulation, we identify distinct features observed in the STM images at low coverages. We propose that the investigation of adsorption of $AlCl_3$ on Ge(001) will improve our understanding of interaction between Lewis-acid molecules and Ge(001) surfaces.

**D-72** **Spatial variation of field emission resonance spectroscopy (FERs) on the Pt(110)-(1x2) surface.** LYO In-whan, CHOI Eunyeoung(*Department of Physics, Yonsei University.*) We investigated Pt(110)-(1x2) reconstructed surface at room temperature using field emission resonance spectroscopy (FERS). The characteristic constant-current conductance spectra show long-range spatial variation over the distance of a few nm. These unusual FER may be associated with the defects in the Pt bulk, whose energy levels are located above the vacuum level. The identity of these defects and the sensitivity of FER to these subsurface structures will be discussed during the talk using the results obtained recently.

**D-73** **Spontaneous orientational ordering of mounds during thin film growth** SEO Jiken, KIM Jae-Sung[1](*Department of Ophthalmic optics, Chodang University. [1]Department of Physics, Sook-Myung Women's University.*) The growth of thin film is conventionally chracterized by the random nucleation of seeds followed by their growth and coalsecence. In the present work, we challenge the basic assumptuion of the random nucleation and isotropic growth of mounds. We perform kinetic Monte Carlo simulation of homoepitaxial growth of Cu on Cu(001) and find that growth of mounds shows orientational preference along [100] direction. This observation is found consistent with the anisotropic Henzler ring observed by spot profile analysis of low energy elctron diffraction (SPA-LEED). The microscopic origin for such anisotropic nucleation and growth of mounds is attributed to anisotropic capture probability of adatomds.



■ SESSION: D [DG13]
10월 24일(금), 11:00 - 12:45
장 소: 401호

**D-74** **Optical Properties Of PZT Thin Films** AHN Jai Seok, SEO Yu seong, KWON Dae Young[1], ZHANG X.D.[1], KIM Bog-Gi[1](*Dept. of Physics, Pusan National Univ. [1]RCDAMP, Pusan National Univ.*) Heat treatment is essential to obtain highly quality ferroelectric thin films for application. The aim of this work was to see the evolution of optical properties of PZT around the optimum growth conditions. PZT thin films were grown on SrTiO3 (001) using an off-axis RF sputtering method. And the films were grown at 400, 500, and 600 °C. Variable angle spectroscopic ellipsometry (VASE) was used for the optical characterization of PZT thin films in the near-IR to UV range (hν = 0.75-6.5 eV). Optical spectra of the films are compared with their x-ray diffraction patterns as a function of annealing temperature.

**D-75** **Relaxor-like behaviour of lead-free (1-*x*)$BaTiO_3$-*x*-$BiScO_3$ ceramics** CHO Jong-Ho, YEO Hong-Goo, SUNG Yeon-Soo, KIM Myong-Ho, SONG Tae-Kwon(*Changwon National University.*) The structural, dielectric and piezoelectric characteristics of lead-free (1-*x*)$BaTiO_3$-*x*$BiScO_3$ ($0 \le x \le 0.45$) solid solution ceramics synthesized by solid state reaction have been investigated. Their polycrystalline structure change from tetragonal ferroelectric phase below at $0.04 < x < 0.08$ to cubic paraelectric phase at $x > 0.08$ and the unknown peaks appears at $x = 0.45$. No morphotropic phase boundary was observed in $BaTiO_3$-$BiScO_3$ ceramic systems prepared by the conventional oxide method. The temperature dependent dielectric constants exhibit that the phase transition becomes more diffuse as $x$ increases. Strong dispersion of the complex relative dielectric permittivity is observed including typical relaxor features such as shift of the permittivity maximum with frequency from $x \ge 0.08$ . The dielectric relaxation obeys the Vogel–Fulcher relationship with activation energy $E_a \sim 0.432$ eV and freezing temperature $T_f \sim 215$ K for $x = 0.35$. The values of piezoelectric coefficient ($d_{33}$) and electromechanical coupling factor ($k_p$) decrease rapidly as with increasing $x$. Ceramics with $x = 0.01$ shows a coercive field of about 6.6 kV/cm and a remnant polarization near 8.5 μC/cm$^2$, which is maximum values for (1-*x*)$BaTiO_3$-*x*$BiScO_3$ systems.

**D-76** **2차원 증성자 위치민감형 검출기에 기반한 단결정 증성자 회절장치 및 해석기술 개발** 이 창희, 문 명국, 김 신애, 천 종규, NODA Yukio[1], ISHIKAWA Yoshihisa[1], KIMURA Hiroyuki[2], WATANABE Mashashi[2](*한국원자력연구원. [1]Tohoku Univeristy. [2]Tohoku Univerisity.*) 결정구조 해석은 물질의 구조와 특성을 이해는 중요한 도구이며, 높은 측정 생산성과 해석에 필요한 충분한 데이타를 얻기 위해 X선 분야에서 image plate, CCD 등 2차원 검출기가 널리 사용되는 것과 달리 중성자회절 분야는 여러 기술적 어려움으로 인하여 상대적으로 드물다. 한국원자력연구원에서는 오랜 개발 시도 끝에 대면적 곡면형 2차원 검출기(curevd 2-dimensional position-sensitve neutron detector, C_PSD)를 개발하였으며, 이에 기

반한 단결정 회절장치와 해석 기술을 일본 동북대 노다교수 그룹과 공동으로 하나로 4축단결회절장치는 물론 일본 JRR-3M의 4축장치인 FONDER를 이용하여 개발과 시험을 진행하고 있다. 이번 발표에서는 C_PSD 제작과 특성 및 초기 이용 결과, C_PSD에 기반한 회절장치의 개념과 데이타 전처리 과정(data reduction)을 보고한다. 이러한 회절장치는 높은 데이타 생산성(throughput)은 물론 신물질 합성시 미지의 넓은 역격자공간의 신속한 탐색은 물론 커다란 단위포를 갖는 유기 물질, 거대분자결정구조, 금속유기물구조체 등의 연구에서 전통적인 4축단결정회절장치의 한계를 극복할 수 있게 해주며, 상호 보완적으로 이용될 것이다.

**D-77** **The measurement of interfacial thermal properties of $Gd_2Zr_2O_7$ thin films by 3 omega method at high frequency range.** 강 준구, 김 종욱[1], 양 호순(*부산대학교 물리학과. [1]부산대학교 기계공학과.*) $Gd_2Zr_2O_7$(Gadolinium Zirconium Oxide)와 같은 파이로클로로(Pyrochlore) 물질의 낮은 열전도도는 최근 열차폐코팅(Thermal Barrier Coating) 물질로 관심을 받고 있다. 또한 마이크로소자의 활용이 활발해 지면서 미세구조에서의 경계면 효과(Interfacial Effect)가 중요해 지고 있다. RF 마그네트론 스퍼터링(RF magnetron sputtering)으로 증착한 박막의 경계면 효과를 확인하기 위해 3ω 방법을 사용하였으나 3ω 방법은 박막과 기판의 열물성에 대한 정보들을 사전에 알고 있어야 하고, 열선의 특성이나 모양에도 영향을 받는 등의 제한사항이 있었다. 이런 물성들의 오차는 실험결과에 영향을 줄 수 있으므로 실험 가능한 주파수 영역을 수십 KHz까지 확장하여 실험을 수행하여 이 문제를 보완하였다. 높은 주파수 영역에서 두께에 따른 박막의 열전도도를 측정하고 $Gd_2Zr_2O_7$ 박막과 $Al_2O_3$ 기판 사이의 경계면 효과를 확인하였으며, 낮은 주파수 영역에서 얻은 결과와 비교하였다.

**D-78** **Ferroelectricity in Highly Ordered Arrays of Ultrathin-Walled $Pb(Zr,Ti)O_3$ Nanotubes Composed of Nanometer-Sized Perovskite Crystallites** KIM Jongok, YANG Sun A, CHOI Yong Chan, HAN Jin Kyu, JEONG Keum Ok, KIM Dong Jik[1], YANG Sang Mo[1], YOON Doohee[2], CHEONG Hyeonsik[2], CHANG Ki-Seog[3], NOH Tae Won[1], BU Sang Don(*Chonbuk National University, Department of Physics. [1]Seoul National University, Department of Physics. [2]Sogang University, Department of Physics. [3]Korea Air Force Academy, Department of Chemistry.*) We report the first unambiguous ferroelectric properties of ultrathin-walled $Pb(Zr,Ti)O_3$ (PZT) nanotube arrays, each with the dimension of 5 nm thick walls and outer diameters of 50 nm [1]. Ferroelectric switching behavior with well-saturated hysteresis loops is observed in these ferroelectric PZT nanotubes with $P_r$ and $E_c$ values of about 1.5 mC $cm^{-2}$ and 86 kV $cm^{-1}$ respectively for a maximum applied electric field of 400 kV $cm^{-1}$. These PZT nanotube arrays ($10^{12}$ nanotubes $cm^{-2}$) might provide a competitive approach toward the development of three dimensional capacitors for the terabyte ferroelectric random access memory.

[1] J. Kim, S. A. Yang, Y. C. Choi, J. K. Han, K. O. Jeong, Y. J. Yun, D. J. Kim, S. M. Yang, D. Yoon, H. Cheong, K.-S. Chang, T. W. Noh, and S. D. Bu, Nano Letters 8, 1813 (2008).

**D-79** **Ferroelectric domain wall dynamics in Epitaxial $Pb(Zr,Ti)O_3$ films** YANG Sang Mo, JO Ji Young, KIM Tae Heon, LEE Ho Nyung[1], YOON Jong-Gul[2], NOH Tae Won (*Department of Physics and Astronomy, Seoul National University. [1]Materials Science and Technology Division, Oak Ridge National Laboratory. [2]Department of Physics, University of Suwon.*) The physics of propagating elastic objects in disordered media with quenched defects is of crucial importance to understand numerous intriguing phenomena in nature, such as growth phenomena of ferroelectric (FE) or magnetic domain walls, contact lines in wetting, and surface of epitaxially grown films. Although the FE domains have recently been intensively studied, but few attempts have been made to explain the FE domain wall dynamics in terms of propagating elastic objects in a disordered medium. Here, we report our studies on the temperature ($T$)-dependent FE domain wall dynamics under various electric fields ($E$).We deposited highly polar epitaxial $PbZr_{0.2}Ti_{0.8}O_3$ thin films on $SrRuO_3$/SrTiO3 (001) substrates by pulsed laser deposition and prepared the Pt top electrode with 100μm diameter [1]. To widen the accessible region of $T$ and $E$, we used switching current measurement results, combined with direct domain wall speed ($v$) data from PFM images by our modified piezoresponse force microscopy technique [2]. We found that $v$ follows the nonlinear dynamic response which has three regimes, i.e., creep, depinning, and flow regimes. We also could obtain values of the two critical exponents, the dynamical exponent $\mu$ and the velocity exponent $\theta$ of approximately 0.9 and 0.7, respectively.

[1] H. N. Lee *et al.*, Phys. Rev. Lett. 98, 217602 (2007) [2] S. M. Yang *et al.*, Appl. Phys. Lett. 92, 252901 (2008)

**D-80** **Directional ferroelectric domain growth in epitaxial $BiFeO_3$ (001) thin films** KIM Tae Heon, ORTIZ Daniel[1], JO Ji Young, YANG Sang Mo, JANG Seung Yup, KIM Yong Su, EOM Chang-Beom[1], NOH Tae Won(*ReCOE &FPRD, Department of Physics and Astronomy, Seoul National University, Seoul 151-747, Korea. [1]Department of Materials Science and Engineering, Univ. of Wisconsin-Madison, Madison, Wisconsin 53706, USA.*) $BiFeO_3$ (BFO) is one of remarkable materials as the next generation memory device since it has a comparable value of remnant polarization ($P_r$) to typical ferroelectric material such as $Pb(Zr,Ti)O_3$ and combined multi-functionality with weak ferromagnetic properties. Then, recent many researches in BFO have been mainly focused on the enhancement and probing of ferroelectric properties. However, detailed studies on ferroelectric domain switching in BFO thin films have been rare since it is difficult to directly observe overall domain evolution with conventional piezoresponse force microscopy (PFM). In this presentation, we investigated the polarization switching behavior in BFO(001) films, using our modified PFM. Interestingly, we observed that much bigger domains in BFO(001) films than that of typical ferroelectric films are nucleatd at a few sites. Moreover, we found that microscopic domain wall motion is affected by ferroelectric domain structure of BFO films. Ferroelectric domains are dominantly switched through domain wall motion along preferred directions. Here, we suggests that this anisotropic polarization switching behavior in BFO(001) film is originated from monoclinally tilted domains. And, such studies on ferroelectric domain switching will be also extended to BFO(101), and (111) films.

■ SESSION: E [EG1]
10월 23일(목), 12:30 - 14:00
장 소: 403호



**E-01** **나노바이오소자 제작을 위한 DNA 격자구조물 연구 (Fabrciation of DNA Nanostructures for Nano-bio devices)** 박 성하(*성균관대학교, 물리학과.*) DNA 나노기술은 DNA가 가지고 있는 생화학적 특성인 자기조립을 이용하여 마이크론 크기의 구조를 제작하는 기술로 나노미터의 정확성으로 구조물을 제어 할 수 있는 첨단과학기술이다. 초기 설계방법에 따라 형태적으로는 선형, 평면 및 입체구조물의 조립이 가능하고, 기능적인 측면에서는 움직임이 수반되는 기계적인 모터와 DNA 구조물을 기판(scaffold)으로 한 나노전자기소자 및 나노바이오센서의 제작도 가능하다. 또한, 몇 개의 DNA가닥에 인위적인 정보를 입력함으로서 컴퓨터의 중요한 기능중의 하나인 Algorithm을 이용한 패턴제작도 실험적으로 가능함이 입증되었다. 본 연구발표에서는 DNA를 이용한 몇 개의 기본 타일(예를 들면, Cross 타일, Double-Crossover 타일, Single-Strand 타일 등)을 이용한 다양한 DNA 나노구조물(1D 나노튜브, 1D 나노리본, 2D 나노격자, 2D 나노트랙 등)이 어떻게 만들어지는지 설명하고자 한다. 이러한 인위적으로 디자인한, 크기 및 직경 제어가 가능한 DNA 나노구조물을 이용하면 다양한 응용 연구가 가능하며, 여기서는 구동가능한 DNA 나노엑츄에이터, 금속을 입힌 DNA 나노와이어, DNA 격자를 이용한 단백질 정렬, 그리고 알고리듬 DNA 격자구조물 제작에 대해서 알아보고자 한다. DNA 분자를 이용한 본 연구의 결과들은 향후 DNA 나노구조물에 다양한 물리적, 생화학적특성을 가진 물질들을-예를 들어 금(Au), 철(Fe)나노입자, 단백질 또는 형광분자와 같은-접합함으로서 대용량의(DNA 1μM로 부피 1mL인 액체 안에서 1014개 이상) 자기조립하는 양자점 셀자동소자, 단일전자트랜지스터, 스핀제어소자, 그리고 다양한 실용적인 바이오센서 개발등으로 진행될 것으로 기대된다. 프로그램이 가능한 DNA 타일에 정보를 입력한 알고리듬으로 조립하면 나노미터의 정확성으로 논리회로의 제작도 가능하리라 본다. 그리고, 이종의 DNA 타일로 제작된 나노채널이나 나노컨테이너는 작은 분자의, 예를 들어 약물과 같은, 수송에도 활용될수 있다. 이는 물리학뿐만 아니라 생물학, 의학분야에서 새로운 패러다임을 제공할 것으로 기대된다.

**E-02** **Position-controlled ZnO nanoflower arrays grown on glass substrates for electron emitter application** 김 용진, 유 진경, 이 철호, 홍 영준, 이 규철(*POSTECH, 신소재공학과.*) There has been tremendous interest in one-dimensional (1-D) semiconductor nanostructures because of their applications to emitters and field emission displays. Of the central importance are the high electron emission and low cost mass production of the nanostructures for the applications to their cold cathode electron emitter. Among numerous 1-D nanostructures, ZnO nanoneedles with a very sharp tip have been considered as one of the best candidate materials for an electron emitter application, thanks to their negative electron affinity and high mechanical stability. Although the ZnO 1-D nanostructures have been studied extensively, there still remain a couple of critical problems for commercial device applications. First, spatial arrangement of 1-D nanomaterials should be optimized for their enhanced and reliable field emission characteristics. For too dense nanomaterials, the local field enhancement at the tips of nanomaterials is reduced while the small number of emitters for low density nanomaterials may result in a low emission current. Nevertheless, a reliable and reproducible method for controlling density and positions of 1-D nanomaterials has rarely been reported. Second, a low material cost is required for the mass production of the electron emitter devices with a competitive price. Glass, generally much cheaper than single crystals, can be the most promising substrate material. In addition, solution-based deposition methods enable the large scale production of nanomaterials, subsequently reducing the production cost of the devices. Accordingly, position- and density-controlled growth of ZnO nanoneedles on glass substrates by a chemical solution method is an important step for mass productions of electron emitter devices. Here, we report on the position-controlled ZnO nanoflowers composed of several nanoneedles with a sharp tip on a conducting glass substrate for field emission device applications. Our controlled selective growth of ZnO nanoflower arrays by CSD offers an opportunity for the fabrication of a high performance electron emitter on glass substrates. ZnO nanoflower arrays exhibited excellent electron emission characteristics showing a low turn-on voltage of 0.13 V/mm at the criterion of 0.1 $mA/cm^2$ and a high emission current of 0.8 $mA/cm^2$ in the applied electric field of 9.0 V/mm, resulting from the well-distributed electric field near the 1-D nanostructure tips. Furthermore, position- and morphology-controlled ZnO nanoflowers can be used as cold cathode electron emitter arrays for field emission microdisplay applications. More generally, we believe that the simple and cheap chemical solution method might readily be expanded to create many other semiconductor nanoflowers on diverse substrates for many device applications.

**E-03** **Strain Relaxation and Texture Evolution of ZnO Nano-rods at Initial Growth Stage** 이 현휘, 정 상태, 이 동렬[1](*포항가속기연구소, 빔라인부. [1]숭실대학교, 물리학과.*) Structural evolution of ZnO nano-rods (NR) at initial growth stage is investigated using x-ray diffraction (XRD), x-ray reflectivity (XRR), and grazing incidence wide angle x-ray scattering (GI-WAXS) methods. ZnO NRs were grown on both c-plane sapphire and quartz substrates by a chemical vapor deposition (CVD) in a horizontal-type reactor. ZnO NRs were grown vertically along c-axis and have in-plane epitaxial relationship, <10-10>// *a*-Al2O3 <11-20>. However, a complicated strain relaxation and texture were introduced at initial growth stage. The strain evolution was measured by high-resolution XRD and the texture of NRs was investigated by an azimuthal angle dependent GI-WAXS. For the detailed measurement of texture evolution on ZnO NRs, a new system of kappa-type 6 circle diffractometer directly combined with MAR345 image plate (IP) is installed at the wiggler beamline-5A (HFXS: High Flux X-ray Scattering) at Pohang Accelerator Laboratory (PAL) in Korea. Both scintillation detector and IP detector can be easily switched on the diffractometer, therefore, XRR, XRD and 2D-GID

measurements are possible.

**E-04** **방사광을 이용한 단결정(samll-molecule)의 3 차원 구조 분석** 김 경화, 권 세진, 이 흥수(*포항가속기연구소*) 단위 격자의 크기가 상대적으로 큰 단백질(macromolecule) 결정 구조 분석이 가능한 빔라인이 2001년부터 완공되어 실험에 사용되고 있다. 이 빔라인을 이용하여 단결정(smallmolecule)의 구조 해석 실험을 수행 할 경우 동일한 실험 기법임에도 불구하고 장비 사용에 있어 많은 위험과 어려움이 따랐다. 이를 개선하기 위해 빔라인의 성능 향상이 진행 되었고, 성공적으로 작업이 진행되어 일반 이용자의 실험 지원을 눈앞에 두고 있다. 사용 가능한 엑스선의 파장은 0.88~2.0Å(14kev~6keV)이고 엑스선의 세기는 $2x10^{11}$ photons/sec에 이르며 $2x10^{-4}$의 분해능($\Delta E/E$)을 나타내고 있다. 이를 이용하면 20μm 이하의 작은 결정에 대한 구조 분석이 가능해 진다. 열에 의해 결정 구조 변화에 대한 연구나 공기와의 접촉을 차단 해야 하는 시료의 경우 액체 질소를 사용하여 90K까지 냉각이 가능한 저온 장치를 이용 할 수 있다. 이와 더불어 수소 저장 등의 실험을 위한 극저온 냉각 장치의 활용도 가능한데, 이는 액체 헬륨을 사용하며 9K까지 냉각이 가능 하다. 설치된 엑스선 회절기의 측정 면적은 210mm x 210mm, 측정 화소는 51μm x 51μm 이고 시료와 회절 이미지 측정기 사이 최소 거리인 60mm일 때 최대 해상도는 0.7Å이다. 신속한 구조 해석을 위하여 Giga Bit 전용 랜과 3.3GHZ/Dual Display, 10CPU 초고속 계산용 서버가 설치되었고 관련 구조 프로그램을 사용 할 수 있도록 전산장비가 마련되었다. 본 논문을 통하여 빔라인이 특성과 이를 활용한 결정 구조분석법에 대해 소개하고, 이미 진행된 연구 결과에 대한 분석을 통해 방사광을 활용한 연구에 대한 이해를 높이고자 한다.

**E-05** **Strain Field Mapping of Zeolite Microcrystals by Coherent X-ray Diffraction** CHA Wonsuk, SONG Sanghoon, JEONG Nak Cheon[1], YOON Kyung Byung[1], HARDER Ross[2], ROBINSON Ian K.[2], KIM Hyunjung(*Sogang University, Interdisciplinary Program of Integrated Biotechnology and Department of Physics. [1]Sogang University, Interdisciplinary Program of Integrated Biotechnology and Department of Chemistry. [2]University College London, Department of Physics and Astronomy.*) Zeolites, crystalline aluminosilicate with uniformly and regularly spaced pores, are used widely in industry for catalysts, adsorbents, ion exchangers and hydrocarbon interconversion. We measured coherent x-ray diffraction (CXD) on zeolite microcrystals to obtain three-dimensional shape and internal strain distribution. The CXD measurements were performed at the beamline 34-ID-C in Advanced Photon Source, USA and employed monochromatic coherent x-rays with wavelength of 1.394Å. The ZSM-5 zeolite microcrystals with size of 2㎛ were attached on Si (100). The CXD patterns were obtained continuously surrounding a (200) and (020) Bragg peak as a function of temperature. We inverted oversampled diffraction patterns using phase retrieval algorithm contained error reduction and hybrid input-output method to obtain three-dimensional shape and internal phase map of the zeolite microcrystals. From the phase map of the inside zeolite microcrystals we found thermal expansion or compression near the edge of the samples along the total wavevector transfer. We observed the changes of thermal induced strain fields with increasing temperature.

* This study was supported by Korea Science &Engineering Foundation, Seoul Research &Business Development program (10816) and Sogang University Research Grant(2007).

**E-06** **Nano-bead structure fabrication by Sequential Ion Beam Sputtering** KIM JiHyun, HA NeulBit, KIM J.-S. (*Sookmyung Women's University.*) 최근 ion beam sputtering을 이용한 자기 조립 방식은 metal, insulator 및 semiconductor의 다양한 기판에 정렬된 nanostructure를 넓은 영역에 손쉽게 만들 수 있다는 장점을 갖고 있어 폭 넓게 연구 되고 있다. 하지만 ion beam sputtering에 의한 표면 식각은 단일 빔 조사로 국한되어, dot 과 ripple 같은 simple한 패턴 형성으로 제한되어 왔다. 최근 이러한 제한을 넘어 다양한 패턴 형성 및 패턴의 질서도 향상을 위한 시도로, 2개 이상의 방향에서 순차적으로 ion beam 을 조사하여 pattern을 형성하는 sequential ion beam sputtering (SIBS)이 제안 된 바 있다. 본 연구진은 SIBS을 이용하여 즉, 첫 번째 oblique incidence ion beam 의 조사로 periodic ripple surface를 만들고 두 번째로 수직 방향으로 ion beam을 조사하여, ripple에 의해 guide된 잘 정렬된 nano dot array를 (nano-bead structure) 형성하였다. 이러한 nano-bead structure는 일차 빔에 의한 2D instability로 인해 1차원의 ripple 패턴이 형성되고, 이어서 2차로 조사된 빔에 의해 1D instability가 일어나 ripple을 따라 0차원의 dot이 형성된 것이다.흥미로운 사실은 flat한 surface에 수직방향으로 ion beam을 조사하였을 때, nano-dot array이가 아닌 기판의 densely closed packed direction을 따라 crossed ripple이 형성된다는 것이다. 이는 flat한 표면에서는 기판의 crystalline의 영향으로 adatom의 diffusion이 두 closed packed direction으로 equivalent하게 일어나기 때문이다.본 연구진은 또한 nano-bead structure 형성에 미치는 초기template의 영향을 살펴보았다. 그 결과 초기 ripple의 wavelength와 무관하게 수직 sputtering 후, initial ripple의 wavelength와 nano-bead의 wavelength가 각각 ~50nm와 ~50nm으로 일정한 값을 가짐을 확인 하였다. 하지만 초기 ripple의 amplitude가 작은 경우, nano-bead structure가 잘 형성되지 못함을 확인 하였다.

■ SESSION: E [EA1]
10월 23일(목), 14:30 - 16:15
장 소: 401호

**EA-01** **3-Dimensional Nanometrology with Atomic Force Microscopy** PARK Sang-il(*Park Systems Corp., KANC 4F, Iui-Dong 906-10, Suwon, Korea 443-270.*) Atomic Force Microscope (AFM) has been widely used to measure and characterize the surface of a sample in nanometer scale. The first generation AFM based on piezoelectric tube scanners has high spatial resolution and performs well in qualitative measurements. However, it suffers from poor repeatability and accuracy due to the background curvature and cross-talk between the x-y-z axes, making it inadequate for quantitative metrology.We developed the second generation AFM, designed and optimized for metrology consideration, with a x-y flexure scanner, decoupled from the z scanner, which has a highly orthogonal

and flat scan, providing adequate repeatability and accuracy for precision nanometrology.[1] The high speed z scanner with minimized drive mass provides a fast z servo response, making true non-contact AFM practical. The second generation AFM has been successfully adopted by hard disk drive industry for measuring the dimensions of Pole-Tip Recession (PTR) in magneto-resistance heads with sub nanometer repeatability.[2]The second generation AFM can also be used in critical angle measurement of microstructures such as reflective LCD display substrates. However, any slight non-orthogonal motion of the z scanner from the x-y scanner movement causes complex distortion in the measured data due to the crosstalk. We have developed a method which can measure the non-orthogonality from the measured data and compensate the effect of the non-orthogonality.[3] In overcoming the limitation of the vertical wall imaging by a flared tip [4], the design concept of the second generation AFM was utilized to measure under-cut structures by intentionally changing the angle of the z scanner.[5] The new 3D AFM can measure and image undercut structures as well as vertical sidewalls for the first time in AFM history.

[1] Joonhyung Kwon, Jaewan Hong, Yong-Seok Kim, Dong-Youn Lee, Kyumin Lee, Sang-min Lee, and Sang-il Park, Rev. Sci. Instrum. 74, 4378 (2003). [2] Joonhyung Kwon, Yong-Seok Kim, Moonseop Hyun, Kwanseok Yoon, Sang-min Lee, and Sang-il Park, Ultramicroscopy, 105, 51 (2005). [3] to be published. [4] Yves Martin and H. Kumar Wickramasinghe, Appl. Phys. Lett. 64, 2498 (1994). [5] to be published.

■ SESSION: E [EG2]
10월 23일(목), 14:30 - 16:15
장 소: 403호

**E-07** **Growth Kinetics and Properties of Thin Cobalt Films Electrodeposited on n-Si(100)** LEE Jong Duk, KIM Hyeon Soo, JEONG Soon Young, KIM Kun Ho, LEE Jeoung Ju (*경상대학교, 물리학과.*) Thin Co films were grown on n-Si(100) substrates by pulsed electrodeposition in 0.1 M $CoCl_2$ electrolyte. In this solution, $Co^{2+}$/n-Si interface showed a rectifying characteristics due to the formation of Schottky barrier and the reduction of $Co^{2+}$ was the dominant process rather than the oxidation. From the potential step experiment, we have known that the formation of Co nuclei in the early deposition stage is proceeded through 3D instantaneous nucleation followed by diffusion-limited growth. It has also been found that the areal nucleus density, $N_0$ of the Co films increases with increasing the pulse potential and has an order of about ~$10^{10}$ $cm^{-2}$ in all potential ranges. The average diameter and average height of Co nanoparticles was about 53.75 nm and 140 mn, respectively. In particular, through the investigation of the magnetic hysteresis loops, it has been confirmed that the shape of hysteresis loop depends on the applied field directions and thin Co films with columnar-shaped Co nanoparticles exhibit uniaxial magnetic anisotropy with the easy magnetization axis parallel to the surface of it.

**E-08** **Thermal Heat Dissipation on Unipolar Resistance Switching in Pt/NiO/Pt Capacitors** CHANG Seo Hyoung, CHAE S. C., LEE S. B., NOH T. W., LEE J. S.[1], KAHNG B.[1], JANG J. H.[2], KIM M. Y.[2], KIM D.-W,[3], JUNG C. U.[4](*ReCOE &FPRD, Department of Physics and Astronomy, Seoul National University. [1]Department of Physics and Astronomy, Seoul National University. [2]School of Materials Science and Engineering, Seoul National University. [3]Division of Nano Sciences and Department of Physics, Ewha Womans University. [4]Division of Department of Physics, Hankuk University of Foreign Studies.*) Resistance switching phenomena have recently attracted lots of interests due to their potential application in nonvolatile memory device which is called resistance random access memory (RRAM). Despite the intensive studies on the mechanism of these resistance switching phenomena, understandings on underlying physics is still lacking. To address one of possible mechanisms, we systematically varied the bottom electrode thickness in Pt/NiO/Pt capacitor structures and investigated their resistance switching behaviors. We observed that the capacitors with thick bottom electrode showed a typical unipolar memory resistance switching, while those with thin bottom electrode showed a threshold resistance switching. Using temperature dependent *I-V* measurement and finite element analysis, we demonstrated that this phenomenon can be occurred due to the thermal stability of conducting filaments. This study indicates that thermal heat dissipation in RRAM is an important factor to control their resistance switching behaviors in Pt/NiO/Pt capacitors.

**E-09** **Investigation on the resistive memory switching mechanism of epitaxially grown NiO thin films** LEE S. R., BAK J. H., PARK Y. D., CHAR K., KIM D. C.[1], SEO S.[1], LI X. S.[1], PARK G. -S.[1](*Seoul N. Univ., Dept. of Physics &Astronomy. [1]Samsung Advanced Institute of Technology.*) NiO thin films have been epitaxially fabricated by pulsed laser deposition on (100) $SrRuO_3$ films prepared on single-crystal (100) $SrTiO_3$ substrates at 500 °C and 700 °C under an $O_2$ pressure of 5 mTorr. A prominent peak due to NiO (200) is observed in the X-ray diffraction spectra and rocking-curve scans of the NiO films grown at 500 °C and 700 °C, with a full width half maximum of 0.92° and 0.75°, respectively. The structures of the NiO films prepared at the two abovementioned temperatures have been characterized from X-ray reciprocal space mapping, indicating negligible differences in their in-plane and out-of-plane lattice parameters. However, the NiO films exhibit distinct I-V characteristics depending on their growth temperature by employing $SrRuO_3$ and Pt as the bottom and top electrode, respectively. Although epitaxial NiO films exhibit bipolar resistive memory switching, only NiO deposited at 500 °C requires the electroforming process before the initialization of the bipolar resistive switching. On the other hand, NiO deposited at 700 °C initially remains in a low-resistance state in the absence of the electroforming process, and its memory switching endurance is considerably poorer. In order to understand the distinct switching behavior of epitaxial NiO at different growth temperatures, in-depth measurements of the initial I-V characteristics and surface images of NiO

are carried out. Our results suggest that defect states of NiO/top electrode interfaces may play a significant role on resistive switching behavior. In addition, temperature dependence of I-V characteristics of the epitaxial NiO films will be presented in order to further characterize the role of NiO/top electrode interfaces.

**E-10** **Changes In Physical Properties Of Zr-incorporated $Gd_2O_3$ Films Grown On Si(100) By $NH_3$-nitridation** LEE Woo-Jung, MA JinWon, CHO Mannho(*연세대학교, 물리 및 응용물리.*) $Gd_2O_3$ and Zr-incorporated $Gd_2O_3$ films grown on Si (100) were annealed under $NH_3$ ambient and investigated by various analysis techniques. For as-grown $Gd_2O_3$ film, Gd-silicide layer was formed in contact with silicon substrate while, for Zr-incorporated or $NH_3$-nitried $Gd_2O_3$ film it was suppressed. We observed the change of lattice constant in Zr-incorporated $Gd_2O_3$ by substituted zirconium with small ionic radius for gadolinium. When concentration of Zr atoms in $Gd_2O_3$ film reach a specific quantity ($Gd_{0.6}Zr_{1.9}O_{4.3}$) phase transition occurred from cubic $Gd_2O_3$ to monoclinic $ZrO_2$. However, it disappeared after $NH_3$ nitridation at 900℃. Most of the nitrogen atoms were piled up near the interface in the films and the concentration of incorporated N increased as Zr content and $NH_3$ annealing temperature increased. Moreover, nitrogen atoms preferred bonded to Zr-silicate rather than $ZrO_2$ directly. These incorporation behaviors of nitrogen into Zr-incorporated $Gd_2O_3$ film affected thermal stability and crystalline structure.

**E-11** **Study of Structure and Dynamics of Segregation layer in Diblock Copolymer Films** SONG Sanghoon, CHA Wonsuk, LEE Heeju, LI Xiaolong, JIANG Zhang[1], NARAYANAN Suresh[1], RUEHM Adrian[2], SINHA S. K.[3], KIM hyunjung(*Sogang University, Department of Physics &Interdisciplinary Program of Integrated Biotechnology. [1]Argonne National Laboratory, Advanced Photon Source. [2]Max Planck Institute for Metal Research. [3]Univ. of California San Diego, Department of Physics.*) We have investigated the structure and dynamics of supported block copolymer films of poly(styrene)-b-poly(dimethylsiloxane) (PS-b-PDMS) in the spherical phase, i.e., PDMS cores surrounded by PS shells by x-ray photon correlation spectroscopy (XPCS) in grazing angle geometry. It is interesting to investigate the dynamics as a function of temperature since the glass transition of PDMS (-120°C) is remarkably lower than the glass transition of PS (100°C). The temperature range studied was between 160-210°C, much higher than the glass transition with the thicknesses from 40nm to 600nm. In the process of analyzing the surface dynamics from XPCS results, we applied hydrodynamic theory for surface capillary waves.We found that the PDMS-rich layer near the surface appears at the temperature higher than the glass transition temperature by x-ray reflectivity and x-ray photoelectron spectroscopy (XPS). We found a universal scaling of the dynamics even with bilayer model. From the fitting with the bilayer model, the viscosities form both of the layers are obtained.
* This work was supported by Korea Science & Engineering Foundation, Seoul Research and Business Development Program (10816), and Sogang University Research Grant (2007). Use of the Advanced Photon Source was supported by the US Department of Energy, Office of Science, Office of Basic Energy Science, under Contract No. DE-AC02-06CH11357

**E-12** **XPS와 UPS를 이용한 ITO/MoO3/NPB 계면에서의 정공 주입 향상의 원인 연구** 이 현복, 이 연진[1], 한 결, 전 평은, 김 현성(*연세대학교 물리학과. [1]한국표준과학연구원.*) 최근 OLED 소자 성능 향상을 위해 사용되는 물질로 주목받고 있는 전이 금속 중 MoO3를 ITO와 NPB 계면에 삽입하여 in situ로 XPS와 UPS 측정을 수행하고, MoO3를 삽입하지 않은 것과 비교 분석하였다. MoO3 층을 삽입한 박막은 큰 계면 쌍극자를 형성하게 되면서 MoO3 를 삽입하지 않은 것과 비교하여 정공 주입 배리어가 월등히 줄어든 것을 관찰할 수 있었다. 그리고 NPB의 밴드 갭 사이에 새로운 전자 상태가 나타나는 것을 볼 수 있었는데 이를 통해 MoO3 층의 삽입이 정공의 Ohmic 주입을 하도록 도와준다는 것을 증명할 수 있다. 이 두가지 요소를 통해 MoO3 층의 삽입으로 왜 OLED의 소자 성능이 향상되는지에 대해 증명하였다.

**E-13** **Study on chemical and structural properties in ALD-$HfO_2$ grown on *n*-GaAs (100) substrate as functions of initial surface states and post-annealing temperature** KIM C. Y., LEE S. Y., CHO M. -H., YI Y.[1], AN C. –H.[2], KIM H.[2], LEE H. J.[2](*Institute of Physics and Applied Physics, Yonsei University. [1]Advanced Technology Group, Korea Research Institute of Standard and Science. [2]School of Advanced Materials Science and Engineering, Sungkyunkwan University.*) We investigated the chemical and structural properties in the $HfO_2$ film grown on the GaAs substrate as a function of post-annealing temperatures. $HfO_2$ films were deposited onto *n*-type GaAs (100) substrates by means of an atomic layer deposition process and a rapid thermal annealing was carried out at 600 °C and 700 °C under an $N_2$ ambient. From x-ray photoelectron spectroscopy results, it was revealed that the chemical bonding state at the interface of $HfO_2$/GaAs was significantly related on initial surface states and dependent on post-annealing temperatures. Through combining high resolution transmission electron microscopy and medium energy ion spectroscopy, moreover, the changes in crystalline structures of $HfO_2$ films was observed to a well-ordered crystalline film as increasing annealing temperatures. The Ga oxides formed within the films during the annealing process affect the values of valence band offsets and energy band gaps of $HfO_2$, which is in good agreements with the theoretical prediction of the band alignment in $HfO_2$/GaAs.

■ SESSION: E [EG3]
10월 23일(목), 16:30 - 18:15
장 소: 207호

**E-14** **Fluorescence Properties of $Eu^{3+}$-doped $YBO_3$ and $Li^+$-modified $YBO_3$ Phosphors** R. Balakrishnaiah, SEO Seong Ji[1], KIM Dong Woo[1], YI Soung Soo[1], JANG Kiwan[2], LEE Ho

Sueb[2], JEONG Jung Hyun[3](*Department of Electronic Materials Engineering, Silla University, Busan 617-736, Republic of Korea and Department of Physics, Changwon National University, Changwon, 641 – 773, Republic of Korea. [1]Department of Electronic Materials Engineering, Silla University, Busan 617-736, Republic of Korea. [2]Department of Physics, Changwon National University, Changwon, 641 – 773, Republic of Korea. [3]Department of Physics, Pukyong National University, Busan 608-737, Republic of Korea.*) Research interest on lanthanide (Ln)-doped materials is rapidly growing in the present generation due to their potential applications in the fields such as non-linear optical (NLO) materials. These materials found wide useful in the development of plasma display panels (PDP), field emission displays (FED) and electro-luminescent panels. Recently, Ln-doped orthoborate phosphors have attracted much attention due to their high stability, low synthesis temperature, high VUV absorption and exceptional optical damage threshold. Among Ln doped materials, $Eu^{3+}$-doped materials found the most interesting due to the simple lower energy levels scheme of $Eu^{3+}$ ions as well as its applications in the fields such as red emitting phosphor by its intense, narrow and monochromatic red emission around 610 nm as a result of $^5D_0 \rightarrow {}^7F_2$ transition. Incorporation of modifiers such as $Li^+$, $La^{3+}$, $Sc^{3+}$, $Bi^{3+}$, etc. will further enhance the luminescence characteristics of $Eu^{3+}$ ions. In our present work, $Eu^{3+}$-doped $YBO_3$ and $Li_xEu_yY_{(1-x-y)}BO_3$ phosphors were prepared by solid state reaction method for x = 0 &0.1 and y = 0.05 0.1, 0.15 and 0.2 mole concentrations. The synthesized materials were characterized by X-ray diffraction (XRD), scanning electron microscopy (SEM), excitation, emission and lifetime measurements. The dependence of various optical and morphological properties of the prepared materials on $Eu^{3+}$ ion concentration has been discussed and the results are compared with those reported in earlier literature.

* Acknowledgements: This work was supported by Korea Research Foundation grant funded by the Korean Government (KRF-J00902).

**E-15** **Site-selective laser-excitation spectroscopy of $Eu^{3+}$ ions doped in $K_2YF_5$ crystals** 장 경혁, 김 은식, 시 량, 서 효진(*부경대학교.*) Luminescence and excited-state dynamics of $Eu^{3+}$ in $K_2YF_5$ crystals are investigated by site-selective laser-excitation spectroscopy at different temperature. The $K_2YF_5$:$Eu^{3+}$ crystals with different $Eu^{3+}$ concentrations (0.1, 1.0, 6.0, 30 and 100 mol %) were grown by the hydrothermal method. The excitation spectra of the $^7F_0 \rightarrow {}^5D_0$ transition obtained by monitoring the emission due to the $^5D_0 \rightarrow {}^7F_J$ (J=1, 2, 3,…,6) transitions exhibit two strong lines together with four weaker lines. The weaker lines increase in intensity for high $Eu^{3+}$ concentrations. Emission spectra were obtained by tuning the dye laser to resonance with each line in the excitation spectra. Two kinds of decay with long and short decay times are detected for the selectively excited emissions. The results indicate that there exist at least six different sites for $Eu^{3+}$ in $K_2YF_5$ lattice. The exchange interaction in $Eu^{3+}$-$Eu^{3+}$ pair is responsible for the short decay times while, the long decay times are ascribed to the isolated $Eu^{3+}$ ions. In this presentation, the results are discussed in relation with one dimensional chain structure of $K_2YF_5$ lattice.

**E-16** **Anisotropic Mobility of Organic Semiconductor: tetramethyltetraselenafulvalene (TMTSF)** KIM Ja-Yeon, YUN Mira, LEE Injae(*Department of Physics, Research Institute of Physics and Chemistry, Chonbuk National University.*) We report the studies anisotropic electrical transport of an organic single crystal semiconductor TMTSF (tetramethyl tetraselena fulvalene) in the field effect transistor geometry. The single crystal TMTSF was synthesized by physical vapor deposition (PVD). The structure of the synthesized crystals was characterized by using a four circle X-ray diffraction. The stamp-type organic FET device was fabricated using Parylene-C as a gate insulator on an elastomeric substrate Polydimethylsiloxane (PDMS). The extra flexible stamp-type device helps to make an intimate contact between the contact pads and the semiconducting organic single crystal TMTSF. Also, it minimizes stress exerted on the organic single crystal while warranting reversible use of the device. Anisotropic mobility of the free standing film type single crystal TMTSF semiconductor was measured in various crystal axes relative to the direction of the source-drain electrode. The maximum field effect mobility was obtained as 3.96 $cm^2$/Vs (saturation region) which is an order of magnitude higher than the value reported previously on single crystal TMTSF.

**E-17** **Photo-controlled Trapped Electron Density and Memory Effect in Soluble Organic Thin Film Transistors** 조 미연, 한 윤덕, 박 동혁, 김 경환[1], 조 민주[1], 최 동훈[1], 주 진수(*고려대학교 물리학과. [1]고려대학교 화학과.*) 용해 가능한 star-shaped oligothiophene 분자인 4(HPBT)-benzene, 4(HP3T)-benzene과 TIPS-pentacene을 이용한 유기 박막 트랜지스터를 제작하였고, 전기 및 광 반응 특성을 연구하였다. 4(HPBT)-benzene을 이용한 광 트랜지스터는 낮은 세기의 광(6.8 ~ 30 μW/$cm^2$)에서도 높은 광 반응도를 보였고, 이러한 민감한 광 반응 특성을 사용하여 낮은 세기의 광과 낮은 게이트 전압을 이용하여 ~$4\times10^4$의 높은 점멸비를 얻을 수 있었다. 광 유도된 전하들은 게이트 전압에 의해 반도체-절연체 계면에 트랩된 전자 밀도를 변화시키는데, 이를 이용하여 광 트랜지스터의 문턱전압을 조절하고 메모리 효과를 구현할 수 있었다. 특히, TIPS-pentacene을 이용한 트랜지스터에서는 광을 이용하여 구현한 메모리 효과가 어두운 조건에서보다 50배정도 큰 on/off 전류 비율을 보였다. 문턱전압의 변화로부터 게이트 전압에 의해 조절 가능한 트랩된 전자 밀도를 구하여 비교하였다.

**E-18** **상대습도 변화에 따른 실리콘 1 kg Sorption Artefacts의 흡착 질량 연구** 정 진완, 이 성준, 김 광표(*한국표준과학연구원.*) 이전에 발표한 결과를 분석 검토한 결과 Sorption Artefacts (SAs)의 미소한 부피차 때문에 부력의 영향이 나타났다. 불확도 평가를 한 결과 부력의 영향이 흡착 질량보다 크게 나타나 실험 결과를 평가하는데 어려움이 있었다. 이에 따라 SAs의 부피차를 최소화하기 위하여 재가공하였고 실험 결과 새로운 결과를 얻었고 상대습도 약 2 %-70 % 범위에서 10 % 별로 구간을 나누어 습도 발생장치를 이용하여 상대습도를 변화시키면서 흡착질량의 변화를 측정하였고 그 결과를 발표하고자 한다.

**E-19** **고감도 가이거 모드 실리콘 광센서 (SiPM)의 설계와 제작** 이 혜영, 나 고운, 김 지은, 남 신우, 이 직, 박 재형, 박 일흥(*이화여자대학교*) SIPM(Silicon Photomultiplier)은 제한된 가이거 모드에서 동작하는 반도체 광센서로 광전증배관 정도의 신호증폭율로 단일광자의 검출에 이용될 수 있으면서도 크기가 작고 자기장의 영향을 받지 않는 등 장점이 많다. 이 광 센서는 저항이 낮은 P형 기판 위에 형성된 수 마이크로 미터 두께의 에피택시 층 안에 1000개 정도의 수십 마이크로미터 크기 P-N 접합 배열을 조성하여 제작된다.최근에 제작한 시작품 센서의 설계과정과 시뮬레이션, 공정과정을 설명하고 이 SIPM 광센서의 누설전류 등의 전기적인 특성 및 광특성 측정결과를 논의한다.

**E-20** **극한 대기 현상 관측 우주 망원경을 위한 MEMS 마이크로미러 어레이** 전 진아, 김 지은, 나 고운, 남 신우, 박 재형, 박 일흥, 서 정은, 이 직, 정 애라, GARIPOV G[1], KHRENOV B[1], KLIMOV P[1], 김 민수[2], 김 용권[2], 유 병욱[2], 진 주영[2], 박 용선[3], 유 형준[3](*이화여자 대학교, 물리학과. [1]DV Skobeltsyn Institute of Nuclear Physics, Moscow State University. [2]서울대학교, 전기컴퓨터공학부. [3]서울대학교, 물리천문부.*) 극한 대기 현상을 관측하기 위한 망원경인 MTEL(MEMS Space Telescope for Extreme Lightning)의 핵심 부품으로서 MEMS(Micro-Electro-Mechanical Systems)기술을 이용한 초소형 마이크로미러를 설계 및 제작하였다. 제작된 마이크로미러는 350μm x 350 μm 의 크기를 가지며 기존의 평면 거울에 비해 회전속도가 빠르고 정확한 제어가 가능하며 전력소모를 크게 줄일 수 있는 장점이 있다. 마이크로미러는 8 x 8 어레이로 배열되어 총 3 mm x 3 mm 로 제작되었으며 콤 구조로 이루어진 마이크로 엑츄에이터의 정전 구동에 의해 2축으로 동작한다. 2축 방향의 구동을 조정하여 임의의 방향에서 발생되는 관측 대상을 1 ms 이내의 빠른 속도로 추적할 수 있다. 마이크로미러를 장착한 망원경(MTEL) 의 우주 환경 테스트가 현재 진행되고 있으며 러시아 Tatyana 2 위성의 주탑제체로서 2008년 11월 발사 예정이다. 본 발표에서는 MTEL을 위해 제작된 마이크로미러의 설계, 제작 및 성능과 더불어 망원경의 발사 후 관측을 위한 지상에서의 테스트 결과에 대해 이야기 하고자 한다.

■ SESSION: E [ET1]
10월 24일(금), 09:00 - 10:50
장 소: 403호

**ET-01** **Graphene: a flat carbon wonderland** SON YOUNG-WOO(*KIAS.*) After successful isolations of graphene - a single layer of graphite, it has been a cornucopia of interesting physical phenomena. In this tutorial, I will briefly describe basic properties of ideal graphene and its engineered structures and then will discuss several issues and problems related with them.

**ET-02** **Progressive Reports of Graphene Experiments at Columbia University** KIM Philip(*Columbia University.*) In this presentation, we will review some of recent experimental developments in graphene research at Columbia University University. First, we will discuss the enhancement of carrier mobilities in suspended graphene samples and the strong temperature dependent conduction in the samples. Second, the nature of these QH states near the charge neutral Dirac point will be discussed as a single particle theory breaks down. We will discuss the transport and IR measurement results that reveal the role of the many-body effects due to the electron-electron interaction in graphene near the Dirac point. In addition, the role of disordered edges in graphene nanostructures will be discussed in the context of localization and variational range hopping conduction. Finally we will discuss the quantum mechanical effects in transport in graphene heterojucntions. Progressive Reports of Graphene Experiments at Columbia University University

■ SESSION: F [FG1]
10월 23일(목), 12:30 - 14:15
장 소: 프레스센터

**F-01(초)** **Mutation rate threshold under changing environments with the sharp-peak fitness function** ANCLIFF, Mark, PARK, Jeong-Man(*가톨릭대학교 물리학과.*) We investigate the evolution of biological organisms under changing environmentsusing the parallel mutation-selection model for quasi-species with the sharp-peak fitness function. While in the static case with the sharp-peak fitness function $f(\xi)=A \delta_{\xi,N}$ a threshold $\mu^{s}_{\rm th}=A$ appears as an upper bound on the mutation rate above which no effective selection can occur, in the dynamic case where the position of the sharp-peak oscillates between $\xi = N$ and $\xi = 0$ with period $T$ the threshold on the mutation rate is found to be $\mu^{d}_{\rm th} = A/2$, and the phase diagram on the mutation rate and fitness phase space is modified according to the new threshold. We also calculate the stationary values for the maximum and minimum population of the master sequence.

**F-02** **Finite-Size Effects of Phase Transitions in *K*-Satisfiability (*K*-SAT) Problem** LEE Sang Hoon, HA Meesoon, JEON Chanil, ARDELIUS John[1], JEONG Hawoong(*Department of Physics, KAIST. [1]Swedish Institute for Computer Science (SICS), Kista, Sweden.*) We numerically study various phase transitions in the well-known random *K*-satisfiability (*K*-SAT) problem, which is a representative non-deterministic polynomial (NP)-complete problem in computer science. In order to solve the random *K*-SAT problem, stochastic local heuristic search algorithms have been suggested and widely studied. In such algorithms, the so-called optimal value of noise parameters are used, which corresponds to the role of temperature in physical systems. However, the systematic approach to find the optimal value and its finite-size effects are hardly discussed on the SAT/UNSAT transition and the solution space structural phase transitions, like freezing, condensation, and clustering of solutions. Using the average SAT (ASAT) algorithm, we systematically characterize various phase transitions as the density of constraints and the noise parameters vary, respectively. We measure the time to find solutions, the number of unsatisfied clauses (the so-called energy), and the "specific heat" in order to investigate their finite-size effects. Besides the random *K*-SAT problem, we propose the TreeCNF problem, where we are able to systematically control the loop structure among variables and clauses, and investigate the effect of loops in the *K*-SAT problem and compare it with the random one.

**F-03** **Driven Contact Process with a long-term memory** HA Meesoon, KWON Sungchul[1], PARK Hyunggyu[2](*KAIST, 물리학과. [1]경희대학교, 물리학과. [2]KIAS, 물리학부.*) The pair contact process with diffusion (PCPD) has recently attracted considerable interest, because of a possibility of a new universality class, which is distinct from well-established directed percolation (DP) and directed Ising (DI)/ parity-conserving (PC) classes. Although various scenarios have been suggested based on numerical and field-theoretical results,its critical properties are not yet clarified. Most recently, it has been reported that there is the long-term memory by solidary particles in the PCPD model as the main source of this new universality class, and also suggested that there is a possibility of continuously varying critical exponents depending on the memory strength. Moreover, it is found that the external driving is relevant to the PCPD while it is irrelevant to the models of the DP or the DI/PC class. In this study, we propose a DP-based cyclically coupled model, namely the contact process with power-law decay feedback (CPP) where we can directly control not only the memory strength but also its power-law tail exponent. We discuss how the long-term memory,caused by power-law type feedbacks, plays a crucial role in the continous varying critical behaviors of the CPP. By introducing the branching bias, we show thatthe external driving is relevant to the CPP, like the driven PCPD. Our numerical simulation results strongly support that the PCPD universality class should be distinct from the DP or the DI/PC class.

**F-04(초)** **Submicrometric surfaces and interfaces out of equilibrium** CUERNO Rodolfo(*Universidad Carlos III de Madrid.*) The recent widespread interest in processes occurring at micro and nanometric scales has increased the physical relevance of the surfaces and interfaces constituting system boundaries, both at and far from equilibrium. In the latter case, universal properties occur, such as scale invariance (surface kinetic roughening), surface pattern formation or domain coarsening. However, descriptions of these systems feature limited predictive power when based merely on universality principles. We will consider [1] examples from Materials Science at nano and submicrometric scales, that underlie the importance of describing growing surfaces by means of (phenomenological) constitutive laws, in order to correctly describe the rich behaviors experimentally found across many different systems. Additionally, this approach provides new generic models that are also of interest in the wider contexts of Pattern Formation and Non-Linear Science. One of these examples will be provided by non-conserved interface growth systems whose dynamics results from the interplay between diffusive matter transport and aggregation kinetics at the interface as, e.g., in thin film production by chemical vapor deposition and electrochemical deposition.
[1] R. Cuerno, M. Castro, J. Muoz-Garca, R. Gago, and L. Vzquez, Universal non-equilibrium phenomena at submicrometric surfaces and interfaces, Eur. Phys. J. Special Topics 146, 427441 (2007). [2] M. Nicoli, M. Castro, and R. Cuerno, Unified moving boundary model with fluctuations for unstable diffusive growth, submitted, Phys. Rev. E 78, 021601 (2008).

**F-05** **Unusual dynamic roughening of vapor-born polymer films** LEE InJae, YUN Mira(*Chonbuk National University, Department of Physics.*) The surface morphologies of poly(chloro-p-xylylene) films weremeasured using atomic force microscopy and

analyzed within the framework of the dynamic scaling theory. The evolution of polymer filmsgrown with fixed experimental parameters showed drastic changes ofdynamic roughening behavior, which involve unusually high growthexponent (beta = 0.65+- 0.03) in the initial growthregime, followed by a regime characterized by beta ~ 0, andfinally a crossover to beta = 0.18+- 0.02 in a steady growthregime. Detailed scaling analysis of the surface fluctuation inFourier space in terms of power spectral density revealed a gradualcrossover in the global roughness exponent, analogous to a phase-transition between two equilibrium states, from a morphology defined by alpha = 1.36+-0.13 to the other morphology characterized by alpha = 0.93+-0.04 as the film thickness increases. Our experimentalresults which significant deviate from the well established descriptionsof film growth clearly exhibit that the dynamic roughening of polymerfilm is deeply affected by strong molecular interactions andrelaxations of polymer chains. I will also discuss briefly unusual turbulent behavior of the interface of the polymer films.

F

■ SESSION: F [FG2]
10월 23일(목), 14:30 - 16:30
장 소: 202호

**F-06** **Dynamics and Directionality in Complex Networks** SON Seung-Woo, KIM Beom Jun[1], HONG Hyunsuk[2], JEONG Hawoong(*KAIST, Dept. Physics. [1]Sungkyunkwan Univ., Dept. Physics. [2]Chonbuk National Univ., Dept. Physics.*) We investigate how we can improve the synchronizability of complexnetworks simply by changing the link direction while conservingthe local linking cost and topology. Performing the linearstability analysis of synchronization and numerical simulation ofKuramoto model on the directed networks, we find that while randomassignment of link directions generally weakens the degree ofsynchronization, properly organized directionality can enhance thenetwork synchronization systematically. In this respect, wesuggest a simple method of changing link direction accordingly tothe larger residual degree starting from small residual degreenodes. This result provides the plausible applications to controlthe synchronizability of the system in various fields.

**F-07** **Dynamical Responses of the Quasiperiodically Forced Hodgkin-Huxley Neural Oscillator** LIM Woochang, KIM Sang-Yoon[1](*아주대학교, 물리학과. [1]강원대학교, 물리학과.*) We study dynamical responses of the quasiperiodically forced Hodgkin-Huxley (HH) neuron model. A self-sustained oscillation (corresponding to a spiking state) is induced in the HH model when the dc stimulus passes a threshold value. This HH oscillator is then quasiperiodically forced at two incommensurate frequencies. In the periodically forced case (i.e., in the presence of only one ac stimulus source), a transition from a periodic to a chaotic oscillation occurs through an infinite sequence of period-doubling bifurcations. Effect of the quasiperiodic forcing on this period-doubling route to chaos is particularly investigated by adding another independent ac stimulus source. Strange nonchaotic (SN) oscillations (that are geometrically strange but have no positive Lyapunov exponents) are thus found to exist between the regular and chaotic oscillations as intermediate states. Due to their high phase sensitivity, SN oscillating states have strange fractal geometry, leading to aperiodic "complex" spikings, as in the case of chaotic oscillations. Variousdynamical routes to SN oscillations are identified, and they are found to be the same as those in the quasiperiodically forced logistic map (which is a representative period-doubling system).

**F-08** **Segregation in reaction-diffusion kinetics on fractal scale-free networks** YUN Chang-Keun, KAHNG Byungnam, KIM Doochul(*Department of Physics and Astronomy, Seoul National University.*) For reaction-diffusion process A+B→0 with equal initial densities on regular lattices or fractal structure in Euclidean space, particle density decreases with time as $t^{-\alpha}$, where α is related to spectral dimension $d_s$, and is equal to or smaller than 1. However recent studies on random scale-free networks show that α is related to degree exponent gamma, and can be larger than 1. Here, we examine the temporal evolution of particle density on fractal scale-free networks, finding that the exponent α is equal to or smaller than 1 and related to the spectral dimension $d_s$ . This result comes from the fact that the fractal scale-free network contains local hubs, which are separated from each other. Thus, segregation effect governs the exponent α. To confirm this effect, we perform the reaction kinetics on complex networks with modules within them as well as rewired networks from the modular network, so that the modules are destroyed. We obtain that indeed the particle density decays slowly in the modular networks in comparison with that on the network without modules. Since many complex networks in real world contain modules within them, segregation effect has to be taken into account when we consider kinetic problems involving more than one species.

**F-09** **Community identification in directed networks** KIM Young-Do, SON Seung-Woo, JEONG Hawoong(*KAIST.*) In the past, the most common approach to community identification of directednetworks has been to ignore edge directions and apply methods developed for undirected networks. Recently, E. A. Leicht published a work on community identification of directed networks, which is a generalization of the widely used community finding technique of modularity maximization in undirected networks. However,our investigation of this method shows that this method combines two effects together to divide networks into communities. One effect is caused by the traditional modularity of undirected networks, and the other effect is to group nodes of larger out-degree (or larger in-degree) into the same community. It is doubtful that this approach is a proper method to exploit directional information. We propose an altanative definition of modularity which is applicable to directed networks.

**F-10** **Priority Queue Systems with Bursty Input/Output**

**Tasks** KIM, J.S., MASUDA, N.[1], KAHNG, B.(*CTP &FPRD, School of Physics and Astronomy, Seoul National University. [1]Graduate School of Information Science and Technology, The University of Tokyo.*) The priority queue systems have been intensively studied as a model of diverse complex systems with bursty dynamics. The authors previously introduced a priority queue model whose number of input tasks is given by a power law, based on the observation of massive digital records for human activities. In this talk, we present recent progress in such class of models, including the one with bursty execution of tasks. Also we discuss the relation between the queue model and the Bak-Sneppen model and Levy's flight random walk problem.

**F-11** **Power Spectrum of Packet Traffic Flow on Scale-free Networks** KIM kanghun, KAHNG byungnam, KIM Doochul(*서울대학교 물리학부.*) We study the dynamics of traffic flow on scale-free networks under dynamic routing and queuing protocols. Based on simulations, we find that near the jamming transition point, the power spectrum of packet traffic flow exhibits a crossover between two $1/f^{\alpha}$-type behaviors with exponent $\alpha = 1$ ($1 < \alpha < 2$) in low (high) frequency regime. This crossover is rooted from a characteristic waiting time of packets in the queue.

**F-12** **Analysis on the Movement of Oil Droplet Controlled by Thermo-Chemical Method** SONG Chaeyeon, KIM Kipom[1], LEE Kyuyong, PAK Hyuk Kyu(*Pusan National University, Physics department. [1]University of California, Santa Barbara, Department of Materials.*) Through the thermo-chemical control of a liquid droplet on a solid substrate, we investigated the motion of the droplet and the underlying mechanism. Depending on the contact angle of the running droplet on the substrate with a chemical gradient coating, we observed two different behaviors for the droplet under local laser heating: reversing for a contact angle larger than a critical value (~90°) and passing for a smaller value. The motion at the laser heating position was found to be closely related to the contact angle change, indicating that capillary flow plays an important role in the thermally-induced motion of the droplet.

**F-13** **High accuracy template based modeling by global optimization** JOO Keehyoung, LEE Jinwoo, LEE Sunjoong[1], SEO Joo-Hyun[2], LEE Sung Jong[3], LEE Jooyoung(*Korea Institute for Advanced Study, School of computational scineces. [1]Hanyang University, Department of Physics. [2]Seoul National University, School of Chemical and Biological Engineering. [3]University of Suwon, Department of Physics.*) For high-accuracy template-based-modeling of CASP7 targets, we have applied a procedure based on the rigorous optimization of score functions at three stages: multiple alignment, chain building, and side-chain modeling. We applied the conformational space annealing method to a newly developed consistency based score function for multiple alignment. For chain building, we optimized the MODELLER energy function. For side chain modeling, we optimized a SCWRL-like energy function using a rotamer library constructed specifically for a given target sequence. By rigorous optimization, we have achieved significant improvement in backbone as well as side-chain modeling for TBM and TBM/HA targets. For most TBM/HA targets (17/26), the predicted model was more accurate than the model one can construct from the best template in a posteriori fashion. It appears that the current method can extract relevant information out of multiple templates.

■ SESSION: F [FG3]
10월 24일(금), 09:00 - 10:45
장 소: 202호

F

**F-14** **Diffusion of Adsorbed Polymer on Corrugated Surface** JEON Chanil, JEONG Hawoong, JUNG Youngkyun[1] (*KAIST, 물리학과. [1]KISTI, 슈퍼컴퓨팅센터.*) We study the dynamics of the flexible polymer adsorbed on two dimensional solid surface using Molecular Dynamics simulation. In particular, we focus on the effect of the corrugation of the surface on the dynamical behavior of the adsorbed polymer. Recently, T. G. Desai *et al.* studied the adsorbed polymer with analytically smooth surface and found that the diffusion coefficient scales as $D \sim N^{-3/4}$, where $N$ is the degree of the polymerization [Phys. Rev. Lett. 98, 218301 (2007)]. Contrary to their results with analytically smooth surface, we observe that the polymer diffusing on the real atomic surface shows more weak scaling $D \sim N^{-1}$. We compare our results with some recent experiments.

**F-15** **Polymer Translocation in Crowded Environments** KIM Yong Woon, GOPINATHAN Ajay[1](*School of Physics, KIAS. [1]School of Natural Sciences, University of California at Merced.*) We study the effect of the crowded environmets on the translocation of a polymer through a pore in amembrane. By systematically treating the entropic penalty due tocrowding, we show that the translocation dynamics aresignificantly altered, leading to novel scaling behaviors of thetranslocation time in terms of chain length. We also observe newand qualitatively different translocation regimes depending uponthe extent of crowding, transmembrane chemical potentialasymmetry, and polymer length.

**F-16** **Incorporation of Quantum Dots into the Lipid Membrane of Giant Unilamellar Vesicles and Theoretical Consideration of its Stability** 이 규용, 위 행섭, 양 호순, 박 혁규 (*부산대학교, 물리학과.*) We prepare QD-Liposome Complexes (QLCs), which are the giant unilamellar vesicles (GUVs) with quantum dots (QDs) incorporated in the membrane bilayer. We use asolectin lipids, single phosphatydilcholine (PC) lipid and trioctylphosphine oxide(TOPO)-coated CdSe QDs with the core size ranging 3-6 nm. Spin coating method in conjunction with electroformation technique yields vesicles with highly homogeneous unilamellar structure of the size up to 200 microns. In addition, we make a model for the QD size effect on QLC formation in terms of molecular packing parameter without any free energy calculations.

As a result, this model predicts that TOPO-coated QDs below a certain critical size (~4 nm) can stably reside in the membrane of 4~5 nm in thickness, which is well consistent with the present experimental results.

**F-17** **Computability of entropy and information in classical Hamiltonian systems** KIM Sungyun(*아태 이론물리센터.*) We consider computability of entropy and information in classical Hamiltonian systems. We define information and information capacity in classical Hamiltonian systems through relative entropy with respect to the reference probability distribution and probability measure. Using recursively enumerable nonrecursive sets, it is shown that even though the initial information and the Hamiltonian are computable the time evolution of information and information capacity may not be computable.

**F-18** **slip velocity and velocity inversion in cylindrical Couette flow** KIM Sangrak(*Kyonggi University.*) The relation between slip velocity and velocity inversion in cylindrical Couette flow is investigated by using Navier-Stokes equation coupled with MD simulation. With the simulated slip velocities we can explain the behavior of velocity inversion in cylindrical Couette flow.

**F-19(초)** **Ergodicity and Chaos in a system of harmonic oscillators** LEE M Howard(*University of Georgia and KIAS.*) A system of two independent harmonic oscillators with incommensurate frequencies (the ratio of the two frequencies is an irrational number) is known to exhibit chaotic behavior. That is, their trajectories on the phase space are not closed. Thus after a very long time, they may possibly fill the surface of the phase space densely. Many have regarded such a possibility as a sign of ergodicity. It is in fact what Boltzmann conjectured for being ergodic. We prove that for systems of finite degrees of freedom (two oscillators included), the time and ensemble averages are not equal. Therefore these systems may be chaotic but not necessarily ergodic. The denseness of the phase space in trajectories is only a necessary condition for ergodicity much as irreversibility is [1]. In addition we show that a system of infinitely many oscillators can be ergodic provided that the frequencies are still incommensurate. This proof is by the ergodicity condition given in [2].
1. M H Lee, Phys Rev Lett 98, 190601 (2007) "Why irreversibility is not a sufficient condition for ergodicity."2. M H Lee, Phys Rev Lett 87, 250601 (2001) "Ergodic theorem, infiniteproducts and long time behavior in Hermitian models"

■ SESSION: K [KI1]
10월 22일(수), 14:00 - 16:00
장 소: 402호

**KI-01** **Next Generation Solar Cell due to Nitride Semiconductors** MATSUOKA Takashi*, USAM Noritaka[1], YAMAMOTO Akio[2](*Institute for Materials Research, Tohoku University 2-1-1 Katahira, Aoba-ku, Sendai, Miyagi 980-8577, Japan, CREST, Japan Science and Technology Agency. [1]Institute for Materials Research, Tohoku University, 2-1-1 Katahira, Aoba-ku, Sendai, Miyagi 980-8577, Japan. [2]Dept. of Electrical and Electronics Eng., Graduate School of Engineering, University of Fukui, 3-9-1 Bunkyo, Fukui 910-8507, Japan.*)
The environment-friendly energy is indispensable for to establish the sustainable society. For this purpose, it is natural to use the solar energy coming from the outside of the earth. Solar cells converting the solar energy to the electrical one have been studied by using silicon. It is expected to generate much more electrical energy and the multi-junction cells are promising. The state-the-art of the maximum conversion efficiency has been realized 46% by using four junctions. This cell is constructed with a few kinds of semiconductors because usual semiconductors can not cover all the spectrum range of the sun light. Nitride semiconductor InGaAlN can cover from the infra-red to ultra-violet. The solar cell, which consists of a Si junction sandwiched with two junctions of InGaN and InN with a bandgap of 1.4eV and 0.7 eV, respectively, has been simulated to have an efficiency of 36%. In the presentation, the aspects of solar cell studies in the world will be shown and the problems in the fabrication of nitride solar cells are discussed.

**KI-02** **Structural and optical properties of asymmetrically coupled GaN/$Al_xGa_{1-x}N$/GaN bounded by $Al_xGa_{1-x}N$ multi-quantum wells grown by molecular beam epitaxy** PARK Young S. (*Quantum Functional Semiconductor Research Center, Dongguk University, Seoul 100-715, Korea.*) In biaxially strained III-nitride heterostructures grown in the wurtzite structure with the *c*-axis parallel to the growth direction, giant piezoelectric and spontaneous polarization effects are expected to be present as a consequence of the non-centrosymmetry of the wurtzite structure. Actually, for fully strained GaN on AlN piezoelectric fields as high as several MV/cm are expected. These values are more than an order of magnitude larger than the piezoelectric fields that can be found in zinc blende semiconductors for the same amount of strain. If spontaneous polarization effects are present and are as large as predicted, then a new degree of freedom in engineering the electric fields within a structure can be envisaged. The samples were grown on a (0001) sapphire substrate by molecular beam epitaxy (MBE) using radio frequency activated nitrogen radicals. CMQW structures used here consist of 50 sets of unintentionally doped GaN(10 Å)/$Al_xGa_{1-x}N$(x Å)/GaN (20 Å) bounded by 100 Å layer thickness of $Al_xGa_{1-x}N$ barriers. In order to systematically study the effect of the inserted layer on PL spectra, a serious of the samples were grown, changing the thickness ($T_{ib}$) of the inserted layer from 0 to 32 Å. In order to evaluate the crystal quality of the samples rocking curve measurements for GaN (00×2) plane were carried out. The full width at half maximum (FWHM) of the GaN buffer layer was approximately 30 arcsec. The $\omega/2\theta$ scans around GaN (00×2) reflection for the samples were employed. These scans clearly showed high order satellite diffraction peaks up to m = -4, indicating a good layer periodicity. Due to the highly-organized structure, the peak positions for the satellite peaks as well as the GaN buffer (or substrate) layer are clearly resolved. To better understand the overall strain state of the SL with respect to the GaN layer, reciprocal space maps (RSM) were obtained for the asymmetric (10×5) reflection of the GaN layer and the SL. The spread of diffraction intensity is related to the orientation distribution and decrease in the coherency of the scattering along the structure. More detailed optical properties will be discussed later.

**KI-03** **Electronic structure of ZnO-based oxide semiconductors** LEE Woo-Jin, CHOI Eun-Ae, BANG Junhyuk, RYU Byungki, CHANG Kee Joo(*Department of Physics,Korea Advanced Institute of Science and Technology, Daejeon 305-701, Korea.*)
The homologous oxides $LnMO_3(ZnO)_m$ (Ln = In, Lu, Yb, or Tm, M = Al, Ga, In, or Fe, and m = integer) are composed of an alternating stack of a $LnO_2$ layer and a $MO(ZnO)_m$ block. Due to the spatial confinement of electrons in the 2-dimensional layer, the layered structure is regarded as a natural superlattice which exhibits the quantum effect in the electronic properties. Among the homologous series, $In_2O_3(ZnO)_m$ and $InGaO_3(ZnO)_m$ have attracted much attention because of potential applications for transparent conducting oxides and optoelectronic devices. For practical applications, it is important to study the electronic structure of these materials. In this work we report the results of first-principles density functional calculations for the atomic and electronic properties of $InGaO_3(ZnO)_m$. We investigate the stability and electronic structure of various structures for the distribution of the Ga atoms. We find that hole carriers are spatially confined to specific regions of the ZnO layers whereas no clear confinement occurs for electron carriers. We discuss the effects of hole confinement and increasing ZnO layers on the band gap.

**KI-04** **Giving a new direction to ZnO** YAO Takafumi (*Center for Interdisciplinary Research, Tohoku University, Aramaki-Aoba, Aoba-Ku, Sendai, Japan 980-8078.*) ZnO possess various attracting properties in terms of device applications. Wide bandgap, large exciton binding energy, high saturation velocity of electron, piezoelectricity, spontaneous polarization, almost the same lattice constants as GaN, just name a few. Research efforts on ZnO are mainly directed to the applications to light-emitting devices, TFTs, TCOs, and sensors. Some of those researches have succeeded, while the rest need more investigation. I would like to introduce our two projects which include the application of ZnO to nonlinear optical devices based on excitonic processes and the growth of GaN thick layers on ZnO templates by suppressing diffusion at the GaN/ZnO interface. Such efforts may help broaden the horizon of ZnO research.

■ SESSION: K [KI2]
10월 22일(수), 16:20 - 18:20
장 소: 402호

**KI-05** **Acceptor Level due to Carbon in (1-101)GaN** SAWAKI Nobuhiko(*NAGOYA UNIVERSITY, Department of Electronics and Akasaki Research Center, Furo-cho 3C-1, Chikusa-ku, Nagoya 464-8603, JAPAN.*) In the improvement of LD's made of III-nitrides, low resistive or highly doped p-type conduction in these materials is one of the important issues. Various elements as the dopant have been studied so far, and the p-type conduction has been available by Mg doping followed by EB or heat treatment. The role of carbon has been studied in (0001)GaN and it has been shown that C creates deep levels to make the material semi-insulating. In this study, the p-type doping in a (1-101)GaN grown by selective MOVPE on a patterned (001)Si substrate is investigated. It is found that Mg doping shows weak self-compensation effects and C creates a shallow acceptor level. The phenomena are explained by the efficient activation of the Mg and the efficient replacement of N with C, respectively, at the top most surface of the (1-101)GaN during the growth.

**KI-06** **Energy relaxation dynamics of high density electron-hole plasma in GaN** KYHM K.*, YI K. S.[1], KIM J. S.[2] (*Dept. of Physics Education, Research Center for Dielectric Material and Advanced Matter Physics, Pusan National University, Pusan 609-735, Korea. [1]Dept. of Physics, Research Center for Dielectric Material and Advanced Matter Physics, Pusan National University, Pusan 609-735, Korea. [2]Research Center for Dielectric Material and Advanced Matter Physics, Pusan National University, Pusan 609-735, Korea.*) Hot carrier dynamics is useful to provide fundamental understanding for light emitting device operation and failure of the initial device's fast-response. Although energy relaxation is interpreted in terms of various carrier-phonon interactions, correction of the many-body effect is demanding as the density increases. In particular beyond the critical high density, so-called exciton-Mott density, collective behaviour of electron-hole plasma (EHP) requires to include screening in the phonon interactions. In this work, the energy loss rates of EHP are obtained numerically by following the approach of Pugnet *et al*. with a use of the Kogan formula extended to degenerate electron-hole plasma [1, 2]. Various carrier-phonon interactions are taken into account such as acoustic deformation-potential, piezoelectrical couplings, and the couplings to polar and nonpolar optical phonons by employing interaction-specific screened electron-phonon matrix elements. The screening of the electron-phonon interactions is included within the random phase approximation, in which the carriers are assumed to respond as independent particles to the total electrostatic potential. This model was compared with experimental data for high carrier density (~ $10^{19}$ $cm^{-3}$), where the relaxation of the average carrier energy was measured by the transient absorption spectrum.

* References [1] S.H. Kogan, Fiz. Tverd. Tela (Leningrad) 4, 2474 (1963). [Sov. Phys.--Solid State 4, 1813 (1963)] [2] M. Pugnet, J. Collet, and A. Cornet, Solid State Commun. 38, 531 (1981).

**KI-07** **Present status of electron and hole properties of InN** ISHITANI Y., FUJIWARA M.[1], WANG X.[1], CHE S.B., YOSHIKAWA A.(*Graduate school of Electronics and Electrical Engineering, Chiba University, Japan, Venture business Laboratory, Chiba University, Japan. [1]Graduate school of Electronics and Electrical Engineering, Chiba University, Japan.*) Recently the crystal quality of InN is being improved. Now the residual electron density has reduced to the order of $10^{17}cm^{-3}$. The experimental Hall electron mobility is about 3000 $cm^2/Vs$ or less. The effects of threading dislocations and point defects are not clarified. Further the hole properties also remain unclear even though the p-InN has been recently achieved. However there is a barrier in the analysis of carrier transport properties: high density electron accumulation around the surface or interface. We have overcome this barrier by infrared spectroscopy and characterized the electron and hole properties outside the accumulation layers. InN layers with the thickness up to 5μm were gown on GaN layers on (0001) $\alpha$-$Al_2O_3$ or GaN substrates. Measurements were conducted at room temperature by infrared reflectance and spectroscopic ellipsometry. We obtained the carrier mobilities by taking the plasmon energy broadening as lifetime broadening. The LO phonon – plasmon coupling states were observed in infrared spectra. It was found that surface electron accumulation shows the negligible effect on the spectra, while the electrons accumulated around the interface between a substrate modulate the spectra. Thus we extracted the carrier properties outside the accumulation layers. Figure 1 shows optical electron mobility $\mu^{opt}_{\perp}$, for the plasmon vibration vertical to the c-axis, which nearly reaches to 5000 $cm^2/Vs$. The analysis on anisotropy in plasmon damping reveals the large effect of threading dislocations or columnar grain boundaries on electron mobility. Figure 2 shows the Mg density dependence of the carrier density and mobility. Just in the region (II) where net acceptors were found by electrolyte capacitance-voltage measurements, the low mobility for holes is found. The hole density up to $10^{19}$ $cm^{-3}$ and mobility of 25 – 70 $cm^2/Vs$ were observed.

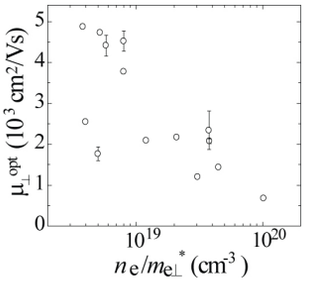


Fig.1. Optical electron mobility $\mu_{\perp}^{opt}$.

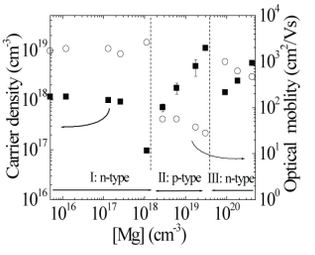


Fig.2. Dependence of carrier density and optical mobility on [Mg].

**KI-08** **The Way to the Growth of High Quality InN** KIMURA Takeshi, LIU Yuhuai, SHIMADA Taka-aki[1], HIRATA Masaki[1], WAKABA Masaki[1], NAKAO Masashi[2], JI Shi-Yang[1], MATSUOKA Takashi*(*Institute for Materials Research, Tohoku University, 2-1-1 Katahira, Aoba-ku, Sendai, Miyagi 980-8577, Japan, CREST, Japan Science and Technology Agency. [1]Institute for Materials*

*Research, Tohoku University, 2-1-1 Katahira, Aoba-ku, Sendai, Miyagi 980-8577, Japan. [2]Future ICT Research Center, National Institute of Information and Communications Technology, 588-2 Iwaoka, Nishi-Ku, Kobe, 651-2492, Japan, CREST, Japan Science and Technology Agency.*) The MOVPE growth of InN by a horizontal reactor is compared with that by a vertical reactor. The phase diagram does not almost depend on the reactor structure, but rather the parameters such as V/III ratio and the growth temperature. The growth rate of InN in the horizontal reactor significantly increases in comparison with the vertical reactor due to the reduction of the stagnant layer thickness, the increases in the source supply to the substrate surface and the high concentration of source gases by narrowing the flow channel. For the horizontal reactor, the polycrystalline phase appeared in the case of the low carrier-gas flow-rate and disappeared for the high carrier-gas flow-rate. These data suggest that increasing the carrier gas flow rate can suppress the gas phase reactions. In the case of the horizontal reactor, InN can be obtained at temperatures as high as 625ºC, compared with the maximum growth temperature of 575ºC in the vertical reactor. But the growth rates significantly decrease above 600ºC due to the decomposition of the InN. The above results are of great importance to pave the way to the growth of high quality InN with MOVPE.

■ SESSION: K [KI3]
10월 23일(목), 09:00 - 10:30
장 소: 402호

**KI-09** **Fabrication of InGaN-based light-emitting diodes with nano-particle embedded p-type electrodes** KWAK Joon Seop(*Department of Materials Science and Engineering, Sunchon National University, Sunchon, Jeonnam 540-742, Korea.*) GaN and related compounds are receiving great attention as optoelectronic devices such as light emitting diodes (LEDs). Achievement of high luminous intensity by flip-chip LEDs (FCLEDs) with Ag reflector or using top emitting LEDs (TELEDs) with highly transparent ITO contacts is required to improve the external quantum efficiency (EQE) and light output of LED. However, since the work function of Ag and ITO is lower than 5.0 eV, it is difficult to produce low-resistance p-type electrode with Ag or ITO only. In this study, in order to develop ohmic contact materials having low contact resistance and high transmittance, nano-particle embedded p-type electrodes for FCLEDs or TELEDs were suggested. In order to elucidate the mechanism for forming a low resistance ohmic contact by the nano-particle structured ohmic contact materials, we proposed the carrier transport model in which the carriers flow from the metal directly to the dense deep level defect band, and also suggested that a formation of inhomogeneous Schottky barriers at the p-GaN/Ag reflector or p-GaN/ITO interface due to the breaking-up of the ohmic contact materials may increase current flow, followed by further reduction of contact resistance.

**KI-10** **Formation of AlN Film by Sapphire Nitridation and Its Polarity Determination** FUKUYAMA Hiroyuki(*Institute of Multidisciplinary Research for Advanced Materials (IMRAM), Tohoku University.*) Aluminum nitride (AlN) is an ideal candidate as a substrate material for AlGaN-based nitride semiconductor devices for the deep-UV LED and LD from the viewpoints of lattice mismatch and transparency to UV light. High-quality single crystalline AlN films have been fabricated by nitriding sapphire by $N_2$-CO gas mixtures with a precise control of driving force of the nitridation reaction based on the phase stability diagram of the AlN-$Al_2O_3$-C-$N_2$-CO system at elevated temperatures. $Al_2O_3(s) + 3C(s) + N_2(g) = 2AlN(s) + 3CO(g)$. This process provides the <0001>-axis oriented AlN film as large as 2 inch in diameter on both (0001) and (11-20) planes of sapphire substrate. However, details of the nitridation and its polarity have not been clearly understood yet. In the present study, the reaction mechanism of the nitridation method is discussed. A kinetic model for describing the nitridation process is presented. In addition, polarity of the AlN film is studied by convergent-beam electron diffraction (CBED).

**KI-11** **Reduction of Leakage current and current dispersion in AlGaN/GaN HFET** LEE Jung-Hee(*School of Electrical Engineering &Computer Science, Kyungpook National University,Republic of Korea.*) We proposed two different methods for reduction of leakage current and current dispersion in AlGaN/GaN HFET. The first is introducing a novel Si delta-doped layer/p-GaN back barrier instead of conventional semi-insulating GaN buffer layer. The p-GaN back barrier is very effective in blocking the current flow through isolation layer below the channel layer. Also, Si delta doping makes the reduction of the current dispersion by changing charge distribution. Second is employing a $Ar^+$ implanted device isolation instead of MESA isolation. This planar type device, which exhibited no degradation in 2DEG mobility and carrier concentration, eliminates the sidewall leakage current and surface damage caused by plasma etching to define mesa in the fabrication of conventional AlGaN/GaN HFET and hence greatly reduces the buffer (between device and device) and gate leakage currents and considerably improves the electrical characteristics such as high drain current density and high transconductance. In addition, the $Ar^+$ implanted AlGaN/GaN HFET exhibits low current dispersion which is believed to be due to inactivating the surface outside of the active area and hence reducing the leakage current between pad metals.

■ SESSION: K [KI4]
10월 23일(목), 10:45 - 12:15
장 소: 402호

**KI-12** **Epitaxial Growth of GaN-on-Si LED** BAEK J. H., KIM Gang Ho, LEE Seung-Jae(*LED Device Team, Korea Photonics Technology Institute, Gwangju 500-460, Korea.*) Silicon substrate is cost-effective, scalable in size and has well-characterized electrical

and thermal properties. In addition, GaN-on-Si techniques are very promising in OEICs and micro-electro-mechanical systems (MEMSs) based on mature Si technologies. Despite these advantages, silicon has not been widely used as a substrate material for GaN growth owing to several problems. This talk deals with recent technical approaches on GaN-on Si LED at KOPTI. Crack-free GaN epitaxial device structures emitting at 460 nm were grown on the plateau of patterned Si(111) substrates by metalorganic chemical vapor deposition. The light-emitting diodes were fabricated through a wafer bonding process with Si receptor wafers having a high reflective metal reflector. The characteristic performances of the wafer bonded LEDs showed 8.3mW at 20mA with forward voltage of as low as 3.1V.



**KI-13** **Recent progress in the growth of GaN single crystals using the Na flux method** KAWAMURA Fumio*, KATSUIKE Satoshi, HIRABAYASHI Yasuhiro, KITANO Yoshihiro, IMADE Mamoru, YOSHIMURA Masashi, KITAOKA Yasuo, MORI Yusuke, SASAKI Takatomo (*Division of Electrical, Electronic and Information Engineering, Graduate school of Engineering, Osaka University, 565-0871 Yamadaoka 2-1, Suita, Osaka, Japan.*) We applied the LPE (liquid phase epitaxy) to the Na flux method for achieving an enlargement of crystal size. Although large crystals could be grown by LPE, low growth rate has been pointed out as one of disadvantageous for industrial use. Generation of poly-crystals on the crucible is the reason for the low growth rate, because those preferentially consume the nitrogen dissolved in the solution rather than LPE. We tried some attempts to solve this problem and found that "Applying the thermal convection" and "Addition of carbon" can suppress the generation of poly-crystals and can increase the growth rate.

**KI-14** **GaN on Patterned $N^+$ Ion Implanted Si** BYUN Dongjin(*Department of Material Science and Engineering, Korea University.*) Epitaxial lateral overgrowth (ELO) and selective area growth (SAG) of GaN on the ion implanted (111) Si substrates with stripe patterns were attained using metal organic chemical vapor deposition. The Si substrates were irradiated by 37.5 KeV $N^+$ ions at different doses. The periodic patterns of 4㎛ width stripes of nitrogen ions with a periodicity of 12㎛ were featured on the (111) Si substrate parallel or perpendicular to the [1-10]. GaN were grown on the prepared substrate using AlN as a buffer layer, then the ELO GaN and SAG GaN were obtained according to the direction of the patterns. The epitaxial grown GaN and the $N^+$ implanted substrate were characterized. The ion implantation at high dose rate (more than $1x10^{17}$ $cm^{-2}$) creates 100-nm-thick subsurface damage in Si substrate as shown in Fig. 1(b). On the damaged region, MOCVD-grown GaN/AlN films are polycrystalline which acted as self-mask with no increase in thickness during the ELO and SAG of GaN. For the ELO process, complete coalescence is achieved after around 3-um of growth in the (0001) direction [Fig. 2 (b)]. Reduced dislocation density of the ELO GaN is evidenced by TEM and cathodoluminescence microscopy.

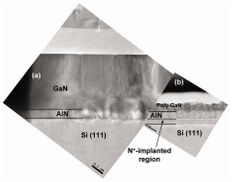


Fig. 1. Cross-sectional TEM images perpendicular to the <1-100>$_{GaN}$ direction of the GaN layers grown on (a) AlN/ bare-Si (111) and (b) AlN/$N^+$- implanted-Si (111)

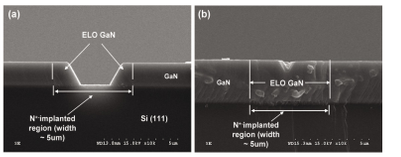


Fig. 2. Cross-sectional SEM images perpendicular to the <1-100>$_{GaN}$ direction of the ELO GaN structures with duration of (a) 30 min and (b) 80 min

■ SESSION: K [KG1]
10월 23일(목), 16:30 - 18:30
장 소: 402호

**K-01(초)** **Characterization of InGaN Quantum Dots Grown on Nano-sized Anodized Aluminum Oxide Pattern** DO Hyung-A, PARK Joonmo, MOON Se-Hoon, RYU Sang-Wan (*Department of Physics, Chonnam National University.*) InGaN quantum dot (QD) is very interesting structure for green and yellow emission from GaN based light emitting devices. However, conventional Stranski-Krastanov growth was not successful to grow high density and small-sized GaN based QDs. In this study, we have fabricated InGaN QD based on nano-patterns and its optical characteristics were measured. For the nano-pattern, 1 μm thick aluminum was deposited on $SiO_2$/GaN/sapphire substrate and was anodized to form hexagonal nano pores. The size of nano pores was around 80 nm and its periodicity was 120 nm. The nano-pattern was transferred to $SiO_2$ layer by reactive ion etching. The sample was used to grow GaN/InGaN/GaN quantum dot/barrier structure in the pores. With the temperature over 970°C, the growth occurred only inside the pores and QD was fabricated. A pyramidal shape growth was observed and, with the control of dot/barrier thickness, the QD shape and location could be optimized. Because the QD is apart from the regrown interface, the QD showed high luminescence intensity and narrow spectral width.

**K-02(초)** **Electrical and structural properties of high-k Er-silicate gate dielectric formed by interfacial reaction between Er and $SiO_2$ films** CHOI Chel-Jong*, JANG Moon-Gyu[1], KIM Yark-Yeon[1], JUN Myung-Sim[1], KIM Jin-Gyu[2](*Department of Semiconductor Science &Technology, Chonbuk National University, Jeonju 561-756, Korea. [1]IT Convergence Technology Research Division, Electronics and Telecommunications Research Institute (ETRI), Daejon 305-700, Korea. [2]Division of Electron Microscopic Research, Korea Basic Science Institute (KBSI), Daejeon 305-333, Korea.*) We investigate the electrical and structural properties of high-k Er-silicate film formed by the interfacial reaction between Er and $SiO_2$ films. The increase in rapid thermal annealing (RTA) temperature leads to the reduction of the interface trap density ($D_{it}$) by one order of magnitude, indicating the improvement in the interface quality of Er-sili-

cate gate dielectric. The increased capacitance value of Er-silicate gate dielectric with thermal treatment is attributed in part to the reduction of $SiO_2$ thickness and to the increase in the relative dielectric constant of Er-silicate film caused by the chemical bonding change from Si-rich to Er-rich silicate. The *in-situ* heating high-voltage electron microscopy (HVEM) operated at 1.25 MeV reveals that the thermally driven Er diffusion through Er-silicate film is responsible for the further reaction with the remained $SiO_2$ film, resulting in the thickness evolution of Er-silicate film. The effective work function ($F_{m,eff}$) of Er metal gate, extracted from the relations of equivalent oxide thickness (EOT) versus flat-band voltage ($V_{FB}$), is calculated to be ~ 2.86 eV.

**K-03** **Radiative Carrier Lifetime of GaAs Quantum Nanostructures** 김 종수, 강 훈수, 변 지수, 정 문석, 조 남기[1], 박 성준[1], 송 진동[1], 최 원준[1], 이 정일[1], 김 준오[2], 이 상준[2], 노 삼규[2], 김 진수[3], 임 재영[4], 김 인수[5](*광주과학기술원 고등광기술연구소. [1]한국과학기술연구원 나노소자연구센타. [2]한국표준과학연구원 첨단산업측정그룹. [3]전북대학교. [4]인제대학교 나노공학부. [5]경운대학교.*) In the present work, using the nature of Ga migration on the GaAs surface, we fabricated GaAs QDs and coupled quantum ring (CQR) structures. The structural and optical properties of GaAs quantum nanostructures (QNSs) were investigated by atomic force microscopy (AFM), photoluminescence (PL), and time-resolved PL. For investigation of the optical properties, the samples were excited by a pulsed laser with a wavelength of 400 nm and pulse duration of 120 fs.The GaAs QNSs were grown by molecular beam epitaxy on a GaAs substrate. A 300 nm thick GaAs buffer layer and a 100 nm thick AlGaAs barrier were grown at the substrate temperature (Ts) of 580 °C. The total amount of Ga was 3.75 ~ 5 monolayers (ML) deposited on the AlGaAs layer with the Ga flux of $3.7\times10^{-7}$ Torr without arsenic supply. For crystallization of the Ga droplets to GaAs QNSs, arsenic was introduced at Ts of 200 °C. To manipulate the shape of the GaAs QNSs, the arsenic flux was controlled from ~$10^{-7}$ to ~$10^{-5}$ Torr. After the crystallization and subsequent thermal process at Ts of 420 °C, a 50 nm thick AlGaAs layer capped the GaAs QNSs. Finally, a 10 nm thick GaAs layer was deposited at Ts of 580 °C as a capping layer.To investigate radiative carrier lifetime (τ) of GaAs QNSs with different shapes and densities, we chose three kinds of GaAs QNSs such as low density GaAs QDs, single QRs, and coupled double QRs. The GaAs QDs showed monotonic increment of τ with increasing emission wavelength while the QRs have small changes of τ in wide emission wavelength range. In particular, in the case of double QRs, we observed double exponential PL decay characteristics at the emission wavelength from 680 to 720 nm with slow and fast decays. When the emission wavelength over 720 nm, we observed the single exponential PL decay with a small change of τ with increasing the emission wavelength. In addition, τ for the high-density QD sample showed the strong increment with the QDs size and quenching behavior, while τ for the low-density QD sample slowly increases with increasing the QDs size.

**K-04** **Ultraviolet-blue emission from crystalline Si/silica core/shell nanowires grown from Si-rich oxides using a Ni catalyst** 김 성, 황 성원, 김 혜룡, 최 석호, 김 태현[1], ELLIMAN R. G.[1](*경희대 국제캠퍼스 응용물리 전공. [1]호주국립대학교 전자재료공학과.*) Crystalline Si/silica core/shell nanowires (NWs) are produced by annealing Ni-coated Si-rich $SiO_x$ (SRO) films at 1100 °C under a $N_2$ ambient. The SRO films of 100 nm were deposited on p-type (100) Si wafers by PECVD under varying conditions of silicon concentration ($n_{Si}$), and a Ni film of 10 nm was coated on top of the SRO films by rf sputtering. The diameter of individual NWs is relatively constant along their length although some of them exhibit kinks and twists, as confirmed by SEM and high-resolution TEM (HRTEM). The average diameter of NWs increases from 48 to 157 nm as $n_{Si}$ increases from 37 to 43 at. %. The NWs with $n_{Si}$ = 37 at. % are amorphous $SiO_x$ (silica), as analyzed by HRTEM and XPS. In contrast, the NWs with $n_{Si}$ = 43 at. % show clear HRTEM images of core/shell structures. Electron energy loss spectroscopy analysis also confirms the core/shell structures. The room temperature photoluminescence (PL) spectra of the NWs have two major emission bands in the near UV (381 nm) and blue (435 nm) ranges at $n_{Si}$ = 43 at. %, whilst at $n_{Si}$ = 37 at. %, only a blue band is observed. These results suggest that the UV PL bands are closely correlated with the core/shell structures of the NWs. The PL intensity of the NWs with $n_{Si}$ = 43 at. % is more than 30 times enhanced by 6 h irradiation, especially above ~ 380 nm. In contrast, free-standing NWs show no such irradiation-time behaviours, indicating the light-induced PL enhancement possibly results from the oxygen-related defect states at the $SiO_x$/Si wafer interface.

**K-05** **The Effect of Isoelectronic C Impurities on B Diffusion in Si** 좌 상훈, 방 준혁, 장 기주(*Department of Physics, KAIST.*) Carbon incorporation into Si has been thought to be a solution to the transient enhanced diffusion (TED) of B dopants in the process of thermal annealing. There have been several theoretical and experimental attempts to explain the suppression of B diffusion in the presence of C. It is believed that Si self-interstitials, which play an important role in B diffusion, are trapped by the C atoms. However, it is still not clearly understood how the B dopants interact with the C impurities and what are the diffusion pathways of B. In this work, we investigate the atomic structure and the electronic properties of complexes consisting of the C, B, and Si self-interstitial and the diffusion pathways of B in C-doped Si using first-principles calculations. We consider various configurations for a C-B complex, and find that a <100> split-interstitial is the most stable complex. Our calculations show that it costs a very high energy of about 3 eV for the B atom to diffuse from the stable C-B complex, indicating that the B dopant is indeed trapped in the neighborhood of the C atom.

**K-06** **Electronic Structure of Oxygen Vacancy in Amorphous $HfSiO_4$** CHANG Kee Joo, NOH Hyeon-Kyun, RYU Byungki(*Department of Physics, KAIST.*) We perform first-principles theoretical calculations to study the atomic and electronic prop-

erties of amorphous $HfSiO_4$. We use molecular dynamics simulations to generate the amorphous phase of $HfSiO_4$, and find that the average coordination numbers of the Si, O, and Hf atoms are 4.02, 2.66, and 6.25, respectively. The density of amorphous $HfSiO_4$ is estimated to be smaller by 7-9 % than the crystalline phase. The pair-correlation function shows that the Si-O and Hf-O bonds have the bond lengths of 1.66 and 2.14 Å, respectively. We also examine the defect properties of an O-vacancy and discuss the degradation mechanism in metal-oxide-semiconductor (MOS) devices. In the amorphous phase, various O-vacancies exist, with different numbers of the Hf and Si atoms in the neighborhood. It is suggested that O-vacancies with only the Hf atoms in the neighborhood cause the threshold voltage shift and the transient charging effect in $HfSiO_4$.



**K-07** **Effect of laser spike annealing on the electrical and optical properties of ultrathin hafnium oxide high-k dielectric stacks**
PARK Joon Won, CHUNG Heayang, LIM Daeyung, KIM Dong Hak, CHANG You Min[1](*kyunghee university department of physics. [1]FST corp. R&D center.*) We performed a systematic study on the effect of laser spike annealing (LSA) on the electrical and optical properties of ultrathin hafnium oxide high-k dielectric stacks. Equivalent oxide thickness (EOT) extracted from C-V measurements decreased for dielectric stacks annealed at low laser powers. However with increasing laser power, EOT re-increased, likely due to $SiO_2$ interfacial layer growth. C-V curves of LSA high-k dielectric stacks showed less positive fixed charge as compared to rapid thermal annealed one. On the other hand, C-V hysteresis revealed enhanced charge trapping/detrapping behavior for all the LSA high-k dielectric stacks. Photoluminescence measurements showed a similar trend, displaying enhanced defect luminescence from LSA dielectric stacks. Charge trapping defects seem to be created during rapid heating and/or cooling processes of LSA. We performed post-LSA, low thermal budget anneals in various gas ambient, but they don't seem to effectively quench or passivate the LSA created defects.

**K-08** **Optical Switching based on Carbon Nanotube**
임 한얼, 유 제황, 손 병택, 임 준원, S. Manivannan, 장 진, 박 규창, 김 응범[1], 신 철우[1], 윤 정기[1](*경희대학교 정보디스플레이학과 차세대디스플레이연구센터. [1]DRTECH.*) 탄소나노튜브(CNTs)의 다양한 형태와 우수한 물리적 특성은 낮은 임계전계에서도 높은 전자방출을 가능하게 하므로 Field emission display (FEDs)나 X-ray electron source와 같은 전자방출 소자로서의 연구개발이 현재 활발히 진행되고 있다. 본 연구에서는 탄소나노튜브와 비정질 셀레늄을 이용하여 광학 스위칭이 가능한 구조를 연구하였다. 먼저 기 연구된 레지스트패터닝법(resist assisted patterning, RAP) 으로 성장된 탄소나노튜브를 Cathode로 이용하였고 높은 Avalanche gain으로 X-ray imaging에 사용되는 비정질 셀레늄을 광반응 Anode로 적용하여 diode type의 구조로 연구를 진행하였다. 이를 통해 광학 스위칭이 가능한 구조, 광반응에 적절한 형태의 탄소나노튜브 성장 연구, 비정질 셀레늄의 광반응 특성 및 광반응 메커니즘에 대한 연구하였다. 결과적으로 조사되는 광량에 따라 전자방출특성이 변화하는 특성을 얻을 수 있었고, 이는 Optical sensor 로의 응용가능성을 보여주었다.

■ SESSION: K [KT1]
10월 23일(목), 18:30 - 20:00
장 소: 402호

**KT-01(초)** **X-선 응용 박막 구조특성 분석** 김 창수(*한국표준과학연구원.*) X-선을 이용한 박막의 구조특성의 평가는 구조특성 자체의 이해뿐 아니라 소자의 물성 및 그 관련성을 이해하기 위한 중요한 분야이다. 양질의 소자를 제작하기 위해서는 원하는 구조특성을 갖는 박막이 요구되고 따라서 이것은 정확한 구조특성 평가가 선행되어야 한다. 본 강의에서는 박막의 구조특성 분석을 위한 고분해능 X-선 회절법(HRXRD:High Resolution X-Ray Diffractometry)과 X-선 반사율 측정법(XRR:X-Ray Reflectometry)에 대하여 알아본다. 단일층과 초격자(MQW) 등의 에피막의 결정성, 격자변형, 두께 등의 구조특성을 분석하기 위한 HRXRD에서는 로킹커브(rocking curve)와 ω 및 ω/2θ 측정에 대한 이해와 측정방법 등을 알아본다. 또한 역격자 공간의 산란강도 지도(RSM: Reciprocal Space Map)에 관한 측정 및 분석방법의 이해 그리고 이것을 통한 에피층의 구조특성을 분석한다. 박막의 두께, 거칠기(roughness) 및 밀도를 측정하기 위한 XRR에서는 간단한 이론, 측정 및 분석 방법 등의 이해와 이를 통한 구조특성 분석의 예를 살펴보고 그 결과들의 신뢰성에 대하여 논의한다.

**KT-02(초)** **광전자 분광기술의 기초와 응용 (Introduction to X-ray Phtoelectron Spectroscopy)** 박 용섭(*경희대학교 물리학과.*) 본 튜토리알에서는 기본적인 고체물리 지식을 가진 대학원생들을 대상으로 표면분석 기법으로 널리 사용되는 광전자분광기술 (XPS)에 대해서 살펴본다. 우선 XPS의 원리에 대해서 소개하고, 진공 및 분석 장비의 개요, 데이터 분석법과 응용에 이르기 까지 광전자 분광기술 전반에 대해서 소개한다.

■ SESSION: K [KF1]
10월 24일(금), 09:00 - 11:00
장 소: 402호

**KF-01(초)** **나노물리 소자의 바이오 측정 및 세포 조절에의 응용** 홍 승훈(*서울대학교.*) 최근 나노기술의 발달에 따라, 새로운 나노물리 소자 및 소재를 이용하여 중요한 생물학적 문제를 풀려는 노력이 활발해지고 있다. 본 발표에서는, 나노트랜지스터 등 나노물리 소자가 바이오 분자의 검지나 그 작용 연구에 어떻게 활용될 수 있는지 논의한다. 또한, 탄소나노튜브, 나노선 등 나노재료들의 표면 패턴이 세포의 생장 조절에 어떤 영향을 미치는지에 대해서도 간단히 소개한다.

**KF-02(초)** **나노메디컬 연구 현황** 유 경화(*연세대학교.*) 나노메디컬 기술이란 나노기술을 질병의 진단 및 치료에 응용하고자 하는 기술이다. 최근 이 분야 연구가 세계적으로 활발하게 진

행되고 있는데 본 발표에서는 주로 나노진단 관련 연구 현황 및 전망에 대해 발표하고자 한다. 나노진단 기술의 궁극적인 목표는 단일 세포 수준에서의 조기 진단이다. In vitro 진단을 위해서는 다양한 종류의 나노바이오 센서가 연구되고 있는데 여기서는 주로 전기적 특성 측정을 이용한 나노바이오 센서를 소개하겠다. 또한 나노메디컬 기술을 이용하면 진단과 치료가 동시에 가능한 다기능 나노 플렛폼의 개발이 가능할 것이라는 기대를 가지고 활발한 연구가 진행되고 있는데 다기능 나노 플렛폼 연구의 최근 동향을 소개하고자 한다.

**KF-03(초)** **Nano-Bio Technology for New Biomedical Science** 문 대원(*KRISS.*) 최근 새로운 개념으로 표준연에서 추진 중인 레이저, 이온빔, 나노탐촉자, 등을 활용한 나노 바이오 융합 무표지 단일세포 측정기술을 요약하여 소개하고 이를 통한 새로운 바이오의료 과학기술의 도출 가능성에 대하여 토의하고자 한다. 비선형 라만 현미경인 coherent anti-Stokes Raman scattering(CARS), 반도체 극미량 분술물 분석기술인 secondary ion mass spectrometry (SIMS), 등 나노기반 바이오 융합 측정기술을 통하여 개발한 단일세포, 생체계면 분석 기술이 바이오의료 분야에 제시하는 새로운 가능성을 동맥 경화라는 주요 질병의 진단과 발생기작 연구를 예로 들어 보여 주고자 한다. 이와 같이 나노바이오 융합기술이 가져올 새로운 과학기술 분야의 변화와 문제점도 같이 토의하고자 한다.

**KF-04(초)** **CMOS platform for ubiquitous molecular sensor** 박 영준(*서울대학교.*) Nano System Institute(NSI) has been concentrating on the integration of the Nano structure on the CMOS platform with minimal process steps added to the conventional CMOS process, thereby easy transfer from the Nano related technology to the massive CMOS process line is possible. For this, as an example, we devise 2 methods; special pad structures appropriate for the sensor applications and introduction of the self aligned contact scheme between the aluminum and Nano structure. In this presentation, the sensor application of the technology based on the carbon nanotube (CNT) sensor array integrated on top of the CMOS chip is explained. In the methods, the CNTs networkas an semiconductor layer is formed on top of each sensor cell site of the fabricated chip after the CMOS chip is fabricated using the standard CMOS process. According to applications, the functionalization of the CNT surface (and/or the oxide surface) is performed to obtain the change in the conductance of the CNT layers due to the chemical reaction. Then the sensing circuit in the chip converts the information to a digital code. For the sensor circuit, the timing discriminatormeasures RC (CNT-Resistor &Capacitor) time constant and generates triggering signal depend on the change of the CNT's conductance. Time-to-Digital Converter (TDC) is used to measure the timing interval which is generated in timing discriminator. The delay-locked-loop is used to compensate the variation of buffer delay cell against process variations, temperature and power supply change. As demonstration examples, the glumamine - glutaminase reaction, the HSA –aptamer reaction, DNA-DNA hybridization have been tried for arrays builton the CMOS platform. The initial results show that the sensitivity and selectivity are in the range to be used as the general platform for electrochemical sensing of the molecule reactions based on the CMOS pad structure and Nano structure integration.

■ SESSION: K [KG2]
10월 24일(금), 11:00 - 13:20
장 소: 402호

**K-09(초)** **Unique characteristics of excitonic matter in cuprous oxide ($Cu_2O$)** JANG Joon Ik(*Department of Physics, Northwestern University.*) A direct-gap semiconductor $Cu_2O$ provides a model system for studying thermodynamics as well as population and relaxation kinetics of excitonic matter owing to its unique crystal structure. As a bound state of an electron and a hole, an exciton can be optically created and makes itself visible by radiative recombination. If excitons can be raised to sufficient densities, they may undergo Bose-Einstein condensation. From the perspective of fundamental exciton physics, renewed interest came with the observation of exciton polaritons. A polariton is a quantum superposition of an exciton and a photon, where the initial coherence with a definite wavevector is primarily determined by the incident laser pulse. In this talk, I will talk about the difficulty in reaching the exciton condensate primarily arising from the formation of short-lived "dark" biexcitons (excitonic molecules). Also I will present various experimental results strongly indicating the half-matter/half-light character of polaritons.

**K-10** **Molecular Random Approach in Lithography Process and Self-Assembly for below 20 nm Pattern Formation: How to model Moleclar Lithography Process and Self-Assembly** 김 상곤(*한양대학교 응용물리학과.*) 20 nm 이하 패턴 형성을 위해서 1.7 nm CD (critical dimension)과 1 nm 이하의 LER (line edge roughness) 과 LWR (line width roughness) 조절이 필요하다. 일반적으로 감광제를 구성하는 포리머 분자들의 하나는 1 nm 보다 크다. Molecular glass 는 분자들을 작게 만들고 LER 를 향상시키지만, dimensional 조절은 어려워 self-assembly 공정이 필요하다. 논문에서는 Monte Carlo를 기초로 한 molecular 감광제의 리소그래피 공정과 self-assembly 공정을 전산모사하고 실험결과와 비교하였다. 또한 aerial image contrast, photoacid generator, acid diffusion length, quencher, acid 그리고 quencher diffusion coefficients, and polymer size에 대한 LER 의 변화를 분석하였다.

**K-11** **The Structural Properties of Crystalline $InGaO_3(ZnO)_m$** CHANG Kee Joo, LEE Woo-Jin, CHOI Eun-Ae, BANG Junhyeok, RYU Byungki(*Physics, KAIST.*) Recently, $InGaO_3(ZnO)_m$, which belongs to the homologous oxides, has attracted much attention because of potential applications to transparent and optoelectronic devices. In this work, we investigate the structural properties of $InGaO_3(ZnO)_m$ (m = 1 - 6) using first-principles calculations within the density functional theory framework. We consider three different structures, where the Ga atoms are ran-

domly distributed in two central layers of a $GaO(ZnO)_m$ block of the layered structure, and form a flat boundary and a zigzag modulated boundary. It is generally found that the flat boundary structure is energetically less favorable because tensile strains are loaded in the ZnO layers due to the lattice mismatch between the Ga-O and Zn-O layers.On the other hand, in the Ga-modulated boundary structure and the random distribution of the Ga atoms, the structural stability is much enhanced as strains are properly released. For each structure, we discuss the stacking sequence of metal-O layers and the polarities of the ZnO layers.

**K-12** **산화물 박막에 대한 파워 효과** 이 봉주, 백 경철, 오 병우(*조선대학교, 물리학과.*) 반도체 공정에서 유전물질(dielectric material)로 이용도고 있는 $SiO_2$는 유전 상수(k)가 작기 때문에 메모리 용량이 기가(giga)급인 소자에서 그 두께가 5nm 이하로 얇아지게 되었으나, 전자 터널링(electron tunneling) 현상에 기인한 누설전류(leakage current)에 의해 적용상에서 한계에 도달하였다. 따라서 기존의 $SiO_2$(k=3.9~5.0)를 대체할 재료로 $Al_2O_3$ (k=8~10), $ZrO_2$(k=25) 및 $HfO_2$(k=30) 등이 연구되고 있다. 이 들은 유전상수가 $SiO_2$ 보다 크기 때문에 보다 두꺼운 상태에서 적정 유전 특성을 가질 수 있다. 그렇지만 Si 기판과 전극(electrode)과의 열적 안정성이 확보되어야 할 뿐만 아니라, 적정 에너지 밴드 갭(energy band gap) 및 결함이 없는 미세구조를 가지고 있어야 우수한 누설 전류 특성이 유지되어야 하며 또한 공정상의 적합성, 오염 등의 많은 문제가 해결되어야 $SiO_2$를 대처할 수 있으므로 증착 공정 개발에서부터 물질 평가에 이르기 까지 많은 연구가 이루어지고 있다. $Al_2O_3$, $HfO_2$, 더불어 $ZrO_2$는 높은 온도에서도 실리콘과 열 안정성이 우수하며 이중 $ZrO_2$는 비교적 높은 유전상수를 비롯하여 넓은 에너지 밴드 갭(energy band gap), 실리콘과의 접촉시에 높은 열적 안정성과 더불어 Si 기판에 증착 되었을 때 상당히 높은 장벽 높이를 가지고 있기 때문에 장래성이 있는 금속-산화물 박막을 형성할 수 있다. 또한 $ZrO_2$는 높은 용융점, 굴절율, 경도값을 가지고 있으며 낮은 열용량과 우수한 내식성을 갖고 있어 과학기술 분야에서 많은 주목을 받고 있으며, 광학 코팅제를 비롯하여 큰 크기의 집적회로에서의 유전체층,높은 큐리온도(curie temperature)에서 산화물 초전도체의 버퍼층, 평판 디스플레이에서 활성층의 용도로 각광받고 있으며, 티타늄보다 강도가 2~3배 강하고 탄성 및 내식성 등이 뛰어나 향후 플라스틱을 대체할 것으로 기대되는 첨단 신소재이기도 한다. 이미 골프클럽의 소재로 상용화 된 바 있으며, 이동전화, 개인 휴대 단말기의 케이스 등 전자기기 뿐만 아니라 의료용 기기, 자동차, 방위 산업 등에 폭넓게 응용되며 건물 벽면, 유리, 거울, 타일 등에 쉽게 코팅할 수 있는 광촉매로의 역할도 하고 있다. 본 연구에서는 RF-sputtering법에 의한 $ZrO_2$ 박막을 형성하는데, 파워증가에 의한 변화를 연구하기 위하여 X-ray diffraction(XRD), ellipsometry등을 이용하여 증착율을 비교 분석하였고, SEM과 AFM을 통한 표면의 모포러지 변화를 관찰하였다.

**K-13** **Spin effects on Collective modes in a 2D array of DMS quantum dots** KIM Nammee, KIM Heesang(*Dept. of Physics, Soongsil University.*) The intra-band collective excitation of a two dimensional(2D) diluted magneticsemiconductor (DMS) quantum dot (QD) array is investigated, including the *s-d* exchange interaction, the spin splitting and the Coulomb interactions inside a dot and between dots. We obtain more branches of collective modes than those of the single dot excitation or collective modes without spin splittings due to the result of degeneracy breaking by the Coulomb interaction and the giant Zeeman splitting. The B dispersion of collective excitation energy for multi carriers per dot has discontinuity due to the carrier transfer between energy levels. The depolarization energy shift in a DMS QD array is found to be predominantly due to inter-dot coupling.

**K-14** **Fabrication and Characterization of Mn-doped ZnO Nanocrystals into a $SiO_2$ Layer** LEE Youngmin, YOO Seungyong, CHO Hyunchil, KIM Deuk Young, KANG Tae Won[1], LEE Sejoon[1](*Dongguk Univ., Dept. of Semiconductor Science. [1]Dongguk Univ., Quantum-fuctional Semiconductor Research Center.*) The fabrication of ferromagnetic Mn-doped ZnO (ZnMnO) nanocrystals into a $SiO_2$ layer and their electrical tunneling transport properties have been investigated. The formation of ZnMnO nanocrystals was performed by irradiation of ultra thin ZnMnO layer using 248 nm KrF excimer laser. After the formation of the ZnMnO nanocrystals into a $SiO_2$ layer, the tunneling transport properties were evaluated through the fabrication of metal-oxide-semiconductor (MOS) capacitors. The MOS capacitors showed the clear memory window with flat-band voltage shifts ranging from 0.73 V to 1.25 V. Here, the control of memory window was achieved by changing the size and density of nanocrystals through the control of laser power density. In addition, to use the spin-functionality of ferromagnetic ZnMnO nanocrystals, back-gated spin-tunneling MOS diodes have also been fabricated. The fabricated devices clearly showed the step-likely increased current staircases attributing to tunneling transfer of carriers, and surprisingly, the current-oscillation packets were observed at each current staircase. The peak-to-valley ratio of the packets showed a dependence on the magnetic properties of the ZnMnO nanocrystals, and it indicates that the current oscillation packets observed at the tunnel-bias-state for the MOS diodes are attributed to the non-linear resistance due to the spin repulsion during spin tunneling processes.

**K-15** **성장 시간과 온도에 따른 ZnO 나노구조물의 형상변화와 광학적 특성 평가** 최 민열, 이 삼동, 김 상우(*금오공과대학교 신소재시스템공학부 정보나노소재공학전공.*) ZnO는 일반적으로 상온에서 3.37 eV의 직접 천이형의 넓은 밴드갭과 60 meV의 큰 엑시톤 결합에너지, 압전특성 등과 같은 독특한 특성을 가지고 있다. 따라서 나노선, 나노막대, 나노튜브와 같은 1차원 ZnO 나노 구조물의 합성방법 개발 및 특성평가와 더불어 합성한 ZnO나노구조물을 소자에 적용하기 위한 연구들이 활발이 이루어지고 있다. 독특한 특성의 나노크기의 ZnO구조물을 LED, 태양전지, 센서와 같은 소자에 적용하기 위해서는 원하는 형상의 ZnO를 합성할 수 있어야 한다. ZnO는 일반적으로 c-축 성장하려는 경향이 강해서 wire, rod 형태의 1차원 구조물로 잘 성장하지만, 성장조건에 따라서 belt, wall, wire, niddle, sphere와 같은 다양한 형상의 구조물로도 성장한다. 따라서 1차원 ZnO 나노구조물 합성 mechanism과 성장조건 확립이 필요하다. 본 연구에서는 ZnO 나누구조물을 금 촉매가 증착된 GaN기판 위에 열화학 기상증착법

을 이용하여 성장시켰으며, 성장시간과 온도에 따른 형상 변화를 FE-SEM을 이용하여 조사하였으며, 성장 시간과 온도에 따라서 wall과 wire 그리고 이종접합 형태의 구조물이 형성된 것을 확인하였다. 이러한 결과를 바탕으로 nanowire 형성 mechnism을 분석하였다. 또한 합성된 ZnO 나노구조물의 결정구조를 XRD를 이용하여 조사하였으며, 상온 PL측정을 통한 광학적 특성도 평가하였다.

**K-16** **저온 습식화학방법을 통해 성장된 ZnO 나노로드의 정렬에 의한 GaN 기반 발광다이오드 (light-emitting diodes)의 광추출율 향상** 이 삼동, 김 경국[1], 박 재철[1], 김 상우(*금오공과대학교 신소재시스템공학부. [1]삼성종합기술원 반도체 소자 연구실.*) 최근, GaN 기반 발광다이오드의 연구에 있어서, 고휘도 (high-brightness) 발광다이오드 (LED)를 위한 광추출율 향상에 대한 연구가 가장 중요한 화제가 되고 있다. 이에 본 연구에서는 광추출율 향상을 위해, ITO (indium tin oxide) 투명전극 위에 ZnO 나노로드 (nanorod)를 정렬시킨 GaN기반 LED를 구현하였다. ZnO 나노로드는 습식화학방법을 통하여 90 ℃의 낮은 온도에서 합성되었다. 20 mA 전류주입(current injection) 하에서, ITO 위에 ZnO 나노로드를 정렬시킨 LED의 광출력효율은 ITO만 있는 기존의 LED와 비교했을 때 56 % 이상 두드러지게 증가하였다. ZnO 나노로드 정렬에 의한 광추출율의 증가는 LED 표면에서 side walls의 형성과 거친 표면에 의한 다광자 산란 (multiple photon scattering)에 의한 결과이다. 본 연구를 통하여 유망한 응용 분야인 고효율 LED를 구현할 수 있을 것으로 기대한다.

**K-17** **Structural and optical properties of Al doped ZnO thin-films** 한 상욱, 서 수영[1], 곽 창하[1], 김 선효[1], 박 순홍[2](*전북대학교, 사범대학 물리교육학과. [1]포항공과대학교 신소재공학과. [2]포항산업과학기술연구원, 신금속재료팀.*) We present the structural and optical properties of Al-doped single-crystal ZnO films synthesized on Al2O3 substrates by a RF-magnetron sputtering procedure. The structural properties of the films were characterized by x-ray diffraction (XRD) measurements. The XRD measurements demonstrated that the films had a hexagonal wurtzite phase with a strong c-axis orientation. We did not observed any extra peak from the XRD measurements. The lattice constant c was linearly increased with Al doping ratio. These strongly implied that Al atoms were randomly substituted for the Zn atoms. The optical and chemical properties of the Al-doped ZnO films were investigated by photoluminescence(PL) and x-ray photoelectron spectroscopy measurements, respectively. We will compare the structural and optical properties with electrical properties of the films.

**K-18** **Impact of Electrical Carrier Conductivity on Ferromagnetic Properties for As-doped p-type ($Zn_{0.93}Mn_{0.07}$)O Layers** BONG Hajong, SHIM Dahye, SEONG Junje, LEE Sejoon[1], KANG Tae Won[1], KIM Deuk Young(*Dongguk University, Department of Semiconductor Science. [1]Dongguk University, Quantum-functional Semiconductor Research Center.*) The dependence of ferromagnetic properties for As-doped *p*-type ($Zn_{0.93}Mn_{0.07}$)O layers on their hole conductivity has been investigated. The control of the hole conductivity was performed through the modification of negative background-charge densities by controlling the oxygen partial pressure ($P_{O2}$) during the initial growth stage before As doping. For measurements of temperature-dependent resistivity and temperature-dependent magnetization, it was clearly observed that the Curie temperature and spontaneous magnetization for the As-doped *p*-type ($Zn_{0.93}Mn_{0.07}$)O layers are systematically increased as the hole conductivity increases. The similar behavior was also observed for the electron spin resonance measurements. By means of Raman spectroscopy, Hall-effect electrometry, and x-ray photoelectron spectroscopy measurements, we found out that the incorporated $Mn^{2+}$ ions and As dopants get more stabilized as the $P_{O2}$ increases; *i.e.*, the increase of $P_{O2}$ during the initial growth stage before As doping leads not only to the increase of hole conductivity but also to the increase of magnetic anisotropy for the samples. Therefore, as a result, the improvement of ferromagnetic properties with the increase in the hole conductivity can be ascribed to originate from the increase of long-range ferromagnetic coupling between stabilized $Mn^{2+}$ ions and hole carriers donated from stably incorporated As acceptors.

**K-19** **Preparation and improvement of $Be_xZn_{1-x}O$ films** PARK Dae-Sung, KIM Jung-Hyun, YU Ji-Hyun, JEONG Tae-Soo[1], YOUN Chang-Joo(*School of Semiconductor and Chemical Engineering, Chonbuk National University. [1]Semiconductor Physics Research Center, Chonbuk National University.*) $Be_xZn_{1-x}O$ alloy material has shown potential in optical and electrical properties for $Be_xZn_{1-x}O$/ZnO multiple quantum well in the ZnO-based device applications. However, the study of growth mechanism of $Be_xZn_{1-x}O$ film is still limited to further understand the relationship between film properties and growth conditions. This work is therefore undertaken to study the dependence of the properties of $Be_xZn_{1-x}O$ films prepared by simultaneous reactive RF sputtering on Be composition. After deposition, post-annealing at various temperature ranging was performed to improve the film properties. The effect of Be composition and post-annealing temperatures on the morphological, structural and optical properties were studied by using scanning electron microscopy (SEM), X–ray diffraction (XRD) and UV visible infrared spectrometer.

# 포스터발표논문 초록

■ SESSION: P1
10월 23일(목), 14:30 - 16:15
장 소: 제3전시장

**Dp-001** **Optical phonons and excitons in semiconductor nanostructures** 송 지선, 이 경연, 노 희석, HONG T. B.[1], TITOVA L. V.[1], MISHRA A.[1], SMITH L. M.[1], JACKSON H. E.[1], YARRISON-RICE J. M.[2], 최 영진[3], 최 경진[3], 박 재관[3](*전북대학교, 물리학과. [1]Department of Physics, University of Cincinnati, USA. [2]Physics Department, Miami University, USA. [3]한국과학기술연구원, 나노재료연구센터.*) CdS 반도체 나노구조에 대한 라만 산란 및 저온 발광 실험 결과를 보고한다 [1-3]. 단일 CdS 나노시트에 대한 저온 cw 발광 실험을 통해 방출되는 빛이 *c*-축에 수직한 방향으로 매우 편광 되어 있음을 알았다. 발광 스펙트럼은 A와 B 유형의 엑시톤 선으로 구성되는데 특이한 사실은 나노시트마다 발광 반응이 제각기 다르며 심지어 나노시트의 위치 변화에 따라서도 발광 반응이 다르다는 것이다. 이를 이해하기 위해 전체 단일 나노시트로부터 발광 이미징을 얻었는데, 나노시트의 길이 방향으로 가장자리 부분에서는 A 엑시톤과 연관된 반응이 중심 부분에서는 B 엑시톤과 연관된 반응이 강하게 나타났다. 시분해 발광 실험을 통해서 이들 엑시톤의 재결합 수명이 약 200 ps 정도임을 파악했는데 이는 나노와이어에서의 엑시톤 수명보다는 길지만 덩어리 물질에서의 수명 보다는 짧은 것이다. 라만 산란 실험은 엑시톤 특성의 이해에 도움을 준다. 단일 나노시트로부터의 라만 스펙트럼에서 매우 강한 다중 광학포논 반응이 관측되었다. 이와 대조적으로 나노와이어로부터의 라만 산란 스펙트럼은 매우 약한 다중 포논 반응을 나타낸다. 강한 다중포논 반응은 나노시트가 나노와이어 보다 향상된 결정성을 지님을 시사하는 것이다. 특히 라만 산란 반응이 단일 나노시트의 위치에 따라 약간씩 다르게 나타나는데 이는 미세한 격자상수의 변형을 나타낸다. 나노시트에서의 결정성의 향상은 엑시톤 수명의 증가와 연관이 있고 격자상수의 변형은 공간적으로 비균질적인 엑시톤 특성과 연관이 있으리라고 본다.
[1] K.-Y. Lee *et al.*, Appl. Phys. Lett. 91, 201901 (2007). [2] H. Rho *et al.*, Appl. Phys. Lett. 92, 013111 (2008). [3] T. B. Hong *et al.*, Appl. Phys. Lett. 92, 143112 (2008)

**Dp-002** **$BaTiO_3$ @X 강자성 나노입자들의 방사광 분광 연구 (X= gamma-$Fe_2O_3$, $Fe_3O_4$, alpha-$Fe_2O_3$, Fe)** 김 대현, 이 현진, 김 그라시아, 강 정수, 구 용성[1], 정 종훈[1], 이 한길[2], 김 재영[2](*가톨릭대학교 물리학과. [1]인하대학교 물리학과. [2]포항가속기연구소.*) 최근 일부 산화물에서 다강성 (multiferroic) 성질이 발견됨에 다기능을 가진 신물질의 개발에 대한 연구가 활발해 지고 있다. 한편 강유전체를 이용한 복합나노 (nano-composite) 입자들의 연구로부터 나노입자들의 모양, 크기, 제조조건 등을 조절함으로써 복합나노 입자의 여러 가지 물리적 성질들을 조절할 수 있음이 발견되었다[1]. 그러므로 자성과 강유전성(ferroelectric)을 동시에 가지는 다기능 물질의 후보로 복합나노물질이 속할 수 있다. $BaTiO_3$를 핵(core)으로 사용하여 그 표면에 강자성물질의 껍질(shell)을 씌운 $BaTiO_3$@gamma-$Fe_2O_3$ 형의 core@shell 나노입자에서 매우 큰 자기유전 (magnetodielectric :MD) 현상이 발견되었는데, 이렇게 큰 MD 결합의 원인으로 나노입자의 제조 온도, 자성체 껍질층의 두께, 계면 근처에서의 살창의 어긋남 등이 고려되었다 [2]. 이러한 발견은 강유전체@강자성체 core@shell 나노입자들에서 강자성 껍질층과 계면의 전자구조가 core@shell 나노입자들의 물성을 결정하는데 매우 중요하다는 것을 나타내며, 그러므로 다기능 신물질의 연구 분야에서 core@shell 나노입자들의 전자구조 연구가 매우 중요하겠다. 본 연구에서는 연x-선 방사광을 사용한 광흡수 분광법 (x-ray absorption spectroscopy: XAS)과 x-선 자기원형이색선분광법 (x-ray magnetic circular dichroism: XMCD)을 이용하여 core@shell구조의 $BaTiO_3$@X (X=gamma-$Fe_2O_3$, $Fe_3O_4$, alpha-$Fe_2O_3$, Fe) 나노입자들의 전자구조를 연구하였다. 특히 껍질층과 계면 근처에 있는 Fe, Ti 등의 전이 금속 이온들의 원자가와 스핀 상태를 결정하였다. 우리의 XAS와 XMCD 실험 결과는 Fe 이온들이 대부분 3가($Fe^{3+}$) 상태에 있으며, 계면 근처의 Ti 이온들은 거의 4가($Ti^{4+}$) 상태라는 사실과 $BaTiO_3$@X 나노입자들의 계면 근처에 있는 Ti 이온들의 유도 스핀분극 효과는 무시할 정도로 작다는 것을 보여 주었다. 이 발표에서 $BaTiO_3$@X 나노입자들의 전자구조가 물성에 미치는 역할에 관하여 논의하고자 한다.
[1] S. Mornet, et al., Chem. Mater, 19, 987 (2007). [2] Y. S. Koo, et al., Appl. Phys. Lett. 91, 212903 (2007).

**Dp-003** **니켈 디실리사이드 나노 결정의 메모리 특성** JANG Yoo-Sung, YOON Jong-Hwan(*강원대학교, 물리학과.*) 금속 실리사이드를 이용한 비휘발성 메모리 소자는 5nm 이하의 얇은 tunnel oxide층의 사용이 가능하여 기존의 비휘발성 메모리 소자의 단점을 극복할 수 있고 공정의 단순함과 적은 제작비용등과 같은 많은 이점을 가지고 있다. 이 논문은 silicon-rich-silicon oxide층안에 니켈 디실리사이드 나노결정의 직접성장에 관한 연구이다. silicon-rich-silicon oxide 층은 Czochralski silicon wafers (100)에 기판온도 300℃에서 plasma-enhanced chemical vapor deposition (PECVD) 방법으로 제조하였다. 니켈 디실리사이드 나노결정은 silicon-rich-silicon oxide층 사이에 아주 얇은 Ni층을 전통적인 증착방법으로 코팅한뒤 고온에서의 열처리를 통해 형성하였다. 이렇게 형성된 구조는 메모리 소자로써 뚜렷한 C-V특성을 나타내었고 -12V와 12V사이를 sweep했을때 약 11V의 memory window가 측정되었다. 또한 gate에 pulse voltage를 적용함으로써 program / erase 각각의 C-V 특성을 얻고 retention 과 endurance 특성을 연구하였다.

**Dp-004** **Polarized Micro Raman Spectroscopy of Bi-layer Graphene** MOON Hyerim, YOON Duhee, CHEONG Hyeonsik, SON Young-Woo[1](*Sogang University. [1]Korea Institute for Advanced Study.*) Graphene has a hexagonal structure of a monolayer which consists of carbon atoms. The thickness of monolayer graphene is about 0.34 nm. Graphene is isolated from a graphite flake using micromechanical cleavage with adhesive tape. The $sp^2$ hybrid covalent bonds in the plane result in strong interactions in plane but weak interactions out of plane. In our previous work on polarized micro-Raman spectroscopy of single layer graphene, Raman *G* band (~1586 $cm^{-1}$) is isotropic and *2D* band (~2686 $cm^{-1}$) strongly depends on relative polarizations of the incident and scattered photons. This strong polarization dependence originates from inhomogeneous optical absorption and emission mediated by resonant electron-phonon interaction. In bilayer graphene, Raman *2D* band can be decomposed into four Lorenztian peaks which can be

interpreted in terms of the four transition paths in the double resonance Raman (DRR) processes. In this work, we will report on the polarization dependence of Raman *2D* band of bilayer graphene. The polarization dependences of the four components of the *2D* band are studied in detail and compared with theoretical analysis.

**Dp-005** **Structure and Morphology of Vanadium Oxide Nanotubes** LEE Cheol Eui, SHIM Eui Taek, PARK Jun Kue, KWON Hyo-Cheon, LEE Kyu Won(*Korea university.*) Vanadium oxide nanotubes (VOx-NTs) were obtained from the composites of alkylamines and vanadium oxide gels by using a hydrothermal treatment (180-200 oC, 6-8 days). The structure and morphology of the VOx-NTs with hexylamines, octylamines and decylamines were characterized by X-ray diffraction, scanning electron microscopy and Fourier transform infrared spectroscopy. The nanotubes were found to have outer diameters from 30 nm to 100 nm and inner diameters from 10 to 30 nm with lengths up to several micrometers.



**Dp-006** **Luminescence properties of $Eu^{3+}$-doped Y-Al-O system phosphors** 문 병기, 정 홍채, 박 진영, GANJI Seeta RamaRaju, 정 중현, 김 중환[1], 최 혜영[1](*부경대학교, 물리학과. [1]동의대학교, 물리학과.*) YAG:$Eu^{3+}$ is well-known as an efficient phosphor for field emission displays (FEDs) so that it motivate a lot of interest to improve their luminescent performance. It is well known that $Eu^{3+}$ emission depends on effect of crystal field. In this work, $Eu^{3+}$-doped Y-Al-O system phosphors [$Y_3Al_5O_{12}$ (YAG), $Y_3AlY(AlO_4)_3$ (YAYG), $YAlO_3$ (YAP), $Y_4Al_2O_9$ (YAM)] were prepared by means of solvthermal reaction method. Their excitation spectra and emission spectra along with decay curves were measured at room temperature and the relationship between the structures and the photoluminescence properties of the phosphors have been studied. YAG:$Eu^{3+}$ and YAYG:$Eu^{3+}$ has cubic garnet phase (centrosymmetric $D_{2h}$ site symmetry) without any impurity phase and the lattice constants were 12.02 and 12.06 Å, respectively. YAP:$Eu^{3+}$ and YAM:$Eu^{3+}$ have orthorhombic perovskite ($C_s$ site symmetry) and monoclinic phases ($C_1$ site symmetry), respectively. The excitation spectra of $Eu^{3+}$-doped Y-Al-O system phosphors consists of charge transfer band (CTB) of $Eu^{3+}$-$O^{2-}$ associated with short ultraviolet and f-f transition with $^7F_0$-$^5L_6$ (395 nm). The emission spectra were composed of $^5D_0 \rightarrow {}^7F_j$ (j= 0, 1, 2, 3) emission lines of $Eu^{3+}$. the emission spectra of YAG, YAYG phosphors is dominated by the orange emission due to $^5D_0 \rightarrow {}^7F_1$ (590 nm) transition with inversion symmetry, and the emission spectra of YAP, YAM phosphors is dominated by the red emission owing to their $^5D_0 \rightarrow {}^7F_2$ (620 nm) transition with no inversion symmetry. $Eu^{3+}$-doped Y-Al-O system phosphors are discussed with necessary details in relation to their complex structures.

**Dp-007** **Enhancement of $Tb^{3+}$ emission through the energy transfer between $Tb^{3+}$ and $Dy^{3+}$ in GAG** 문 병기, 박 진영, 정 홍채, GANJI Seeta RamaRaju, 정 중현, 김 중환[1](*부경대학교, 물리학과. [1]동의대학교, 물리학과.*) Aluminum garnets have been studied widely in the applications of optoelectronics and lasers due to their stable chemical and physical properties. It is well known that $Tb^{3+}$and $Dy^{3+}$ are the promising activators in green ($^5D_4 \rightarrow {}^7F_5$) and blue ($^4F_{9/2} \rightarrow {}^6H_{15/2}$), yellow ($^4F_{9/2} \rightarrow {}^6H_{13/2}$) regions, respectively. In this paper, we report on the structural and luminescent properties of $Dy^{3+}$ -doped GAG: $Tb^{3+}$ phosphors by means of solvthermal reaction method. The powders were sintered at 1400 $^oC$. The samples had garnet structure with cubic phase. Increasing the concentration of $Dy^{3+}$, the lattice constants is decreased. The emission spectra of GAG:$Tb^{3+}$,$Dy^{3+}$ phosphors show mainly green emission at 545 nm due to $^5D_4 \rightarrow {}^7F_5$ ($Tb^{3+}$) and weak blue emissions at 480 nm due to $^5D_4 \rightarrow {}^7F_6$ ($Tb^{3+}$) and $^4F_{9/2} \rightarrow {}^6H_{15/2}$ ($Dy^{3+}$) and yellow emission at 585 nm due to $^5D_4 \rightarrow {}^7F_4$ ($Tb^{3+}$) and $^4F_{9/2} \rightarrow {}^6H_{13/2}$ ($Dy^{3+}$). Increasing the $Dy^{3+}$ ions concentrations, $Tb^{3+}$ emission was increased because the distance between the activator and donor is decreased. So, the efficient energy transfer occurred between $Dy^{3+}$ and $Tb^{3+}$ ions. The decay curve was measured and probability of the energy transfer was investigated.

**Dp-008** **Theoretical study of encapsulation of anticancer drug into carbon nanotubes** LOC Duong Dinh, KIM Gunn, LEE Young Hee(*SKKU.*) Carbon nanotubes (CNTs) are good candidates for drug delivery. Based on the local density approximation, we performed density functional theory calculations to study the energetics of cisplatin (an anticancer drug) inside CNTs. The energy profile for encapsulation process are calculated. It is found that the cisplatin molecule can enter the (10,10) CNT with no activation barrier. The encapsulation energy is approximately 0.12 eV (endothermic), which implies that encapsulation and release of cisplatin may be possible using the CNTs with diamter of ~1.4 nm. We will also discuss encapsulation of cisplatin into CNTs with smaller diameter.

**Dp-009** **First principles study of hydrogen storage in Ca doped graphenes** 김 규봉, 지 승훈, 임 석호[1], 박 노정[1](*포항공대 물리학과. [1]단국대 응용물리학과.*) Recently, transition metal (TM)-dispersed porous materials have been suggested as plausible candidates for hydrogen storages that possess optimal hydrogen binding characteristics. A serious problem in this approach is that TM atoms tend to aggregate instead of being atomistically dispersed, which results in the deterioration of hydrogen uptake. Here we investigate the hydrogen adsorption on Ca atoms dispersed on graphene using ab initio methods. We observe that the clustering energy of Ca atoms is much smaller than that of TM atoms, which indicates that Ca can be almost free of clustering on graphene. Our study shows that the s- and d-orbital charge states of Ca atom has crucial role in hydrogen adsorption mechanism on that complex. Such Ca charge states on various graphene doping conditions and the corresponding hydrogen adsorption properties are studied

**Dp-010** **Sol-Gel Synthesis and Optical Properties of $Ca_2SnO_4$: $Eu^{3+}$ Phosphors** FU Zuoling, 문 병기, 양 현경, 최 병춘, 정 중현(*부경대학교, 물리학과.*) The development of flat panel displays, such as field emission displays (FEDs), plasma dis-

play panels (PDPs) and thin film electro-luminescent devices (TFEL), has always been accompanied by improvements in the phosphor used. Many efforts have been made to discover host materials as well as activators with high performance for phosphor applications [1, 2]. Alkaline earth stannate is drawing more and more attention for new phosphors. Chau et al. [3] reported $Sr_2SnO_4:Eu^{3+}$ phosphor. Kim and his coworkers [1] reported a new excellent luminescent phosphor, $Mg_2SnO_4$: $Mn^{2+}$ for application in PDPs. Generally, the luminescent properties of phosphors are strongly dependent on the crystal structure of the host materials. The structure of $Ca_2SnO_4$ consists of chains of $SnO_6$ octahedra which are linked by edges. The calcium ions are surrounded by seven oxygen ions in an arrangement of low symmetry. $Ca_2SnO_4:Eu^{3+}$ can be prepared by solid state reaction and temperatures up to 1300°C are necessary[4], and $CaSnO_3$ is formed as an intermediate product which reacts further with CaO to form the orthostannate. However, in this paper, the $Ca_2SnO_4:Eu^{3+}$ phosphor was prepared by low temperature sol-gel method. The influence of calcined temperature and time on structure of $Ca_2SnO_4:Eu^{3+}$ was investigated by using X-ray powder diffraction (XRD). The experimental results show that the dried gel was crystallized to the pure orthorhombic phase after calcination at 900°C in air for 6 hours. These phosphors have displayed bright red color under a UV source. The richness of the red color has been verified by determining their color coordination from the CIE standard charts, and this red emission has been assigned to $^5D_0 \rightarrow ^7F_2$ electric dipole transition at 616nm and 620nm.The excellent luminescence properties make it possible as a good candidate for plasma display panel (PDP) application.

**Dp-011** **Fabrication and Characterization of the Ultrasmall Split Gate Type of GaAs Quantum Dots** SEO YoHan, KIM YoungSang, JEON HanKyung, JEONG HeeJun(*한양대학교 응용물리학과.*) We present fabrication and electrical characterizations of the lithographically defined ultrasmall quantum dot device based on GaAs/AlGaAs heterostructure with a two-dimensional electron gas (2DEG) which is located 60nm beneath the surface. Quantum dot device, which is composed of fully tunable metal split gates, is defined by electron beam lithography technique. By adjusting the pinch-off gate voltages, electrical potential barriers are formed thus electrons are confined in an electronic island. Low temperature measurements of our device show a Coulomb blockade oscillation as a function of plunger gate voltages due to the quantum confinement and the electron charging effect. We obtain Coulomb diamond shapes of two dots from two-dimensional plots of conductance via gate and source-drain bias and find the charging energies of 2.2 and 4.41 meV, respectively. Large Coulomb energy gives a possibility of potential applications quantum dot devices functioning in high temperature condition.

* This work was supported by the Korea Research Foundation Grant funded by the Korean Government (MOEHRD) (KRF-2006-331-C00120).

**Dp-012** **Nonperturbative Dynamical Theory on the Double Quantum Dot** HWANG Sun-Yong, KIM Seongjin[1], YI juyeon[1] (*고려대학교 물리학과. [1]부산대학교 물리학과.*) We theoretically investigate the double quantum dot (DQD) system via the nonperturbative dynamical theory (NDT). The system we study is composed of two quantum dots connected to the single lead, which are also coupled to each other by kinetic hoppings. We consider the on-site Coulomb repulsion within the Anderson Model exhibiting the Kondo resonance. With focus laid on the effects of inter-dot hopping, we calculate the density of states and examine the variation of resonant properties.

**Dp-013** **The effect of dispersants in dispersing carbon nanotubes for flexible transparent conducting film** PARK hyeon ki, 김 기강, 김 수민, 배 정준, GENG Hong Zhang(*성균관 대학교.*) Carbon nanotubes (CNTs) were dispersed by using different dispersants in aqueous solution; anionic sodium dodecylbenzene sulfonate (NaDDBS), non-ionic triton X-100 (TX-100), and cationic cetyltrimethylammonium bromide (CTAB). The flexible transparent conducting films (TCFs) were prepared by using the prepared CNT solution with spray method. The TCFs were then immersed in acidic solution ($HNO_3$) for some time. The variation of the sheet resistance by acid treatment depend on the interaction energy between dispersant and CNTs. The interaction nature was characterized by UV-Vis-NIR, Raman spectrum, electrophoretic light scattering and scanning electron microscopy.

**Dp-014** **Influence of Surface Morphology on Adsorption Behavior in ZnO Nanowire Field-effect Transistors** OH Hwangyou, LEE Jeong-O[1], KIM Sang Sub[2], CHOI Heon-Jin[3], KIM Ju-Jin[4](*Department of Physics, Chonbuk National University &Department of Materials Science and Engineering, Yonsei University. [1]Advanced Material Division, Korea Research Institute of Chemical Engineering. [2]Department of Materials Science and Engineering, Inha University. [3]Department of Materials Science and Engineering, Yonsei University. [4]Department of Physics, Chonbuk National University.*) We fabricated field-effect transistors (FETs) using ZnO nanowires with different structures and studied the effect of the adsorption of gas molecules on the electrical properties of the obtained nanowire devices. Although they were grown on the same substrate and under the same synthesis conditions, the devices showed completely different adsorption behaviors depending on their surface structures. Some FETs underwent oxidative adsorption reactions whereas others underwent reductive adsorption reactions in ambient air. In addition to these differences in adsorption behavior, our experimental results show that the electron mobilities in the ZnO nanowire devices are also closely related to their surface structure.

**Dp-015** **Electric property of graphite oxides** JIN MeiHua, JEONG Hae-Kyung, YU Woo Jong, KANG Bo Ram, JANG Jin Ho, LEE Young Hee(*Department of Physics, BK21 Physics Division, Center for Nanotubes and Nanostructured Composites, Sungkyunkwan Advanced Institute of Nanotechnology, Sungkyunkwan University, Suwon 440-746, Korea.*) We have synthesized graphite

oxide by simplified Brodie method and characterized IV characteristics at room temperature. Graphite oxide shows p-type semiconducting behavior and its on-off ratio decreases as thickness of graphite oxides increases. Detail characteristics of graphite oxides were investigated using x-ray photoelectron spectroscopy, x-ray diffraction, Fourier transformed infra red spectroscopy, and atomic force microscopy.

**Dp-016** **Zero Temperature Phase Diagram And Magnetic Excitations Of Bilayer Graphene And Nanoribbon System.** 문 경순, 임 준원(*연세대학교.*) We theoretically study the magnetic phase diagram of bilayer graphene system based on the Hubbard-type Hamiltonian. By varying the doping and the strength of the on-site Coulomb repulsion, we establish the zero temperature phase diagram of the system by solving the Hamiltonian within the Hartree-Fock approximation and investigate the low-lying excitation spectrum such as spin waves. It is generally believed that the bulk graphene system is nonmagnetic. However, graphite nanoribbons can support the edge ferromagnetism due to the strong magnetic fluctuations at the edges. We attempt to obtain the effective energy functional by applying the Hartree-Fock method with the inclusion of the variational parameters and study the edge magnetic excitations of both single and bilayer graphite nanoribbons.

**Dp-017** **Influence of Diameter on the Photoresponse in a Networked Zinc-oxide Nanowire Photodetector** HA Ryong, PYUN Jae-Chul, OH Hwangyou, CHOI Young-Jin[1], PARK Jae-Gwan[1], CHOI Heon-Jin(*Department of Materials Science and Engineering, Yonsei University. [1]Nano-Materials Research Center.*) We report on the photoresponses of networked ZnO nanowire photodetectors fabricated by using a simple, mass-scalable process. ZnO nanowires were synthesized by using a carbothermal reduction process, and the diameter of the nanowires was controlled by using the thickness of the gold catalyst. The photoresponse was measured by using photodectors fabricated with nanowires of 80 nm and 300 nm in diameter. The photoresponse showed no dependence on the diameter of the nanowires in the wavelength range of 200 ~ 370 nm, which is attributed to the effects of photo-generation and photolysis on the surface nanowires, while it showed a dependence on the diameter in the wavelength range of 370 ~ 650 nm.

**Dp-018** **Field Emission Property Of Transparent Ultra-thin Carbon Nanotube Film On ITO Glass** JANG Eunsoo, GOAK Jeungchoon, KIM Myungsu, LEE Hansung, LEE naesung(*Faculty of Nanotechnology and Advanced Materials Engineering, Sejong University, Seoul 143-747.*) Carbon nanotubes (CNTs) are considered as an electron field emitter due to their superior electrical, mechanical, and chemical properties. Several applications using CNTs as field emitters have been demonstrated such as field emission display (FED), backlight unit (BLU), and X-ray source. In this study, we applied a simple and efficient process to fabricate a transparent ultra-thin CNT film. First, we prepared CNT aqueous solution by ultrasonically dispersing purified single-walled carbon nanotubes (SWCNTs) in deionized water with sodium dodecyl sulfate (SDS). After centrifugation, SWCNTs at ~ 50 wt. % was present in the supernatant. To obtain CNT film, well-dispersed CNT solution in a milliliter or even several tens of micro-litters was deposited onto porous alumina membrane through the vacuum filtration process. Then, the alumina membrane was solvated by 3 M NaOH solution and the floating CNT film was easily transferred to indium-tin-oxide (ITO) glass defined as 1 x 1 $cm^2$ with film mask. The transmittance of as-prepared ultra-thin CNT film measured by UV-Vis spectrophotometer was from 68 % to 97 % depending on the amount of CNT aqueous solution and, after roller-activation, varied from 93 % to 98 %, regardless of CNT quantity. This ultra-thin CNT film showed a very high peak current density of field emission up to 30 mA/$cm^2$ at 7.23 V/μm and uniform field emission images on phosphor, which seems very promising to be applied to vacuum microelectronics such as microwave power amplifiers and X-ray sources.

**Dp-019** **Pulsed Laser Deposition 방법으로 증착한 $Gd_2Zr_2O_7$/YSZ 박막의 물리적 특성과 열전도성** 정 고은, 배 종성[1], 양 호순(*부산대학교 물리학과. [1]한국기초과학지원연구원 부산센터.*) Pyrochlore 구조의 $Gd_2Zr_2O_7$ 는 낮은 열전도성을 가지는 물질로서 열차단에 효과적인 물질로 주목 받고 있다. Pyrochlore 구조를 가지는 물질들이 낮은 열전도성을 나타내는 것은 Fluorite 구조에서 8a위치의 산소 음이온 한 개가 비어 있는 구조이므로 산소 vacancy로 인하여 포논의 평균 자유거리가 줄어들기 때문이다. 지금까지 $Gd_2Zr_2O_7$연구가 분말형태를 처리하여 이용한 것과는 달리 본 연구는 $Gd_2Zr_2O_7$ 박막을 증착하여 그의 특성을 연구하였다. $Gd_2Zr_2O_7$ 박막을 yttria-stabilized zirconia (YSZ) 기판 위에 펄스화 레이저 증착 방법(Pulsed Laser Deposition)을 이용하여 제작하였다. 기판 YSZ와 $Gd_2Zr_2O_7$ 는 유사한 격자 상수를 가지기 때문에 epitaxial한 $Gd_2Zr_2O_7$박막을 증착시킬 수 있다. 산소 분압과 기판 온도 변화를 주어 epitaxial한 $Gd_2Zr_2O_7$ 박막을 증착하는 조건을 최적화하고, 박막의 결정성, 표면 거칠기를 XRD pattern과 AFM으로 확인하였다. 증착된 $Gd_2Zr_2O_7$ 박막의 열전도성은 3ω방법을 이용하여 측정하였다. 보고된 $Gd_2Zr_2O_7$ 의 열전도도와 비교 분석하여 기판과 박막의 경계면이 박막의 열전도도에 미치는 효과를 분석하였다. 한편 sputtering방법으로 증착된 $Gd_2Zr_2O_7$ 박막의 열전도도와 비교하여 증착 방법에 따른 박막의 특성을 비교 분석하였다.

**Dp-020** **SiC 나노분말의 크기에 따른 소결체의 여러 가지 특성 분석** 유 인근, 김 성훈(*국가핵융합연구소(NFRI).*) SiC는 금속보다 가벼우면서도 다이야몬드 다음으로 경도가 높기 때문에 산업적으로는 공구, 기계 및 장비의 부품, 우주선의 반사경, 저항발열체, 연마포, 화학반응 용기 등 다방면으로 활용되고 있다. 뿐만아니라 녹는점이 2700℃ 이상이고 1000℃ 이상의 고온에서도 기계 및 열적 특성이 우수하며 비교적 안정되어 있는 물질이다. 최근에는 중성자 조사에서도 금속성 재료보다 안정되고 방사화가 잘되지 않기 때문에 핵융합로 구조재료로 개발하기 위하여 많은 연구가 뒤따르고 있다. 핵융합로 구조재료 활용되기 위해서는 기계 및 열적특성과 저방사화 특성이 우수해야한다. 먼저 분말분석(크기, 구조, 불순물 농도 등)을 통해서 얻어진 결과를 토대

로 SiC 단미재료를 hot press법으로 제조했다. 제조된 시료의 기계적 특성과 미세구조 및 밀도 등과 분말 특성과의 상관관계를 분석했다. 그 결과, 소결체의 기계적 강도는 분말의 크기가 작을 수록 큰 것을 알 수 있었다. 미세구조 분석 결과, 분말이 작을 수록 결정이 보다 치밀화 되어 있는 것을 관찰 할 수 있었으며 밀도 또한 높은 것을 확인할 수 있었다. 그렇지만 분말에서 관찰된 Cu, Fe, Ba 등의 불순물과 산소의 농도가 시료의 기계적 특성에 미치는 영향은 파악하기가 쉽지 않았다.

**Dp-021** **Aging effects of Ar ion treatment on screen-printed carbon nanotubes** KIM Chang-Duk, JUNG Woo-Sik, LEE Hyeong-Rag[1](*School of Display and Chemical Engineering, College of Engineering, Yeungnam University. [1]Department of Physics, Kyungpook National University.*) The aging effect of argon ion treatment on the field emission (FE) and luminescent properties of screen-printed carbon nanotubes (SPCNTs : SWNT, DWNT, MWNT) with square pixels was examined, to further improve field emission displays (FEDs) applications. The emission current of carbon nanotubes was unstable during the initial anode voltage scans related to a type of aging process. However, the turn-on voltage was shifted to the high voltage side in the subsequent anode voltage sweep. The Fowler–Nordheim slopes were dynamically changed with successive anode voltage scans. The saturated turn-on voltage and emission current could be the result of a type of purification process during the field emission. Persistent problems associated with SP-CNTs such as bent or/and buried CNTs and the degradation of binder-residue-induced emission were improved as a result of the permanent straightening of CNTs and protruding CNTs from binders by the irradiation treatment. The findings here in suggest that ion irradiation treatment is an effective method for achieving uniform FE and for reducing the aging time of SP-CNTs.

**Dp-022** **Stimulated Stokes and Anti-Stokes Raman scattering Process of G-mode Vibrations in SWNT** 김 지희, 이 기주, 임 용식[1], E. H. Haroz[2], J. Kono[2](*충남대학교, 물리학과. [1]건국대학교, 응용물리학과. [2]3Department of Electrical and Computer Engineering, Rice University, USA.*) By using spectrum-resolved detection in pump-probe experiment, we have performed the variations of coherent G-mode oscillations in SWNT. Ultrashort pulses had sub-10fs pulse duration and the spectrum covered a 200 nm broad spectral range with a Kerr-lens mode-locked Ti:sapphire laser. The spectrum-resolved detection was performed by placing a series of 10nm-step Bandpassfilter in the probe beam path after the sample. The intensity of coherent G-mode oscillations as a function of detection wavelength varies around the center of the spectrum and it is related to stimulated anti-Stokes or Stokes Raman scattering process. Then by controlling the dispersion of ultrashort pulses, we could drive one process between SSRS and SARS.

**Dp-023** **Structural Properties of NiO Thin Films Deposited by Reactive Sputtering Method** SHIN Hye min, LEE Yun man, LEE Sang Hwa, KIM Jae-Yong(*Hanyang University, Department of Physics.*) Recently, nickel oxide (NiO) has been re-studied for a nano device material due to its excellent optical, electrical, and magnetic properties with chemical stability. NiO films have been used as an antiferromagnetic layer, p-type transparent conducting films, electrochromic display devices and functional sensor layer for a chemical sensor. In these senses, we investigated the crystalline structure and morphology of NiO thin films to study the reaction between the reactive gas and sputtered atoms on the substrate resulted in the formation of the compound layer. We have grown NiO thin films on Si (100) substrates using reactive magnetron sputtering method. Samples were deposited from a Ni target in different oxygen reactive flows. The total gas pressure and the distance between target and substrate were maintained constant. We also prepared NiO thin films at various substrate temperatures (from room temperature to 500 °C). The combined influence of oxygen flow and substrate temperatures on the crystalline structure and surface roughness of the films were investigated by using X-ray diffraction (XRD). The XRD measurements showed that almost single phase of NiO films were formed arranging with polycrystalline structure. The detailed studies on structural properties of NiO thin films will be presented.

**Dp-024** **Fabrication of Carbon nanotubes Field-Effect Transistor Using Inkjet Printing Technique.** LEE YoungHee, LEE DaeSik[1], LIM Seong Chu[1], KIM KiKang[1](*Department of Physics1, Center of Nanotubes and Nanostructured Composites2, SKKU Advanced Institute of Nanotechnology3 Sungkyunkwan University. [1]Sungkyunkwan University.*) Ink-jet printing is an important process for placing active electronics on plastic substrates. We demonstrate ink-jet printing as a viable method for large area fabrication of carbon nanotube CNT thin film transistors (TFTs). single walled-carbon nanotubes (SWCNTs) were dispersed in a bisolvent using Nafion. Although Not too high viscosity, CNT-INK is well purged we want the position. It is changed contact angle and surface tension that depend on water and isopropanol ratio. We have ink jetted the aqueous CNT solution on a siIicon oxides (SiO2) substrate using ink jet-printer that is equipped with a nozzle of 50 mm in a diameter. our devices exhibit field effect behavior with ON/OFF current ratio of up to 1000.

**Dp-025** **Method of Removing Bulge Formed by Nanoindentation of PMMA using Atomic Force Microscopy** SHIN ChaeHo, JEON InSu[1], JEON Seung Hee[1], PARK Junghwan[1], KHIM Zheong. G.[1](*Seoul National University, Interdisciplinary Program of Nano-Science and Technology. [1]Seoul National University, Department of Physics and Astronomy.*) Unavoidable formation of bulge during the indentation process is a serious obstacle in the application of atomic force microscope (AFM) indentation technique. Frequently the indentation pattern is made on a soft photoresistor layer such as polymethyl methacrylate (PMMA) by AFM. We found a new and easy method of removing bulge of PMMA formed during indentation process by using a solution of de-ionized (DI) water and isopropanol (IPA). We can remove bulge by applying an electric field (AC or DC) or sonication in this solution. The solution used in

this work is mixture of DI water and IPA. The mixing ratio of DI water and IPA is a very important factor. In this experiment, we found the adequate mixing ratio of DI water and IPA ranges from 1:5 to 1:9, and studied the effect of applied agitations such as electric field or sonication. Our experiment clearly demonstrates that this method can remove bulge of PMMA formed during AFM indentation process very effectively. This simple method of removing bulges can be a valuable process in manufacturing nano-devices by using AFM indentation.

**Dp-026** ***Ab Initio* Study of Point Defects in Si/Ge Core-Shell Nanowires** LEE Hyungjun, CHOI Hyoung Joon (*Department of Physics and IPAP, Yonsei University.*) We have investigated the effects of point defects in Si/Ge core-shell nanowires by first-principles calculations. We introduce either impurities or structural defects into Si/Ge core-shell nanowires and describe their atomic and electronic structures using norm-conserving pseudopotentials with Kleinman-Bylander's nonlocal projectors and the local density approximation for the exchange-correlation potential. Effects of point defects on the atomic and electronic structures in Si/Ge core-shell nanowires are analyzed by calculating band structures and local density of states.
* This work was supported by the KRF (KRF-2007-314-C00075) and by the KOSEF Grant No. R01-2007-000-20922-0. Computational resources have been provided by KISTI Supercomputing Center (KSC-2008-S02-0004).

**Dp-027** **Saccharide-Mediated Soft Cutting of Thin Mutiwall Carbon nanobutes** KYU Lee, YOUNG HEE Lee(*Department of Physics, Center for Nanotubes and Nanostructured Composites, Sungkyunkwan Advanced Institute of Nanotechnology, Sungkyunkwan University, Suwon 440-746, Republic of Korea.*) Commercially available, thin multiwall carbon nanotubes (T-MWCNTs) were inherently entangled and had long length, so it made difficult to disperse well. Length control of CNTs was important to disperse but also, to fabricate the one-dimensional building blocks for advanced nano-scale structures and fictionalization at CNTs ends. Length control of CNTs was achieved by the sacchared-mediated soft cutting. Shorted CNTs had ~ 300 nm length distribution, and Scanning electron microscopy (SEM), and dynamic light scattering (DLS) were used to determine the CNTs length distribution.

**Dp-028** **Resistive Switching Characteristics of Electrochemically Deposited Epitaxial Cuprous Oxide($Cu_2O$) Thin Films** PARK BaeHo, KANG Sung-Oong, HONG SaHwan, HWANG InRok, CHOI JinSik, CHOI JungAe, OH GwangTaek(*Department of Physics, Konkuk University.*) Electrochemical deposition method for fabricating epitaxial cuprous oxide ($Cu_2O$) thin films was introduced and resistive switching properties were also investigated. By controlling parameters of electrodeposition process (concentration of reacting solutions, temperatures of reaction, pH of solutions, applied potentials, etc.,), epitaxial $Cu_2O$ thin films with the thickness of ~100 nm in a diameter could be effectively deposited on a series of conducting substrates such as Pt, Au, and Ir. Growth mechanism of epitaxial $Cu_2O$ thin film was suggested on a basis of Stranski-Krastanov growth mode in which critical thickness of $Cu_2O$ thin film fabricated in our system was observed to be around 100 nm. Additionally, we studied the crystal structure and epitaxity of $Cu_2O$ thin films using TEM and HRXRD analysis. The resistive switching properties of epitaxially grown $Cu_2O$ thin films were characterized to have unipolar resistive switching properties.

**Dp-029** **Effect Of Hydrogen Amount On cm-long Single-Walled Carbon Nanotube (SWCNTs) Arrays** CHAE Seung Jin, JANG Jin Ho[1], LEE Il Ha, LEE Young Hee[2](*School of Nanoscience and Nanotechnology SKKU Advanced Institute of Nanotechnology (SAINT). [1]Department of Physics Center for Nanotubes and Nanostructured Composites (CNNC). [2]School of Nanoscience and Nanotechnology (SAINT), Department of Physics CNNC.*) Horizontally aligned single-walled carbon nanotubes (SWCNTs) were synthesized using laminar flow in the thermal chemical vapor deposition (CVD). Fe catalyst from $FeCl_3$ in ethanol has been used to produce long single-walled carbon nanotube (SWCNTs) arrays. The catalysts were prepared on the Si substrates by stamping. The mixture of $CH_4$, $H_2$, and Ar were introduced into chamber at 1000 $^oC$ during the growth. The extremely low flow rate of $CH_4$ (8 sccm) was one of the important factors. We controlled amount of hydrogen in order to investigate the hydrogen effect. This was confirmed by scanning electron microscopy (SEM), raman spectroscopy, and atomic force microscopy (AFM).

**Dp-030** **Improved Structure of Ti-Zr-Ni Quasicrystals by Hydrogen Absorption** KIM Jae-yong, JEON Jae-kyun, LEE Sanghwa, LEE Yun-man, SHIN Hye-min, CHOI Soo-bin, LEE Jung-gil, KIM Eui-kwon(*Hanyang University.*) Surprisingly, after absorption of hydrogen in Ti-Zr-Ni quasicrystals, we discovered that the coherence length of quasicrystal was increased approximately from 110 to 270 Å. Thin metallic ribbons of quasicrystals (20 μm thick) were prepared by an arc-melting and subsequent rapid quenching in an Ar atmosphere. Structural properties were investigated by using x-ray diffraction (XRD) and transmission electron microscope (TEM). The possible explanation for the stabilization of the quasicrytal phase by hydrogen will be discussed.

**Dp-031** **Thermal Conductance Measurement of Pd-CNT Composites using Micron-Sized Suspended Structure** 서 기성, 박 정훈, 조 명래, 이 병양, 홍 승훈, 박 윤(*서울대학교 물리천문학부.*) As carbon nanotubes (CNTs) have a unique structure and remarkable physical properties, CNT composites have attracted much attention from many researchers. Especially the thermal properties of composite materials incorporating CNTs have been studied intensively, as CNTs are known to possess excellent thermal transport properties [1-5]. For example, thermal conductivity of CNT is known to be much larger than that of metals such as Ag, Au, Cu and Al. As Pd has good wetting property on the CNT surface, thermal conductance measurement can be useful to investigate the in-

teraction between Pd and CNT. To study the thermal conductance of Pd-CNT composite, we have fabricated micron-sized suspended structures. By using e-beam lithography and metallization, two thermometers have been patterned on GaAs substrates. Thermal links made of Pd-only or Pd-CNT composite also have been patterned between the two thermometers. Then GaAs substrate has been selectively etched to form suspended structures. We will show the fabrication methods and preliminary measurement data on the thermal conductance of Pd-CNT composite.

† parkyd@phya.snu.ac.kr

[1] J.A. Eastman *et al.*, Appl. Phys. Lett. 78, 718 (2001).[2] S.U.S. Choi *et al.*, Appl. Phys. Lett. 79, 2252 (2001).[3] M.J. Biercuk *et al.*, Appl. Phys. Lett. 80, 2767 (2002).[4] R. Ramasubramaniam *et al.*, Appl. Phys. Lett. 80, 4647 (2003).[5] H.Q. Xia *et al.*, Appl. Phys. Lett. 94, 4967 (2003).

**Dp-032** **Graphene Single Electron Transistor fabricated by FIB** 노 현호, 이 상돈[1], 김 진희[1], 김 정구(*서울대학교, 물리천문학부. [1]한국표준과학연구원.*) Graphene, the monolayer of graphite, is a good candidate for validating 2-D quantum transport phenomenon. We investigate electrical transport through the mechanically exfoliated graphene for observing such phenomena. Especially, graphene nano structures fabricated by Focused Ion Beam(FIB), operate as single electron transistor. The device consists of a graphene island connected with narrow graphene constrictions. Laterally disposed local gates and conventional back gate are also employed to tune the device.

**Dp-033** **Enhanced Elastic Modulus and Thermo Mechanical Behavior ofMicromechanical Resonators from Metal-Carbon Nanotube Nanolaminates** 박 정훈, 김 영덕, 홍 승새[1], 이 병양, 이 승란, 장 재혁[2], 김 미영[2], 차 국린, 홍 승훈, 박 윤(*서울대학교 물리천문학부. [1]Department of Applied Physics, Standford University. [2]서울대학교 재료공학부.*) We report on the mechanical properties of nanolaminate composed of metallic thin-film and 2-D swCNT network, including the effects of thermally induced stress. Elastic properties are characterized by dynamic and quasi-static flexural measurements. Before flexural measurements, the resulting nanolaminates are fashioned into suspended doubly-clamped micromechanical beams with varying widths (<5 μm) and lengths (< 50 μm), in a scalable process. From both measurements, we observe a significant enhancement of the Young's modulus of Al/CNT nanolaminate compared to equivalent Al beams *sans* CNT. Furthermore, from large amplitude flexural measurements, beam resonators with Al/CNT nanolaminate have increased strengths and significant suppression of the nonlinear response. Such characteristics along with $\sqrt{(E/\rho)}$ values higher than that of Si and approaching that of AlN and SiC make these metallic-CNT nanolaminates an ideal candidate material for micro- and nano-mechanical resonator. Thermally induced stress in film determines thermo mechanical behavior of beam resonator; natural resonant frequency, quality factor and nonlinearity. We investigate the thermo mechanical behavior of beam resonators with Al/CNT nanolaminate compared to Al beam resonator using heating with applied DC power and temperature cycling by external heating source.

*This work is partly supported by Seoul R&BD program and MOCI

**Dp-034** **Synthesis of carbon nanotube fibers from vertical CVD** 김 태민, 송 우석, 김 유석, 이 미현, 장 성원, 최 원철, 박종윤(*나노물리연구실, 물리학과.*) 탄소나노튜브(carbon nanotube, CNT)의 다양한 합성 방법 중 화학기상증착법(chemical vapor deposition, CVD)은 아크방전법(arc-discharge), 레이저 증발법(laser-ablation)에 비해 양질의 탄소나노튜브의 합성이 가능하다. 하지만 극소량의 탄소나노튜브가 합성되기 때문에 대량생산이 어렵다는 단점을 지닌다. 최근 이러한 문제를 해결하기 위한 방법으로써 탄소 공급원(carbon feedstock)과 기체 형태의 촉매(catalyst)를 고온의 수직로(vertical CVD)에 연속적으로 주입하여 대량의 탄소나노튜브를 합성하고, 섬유형태로 제작하는 방법이 보고된바 있다. 이러한 방법으로 합성된 탄소나노튜브섬유는 약 40 N/tex의 우수한 기계적 강도를 지니기 때문에 앞으로의 항공우주산업, 자동차, 전기전자, 통신(안테나), 환경산업 등 다양한 분야에 응용가능성을 지닌다. [1, 2] 본 연구에서는 연속적인 탄소공급원과 탄소나노튜브의 수집이 가능한 수직로를 이용하여 고순도 탄소나노튜브를 대량 합성하였다. 탄소공급원인 에탄올(ethanol, $CH_3CH_2OH$)에 촉매인 페로센(ferrocene, $Fe(C_5H_5)_2$)을 0.25～10 wt%로 혼합한 후 수직로에 주입하였으며, 이때 수직로 내부의 온도를 1150 ℃로 유지시켰다. 에탄올과 페로센의 비율과 합성 활성제로 사용된 싸이오펜(thiophene, $C_4H_4S$)의 첨가에 따른 탄소나노튜브의 구조적 특성 변화를 연구 하였다. 합성된 탄소나노튜브의 기하학적 구조를 주사전자 현미경(scanning electron microscopy, SEM)과 투과전자현미경(transmission electron microscopy, TEM)을 통해 관측하였고, 순도 및 결정성의 정보를 열분석(thermogravimetrci analysis, TGA)과 라만 분광법(Raman spectroscopy)을 통해 분석하였다.

[참고문헌] 1. Ya-Li Li, Alan H. Windle. Science 304, 276 (2004) 2. Marcelo Motta, Alan H. Windle. Adv.Mater.19, 3721(2007)

**Dp-035** **PMMA/MWNTs composite nanofibers fabrication by electrospinning** 이 미현, 장 성원, 최 원철, 박 종윤(*성균관대학교 물리학과.*) Carbon nanotubes (CNTs) possess remarkable electrical and mechanical properties coupled with good chemical stability due to their unique nanostructure. Thus, polymer composites reinforced with CNTs are considered to have many engineering potentials such as battery electrodes and electronic devices. Electrospinning is a fast and simple process for fabrication of nanofibers. Polymer nanofibers can be utilizing in a wide range of applications such as filters, porous electrode, biomaterials, composite reinforcement. In this study, we attempted to produce electrospinned nanofibers by using the PMMA/MWNTs composite. It was well known that a nanofiber contained the CNTs will be enhanced in mechanical and electrical properties.[1, 2]. We investigated surface morphology and internal geometry of electrospinned PMMA nanofibers with axial aligned-MWNTs by scanning electron microscope (SEM) and transmission electron microscopy (TEM), respectively. The mechanical and electrical properties of PMMA/MWNTs composite nanofiber were measured by four-prove method and universal test machine (UTM).

**Dp-036** **NEMS(Nanoelectromechanical systems) Resonators Of Carbon Nanotube Network And Metal-Carbon Nanotube Composites** 조 성완, 박 정훈, 김 영덕, 이 병량, 이 승란, 홍 승훈, 박 윤(*서울대학교 물리천문학부.*) Carbon nanotubes have been spotlighted for its great potential as a promising material as well as the future candidate for nano-scale electronics and mechanics, with CNT's unique electrical and mechanical properties. NEMS structure combined with CNT can be applied to elucidate the nanotube's physical properties as well as further applications. Furthermore, metal based NEMS resonator structures are of interest due to higher optical reflectivity, ductility, and conductivity compared to insulator- and semiconductor- based NEMS structures. We present NEMS beam and torsional resonator structures fabricated from palladium and palladium-carbon nanotube (CNT) composite to discriminate the effect of CNT. In addition, we realize NEMS structures suspended by carbon nanotube on GaAs surface by adopting highly selective wet-etching and reactive ion etching techniques. The resonators are electro-statically driven and are detected at room temperatures under moderate vacuum conditions using optical modulation techniques.

**Dp-037** **Synthesis and characterization of SiC nanotube grown by using a metal catalyst** 정 민욱, 박 종윤, 최 원철, 백 재윤, 송 우석(*나노물리연구실, 물리학과.*) Silicon carbide nanotubes(SiCNT) were successfully synthesized by reaction of CH4 on melting surface of Si powder with Al catalyst. The synthesis was performed at 1300℃~1400℃ with Ar atmosphere. Structure and chemical composition of the synthesized SiCNT were studied by Scanning Electron Microscopy(SEM), Transmission Electron Microscopy(TEM), X-ray Diffraction(XRD) and Raman Spectroscopy (RS), where the outer diameter was 1μm and the length was several ten μm.

**Dp-038** **First-principles study of boron impurities in MgO** HAN Jinhee, CHOI Hyoung Joon(*Department of Physics and IPAP, Yonsei University.*) We study interstitial and substitutional boron impurities in MgO by an ab-initio density-functional pseudopotential method. The local density approximation is used for the exchange correlation energy and pseudo-atomic orbitals for wavefunction expansion. Structural deformations around the impurities are obtained by minimizing the total energy. Electronic structures near the impurities are analyzed to find out occurrence of any mid-gap state.

* This work was supported by the KRF (KRF-2007-314-C00075), the KOSEF Grant No. R01-2007-000-20922-0, and KISTI Supercomputing Center (KSC-2008-S02-0004).

**Dp-039** **Controlled growth of single-walled carbon nanotubes using Mo/Fe/Al tri-metal layer and their field emission characteristic** NGUYEN Tuan Anh, SONG wooseok, JUNG daesung(*성균관대학교 물리학과.*) Carbon nanotubes (CNTs) have intriguing electrical and physical properties, which make attractive building block in multifacet applications such as CNTs-based field effect transistor (CNTs-FET), logic gate, gas sensor, and solar cells. Specially, CNTs have been widely studied as field emitter, showing promising properties due to their high aspect ratio and chemical an thermal stabilities. Controlling the geometrical parameters such as length, diameter, and density of CNTs is a crucial issue for application of CNTs field emitter. Here, we investigated the control of CNTs geometry employing the Mo as a barrier layer on Fe/Al catalytic films, which confirmed by scanning electron microscopy, transmission electron microscopy, and resonant Raman spectroscopy with excitation wavelength of 514 nm and 633 nm. The decrease of CNTs density and diameter can be attributed to increasing the thickness of Mo top-layer from 0 to 5 nm. Additionally, we performed that the effect of Mo top-layer incorporated with Fe catalytic nanoparticles was studied by X-ray photoelectron spectroscopy and X-ray diffraction. Finally, the field emission characteristics of geometrically controlled-CNTs were carried out. This technique could be provided for application of field emission display that employ the CNTs.

**Dp-040** **Spinning of Carbon Nanotube Yarns from Vertically Aligned CNT Arrays** KIM Sang Yong, LEE Soonil, KOH Ken Ha(*Division of Energy Systems Research, Ajou University, Suwon, KOREA.*) The strategy of carbon nanotube yarns from vertically aligned carbon nanotube (VA-CNT) arrays was studied. VA-CNT arrays with the height was above 2 mm were synthesized using low pressure chemical vapor deposition(LPCVD) on silicon wafer sputtered aluminum and iron thin layer sequently. Acetylene as feedstock gas was supplied by mass flow controller to grow CNT arrays with argon gas. The grown VA-CNT arrays were characterized by scanning electron microscopy (SEM), thermogravimetric analysis (TGA) and Raman spectroscopy. We achieved the spinning of CNT yarns with 2.5 cm length from grown VA-CNT arrays and the study to elongate continuous yarns are going on progress.

**Dp-041** **Synthesis of thin graphite layers on Ni surface using remote RF plasma-enhanced CVD** KIM Eun Sung, HAN Gang Hee, KIM Ki Kang, CHAE Seung Jin[1], FETHULLAH Güneş[1], LEE Young Hee[2](*BK 21 Physics Division, Department of Physics, Center for Nanotubes and Nanostructured Composites (CNNC), Sungkyunkwan University. [1]BK 21 Physics Division, School of Nanoscience and Nanotechnology, SKKU Advanced Institute of Nanotechnology (SAINT), Center for Nanotubes and Nanostructured Composites (CNNC), Sungkyunkwan University. [2]BK 21 Physics Division, Department of Physics, School of Nanoscience and Nanotechnology, SKKU Advanced Institute of Nanotechnology (SAINT), Center for Nanotubes and Nanostructured Composites (CNNC), Sungkyunkwan University.*) We have synthesized thin graphite layers using remote RF plasma-enhanced chemical vapor deposition (PE-CVD) with gas mixture of $H_2$ and $C_2H_2$. By changing some of experimental variables like plasma power, process time and gas mixture ratio, we have tried to growth uniform thin graphite layers. For the synthesis, Ni 500 nm on the $SiO_2$ substrate which is deposited by E-beam evaporation was used. There was reduction process by $H_2$ gas before growth

process. After growth process, we added $H_2$ purging time to remove amorphous carbon on the synthesized layer. Graphite layers were characterized by high-resolution transmission electron microscopy (HRTEM), Raman analysis, field-emission scanning electron microscope (FESEM), and X-ray diffractometer (XRD).

**Dp-042** **전기 방사법을 이용한 PMMA/PAN/MWNTs 복합 나노섬유의 제작 및 물리적 특성연구** 장 성원, 이 미현, 김 태민, 최 원철, 박 종윤(*나노튜브 및 나노복합구조 연구센터, 성균관대학교 BK21 물리연구단.*) 전기 전도성 고분자(electrical conducting polymer)는 도핑 정도에 따라 부도체에서 도체 범위의 전도성을 가지는 재료로써 전자 소자 또는 인공 근육으로의 응용을 목적으로 전기적, 물리적 특성을 향상시키기 위한 연구가 활발히 진행되고 있다. 나노섬유의 제조방법은 템플레이트법, 자기 조립성을 이용한 방법, 레이저를 이용한 고속연신법과 전기방사법이 있다. 이 중에서도 전기방사법은 간단하고 대부분의 고분자 용액으로부터 나노섬유 제조가 가능하며, 고분자뿐만 아니라 무기물 및 복합소재의 방사가 가능하다는 장점을 지닌다. 고분자 소재 중 전기 전도성 고분자(electrical conducting polymer)는 도핑 정도에 따라 부도체에서 도체 범위의 전도성을 가지는 재료로써 전자 소자 또는 인공 근육으로의 응용을 목적으로 전기적, 역학적 특성을 향상시키기 위한 연구가 활발히 진행되고 있다. 이 중 대표적인 PAN(poly acrylonitrile)은 전기 전도성과 보온성, 탄력성이 우수한 반면 강도가 약한 단점을 지닌다. 이러한 단점을 보안하기 위해 carbon nanotubes(CNTs)와의 복합체를 제조함으로써 기계적 강도를 향상 시킨 연구 결과가 보고된바 있다. 본 연구에서는 PAN과 multi-walled caron nanotubs (MWCNTs)가 혼합된 복합 나노섬유의 투명도(transparency)와 강도를 향상시키기 위하여 PMMA(polymethyl methacrylate)를 첨가하여 나노섬유를 전기방사법으로 제작 하였다. 제작된 나노섬유의 기하학적 구조를 주사전자 현미경(scanning electron microscope)과 투과전자 현미경 (transmission electron microscope)을 통해 분석하였고, 전기적 특성을 4-prove을 이용하여 측정 하였다.
참고 문헌 1. Min Kyoon Shin et al., Sensors and Actuators B, 134, 122 (2008). 2. Yuya Ishii et al., Materials Letters, 62, 3370 (2008)

**Dp-043** **The active resonator array for artificial cochlea** PARK Hee Chul, SONG Taegeun, AHN Kang-Hun(*충남대학교, 물리학과.*) Inspired by the outstanding frequency selectivity of the ear, we propose an artificial cochlea based on the electromechanical system. The basilar membrane is mimicked by the array of resonators which have different resonant frequency depending on the position. The active process in the hair cells in the cochlea is mimicked by an electronic feedback loop. We show that the proposed system shows enhanced frequency selectivity with the aid of the implemented active feedback loop. Through finite element simulation, we design an experimentally realizable structure for the artificial cochlea.

**Dp-044** **Density functional theory를 이용한 Orthorhombic-NiSi/Si (010)에 Pd 원자 치환의 구조 연구** 김 대희, 서 화일[1], 김 영철(*한국기술교육대학교, 신소재공학과. [1]한국기술교육대학교, 정보기술공학부.*) CMOS에서 source, drain, 그리고 gate의 접촉 저항을 감소시키는 금속 실리사이드 물질 중에서, NiSi는 낮은 형성 온도, 적은 실리콘 소모량, 선 폭이 작아짐에 따른 면저항의 감소 등의 장점 때문에 45 nm 노드에 적용되고 있고, 22 nm 노드까지 적용될 것으로 예상된다. NiSi는 $TiSi_2$와 $CoSi_2$보다 열 안정성이 우수하지 못하다. NiSi의 열 안정성을 개선시키기 위하여 금속을 첨가한 연구가 진행되어오고 있다. Y. C. Kim *et al.*은 LEAP를 이용하여 NiSi/Si 구조에 Pd 원자를 첨가하게 되면 Pd 원자가 계면 쪽으로 편석 (segregation) 된다고 보고하였다. 본 연구는 Y. C. Kim *et al.*의 실험적 결과를 계산으로 평가하기 위해 orthorhombic-NiSi (010)과 Si (010)을 접합시켜 계면을 형성한 후 Pd 원자를 첨가하였다. NiSi의 대표적인 B2와 orthorhombic 구조 중에서 에너지 관점에서 안정한 orthorhombic-NiSi (010)를 Si (010)과 접촉시켰으며, 또한 Si 기판과의 에피택시 접합 (epitaxy contact)을 위하여 orthorhombic-NiSi (010)의 격자 상수를 *a* 축과 *c* 축으로 각각 +6.15 %, –1.36 % 수정하였다. 1x4x1 orthorhombic-NiSi (010)와 1x2x1 Si (010) 두 초격자 구조를 접합시키면 계면 사이의 거리가 1.6 Å이 된다. 이는 orthorhombic-NiSi (010) 단위 격자 간의 거리와 유사하게 두 초격자 구조 사이의 거리를 형성한다는 것을 알 수 있다. Orthorhombic-NiSi/Si (010) 초격자 구조에 Pd 원자를 치환하게 되면 Si 원자보다 Ni 원자 자리에 치환되는 것이 에너지 관점에서 안정하였으며, 또한 계면에 위치한 Ni 원자 자리에 Pd 원자가 치환되었을 때 에너지 관점에서 가장 안정하였다.

**Dp-045** **Surface Energy Calculation of ZnO and ZnS** 나(NA) 성호(Sung-Ho), 박(PARK) 철홍(Chul-Hong)(*Pusan National University, Physics/RCDAMP.*) The surface energy of major surfaces of ZnO are estimated by the first principles calculation based on the density functional theory. Selected surfaces are (0001), (101'0), (112'0), (101'1), and (112'1) surfaces of wurtzite ZnO. (110) surface of zincblende ZnO is included for comparison. ZnS surfaces are studied similarly.

**Dp-046** **Monte-Carlo simulation of electron penetration in solids** LEE Cheol Eui, LEE Su Cheol, LEE Kyu Won, YOON Sungmin(*Department of Physics, Korea University.*) Characteristics of electron penetration in solids, such as energy losses and distributions of scattered electrons, have been calculated by using a Monte Carlo method. Following previous studies, the Gryzinski's model was employed to calculate the inelastic scattering cross-section. The elastic scattering cross section was obtained from the modified screened Rutherford cross section in comparison to the Mott cross section, which gives a much better backscattering probability in Aluminum. Back scattered electrons from silicon give rise to electron beam broadening in PMMA/Si film. While the electron beam broadening was narrowed with increasing incident energy, overspreading became serious. The overspreading effect was reduced by using a blocking layer.

**Dp-047** **Effects of a Single In Adsorbate on the Au/Si(111)-√3x√3 Surface: DFT Calculations** PARK Jae Hwan, KANG Myung Ho(*포스텍 물리학과.*) We investigate the effects of a single In adsorbate to the structural and electronic properties of the Au/Si(111)-√3x√3 surface by using density-functional theory

calculations. It is found in our 3x3 supercell calculations that the In atom prefers a Au-free T4 site as the most stable site. We find there is a diffusion pathway from a T4 site to another T4 site with a low energy barrier of about 0.3 eV, which provides a way of explaining the room-temperature hexagonal STM images of In atoms observed at low In coverages as an image of a rapidly hopping In adsorbate. The changes in band structure induced by In adsorption are quantified and used to discuss the In-derived elimination of the domain walls of the Au/S(111) surface.

**Dp-048** **Surface and Photoluminescent examinations of lithium incoporated $GdVO_4:Eu^{3+}$ phosphor grown by pulsed laser deposition** BAE J. S, PARK S. S, KIM J. P, HONG T. E, JEONG J. H[1], PARK S[2](*Busan center, Korea Basic Science Institute, Busan 609-735, Korea. [1]Department of Physics, Pukyong National University, Busan 608-737, Korea. [2]Department of Physics, Pusan National University, Busan 609-735, Korea.*) The influence of lithium doping on the crystallization, the surface morphology, chemical states, ion distribution and the luminescent properties of pulsed laser ablated GdVO4:$Eu^{3+}$ thin film phosphors grown on GaN/$Al_2O_3$ substrate were investigated by using x-ray diffraction (XRD), scanning electron microscope (SEM), x-ray photoelectron spectroscopy (XPS), secondary ion mass spectroscopy (SIMS), and spectrophotometer, respectively. The crystallinity, the surface morphology, and the photoluminescence of phosphors highly depended on the Li-doping and deposition condition, in particular, a deposition temperature and oxygen pressure. $Li^+$-doping was found to be effective not only for the enhanced crystallinity but also for the luminescent brightness of $GdVO_4:Eu^{3+}$ thin film phosphors. The enhanced luminescence intensity caused by the additional Li-ion doping may be attributed to the efficient energy transfer due to better crystallization. The details of mechanism will be discussed in this presentation. Furthermore, XPS measurements showed two Gaussian components of O1s spectrum assigned to Gd-O and V-O, respectively, in all films. The SIMS analysis indicated that Li ion were detected for Li-doped $GdVO_4:Eu^{3+}$ film and there was not concentration variation of other elements.

**Dp-049** **The electron density and interface roughness dependant electrical properties of ferroelectric semiconductor $PbZr_{0.52}Ti_{0.48}O_3$ thin films** KIM Hyunjun, PARK Sungmin, KWON Hyosang, LI Xiaolong, PAK Jaymoon, SONG Sanghoon, KIM Hyunjung, CHEONG Hyeonsik, PARK Gwangseo, PARK Doyoung(*Department of Physics, Sogang University.*) We have investigated the electron density and interface roughness dependant electrical properties of ferroelectric semiconductor $Pb(Zr_{0.52}Ti_{0.48})O_3$ thin films on Pt(111)/Ti/$SiO_2$/Si substrate. It is found that their crystal symmetry belongs to rhombohedral by using Raman spectra. In order to examine the electron density (equally can be considered as mass density) and the roughness of the interfacial layer, a grazing incidence x-ray specular reflectivity (XRR) was employed. Pt/PZT/Pt capacitor showed two significant electrical properties. The one is that the hole concentration increases with the decrease of the electron density. The other one is that the built-in voltage, which arises from the junction between PZT layer and the bottom Pt electrode, increases as the interface roughness increases. In this study, we will present, for the first time, that the electron density and the interface roughness extracted from the XRR results can be used to investigate the change of the hole concentration and the built-in voltage.

**Dp-050** **Study of ZnO Self-limiting growth** NOH S.J., LEE D.H., KWON S.R., LEE S.K., LEE J.H., KIM H.S., HYUN J.W.(*Department of Applied Physics, Dankook University.*) Zinc oxide (ZnO) has rapidly emerged as a promising material for future devices such as transparent flexible display, semiconductor, and optoelectronics owing to its large band gap of 3.37 eV(large exciton binding energy of 60 meV). In this study, we will report the self-limiting growth of ZnO films on various substrates by using Atomic Layer Deposition (ALD) at low temperatures. Diethylzinc (DEZn) was used as the zinc precursor, $H_2O$ as the oxidant, and argon as the carrier and purge gas. Self-limiting growth of ZnO was successfully obtained. The deposition characteristics and film properties were investigated using field emission scanning electron microscopy (FESEM), X-ray diffraction (XRD), auger electron spectroscopy (AES), etc.. The detail results will be presented.
* This work was supported by the Korea Science and Engineering Foundation (KOSEF) grant funded by the Korea government (MEST)(No.R01-2008-000-10294-0).

**Dp-051** **Characterization of Al-doped ZnO deposited on the polymer substrate treating with plasma** KIM JONG-PIL, PARK SANG-SIN[1], BAE JONG-SEONG, CHO CHAE-RYONG[2] (*Nano-Surface Technology Research Team, Korea Basic Science Institute. [1]Nano-Surface Technology Research Team, Korea Basic Science Institute, Department of Physics, Pusan National University, Busan 609-735. [2]Department of Nanomedical Engineering, Pusan National University,.*) Plasma treatment of polymer has been utilized broadly in surface modification to increase material adhesion and improve compatibility, etc. It involves the interaction of the plasma-generated excited species with a solid interface and results in a physical and/or chemical modification of the first few molecular layers of the surface, while maintaining the properties of the bulk. In this study, Polyethylene terephthalate (PET) and polyethersulfon (PES) films was treated by atmospheric pressure plasma. $O_2$/Air gas was used with maintained constant gas flow rate. The exposure time fixed at 10 min. Then, we deposited Al-doped ZnO (AZO) on the polymer by RF sputtering process. The effects of the plasma modification were investigated in order to understand the adhesion with Al-doped ZnO. We described the phase formation, chemical bonding states, and optical properties of Al-doped ZnO thin films. Surface chemical composition analysis and binding energy was performed using X-ray photoelectron spectroscopy (XPS) and Fourier transform infrared spectroscopy(FT-IR). Surface morphology was analyzed by scanning electron microscopy (SEM) and atomic force microscopy (AFM).

* Authors to whom the correspondence should be addressed jpkim@kbsi.re.kr
* This work was supported by grant the SMEs Technology Innovation Program (S1028273)

**Dp-052** **Physical Properties of NO Molecules on MgO (100) Powder Surface Measured by Adsorption Isotherm** LEE Jeonggil, KIM Euikwoun, LEE Sangwha, SHIN Hyemin, KIM Jae-yong, LEE HyunHwi[1], LEE Dongryul[1](*Hanyang university, Department of Physics. [1]Pohang Accelerator Laboratory.*) The adsorption isotherm of gas molecules on adsorbent has drawn much attention because of the useful information about the fine structure of the adsorbed gas molecules on surface. We investigated nitric oxides (NO) gas molecules on MgO surface to study the physical / chemical interaction of NO molecules adsorbed on MgO surface. The meso- sized MgO(100) powder were synthesized by rf-power induction method. NO adsorption isotherm on MgO data were measured by using a computer-controlled isotherm apparatus below the triple point (108.9K). The structure of NO gas on MgO surface was investigated by X-ray diffraction at High Flux Materials Science Beamline (PAL-5A) of the Pohang Accelerator Laboratory. The adsorption isotherm data showed that NO molecules form two atomic layers on a MgO surfaces. The atomic layer formation was confirmed by analyzing the thermodynamic properties including 2-dimensional compressibility and the heat of adsorption values. The X-ray diffraction results revealed that the NO molecules form an 1 x 1 commensurated structures on MgO.

**Dp-053** **Density functional theory를 이용한 Si (001) 표면의 In 원자 흡착 연구** 김 대현, 김 대희, 백 승빈, 서 화일[1], 김 영철(*한국기술교육대학교, 신소재공학과. [1]한국기술교육대학교, 정보기술공학부.*) J. Nogami et al.은 III 또는 IV 족 원자가 흡착된 Si (001) 표면을 STM으로 분석하여 III 또는 IV 족 원자가 일차원으로 성장하는 것을 보고하였다. 본 연구는 DFT (density functional theory)를 이용하여 III 또는 IV 족 원자 중에서 In 원자를 Si (001) 표면에 흡착시켰을 때 에너지 관점에서 안정한 표면 흡착 위치를 찾았다. Si (001)-(2×1) 표면에서 In 원자는 평행한 두 개의 dimer 사이, dimer 열 사이, 나란한 두 개의 dimer 사이가 국부적으로 안정한 위치라는 것을 알 수 있었다. 세 개의 위치 중 에너지 관점에서 가장 안정한 위치는 평행한 두 개의 dimer 사이였다. 다른 두 위치에서 평행한 두 개의 dimer 사이로 In 원자가 이동할 때의 energy barrier는 각각 0.005 eV, 0.1 eV로 낮다. 따라서 다른 두 위치에 흡착된 In 원자는 평행한 두 개의 dimer 사이로 쉽게 이동한다. In 원자를 평행한 두 개의 dimer 사이에 흡착시키고, 두 번째 In 원자를 가능한 위치들에 추가적으로 흡착시켰다. 평행한 두 개의 dimer 사이에 위치한 In 원자에서 Si valley를 건너뛴 평행한 두 개의 dimer 사이에 추가로 In 원자가 흡착될 때 가장 안정하다.

**Dp-054** **증착 조건에 의한 YSZ 박막의 결정성에 관한 연구** 박 상신, 배 종성[1], 정 의덕[1], 김 영철, 박 성균(*부산대학교 물리학과. [1]한국기초과학지원연구원 부산센터.*) Epitaxial 한 산화물 박막을 만들기 위한 여러 가지 방법 중Yttrium-stabilized zirconia (YSZ) 박막을 완화층으로 이용한 연구가 활발히 진행되고 있다. 특히 양질의 산화물 박막을 증착하기 위해서는 완만한 표면을 가진 epitaxial한YSZ 완화층이 필요하다. [1] 본 연구에서는 epitaxial한 YSZ 완화층의 초기 성장 매커니즘을 알기 위해서 pulsed-laser deposition를 이용하여YSZ 완화층을 성장시켰다. 증착 시 체임버 내의 산소 분압과 증착 시간을 변화시켜 $Al_2O_3$ 기판 위에 증착된 YSZ 박막은 체임버 내의 산소 양에 따라YSZ 박막의 성장 방향이 바뀌는 것을 x-ray diffraction 를 통해 확인할 수 있었다. 진공 중에서 증착한 YSZ박막은 (111) 방향으로 성장하였으나 산소 주입 후, (002) 방향의 peak도 확인할 수 있었다. 또한 산소의 양이 증가할수록 (111) 방향의 peak은 감소하였고 (002) 방향의 peak은 점차적으로 증가하였다. YSZ 박막의 성장 방향은 산소 분압 뿐 아니라 증착 시간에 따라서도 차이를 보였다. 증착 시간이 5배 증가한 경우 (002) 방향의 반치폭은 13% 줄어들었으며, peak 면적은 2배 증가하였다. 하지만 증착 시간이 10배로 증가하게 되면 (002) 방향으로의 성장은 오히려 감소하게 되고 (111) 방향의 반치폭이 줄어들며, peak 면적도 증가하였다. 본 실험에서와 같이 $Al_2O_3$ 기판 위에 증착한 YSZ 박막은 체임버 내의 산소 분압과 증착 시간에 의해 prepared orientation이 바뀌는 것을 알 수 있었다.

[1] G. Garcia, J. Santiso, J.A. Pardo, A. Figueras, Applied Surface Science, 233, 191 (2004)

**Dp-055** **First-Principles Study Of Clean Ge(001) Surface And Its Defect Structure.** HONG Suklyun, SONG Jaehoon, SUNG Dongchul, RYOU Junga, KIM Sehun[1], JUNG Soon Jung[1](*Sejong Univ., Physics. [1]KAIST, Chemistry.*) The weakness of the $\pi$-bond across the Ge dimer on the Ge(001) surface allows the dimer to be tilted, which imparts a zwitterionic-like property to the dimer. In the scanning tunneling microscopy (STM) images, these buckled dimer regions having *c*(4x2) and occasionally *p*(2x2) structures are observed with symmetric dimer regions having 2x1 structure. Recently, the empty-state STM images for the clean Ge(001) surface were clearly observed [2]. The empty-state images show a strong bias dependence and are very similar to the filled-state images at higher bias voltages. To explain this resemblance at high biases, we perform density functional theory (DFT) calculations for the clean Ge(001) surface. Examining the projected density of states, we explain well the bias dependence of the STM images, and the simulated images are in accordance with the experimental observation. It is well known that the clean Si(001) surface has several types of point defects—type *A*, *B*, and *C*. Type-*A* and *B* defects have been identified as one and two-dimer vacancies (DVs), respectively, while type-C defects are clearly identified as dissociated water molecules [2]. Similarly to the Si(001) case, we investigate those surface defect types on the clean Ge(001) surface. DFT calculations are done for the Ge(001) surface with one and two DVs, and adsorbed water molecules, respectively. The simulated images are compared with the available experiment and with the Si(001) case.

**Dp-056** **Electronic and Optical Properties of $Al_2O_3/SiO_2$ Dielectric Thin Films and Compared to $\gamma$-$Al_2O_3$ Thin Films** 이 은경, DAHLANG Tahir, 최 은혜, 강 희재(*충북대학교, 물리학과.*) $Al_2O_3/SiO_2$ thin films as gate dielectrics have been proposed to

overcome the problems of tunneling current and degradation mobility in achieving a thin equivalent oxide thickness. An extremely thin $SiO_2$ layer is used in order to separate the carrier in MOSFET channel from the dielectric field fluctuation caused by phonons in the dielectric which decreases the carrier mobility. The electronic and optical properties influenced the device performance to a great extent. In this study, the band gap and the optical properties of $Al_2O_3/SiO_2$ thin films were obtained from the experimental inelastic scattering cross section of reflection electron energy loss spectroscopy (REELS) spectra. The bandgap of $Al_2O_3/SiO_2$ thin films slightly increases from 6.5 eV to 7.5 eV after annealing due to the bond structure change in of $Al_2O_3/SiO_2$. The optical properties' e.g., index refractive ($n$), extinction coefficient ($k$) and dielectric function ($\varepsilon$) of $Al_2O_3/SiO_2$ after annealing were obtained from REELS spectra by using QUEELS-$\varepsilon(k, \omega)$-REELS software shows similarity electronic and optical properties of $\gamma$-$Al_2O_3$.

**Dp-057** **Electronic and Optical Properties of Zr Silicate Thin Films** DAHLANG Tahir, 이 은경, 최 은혜, 강 희재(*충북대학교, 물리학과.*) Zr silicates thin films as gate dielectrics have been proposed to overcome the problems of tunneling current and degradation mobility in achieving a thin equivalent oxide thickness. The electronic and optical properties influenced the device performance to a great extent. In this study, the electronic and optical properties of Zr silicates $(ZrO_2)_x(SiO_2)_{1-x}$ (x=1, 0.75, 0.50, 0.25)thin films were obtained from the experimental inelastic scattering cross section of reflection electron energy loss spectroscopy (REELS) spectra. The bandgap of $(ZrO_2)_x(SiO_2)_{1-x}$ thin films was 5.30±0.05 eV and increase to 5.85±0.05eV for x=0.25. The optical properties, e.g., dielectric function ($\varepsilon$), index refractive ($n$), and extinction coefficient ($k$) of $(ZrO_2)_x(SiO_2)_{1-x}$ thin films were obtained from REELS spectra by using QUEELS-$\varepsilon(k, \omega)$-REELS software. The effects on the optical properties of the $ZrO_2$ composition on films are discussed. In addition, some other recent experiments are compared with our results.

**Dp-058** **First-principles study of atomic and electronic properties of graphene on metal (Ru, Pt) slabs** GOH Jung Suk, CHOI Hyoung Joon(*Department of Physics and IPAP, Yonsei University.*) We have studied contact properties of graphene-metal systems for two metals, Ru and Pt based on first-principles methods. We determine atomic superstructures of these systems in considering commensuration which experimental results represent. Our analysis shows equilibrium distances, potential barriers and cohesive energies of graphene-metal systems. We compare the experimental results of the scanning tunneling microscopy with calculating local density of states. To understand electronic band structures of the graphene layer on metal surfaces, we simulate angle-resolved photoemission spectroscopy.

* This work was supported by the KRF (KRF-2007-314-C00075) and by the KOSEF Grant No. R01-2007-000-20922-0. Computational resources have been provided by KISTI Supercomputing Center (KSC-2008-S02-0004).

**Dp-059** **자성체/초전도체 이층박막 La0.7Sr0.3MnO3/YBa2C3O7-δ와 LaNiO3/YBa2C3O7-δ에서 근접효과와 전기적/자기적 특성 분석** DHO Joonghoe, KI Sanghoon, ZHANG X. D., LI Jian(*경북대학교 물리학과.*) 자성체/초전도체 이층박막 La0.7Sr0.3MnO3/YBa2C3O7-δ와 LaNiO3/YBa2C3O7-δ에서 근접효과와 전기적/자기적 특성 분석, 기상훈, 리찌엔, 장사오동, 도중희*(경북대학교 물리학과) 강자성체(F)와 초전도체(S)를 근접시키면 경계면에는 서로 경쟁하는 질서도 매개변수를 가지게 된다. 즉, 강자성체는 전자의 스핀들이 서로 같은 방향으로 정렬하려고 하는 반면, 초전도체는 쿠퍼쌍을 이루는 전자들의 스핀은 서로 반대로 정렬하게 되기를 요구한다. 지금까지 자성체로부터 초전도체로 스핀 편극된 전도전자들의 주입에 대한 연구와 두 물질 사이의 근접효과에 대한 연구결과들이 많이 보고되어 왔다. 예를 들면, SrRuO3/YBa2C3O7-δ와 같이F-S구조 이층박막에서 초전도성을 보이는 임계온도가 초전도체 단일박막보다 낮은 것으로 보고되었다. 두 물질을 근접시킴으로서 관찰되는 현상은 계면거침도, 계면확산, 계면합금반응과 같은 경계면에서의 무질서도에 의해 쉽게 영향을 받는다. 이번 실험에서는 서로 같은 결정구조와 비슷한 격자 상수를 가지는 산화물 이층박막 La0.7Sr0.3MnO3(LSMO)/YBa2C3O7-δ와 LaNiO3(LNO)/YBa2C3O7-δ를 제작하고 전기적/자기적 특성을 조사하였다. 여기서는 초전도체 YBCO를 반금속성 강자성체 LSMO와 금속성 상자성체 LNO의 두 가지 다른 성질의 자성체로 근접을 시켰다. 두 가지 형태의 시료는 (100)SrTiO3기판 위에 펄스 레이저 증착법을 이용하여 에피탁시 이층박막으로 성장 시켰다. 이렇게 제작된 이층박막의 표면형상, 박막 두께, 성분분석, 결정구조를 SPM, SEM, EDX, XRD 등을 이용하여 분석하였다. 이층박막 LSMO/YBCO, LNO/YBCO의 전기적/자기적 특성을 온도와 자기장의 함수로 측정하였다. 두 가지 형태의 이층박막의 초전도 임계온도가 단일 YBCO박막의 초전도 임계온도와 비교했을 때 약간 낮아지는 것을 확인하였고 외부 자기장 하에서 온도에 따른 저항의 변화를 측정하였다.

**Dp-060** **Fabrication of YBCO weak links by a focused ion beam technique** HONG Sung-Hak, LEE Soon-Gul(*Korea University.*) This presentation reports the results of our recent study on the characteristics of $YBa_2Cu_3O_7$ weak links prepared by a focused-ion-beam (FIB) milling technique. $YBa_2Cu_3O_7$ thin films were deposited on sapphire substrates by a pulsed laser deposition method at 400-mtorr $O_2$ partial pressure and 790 ℃ substrate temperature. Prior to the weak-link fabrication, 130~150nm thick $YBa_2Cu_3O_7$ films were patterned into 2~5 mm bridges by a photolithography-with-argon-ion-milling technique. Superconducting weak links were formed on the prepatterned microbridges by FIB milling. We prepared various types of weak links and compared their transport properties. They are FIB-defined nano-constrictions, focused-ion-needle-beam scribed weak links, and the bridges patterned on FIB-indented lines of substrate. We studied the current-voltage characteristics, the critical current density and the normal-state resistance as functions of temperature. The bridges showed variety of transition properties including Josephson coupling and flux flow behaviors. Details of sample preparation and the bridge properties will be discussed.

**Dp-061** **Experimental study on the transision properties of $MgB_2$ nanobridges** 홍 성학, 이 순걸, 강 원남[1], 김 동호[2](*고려대학교. [1]성균관대학교. [2]영남대학교.*) The technology to produce reliable and reproducible $MgB_2$ Josephson junctions is a prerequisite for electronic application of $MgB_2$ films. Recently many research groups have tried to make various types of $MgB_2$ Josephson elements, such as in-situ deposited trilayer structures with an artificial barrier and focused-ion-beam (FIB) defined bridges. Up to the present the properties of those were not good enough for application mainly due to low $T_c$ and poor reproducibility. In this work, we have studied fabrication and transition properties of $MgB_2$ nanobridges with and without a natural grain boundary crossing the bridges by using the FIB writing technique. The thickness of $MgB_2$ films was 500-700 nm and the nominal width of the bridges was 100-150 nm. The success rate of the bridge fabrication was nearly 100% and all the fabricated bridges had $T_c$ of 38-40 K. Very near $T_c$, current-voltage (I-V) curves showed RSJ behaviour, implying that the Josephson effect was dominating, and at low temperatures, they showed large excess currents due to the flux flow effect. More details on the fabrication process and the nanobridge properties will be discussed.

**Dp-062** **Detection of Fluxoid Quantum in a Superconducting Niobium Micro Ring Using a Micro Hall Array Sensor** KAHNG Yung Ho, JOO Sungjung[1], KIM Yun Won[2], LEE Kyu Won, KIM Mun Seog, HONG Jinki[1], RHIE Kungwon[1], LEE Soon-Gul[1], CHOI Jae-Hyuk(*KRISS. [1]Korea University. [2]KRISS and Korea University.*) Fluxoid quantization in superconductors has been experimentally observed since 1961. Tubular samples were used in early experiments rather than rings due to technical difficulty and this had complicated the interpretation of the data. With development of lithographic technology, micro-size-patterned thin film samples became available recently for studying superconducting properties. For such samples, magnetic detection is also a technical challenge to overcome because the quantized fluxoid signal is very small. Here we report detection of fluxoid quantum in a superconducting niobium micro ring using a micro hall array sensor where niobium ring was directly patterned onto a silicon dioxide pacified micro hall sensor. The whole measurements were done in a physical property measurement system (PPMS, Quantum Design, Inc.). We also describe an experimental scheme to control magnetic field with ten times higher resolution than the apparatus specs by using a simple current divider.

**Dp-063** **Mixed rare rarth HTS (Nd-Eu-Gd)$Ba_2Cu_3O_{7-d}$ thin films grownth by pulsed laser deposition for coated conductor** KO Rock-Kil, BAE Sung-Hwan[1], JUNG Myung-Jin[1], JANG Se-Hoon, SONG Kyu-Jeong[2], SOHN Myung-Hwan, OH Sang-Soo, KIM Young-Cheol[3](*Korea Electrotechnology Research Institute. [1]Seoul National University, Materials Science &Engineering. [2]Chonbuk National University, Physical Education. [3]Pusan National University, Physic.*) In order to investigate the possibility of using mixed rare earth $(Nd_{1/3}Eu_{1/3}Gd_{1/3})Ba_2Cu_3O_{7-x}$ (NEG123) as the superconducting layer of the HTS coated conductor, the NEG123 thin film was deposited epitaxialy on LAO(100) single crystal and IBAD_YSZ metal templates by pulsed laser deposition. Systematic studies were carried out to investigate the influences of deposition parameters of PLD on the microstructure, texture and superconducting properties of NEG-123 coated conductor. Deposition at oxygen partial pressure of 600 mTorr was needed to routinely obtain high quality NEG123 films with $J_C$'s (77 K) over 2 MA/cm$^2$ and Tc's over 90 K. We verified from magnetization study that the NEG123 has an improved in-field Jc as the field increases at temperatures between 10 K and 77 K compared with Gd123. The $J_C$ (77 K, self field) and the value of onset $T_C$ of NEG123 thin film on LAO substrate was 4.0 MA/cm$^2$ and 92 K, respectively. We fabricated coated conductors with NEG123 film as the superconducting layer which have Ic and Jc over 40 A/cm-width and 1.6 MA/cm$^2$ at 77 K, self field. This study shows the possibility of using NEG123 film as the superconducting layer of the HTS coated conductor which can be used in high magnetic field power electric devices.

**Dp-064** **Initial Suppression of $T_c$ in Optimally Doped $Bi_2Sr_{1.6}Re_{0.4}Cu_{1-x}Zn_xO_{6+d}$ (Re = La, Pr, Nd, Sm, and Eu)** KIM G.C., PARK I., KIM Y.C.(*Department of Physics, Pusan National University.*) We have investigated the initial suppression of the superconducting transition temperature, $T_c$, by Zn substitution in $Bi_2Sr_{1.6}Re_{0.4}Cu_{1-x}Zn_xO_{6+d}$ (Bi(Re)-2201) with single $CuO_2$ plane. In our study, we proposed a phase diagram of Bi(Re)-2201 as a function of the degree of disorder outside the $CuO_2$ plane. The initial suppression rate of $T_c$, described well by considering the enhancement of pseudogap by the out-of-plane disorder, increased with the degree of disorder.

**Dp-065** **Temperature Dependence of Critical Current Density in Iron –Based High-$T_c$ Superconductor $SmFeAsO_{0.85}$** AHMAD Dawood, PARK Park, KIM G.C., REN Zhi-An[1], KIM Y.C.(*Department of Physics, Pusan National University. [1]National Laboratory for Superconductivity, Institute of Physics.*) Critical current density of new iron-based high $T_c$ superconductor made by solid state reaction was obtained by Bean's critical state model from magnetization data. The flux pinning force density follows the scaling behavior at different temperature, which is the sign of single pinning mechanism activated at all temperatures. Temperature dependence of critical current density analyzed by collective pinning model shows that pinning sites due to spatial fluctuation of the mean free path of the charge carrier have the most prominent role in flux pinning properties of $SmFeAsO_{0.85}$ superconductor

**Dp-066** **초전도-강자성체 접합 구조의 상태 밀도 계산** 홍 승환, 이 나영, 최 한용(*성균관대학교 물리학과.*) 강자성체-초전도체-강자성체 접합 구조의 상태 밀도 함수를 연구하였다. 접합면에 평행한 방향을 z,x 축으로, 접합면에 수직인 방향을 y축으로 두었고 강자성체의 자기화 방향은 접합면에 평행한 방향이다. z,x 방향으로는 자유 파동 함수로 두었고 접합면에 수직인 y방향 성분은 물질의 양 끝에서 파동함수를 0으로 두는 경계 조건을 적

용하였다. 운동량 공간에서 Bogliubov-de Gennes(BdG) 방정식을 자체 일관적인(self-consistency) 방법으로 풀어 초전도체 질서매개변수 (order parameter) Δ 을 결정하였다. 초전도체-강자성체 층의 두께를 변화시켜가면서 단일 쌍 진폭 함수 (singlet pair amplitude function)와 세겹 쌍 진폭 함수(triplet pair amplitude function), 국소 자기화(local magnetization), 국소 상태 밀도 함수(local density of state)를 계산하였고 접합면에서 초전도체 또는 강자성체로의 깊이에 따른 단일 쌍 진폭 함수와 세겹 쌍 진폭 함수의 변화를 보았다. 강자성체-초전도체-강자성체의 자기화 방향이 평행인 경우와 반평행인 경우를 계산하여 세겹 쌍 진폭 함수와 국소 상태 밀도 함수를 비교하였다.

**Dp-067** **Extraction of the self-energy and gap function from ARPES experiments for high $T_c$ superconductor $Bi_2Sr_2CaCu_2O_{8+\delta}$.** BOK Jin Mo, YUN Jae Hyun, CHOI Han-Yong(*Department of Physics and Institute for Basic Science Research, SungkyunKwan University, Suwon 440-746, Korea.*) We report the self-energy and gap function extracted from the angle resolved photoemission spectroscopy (ARPES) experiments for high $T_c$ superconductor $Bi_2Sr_2CaCu_2O_{8+\delta}$ for the optimally doped. In this analysis, we assume that the self-energy has no momentum dependence and gap function has the *d*-wave form. then, the self-energy at a chosen energy may be obtained by fitting the momentum distribution curve of the ARPES intensities to two Lorentzian form for treating bilayer splitting along the nodal cut where the paring function vanishes. For the paring function, we will use the relation that the normalized momentum integrated intensity is equal to the superconducting density of states. We will show how the self-energy and gap function evolve as the temperature is lowered below $T_c$ and compare with other studies.

**Dp-068** **Effect of Nb Doping on Superconductivity of (Ru1-xNbx)Sr2(R1.4Ce0.6)Cu2Oz** LEE H.K., BAE S.M., LEE J.M.(*Kangwon National University Department of Physics.*) We investigated the effects of Nb doping on the structural and superconducting properties of (Ru1-xNbx)Sr2(R1.4Ce0.6)Cu2Oz(R=Nd, Sm). X-ray diffraction data reveal that nearly single-phase samples are found to exist in the range from x = 0.5 to 1.0 and from x = 0 to 1.0 for R = Nd and R = Sm, respectively.All samples with R = Sm show superconducting transition behavior and Tc decreases slightly with increasing x in consistent with RT thermoelectric power measurements. On the other hand, the maximum Tc for the R = Nd system was observed around x = 0.2. The experimental results are discussed in connection with the structural and magnetic properties.
* This work was supported by KRF(KRF-2007-313-C00204).

**Dp-069** **Peltier current leads.** KIM sanghoon(*경북대학교, 물리학과.*) For superconducting electronics, we need current leads, which connect cryostats system at the liquid helium temperature or liquid nitrogen temperature and power supply at the room temperature. Because of The temperature difference between cryostats and room temperature two major losses electric power losses and thermal losses occurred. We have developed 100A Peltier current lead that fabricate from P-type and N-type Peltier element(Bi2Te3 based) for DC operation testing. We confirmed two major losses reduced. For application of superconducting electronics which it appropriate at higher current we are willing to reduce the ohmicresistance and to find optimized configuration shape.

**Dp-070** **Growth of $Eu_{1-x}K_xFe_2As_2$ single crystals** KHIM Seung Hyun, KIM Hyung-Jin, LIU Yong, NAM Dong Hak, LIM Soon Ho, STEWART G. R.[1], KIM Kee Hoon(*FPRD, Department of Physics and Astronomy, Seoul National University, Seoul 151-742, Republic of Korea. [1]Department of Physics, University of Florida, Gainesville, Florida 32611-8440, USA.*) We have grown single crystals of $Eu_{1-x}K_xFe_2As_2$ compounds by the Sn flux method. The transport and magnetic properties were investigated in both H⊥c and H||c configurations to study the possible superconducting properties of the as-grown single crystals. The role of Eu on the superconducting properties of the single crystals will be further discussed in comparison with other compounds with Ba or Sr ions.

**Dp-071** **The distribution analysis of critical temperature in YBCO thin film using low temperature scanning laser microscopy (LTSLM)** PARK sangkook, KIM maengjun, RI hyeongcheol(*경북대학교 물리학과.*) Low temperature scanning laser microscopy (LTSLM) can be used for a two-dimensional display of various sample responses arising from the localized excitation. As shown in many experiments, LTSLM becomes particularly interesting when applied to superconductors. By using the $YBa_2Cu_3O_7$ thin film on a $Al_2O_3$ substrate, we have measured the distribution of the critical temperature. We suspected the shorter once exposed laser beam time constant , the better signal to noise ratio we can get with eliminating whole substrate heating effect. We modified laser beam configuration by adopting maximum 3kHz modulated laser beam which is produced by mechanical opto chopper as needed.

**Dp-072** **The development of LTSLM that can be used for the spatially resolved critical temperature distribution of superconductor coated conductor** RI Hyeong Cheol, KIM MaengJun, PARK SangKook(*경북대학교 물리학과.*) For the application of large current transporter using superconductor coated conductor, our research has lived up to the demand to ensure a homogeneity of the representative superconducting properties such as critical temperature and critical current density. Selectively heated region by Si-Diode laser gives us resistance's variation that depends on the local property. Resistance variation can be detected by lock-in amplifier referenced by 3 KHz modulated mechanical chopper. However, as long as laser is incident throughout cryostats's optical view port , there still remains light from environment. In order to reduce the effect of environmental photon, laser power is transmitted not through air but optical fiber. A comparison of signal between before and after superconducting specimen's isolation from external white light has been done.

**Dp-073** **Optical Properties and Electronic Structures of (GeTe, $Sb_2Te_3$) Pseudo-binary Compound Thin Films** 이 호선, 박 준우, 강 윤선[1], 이 태연[1], 서 동석[1], 김 기준[1], 김 철규[1], 강 윤호[1], DA SILVA Juarez L. F.[2], WEI Su-Huai[3](*경희대학교. [1]삼성전자. [2]NREL. [3]NREL, USA.*) We measure the dielectric functions of (GeTe, $Sb_2Te_3$) pseudo-binary thin films by using spectroscopic ellipsometry. We anneal the thin films at various temperatures. According to x-ray diffraction, the as-grown thin films are amorphous and the annealed films have metastable and stable crystalline phases. By using standard critical point model, we obtain the accurate values of the energy gap of the amorphous phase as well as the critical point energies of the crystalline thin films. The optical gap (indirect band gap) energy of the amorphous (crystalline) thin films is estimated by the linear extrapolation of aborption coefficients. As the Sb to Ge atomic ratio increases, the optical (band) gap energy of amorphous (crystalline) phase decreases. Standard critical point fitting show several higher band gaps. The electronic structures and the dielectric functions of the amorphous and crystalline thin films are calculated by using density functional theory and are compared to the measured ones. The band structure calculations show in stable phase that GeTe, $Ge_2Sb_2Te_5$, and $Ge_1Sb_2Te_4$ have indirect gap whereas $Ge_1Sb_4Te_7$ and $Sb_2Te_3$ have direct gap. The measured indirect band gap energies match well with the electronic band structure calculations.

**Dp-074** **$CaCu_3Ti_4O_{12}$ 유리-세라믹 : 지수 법칙과 임피던스 해석을 통한 유전완화 및 전기 전도 특성** 송 철호, 김 맥, 최 현우, 김 영훈, 양 용석(*부산대학교 나노과학기술대학, 나노융합기술학과.*) $CaCu_3Ti_4O_{12}$ (CCTO) 세라믹은 상온에서 높은 유전율($\sim10^4$)을 가질 뿐만 아니라 300 ℃를 중심으로 완화형 유전 봉우리가 나타나는 새로운 유전체이다. CCTO는 축전기, 센서, 엑츄에이터, 메모리 소자 등 전자 전기 소자에 널리 이용될 수 있다. 지금까지 다결정 CCTO 세라믹에 대한 유전 완화, 불순물 효과, 결정경계 효과 및 제조 방법에 따른 전기 전도 특성 변화 등 많은 연구가 이루어져 왔으나, CCTO 유리에 대한 유전완화 및 전기 전도 특성에 대한 연구는 없는 상황이다. 본 연구에서는 급속 냉각법을 통해 처음으로 비정질 CCTO를 제조하고 지수법칙과 임피던스 해석을 통해 유전완화 및 전기 전도 특성을 연구하였다. 온도에 따른 유전상수 그림에서 유리의 결정화에 의한 완만한 봉우리를 발견하였다. 지수법칙과 임피던스 해석을 통해 구한 dc 와 ac 전도에 대한 활성화 에너지가 비슷한 것을 통해 이 두 방법이 CCTO 유리의 전기 전도 및 유전완화 기구를 이해하는데 중요한 정보를 제공하는 것을 알 수 있었다. 또한, 제조된 비정질의 결정화를 통해 CCTO 세라믹을 제조하였으며, 기존의 여러 방법(고상 반응법, 불순물 첨가, 솔-젤 법)을 통해 제조된 세라믹의 유전 특성과 비교 분석하였다. 그 결과, 높은 유전상수를 지니면서 낮은 유전손실 값을 가지는 CCTO 세라믹을 제조하는 새로운 방법을 제시하였다.

**Dp-075** **결정 및 비정질 $(Li_{1-x}Na_x)_2B_4O_7$의 전기적 특성 연구** 김 맥, 송 철호, 최 현우, 임 영훈[1], 양 용석(*부산대학교 나노과학기술대학, 나노융합기술학과. [1]세명대학교, 교양과정부.*) 혼합 알칼리 효과는 한 종류의 알칼리가 포함된 물질에 다른 알칼리를 치환함으로써, 이온 거동과 관련된 이온 전도도, 이온 확산, 유전 완화 등의 특성이 비 선형적으로 변하는 현상이며, 주로 유리에서 나타난다. 최근 혼합 알칼리 효과의 근원 및 소자로의 응용성에 대한 연구가 활발하게 이루어지고 있다. 본 연구에서는 $(Li_{1-x}Na_x)_2B_4O_7$의 결정 및 비정질의 전기적 특성을 Jonscher의 보편 법칙을 이용하여 해석하였다. 결정과 비정질 시료의 확인은 엑스선 에돌이 (XRD)를 이용하였다. 비정질 $(Li_{1-x}Na_x)_2B_4O_7$에서는 dc 전기 전도도 및 dc 활성화 에너지가 강한 혼합 알칼리 효과를 보였다. 혼합 알칼리 효과는 온도가 낮을수록, 두 알칼리 이온의 크기 차이가 클수록 강하게 나타났다. 결정에서는 dc 전기 전도도 값이 비정질 보다 낮고, 혼합 알칼리 효과가 사라지는 것을 발견했다. RMC(reverse Monte Carlo) 시뮬레이션과 bond-valence technique을 결합한 모델에 의하면, 비정질에서 두 알칼리 이온이 마구잡이로 존재할 때 몰 비가 가까울수록 전도 방해 효과로 인해 이온 전도도가 감소하게 된다. 그러므로 규칙적인 구조를 지니는 결정에서는 전도 방해 효과가 발생하지 않으므로 혼합 알칼리 효과가 사라짐을 확인하였다.

**Dp-076** **$xLi_2O$-$(1-x)B_2O_3$ 비정질의 결정화 기구 및 열 특성 연구** 이 상민, 최 현우, 송 철호, 김 맥, 김 영훈, 진 근영, 양 용석(*부산대학교 나노융합기술학과.*) $Li_2B_4O_7$ 세라믹 또는 비정질은 전기광학 소자, 압전 소자, 고에너지 검출기 등으로 사용되어 많은 연구가 되고 있다. 이 물질의 일반적인 화학식은 $xLi_2O$-$(1-x)B_2O_3$와 같이 표현된다. 일반식에서 x=0.33인 경우에 결정 및 비정질 형성이 잘 되며 많은 응용이 이루어지고 있다. 한편 비정질 형성 측면에서 보면 x가 0.33보다 작은 경우 비정질 제조가 용이하나 그 이상인 경우는 어렵고 특히 x가 0.5보다 큰 경우에 대한 비정질 제조 및 연구는 거의 없다. 본 실험실에서는 x=0.5 0.55, 0.6, 0.65인 비정질을 성공적으로 제조하였다. 본 연구에서는 이와 같이 제조한 비정질의 결정화 기구 및 열 특성을 DSC, DTA, XRD, AFM, SEM, CCD 카메라를 이용하여 조사하였다. x=0.33일 경우 DSC 곡선에서 발열봉우리가 하나 발견되었으나, x=0.5 이상에서는 준안정 결정 및 안정상 결정형성에 대응되는 두 개의 발열봉우리가 나타났으며, x가 증가할수록 두개의 발열 봉우리 사이의 온도 간격이 늘어남을 볼 수 있었다. x의 증가에 따라 유리전이 온도, 결정화 온도, 발열봉우리 온도 등이 감소하는 것으로 보아 Li이 결정화에 미치는 영향이 많음을 알 수 있었다. 또한 비정질 형성 능력의 척도가 되는 과냉각 구간의 온도 범위와 녹는점 관계로부터 Li 양이 증가할수록 비정질 형성 능력이 급속히 작아짐을 알 수 있었다. 핵생성과 성장에 대한 모델을 구조 변화 그리고 열분석 곡선에 적용하여 $xLi_2O$-$(1-x)B_2O_3$ 비정질의 결정화 기구를 규명하였다.

**Dp-077** **비정질 유전체 $2LiTaO_3$-$SiO_2$의 유전 특성 연구** 김 영훈, 김 맥[1], 송 철호[1], 최 현우[1], 양 용석[1](*부산대학교 나노정보소재공학과. [1]부산대학교 나노융합기술학과.*) $LiTaO_3$ 계는 $ABO_3$ 형 강유전체로써 압전, 광학, 표면 탄성파 성질이 우수하며, 응용성에 대한 연구가 활발히 이루어지고 있다. $LiTaO_3$의 결정과 세라믹, 박막에 대한 전기적, 광학적, 구조적 특성에 대한 연구는 활발한 반면, 비정질에 대한 연구는 거의 이루어지지 않고 있다. 최근 이러한 강유전체에 대한 비정질 및 비정질-세라믹에 대한 연구가 나노 형성, 신물질, 새로운 기능성 소재/소자 개발에 연관되어 많은 관심을 받기 시작하고 있다. $LiTaO_3$ 비정질은 투명성이 좋고 나노 형성이 용이하여 응용성이 매우 클 것으로 기대되나 높

은 용융온도와 낮은 열전도 때문에 비정질 제조가 매우 까다롭다. 본 실험실에서는 비정질 $LiTaO_3$에 비정질 형성제 $SiO_2$를 첨가하여 $LiTaO_3$ -$SiO_2$ 비정질을 성공적으로 제조하였다. 비정질 형성제 첨가는 비정질 제조뿐 아니라 응용 시 대량 제조에 용이하다. 본 연구에서는 비정질 $LiTaO_3$ -$SiO_2$의 온도와 주파수에 따른 유전 특성을 조사하였다. 지수법칙과 Cole-Cole 식을 사용하여 전기 완화 및 dc, ac 전도도를 구했으며 이온 깡총뛰기에 의해서 나타나는 전기 전도에 대한 활성화 에너지를 구하였다. 또한 이러한 전기 완화 및 전기 전도도를 비정질/나노결정 계에 대하여도 비교 연구하였다.

**Dp-078** **Synthesis of $Pb(Zr_{0.52},Ti_{0.48})O_3$ Nanodot Arrays Using Ultra Thin Porous Alumina Membranes** YANG Sun A, CHOI Yong Chan, BU Sang Don(*Department of Physics, Chonbuk National University.*) We report the synthesis and characterization of ferroelectric $Pb(Zr_{0.52},Ti_{0.48})O_3$ (PZT) nanodot arrays. The PZT nanodot arrays were synthesized by spin-coating deposition of PZT precursor solutions using ultra thin porous alumina membranes (UT-PAMs) as template. UT-PAMs of ~300 nm thickness were prepared on Si substrate by two-step anodization method to form PZT nanodot arrays of uniform size in large area. Hexagonally ordered arrays of PZT nanodot were obtained by etching UT-PAMs selectively with 5 wt. % NaOH solution. The average diameter and interdot spacing of synthesized PZT nanodot arrays are consistent with diameter and interpore distance of nanopores of UT-PAMs, respectively, which could be controlled by tuning of the geometrical structure of UT-PAMs. We also investigated the effect of spin-coating conditions and sol properties on the morphology of the nanodots. These PZT nanodot arrays may provide a fundamental step to study peculiar physical properties of ferroelectric nanostructures, such as size-effect and toroidal ordering. It can be also applied to commercial field for fabrication of PZT-based nanodevices.

**Dp-079** **Polarized Micro- Raman Study of Molecular Wire** LIM Hyunjin, CHEONG Hyeonsik, JEONG Nak Cheon[1], YOON Kyung Byung[1](*Sogang University, Department of Physics. [1]Sogang University, Department of Chemistry.*) Nano-materials have been studied extensively due to their interesting properties and the potential for the applications to optoelectronic device, high speed semiconductor, and so on. Quantum dot, nanowire, nanorod are examples of the nano-materials. Among these structures, molecular wire is the thinnest of quantum confinement nano-materials. In this study, we focus on the optical property of molecular wire using micro-Raman spectroscopy. ETS-10 (Engelhard corporation Titanosilicate) is a crystalline microporous titanosilicates and has regularly organized titanium (Ti) - oxygen (O) molecular wires. The crystal has dimensions of about 15 ㎛ x 15 ㎛ x 3㎛ (width x length x height). Each molecular wire of Ti-O is isolated from other wires. Polarized micro- Raman spectra are obtained with a half lambda waveplate and a polarizer at different points of ETS-10 - center, side and edges. Because Ti-O stretching mode (724 $cm^{-1}$) is related directly to molecular wire, the intensity and shape (FWHM) of this peak can be the fingerprint of the crystal quality. High intensity and a sharp peak shape show the good quality of the crystal and the long length of molecular wire. The polarization direction of the incident beam was determined by one of the axes of the crystal, and the micro-Raman spectra were obtained while changing the angle of analyzer from 0° to 360°. Data from all three measurements show the same angle dependence and approached the function of $\cos^2\theta$ ($\theta$: analyzer angle), though the intensity at the center is lower than others. From these results, we can understand the angle dependence of Ti-O stretching mode from ETS-10 and the arrangement directions of molecular wires.

**Dp-080** **High Temperature High Pressure Simulation : report of on-going research in PNU CSSP Lab** 나(NA) 성호(Sung-Ho), 남(NAHM) 호현(Ho-Hyun), 김(KIM) 맹숙(Maeng-Sook), 강(KANG) 일준(Il-Joon), 최(CHOI) 기식(Kee-Shick), 박(PARK) 철홍(Chul-Hong)(*Pusan National University, Physics/RCDAMP.*) The state of condensed matter under high pressure and high temperature can be simulated by using the phonon dispersion relation acquired by the density functional theory. So far we have been testing our methodology with known materials. And now we continue to study about tin(Sn) and $MgSiO_3$. Further application and method improvement will be made.

**Dp-081** **Density functional theory를 이용한 CaO로 안정화된 $ZrO_2$의 산소 공공 연구** 이 병언, 김 대희, 김 영철(*한국기술교육대학교, 신소재공학과.*) 칼슘으로 안정화된 산화지르코늄 (calcia-stabilized zirconia, CSZ)은 산소 센서와 고체 산화물 연료전지 (Solid oxide fuel cells, SOFCs)의 전해질로써 많이 사용되는 물질이다. 본 연구는 DFT를 이용하여 산화칼슘(CaO)으로 안정화된 산화지르코늄 ($ZrO_2$)에서의 산소공공 이동에 대해 계산하였다. 2x2x2로 확장된 산화지르코늄은 32개의 지르코늄 원자와 64개의 산소 원자로 구성되어 있으며, 중앙에 위치한 지르코늄 원자를 칼슘 원자로 치환하였고 이 때에 전하균형조건을 만족시키기 위하여 산소 공공을 만들어주었다. 산소공공의 위치는 칼슘 원자로부터 거리가 가까운 순서대로 1st, 2nd, 3rd, 4th 순으로 만들었으며, 각각의 전체 에너지는 상대적으로 0, -0.2, 0.4, 0.4 eV 로 칼슘 원자로부터 두 번째로 가까운 위치에 산소공공이 만들어졌을 때 가장 유리함을 알 수 있었다. 산소 공공이 칼슘으로부터 일정거리 이상 멀어지면(3rd, 4th) 전체 에너지는 비슷한 값을 가짐을 알 수 있었다. 또한 본 연구에서는 두 산소 공공사이의 에너지 장벽을 계산하였다. 1st와 2nd에서 산소공공이 이동할 경우 에너지 장벽은 0.1 eV 정도로 매우 낮게 나왔으며, 2nd와 3rd 그리고 3rd와 4th에서의 에너지 장벽은 0.45 eV 이다. 따라서 산소 공공은 상대적으로 에너지 장벽이 낮은 1st와 2nd 위치를 통로로 하여 이동할 것이다.

**Dp-082** **A Numerical Study on the Lattice Constant Dependence of Resonance Frequencies of Cut-wire Pair Structure** TUNG N. T., CHO M. H., LAM V. D., PARK J. W., LEE Y. P.(*Quantum Photonic Science Research Center and Department of Physics, Hanyang University.*) Recently, a new area of research, left-handed materials (LHMs), has been investigated intensively because of their fascinating properties and novel applications. To obtain the

LH behavior, these materials should have a negative permeability (μ <0) and a negative permittivity (e <0) simultaneously over a certain frequency range. A negative permittivity medium can be easily obtained by a periodic array of wires. However, obtaining m <0 is still a major challenge for researchers since it occurs only in a narrow frequency band. In this research, we studied theoretically the transmission properties of the cut-wire pair structures which could be utilized as the magnetic components for providing m <0 to construct the LHMs. It was found that the resonance frequencies depend strongly on the lattice constant of the cut-wire pair structure. Our theoretical results are in good agreement with the experimental data. The numerical analysis was performed using the transfer-matrix method.

**Dp-083** **The phase separation and balance of the (1-*x*)$BiScO_3$-*x*$PbTiO_3$ at Morphotropic Phase Boundary** 김 봉주, PENG tong, 권 대영, 김 복기(*Department of Physics and Research Center for Dielectric and Advanced Matter Physics.*) We have studied the temperature-dependent neutron powder diffraction experiments on the new ferroelectric (1-*x*)$BiScO_3$-*x*$PbTiO_3$ (*x*=0.62, 0.64 and 0.66) systems. within the morphotropic phase boundary regime. In all samples, the monoclinic phase and tetragonal phase is coexisted in the ferroelectric phase. The details of structural analysis results introduced a subtel balance between the coexisting two phases. Such subtle balance is suggested to be sensitive to external electric field, and its contribution have a responsible for the enhanced electromechanical properties observed in $x$ = 0.64. Our result show the phase separation with a subtle balance between two phases are crucial to understand the unique properties at morphotropic phase boundary in new ferroelectric (1-*x*)$BiScO_3$-*x*$PbTiO_3$ systems.

**Dp-084** **In-situ x-ray photoemission spectroscopy and resistance switching behavior of NiO thin film** CHAE Seung Chul, PARK Soo Hyun, NOH Tae Won(*서울대학교 물리천문학부.*) Unipolar resistance switching behavior of NiO thin film has attracted attention due to the possibility for next generation nonvoltile memory. Issues of considerable attention are the clarification of key parameter which determine the overall switching operation and improvement of practical switching operation. However, although tremendous research effort was dedicated to these issues, the clear understanding on resistance switching is quite far. In this presentation, we report the in-situ x-ray photoemission spectroscopy (XPS) and resistance switching behavior of NiO thin film. NiO thin films were fabricated by using pulsed laser deposition technique. According to the oxygen partial pressure during the NiO film growth, the non-stoichiometry of NiO thin films were confirmed and different resistance switching behavior were observed. These indicate that the stoichiometry of as-grown NiO thin film could be attributed to the occurrence of unipolar resistance switching in NiO thin film.

**Dp-085** **$^1$H Nuclear Magnetic Resonance Measurements of $RbNH_4SO_4$** HAN Kee sung, KANG Ki Hyeok, MEAN Byoung Jean, CHOI Heon Hwa, LEE MooHee, LIM Ae Ran[1](*Department of Physics, Konkuk University, Seoul, 143-701, Korea. [1]Deparment of Science Education, Jeonju Univertsity, Jeonju, 560-759, Korea.*) $RbNH_4SO_4$ crystal is known to be a family of oriented glasses and possess complex phase transitions. The crystal structure of $RbNH_4SO_4$ is an orthorhombic phase *Pnma* at room temperature. $RbNH_4SO_4$ exhibits the transitions at 189 K and 120 K. However, the structural characteristics and nature of phase transitions in the crystal are not clearly understood. In this presentation, $^1$H nuclear magnetic resonance (NMR) experiments have been performed to investigate the role of proton in the phase transitions of $RbNH_4SO_4$ in the temperature range of 65~300 K at 7 T. As temperature decreases, the $^1$H NMR spectra obtained from $T_1$ and $T_{1r}$ measurements shift to the high frequency below 189 K and the shift becomes larger below 120 K. The linewidth does not change in all temperature regions. The measured value of $T_1$ decreases as temperature decreases down to ~150 K, where it starts to increase. On the other hand, the measured value of $T_{1r}$ decreases with decreasing temperature and the decrease-rate becomes larger below ~150 K. These temperature dependences of $T_1$ and $T_{1r}$ show that the proton dynamics abruptly changed around 150 K.

**Dp-086** **Rubidium Dynamics in $RbNH_4SO_4$ by Using $^{87}$Rb NMR** CHOI Heon Hwa, KANG Ki Hyeok, HAN Kee Sung, MEAN Byoung Jean, LEE MooHee, LIM Ae Ran[1](*Department of Physics, Konkuk University, Seoul, 143-701, Korea. [1]Deparment of Science Education, Jeonju Univertsity, Jeonju, 560-759, Korea.*) $RbNH_4SO_4$ exhibits complex phase transitions including those at 189 K and 120 K. However, the structural characteristics and nature of phase transitions in the crystal are not well understood. In this presentation, $^{87}$Rb nuclear magnetic resonance (NMR) experiments have been performed to investigate the role of rubidium in the complex phase transitions of $RbNH_4SO_4$ in the temperature range of 70~300 K at 7 T. The spectrum shows 2 peaks, denoted as I and II, which are, respectively, 97.645MHz and 97.667MHz at room temperature. Above 189 K, the measured value of $T_1$ of the peak I is almost same as than that of the peak II. Below 189 K, it becomes much larger than that of the peak II. The measured value of $T_1$ for both I and II rapidly decreases as temperature decreases toward 120 K, where the rapid decrease starts to be reduced and $T_1$ is temperature-independent below 100 K. These temperature dependences of $T_1$ show that the rubidium dynamics abruptly changed around 189 K and 120 K.

**Dp-087** **Twisted Pair Cryogenic Low Pass Filters** REHMAN Mushtaq, 류 상완, 송 운[1], 정 연욱[1](*전남대학교, 물리학과. [1]한국표준과학연구원.*) For precision transport experiments, low pass filters are usually required to block external interference. However, since filters designed for the RF frequencies often don't work at microwave frequencies, a separate low pass filter such as copper powder filter has been used widely, even though it is bulky for many applications. We fabricated a low pass filter consisting of twisted pair of manganin wires wrapped in a copper tape, which can be made compact. We measured its microwave transmission

characteristic with various filter parameters such as length, insulation thickness and twisted turns per unit length. The constructed filter with length of one meter showed a high attenuation (more than 60 dB at 1 GHz) with cutoff frequency of about 8 MHz. This result is in good agreement with the theoretical model, which assume the cable as a resistive transmission line. Comparison with copper powder filter will also be presented.

**Dp-088** **Building functional bio-architecture by surface templated layer-by-layer assembly on micro-patterned surface**
KIM Dongchung, KANG Dae Joon(*성균관대학교 물리학과.*)
We successfully build functional bio-architecture with two different active enzymes on pre-patterned surfaces created by photolithography using a sequential layer-by-layer (LBL) assembly. The modified enzymes, avidin/biotin-lactase oxidase (LOD) and avidin/biotin-horse raddish peroxidase (HRP), are attached together in close proximity and mediate coupled reaction that result in the production of a colored dye in the presence of L-lactate (Figure). Atomic force microscopy (AFM) and fluorescence images clearly show a regular, successively well-controlled LBL-assembled bio-architecture with the active two enzymes on the μ-patterned surface. Further, we show that the assembled enzyme structures are functional and that the bio-architecture has viable biosensing applications.

**Dp-089** **Superfluidity of Deuterium-Doped para-$H_2$ Clusters**
심 수민(*건국대학교 물리학과.*)
We have calculated the low-temperature properties of mixed clusters of $(D_2)_M(H_2)_N$ by using the path-integral Monte Carlo method. Hydrogen clusters doped by two additional deuterium molecules, $(D_2)_2(H_2)_N$ with $10 \le N \le 18$, show noticeably reduced superfluid fractions at 1.6 K when compared to pure hydrogen clusters of the corresponding sizes. This indicates that $D_2$ impurity molecules interrupt Bose exchange among hydrogen molecules. In addition, the radial density distributions of $D_2$ and $H_2$ molecules are deliberated as a function of the cluster size. When clusters of smaller sizes with $N \le 14$, one $D_2$ molecule is located around the cluster center and the other $D_2$ molecule is around 3.7Å from the center. However, for the clusters of larger sizes with $N \ge 15$, two $D_2$ molecules are located around 1.7Å from the cluster center and the $H_2$ density distributions seem to be more structured. Additionally, the clusters at specific sizes show conspicuously suppressed superfluid fractions than those of the neighboring sizes. This magic number behavior is also reflected in the energy differences between the adjacent cluster sizes. We find that $(D_2)_M(H_2)_{20}$ clusters have totally quenched superfluid fraction at 0.8 K when M = 3, which is believed to be due to the magic number stability of the hydrogen clusters. And mixed clusters of $(D_2)_M(H_2)_{20}$ with $M \ge 4$ are also shown to have entirely quenched superfluid fractions because of strong impurity effects. Furthermore, the radial density distributions of $D_2$ and $H_2$ molecules are discussed as well. As the number of impurity molecule becomes larger, $H_2$ density distributions are found to be well separated from $D_2$ density distributions.

**Dp-090** **온도와 전기장에 따른 블루페이즈 도메인의 크기 변화**
이 호현, H. Kikuchi[1], 김 종현(*충남대학교, 물리학과. [1]Kyushu Univ.*)
일반적으로 블루페이즈는 카이럴 액정이 등방상으로의 상전이 중에 작은 온도 영역에서 나타내는 상이다. 블루페이즈에서 크기와 모양이 다른 결정의 도메인들이 무작위로 나타난다. 본 연구에서는 블루페이즈가 나타나는 액정셀에 온도를 바꾸면서 전기장을 인가하여 도메인의 크기 변화를 관찰하였다. 전기장의 크기, 주파수에 따라 도메인이 나타나는 온도, 나타내는 온도영역, 크기등이 달라졌다. 도메인의 크기 변화는 광학현미경을 이용하여 온도에 따라 관찰하였다. 또한 분광기를 써서 반사광의 변화를 연구하였다.

■ SESSION: P1
10월 23일(목), 14:30 - 16:15
장 소: 제3전시장

**Kp-001** **Physical Vapor Transport에 의한 CdSxSe1-x(0** 김 유리, 정 재훈, 김 경호, 송 만석, 윤 현식, 배 세환, 김 용, GAO Qiang[1], TAN H.Hoe[1], JAGADISH Chennupati[1](*동아대학교 신소재물리학과. [1]The Australian National University.*) 반도체 nanostructure의 다양한 특성은 전자공학과 광학적 소자로의 적용가능성에 있어서 주목 받고 있다. 이로써 반도체 nanosturcture는 결정학적, 광학적인 특성의 조절이 요구된다. 본 실험은 간단한 장치인 single-zone quartz tube furnace를 이용하여 nanostructure를 성장시키고 micro-PL을 관찰하였다. 성장온도를 증가시킴에 따라 nanowire에서 nanosheet로 구조변화가 일어남을 관측하였다. 그리고CdSe나노박판에 후속으로 CdS 나노박판을 측면으로 성장하는 새로운 측면 나노박판 헤테로구조를 관측하고 micro-PL 측정 및 polarization anisotropy를 측정하였다.
* We acknowledge support by the Korean Science and Engineering Foundation (KOSEF) through Grant No. Fol-2007-000-10087-0.

**Kp-002** **Growth and Structural Properties of M-plane ZnO Films on Sapphire Substrates by Plasma-Assisted Molecualr Beam Epitaxy** KIM Jung-Hyun, HAN Seok Kyu, HONG Soon-Ku, LEE Jae Wook[1], LEE Jeong Yong[1], SONG Jung-Hoon[2], YAO Takafumi[3](*Department of Advanced Materials Engineering, Chungnam National University. [1]Department of Materials Science and Engineering, KAIST. [2]Department of Physics, Kongju National University. [3]Center for Interdisciplinary Research, Tohoku University.*) ZnO has been extensively studied for its applications in light emitters and detectors in the ultraviolet (UV) spectral region. Recently, researches on the growth of nonpolar ZnO films have been received much attention. Several results have been reported on the growth of nonpolar A-plane ZnO on R-plane sapphire substrates by MOCVD or by PAMBE. Recently, we have investigated strong anisotropies in structural and optical properties of A-plane ZnO on R-plane sapphire substrates. However, in contrast to the A-plane ZnO growth, it is known that the growth of single crystalline and uniaxial M-plane ZnO without a mixture of C-plane ZnO on M-plane sapphire substrate is not so easy. Very recently, M-plane ZnO growth on cubic (001) MgO substrate by PAMBE has been reported but, a little amount of C-plane mixture was not fully avoided. In this study, we report investigations on growth and structural properties of ZnO films grown on M-plane sapphire substrates by PAMBE. The ZnO films were grown at a wide range of substrate temperatures between 100 and 800°C with fixed II/VI ratio conditon. In addition, growth at different II/VI flux ratio were carried out at fixed substrate temperature of 600°C. All the growth procedures were monitored by in-situ reflection high energy electron diffraction (RHEED). Surface morphologies of the grown films were investigated by atomic force microscope (AFM) and growth orientation was examined by x-ray diffraction (XRD). Detailed XRD analysis of the grown ZnO films showed that nonpolar (10-10) M-plane ZnO films with negligible (but existing) weak reflection of (10-13) or (0002) plane could be grown under the limited growth conditions, which indicates difficulties of genuine M-plane ZnO. Structural properties of the grown films were investigated by transmission electron microscope (TEM) analysis. The detailed results will be presented.

**Kp-003** **Oxygen vacancy clustering in perovskite oxides** CUONG Do Duc, LEE Jaichan(*School of Materials Science & Engineering, SungKyunKwan University, Suwon 440-746, Korea.*) Recently, perovskite oxides materials have been extensively studied because of their technical importance and the fundamental interest in the physics of their phase transitions. Physical and chemical properties of these materials can be strongly modified with the introduction of various kinds of defects. Among them, oxygen vacancy has been well known as a fundamental defect in perovskite oxides, which give critical impact on physical properties, especially on transport properties. In our previous reports, the oxygen vacancies in $SrTiO_3$ have been found to be interacted to each other along Ti-Vac direction and lead to the oxygen vacancy clustering along [001] direction [1]. This behavior may be extended for other perovskite materials. In this study, we used the first principles calculation to study oxygen vacancies in other ferroelectric materials including $PbTiO_3$ and $BaTiO_3$. The electron localization has been seen in these structures with certain configurations of oxygen divacancy for both two materials, in which the electron localization appears prominently in $PbTiO_3$ which has high ferroelectricity. The orbital symmetry plays the important role for the localization of electron. By this study, the oxygen vacancy clustering is also suggested in these materials
[1] D. D. Cuong *et al.,* Phys. Rev. Lett. 98, 115503 (2007).

**Kp-004** **Au 촉매가 증착된 ZnO/$SiO_x$ 박막으로부터 형성된 나노선의 구조 및 발광 특성 연구** 김 창오, 신 동희, 김 성, 홍 승휘, 최 석호(*경희대 국제캠퍼스 응용물리 전공.*) 이온빔 스퍼터링에 의해서 Si (100) 기판 위에 100 nm 두께의 $SiO_x$ 박막을 증착한 후 RF 스퍼터링 증착법을 사용하여 30 nm 두께의 ZnO 박막을 증착하였다. $SiO_x$의 x 값은 0.8부터 1.8까지 변화시켰으며 XPS를 사용하여 확인하였다. ZnO/$SiO_x$ 박막 형성 후RF 스퍼터링를 이용하여 10nm의 Au 박막을 증착하였다. 이렇게 증착된 Au/ZnO/$SiO_x$ 박막들은 급속 열처리기 (RTA)로 700°C에서 30분간 열처리 한 후 이어서 1100°C에서 20분 간 열처리하였으며 SEM 분석에 의해 표면에 나노선들이 형성되었음을 확인하였다. 각각의 x값에 대하여 형성된 나노선들은 대부분이 방향성 없이 형성되었으나, 나노선의 직경은 거의 균일하게 형성되었음을 확인할 수 있었다. 각각의 x값에 따른 나노선의 광루미네센스 (PL) 띠는 ZnO의 밴드끝 (near band edge, NBE) 발광에 기인하는 자외선 영역에서 관찰되었다. 나노선의 PL 세기는 x 값이 0.8부터 1.2까지 증가함에 따라 감소하며, 1.2 이상부터는 증가하였다. 또한, 나노선의 ZnO NBE와 관련된 PL 띠 에너지는 x 값이 0.8부터 1.2까지 증가함에 따라 적색 천이하며, x값이 1.2에서 1.8로 증가함에 따라서는 청색 천이하였다. x =1.4 이상에서는 ZnO의 NBE PL과 함께 750nm근처에서 Si 나노결정과 관련된 PL띠가 관찰되며, x값이

1.4에서 1.8로 증가함에 따라 Si 나노결정과 관련된 PL 띠 에너지는 청색 천이하였다. 이러한 실험결과를 바탕으로 나노선의 구조와 PL 특성과의 상호관계 및 그 발광 메커니즘을 규명하고자 한다.

**Kp-005** **Growth-point defect for $AgGaS_2$ single crystal thin film by hot wall epitaxy** HONG KWANGJOON(*DEPARTMENT of PHYSICS, CHOSUN UNIVERSITY.*) To obtain the single crystal thin films, $AgGaS_2$ mixed crystal was deposited on thoroughly etched semi-insulating GaAs(100) substrate by the hot wall epitaxy (HWE) system. The source and substrate temperatures were 590 ℃ and 440 ℃, respectively. After the as-grown $AgGaS_2$ single crystal thin films was annealed in Ag-, S-, and Ga-atmospheres, the origin of point defects of $AgGaS_2$ single crystal thin films has been investigated by the photoluminescence(PL) at 10 K. The native defects of $V_{Ag}$, $V_S$, $Ag_{int}$, and $S_{int}$ obtained by PL measurements were classified as a donors or acceptors type. And we concluded that the heat-treatment in the Ag-atmosphere converted $AgGaS_2$ single crystal thin films to an optical n-type. Also, we confirmed that Ga in $AgGaS_2$ crystal thin films did not form the native defects because Ga in $AgGaS_2$ single crystal thin films existed in the form of stable bonds.

**Kp-006** **ZnO 박막의 두께에 따른 $ZnO/SiO_x$ 이질접합 박막의 구조적 및 발광 특성 연구** 신 동희, 김 창오, 김 성, 남 지선, 오 형택, 최 석호(*경희대 국제캠퍼스 응용물리 전공 및 자연과학종합연구원.*) 각각 다른 x값을 가지는 $ZnO/SiO_x$ 이질접합 박막의 각 층을 RF 스퍼터링과 이온빔 스퍼터링으로 제작하였으며, 광루미네센스 (PL), high-resolution TEM (HRTEM), XPS 등을 이용하여 ZnO의 두께 변화에 따른 구조적 및 발광 특성을 연구하였다. 실리콘 (100) 기판 위의$SiO_x$박막의 두께는 100nm이며, x값은 0.8에서1.8까지 변화시켰다. 각각의 x값을 가지는 $SiO_x$기판 위에 10 – 100 nm의 ZnO박막을 증착한 후 900°C에서 3분간 산소분위기에서 급속 열처리를 하였다. $ZnO/SiO_X$ 박막에서 ZnO의 밴드 끝 (near band edge, NBE) 발광에 기인하는 자외선 (UV) PL과 함께 결함 (defect)와 관련된 가시 광선 영역의 PL띠가 관찰되었다. NBE-PL 세기는 ZnO의 두께가 10부터 50nm까지 증가함에 따라 증가하며, 70nm 이상일 때는 감소하였다. 각각의 x값에서 결함 PL의 세기는 50nm 두께의 ZnO에서 가장 작았다. 또한 ZnO의 두께가 10 부터 50nm까지 증가함에 따라 NBE PL 띠는 청색천이하며, 70 에서 100nm로 증가함에 따라서는 적색천이를 하였다. HRTEM분석결과, ZnO의 두께가 10에서 50nm로 증가함으로써 ZnO박막은 나노결정 구조에서 거의 단결정 구조로 변화하였으며, 70에서 100nm로 증가함에 따라서는 기둥모양 (columnar)의 낟알 (grain)들을 가지는 다결정 구조가 관찰되었다. 이러한 구조는 ZnO 두께가 50nm 일 때 PL의 세기가 가장 크게 나타나는 것과 깊은 관련이 있는 것으로 보인다.

**Kp-007** **H-passivation-enhanced photoluminescence from $SiO_2$ films containing Si nanocrystals** JUNG Yoon-Jin, YOON Jong-Hwan(*강원대학교, 물리학과.*) Si nanocrystals embedded in silicon dioxide films are exposed to an atomic hydrogen plasma at different temperatures. Photoluminescence (PL) intensity from the nanocrystals is shown to increases with increasing exposure time, followed by saturation that depends on the exposure temperature. The saturation level depends on the final exposure temperature and shows no dependence on the thermal history of exposure. This behaviour is shown to be consistent with a model in which the steady-state passivation level is determined by a balance defect passivation and depassivation by hydrogen. The activation energy for the passivation reaction being larger than that for the depassivation reaction. Comparison between samples annealed in atomic and molecular hydrogen confirmed that atomic hydrogen leads to a greater level of passivation than molecular hydrogen, and that samples passivated in atomic hydrogen show a very fast initial (T <500 oC) depassivation compared to those passivated in molecular hydrogen.

**Kp-008** **가지가 있는 에피택시 Ge 나노선의 성장조절** 정 재훈, 김 경호, 김 유리, 송 만석, 윤 현식, 김 용, GAO Qing[1], TAN H. Hoe[1], JAGADISH Chennupeti[1](*동아대학교 물리학과. [1]The Australian National University.*) Lamp Heated CVD(Chemical Vapor Deposition)법에 의해 GaAs 기판에 Epitaxy한 Ge Nanowires(NWs)를 1차 성장한 후 2차 성장으로 가지가 있는 Ge NWs를 성장하였다.Ge NWs는 VLS(Vapor-Liquid-Solid) 메커니즘을 통해 성장하며, 촉매로는 1차 성장에 50nm Au colloid 용액, 2차 성장에 Au colloid 용액이나 Evaporation을 이용하여 얇은 Au 층을 성장시켜 사용하고, source gas로는 diluted GeH4를 사용하였다. Au 입자들을 기판 표면에 고정시키기 위해 APTES 용액에 기판을 1분간 담근 후, Au colloid 용액을 살포하였다.Au와 Ge의 공융점 온도 근방인 섭씨 320 - 380 도 사이 온도에서 10 Torr 압력에 1시간씩 2차에 걸쳐 성장시킨 샘플은 FE-SEM(Field ion Scanning Microscope)을 이용하여 가지가 있는 Ge NWs의 이미지를 관찰하였다. 각 샘플의 평면과 단면 SEM 이미지를 통해 가지가 있는 Ge NWs의 성장방향과 모양을 분석하였다.

* This work was supported by the Korean Reserch Foundation Grant Funded by the Korean Goverment (MOEHRD) (KRF-2007-313-C00222)

**Kp-009** **SiC 나노 입자가 있는 나노 부유 게이트 메모리 소자의 온도 변화에 따른 전기적 특성 연구** 이 태희, 이 동욱, 김 선필, 김 은규, 신 진욱[1], 조 원주[1](*한양대학교 물리학과. [1]광운대학교 전자재료공학과.*) 차세대 비휘발성 메모리는 상변화 메모리 (PRAM), 폴리머 메모리 (PoRAM) 등과 같이 기존의 플래시 메모리와 DRAM 성능의 한계라 제기되는 빠른 쓰기 및 지우기 동작, 오랜 기간 보존할 수 있는 능력에 대한 해결책을 동시에 제시한다는 점에서 폭넓게 연구되어지고 있다. 그 중, 나노 부유 게이트 메모리 소자 (Nano-floating gate memory : NFGM)는 실리콘 기판의 채널로부터 들어오는 전자를 수 나노 미터 크기의 나노 입자에 저장한다는 점에서 기존의 플래시 메모리 구조와 다르다. 본 연구는 실리콘 공정에 적합하며 일함수가 4 eV 이상인 SiC 나노 입자를 사용하여 NFGM 소자를 제작 하였다. 공정은 *p*-type의 silicon-on-insulator 기판에 $O_2$ 분위기에서 4.5 nm의 $SiO_2$를 건식 산화법으로 성장시킨 이후에 12 nm 두께의 SiC 박막을 radio-frequency magnetron sputtering을 이용하여 증착시켰다. 그리고 기판에 50 nm의 $SiO_2$를 증착시키고, SiC 나노 입자를 형성시키기 위하여 900 ℃에서 3분 동안 질소 분위기에서 1차 열처리를 실시하였

다. 이후 컨트롤 층으로 $SiO_2$를 30 nm 증착시키고, rapid thermal annealing 과정을 통하여 900 ℃에서 30초 동안 질소 분위기에서 2차 열처리를 실시하였다. 마지막으로 thermal evaporator를 이용하여 150 nm의 Al을 증착한 후 포토리소그래피와 에칭 공정을 통하여 게이트 전극을 형성하고, 소스-드레인 영역에 도핑과정을 실시한다.제작된 SiC NFGM의 전기적 특성을 확인하기 위하여 HP-4156A semiconductor parameter analyzer를 이용하였으며 특히 측정 온도를 상온부터 최대 200 ℃까지 변화시키면서 온도에 따른 문턱전압 이하 영역의 전달특성 ($V_G$-$I_D$)과 출력특성 ($V_D$-$I_D$), 전압 인가에 따른 문턱전압의 이동, 그리고 retention 특성을 살펴보았다. 그리고 소자 내에 SiC 나노 입자의 형태 및 분포 상태를 확인하기 위하여 전계방출투과전자 현미경을 이용하였다.

**Kp-010** **Growth of the carbon nanotips with resist-assisted patterning process** 손 병택, 유 제황, 임 한얼, 임 준원, S. Manivannan, 장 진, 박 규창(*경희대학교 정보디스플레이학과 차세대디스플레이연구센터.*) 본 연구에서는 기 연구된 레지스트를 이용한 패터닝 (Resist-Assisted Patterning) 법을 이용하여 우수한 구조적 특징과 전자방출 특성을 갖는 튼튼한 탄소나노튜브 (Robust CNT)를 개발하였다. 이는 실리콘 기판 위에 단층막/니켈 형성 후, 플라즈마화학기상증착 (plasma enhanced chemical vapor deposition) 법을 이용한 성장 조건을 변화시켜 구조적으로 안정된 팁을 얻을 수 있었다. 결과적으로 전자주사현미경 (scanning electron microscope)을 이용하여 탄소팁의 하부 직경은 마이크로미터의 크기라는 것을 알 수 있었고, 팁의 상부는 나노크기의 매우 뾰족한 형상을 볼 수 있었다. 그리고, 물리적 스트레스를 가한 이후, 전자주사현미경(Scanning electron microscope)을 이용하여 팁의 하부를 관찰한 결과, 탄소나노튜브와 기판 사이의 접착력 (adhesion)이 매우 강한 것을 볼 수 있다. 따라서 지금까지 탄소나노튜브와의 형상과는 전혀 다른 안정된 구조물을 얻을 수 있었다. 이러한 탄소팁의 구조물은 안정된 전자방출 특성과 구조적 안정성으로 장수명의 에미터 소자 적용에 큰 기대가 될 것이다.

**Kp-011** **Growth of CNTs on metal substrate for X-ray sources** 임 준원, 유 제황, 임 한얼, 손 병택, S. Manivannan, 장 진, 박 규창, 최 해영[1], 김 종욱[1](*경희대학교 정보디스플레이학과 차세대디스플레이연구센터. [1]한국전기연구원.*) 탄소나노튜브 (CNTs) 는 다양한 형태와 물성을 지닌 특성으로 인하여 나노전자 산업분야로 활발하게 응용되고 있다. 그 중에서도 낮은 임계전계에서의 높은 전자방출 특성으로 인하여 다양한 전자방출소자로의 연구가 활발히 이루어지고 있다. 특히 엑스레이 방출원으로의 적용시, 기존의 열전자 방출을 이용한 소자를 대신하여 간편하고 고효율 소자로의 응용이 가능하다. 이는 장수명 엑스레이 램프의 전자 방출원으로 기대되고 있다. 본 연구에서는 기 연구된 레지스트 패터닝법(resist assisted patterning, RAP) 을 이용하여, 금속 기판 위에 높은 전류 방출특성을 갖는 탄소나노튜브 에미터 어레이 (carbon nanotube-field emitter array, CNT-FEA)제작기술을 연구하였다. 금속 기판은 실리콘 기판이나 유리 기판에 비해 높은 온도에서 공정이 가능하고 기판 재료 단가가 저렴하며, 가공성이 뛰어나고 구부러질 수 있다는 장점이 있다. 이러한 금속 기판 위의 CNT-FEA 의 전자방출특성에 관하여 연구하여 이를 실리콘 기판 위의 CNT-FEA 의 전자방출 특성과 비교하고 그 이유를 분석하였다. 결과적으로 금속 기판 위의 CNT-FEA 의 우수한 전자방출 특성을 얻을 수 있었으며, 이를 엑스레이 전자 방출원으로 이용하여 우수한 특성의 엑스레이 이미지를 얻을 수 있었다.

**Kp-012** **CdSSe 삼원계 나노구조의 투과전자현미경 분석** 윤 현식, 김 경호, 정 재훈, 김 유리, 송 만석, 김 용, 배 세환(*동아대학교 물리학과.*) CdSSe 나노구조는 S/Se 의 조성변화에 따라 가시영역에서 발광파장이 변화하여 광소자에 매우 유용한 나노물질체계이다. 이전의 연구에서 physical vapor transport 에 의하여 성장한 CdSSe 나노구조가 성장온도에 따라서 nanowire, nanobelt, nanosheet 로 구조 변화가 일어남을 관측한 바 있다. CdS 나 CdSe nanobelt 의 투과전자현미경에 의한 원자배열관측은 많이 보고되었으나 삼원계 CdSSe 의 투과전자현미경에 의한 보고는 많이 않다. 따라서 본 연구에서는 이 삼원계 나노구조체의 원자구조를 투과전자현미경으로 관찰하고자 한다. 특히 CdSSe 시료의 경우에 micro-PL 실험에서 CdS와 CdSe 가 공존하는 경우도 관찰된 바 어떤 경우에 이러한 성장이 일어나는지 투과전자현미경으로 관찰하고 성장모형을 제시하고자 한다.

**Kp-013** **Effect of the workfunction of metal nanoparticles on the nonvolatile flash memory.** KIM Dong Hak, LIM Daeyoung(*Kyung Hee University.*) It has been proposed that nonvolatile flash memory based on metal nanoparticle can have several advantages over conventional ones, mainly because of the possibility of workfunction engineering. To study the effect of metal workfuction on memory properties, we fabricated floating gate MOS structures based on Pt, Au, and Cr nanoparticles and measured their properties. We found easier programming and erasing, larger memory window for low workfunction metal as compared to higher workfunction ones. All the structures showed comparable retention characteristics. The structure of tunneling oxide also strongly affected the memory properties.

**Kp-014** **Interrelation between Luminescence and Structural Properties of Plasma Power Controlled SiNx Films by using PECVD** 한 문섭, 장 승훈, 고 창훈, 정 기영(*서울시립대학교 물리학과.*) Visible light emission from silicon with nano-sized structures at room temperature has been reported. For this enormous potential for optoelectronic device application, the various nano-sized silicon composites have been studied by many researchers. In this work, we investigate the optical and structural properties for the nano-structured silicon nitride films by using plasma-enhanced chemical-vapor deposition (PECVD). We controlled the peak position of photoluminescence (PL) in the red-visible range by adjusting the plasma power of reactant gas. We observed that the PL peak shifted toward the higher energy and the PL intensity became stronger with increasing the plasma power from 20 W to 60 W. In order to interpret more deeply the optical properties, we employed Raman scattering spectroscopy (RSS) and x-ray diffraction (XRD). In Raman spectrum, as the plasma power decrease, the presence of a silicon amorphous phase can be observed more. Also, we confirmed that XRD data showed similar behavior. According to these results, we report interrelation between luminescent and structural properties of plasma power controlled SiNx films.

**Kp-015** **Terahertz Time-Domain Spectroscopy of Doped Si** LEE Cheol Hyeok, CHOI Kyu-jin, HONG Tae Yoon, KIM Min Ho, KIM Jae Hoon(*Yonsei University.*) The terahertz range, which spans the spectral region of 0.05-5 THz (1.5-150 cm-1), lying between the microwave (electronics) and the infrared (optics) regions, has been relatively unexplored up to now. Intense broadband-tunable sources and efficient ambient-temperature detectors were scarce in this spectral region. However, recent advances in ultrafast pulsed lasers and semiconductor fabrication technology have provided us with a means to explore the terahertz gap based on the principle of timedomain Fourier-transform pulse spectroscopy. We have carried out THz transmission measurements on lightly doped p-Si and determined the frequency-dependent conductivity, dielectric function, optical constants, and loss function. Our method, suitable for solids with low-density free carriers, is based on exact numerical solutions of coupled nonlinear equations with the experimental amplitude reduction and phase shift upon terahertz transmission.



**Kp-016** **Origin of One-Side Long Extension of Coulomb Blockade Regime for Single Electron/Hole Transistors** HYUN Youmee, KIM Hyungjun, KIM Deuk Young, KANG Tae Won[1], LEE Sejoon[1], TOSHIRO Hiramoto[2](*Dongguk Univ., Dept. of Semiconductor Science.* [1]*Dongguk Univ., Quantum-fuctional Semiconductor Research Center.* [2]*Univ. of Tokyo, Institute of Industrial Science.*) The single electron/hole transistor (SET/SHT) having an ultra narrow Si nanowire-channel were fabricated and it was confirmed that they show the clear Coulomb blockade oscillation (CBO) at room temperature. For the contour plot of $I_D$ as functions of $V_G$ and $V_D$, peculiarly, the SET and SHT demonstrated the long-range-extended Coulomb blockade (CB) regime. The shape of the extended CB regime was quite long and cuspidal. In addition, the extended CB regime appeared in only positive $V_D$ bias direction. In the extended CB regime, the negative differential conductance (NDC) oscillation was clearly demonstrated, and the modulation of NDC and CBO peak positions was observed to be precisely performed. In order to clarify the origin of the one-side-extension of CB regime, we characterized the carrier transport properties in each current flow direction by switching the source and the drain. And then, to make an experimental allusion more definite, we also simulated all kinds of possibilities based on experimental results. As a result, we found that the one-side-extension of CB regime is attributed to the difference in tunneling probabilities between tunneling-in and tunneling-out of carriers due to the asymmetric barrier structure in source and drain regions.

**Kp-017** **Inductively Coupled $CF_4$ Plasma Etching Of Germanium** KIM T.S., YANG H.Y., JUNG M.R., CHOI S.S., KIL Y.H., SHIM K.H.(*Semiconductor Physics Research Center, Department of Semiconductor Science and Technology, and Department of Physics, Chonbuk National University.*) We have investigated etch rate, etch profile and surface for Ge as a function of varied $CF_4$ flow rate, inductively coupled plasma (ICP) power and work pressure, which used inductively coupled $CF_4$ plasma for the Ge substrate etching. It was found that the peak etch rate is at 40 sccm $CF_4$ flow rate. The etch rate of Ge decreases from 5138 to 3588 Å/min as $CF_4$ flow rate increases from 40 to 60 sccm. The etch rate of Ge increases from 2583 to 5138 Å/min as ICP power increases from 100 to 400 W, whereas the etching rate of Ge decreases from 4450 to 3549 Å/min as work pressure increases from 10 to 20 mTorr when ICP power is 200W. When pressure is 20mTorr at 200W, the etching rate of Ge decreases compared with 10mTorr. But it has been found that its surface is more smooth than other etched surfaces.

**Kp-018** **Effects of Two-Step Growth Conditions on Structural Properties of (11-20) ZnO Films Grown on Sapphire Substrates by Plasma-Assisted Molecular Beam Epitaxy** HAN Seok Kyu, KIM Jae Goo, KIM Jung-Hyun, HONG Soon-Ku, LEE Jae Wook[1], LEE Jeong Yong[1], SONG Jung-Hoon[2], YAO Takafumi[3] (*Department of Advanced Materials Engineering, Chungnam National University.* [1]*Department of Materials Science and Engineering, KAIST.* [2]*Department of Physics, Kongju National University.* [3]*Center for Interdisciplinary Research, Tohoku University.*) ZnO has been extensively studied for its applications in light emitters and detectors in the ultraviolet (UV) spectral region. Recently, researches on the growth of nonpolar ZnO films have been received much attention. Several results have been reported on the growth of nonpolar A-plane ZnO on R-plane sapphire substrates by MOCVD or by PAMBE. Recently, we have investigated strong anisotropies in structural and optical properties of A-plane ZnO on R-plane $Al_2O_3$ substrates. The ZnO films showed typical anisotropic surface morphology with stripes running along the <0001> direction, where the average width of the stripes changes with thickness of the film. On the other hand, it is well known that surface morphology of polar ZnO films is strongly dependent on II/VI ratio. We have found that the surface morphology of nonpolar ZnO films changes strongly with the II/VI ratio, too. Recently, Hollander et al. reported growth of a-plane GaN films with reduced structural anisotropy and improved crtstal qualty by employng two-step growth, where different V/II ratio is applied in metal organic vapor deposition (MOCVD). In this study, we applied two-step growth; the first step ZnO films with different thicknesses were grown by the pre-determined Zn-rich (O-rich) growth condition and then the second step ZnO films were grown by the O-rich (Zn-rich) growth condition, where the total ZnO film thickness was maintained to about 280 nm. The surface morphology and roughness of grown ZnO thin films were investigated by atomic force microscopy (AFM) measurement. Structural properties of grown ZnO films were analyzed by high resolution x-ray diffraction (HRXRD) measurement and high resolution transmission electron microscope (HRTEM). Surface morphology and structural properties are changed depending on the combination of two steps. The detailed results will be presented.

**Kp-019** **Study on Properties of ZnO Films Grown on C-plane Sapphire Substrates as a Function of Low Temperature ZnO and MgO Buffer thickness by PAMBE** KIM Jae Goo,

HAN Seok Kyu, YANG Sang Mo, HONG Soon-Ku, LEE Jae Wook[1], LEE Jeong Yong[1], SONG Jung-Hoon[2], YAO Takafumi[3] (*Department of Advanced Materials Engineering, Chungnam National University. [1]Department of Materials Science and Engineering, Korea Advanced Institute of Science and Technology. [2]Department of Physics, Kongju National University. [3]Center for Interdisciplinary Research, Tohoku University.*) ZnO is a optoelectrically available II-VI compound semiconductor with wide band gap energy of 3.37 eV and large exciton binding energy of 60 meV at room temperature. (0001) $Al_2O_3$ substrate has been widely used as a substrate of the ZnO film. But, ZnO films directly grown on (0001) $Al_2O_3$ showed poor crystalline quality because of the large lattice mismatch of about 18% between ZnO and (0001) $Al_2O_3$. In order to improve crystal qualities of the ZnO films, the growth process using the MgO buffer layer and the low temperature (LT) ZnO buffer layer has been developed by plasma-assisted molecular beam epitaxy (PAMBE).We reported the effects of the MgO buffer thickness when ZnO films grown on (0001) $Al_2O_3$ substrates. And it is reported that the polarity of the ZnO films with the MgO buffer changes as the thickness of the MgO buffer; O-polar ZnO films grow when the MgO thickness is thinner than about 3nm, while Zn-polar ZnO films grow when the MgO thickness is thicker than about 3nm. However, the effects of LT-ZnO buffer layers with a relation of MgO buffer thickness have not been systematically investigated. In this study, we investigated the effects of the LT-ZnO buffer thickness with a relation of the MgO buffer thickness. All the growth procedures were monitored by in-situ reflection high energy electron diffraction (RHEED). Surface morphologies and crystalline quality of the ZnO films were investigated by atomic force microscope (AFM) and high resolution x-ray diffraction (HRXRD), respectively. And optical properties of the ZnO films were investigated by photoluminescence (PL) measurements. We confirmed that the properties of the ZnO films were changed depending on the thickness of the LT-ZnO as well as of the MgO buffer. The detailed results will be presented.

**Kp-020** **Study on ZnO Nanorods Prepared by Hydrothermal Growth Followed by Chemical Vapor Deposition for Gas Sensors** KANG Dong-Suk, HAN SeokKyu, HONG Soon-Ku, KIM HyoJin, SONG Jung-Hoon[1], KIM DoJin, KIM Min-Jung[1], SONG Jae-Ho[1], LEE JaeWook[2], LEE JeongYong[2](*Department of Advanced Materials Engineering, Chungnam National University. [1]Department of Physics, Kongju National University. [2]Department of Materials Science and Engineering, KAIST.*) Zinc oxide with a direct-wide-band gap energy of 3.37eV at room temperature and an exciton binding energy of 60mV has received increasing attention due to their potential applicability to emitters, and chemical and bio sensor. Lots of works have been reported on the ZnO nanostructures synthesized by chemical vapor deposition (CVD) with or without catalyst. Aqueous solution based hydrothermal growth (HG) is an alternative way to synthesize ZnO nanostructures, which can be performed at a low temperature of about 90°C.In this study, we have synthesized vertically aligned ZnO nanorods without using any catalyst. Instead, a thin ZnO layer deposited by sputtering on $SiO_2$/Si substrate was used for the seed layer. First, ZnO nanorods were synthesized by HG using $Zn(NO_3)_2{\cdot}6H_2O$(0.1M) and $(CH_2)6N_4$(0.1M) as source material for 3 h at 95°C. From plan-view and cross-sectional SEM micrographs, we confirmed that Well aligned ZnO nanorods with hexagonal cross-section were synthesized. On these ZnO nanorods, the second step growth of ZnO nanorods were carried out by CVD using ZnO:C powder as source material for 20 min at 1000°C. Vertical ZnO nanorods with a high aspect ratio (~100nm diameter and ~6mm length) were synthesized. The morphology of ZnO nanorods were observed by FE-SEM. The growth orientation and crystalline qualities of ZnO nanorods were analyzed by XRD measurement. And, the optical properties of the samples were analyzed by PL measurements. Finally, gas sensor applications of these ZnO nanorods are tested by making a simple sensor structure with top platinum contact. Detailed properties of the synthesized ZnO nanorods and sensors will be presented.

**Kp-021** **Epitaxial Growth of ZnO Films on (111) Si Substrates: Effects of Zn Pre-exposures Followed by In-Situ Oxidation Processes** YANG Sang Mo, HAN Seok Kyu, KANG Dong-Suk, KIM Jae Goo, HONG Soon-Ku, LEE Jae Wook[1], LEE Jeong Yong[1], SONG Jung-Hoon[2], YAO Takafumi[3](*Department of Advanced Materials Engineering, Chungnam National University. [1]Department of Materials Science and Engineering, KAIST. [2]Department of Physics, Kongju National University. [3]Center for Interdisciplinary Research, Tohoku University.*) In recent years, zinc oxide (ZnO) has received considerable attentions for the possibility of its application in high-efficiency optoelectronic devices, such as light emitting devices and laser diodes. For these applications, ZnO film has been grown by several growth methods, such as pulsed laser deposition, sputtering, chemical vapor deposition and molecular beam epitaxy. Among these methods, MBE growth method is most promising due to facility of atomic layer control during the epilayer growth and film growth under ultra high vacuum condition.Growing epitaxial ZnO films on Si substrate is attractive in considering a cost and an availability of large-sized substrate. In addition, growth of wide band gap wurtzite ZnO on cubic Si substrate has potentials of applications in employment of well-developed silicon integrated technology in to functional device fabrications. However, it is difficult to grow single crystalline ZnO films on Si substrates because of generation of amorphous $SiO_x$ layer at the Si surface at the very beginning of the growth that is being performed under oxygen ambient. In order to prevent the formation of an oxide layer at the ZnO/Si interface, Fujita et al. employed the Zn pre-exposure and Wang et al. employed the Mg pre-exposure prior to the ZnO growth. Although the growth of single crystalline ZnO films on Si have been reported, detailed and schematic investigations on pre-exposure followed by ZnO growth are not studied although it is believed to be critical in growing single crystalline, high quality ZnO films on Si substrates.In this study, we report epitaxial growth of ZnO films on (111) Si substrates by PAMBE, where emphasis is given on the effects of Zn pre-exposure conditions followed by in-situ oxidation processes of the Zn layer. The Zn pre-exposures and the followed

oxidation processes are monitored by in-situ RHEED. The ZnO films with different in-situ oxidation processes have been investigated by XRD technique including pole figure measurements and HRTEM analysis. The crystal quality of ZnO films is changed with the oxidation processes whether the oxidations were performed by using oxygen gas or radical, and the oxidation time. Additionally, we introduced low temperature ZnO buffer layer before high temperature ZnO growth for high crystal quality of epitaxial ZnO films. The details will be presented.

**Kp-022** **Effects of RTA Temperature on the Optical Properties of ZnO Thin Films Grown by PLD** 조 신호(*신라대학교 전자재료공학과.*) The effects of rapid thermal annealing (RTA) temperature on the optical properties of ZnO films are investigated. The ZnO films are grown on Si (100) substrates by pulsed laser deposition. The crystallographic structure and surface morphology are studied by X-ray diffraction and atomic force microscopy, respectively. The crystalline orientation of ZnO (002) plane is not changed, but the full width at half maximum decreases with increasing RTA temperature. The steady-state photoluminescence spectra of the ZnO films at 13 K exhibit neutral bound excitons peak at 3.357 and 3.330 eV. As the temperature increases, the intensity of two bound excitons peak rapidly decreases and a free exciton peak is dominant above 180 K. The carrier lifetimes, obtained by using a least-square fit of the data, are found to significantly depend on the annealing temperature, indicating that the fast lifetime of 40 ps occurs at the sample annealed at 800°C.

**Kp-023** **Nitrogen and Aluminum Codoped ZnO Thin Films grown by RF Magnetron Sputtering** 조 신호(*신라대학교 전자재료공학과.*) Nitrogen and aluminum codoped ZnO (NAZO) thin films were grown on glass substrates with changing the nitrogen flow ratio by radio-frequency magnetron sputtering. The structural, optical, and electrical properties of the NAZO films were investigated. The surface morphologies and the structural properties of the thin films were analyzed by using the X-ray diffraction and scanning electron microscopy. The NAZO thin film, deposited at nitrogen flow ratio of 0%, showed a strongly c-axis preferred orientation and the lowest resistivity of $3.2\times10^{-3}$ Ωcm. The intensity of ZnO (002) diffraction peak was decreased gradually with increasing the nitrogen flow ratio. The optical properties of the films were measured by UV-VIS spectrophotometer and the optical transmittances for all the samples were found to be an average 90% in the visible range. Based on the transmittance value, the optical bandgap energy for the NAZO thin film deposited at nitrogen flow ratio of 0% was determined to be 3.46 eV. As the nitrogen flow ratio was increased, the carrier concentration and the hall mobility were decreased, but the electrical resistivity was increased.

**Kp-024** **Identification of The 3326 $cm^{-1}$ Infra-red Absorption Line in ZnO** CHANG Kee Joo, BANG Junhyeok(*Department of Physics, KAIST.*) Zinc oxide (ZnO) has attracted much attention because this material has a large band gap and a large exciton binding energy. It is known that as-grown ZnO exhibits the *n*-type conductivity. Hydrogen is considered as a promising candidate for the origin of the *n*-type conductivity. Recent experiments suggested that two infra-red absorption peaks observed at 3326 and 3611 $cm^{-1}$ are related to hydrogen. Although it is believed that the origin of the 3611 $cm^{-1}$ line is an isolated interstitial hydrogen at a bond-centered site, it is not clearly understood what causes the 3326 $cm^{-1}$ line. In this work, we perform local-density-functional calculations to investigate the atomic and electronic properties of defect complexes, such as $V_{Zn}$-H and Ca-H, in ZnO. Considering the energetics of various configurations and the orientation of the H atom, we suggest that the 3326 $cm^{-1}$ absorption line is caused by a Ca-H complex.

**Kp-025** **Annealing Effects of ZnO Nanorod Thin Films Dispersed with Solvents** LEE Cheol Eui, PARK Jun Kue, SHIM Eui-Taek, KIM Minseok, LEE Eunmo, LEE Kyu Won(*고려대학교 물리학과.*) Thin films using zinc oxide (ZnO) powder as the reactant, and water, methanol and chloroform as reaction solvents are investigated. The morphology as well as crystallization mechanism of the powder and the thin film sampes were characterized by X-ray diffractometer (XRD), scanning electron microscopy (SEM) and IR spectra methods. Also, optical properties of the ZnO nanorod were investigated by the photoluminescence (PL) measurements. The thin film crystallinity is better with water than with any other solvent.

**Kp-026** **CdS 단결정 박막의 두께 변화에 따른 타원분광학적 특성 연구** 김 대중, 최 용대[1], 이 종원[2], 서 정철[3](*목원대학교 테크노과학연구소. [1]목원대학교 기술마케팅학과. [2]한밭대학교 신소재공학부. [3]원광대학교 반도체 광 디스플레이학부.*) 고품질의 CdS 박막들은 소스 온도에 변화를 주어 두께를 조절하였으며, 열벽 적층 성장법을 이용하여 GaAs (111) 기판위에 성장시켰다. 성장된 CdS 박막들은 X-선 회절 패턴을 분석한 결과 육방정 구조(hexagonal structure)를 갖는 것으로 확인되었고, 결정성을 알아보기 위하여 HRXRD를 측정하였다. 박막의 표면 상태를 알아보기 위하여 Nomarski 간섭현미경과 AFM을 이용하여 관측하였고, SEM/EDX를 이용하여 박막들의 성분비를 알아보았다. 또한 성장된 박막들의 광학적 특성을 알아보기 위하여 분광학적 엘립소미트리를 사용하여 실온에서 2.0-8.5 eV 사이 포톤에너지 범위에서 측정하였다. 측정된 데이터들로부터 유사 유전함수 스펙트럼 $\langle\varepsilon(E)\rangle=\langle\varepsilon_1(E)\rangle+i\langle\varepsilon_2(E)\rangle$에 나타난 $E_0$, $E_{1A}$, $E_{1B}$, $E_2$, $E_0$` 와 같은 임계점 구조를 관측하였다. 또한 이차미분을 통하여 획득한 임계점 피크들의 두께 변화 의존성을 연구하였다. 박막의 복소 유전함수와 밀접한 관계를 가지고 있는 굴절지수 n(E), 소광계수 k(E), 반사계수 R(E) 그리고 흡수계수 α(E)와 같은 광학적 특성 등을 연구하였다. 특히, 두께 변화에 따른 임계점 피크들의 이동과 넓어짐을 관측할 수 있었고, 이러한 결과는 GaAs 기판과 CdS 박막사이의 스트레인과 밀접하게 연관되어 있다는 것을 알 수 있었다.
* (본 연구는 학술진흥재단의 지원을 받아 연구되었음; KRF-2005-075-C00012)

**Kp-027** **The epitaxial growth of the ZnS thin films deposited by pulsed laser deposition** CHUNG Jun-Ki, SONG Tae

Kown[1], KIM SangSu[2], KIM Won-Jeong[2](*Institute of Industrial Technology, Changwon National University. [1]Department of Ceramics, Changwon National University. [2]Department of Physics, Changwon National University.*) The epitaxial ZnS thin films were deposited on sapphire (*c*-cut $Al_2O_3$) substrates by pulsed laser deposition (PLD). The PLD of ZnS target produced by spark plasma sintering (SPS) has been carried out by using excimer laser (248 nm). SPS was performed with a heating rate of 100 °C/min at 1100 °C and pressures in a vacuum atmosphere. The die and punch material was made of graphite with a 25 mm diameter. ZnS films were deposited at a various substrate temperatures (400 °C - 725 °C) with a fixed $P(O_2) = 10^{-5}$ Torr, and the thickness of the films are estimated to be about 300 nm. The elemental composition of ZnS films was confirmed by energy dispersive analysis by X-ray (EDAX) technique. Structure, surface morphology and optical properties of as-deposited films were characterized by X-ray diffraction (XRD), scanning electron microscopy (SEM) and UV-spectrophotometer, respectively. Results of the x-ray diffraction analysis, the intensity of ZnS (0 0 0 2) peak increases while the full width at half maximum (FWHM) values of ZnS (0 0 0 2) peak decreases with the increase of the substrate temperature. As deposition temperature increases, surface roughness increased. Transmission spectra indicate a high transmission coefficient (~80%). The optical energy gap obtained from the transmittance spectra is about 3.56 – 3.73 eV.

* This work was partially supported by the Korea Research Foundation Grant funded by the Korean Government (MOEHRD, Basic Research Promotion Fund) (KRF-2007-313-C00224).

**Kp-028** **버퍼층의 종류에 따른 GaZnO의 광학적 및 전기적 특성** 김 형준, 조 현칠, 유 승용, 현 유미, 이 영민, 봉 하종, 심 다혜, 성 준제, 김 득영, 이 연환[1], 우 용득[2](*동국대학교 반도체과학과. [1]동국대학교 정보통신공학과. [2]우석대학교 기계자동차공학과.*) 투명한 기판(Polyethersufone(PES)위에 RF 마그네트론 스퍼터법으로 $SiO_2$, $Al_2O_3$, ZnO 등 각기 다른 버퍼층을 약 50 nm의 두께로 증착 후 Ga-doped ZnO 박막을 증착하였다. ZnO를 버퍼로 사용한 경우의 가시광영역에서 약 80% 이상의 투과율을 보였고, 전기적 비저항 특성은 약 $9\times10^{-3}$ Ωcm의 값을 나타냈다. 또한 $SiO_2$ 버퍼층의 경우 가시광 영역에서 약 80% 이상의 값을 보였으나, ZnO 버퍼층과는 다르게 400~500nm 범위에서 투과율이 다소 감소된 것을 관찰할 수 있었고, 비저항도 약$6\times10^{-1}$Ωcm의 값으로 낮은 값을 보였다. $Al_2O_3$ 버퍼층을 사용한 경우 가시광 영역에서 약 70%의 투과율이 관찰되었으며, 또한 400~500nm와 800~1000nm 범위에서 투과율이 약간 감소된 것이 확인되었고, 약 $8\times10^{-2}$Ωcm의 비저항을 나타내었다. 이는 버퍼층의 종류에 따라 전기적 특성 및 광학적 특성에 영향을 미치는 것을 알 수 있고, $Al_2O_3$의 경우 $SiO_2$ 버퍼층에 비해 전기적 특성은 향상되지만 투과율 특성은 감소되는 것을 알 수 있었다.

**Kp-029** **Study of Ferromagnetism Property of $Zn_{0.97}Mn_{0.03}O$ Diluted Magnetic Semiconductors Grown on Al2O3(0001) Substrate According to Oxygen Vacancy.** CHA Su-young, KIM Won-kyung, CHO Yong chan, JEONG Se-young(*Department of Nano Fusion Technology, Pusan National University, Miryang 627-706, Korea.*) For last several years, the great potentials of diluted magnetic semiconductors (DMSs) have brought world-wide research efforts into spintronics. Also, (Ga,Mn)As, (In,Mn)As, and MnGe systems have been frequently reported due to their magnetic and transport properties such as strong sp-d exchange interactions or extraordinary Hall effect. However, the Curie temperature(TC) of these materials have been limited to 140K which is far from that required for practical device applications. Since many researchers investigated that hole-mediated Mn-doped ZnO could achieve a high Curie temperature(TC), there has been much interest in Mn-doped ZnO as a potential candidate for DMSs with high TC. Especially, in II–VI semiconductors ZnO, transition metals including cobalt and manganese ions have been examined as dopants in semiconductor for introducing ferromagnetism. The origins of room temperature ferromagnetism in ZnMnO are now on debating. In this research, we investigated the relation between carrier density and ferromagnetism depending on the growth conditions. We report the growth of Mn doped ZnO with 300 nm thick deposited by radio-frequency magnetron sputtering system. The structural properties were analyzed by X-ray diffractometer(XRD) and the surface morphology and thickness were characterized by scanning electron microscope(SEM). Optical bandgap and transmittance were investigated by UV-VIS-NIR spectrophotometer. Hall effect and magnetic properties were measured with Van der Pauw method, superconducting quantum interference device(SQUID) and magnetic circular dichroism(MCD), respectively.

**Kp-030** **Effect of N-addition on the structural and optical properties of ZnO thin film** 김 준관, 임 정욱, 김 현탁[1], 윤 선진(*한국전자통신연구원, MIT 소자팀 - 과학기술연합대학원대학교, 차세대소자공학과. [1]한국전자통신연구원, MIT 소자팀.*) The effect of nitrogen (N)-addition to ZnO thin films on the structural and optical characteristics was investigated for the phosphor application. ZnO thin films were deposited on $SiO_2$-coated Si substrate with a thickness of 150 nm using rf-magnetron sputter deposition technique under various ratios of Ar and $N_2$. The composition analysis showed that a trace amount of N existed in the N-doped ZnO film. The grain size slightly decreased with increasing $N_2$ content in deposition ambient and the lattice parameter of *c*-axis increased with increasing $N_2$, and the peak slightly shifts towards lower $2\theta$ angle side. The results showed that the crystallinity degraded and the tensile stress was increased due to N-addition in the films. While undoped ZnO showed no emission in visible region, N-doped ZnO exhibited the broad emissions in PL measurement. The position of the highest intensity peak of N-doped ZnO was shifted from 600 to 660 nm with increasing $N_2$ content from 17 % to 33 % in the deposition ambient. These results implicated that the microstructure and the energy state of the defect level can be effectively controlled by varying $N_2$ content in the deposition ambient.

**Kp-031** **PVA(polyvinyl alcohol)에 도핑된 CdS 나노결정의 물리적 특성** 하 성용, 유 동선, 김 일곤, 이 정두, 정 재영, 장 옥흔(*창원대학교, 물리학과.*) 유리 기판 위에 PVA-CdS 나노 결

정을 흡착시키고, 물리적 특성을 조사 하였다. 몰 농도가 다른 $CdCl_2$(0.1mM, 0.5mM, 0.7mM, 1mM, 3mM, 5mM)를 PVA와 혼합하여, PVA-$Cd^{2+}$결합체를 만들었으며 이를 유리 기판에 캐스팅 하였다. PVA-$Cd^{2+}$결합체를 0.5mM의 $S^{2-}$이온이 내재된 $Na_2S$와 NaOH 수용액에 담금으로써 PVA-CdS 나노결정을 만들었다. PVA-$Cd^{2+}$ 결합체의 FT-IR spectra 측정을 통해서 PVA모체 속의 OH와 치환된 $Cd^{2+}$의 양을 정성적으로 추정하였다. PVA-CdS 시료의 광흡수 측정 결과 $Cd^{2+}$의 몰 농도가 높아짐에 따라 absorption edge가 장파장 쪽으로 이동함을 확인하였는데 이는 $S^{2-}$의 몰 농도가 일정함에도 불구하고 $Cd^{2+}$몰 농도의 증가에 따라 합성된 CdS 나노 결정의 크기가 커짐을 의미한다. 합성된 CdS 나노 결정의 optical gap은 2.51-2.74eV로 계산되었다. XRD 측정결과 PVA-CdS 나노 결정은 cubic phase의 결정성을 보였으며 XRD intensity를 이용하여 계산된 나노 결정의 반경은 5-8nm 였는데 이는 Brus의 식에 의해 계산된 값과 거의 일치하였다.

* 본 연구는 한국과학재단(2008-0067-0000)의 지원을 받아 연구되었음.



**Kp-032** **p-타입 실리콘 위에 올린 실리콘 나이트라이드 박막 연구** 윤 성민, 남 윤성, 이 상욱, 장 동기, 백 경선, 장 수경(*연세대학교 물리학과.*) 비휘발성 메모리인 전자트랩플래시는 트랩이 많은 나이트라이드라는 물질을 절연체로 사용해 그 구멍 속에 전하를 채워 0과 1을 구분하게 하는 방식으로 기존에 도체인 플로팅 게이트가 데이터를 저장하던 것을 부도체인 나이트라이드가 대신함으로 인접한 셀과의 간섭을 원천적으로 차단할 수 있게 된다. 메모리 특성은 나이트라이드의 트랩 농도와 준위에 의존하게 된다. 본 연구에서는 p-타입 실리콘 위에 올린 실리콘 나이트라이드 박막의 캐패시턴스-전압 및 포토루미네센스를 측정하여 트랩 특성을 연구하였다.

**Kp-033** **비정질 SiN 박막 위에 올린 ZnSe의 특성 연구** 장 동기, 남 윤성, 이 상욱, 윤 성민, 백 경선, 장 수경(*연세대학교 물리학과.*) 비정질 또는 다결정 ZnSe 박막은 LED, 태양전지셀 등의 응용 가능성을 보이고 있다. 비정질 기판은 그 위에 올린 시료에 다양한 방향과 크기의 스트레인을 주고 재결정화나 그레인의 형성을 유도한다. 이에 본 연구에서는 비정질 SiN 박막 위에 ZnSe를 증착시켜 SEM으로 관측한 결과, 약 100 나노미터 크기의 피라미드 모양의 그레인들이 형성되었음을 확인하였다. 이는 N-dangling bond와 관련한 것으로 예상되며 PL 스펙트럼을 통하여 질소와 관련한 피크들을 관측하고 연구하였다.

**Kp-034** **Electrical and Magnetic Properties of Co Doped ZnO Diluted Magnetic Semiconductor** KIM Jae-Hoon, SONG Hooyoung, KIM Eun Kyu(*Quantum-Function Spinics Lab. and Department of Physics, Hanyang University.*) Diluted magnetic semiconductors (DMS) are important materials for semiconductor spintronics applications. ZnO and GaN are typical materials of wide-bandgap semiconductors. The ZnO has much interesting for a based material for DMS, because of its theoretical high Curie temperature. In this study, the Co doped ZnO DMS was grown by pulsed laser deposition (PLD) system that has an advantage to control the composition ratio of the grown film from the mixture target. Here, the Co atoms were used as a magnetic impurity. A Mn doped ZnO films were also grown to compare the Co doped ZnO films. A hydrogen annealing to these films was tried to improve their magnetic and electrical properties. The defect states in these films were investigated by using deep level transient spectroscopy (DLTS) and photoluminescence measurements. For DLTS measurement, a Ti/Au was deposited over the large area of the sample to form an Ohmic contact and Au electrodes were used for Schottky contact. On the prepared sample the DLTS measurements were performed at temperature range from 20 K to 350 K.

**Kp-035** **Cr이 첨가된 ZnO 박막에서 엑시톤-포논 상호작용에 관한 고찰** 심 다혜, 봉 하종, 성 준제, 이 영민, 유 승용, 김 형준, 조 현칠, 현 유미, 이 세준[1], 조 용훈[2], 김 득영(*동국대학교 반도체과학과. [1]동국대학교 양자기능반도체연구센터. [2]한국과학기술원 물리학과.*) 본 연구에서는 자체 제작된 타깃을 이용하여 Pulsed laser deposition (PLD) 법으로 Cr이 첨가된 ZnO ($Zn_{0.975}Cr_{0.025}O$ 와 $Zn_{0.85}Cr_{0.15}O$) 박막을 성장하였다. 이들 박막의 광학적 특성을 알아보기 위해 PL을 측정한 결과, 근접 밴드간 전이와 녹색발광이 관찰되었다. 특히, 이때 중성 구속 엑시톤의 반치폭이 약 ~7 meV로 매우 작은 값을 보였다. 온도의존성 PL 측정을 통해 중성 바운드 엑시톤 방출 피크가 온도가 증가함에 따라 red-shift되는 것을 알 수 있었다. 엑시톤 방출 피크의 변화의 원인을 확인 하기 위해 Bose-Einstein 접근법을 사용해 온도 의존성 엑시톤 파라미터를 추출하였고, 이를 통해 Cr이 첨가된 박막의 엑시톤과 포논의 상호작용을 확인하였다. 결론적으로 본 실험에서 ZnO내에 Cr이 첨가됨에 따라 격자진동을 일으키며 이는 엑시톤 발광 특성에도 영향을 미치는 것으로 판단된다.

**Kp-036** **Ion-beam을 이용한 박막 표면 특성 변화에 대한 연구** OH gwangtaek, CHOI Jinsik, JEON SangHo, HWANG Inrok, HONG Sahwan, CHOI JungAe, KIM Yoensoo, YOON InSung, YOON HeeSun, YALISHEV Vadim, PARK BaeHo(*건국대학교 물리학과.*) 기존의 flash memory는 동작속도가 느리고 읽고 쓰는 횟수가 제한적이며 정보집적도 등의 기술적인 한계가 드러남에 따라 기존의 메모리를 대체할 만한 차세대 메모리에 대한 요구가 거세이지고 있다. 이에 따라 FRAM(Ferroelectric Random Access Memory), MRAM(Magnetic Random Access Memory), PRAM(Phase-change Random Access Memory), ReRAM (Resistance Random Access Memory)등의 비휘발성 메모리소자가 개발 중에 있으며, 특히 저항 변화 현상을 이용한 ReRAM은 제작이 용이하고 빠른 동작속도와 낮은 동작전압, 높은 직접도 등 차세대 메모리의 좋은 조건들을 갖추고 있어 많은 연구가 이루어져 왔지만, 여전히 그 동작 mechanism에 대해서는 명확히 밝혀진 바가 없다. 기존의 많은 연구에서 switching 현상에 대해 많은 가설들이 제시되었고 binary oxide의 unipolar switching에 대해서는 conducting filament의forming과 rupture로 switching 현상을 설명하고 있으나, oxygen vacancy, grain boundary 등과 같은 defects가 switching 현상의 지배적인 원인으로 알려져 있어서 있을 뿐, 그 또한 명확하지 않다.특히, 메탈과 oxide의 인터페이스에서의 결함이 filament의 형성에 큰 영향을 미칠 것으로 예상되고 있어, 본 연구에서는 표면의 defect를 제어함으로 switching 현상에 대해 알아보고자 하였다. 본 연구에서는 switching을 보여주는 $ZrO_2$ 박막을 제작하여 박막의 상.하부의 표면을 개질함으로써 defect가 forming되

는 과정에 큰 영향이 있음을 확인하였다. Ion-beam은 특정 이온으로 박막 표면에 충격 줌으로써 물질의 상태를 (친수성<->소수성) 변화 시켜주거나 표면을 다듬어 줌으로 RMS를 줄여주는 효과를 가져다 준다. 우리는 이러한 Ion-beam을 사용하여 다양한 처리조건에서의 박막 표면의 변화를 AFM(Atomic Force Microscopy)을 이용해 분석하였으며, 하부전극의 표면을 변화시킴으로써 박막의 형성에 어떤 영향을 미치는지 측정하였다. 박막의 defect의 변화를 줌으로써 이에 따른 전기적 특성을 연구하였다.

**Kp-037** **Advanced properties as alternative RRAM of EuO thin films** CHOI JungAe, CHOI Jinsik, HWANG Inrok, JEON SangHo, HONG SaHwan, OH Gwangtaek, KIM YeonSoo, YOON InSung, YOON HeeSun, YALISHEV Vadim, PARK BaeHo(*건국대학교 물리학과.*) Resistive random access memory (RRAM), among non-volatile memory fields, which utilizes resistive switching properties of oxide materials is an attractive part. Therefore, several materials to reveal RRAM properties, which show reproducible swithcing phenomena, are studied. Among studying materials, we had interesting about $Eu_xO_y$ as RRAM material. Especially, we have focused to study structural and electrical properties of $Eu_xO_y$ thin films as RRAM materials. Before this study, we performed several experiments: to depositt $Eu_xO_y$ thin films on Ir substrate by using EuO target and Radio Frequency (RF) sputter, to measure the structural properties of the films by using X-ray diffraction (XRD), and to analyze the electrical properties of the films by using Kithley 2400 and probe station. From those experiments, we make sure that there is the reproducible switching phenomena in $Eu_xO_y$ thin films, that is, the switching properties were shown from poly-crystalline behaviors and mixed structures of $Eu_2O_3$ and $Eu_3O_4$. Additionally, interesting switching properties of the films were revealed. Therefore, in this study, we perfomed advanced experiments: to deposit the films at several conditons, to measure surface properties of the films by using Atomic Force Microscope (AFM), and to analyze the electrical properties of the films. From these study, we confirmed the interesting reproducible switching properties shown in $Eu_xO_y$ thin film is dependent on an atomic structure of the films.

**Kp-038** **Synthesis and Optical Characterization of Single-Crystalline Zinc Oxide Nanowires** SUH Duk-Il, BYEON Clare C., KIM Bok Hyeon, LEE Jongmin, LEE Sang-Kwon[1], LEE Chang-Lyoul(*Advanced Photonics Research Institute, Gwangju Institute of Science and Technology. [1]School of Semiconductor and Chemical Engineering, Chonbuk National University.*) Low-dimensional semiconductor nanowires offer many opportunities for the assembly of nanoscale electronic/photonic devices and arrays by the bottom-up approach. We have synthesized single-crystalline ZnO nanowires by using chemical vapor deposition and gold(Au)-assisted catalytic growth mechanism varying the growth temperature. We also discussed associated material properties. Field-emission scanning electron microscopy (FE-SEM) images of nanowire arrays show that ZnO nanowires are ordered and uniform size with diameter of ~100 nm and up to 5 μm in length. PL measurements showed a strong bandedge emission at ~ 380 nm without any defect.

**Kp-039** **MOCVD 방식으로 나노다공성 알루미나 마스크를 이용한 ZnSe 나노점 형성** 이 상욱, 남 윤성, 윤 성민, 장 동기, 백 경선, 장 수경(*연세대학교 물리학과.*) 나노미터 크기의 집적회로 소자를 만들기 위한 노력으로 나노다공성 알루미나 마스크를 이용하여 나노구조물을 제조하는 패턴방법에 대한 연구가 많이 진행되고 있다. 종횡비(직경에 대한 길이의 비)가 높아지면 열역학 에너지만으로 시료가 구멍 안으로 들어갈 확률은 줄어들게 된다. 이러한 이유로 전기적인 반응을 이용하여 구멍 안으로 빨려 들어가게 만드는 경우가 많고, 특히 화합물을 성장시키려는 경우는 이 과정 이후에 여러 화학적인 반응의 단계를 통해 형성하게 된다. 하지만 반도체의 경우 다단계의 시료 형성과정은 원치 않는 불순물의 첨가, 계면 준위의 형성 등의 효과를 일으켜 반도체 특성 조절에 또 다른 문제를 낳게 된다. 본 연구에서는 종횡비를 조절하여 MOCVD 증착의 한 단계만으로 ZnSe 나노점을 형성하고 그 특성을 조사하였다.

**Kp-040** **Post-annealing and Hydrogen Plasma Treatments for Non-polar ZnO Films Grown by Pulsed Laser Deposition** SONG Hooyoung, KIM Jae-Hoon[1], KIM Eun Kyu[1], HWANG Sung-Min[2](*Quantum-Function Spinics Lab. and Department of physics, Hanyang University, Seoul 133-791, Korea, Energy-nano Materials Research Center, Korea Electronics Technology Institute, Gyeonggi-do 463-816, Korea. [1]Quantum-Function Spinics Lab. and Department of physics, Hanyang University, Seoul 133-791, Korea. [2]Energy-nano Materials Research Center, Korea Electronics Technology Institute, Gyeonggi-do 463-816, Korea.*) ZnO as a wurtzite semiconductor has been intensively studied because of its large exciton binding energy (~60 meV). High exciton binding energy is the one of the most important factor which confirms the internal quantum efficiency of optoelectronic devices. However, the optoelectronic or electronic devices based on ZnO oriented along the c-axis cause malfunctions, which are produced by the axis-dependent strong piezoelectric polarization. In this study, we prepared non-polar ZnO films oriented along the (11-20) plane called a-plane by pulsed laser deposition. To deposit a-plane ZnO films, we choose the r-plane sapphire substrate. And a-plane ZnO films were grown at various ambient gas and temperature conditions. After finding optimized growth condition, a-plane ZnO films were annealed at 600~900℃ by rapid thermal annealing system for the recrystallization. After the deposition process, the hydrogen plasma treatment was performed on the surface of the ZnO films to control defect states and carrier concentration. Characteristics of annealed and plasma irradiated samples were analyzed by high-resolution x-ray diffraction, scanning electron microscope, atomic force microscope, cathodoluminescence, spectral and time-resolved photoluminescence.

**Kp-041** **Fabrication and field-emission characteristics of position-controlled AlN/ZnO coaxial nanotube heterostructure arrays** YI Gyu-chul, CHO Jeonghui, KIM Yong-Jin, HONG Young Joon(*포항공과대학교 신소재공학과.*) There has been an enormous interest in 1-dimensional (1-D) wide band gap semi-

conducting nanostructures for field-emission device applications due to their excellent electron emitter characteristics with sharp tip and low electron affinity. Among numerous semiconductor nanostructures, 1-D ZnO nanostructures have been extensively studied because they can be easily prepared with diverse morphologies by many different methods including metal-organic chemical vapor deposition and chemical solution deposition. Recently, we reported on the position-controlled growth of ZnO nanotubes and nanoflowers arrays and enhanced field-emission characteristics due to well-ordered spatial arrangement of 1-D nanomaterials. In spite of the excellent electron emitter characteristics of ZnO nanotube ordered arrays, the electron emission characteristics can be further improved by coating a nitride layer on the nanostructure arrays because an electron affinity of nitrides is much lower than that of ZnO. Here, we report on the fabrication of position-controlled AlN/ZnO coaxial nanotube heterostructure arrays and their field-emission characteristics.



**Kp-042** **Effect of gate bias sweep rate on the electronic properties of ZnO nanowire field effect transistors** MAENG Jongsun, JO Gunho, KWON Soon-Shin, SONG Sunghoon, SEO Jaeduck, KANG Seok-Ju, KIM Dong-Yu, LEE Takhee(*Gwangju Institute Science and Technology (GIST), Department of Materials Science and Engineering.*) ZnO nanomaterials have been widely applied as building blocks for nanoscale transistors, sensors, optoelectronics, and piezoelectric devices. The large surface area to volume ratio of ZnO nanowires have an influence on conductivity by adsorption and desorption of ambient oxygen. Adsorbed oxygens that bind the electrons localized at the nanowire surface become oxygen ions in the forms of $O^-$, $O^{2-}$, or $O_2^-$, resulting in a surface depletion in the nanowire channel. We will present the effects of gate bias sweep rate on the electronic characteristics of ZnO nanowire field effect transistors (FETs) under different environments. The adsorption of oxygen on ZnO nanowire surface is dependent on the gate bias sweep rate. The current, threshold voltage, and carrier density were sensitively dependent on the gate bias sweep rate. Slower gate bias sweep rates result in larger depletion regions in the nanowire channel with more oxygen adsorption for longer gate biasing time, resulting in reduction of current and carrier density and shift of gate bias in the positive gate bias direction.. Particularly, we characterized and compared the effects of the gate bias sweep rate for ZnO nanowires FETs under different oxygen environments; when the nanowire FETs were characterized in ambient air or $N_2$–filled glove box with or without passivation.

**Kp-043** **Fabrication of Nano-electrodes and Transport Characteristics through Single and Coupled InAs/GaAs Quantum Dots** 노 삼규, 김 준오[1], 이 상준, 정 관수[2], 최 정우[1], 황 종승[3], 오 정현[4], 안 도열[4], 황 성우[3](*한국표준과학연구원 전략기술연구부. [1]경희대학교 물리학과. [2]경희대학교 전자컴퓨터공학부. [3]고려대학교 나노기능소자연구센터. [4]서울시립대학교 양자정보처리연구센터.*) The vertical transport behavior in single and coupled InAs/GaAs quantum dots (QDs) has been investigated by low-temperature current-voltage (I-V) measurements. In order to characterize the electron tunneling through only a few QDs, two-terminal vertical device structure with a nanoscale top electrode was designed. The nano-electrodes were fabricated on single- and double-stacked InAs QD *ensembles* that were grown by the Stranski-Krastanow mode. For isolation between the top electrode and the bottom QD substrate, thin $SiO_2$ layers were deposited on the QD substrates. PMMA was spin-coated on the front surface of samples, and the top nano-hole electrode with a 160-nm diameter was patterned by a standard e-beam lithography process. The device was completed by Au-evaporation just on the patterned nano-holes, using a shadow mask with large circular openings. Because $SiO_2$ film is a good insulator, a top electrode *sees* only a few QDs through a nano-hole. The I-V characterization of devices was performed by using semiconductor parameter analyzer at a temperature of 4.5 K. Distinguished peaks and oscillatory behaviors were observed in the conductance curve at specific voltage regions. The conductance peak separations for single-stacked QDs are 135/85/70 meV and 70/55/50 meV for small/medium/large QD, whose value corresponds to the sublevel energy spacing of s-p and p-d states, respectively. The origin of conductance oscillations observed in coupled QD is not clear yet, and the measurements at 100 mK are now under plan.

**Kp-044** **Optical and Electrical Activation Studies of Si-Implanted $Al_{0.45}Ga_{0.55}N$** RYU Mee-Yi, MOORE Elizabeth A,[1], YEO Yung Kee[1], HENGEHOLD Robert L.[1](*Kangwon National University, Department of Physics. [1]Air Force Institute of Technology.*) Both optical and electrical activation studies of Si-implanted $Al_{0.45}Ga_{0.55}N$ have been made as a function of ion dose and anneal temperature by using the cathodoluminescence (CL) and temperature-dependent Hall-effect measurements. The CL intensity of near band emission increases as the anneal temperature is increased up to 1300 $^oC$, indicating a successive implantation damage recovery with increasing anneal temperature. The carrier concentration (activation efficiency) and Hall mobility also increased with anneal temperature, which agree well with the CL results. The results of Hall-effect measurements show that nearly 100% electrical activation efficiencies were obtained from the Si-implanted $Al_{0.45}Ga_{0.55}N$ samples for doses of $1x10^{14}$ and $5x10^{14}$ $cm^{-2}$ after annealing at 1350 $^oC$ and for a dose of $1x10^{15}$ $cm^{-2}$ after annealing at 1250 $^oC$. The effective Si donor ionization energy decreased with increasing carrier concentration as the anneal temperature increased and/or the implanted ion dose increased. The obtained ionization energies (~2.8-14 meV) are much lower than the predicted energy of about 59 meV. These low ionization energy can be attributed to the formation of a degenerate conduction band merged with impurity band resulting from exceeding the Mott transition concentration.

**Kp-045** **질화물 LED의 발광효율 향상을 위한 표면 위에 Alumina powder의 도포와 surface texturing 방법** 양 계모, 김 태기, 김 승환, 배 성준[1], 심 규환, 임 기영(*전북대학교, 반도체화학공학부, 반도체물성연구소. [1](주)옵토웰.*) 본 연구는 질화물

LED 내부에서 발생된 광을 효과적으로 외부로 추출함으로써 고효율 발광특성을 실현하고자, MOCVD방법으로 사파이어 기판 위에 성장한 질화물 LED 시료의 투명전극 위에 GaN 박막(n=2.5)과 공기(n=1)의 중간 정도의 굴절율을 가지는 투명한 Alumina powder(n=1.6)의 도포를 시도하였으며, 도포된 파우더를 거친 표면을 갖는 투명전극의 형성을 위한 mask로서 사용하여, 파우더가 도포된 거친 표면의 투명전극을 갖는 질화물 LED를 제작하였다. 또한, 파우더 도포조건과 투명전극 에칭조건을 다양하게 변화를 주어, LED 특성에 미치는 영향을 연구하였다.

**Kp-046** **Indium interruption growth법으로 성장시킨 InAs 양자점의 광학적 특성 연구** 이 희종, 류 미이, 김 진수[1](*강원대학교, 물리학과. [1]전북대학교, 신소재공학부.*) S-K (Stranski-Krastanove) 성장 모드로 GaAs (100) 기판 위에 분자선에피택시 (molecular beam epitaxy, MBE)을 이용하여 성장한 InAs 양자점의 광학적 특성을 PL (Photoluminescence)와 TR-PL (Time-Resolved PL)을 측정하여 분석하였다. 실험에 사용한 시료는 InAs 양자점 성장 동안 As는 계속 공급하면서 In 셔터를 1초 열고, 9초, 19초, 29초, 또는 39초 셔터를 닫는 방식 (Indium interruption growth법)을 이용하여 성장하였다. 또한 양자점 성장 동안 In 공급을 중단하지 않고 30초 동안 성장한 시료를 기준 시료로 사용하였다. In interruption 시간을 조절함으로써 양자점의 PL 피크의 위치가 상온에서 1200 nm에서 1300 nm까지 변화되었고 PL 특성도 변화하였다. 또한 양자점을 이용한 소자 제작 시 양자점 내의 에너지 레벨 사이에서의 carrier dynamics가 중요하므로 In interruption growth법으로 성장한 시료들의 carrier lifetime을 측정하였다. In interruption 시간을 조절함으로써 양자점의 크기와 밀도를 조절할 수 있으므로 원하는 파장대의 양자점을 성장할 수 있다.

**Kp-047** **Strain Modification in GaSb/InAs Type-II Superlattices** KIM Jun Oh, LEE Sang Jun, KIM Chang Soo, NOH Sam Kyu, CHOE Jeong Woo[1], KRISHNA Sanjay[2](*Center for Advanced Measurements and Instrumentations, Korea Research Institute of Standards and Science. [1]Department of Physics, Kyung Hee University. [2]Electrical and Computer Engineering Department, University of New Mexico.*) It has been already demonstrated that the infrared (IR) photodetectors based on GaSb/InAs strained superlattice (SLS) are excellently operated up to room temperature by virtue of low thermal ionization attributed to type-II band alignment which electrons are confined in InAs layer whereas holes in GaSb layer. In this study, we present structural and optical characteristics of the GaSb/InAs type-II SLs with different layer thicknesses grown by molecular beam epitaxy (MBE). For the modulation of transition energy, the layer thickness of GaSb and/or InAs was changed from 4/4 monolayers (MLs) to 8/21 MLs at a fixed period of 50. The high-resolution x-ray diffraction (HR-XRD) measurement and the infrared photoluminescence (IR-PL) spectroscopy have been conducted for monitoring the strain modification and analyzing the miniband alignment. The HR-XRD curves taken from GaSb/InAs SLS with different layer thickness show that their satellite peaks are well developed up to $\pm$3rd order and the 0th-order peak gradually moves to the reference position of GaSb buffer peak as the layer becomes thicker. The inter-miniband transition mechanism in GaSb/InAs SLS structures will be discussed on the basis of IR-PL spectra.

* This work was supported by the Korea Foundation for International Cooperation of Science and Technology (KICOS) through a grant provided by the Korean Ministry of Science and Technology (MOST) in 2007 (No. 2007-00011) for GRL project.

**Kp-048** **MOCVD 성장 조건에 따른 GaN nanowire의 특성** 신 대근, 우 시관, 오 병성, 김 태규[1], 이 형규[1], 김 창수[2](*충남대학교 물리학과. [1]충북대학교 전기전자 컴퓨터 공학부. [2]한국표준과학연구원.*) 일차원 구조체인 nanowire는 nanophotonics와 nanoelectronics에 가장 기본이 되며 그 응용 가능성이 높다. 특히 GaN nanowire는 청색 발광 및 기억소자의 응용가능성 때문에 관심을 끈다. Ni을 수십 Å의 두께로 올린 Si(100)기판을 사용하여 Metal-Organic Chemical Vapor Deposition (MOCVD)법으로 GaN nanowire를 성장 시켰다. Ni은 고온에서 droplet이 되어 catalyst 역할을 하게 된다. 성장조건에 따른 변화를 연구하기 위하여 GaN nanowire 성장에 적합한 기판온도를 찾아보았다. 또한 Ⅴ-Ⅲ 비율도 변화시켰다. GaN nanowire의 길이는 수 ㎛, 지름은 수백 ㎚ 정도로 성장되었다. PL, FE-SEM, XRD 등으로 구조적, 광학적 특성을 살펴보았다.

**Kp-049** **Analysis of energy levels in p- and n-type InAs/GaAs quantum dots by deep level transient spectroscopy measurements** KIM Jin Soak, KIM Eun Kyu, KIM Jun Oh[1], LEE Sang Jun[1], NOH Sam Kyu[1](*Department of Physics and Quantum-Function Spinics Laboratory, Hanyang University, Seoul 133-791, Korea. [1]Korea Research Institute of Standards and Science, Deajeon 305-600, Korea.*) Energy level properties of InAs/GaAs self-assemble quantum dots were analyzed by using deep level transient spectroscopy (DLTS) methods with minutely changing conditions such as filling pulse width. In order to find information for the not only conduction band but also valence band, p- and n-type samples were used either. The InAs/GaAs QD system was grown on $n^+$- and $p^+$-GaAs substrate by a molecular beam epitaxy method. The GaAs buffer and capping layers were grown at 570 $^oC$ with $5\times10^{16}$ $cm^{-3}$ doping concentrations, and InAs QD was grown at 495 $^oC$. A thickness of the capping layer was 350 nm. Finally, a Schottky diode structure with the QD system was made to measure capacitance changing by applied biases. From calculated depth profile and C-V data of the n-type QD system, a carrier accumulation peak was clearly observed at ~350-nm depth. The bias ranges for the DLTS measurement were determined by this information. Then, the pulse condition for DLTS was varied. And then, the information for the conduction and valence band of the QD system could be derived from the DLTS measurements

**Kp-050** **접합과도용량분광법을 이용한 복층 InAs/GaAs 양자점 시스템의 에너지 준위 연구** 이 윤일, 김 진석, 김 은규, 김 준오[1], 이 상준[1], 노 삼규[1](*한양대학교, 물리학과. [1]한국표준과학연구원.*) 양자점(QD)은 수소원자나 상자속의 입자와 같이 매우 작게 제한된 영역에 불연속적인 에너지 준위가 분포되어 있는 상태함수 구조를 가지고 있다. 양자점 시스템 안에서 전자

나 흘은 불연속적인 에너지 분포를 가지면서 존재하게 되고 이런 성질은 레이저 다이오드나 양자논리소자와 같은 다양한 구조에 응용 가능하다. 특히, GaAs나 InP를 기반으로 하는 자기조립 InAs 양자점 시스템은 그 에너지 구조 상 1.3 ~ 1.55 ㎛ 영역에서 동작할 수 있기 때문에 광통신에 사용되는 레이저 다이오드 및 광다이오드에 광범위하게 사용되고 있다. 따라서, 양자점 시스템에 대한 이론적인 연구나 응용을 위한 연구가 활발히 이루어지고 있다. 대부분의 경우 양자점 구조의 측정은 photoluminescence와 같은 광학적인 방법으로 하는데, 전자소자로의 응용 및 소자 효율 증대를 위해서는 전기적인 물성측정과 병행되어야 한다. 본 연구에서는 InAs/GaAs 양자점 시스템의 에너지 준위 특성을 전기용량 (C-V) 측정과 접합과도용량분광법 (DLTS) 을 통하여 분석하였다.

**Kp-051** **혼합소스 HVPE-비형광체 White-LED의 발광 메커니즘 분석** 안 형수, 이 아름, 전 헌수, 홍 상현, 김 은주, 한 영훈, 김 경화, 하 홍주, 양 민, 황 선령[1], 김 석환[2], 조 채용[3](*한국해양대학교, 나노반도체공학과. [1]삼성전자 주식회사. [2]안동대학교, 물리학과. [3]부산대학교, 나노메디컬공학과.*) 최근 백색 LED는 백열전구를 대체할 차세대 조명 광원으로서 각광받고 있다. 전 세계적으로 활발하게 진행되고 있는 백색 LED를 구현하기 위하여 고휘도 RGB발광 다이오드들의 조합, 다층구조나 웨이퍼 접합 등을 통한 단일 칩 발광 다이오드 구현, 청색다이오드와 황색 형광체 조합, 자외선 다이오드와 형광체를 여기시키는 방식이 개발되어 다양한 응용 분야가 기대된다. 본 연구에서는 n-GaN templated 사파이어 웨이퍼를 사용하여 InAlGaN/AlGaN 이중이종접합구조(Double Hetero)를 혼합소스 HVPE 법과 multi-sliding boat를 사용하여 제작하였다. 제작된 LED 소자의 EL 특성은 403 nm ~ 410 nm 부근의 main peak와 550 nm ~ 610 nm 부근의 넓은 파장 영역으로 인해 백색 발광이 관측되었다. 이러한 원인과 그 메커니즘을 분석하기 위하여 활성층에 대해 PL(Photoluminescence), CL(Cathodlumicesence), XPS(X-ray photoelectron spectroscopy)를 각각 측정하였다. PL 측정 결과 357 nm 부근에서 나타나는 peak는 사파이어 위에 성장된 GaN층에 의한 peak로 판단되며 550 nm ~ 610 nm 부근에서 나타나는 peak는 Al과 In의 불순물 결합에 의한 yellow 준위의 영향이라고 판단된다. 또한 CL 측정 결과도 PL과 마찬가지로 비슷한 부근에서 peak가 관찰되었다. XPS 측정결과, Al 조성이 14 %, In 조성이 3 %임을 알 수 있었다.본 실험에서 제작된 비형광체 백색 LED는, GaN의 방출 파장과 Al, In과 관련된 방출파장이 합성되어 백색광 파장이 방출된다고 판단된다. 혼합소스 HVPE법은 기존의 HVPE와 달리 소스를 혼합하여 주입하기 때문에 Cl 전구체가 각 소스들을 한번에 이동시키고, NH3에서 N이 이동되어 표면 위에 확산되어 화학적, 물리적으로 결합할 것으로 예상된다. 각 원소의 조성비와 반응성에 따라 In이 풍부한 영역에 InGaN계열이 형성되고 Al 풍부한 영역에 AlGaN이 형성되어 임의의 cluster를 형성하고 제한적인 구간별로 여러 원자들이 아주 다른 크기로 성장되어서, 이로부터 서로 다른 파장대의 빛의 방출이 합쳐져 육안으로는 백색이 관측된다고 판단된다. 따라서 기존의 형광체 LED와 차별화된 혼합소스 HVPE LED의 성장 메커니즘이라고 해석되며 비형광체 백색 LED의 제작 가능성이 기대된다.

* 본 연구는 2008년도 재단법인 부산테크노파크의 지원에 의하여 연구되었음 *

**Kp-052** **비형광체 백색 HVPE-LED램프의 광 특성** 안 형수, 김 은주, 전 헌수, 홍 상현, 한 영훈, 이 아름, 황 선령[1], 김 석환[2], 김 상묵[3](*한국해양대학교 나노반도체학과. [1]삼성전자 주식회사. [2]안동대학교 물리학과. [3]한국광기술원.*) 현재 백색 LED는 모바일 디스플레이의 백라이트나 표시등, 전조등이 주를 이루어 한정적으로 응용되어왔지만 최근에 고효율의 백색 LED 조명 상용화를 위하여 생산 단가를 낮추기 위한 연구가 활발히 진행 중이다. 백색 LED를 조명으로 사용하기 위하여 갖추어야 할 조건으로 광출력, 고휘도, 고효율과 같은 특성 뿐 아니라 이를 조절하고 질을 향상시키기 위하여 CCT (Correlated color temperature : 상관색온도 ), CRI (Color rendering index : 색 연색성 계수) 등 과 같은 백색 LED의 특성 분석이 필요하다. 색 CRI는 태양광을 물체에 비출 때 15 개 의 기준색상을 인지하는 정도로서, 0 이상 100 까지의 수치를 가진다. CCT는 빛의 색이 고온의 고체에서 나오는 빛과 비교할 때 광속을 상관시켜 표시한 것 즉, 발광체의 온도를 나타내는 방법 중 하나로서, 온도가 높을수록 눈이 부시고 푸른 색을 띠는 백색이 된다. 백열전구처럼 따뜻한 느낌의 백색인 경우 그 이상으로 높다. 일반적인 백색 LED의 경우 3200 K 및 5500 K에서 60-70 정도의 CRI를 제공하며 이상적인 백색 LED는 6500 K에서 색좌표 (x=0.313, y=0.329)값을 가진다. 본 연구에서는 혼합소스 HVPE(Hydride Vapor Phase Epitaxy)을 사용하여 활성층이 GaN(Al, In)을 기반으로 한 단일 칩 형태의 비 형광체 백색 LED를 제작하고, 패키징 후 그 특성을 분석하였다. 패키징된 백색 LED의 CRI와 CCT를 측정한 결과, 30 mA의 동작전류에서 CCT는 8900 ~ 10500 K, CRI 값은 76 ~ 87로 측정되었으며, 색좌표는 x=0.26 ~ 0.33, y=0.31 ~ 0.37에서 나타났다. 또한 주입 전류가 증가함에 따라 yellow로 이동하고 있어 기존의 형광체가 있는 백색 LED와 다른 경향을 보였으며, 이는 본 연구의 샘플이 비형광체 백색 LED임을 증명하고 있음을 확인할 수 있었다. 따라서 본 연구에서는 혼합소스 HVPE 방법을 통하여 제작단가가 저렴하고 제작방법이 매우 간편한 단일 칩 형태의 소자인 비형광체 백색 LED램프의 제작 가능성을 확인하였다. 이는 소자 구조, 방열, 패키지 구조 등의 개선을 통하여 저 전력의 고효율 백색 LED 분야에 큰 파급효과를 기대할 수 있을 것으로 판단된다.

* 본 연구는 2008년도 재단 법인 부산테크노파크의 지원에 의하여 연구되었음. *

**Kp-053** **Magnesium Doping Effects of $Al_xGa_{1-x}As$ Epitaxial Layers Grown by Molecular Beam Epitaxy** KIM Min Su, KIM Do Yeob, KIM Tae Hoon, KIM Ghun Sik, CHOI Hyun Young, CHO Min Young, RYU H. H., JEON Minhyun, CHO Guan Sik, KIM Jong Su[1], KIM Jin Soo[2], LEE D. Y.[3], SON J. S.[4], LEEM J. Y.(*School of Nano Engineering, Institute of Nano Manufacturing, Inje University. [1]Nano Photonics Group, Advanced Photonics Research Institute. [2]Division of Advanced Materials Engineering, Chonbuk National University. [3]Lighting Module Research and Development, Samsung Electro-mechanics. Co., Ltd. [4]Department of Visual Optics, Kyungwoon University.*) Magnesium (Mg) doped $Al_xGa_{1-x}As$ epitaxial layers were grown by molecular beam epitaxy (MBE) on (100) GaAs substrates using different growth conditions, including varying Mg cell temperature, Al mole fraction, substrate temperature, and As/Ga beam equivalent pressure (BEP) ratio. The epitaxially grown Mg doped $Al_xGa_{1-x}As$ layers were characterized using Hall measure-

ments and photoluminescence (PL) to investigate their electrical and optical properties, respectively. The carrier concentration by the Hall measurements of the samples decreased from $1.86 \times 10^{17}$ to $4.87 \times 10^{14}$ $cm^{-3}$ with increase in substrate temperature ranged from 530 to 630 ℃. This can be attributed to dramatically decrease in Mg incorporation on Ⅲ-Ⅴ epilayers with increase in substrate temperature. The photoluminescence (PL) spectra of the Mg doped $Al_{0.13}Ga_{0.87}As$ samples with the substrate temperature range were red-shifted ranging from 1.780 to 1.768 eV when p-type doping level increased. The full width at half maximum (FWHM) varied from 19 to 29.6 meV as the spectra were red-shifted. The electrical and optical properties of the Mg doped $Al_xGa_{1-x}As$ samples also depend on the Al mole fraction and As/Ga BEP ratio. In comparison to Be doped AlGaAs samples, the mobilities of Mg doped $Al_{0.13}Ga_{0.87}As$ layers more rapidly increased as the p-type doping concentration was decreased. Since Mg as a p-type dopant is more effective for AlGaAs epilayers grown at 600 ℃ and with hole concentrations below $10^{18}$ $cm^{-3}$, it is expected that Mg could be a reasonable p-type dopant for nanostructured semiconductors fabricated at low temperatures.

**Kp-054** **Photocurrent Spectroscopy of $Al_{0.3}Ga_{0.7}As$/GaAs High Electron Mobility Transistor Structure** 고 병수, 김 정화, 배 인호(*영남대학교 물리학과.*) The electronic properties of $Al_{0.3}Ga_{0.7}As$/GaAs high electron mobility transistor(HEMT) have been investigated by photocurrent(PC) spectroscopy. The PC measurements were performed in temperature range between 18 and 300 K. We observed three peaks at room temperature PC spectra. The peaks at 1.416 and 1.804 eV are related to the GaAs and $Al_{0.3}Ga_{0.7}As$ band gap transitions, respectively. The transition observed at 1.968 eV attributed to the x-valley of $Al_{0.3}Ga_{0.7}As$. The PC intensity increases with increasing light intensity, dc bias voltage and temperature. At low temperature, we observed two signals associated to the surface quantum well and to the two dimensional electron gas(2DEG), respectively. In addition, we have also studied the Varshni coefficients for $Al_{0.3}Ga_{0.7}As$/GaAs HEMT structure.

**Kp-055** **MOCVD 법으로 성장한 GaN 에피층의 전자빔 조사에 따른 깊은준위 결함상태 분석** 하 임경, 이 동욱, 김 진석, 김 은규, 배 성범[1], 이 규석[1], 오 대곤[1], 한 영환[2], 이 병철[2](*한양대학교 물리학과. [1]한국전자통신연구원. [2]원자력연구소 양자광학실험실.*) GaN는 3.4 eV 정도의 넓은 띠 간격이 특징인 물질로 일본의 나카무라에 의해 1993년 청색 발광 소자로 개발된 이래 청색 파장의 발광 다이오드(light emitting diodes-LED), 레이저 다이오드 (laser diode-LD), 자외선 감지기 (UV detector) 등의 광소자 쪽으로 응용되고 있다. 최근에는 양자 구조나 어긋나기(dislocation) 및 결함 구조를 이용하여 출력 효율이나 발광 특성을 조절하려는 노력으로 진행되고 있는데, 반도체 결정에서 어긋나기나 결함은 성장 조건에 의해 성장 과정에서도 발생할 수 있지만, 고에너지로 가속된 입자의 인위적인 조사(irradiation)에 의해서도 생성이 가능하다. GaN 반도체의 경우 전자 소자로 만들었을 때 높은 전압에서 동작할 수 있고, 낮은 누설 전류(leakage current) 특성을 보여 고전압, 고전력 소자(hight power device)로의 응용역시 기대되는데, 익히 알려져 있듯이 스윗칭 (switching) 소자 등에서 전력의 손실을 방지하려면 소수 운반자(minority carrier)의 수명(life time)을 짧게 조절하여야 한다. 적절히 생성된 결함은 소수 운반자를 포획하여 운반자의 수명을 줄여주기 때문에 소자 응용에 매우 중요하다. 이를 위해서는 먼저 GaN 에피층의 전기적 특성들과 박막 내의 결함을 조사하는 것이 우선된다. 본 연구에서는 MOCVD 기법으로 성장된 GaN 에피층에 1 MeV로 가속된 전자빔을 $1\times10^{16}$ $cm^{-2}$ 농도로 조사하여 결함을 생성하였다. 결함에 대한 특성 확인은 쇼트키장벽 다이오드(Schottky barrier diode)구조를 만든 후, 바이어스 전압 및 채움펄스폭의 변화 등 다양한 조건에서 전기용량 (C-V) 및 깊은준위 접합과도용량분광법(Deep Level Transient Spectroscopy-DLTS)을 이용하여 운반자의 공간적인 농도분포와 새롭게 고에너지 전자선에 의해 생성된 결함 상태를 분석 연구하였다.

**Kp-056** **Investigation of magneto-transport properties of GaMnAs:Si ferromagnetic semiconductors** KIM Hyungchan, CHUNG Sunjae[1], YOO Taehee[1], KIM jungtaek[1], LEE Sanghoon[1], LIU X.[2], FURDYNA J. K.[2](*Physics Department, Korea University. [1]Physics Department, Korea University, Seoul, Korea. [2]Physics Department, University of Notre Dame, Notre Dame, Indiana, USA.*) We investigated a series of n-type doped GaMnAs:Si of ferromagnetic semiconductor films by magneto transport. Since Si act as n type dopant, we are able to incorporate Mn up to 10 % in GaMnAs. Though it is reported that the $T_C$ of GaMnAs decreases with increasing Mn concentration above 6%, our GaMnAs:Si samples showed systematic increase of $T_C$ even up to 10%. This indicates the effectiveness of our counter doping technique for improving $T_C$ of GaMnAs-based ferromagnetic semiconductor. The low temperature annealing further increase $T_C$ up to 165 K in GaMnAs:Si with 10% of Mn. The planar Hall resistance measured on the as-grown samples revealed the presence of strong cubic anisotropy and change of uniaxial anisotropy from [-110] to [110] direction with increasing Mn concentration in the series of samples. The systematic change of magnetic anisotropy with increasing temperature was also observed due to the variation of carrier density in the GaMnAs:Si by increasing temperature.

**Kp-057** **Temperature dependent magnetic Anisotropy in (Ga,Mn)As/(In,Ga)As/(Ga,Mn)As tri-layer with different thicknesses of (In,Ga)As spacer layer** LEE Hakjoon, CHUNG Sunjae, CHOI Ilsoo, KIM Yungjun, LEE Sanghoon, LIU X.[1], FURDYNA J.K.[1](*Physics Department, Korea University, Seoul Korea. [1]Department of Physics, University of Notre Dame, Notre Dame In, USA.*) We have investigated the effect of (In,Ga)As spacer layer thickness on magnetic anisotropy on the (Ga,Mn)As/(In,Ga)As/(Ga,Mn)As trilayer structures. The (Ga,Mn)As in the top and the bottom layers of structure have 2.7 % and 3.8 % of Mn composition, respectively. The thicknesses of (In,Ga)As spacer layer varies from 5 nm to 50 nm in the series. The magneto-transport measurements have been carried out with application of magnetic fields within in-plane and out-of plane. The magnetic anisotropy field obtained from temperature dependent angle dependence measurement showed systematic change with spacer layer thickness in the series. To accommodate

the contribution from both layers, we have introduced a parameter, $K_{eff}$/M, called as effect anisotropy barrier, which is the difference of free energy between in-plane easy and [001] direction. The sign of $K_{eff}$ determines the dominance of anisotropy in the sample (i.e., positive for dominant in-plane magnetic anisotropy and negative for dominant out-of-plane magnetic anisotropy). This phenomenon results from the increase of tensile strain on the (Ga,Mn)As by increasing (In,Ga)As spacer layer thickness. The temperature dependence of magnetic anisotropy is further discussed using one of the samples

**Kp-058** **Magneto-transport properties of MnAs/GaMnAs multi-layered structures with and without GaAs spacer** KIM Yungjun, KIM Jungtaek, YOO Taehee, SON Hyunji, CHUNG Sunjae, LEE Sanghoon, LIU X.[1], FURDYNA J.K.[1](*Physics Department, Korea University, Seoul, Korea. [1]Physics Department, University of Notre Dame, Notre Dame, Indiana, USA.*) We have investigated the magneto-transport properties of MnAs/GaMnAs multi-layered structures with and without GaAs spacer. The samples were grown by molecular beam epitaxy technique on (001) GaAs substrate. The thickness of spacer in the one of structures is 1.4 nm. The Curie temperatures ($T_C$ ) of the two samples were estimated from temperature dependent resistivity, which showed peak at 74 and 96 K , respectively, for the samples with and without GaAs spacer. This indicates that the $T_C$ of GaMnAs layer was strongly affected by GaAs spacer. The planar Hall resistance (PHR) and magneto-resistance were also measured to investigate magnetic anisotropy properties. The field scan of PHR data were obtained at every 10 degrees from [110] direction. The two samples showed different transition behavior in the magnetization reversal process indicating influence of GaAs spacer layer on the magnetic anisotropy of GaMnAs layer.

**Kp-059** **MBE - Growth and Properties of Mg-doped InGaAs Epitaxial Layer** 최 현영, 조 민영, 김 군식, 유 경열, 임 광국, 한 영재, 정 동균, 김 도엽, 김 민수, 김 태훈, 임 재영(*인제대학교 나노공학부.*) 분자선 에피택시 방법을 이용하여 GaAs 기판 위에 Mg 불순물이 첨가된 InGaAs 에피층을 성장하고 그 특성을 Hall Effect와 Photoluminescence (PL) 등으로 조사하였다. InGaAs 박막성장 시 박막의 특성 변화를 조사하기 위하여 기판온도, In 조성비, Mg flux ratio 등의 성장 변수를 바꾸면서 성장하였다. InGaAs 에피층 성장 시 As의 beam equivalent pressure (BEP)는 $1\times10^{-5}$ Torr 이었으며, 성장층의 두께는 7500 Å 이었다. In 조성비가 0.156인 InGaAs 에피층에서 약 $2.07\times10^{18}/cm^3$의 정공 농도를 얻을 수 있었으며, 그때 이동도는 약 67 $cm^2/(V\cdot s)$ 이었다. 한편 PL 측정결과 near band-gap (NBG)에 대응하는 피크와 세기가 매우 미약한 결함 및 불순물에 관련된 피크가 관측되었다. 또한 이들 피크에 대하여 온도 및 여기광의 세기에 따른 변화를 측정하였다.

**Kp-060** **Photocurrent Spectroscopy를 이용한 InGaN/GaN 청색 발광다이오드의 활성층 성질 분석에 관한 연구** 송 재호, 김 호종, 안 병준, 이 기원, 최 성철[1], 여 환국[1], 문 영부[1], 송 정훈(*공주대학교, 물리학과. [1]더리즈(주).*) InGaN/GaN 청색 발광다이오드 구조의 양자우물 내에서 강하게 존재하는 압전 전기장은소자 전체의 발광 특성에 매우 중요한 영향을 끼친다. 그러나 현재까지 보고된 압전 전기장의 크기는 0.7 MV/cm 에서 2MV/cm 까지 큰 편차를 보이고 있고, 시료구조 및 측정 방법에 따라 일관되지 않은 결과가보고 되고 있다. 본 연구에서는 photocurrent spectroscopy를 이용하여 InGaN/GaN 청색 발광다이오드에서 활성층의 성질에 관하여 분석하였고, 더 나아가 개별 시료에 대한 압전 전기장 크기의 측정을 시도하였다. Xenon lamp의 백색광을 분광하여 InGaN/GaN 발광다이오드에 조사시켜 입사광의 에너지 변화에 따른 photocurrent를 측정하여 흡수 스펙트럼을 관측하였다. 미세전류 측정계의 최적화를 통하여 높은 Signal/Noise 비를 얻을 수 있었다. 양자우물구조 내에 강하게 인가된 압전 전기장은 Stark 효과에 의해서 흡수 스펙트럼의 tail 상태를 만들고 스펙트럼의 기울기를 변화시킨다. 시료에 역방향 바이어스를 인가했을 때 인가된 전기장은 시료의 압전 전기장의 방향과 반대 방향이다. 입사광의 에너지대한 photocurrent 스펙트럼을 분석하였고, 스펙트럼의 기울기 변화를 관측하였다.외부에서 인가한 바이어스에 의해 총 내부전기장의 세기가 보상될 때, 그 보상 바이어스 값을 통해서 압전 전기장의 크기를 구하는 분석을 시도하였다. 또한 시료구조에 따라 크기가 다른 압전전기장을 보다 정확히 측정할 수 있는 분석틀 확립에 관해 논의할 것이다.

**Kp-061** **Carrier and Piezoelectric Field Dynamics in InGaN/GaN MQW's Studied by Spectrum-resolved Pump-probe Measurements** KIM Chang-seop, CHANG Dong-wook, KIM Ji-hee, YEE Ki-ju, KIM J. C[1], CHOI Y. H[1], NOH M. S[1](*Department of Physics, Chungnam National University. [1]LG Electronics Institute of Technology.*) We investigated the carrier localization process into potential minima of InGaN layers and the subsequent piezoelectric field modifications in InGaN/GaN multiple quantum wells using femtosecond Ti:sapphire oscillator with 400nm center wavelength, around 40 nm FWHM. We have analyzed the carrier lifetime, which was performed spectrum-resolved pump-probe experiments on InGaN/GaN MQW's grown on the hydride vapour phase epitaxy (HVPE) GaN substrate, through the relation between the carrier localization and piezoelectric field. It is interesting that the transmission change by the carrier excitation takes different signs as the detection wavelength is scanned from 405 nm to 394 nm. This spectral results can explained by the modulated Franz-Keldysh effect due to the piezoelectric field screening. With analyzing the spectrum-resolved results measured at different excitation power, we could find that the field screening is affected by the carrier localization and carrier localization process into potential minima occurs around within 50 ps for the measured InGaN/GaN MQW's sample.

**Kp-062** **Light Extraction in InGaN LED with n-GaN nano patterns** PARK Si-Hyun, HONG Jun-Hee(*Dept. of Photonic Engineering, Chosun University.*) n-GaN layer at InGaN-LED was the patterned with the nano-size SiO2 columns by using a self-assembled indium tin oxide clusters as etching mask. The measured total light output power of our LED showed the increase compared to that of the reference LED. The increase of outpour power from PNS-LED depends on the SiO2 column size onto n-type GaN

sub-strate. We performed FDTD simulation on our LED structures and results confirmed with our experimental results.

**Kp-063** **Synthesis of single-crystalline GaN nanorods grown by HVPE** 이 삼녕, 문 진영, 권 해용, 최 윤정, 신 민정, 장 지호, 윤 용주[1], 김 상훈[1], 하 동한[1], 박 승환[2](*한국해양대학교, 응용과학부. [1]한국표준과학연구원, 전략기술부. [2]대구가톨릭대학교, 전기전자공학부.*) GaN, which has a wide and large direct band gap, is one of the most proper materials for light-emitting diodes, and high-temperature and high-power electronic devices. We have studied the conditions for the formation of GaN nanorods by Hydride Vapor Phase Epitaxy (HVPE) method. GaN nanorods were obtained at the conditions of 1:40 flow ratio between HCl and $NH_3$ at growth temperature 650°C. And AlN buffer layer was deposited on a Si(111) substrate for 25 minutes by RF-Sputter before GaN growth. A high density of straight nanorods with diameter of 200~350nm were formed uniformly over the entire substrate. Their synthesis and structural properties are investigated by X-ray diffraction(XRD), scanning electron microscopy(SEM). The XRD pattern indicates that the formed GaN nanorods preferentially oriented in the *c*-axis direction.

**Kp-064** **Growth and Characterization of (1120) A-plane GaN on (1102) R-plane Sapphire** LEE YongSeok, SENTHIL KUMAR MUTHUSAMY, KIM HeeYun, OH TeaSu, CHUNG SangJo, HONG ChangHee, SUH EunKyung(*전북대학교 반도체물성연구소.*) GaN based optoelectronic devices grown on c-plane sapphire substrates posses a strong electric field at the hetero-interfaces due to internal spontaneous and strain-induced piezo-electric polarization which reduces the radiative recombination efficiency. GaN growth in a non-polar direction is proposed to avoid this effect and improve the device quantum efficiency. In this report, we describe the growth and characterization of non-polar (1120) a-plane GaN films on (1102) r-plane sapphire substrate by using metal-organic chemical vapor deposition (MOCVD). We have attempted to achieve smooth surface and good crystal quality GaN layer by optimization of MOCVD growth parameters itself. A nucleation layer was grown at 540 $^{o}$C followed by the growth of un-doped GaN layer at 1100 $^{o}$C. Trimethylgallium (TMGa) and ammonia flows were varied between 20 to 50 sccm and 1000 to 3500 slm, respectively. From scanning electron microscopy (SEM), we observe that the coalescence of GaN grains strongly depends on the ammonia flow and V/III ratio. Degree of coalescence is found to increase with the decrease of V/III ratio. A reasonably good surface and crystal quality a-plane GaN layer was obtained for the V/III ratio of below 500. The full width at half maximum (FWHM) of X-ray rocking curve was measured to be ~1400 arcsec. In photoluminescence, the band-edge peak of GaN is observed at 363 nm along with a stronger yellow luminescence peak. Further improvement in the quality of a-plane GaN will be achieved with optimized growth pressure and substrate nitridation.

* This work was supported by the Korea Research Foundation Grant funded by the Korea Government (MOEHRD)" (KRF-2005-005-J07501).

**Kp-065** **Studies on As-Grown and Heavy Ion Irradiated InAlGaN/GaN Heterostructures** SENTHIL KUMAR Muthusamy, LEE Yong Seok, CHUNG Sang Jo, HONG Chang Hee, SUH Eun Kyung(*전북대학교 반도체물성연구소.*) Group III nitride has strong potential for application in electro-optical devices in the UV to IR spectral range and also in high-power, high-frequency electronic devices due to its high electron-saturation velocity, high critical field, and high stability. Some of the proposed applications for AlGaN/GaN HFETs include nuclear industry monitoring and satellite-based broadband communication. The space environment contains a wide range of high energy particles including electrons, protons and heavy ions in the keV to GeV energy range. Radiation effects from these species cause material degradation and failure of the electronic systems. On the other hand, ion beams are also used for impurity doping and device isolation in semiconductors. In this work, we report 100 MeV Nickel (Ni) ion irradiation effects on the properties of InAlGaN/GaN heterostructure. The heterostructures were grown on c-plane sapphire substrates by using a low-pressure metal organic chemical vapor deposition system. The samples were irradiated with 100 MeV swift heavy Ni ions for a fluence of $5x10^{12}$ $cm^{-2}$ at room temperature. The (0002) x-ray rocking full width at half maximum (FWHM) value of as-grown InAlGaN layer was 254 arcsec and it was not changed by ion irradiation. However, the optical and electrical properties were severely affected by Ni ion irradiation. The PL peak intensity completely quenched after irradiation while its electrical properties turned to be highly insulating due to irradiation induced defects. It indicates that optical and electrical isolation is feasible in this heterostructure by using heavy ion irradiation without damaging the crystalline quality. A combined process of rapid thermal and furnace annealing partially recovered their optical and electrical properties.

* This work was supported by the Korea Research Foundation Grant funded by the Korea Government (MOEHRD)" (KRF-2005-005-J07501)

**Kp-066** **Growth of semi-polar (11-22)GaN on m-plane sapphire** SEO YONG GON, SUH MOON SUHK[1], YOON HYUNG DO[1], HWANG SUNG MIN[1], OH KYUNGHWAN[2] (*Institute of Physics and Applied Physics, Yonsei University; Energy-nano Materials Research Center, Korea Electronics Technology Institute. [1]Energy-nano Materials Research Center, Korea Electronics Technology Institute. [2]Institute of Physics and Applied Physics, Yonsei University.*) Growth of nonpolar and semipolar GaN films on sapphire substrates has been receiving considerable attention to reduce the spontaneous and strain-induced piezoelectric polarization effects. In this study, semipolar (11-22)GaN thin film was grown on m-plane sapphire by metal-organic chemical vapor deposition(MOCVD). Trimethylgallium(TMGa) with hydrogen carrier gas and ammonia were used as the Ga and N sources for the undoped GaN epigrowth. The growth procedure consisted of a 120nm thick GaN

with N2 atmosphere and 2um thick GaN with H2 atmosphere without a low temperature GaN buffer layer. The growth temperatures were 1050°C and 1110°C, respectively. From high-resolution X-ray diffraction measurements, the full width at half maximums of (11-22)GaN rocking curve was near 640 arcsec. We investigated the optical and surface properties of the GaN film analyzed by photoluminescence(PL) spectra and atomic force microscopy(AFM) image.

**Kp-067** **Enhancement of Light Extraction in InGaN- based LED with a high refractive index epoxy microlens array and a packaging dome lens.** PARK SI-HYUN, LEE Hyun-Haeng(*Department of Photonic Engineering, Chosun University.*) We fabricated an InGaN-based LED chip and integrated an epoxy microlens array onto a top p-GaN layer of LED chip where a value of a refractive index of the epoxy is relatively high, ~1.6. Then, a dome lens of another epoxy where the value of a refractive index is medium, ~ 1.5 was packaged onto the microlens integrated LED chip. The effects of microlens on light extraction caused the enhancement of light output. We measured the light output vs current for our LED with microlens and the reference LED without microlens. The increased of light output in our microlensed LED was observed compared with the normal LED. The using of the epoxy with the high refractive index value for the microlens array can contribute to the enhancement of light extraction in LED even after the general epoxy dome lens was packaged onto the LED chip. We performed the ray tracing simulation for our LEDs and confirmed the consistency with our experimental results.

**Kp-068** **ITO투명전극의 습식 식각에 따른 질화물계 반도체 발광다이오드의 광학 및 전기적 특성연구** 홍 창희, 강 지혜, 김 형구, 김 현규, 김 희윤, 유 재형, 한 남(*전북대학교 반도체화학공학부.*) P-형 오믹 접촉을 위한 ITO층에 ITO etchant를 이용한 습식 식각을 하여 GaN LED의 광추출 효율 변화를 관찰하였다. Electron-beam evaporator를 이용하여 ITO를 230nm 증착하고, Rapid Thermal Annealing을 이용하여 열처리하였다. ITO etchant LCE-12K를 45℃로 가열한 상태에서 Sample A는 ITO 전 면적을 wet etch 하였고, Sample B는 PR을 mask로 하여 4um dot pattern으로 국부적인 wet etch를 하였다. 이때 etch 시간을 각각 10s, 20s, 30s로 달리 하여 그 표면을 AFM과 SEM을 이용하여 각 sample의 거칠기를 측정, 관측하였다. 그 결과 시간이 경과함에 따라 거칠기가 증가하고 결정 크기가 커짐을 알 수 있었다. Conventional Sample과 Sample A, Sample B간의 전기적, 광학적인 차이를 Probe station을 이용한 I-V측정과 적분구를 이용한 광량 측정으로 비교, 분석 하였다.

**Kp-069** **나노 임프린트 리소그래피를 이용한 InGaN/GaN LED의 구조 및 광학적 특성** 홍 창희, 김 현규, 김 형구, 강 지혜, 변 경재[1], 이 헌[1](*전북대학교 반도체화학공학부. [1]고려대학교 신소재공학부.*) InGaN/GaN LED는 낮은 발광효율로 인하여 내부양자효율 (IQE), 외부양자효율 (EQE) 향상을 목적으로 많은 연구가 진행 중이다. 본 실험에서는 InGaN/GaN LED의 광추출효율을 향상시키기 위하여 나노 임프린트 리소그라피를 이용하여 LED의 투명전극층에 hole 모양의 나노크기 패턴을 형성하였다. 패턴의 크기는 400nm, 490nm, 540nm로 하였으며, 패턴의 간격은 각각 600nm, 700nm, 800nm 하였다. 전기적인 특성과 광학적 특성을 알아보기 위해 LED공정을 하였으며, probe-station과 적분구를 이용하여 I-V 특성과 EL특성을 알아보았다. I-V특성에서는 conventional LED와 큰 차이가 없었으며, EL특성에서는 490nm의 hole 패턴을 가진 LED가 광량이 약24%로 가장 많이 증가하였다.

**Kp-070** **Comparison of the Alpha Response from a Semi-insulating GaAs Radiation Detector at Variable Chemical Cleaning Conditions** KANG S. M., HA J. H.[1], PARK S. H.[1], KIM H. S.[1], KIM Y. K.(*Hanyang University, Nuclear Engineering. [1]Korea Atomic Energy Research Institute.*) In general, the requirement for a room temperature operation of a semiconductor material for a radiation detection is a large band gap energy such that the thermal generation of the signal carriers is kept to a minimum. The band gap of the GaAs is 1.42 eV and it is sufficiently wide to allow for its use as a radiation detector at room temperature. The properties of the GaAs wafer are a $7.58\times10^7$ ohm-cm resistivity, a 350 μm thickness, and a (100)-oriented type. We prepared 5×5 $mm^2$ samples by using a semiconductor diamond saw. Prior to a metallization process, the surfaces of the GaAs samples were cleaned by three processes, respectively. Metal/semiconductor contacts on the surface were fabricated by using a thermal evaporator in a high vacuum condition. The prototype GaAs detector had circular metal contacts of Ni/Au = 30/100 nm at each side and the diameter of a circular contact was 3 mm. The current-voltage characteristics of the GaAs semiconductor detector were measured by using a HP parameter analyzer with voltage sources. We measured the alpha response evaluated by $^{241}$Am with 5.485 MeV α-ray at room temperature and at an atmospheric pressure.
*Acknowledgments: This work was performed under the long-term nuclear research and development program sponsored by Ministry of Science and Technology of Korea, and supported by the Innovative Technology Center for Radiation Safety(iTRS).

**Kp-071** **PCR chip의 heat-sink로 사용되는 $Al_2O_3$나노유체의 특성 비교** 유 현준, 은 덕수[1], 공 대영[1], 홍 영명, 장 종민[1], 강 태욱[1], 조 영우[1], 장 성재[1], 정 상훈[1], 류 인식[2], 이 종현[1](*경북대학교 센서및디스플레이공학. [1]경북대학교 전기전자컴퓨터공학. [2]경동정보대학 정보통신과.*) 오늘날 MEMS 공정을 이용한 다양한 소형 메커니즘의 개발이 활발히 진행되고 있다. 이러한 MEMS 공정으로 만든 PCR chip은 빠른 반응 시간과 소형화의 이점을 가진다. 특히 PCR 과정에서 반응시간을 줄이기 위해서는 빠른 온도 컨트롤이 요구되어 진다. 이러한 문제를 해결하기 위해서 우수한 열전달 특성을 가진 나노유체를 heat-sink로 사용하면 빠른 온도 제어를 기대할 수 있다. 나노유체의 효과적인 이용을 위해 다양한 측정을 통하여 열전달 특성을 향상 시키는 요인을 파악 하였다. 사용된 나노입자의 크기, 농도, 기본유체의 종류, 분산 정도 등에 따라 제타포텐셜 및 점도, 비정상열선법을 이용한 유체의 열전달 특성 등을 측정하여 가장 효과적인 나노유체를 제작하였다. 또한 나노유체를 사용하기에 적합한 구조의 PCR chip을 설계하여 제작된 나노유체를 적용시켜 효과적인 heat-sink로 사용하였다. 본 논문에

서 제안한 방법으로 빠른 반응 시간을 가지는 소형화된 PCR chip의 제작이 가능할 것으로 기대되어 진다.

* 본 연구는 산업자원부와 한국산업기술재단의 지역혁신인력양성사업으로 수행된 연구결과임.

**Kp-072** **DFR을 이용한 PCR 챔버의 제작 및 시뮬레이션**

홍 영명, 은 덕수[1], 공 대영[1], 유 현준, 장 종민[1], 강 태욱[1], 장 성재[1], 조 영우[1], 정 상훈[1], 류 인식[2], 이 종현[1](*경북대학교, 센서및디스플레이공학. [1]경북대학교, 전기전자컴퓨터공학. [2]경동정보대학, 정보통신과.*) 오늘날 PCR(Polymerase Chain Reaction) 제작 기술의 대부분은 실리콘 벌크 마이크로머시닝과 SU-8 몰드를 이용한 PDMS 제작 기술이 주를 이루고 있다. 본 논문에서는 DFR(Dry Film Resist/Ordyl BF410)을 기반으로 하여 PCR 챔버를 제작하였다. 챔버의 안에는 백금 히터를 내장 하였으며, 기판으로는 글래스를 사용 하였다. 공정에 앞서 챔버의 형태에 따른 온도 분포 특성을 파악하기 위하여 ANSYS 시뮬레이션을 이용한 결과, 챔버의 각 모서리에서 온도 저하가 발생하는 사각형 모양의 챔버 보다 원형 모양의 챔버가 더 우수한 온도 분포 특성을 보였다. 따라서 챔버의 모양은 원형으로 설계되었으며, 소자를 완성한 뒤 열화상 카메라를 이용하여 온도 분포를 측정하고 그 결과를 ANSYS 시뮬레이션과 비교 하였다. 제작된 PCR 챔버의 온도 분포는 시뮬레이션 결과와 일치 하였고, 향후 다른 바이오 소자에도 DFR의 응용이 기대된다. 본 연구는 산업자원부와 한국산업기술재단의 지역혁신인력양성사업으로 수행된 연구결과임.

**Kp-073** **Properties of phoconductor for the $AgInS_2$ epilayers grown by hot wall epitaxy**

HONG KWANGJOON (*DEPARTMENT of PHYSICS, CHOSUN UNIVERSITY.*) A silver indium sulfide ($AgInS_2$) epilayer was grown by the hot wall epitaxy method, which has not been reported in the literature. The grown $AgInS_2$ epilayer has found to be a chalcopyrite structure and evaluated to be high quality crystal. From the photocurrent measurement in the temperature range from 30 K to 300 K, the two peaks of A and B were only observed, whereas the three peaks of A, B, and C were seen in the PC spectrum of 10 K. These peaks are ascribed to the band-to-band transition. The valence band splitting of $AgInS_2$ was investigated by means of the photocurrent measurement. The crystal field splitting, $\Delta cr$, and the spin orbit splitting, $\Delta so$, have been obtained to be 0.150 eV and 0.009 eV at 10 K, respectively. And, the energy band gap at room temperature has been determined to be 1.868 eV. Also, the temperature dependence of the energy band gap, $E_g(T)$, was determined.

**Kp-074** **Growth and electrical properties for $CuGaSe_2$ single crystal thin film by hot wall epitaxy**

HONG KWANGJOON (*DEPARTMENT of PHYSICS, CHOSUN UNIVERSITY.*) A stoichiometric mixture of evaporating materials for $CuGaSe_2$ single crystal thin films was prepared from horizontal electric furnace. Using extrapolation method of X-ray diffraction patterns for the polycrystal $CuGaSe_2$, it was found tetragonal structure whose lattice constant $a_0$ and $c_0$ were 5.615 Å and 11.025 Å, respectively. To obtain the single crystal thin films, $CuGaSe_2$ mixed crystal was deposited on thoroughly etched semi-insulating GaAs(100) substrate by the hot wall epitaxy (HWE) system. The source and substrate temperatures were 610℃ and 450℃, respectively. The crystalline structure of the single crystal thin films was investigated by the photoluminescence and double crystal X-ray diffraction (DCXD). The carrier density and mobility of $CuGaSe_2$ single crystal thin films measured with Hall effect by van der Pauw method are $4.87\times10^{17}$ $cm^{-3}$ and 129 $cm^2/V\cdot s$ at 293K, respectively. The temperature dependence of the energy band gap of the $CuGaSe_2$ obtained from the absorption spectra was well described by the Varshni's relation, $E_g(T) = 1.7998\ eV - (8.7489\times10^{-4}\ eV/K)T^2/(T + 335\ K)$.

**Kp-075** **Growth and temperature dependence of photocurrent spectrum for $ZnIn_2S_4$ sngle crystal thin film**

HONG KWANGJOON(*DEPARTMENT of PHYSICS, CHOSUN UNIVERSITY.*) Single crystal $ZnIn_2S_4$ layers were grown on a thoroughly etched semi-insulating GaAs(100) substrate at 450 ℃ with the hot wall epitaxy (HWE) system by evaporating the polycrystal source of $ZnIn_2S_4$ at 610 ℃prepared from horizontal electric furnace. The crystalline structure of the single crystal thin films was investigated by the photoluminescence and double crystal X-ray diffraction (DCXD). The carrier density and mobility of single crystal $ZnIn_2S_4$ thin films measured with Hall effect by van der Pauw method are $8.51\times10^{17}$ electron/$cm^{-3}$, 291 $cm^2$/v-s at 293K, respectively. The photocurrent and the absorption spectra of $ZnIn_2S_4$/SI(Semi-Insulated) GaAs(100) are measured ranging from 293 K to 10K. The temperature dependence of the energy band gap of the $ZnIn_2S_4$ obtained from the absorption spectra was well described by the Varshni's relation, $E_g(T) = 2.9514\ eV - (7.24\times10^{-4}\ eV/K)T^2/(T + 489\ K)$. Using the photocurrent spectra and the Hopfield quasicubic model, the crystal field energy($\Delta cr$) and the spin-orbit splitting energy($\Delta so$) for the valence band of the $ZnIn_2S_4$ have been estimated to be 167.8 meV and 14.8 meV at 10 K, respectively. The three photocurrent peaks observed at 10 K are ascribed to the $A_1$-, $B_1$-, and $C_{41}$-exciton peaks.

**Kp-076** **Growth-optical properties for $CdIn_2Te_4$ single crystal by Bridgman method**

HONG KWANGJOON (*DEPARTMENT of PHYSICS, CHOSUN UNIVERSITY.*) The single crystals of $CdIn_2Te_4$ were grown by the Bridgman method without the seed crystal. From photocurrent measurements, it was found that three peaks, A, B, and C, correspond to the intrinsic transition from the valence band states of $\Gamma_7$(A), $\Gamma_6$(B), and $\Gamma_7$(C) to the conduction band state of $\Gamma_6$, respectively. The crystal field splitting and the spin orbit splitting were found to be 0.2360 and 0.1119 eV, respectively, from the photocurrent spectroscopy. The temperature dependence of the $CdIn_2Te_4$ band gap energy was given by the equation of $E_g(T) = E_g(0) - (9.43\ ´\ 10^{-3})T^2/(2676 + T)$. $E_g(0)$ was estimated to be 1.4750, 1.7110, and 1.8229 eV at the valence band states of A, B, and C, respectively. The band gap energy of p-$CdIn_2Te_4$ at room temperature was determined to be 1.2023 eV.

**Kp-077** **Elecrical - Photocurrent properties for $CdGa_2Se_4$ single crystal thin film grown by hot wall epitaxy**

HONG

KWANGJOON(*DEPARTMENT of PHYSICS, CHOSUN UNIVERSITY.*) Single crystal $CdGa_2Se_4$ layers were grown on a thoroughly etched semi-insulating GaAs(100) substrate at 420 ℃ with the hot wall epitaxy (HWE) system by evaporating the polycrystal source of $CdGa_2Se_4$ at 630 ℃. The crystalline structure of the single crystal thin films was investigated by the photoluminescence and double crystal X-ray diffraction (DCXD). The carrier density and mobility of single crystal $CdGa_2Se_4$ thin films measured with Hall effect by van der Pauw method are $8.27\times 10^{17}$ $cm^{-3}$, 345 $cm^2/V\cdot s$ at 293K, respectively. The photocurrent and the absorption spectra of $CdGa_2Se_4$ /SI(Semi-Insulated) GaAs(100) are measured ranging from 293 K to 10K. Using the photocurrent spectra and the Hopfield quasicubic model, the crystal field energy(Δcr) and the spin-orbit splitting energy(Δso) for the valence band of the $CdGa_2Se_4$ have been estimated to be 106.5 meV and 418.9 meV at 10 K, respectively. The three photocurrent peaks observed at 10 K are ascribed to the $A_1$-, $B_1$-, and $C_{11}$-exciton peaks.

P1
포스터세션

**Kp-078** **Optical properties and structure of GaInZnO thin films with ion implantation** PARK Jun-Woo, JEONG Pil-Seong, CHOI Suk-Ho, LEE Hosun, ELLIMAN. R.[1], PARK Y.S.[2](*Kyung Hee University, Depart of Applied physics. [1]Australian National University, Electronic Materials Engineering Department. [2]Samsung Asvanced Institute of Technology, Semiconductor Device and Material Laboratory.*) GaInZnO(GIZO) thin films are attraction much interest for their great potential in optoelectronic applications such as flat panel displays, transparent thin film transistors(TTFTs) and flexible TTFTs. GIZO thin films on SiO2/Si substrate were grown by using RF sputtering deposition at room temperature. We implanted the GIZO thin films with $InO^-$ ions and $F^-$ ions. The ion implantation dose density for $InO^-$ ion were $1.4x10^{15}$, 2.7x1015 $cm^{-2}$ and F- ion were $2.5x10^{15}$, $5x10^{15}$ $cm^{-2}$. Then, We annealed thin films between 600℃ and 1000℃. We measured optical properties by using spectroscopic ellipsometry, X-ray diffractometer(XRD) and X-ray photoelectron spectroscopy(XPS). The band gap energy increased with increasing annealing temperature. The band gap energy increased up to 4.65eV with increasing annealing temperature possibly due to the decrease of band tails arising from annealing. Several defect peaks appeared at high annealing temperature for as-grown and implanted films. Specially, implanted films showed an optical structure around 3.6 eV.

**Kp-079** **EUV Multilayer 표면 거칠기에 따른 패터닝 영향** 김 은진, 박 준민, 김 현수, 조 인욱, 김 보배, 정 민희, 유 지혜, 박 승욱, 김 성수[1], 조 한구[1], 오 혜근(*한양대학교 응용물리학과. [1]삼성전자.*) 여러 가지 차세대 리소그라피 기술 중 EUVL (Extreme Ultra-Violet Lithography, 13.5 nm 파장)은 22 nm 이하의 선폭을 갖는 반도체 소자를 만들 수 있는 기술이다. EUVL 시스템에서는 렌즈대신 Mirror를 사용하는 반사형 시스템을 추구한다. 따라서 이 Mirror가 일정량 이상의 빛을 반사해야만 Mask 에서 Wafer까지 정확한 정보를 전달하여 원하는 해상력과 패턴을 얻을 수 있는 것이다. 따라서 Multilayer에서 반사되는 빛의 성질이 상당히 중요하게 되었다. 이 연구에서는 EUV Multilayer의 표면의 거칠기에 따른 반사도 및 진폭과 위상의 변화가 패턴에 주는 영향에 대해 알아 보았다. 일반적으로 Simulation에서는 표면이 매끈하다는 전제 아래 이상적인 73 %의 빛이 반사되는데, Multilayer 의 불완전한 여러 요인 때문에 실제 보고된 반사도는 최대 약 68 % 정도를 넘어서지 못하고 있다. 특히 Multilayer의 표면이 매끄럽지 못하고 울퉁불퉁하게 증착되었을 경우 고르지 못한 표면에서 빛의 진폭과 위상의 변화가 생길 수 있다. 이러한 변화가 EUV 패턴 공정에 끼치는 영향에 대해 알아봄으로써 보다 작은 선폭을 얻음과 동시에 원하는 선폭 조절이 가능하도록 하였다

**Kp-080** **Investigation on the electronic states and the structural properties of the GeSb films** 박 승종, 장 문형, 임 동혁, 조 만호(*연세대학교 물리학과.*) Most chalcogen phase change materials are based on the Te matrix such as GeSbTe (GST), doped SbTe and doped GeTe. So far, the role of the Te atoms in this type of phase change materials are not well understood. Hence, to compare GST and the absence of Te atoms in GST, the phase change characteristics of the GeSb films are investigated. The GeSb films were deposited by ion beam sputtering method in amorphous state at room temperature. Sheet resistance as a functions of the annealing temperatures were measured to confirm the phase change temperature of the films. To investigate the change of the electronic states and the structural properties during phase transition, photoemission spectroscopy (PES) and x-ray diffraction (XRD) were used. Ge K-edge extended x-ray absorption fine structure (EXAFS) were observed to verify the Ge local atomic arrangement. From sheet resistance and XRD data, the phase transition to cubic GeSb phase in the GeSb films occur at higher temperature than typical GeSbTe films of 150 oC. From EXAFS and PES spectra, we confirmed that even though the Ge local atomic arrangement is changed, the Ge-Sb bond is too weak to show the change of the electronic states.

**Kp-081** **Photoluminescience and Structural Properties for $CuInSe_2$ Epilayers** HONG KWANGJOON(*DEPARTMENT of PHYSICS, CHOSUN UNIVERSITY.*) Copper indium diselenide ($CuInSe_2$, CIS) layers were grown on GaAs(100) substrates by the hot wall epitaxy (HWE) method. The optimum temperatures of substrate and source for the growth turned out to be 410 and 620 $^oC$, respectively. The CIS layers were epitaxially grown along the <112> direction and kept up the initial mole fraction during the layer growth. Based on the absorption measurement, the band-gap variation of CIS was well interpreted by the Varshni's equation. But, the energy difference, 180 meV, of the band gap between liquid helium and room temperatures was a very large value unlike that of the reported CIS. Also, from the low-temperature photoluminescence-measurement, the acceptor impurities in the CIS layers confirmed to the native defects of the $V_{Cu}$ and/or $Se_{int}$, which is deeply located at 73.8 meV upper the edge of the valence band.

**Kp-082** **Study on electron charging effect of nano-floating gate capacitor with $WSi_2$ nano-particles** SEO Ki Bong, LEE Dong Uk, LEE Tae Hee, KIM Eun Kyu, SHIN Jin-Wook[1], CHO

Won-Ju[1](*Quantum-Function Spinics Laboratory and Department of Physics, Hanyang University,Seoul 133-791. [1]Department of Electronic Materials Engineering, Kwangwoon University, Seoul 139-701.*) We fabricated the nano-floating gate capacitor with $WSi_2$ nano-particles embedded in silicon dioxide ($SiO_2$) layer. After the growth of 4.5-nm-tunnel oxide layer on *p*-type silicon wafers by thermal oxidation, the $WSi_2$ layer with a thickness of 1~2 nm was deposited on the tunnel oxide layer by sputtering. Firstly the post-annealing process of samples was carried out at 1000 °C for 1 min in rapid thermal process system in nitrogen ($N_2$) ambient to form $WSi_2$ nano-particles. The control oxide layer with 30 nm was deposited by radio-frequency magnetron sputtering. Finally, the second post-annealing was performed at 900 °C for 30 s to improve the control oxide quality, and the 150 nm-thickness of aluminum gate electrode was evaporated by using thermal evaporator system. The spherical shape of $WSi_2$ nano-particles with a size of 2.5~3 nm are conspicuously observed embedded in the $SiO_2$ layer by using field emission transmission electron microscopy. Then, the electrical properties of the nano-floating gate capacitor with $WSi_2$ nano-particles were characterized also by 1-MHz capacitance-voltage measurement.

**Kp-083** **급속 열처리 과정을 이용한 $TiSi_2$ 나노 부유게이트 커패시터의 제작 및 전기적 특성연구** 한 승종, 이 동욱, 이 태희, 서 기봉, 김 은규(*한양대학교 물리학과.*) 나노입자를 기반으로 한 나노 부유 게이트 메모리 (NFGM)는 기존의 플래시 메모리 구조에서 저장전극에 해당하는 부분을 나노 크기의 입자로 구성한 메모리 소자이다. 따라서, 소자의 크기를 줄일 수 있음으로써 소자의 초고집적화를 가능하게 할 수 있다. 또한 저전력 소모, 쓰기/지우기 동작특성이 낮은 동작전압에서도 빠르며, 장기간 데이터를 유지할 수 있는 비휘발성이 우수하다는 점 등의 많은 이점 때문에 차세대 비휘발성 메모리 소자제작을 위한 다양한 연구가 이루어지고 있다. 특히 일함수가 크지만 실리콘 내의 확산 문제를 가지고 있는 금속 나노입자와 달리 현 실리콘 기반의 반도체 공정 적용이 용이한 실리사이드 계열의 나노입자를 적용한 연구가 활발하다. 따라서, 본 연구에서는 실리사이드계열의 화합물 중에서 열화학적으로 안정하며 산화막이나 실리콘기판과의 접착력이 우수한 $TiSi_2$를 열처리 과정을 통하여 수 나노미터 크기의 나노입자로 제조하여, 나노 부유 게이트 커패시터를 제작하였다. *p*-Si기판 (100)에 퍼니스를 이용한 건식 산화과정을 거쳐 4～5 nm 두께의 $SiO_2$ 터널층을 성장시킨 후 $TiSi_2$ 박막을 $Ar^+$ 분위기에서 sputtering 방법으로 5～10 nm 두께로 증착하였다. 그리고 30 ～50 ㎚ 두께의 $SiO_2$ 컨트롤층을 sputter를 이용하여 형성한 이후, rapid thermal annealing를 사용하여, 질소분위기에서 600～900 °C의 온도로 시간조건을 변화해가며 열처리를 실시하여 $TiSi_2$ 나노 입자형성 조건을 확인하였다. 마지막으로 thermal evaporation system을 통하여 Al 전극을 직경 200 ㎛, 두께 150 nm로 증착하였다. 제작된 구조는 metal-oxide-semiconductor 구조이며, $TiSi_2$ 나노 입자의 형성 여부 및 분포 상태를 확인하기 위하여 전계 방출 투과 전자현미경을 이용하였다. 전기적 특성 분석을 위하여 Boonton 7200 1-MHz capacitance-voltage meter와 Agilent 81101A pulse generator를 사용하여 전하 저장 효과, 저장 속도 및 retention 특성을 분석하여 나노 부유 게이트 메모리 소자로의 응용 가능성을 확인 하였다.

**Kp-084** **The properties of Metal/Double-Insulator/Metal Diode** CHOI Kwang Nam, CHUNG Kwan Soo, PARK Jun Woo[1], LEE Hosun[1](*Kyunghee University, Electronic Engineering. [1]Kyunghee University, Physics.*) The advantage of the MIM diode over semiconductor rectifiers is its extremely fast response time and wide bandwidth. These attributes make possible the promise of higher speed detection and mixing of optical radiation. We have fabricated several metal/double insulator/metal diodes (MIIM) using atomic layer deposition. Here, we show metal/double insulator/metal diode applied as a switch element. The diode exhibits good rectifying characteristics at room temperature. We used the electrode material with Pt and insulators were $HfO_2$/ZnO, $HfO_2$/$ZrO_2$ and NiO/ZnO each. The devices were fabricated using the lithographic system and top electrode size were 10~100 $\mu m^2$. The double insulator diode produces an enhanced nonlinearity by incorporating two adjacent oxides instead of the single oxide layer of the MIM diode. In the double insulator diode the mode of tunneling under positive applied biases can be made different from that under negative applied biases resulting in improved asymmetry.

**Kp-085** **전기도금법으로 제작된 구리박막의 특성향상에 대한 연구** 송 유진, 서 정혜, 이 연승, 류 영호[1], 홍 기민[1](*한밭대학교 정보통신공학과. [1]충남대학교 물리학과.*) Electron-beam evaporation 법으로 p-type Si(100)기판에 Cu 와 Ti가 각각 20nm 증착된 Cu seed위에 전기도금법으로 구리박막을 성장시켜, 제작된 구리박막의 특성을 개선하기 위한 도금액 조건을 분석하였다. 전기도금은 정전압방식을 사용하였으며 도금액으로 전해액과 유기첨가제(가속제, 억제제, 평탄제)를 사용하였다. X-선 회절 분석기(X-ray Diffraction), X-선 광전자 분광기(X-ray Photoelectron Spectroscopy), 원자현미경(Atomic Force Microscope), 전계방사 주사전자현미경(Field Emission Scanning Electron Microscope), 4탐침 표면저항측정기(4-point probe) 측정을 통해 전기도금된 구리박막의 물리적 특성과 화학구조를 조사하였다. 가속제와 평탄제의 비율을 증가시켰을 때, 불순물이 줄어들고 결정성이 향상되어 (111)방향을 따라 우선성장 되었음이 발견되었다. 또한 비저항이 2.26μΩcm 에서 1.85μΩcm 로 감소하여 전기전도도가 향상되었다. 적정 유기첨가제의 비율은 구리박막의 전기적, 물리적 특성을 향상시킨다. 이는 불순물의 양과 결정성의 특성으로 해석되며, 구리박막의 비저항에 영향을 미치는 주요인자는 박막의 불순물 상태와 결정성임이 확인되었다.

**Kp-086** **Effects of accelerator in electroplated Cu films** SEO JungHye, SONG YooJin, LEE YounSeoung, RYU Youngho[1], LEE InHyuk[1], HONG KiMin[1], RHA SaKyun[2], KANG SungKyu[2] (*Hanbat National University, Department of Informaion Communication Engineering. [1]Chungnam National University, Department of Physics. [2]Hanbat National University, Department of Materials Engineering.*) In order to investigate the effect of organic additives in electroplated Cu film growth, we estimated the characterization of electroplated Cu films according to the concentration variation of organic additives, especially, accelerator. Prior to Cu film growth by electroplated method, Cu seed layer was deposited onto Ti barrier film of

20 nm which was deposited onto a p-type Si (100) substrate by e-beam deposition. Potentiostatic electrodepositions were carried out using the three terminal methods with a platinum plate as a counter electrode. The plating electrolyte composed of $CuSO_4$, $H_2SO_4$, and HCl, was fixed. The concentrations of suppressor and leveler were fixed to 2.5 mL/L and 2 mL/L, respectively. The concentration of accelerator was changed. The resistivity was measured with a four-point probe and the material properties were investigated with XRD (X-ray Diffraction), AFM (Atomic Force Microscope), FE-SEM (Field Emission Scanning Electron Microscope) and XPS (X-ray Photoelectron Spectroscopy). From these experimental results, we found that an accelerator plays an important role in Cu film growth.

**Kp-087** **Position Shift Analysis in Resist Reflow Process for Sub-50 nm Contact Hole** YOU Jee-Hye, PARK Joonwoo, PARK Joon-Min, KIM Eun-Jin, KIM BoBae, JUNG Minhee, CHO Imwook, KIM Hyunsu, JEONG HeeJun, OH Hye-Keun (*Hanyang University, Department of Applied Physics.*) Contact hole (CH) patterning, specially for sub-50 nm node, is one of the most difficult technique in optical lithography. Resist reflow process (RRP) can be used to obtain smaller CH. RRP is a simple technique that the resist is baked above the glass transition temperature ($T_g$) after the develop process. Heating causes the resist to flow, and results in smaller dimension of CHs. However, RRP is unmanageable method because CH offset caused by pattern position in random array CH. Uniform critical dimension (CD) can be obtained with decreasing the bulk effect through the whole CH array with stronger adhesion force and optical proximity correction (OPC). However, we still have CH position shift problem. Because of a difference in an amount of resist that flow into the hole in random array during the reflow process, position shift occurs. This position shift makes overlay error, and it may exceed the overlay error budget suggested by ITRS roadmap. In this work, we try to find not only uniform CD size of each CH, but also optimum condition for correcting CH position shift by using amended home-made simulation considering the error of bulk effect. Consequently, we confirmed that position shift showed the tendency that CH moved to receding direction from each other, and obtained sub-50 nm CHs in random array by considering the position shift through the amended simulation.

**Kp-088** **High NA Immersion 에서 Resist Reflow Process 와 Hardmask 를 이용한 22 nm 1:1 Line and Space 제작을 위한 Double Patterning** 박 준민, 유 지혜, 김 은진, 김 현수, 조 인욱, 김 보배, 정 민희, 박 승욱, 안 일신, 오 혜근(*한양대학교 응용물리학과.*) ITRS roadmap에 따르면 22 nm half-pitch는 2016년에 이르러서야 가능할 것으로 보인다. 22 nm half-pitch를 위해서는 double patterning 과 극자외선 (extreme ultraviolet lithography, EUVL) 등이 후보로 생각되고 있지만, 아직도 해결하지 문제들과 비용 문제 등이 남아 있다. 따라서 본 연구진은 현재 상용화되어 있는 고굴절 lens 와 유체를 이용하여 개구수 (numerical aperture, NA) 를 1.0 이상 내는 immersion technology를 이용하고, hardmask 를 같이 사용하여 double patterning 에서 resist reflow process (RRP) 를 통한 좁은 space 패턴이 높은 분해능을 가질 수 있도록 하는 새로운 공정 기술을 제안하고자 한다. 일반적으로 RRP 는 contact hole 에서 shrinkage 를 얻을 때 사용하는 방법이다. 그러나 본 연구진은 line and space 패턴에서도 RRP 를 이용하는 공정 기술을 개발하였으며, 이를 이용하여, hardmask 를 사용, substrate 위에 패턴 형성 후 이를 RRP 하여 space를 좁힌 후에 이를 다시 double patterning 한다. 현재 상용화되어 있는 scanner 에서 NA 1.35 에서 40 nm 의 half pitch 의 성능을 내므로 이를 이용하여 44 nm 1:1 line and space 를 제작하고 RRP 를 하면 66:22 nm line and space patterning 이 되고, 이를 double patterning 하면 22 nm 1:1 line and space 를 만들 수 있다. 이를 home-made simulator 와 상용 tool 인 EM-suite 를 이용하여 확인하였다.

**Kp-089** **극자외선 Lithography를 위한 Photoresist의 구성 성분 특성과 표면 거칠기 와의 관계** 김 현수, 조 인욱, 김 은진, 박 준민, 김 보배, 정 민희, 유 지혜, 박 승욱, 오 혜근(*한양대학교 응용물리학과.*) Extreme ultraviolet (EUV) lithography 기술을 22 nm 이하의 패턴을 형성하기 위해 현재 개발 중에 있다. 그러나 line edge roughness (LER) 이나 line width roughness (LWR) 은 이러한 패턴 형성을 하는데 가장 큰 걸림돌 중 하나이다. 기존의 polymer resist 에서는 기본적인 분자의 크기가 크기 때문에 작은 패턴의 형성에 한계를 보이고 있으므로 분자 크기가 작은 molecular resist 의 개발이 활발하게 이루어지고 있다. Molecular resist 에서 패턴에 영향을 미치는 요소로는 물리적 입장에서 분자의 크기와 구조를 생각할 수 있다. Resist 를 구성하고 있는 분자의 크기는 LER 과 LWR 을 좌우하는 중요한 요소이며, 구성 요소가 가지고 있는 구조의 모양 또한 패턴을 형성하는 요소가 된다. 그러므로 우리는 자체적으로 개발한 컴퓨터 시뮬레이션을 이용하여 이것들을 다양하게 변화시키면서 특성을 살펴보았다.이들의 영향을 살펴보기 위해 resist 를 구성하고 있는 photo acid generator (PAG) 와 quencher 등은 기존의 것을 사용하였고 또한 Monte-Carlo 방법을 사용하여 분자들의 위치와 산확산 방향을 구성하였고 이에 따른 LER 과 LWR 의 경향을 분석하였다. 22 nm 패턴의 aerial image 를 얻기 위해 Solid-EUV 를 사용하였고, ChemOffice 를 사용하여 분자의 크기와 구조를 분석하였다

**Kp-090** **EUV Lithography 에서 Resist 재흐름 공정을 통한패턴 거칠기의 축소** 조 인욱, 박 준민, 김 현수, 김 은진, 김 보배, 정 민희, 유 지혜, 박 승욱, 오 혜근(*한양대학교 응용물리학과.*) Extreme Ultra-Violet lithography (EUVL) 는 최근 몇 년 동안 차세대 lithography를 위해 고 EUVL 을 사용하여 22 nm 급의 패턴을 얻을 수 있다고 발표되고 있다. 그러나 거칠기, 민감도, 및 해상도와 같은 문제가 여전히 남아있다. 2007 ITRS roadmap에 따르면, 패턴 거칠기는 22 nm 패턴을 얻기 위해서 1.2 nm 이하가 되어야만 한다. 그러나 패턴 거칠기를 제어하기는 매우 어렵다. 왜냐하면 선폭은 노광 후 굽기 시간, 온도, 산 확산 길이뿐만 아니라 레지스트의 구성 성분과 크기에 의해 결정되기 때문이다.거칠기를 줄이기 위해 새로운 방법을 제안하고자 한다. 표면 거칠기는 현상된 resist에서 레지스트 재흐름 공정 (resist reflow process, RRP)을 통해 매끄러워질 수 있다. 노광, 노광 후 굽기, 현상과정을 거친 표면 거칠기가 있는 패턴을 만들 수 있었다. 표면 거칠기는 photo acid generator 와 quencher 의 양과 크기와 같은 변수를 변화시켜 계산하였다. 유리 상전이 온도 이상으로 구워진 현상된 레지스트

는 흘러갈 것이다. 그리고 resist 의 표면은 고르게 분포될 것이다. 결과적으로, 패턴 거칠기는 RRP 후에 처음보다 더 작아질 것이다. RRP 동안 패턴 거칠기의 감소 비율은 초기의 패턴 거칠기가 크면 더욱 커진다.

**Kp-091** **핫 플레이트 (Hot Plate) 열 분포에 의한 웨이퍼 내부의 온도 변화** 김 보배, 박 준민, 김 현수, 김 은진, 정 민희, 조 인욱, 유 지혜, 박 승욱, 오 혜근(*한양대학교 응용물리학과.*) 초 미세패턴을 형성하기 위해서는 반도체 공정 중 노광후 굽기 (Post Exposure Bake, PEB) 과정이 매우 중요하다. 노광을 통해 얻어진 산은 폴리머를 분해하는데 이 때 분해 반응과 산의 확산은 PEB 온도에 크게 의존한다. 2007 ITRS roadmap에 따르면, 22 nm 이하의 패턴이 전체 과정에서 조절될 수 있는 선폭 (Critical Dimension, CD) 의 범위는 1.9 nm 이다. 하지만 Exposure 공정과 PEB 공정, Develop 공정, Etching 공정 등에서 CD 의 오차가 발생하게 된다. 이 중에서 우리는 PEB 공정에서 발생할 수 있는 약 0.5 nm (4 공정의 산술평균) 이하의 CDU를 만족할 수 있어야 한다. 현재 상품화된 ArF용 photoresist 를 보면, PEB 과정에서 1 도의 온도 차이로 인하여 3 nm의 CD가 변하게 되므로 22 nm node 에 맞는 오차범위를 가지려면 약 0.2 도 (0.5 nm/3 nm x 1 도) 이하의 온도 조절이 필요하다. 하지만 실제 우리가 쓰고 있는 핫 플레이트 (Hotplate) 는 전체 면적이 다 열원으로 균일하게 채워져 있지 못하기 때문에 열원의 위치에 따른 온도 차이가 생기게 된다.우리는 핫 플레이트 내부의 열원과 빈 공간 사이의 온도 차이를 알아보았다. 이러한 핫 플레이트 내부의 온도 차이는 PEB 과정에서 온도 분포에 영향을 미치게 되고 결국 웨이퍼의 제일 위 층인 photoresist 에서 내부 온도 분포 차이가 생기게 된다. 그 결과 CD를 변화시킨다. 우리는 핫 플레이트 내부의 열원의 위치나 구조에 따른 온도 분포를 계산하였고 그에 따른 photoresist 내부의 온도 분포도 계산하였다.

**Kp-092** **32 nm half pitch formation with high NA single exposure** 정 민희, 박 준민, 김 보배, 김 현수, 조 인욱, 김 은진, 유 지혜, 박 승욱, 오 혜근(*한양대학교 응용물리학과.*) ITRS가 발표한 반도체 로드맵에 따르면 2012년과 2017년의 DRAM 1/2 pitch (hp)는 각각 32 nm, 20 nm에 이를 것으로 전망하고 있으나 현재 이용되는 1.35 NA ArF immersion lithography는 40 nm node 이하로 진입하는데 어려움이 있다. 그리하여 double patterning 과 극자외선 (extreme ultraviolet lithography, EUVL) 이 32 nm 이하의 node 를 열어 줄 것으로 예상되고 있지만, 비용 증가와 아직 해결하지 못한 문제로 인해 차세대 기술로서 high-index immersion technology에 대한 연구가 새롭게 대두되고 있다. 기존의 ArF water immersion system은 NA 1.35로 40 nm half pitch를 만들어 냈지만, 최근에는 ArF 파장대에서 LuAG(n=2.14) 렌즈와 3세대 fluid 를 이용 하여1.55 NA 를 실현시키는 연구가 진행되고 있으며, 그에 대한 가능성이 많은 것으로 예상되고 있다. 공정 상수인 $k_1$ factor가0.25 일 때single exposure technology 로32 nm hp를 얻을 수 있다. 1.55 NA 의 high-index immersion technology에서 32 nm 1:1 line and space를 구현하기 위한 illumination, exposure, develop 조건을 commercial simulator 를 이용하여 찾았다. 또한 32 nm 1:1 line and space pattern을 얻기 위한 최적의 1.55 NA single exposure technology의 공정 조건을 찾았다.

■ SESSION: P2
10월 24일(금), 11:00 - 12:45
장 소: 제3전시장

**Dp-091** **Theoretical spin-wave calculation and analysis of $YMnO_3$ &$LuMnO_3$** LEE JUNGHYUN, PARK JE-GEUN (*Department of Physics, Sungkyunkwan University.*) Recently it was shown that multiferroic (Y,Lu)$MnO_3$ manganites exhibit a strong spin-lattice coupling at the antiferromagnetic transition temperatures. This unusually strong spin-lattice coupling is believed to be responsible for the multiferroic behavior of (Y,Lu)$MnO_3$. Therefore, it will be of urgent importance for one to examine and understand the spin-lattice coupling in full details. In this work, we have investigated the spin-lattice coupling through the analysis of the spin wave of $YMnO_3$ &$LuMnO_3$ measured by inelastic neutron scattering technique.In order to analyze the experimental spin waves of $YMnO_3$ &$LuMnO_3$ single crystals, we started Heisenberg Hamiltonian with four interaction terms between Mn atoms ($J_1$, $J_2$, $J_1'$, $J_2'$) and two anisotropy terms ($D_1$ *and* $D_2$). We then calculated the dispersion relation using a linear spin-wave theory through the Primakoff-Holstein transformation. Since we are interested in the possible effects of the spin-lattice coupling, i.e. a difference between $J_1$ and $J_2$, we carefully examined a wide range of $J_1$ and $J_2$ parameter space. And for each given set of the parameters, we carried out our calculations self-consistently. From this rather extensive search of the parameter space, we could find that there are two distinct minima in the $J_1$ and $J_2$ parameter space: one is a local minimum and another is a global minimum. We will discuss our findings in the light of the spin-lattice coupling.

**Dp-092** **Proton irradiation effects on $KH_2PO_4$ studied by NMR and electrical conductivity measurements** LEE Cheol Eui, KWEON Jin Jung, OH In Hwan(*Korea University, Department of Physics.*) Proton irradiation effects on $KH_2PO_4$ (KDP) were studied by means of NMR spin-lattice relaxation time ($T_1$) and electrical conductivity measurements. An increase in $T_1$ was observed after the proton-beam irradiation and is discussed in terms of the proton motions, with decreased activation energy. The high-temperature proton conductivity was modified by the proton-irradiation, which may be attributed to the shortening of the bond distance between the oxygen atoms, as was observed by the neutron diffraction and NMR measurements.

**Dp-093** **전하밀도파 $CeTe_2$단결정의 각분해 광전자분광 연구** 이 현진, 김 대현, 강 정수, 권 용성[1], 김 형도[2](*가톨릭대학교, 물리학과. [1]성균관대학교, 물리학과. [2]포항가속기연구소.*) $Cu_2Sb$형태의 정방정계(tetragonal) 구조를 가진 $RTe_2$ (R=La, Ce)는 전이온도가 매우 높은 ($T_{CDW}$ ~ 1000 K) 전하밀도파 물질계 (charge-density-wave system: CDW)로 알려져 있으며, 전기적 성질과 자기적 성질에서 이방성(anisotropy)이 매우 강하게 보이는데, 이는 $RTe_2$의 준 이차원 구조로 인한 것으로 생각된다. $RTe_2$에서 Te이온은 그 위치에 따라 Te(1)과 Te(2)의 두 종류로 분류되며, Te(1) 이온들로 이루어진 이차원 사각형 모양의 평면층과 Ce 이온들과Te(2) 이온들이 섞여 주름 형태를 이룬 이중층이 번갈아 있다. $RTe_2$에서 R 이온은 3가 상태($R^{3+}$)이며, CDW 전이가 일어 나기 전에는 Ce-Te(2)층은 반도체성 전자구조를 가지지만, Te(1) 평면층은 금속성 전자구조를 가져 전하 운반자가 존재할 것으로 여겨진다. 일반적으로 CDW가 생기는 원인은 페르미면의 nesting 때문으로 알려져 있으나, $RTe_2$에 관한 전자구조 연구 결과에서 [1,2] CDW 형성의 원인과 CDW에너지 갭의 크기, CDW 살창(lattice)의 대칭성 등에 관하여 아직도 논란이 있다. 그러므로 $RTe_2$의 전자구조를 좀 더 자세히 연구하는 것이 중요하겠다. 각분해 광전자 분광법 (angle-resolved photoemission spectroscopy: ARPES)은 페르미면의 nesting과 에너지 갭의 크기 등을 직접 관찰할 수 있는 매우 중요한 실험이며, 준 이차원 구조를 가진 $RTe_2$는 ARPES 실험에 적합한 물질이다. 그러므로 본 연구에서는 $CeTe_2$ 단결정에 대하여 마이크로빔 크기의 방사광을 사용한 ARPES 실험을 수행함으로써 $CeTe_2$의 전자 구조를 연구하였다. 이번 발표에서는 본 연구로부터 결정한 $RTe_2$의 페르미 준위 근처의 에너지 면들의 형태, 에너지 분포 곡선(energy distribution curves)과 운동량 분포 곡선(momentum distribution curves) 등을 발표하고, $CeTe_2$의 전자구조가 CDW 형성에 미치는 역할에 관하여 논의하고자 한다.
[1] D. R. Garcia, et al., Phys. Rev. Lett. 98, 166403 (2007). [2] J.-S. Kang, et al., Phys. Rev. B 74, 085115 (2006).

**Dp-094** **고압 상태에서 bulk Fe 합금들의 결정 구조 및 압축률** 고 영호, 김 광주, 한 충규, 이 용재[1](*국과연. [1]연세대.*) PLS (Pohang Light Source)에 있는 방사광을 이용하여 FeAu, FeB, FePt, 그리고 FeSi에 대한 상태방정식을 55GPa까지 측정하였다. FeSi는 용융된 철과 맨틀 규산염 사이에서의 반응에서 발생되는 주된 부산물들 중 하나로서 지구 내부 구성 물질로 여겨지며, FeAu, FePt는 차세대 데이터 저장 매체 제작에 필요한 자성 소재들 중 하나이다. Fe 합금들은 아크 융해 (arc-melting) 법에 의해 제작되었으며, FeAu, FeB, FePt, 그리고 FeSi에 대한 결정 구조들은 분말 rietveld refinement 방법을 이용하여 풀었다. 그리고, 등온 체적 탄성율 (B)와 등온 체적 탄성율의 압력 미분계수 (B')을 Birch-Murnaghan EOS을 이용하여 유도하였다.

**Dp-095** **Brillouin Light Scattering을 이용한 CoFeSiB의 stripe domain에 대한 불연속적인 스핀파 분산** 하 승석, 윤 정범, 이 석목, 유 천열, 정 명화[1], 김 영근[2](*인하대학교 물리학과. [1]서강대학교 물리학과. [2]고려대학교 신소재공학부.*) 비정질 상태의 CoFeSiB 박막은 크지 않은 자기 결정이방성과 높은 스핀 분극률을 보이기 때문에 자기 메모리 소자의 magnetic tunnel junction(MTJ)의 자유층 물질 중 하나로써 연구가 되어 왔다. Magnetic force microscopy(MFM)로 관찰한 선행 연구의 결과에 따르면 CoFeSiB박막은 특정 크기 이하의 자기장에서 stripe domain을 형태를 가짐이 보고되었다 [1,2]. CoFeSiB의 stripe domain의 자기이방성에 대한 조사를 위해 Brillouin Light scattering(BLS)을 이용하였다. BLS 측정방법은 열적으로 들뜬 스핀 파의 주파수를 측정하여 교환강성, 포화자화, 자기 이방성 등의 자기적 성질을 비 접촉 방식으로 국소적으로 측정할 수 있는 광학적 측정방법이다. 본 연구에서는 BLS를 이용 CoFeSiB 박막에서 stripe domain의 형성 여부에 따른 스핀파 들뜸을 연구하였고, 특히 입사광의 입사각을 조절하여 CoFeSiB 스핀파의 분산관계도 측정하였다. 그 결과, stripe

domain의 존재 여부에 따라 다른 스핀파 분산관계를 관측하였다. 특히 stripe domain이 없을 때에는 연속적인 박막에 대한 스핀파 분산관계를 볼 수 있었지만, stripe domain이 형성되었을 때는 불연속적인 스핀파 분산관계가 관찰되었다. 이 불연속적인 분산관계는 nanowire와 같은 confined magnetic structure에서 관찰되는 현상으로, stripe domain 구조에서 각각의 domain이 스핀파 드뜸의 경계조건으로 작용하여 구조적인 경계 조건과 비슷한 스핀파 거동이 일어나는 것으로 판단된다.

[1] Jungbum Yoon *et al.*, IEEE Transactions on nanotechnology, 7 409 (2008). [2] Jungbum Yoon *et al.*, Current Applied Physics, CAP1322 (2008).

**Dp-096** **강자성체/반강자성체 계에서의 강자성체의 스핀방향전환과 스핀방향전환시의 큐리온도의 감소에 관한 연구**

석 진호, 권 희영, 원 창연(*경희대학교 이과대학 물리학과.*) 강자성체(F)가 반강자성체(AF)와 계면상호작용을 하게 되면 히스테리시스 곡선의 원점이동(exchange bias)이나, coercivity의 증가 등 그 자성구조에 변화가 있게 되어 그에 대한 활발한 연구가 있어 왔다. 그리고 최근에는 그 상호작용이 자성체의 비등방성에도 영향을 주어 자성체에 스핀방향전환 (Spin reorientation transition; SRT)을 일으키는 것이 보고되었다. 우리는 double layered 2 dimensional (F/AF) - Heisenberg model을 바탕으로 하는 Monte-Calro simulation을 통해 상호작용하는 반강자성-강자성박막구조에서 강자성체의 자성구조와 반강자성체와의 결합각도등을 연구하였다. AF 박막의 스핀결합에너지가 AF 박막의 비등방성에너지에 비해 상대적으로 낮은 경우, AF 박막의 비등방성에너지의 효과가 두 계의 상호작용을 통해 자성체에 영향을 주어 자성체의 자성방향이 AF의 자화용이축 (easy axis) 방향으로 정렬된다. 그에 비해, AF 박막의 스핀결합강도가 큰 경우에는 AF 와 F 박막의 자성이 서로 수직 결합되어 F 박막의 자성축이 AF의 자화용이축의 수직방향으로 정렬되는 현상을 관찰하였다. 즉 실험적으로 F/AF 계에서 AF 막의 두께의 변화에 의해 F 박막에 SRT가 일어날 수 있음을 확인하였다. 또한 이러한 SRT 영역에서는 그 자성방향의 자유도 증가에 따라 자성박막의 큐리온도가 스핀방향이 고정되어 있는 경우에 비해 낮을 것으로 예상되는 데, 시뮬레이션을 통해 그 사실을 확인하였다.

**Dp-097** **$Tm_5Si_2Ge_2$ 단결정에 대한 열적 특성과 자기적 특성** 이 찬익, 이 경은, 김 솔지, 권 용성, 이 종수[1], S. Angappane, 박 제근(*성균관대학교 물리학과. [1]Inorganic Materials Group, Samsung Advanced Institute of Technology.*) $Tm_5Si_2Ge_2$ 단결정에 대한 자기적 특성과 열적 특성을 다양한 자기장하에서 온도의 함수와 다양한 온도하에서 자기장의 함수로서 측정하였다. 장거리 반강자성적인 배열과 ac-면 에서의 강자성적으로 결합한 자기적 모멘트들에 의한 특이성이 자기 감수율과 비열 측정에서 8.01K과 5K에서 각각 관측할 수 있었다. spin-flip과 같은 자기적 전이가 $H$=0.5T일 때 $T_N$이하에서 관측되었고, 약한 자기이력도 수반하였다. $T_N$에서의 자기적 엔트로피의 값은 $R$ln2 에 거의 근접하였고, 4$f$의 바닥상태는 결정장 효과에 의해 이중상태로 갈라져 있었다. $H$ // $b$ 결정축의 방향의 자화율과 $H$ // $ac$ 면의 자화율 측정에서 큰 이방성이 관측되었다.

**Dp-098** **Influence of Phonon on the Spin Dynamics in a Hexanuclear Manganese Ring – {Mn6} and its 3D Network**

YOON Sungwon, SUH Byoung Jin, JANG Zeehoon[1](*The Catholic University of Korea, Department of Physics. [1]Kookmin University, Department of Physics.*) We report a $^1$H nuclear magnetic resonance (NMR) and relaxation measurements on a hexanuclear antiferromagnetic (AFM) spin ring and its 3 dimensional network system, in brief {Mn6} and {Mn6}-network, respectively. The study has been aimed at exploring the influence of phonon on the spin dynamics, in particular on the scaling behavior of $^1$H spin-lattice relaxation rate $1/T_1$ commonly observed in AFM molecular rings [1]. The magnetic properties of both systems were observed to be almost identical and characterized by AFM coupling constants $J_1/k_B \approx$ -4.0 K, between the nearest neighbors, and $J_2/k_B \approx$ -1.0 K, between the next-nearest neighbors. Heat capacity has been observed to be different in two systems, whereby the molar heat capacity in {Mn6}-network is smaller and increased less rapidly with $T$ as expected from the more rigid structure of the network system. The $^1$H $1/T_1$ shows a broad peak at low $T$ in both systems similar to the common observation in AFM rings or clusters [1], but the peak positions of two samples are found to be totally different. The peak position of the $^1$H $1/T_1$ in {Mn6}-network shifts to higher $T$, which agrees qualitatively with the slower increase of the heat capacity with $T$ in the network system.

[1] S. H. Baek, M. Luban, A. Lascialfari, E. Micotti, Y. Furukawa, F. Borsa, J. van Slageren, and A. Cornia, Phys. Rev. B 70, 134434 (2004).

**Dp-099** **Study on the Magnetic Properties and the Spin Dynamics of Oxo-Centered {$Mn_3O$} - Type Spin Triangles with 30 T pulsed magnet and NMR**

JANG Zeehoon, YOON Sungwon[1], SUH Byoung Jin[1], HAN Kyunghoon[1](*Kookmin University, Department of Physics. [1]The Catholic University of Korea, Department of Physics.*) We report the results of experimental and theoretical studies on the magnetic properties of two variants of trinuclear oxo-centered Mn complexes, $Mn_3O$-I and $Mn_3O$-II [1]. In the $Mn_3O$-I, three identical $Mn^{3+}$ (S = 2) ions form a nearly equilateral triangle and the $Mn_3O$-II consists of two $Mn^{3+}$ (S = 2) ions and one $Mn^{2+}$ (S=5/2) ion. Temperature dependence of the magnetic susceptibility $\chi$ has been measured with a SQUID magnetometer from room temperature down to 1.8 K. The magnetic susceptibility $\chi$ of both molecules shows a typical behavior for an antiferromagnetic (AFM) spin ring system, whereby $\chi T$ decreases gradually as temperature decreases. Field dependence of magnetization has been measured using a pulsed magnet up to $H$ = 30 T at $T$ = 1.7 and 0.5 K. Magnetization versus field shows a stepwise behavior with broad steps in both compounds. In particular, a sharp step at zero field was detected in the hysteresis loop of $Mn_3O$-II, suggesting the existence of a level anticrossing gap at zero field. Model Hamiltonians of both molecules will be presented with parameters deduced from the fitting of the measured magnetic properties. We also present $^1$H nuclear magnetic resonance (NMR) experiments on $Mn_3O$-II. The $^1$H NMR linewidth strongly depends on both the magnetic field and temperature, and is quantitatively explained by the dipolar inter-

action between proton nuclei and Mn ion spins. A strong enhancement of $1/T_1$ with a peak around T≈15 K, which is a common behavior a AFM coupled rings, was observed and will be discussed in the light of the scaling behavior reported previously [2].
[1] J. B. Vincent, H-R. Chang, K. Floting, J. C. Huffman, G. Christou, and D. N. Hendrickson, J. Am. Chem. Soc. 109, 5703 (1987). [2] S. H. Baek, M. Luban, A. Lascialfari, E. Micotti, Y. Furukawa, F. Borsa, J. van Slageren, and A. Cornia, Phys. Rev. B 70, 134434 (2004).

**Dp-100** **Resonance Study of $LiNbO_3$ Single Crystal Doped with MgO and Fe** YEOM Tae Ho, LIM Ae Ran[1], NOIRET I[2] (*Cheongju University. [1]Jeonju University. [2]Universite de Lille-1.*) Lithium niobate single crystals are technologically important because of piezoelectric effect, optical non-linearties and corresponding potemtial devices. The spin lattice relaxation time and spin spin relaxation time of host nuclei in $LiNbO_3$ crystal doped with Fe or MgO have been investigated with NMR spectrometer as a function of impurity concentration. The variation of $T_1$ and $T_2$ was discussed in detail. From the EPR measurements, MgO-doping made some changes in substitutional $Fe^{3+}$ sites as well as some distortions in the crystal. MgO-doping, however, made not any difference in the spin-lattice relaxation time.

**Dp-101** **반강자성체 없이 강자성체로만 이루어진 계에서 대칭성 붕괴로 일어나는 exchange bias** 부 경미, 권 희영, 원 창연(*경희대학교 이과대학 물리학과.*) 자성체의 히스테리시스 곡선의 원점이동을 보여주는 exchange bias는 자성체가 반강자성체와 상호작용을 할 때 주로 나타나며, 그 원리를 이해하기 위해 많은 연구가 있어왔다. 반강자성체가 없는 경우에는 일반적으로 전체 자성 시스템의 시간 역전 대칭성을 가지기 때문에 exchange bias를 기대할 수 없다. 하지만, 서로 수직의 이등방성을 가지는 두 강자성 박막이 비자성박막을 통해 상호작용하는 계의 경우, 이등방성축이 서로 수직에서 약간 어긋나게 되면, 반강자성체가 없음에도 불구하고 exchange bias를 보여, 실험적으로 Ni/Cu/Co/Cu (1,1,40) 계에서 Exchange bias가 관찰되었다. 우리는 Neel's anisotropy model과 2D Heisenberg model을 바탕으로 한 계산과 Monte-Carlo simulation을 통해 박막에 수평인 자화용이축을 가지는 자성박막1(FM//) 와 박막에 거의 수직인 자화용이축을 가지는 박막2(FM⊥)에서 어떻게 시간 역전 대칭성이 깨지는지, 그리고 그로 인해 어떻게 상호작용이 Exchange bias를 만드는 지를 연구하였다. 그리고 Exchange bias의 크기나 coercivity의 크기가 각각의 박막의 교환에너지, 이등방성에너지, 두 박막간의 자성용이축 사이의 각도, 두 박막사이의 결합에너지 등 에 따라 어떻게 변하는 지 시뮬레이션을 통하여 측정하고, 이를 실험결과와 비교하였다. (FM//)/(FM⊥) 계에서의 exchange bias는 위의 몇 물리적 인자들에 대해 불연속적인 의존도를 보이는 데, 이는 이 계에서의 exchange bias가 불안정한 에너지 상태에서의 대칭성 붕괴로 일어남을 나타낸다.

**Dp-102** **수직이등방성을 가지는 자성박막에서 자발적으로 형성된 줄무늬 자성도메인과 방울무늬 자성도메인 간의 상전이** 홍 상신, 권 희영, 이 응규, 원 창연(*경희대학교 이과대학 물리학과.*) 수직이등방성을 가지는 강자성박막의 경우 같은 방향의 스핀배열을 선호하는 근거리 교환상호작용과 반대방향의 스핀배열을 선호하는 원거리 쌍극자 상호작용에 의해 자발적으로 형성되는 자성 도메인 무늬를 가지게 된다. 외부 자기장이 없는 경우에는, 박막에 대해 위와 아래의 스핀방향을 가지는 자기구역의 넓이 비가 같은 줄무늬를 형성하며, Fe/Cu(001)과 같은 실험 계에서 그에 대한 연구가 진행이 되어 왔다. 우리는 수직의 외부자기장이 이러한 줄무늬자성영역에 미치는 영향을 Monte-Carlo method를 이용한 전산시뮬레이션을 이용하여 연구하였다. 수직인 외부자기장이 존재할 때, 줄무늬 모양의 패턴은 두 가지 형태로 변화하게 됨을 발견하였다. 우선 약한 외부의 자기장이 가해졌을 때에는 외부 자기장 방향의 자기구역의 줄무늬의 폭이 점점 넓어지고 그 반대 방향의 자기구역은 점점 그 폭이 줄어드는 형태로 자기구역의 모양이 변화한다. 하지만 외부자기장의 세기가 점점 강해지면 줄어드는 자기구역은 줄무늬 형태의 모양이 임계의 폭까지 줄어들다가 구역사이의 경계를 최소화하기 위해서 방울 무늬의 형태로 바뀌게 된다. 그리고 이런 자성체의 자기화는 방울의 크기보다는 방울의 수에 의존하게 된다. 시뮬레이션을 통해 구한 줄무늬와 방울무늬 사이의 상태 변화에 대한 임계 조건을 (Fe/Ni)/Cu/Ni/Cu(001)에서의 실험결과와 간단한 수식 모델과 비교하였다.

**Dp-103** **강자성 나노선 소자에서 이중노치에 의한 자구벽의 운동 및 정지 디피닝 자기장에 대한 연구** 최 석봉, 안 성민(*서울대학교 물리천문학부.*) 강자성 나노선 소자에서 노치(notch)에 의한 자구벽의 피닝(pinning)과 디피닝(depinning) 과정에 대해 최근 폭넓게 연구되고 있다. 미국 표준연구소에서 개발한 OOMMF 코드를 사용하여, 정지 및 운동상태인 자구벽의 이중노치에서 일어나는 각기 다른 디피닝 현상에 대해 보고하고자 한다. 정지상태의 자구벽은 초기에 노치에 구속되어 있고, 반면에 운동중인 자구벽은 이동 중인 상태에서 노치를 지나간다. 이 때 각각의 상황에서 노치를 벗어나는데 필요한 최소 자기장을 전자의 경우, 정지 디피닝 자기장(the static depinning field), 후자에서는 운동 디피닝 자기장(the kinetic depinning field)이라고 한다. 특히, 노치 깊이에 따라 정지 디피닝 자기장이 운동 디피닝 자기장보다 여러 배 크게, 확연히 다른 분포를 나타난다. 이 차이는 각기 다른 피닝 세기(the pinning strength)에 의한 것으로, 충분한 에너지를 가진 자구벽은 운동 피닝 세기, $u_K$ (the kinetic pinning strength)를 극복하고 노치를 지나가고, $u_K$ 보다 적은 에너지의 자구벽은 노치에 구속된 후 정지 피닝 세기 $u_S$ (the static pinning strength)상태로 전환된다. 이런 과정은 고전역학의 정지 및 운동 마찰력의 작용과 유사하다.

**Dp-104** **Electronic Structures of Perovskite $SrMn_{1-x}Mo_xO_3$ Studied by XAS** 이 지은, 김 봉재, 김 범현, 민 병일, 이 현진[1], 김 대현[1], 강 정수[1], 정 민철[2], 신 현준[2](*포항공과대학교, 물리학과. [1]가톨릭대학교, 물리학과. [2]포항가속기연구소.*) The electronic structures of $SrMn_{1-x}Mo_xO_3$ with $0 \le x \le 0.5$ have been investigated by means of soft x-ray absorption spectroscopy (XAS). XAS is known to be a powerful experimental tool for studying the valence states and the spin states of transition-metal ions in solids. The measured Mn 2p XAS spectra of $SrMn_{1-x}Mo_xO_3$ exhibit systematic changes with x, indicating that the valance states of Mn ions change from $Mn^{4+}$ to $Mn^{3+}$ and to $Mn^{2+}$ with increasing x. We have also

performed the cluster model calculations for the Mn 2p XAS spectra in order to analyze the measured Mn 2p XAS spectra of $SrMn_{1-x}Mo_xO_3$. We will present the cluster model fitting of the experimental XAS spectra and will discuss on the roles of different physical parameters.

**Dp-105** **양성자빔 조사에 따른 철산화물 나노입자의 뫼스바우어 분광연구** 현 성욱, 김 삼진, 김 철성(*국민대학교 나노전자물리학과.*) 본 연구에서는 철산화물 ($Fe_3O_4$) 나노입자에 양성자빔을 조사함에 따라 자기적 특성의 변화를 알아보고자 하였다. $Fe_3O_4$ 나노입자의 합성을 위하여 고온 열분해법을 사용하였고, 용매로는 phenyl ether를 사용하였으며, oleic acid 와 oleylamine 을 계면활성제로 첨가하였다. 제조된 시료를 직경 0.5 cm의 원형 pellet 형태로 만들어서 1, 5, 10 pC/μm$^2$ 의 양성자빔을 각각 조사하였다. 결정구조를 판별하기 위하여 X-선 회절 실험을 수행하였고, 공간그룹 *Fd3m*을 갖는 스피넬 상이 나타남을 확인할 수 있었다. 진동시료형 자화율 측정기(VSM)를 이용하여 1.5 T 의 외부자기장하에서 실험 결과, 자화율값은 0, 1, 5, 10 pC/μm$^2$ 의 양성자빔을 조사한 시료가 각각 57.2, 60.4, 61.5, 57.8 emu/g 이었고, 보자력은 1.4, 1.8, 1.8, 1.7 Oe 이었다. 또한 미시적인 자성과 명확한 나노 입자의 상을 판별하기 위하여 뫼스바우어 분광 실험을 수행하였다. 상온에서 양성자빔 조사에 따른 각 시료의 뫼스바우어 스펙트럼을 분석한 결과, 원 시료에서는 입자크기에 따른 초상자성 현상으로 인하여 6-line 의 형태가 보이지 않으나, 양성자빔을 조사함에 따라 흡수율이 줄어들면서 6-line의 형태가 살아남을 확인할 수 있었다. 이는 양성자빔 조사를 이용하여 나노입자의 자성 발현이 가능한 것으로, 자성이온의 주입이 없이도 자성의 발현을 제어할 수 있는 것에 대한 증거가 된다고 결론지어진다.

**Dp-106** **The study of Structural, Electrical and Magnetic properties of epitaxial $Eu_{0.5}Sr_{0.5}CoO_3$ thin films** 우 영수, 김 봉주, 권 대영, 김 복기(*Department of Physics and Research Center for Dielectric and Advanced Matter Physics.*) We have investigated the epitaxial Eu0.5Sr0.5CoO3(ESCO) thin films grown on (100)STO and (001)LAO single-crystal substrates by off-axis RF magnetron sputtering method at different substrate temperature. X-ray diffraction patterns at room temperature showed that while ESCO/STO thin films with enlarged unit cells were semiconducting, ESCO/LAO thin films with constricted unit cells were metallic. For all samples, magnetization, M(T), increased below 175K due to the ferromagnetism of ESCO. The inverse magnetic susceptibility, $\chi^{-1}$, was described by using Curie-Weiss law. The resistivity(ρ) data can be explained double-exchange mechanism and strain effect.

**Dp-107** **Mössbauer 분광법을 통한 망간 페라이트의 초상자성 현상 연구** 최 한나, 현 성욱, 심 인보, 김 철성(*국민대학교 물리학과.*) Manganese chloride ($MnCl_2$), iron nitrate를 선구물질로, dodecanoic acid 와 1-dodecylamine을 계면활성제로 사용하여 고온열분해법으로 입자크기별 $MnFe_2O_4$ 시료를 합성하였다. 제조된 입자에 대하여 X-선 회절기(XRD), 진동시료형 자화율 측정기(VSM), 투과전자현미경(TEM), Mössbauer 분광기를 이용하여, 시료의 결정학적 및 자기적 특성을 연구하였다. X-선 회절도를 분석한 결과 결정구조는 inverse spinel 구조이며, 공간 그룹은 *Fd3m*이었다. 또한 scherrer식을 이용하여 그 입자 크기가 6.5, 8, 12, 17 nm임이 확인되었고, 각각의 격자상수는 8.403, 8.415, 8.437, 8.459 Å 로 밝혀졌다. VSM 측정결과 각각의 magnetization($M_s$) 값은 각 크기 별로 각각 31.1, 31.2, 54.2 58.9 emu/g 이며, coercivity ($H_c$) 값은 25.6, 38.7, 32.4, 80.5 Oe로 측정되었다. 또한 Mössbauer 스펙트럼을 상온에서 측정한 결과 6.5 nm 시료의 경우 6-line이 없는 초상자성 현상을 보였으며, 반면 8 nm 시료의 경우 6-line의 형태를 보이고 완벽한 초상자성 현상이 나타나지 않았다. 이로 보아 망간 페라이트의 초상자성 완화 효과는 그 크기에 따라 영향이 미치게 됨을 알 수 있었다.

**Dp-108** **강자성 $Fe_{1/4}TaS_2$의 거대 보자력 현상 연구** 김 성백, CHOI Y. J.[1], ASADA T.[2], PARK S.[1], WU Weida[1], HORIBE Y.[1], CHEONG S-W.[1](*포항공과대학교, 물리학과. [1]Department of Physics and Astronomy, Rutgers University (USA). [2]Research Department, Nissan ARC. LTD. (Japan).*) $TaS_2$ 판상 결정구조 사이에 $Fe^{2+}$ 이온이 삽입되어 초격자를 이루고 있는 강자성 $Fe_{1/4}TaS_2$ 물질에 대하여 거대 보자력이 관측됨을 확인하였고, 투과전자현미경 (TEM) 및 자기력원자현미경 (MFM)을 이용하여 이러한 현상의 근본 원인을 연구하였다. $Fe_{1/4}TaS_2$ 단결정은 chemical vapor transport 방법에 의하여 얇은 판상으로 성장되었으며, 급냉과 서냉의 두 가지 방법으로 후열처리 되었다. 급냉한 시료의 경우 약 7 T의 높은 보자력이 관측되었으며, 서냉한 시료와 후열처리 하지않은 단결정 (as grown) 시료에서는 약 2.7 T 및 4 T로 각각 나타났다. 이때 급냉한 시료의 자기이방성 자기장은 약 59 T로 계산되었다. 모든 시료에서 포화자화값은 열처리 방법에 상관없이 약 4 $u_B$로 $Fe^{2+}$의 high-spin 모멘트를 보이고 있다. 강자성 전이 온도($T_C$)는 급냉과 서냉 그리고 후열처리되지 않은 시료에서 각각 104 K, 159 K, 156 K로 관측되었으며, 이들 강자성 정렬 상태와 보자력 현상의 근본 기구는 $Fe^{2+}$ 이온의 초격자 결정구조에 따른 스핀-궤도 결합 (spin-orbit coupling)으로부터 발현됨을 투과전자현미경 및 자기력 원자현미경 분석 결과로부터 이해할 수 있었다

**Dp-109** **NiFe 자성나노선의 폭방향으로 균일하지 않은 자화상태의 측정** 문 경웅, 이 재철, 신 경호[1], 최 석봉(*서울대학교 물리천문학부. [1]한국과학기술연구원 스핀트로닉스연구단.*) NiFe 자성나노선의 자화역전 현상을 탐구하였다. 두께 20nm의 NiFe 박막에 e-beam 공정을 통하여 폭 600nm 자성나노선을 제작하였다. 자성나노선의 폭이 작기 때문에 자성나노선의 자화방향은 균일할것으로 예상된다. 자기장과 나노선이 이루는 각도를 고정시켜 놓은 상태에서 자기장의 세기를 바꾸어주며 자기저항을 측정하였다. 외부에서 주어진 자기장과 내부의 비등방성에 의해 자화방향이 결정되는데 외부 자기장의 세기가 일정 이상이 되면 나노선의 자화방향이 갑자기 바뀌는 현상이 일어나게 된다. 실제 측정한 결과 자기장과 나노선의 각도가 74도 보다 작을 때 자기장이 증가할수록 한번의 변화를 통해 자화방향이 역전되었다. 하지만 각도가 78도 이상이 되면 자기저항 곡선에서 두번의 큰 변화가 일어나게 된다. 자기저항값에 두번의 큰 변화가 일어나는 현상을 알아보기 위해 마이크로마그네틱시뮬레이션(OOMMF)를 수행하였다. 그 결과 자성나노선의 폭방향에서 중심부분의 자화역전이 먼저 발생하고 자기장의 세기가 더 증가한뒤 가장자리 부분의 자화역전이 일어남을 확인 하였다. 중심부분이 먼저 자화역전 되면 나노선의 자화상태는 폭방향으로 볼때 S자 형태를 가지게 되는데

이는 단자구 이론으로 설명되지 않는 결과이다.

**Dp-110** **퍼멀로이 나노선 노치에서 자기 구역 안정성** 김 준연, 최 석봉(*서울대학교 물리천문학부.*) 자기 메모리 응용을 위해서 강자기 나노선의 자기 구역과 자구벽의 특성에 대한 이해가 필요하다. 특히 자구벽의 제어와 고밀도 소자의 노치 디자인에서 자기 구역의 안정성은 중요한 문제다. 우리는 퍼멀로이 나노와이어의 자기 구역의 안정성을 oommf를 이용하여 수치 계산하였다. 미소자기 계산에 의하면 안정성은 자기 구역의 구성에 민감하다. 즉, 자구벽의 안정성은 transverse 혹은 소용돌이 자구벽이 가장 이웃하는 자구벽과 평행 혹은 반평행 하는 것에 관계 있다. 가장 이웃하는 자구벽이 서로 평행하게 정렬되어 있는 transeverse 자구벽 사이에 자기 구역이 있을 때 그 길이가 가장 짧다. 또 어떤 자구벽의 구성이든 안정한 가장 작은 자구벽의 길이는 나노선 너비의 약 2.4배이다.

**Dp-111** **$ErFe_2O_4$의 Thermoremanent magnetization 현상에 관한 연구** 김 재영, 이 보화(*한국외국어대학교, 물리학과.*) $ErFe_2O_4$ 이 속해 있는 $RFe_2O_4$ ($R$=Y, Ho, Er, Tm, Yb와 Lu)는 $Fe^{2+}$와 $Fe^{3+}$이온이 같은 결정학적인 위치를 차지하는 Rhombohedral 구조를 가지고 있는 일련의 혼합물이다. $RFe_2O_4$ 중 $R$=Tm, Yb, Lu인 화합물에서 thermoremanent magnetization(TRM) 을 볼 수 있는 것으로 알려져 있다. 본 연구에서는 TRM이 일어나는 원인을 분석하기 위해 $ErFe_2O_4$의 다결정체를 고체상태반응법으로 제작하여 자기적 특성을 연구하였다. VSM 을 이용한 온도에 따른 자화율 측정 결과 상전이가 일어나지 않는 온도영역 200 K 이하에서는 field cooling 효과가 나타나지 않음을 확인하였다.

**Dp-112** **Ionic valence and spin structure of $Co_{0.6}Fe_{0.9}Mn_{1.5}O_4$ investigated by XAS and NMR** JUNG Hyunok, LEE Soonchil, LEE H. J.[1], KIM D. H.[1], KANG J. -S.[1], ZHANG C. L[2], CHEONG S. -W.[2](*KAIST, Physics. [1]Catholic University of Korea, Physics. [2]Rutgers University, Physics.*) 우리는 nano checkerboard 구조를 가지는 물질인 $Co_{0.6}Fe_{0.9}Mn_{1.5}O_4$ 의 세가지 종류의 양이온들의 전자가 상태와 자기적 구조에 대해서 XAS와 NMR 측정을 통해서 연구하였다. 시료의 전자가 상태를 알아 보기 위해서 Mn, Co 그리고 Fe 2p XAS 측정을 하였고, 이전 발표된 XAS spectrum과의 비교를 통해서 $Mn^{2+}$, $Mn^{3+}$, $Co^{2+}$, $Co^{3+}$, $Fe^{3+}$ 상태의 이온들의 존재를 확인하였다. 50 MHz에서 610 MHz에 이르는 넓은 주파수 영역에서 4개의 구별되는 NMR 신호를 얻었다. 외부 자기장에 따른 NMR 주파수 이동의 크기와 다른 spinel 구조를 가지는 $MnFe_2O_4$, $Mn_2FeO_4$, $CoFe_2O_4$, $Co_3O_4$의 NMR 결과와의 비교를 통해서 이들은 XAS에서 얻은 4가지 이온상태들에서 나오는 신호임을 확인하였다. XAS와 NMR 측정 결과로부터 얻어진 이온들의 위치 분포를 spinel 물질의 화학식량과 총 전자가 그리고 격자 위치의 비로부터 예상하였고, saturated magnetization의 값과 비교하여 x=0.875를 가지는 $(Mn_x^{2+}Co_{1-x}^{2+})_A[Co_{x-0.4}^{3+}Mn_{1.5-x}^{3+}Fe_{0.9}^{3+}]_BO_4$의 화학식을 가짐을 예측하였다. 양이온들 중 $Fe_{0.9}^{3+}$, $Co_{0.125}^{2+}$, $Mn_{0.625}^{3+}$가 majority spin 이고, $Co_{0.375}^{3+}$, $Mn_{0.875}^{2+}$ 가 minority spin인 ferrimagnet임을 알 수 있었다.

**Dp-113** **Thickness and interface condition dependent magnetic anisotropy of Fe/Co/Cu ultrathin films** KIM Dongyoo, HONG Jisang(*Department of Physics, Pukyong National University.*) Using the full potential linearized augmented plane wave (FLAPW) method, we have explored the thickness-dependent magnetic anisotropy of ultrathin Fe films with 1.5 ML and 0.5ML Co underlayer on Cu(001). In this study, we have assumed that Co have two different interface alloy systems such as $Fe_{0.5}Co_{0.5}$ and $Co_{0.5}Cu_{0.5}$. We find that the CoCu interface alloy systems always have perpendicular magnetic anisotropy (PMA) to the film's surface. However, FeCo interface alloy systems show spin reorientation transition (SRT) phenomenon. In addition, theoretically calculated X-ray absorption spectroscopy (XAS) and X-ray magnetic circular dichroism (XMCD) will be presented.

**Dp-114** **자성이 촉매작용에 미치는 영향에 대한 제일원리계산: CO/Pd(111)** 홍 순철, 권 오룡(*울산대학교.*) 촉매로 널리 사용되고 있는 전이금속 (Ni, Pt, Pd, Rh 등)은 자성을 띠고 있거나 거의 자성을 가지려하는 성향이 있다. 이중 특히 덩치 Pd는 Fermi 에너지 준위에서 큰 상태밀도가 가지고 있어 자기 감수율이 원소 중에서는 가장 크다. 약간의 환경 변화로 자성을 띨 가능성이 높은 것으로 알려져 있다. Pd(001) 표면에 대한 선행 연구에서 인위적으로 격자 상수를 변화시켜 자성을 조절하여 자성과 촉매 작용을 연구한 결과, 자성과 촉매 작용은 밀접한 관계가 있는 것으로 밝혔다. 자성이 있는 특수한 조건에서의 Pd(001) 표면이 자성을 가지지 않는 Pd(001) 표면보다 CO 분자의 흡착과 해리에 대하여 촉매작용이 활발할 것으로 예측되었다. 본 연구에서는 Pd(111) 표면의 촉매 작용에 대한 제일원리계산을 수행하였다. 계는 Pd의 면심입방구조(fcc)의 Pd(001) 5층으로 구성된 단일판을 사용하였고 원자 구조에 대한 예비 결과를 얻기 위해 PAW_LDA 유사퍼텐셜을 도입한 VASP(Vienna Ab-initio Simulation Package) 이용하였고 그 결과를 바탕으로 자성 연구에서 가장 적합한 FLAPW(Full-potential Linearized Plan Wave)를 사용하여 더욱 명확한 결과를 도출하였다. CO 분자 흡착이 가장 용이한 것으로 알려져 있는 Pd(111) 표면에서 상자성(PM)의 안정화된 구조를 찾기 위하여 격자상수를 변화시키면서 총에너지를 계산하여 가장 안정화된 표면구조를 찾았다. 그리고 가장 안정화된 상자성(PM) 구조와 가장 강한 자성을 띠는 강자성(FM) 구조에 CO 분자를 흡착시켜 CO의 상태를 상호 비교하였다. 상태 변화와 촉매 작용과의 상관관계를 상세하게 논의할 예정이다.

**Dp-115** **MBE Growth, Magnetic and Transport Properties of Epitaxial MnP Thin Tilms** CHOI Jeongyong, KIM Jae Hwi, CHO Sunglae, KIM Yong-Hamb[1], LEE Min-Kyu[1](*Department of Physics, University of Ulsan. [1]Division of Advanced Technology, Korean Research Institute of Standards and Science.*) For the past many decades, MnP has been widely studied because of its unique magnetic properties. The crystal structure of MnP is an orthorhombic with the lattice constants of a= 5.916 Å, b= 5.260 Å, and c= 3.173 Å, which is distorted from the NiAs-type hexagonal crystal structure. Up to now, the single crystals of MnP which was grown by the Bridgman method have been mostly used for physical property studies such as nuclear magnetic resonance (NMR) and neutron scattering. We have grown MnP thin film directly on semi-insulating GaAs(100) substrate by MBE. Standard and cracking effusion

cells are used for Mn and P evaporations, respectively. The growth was monitored with reflection high energy electron diffraction (RHEED). The growth temperatures of MnP were 300 and 500 ℃ and growth rate of Mn was 0.25 Å/s under phosphorus ambience. We have grown 500 Å and 1 μm MnP thin films. The crystal structure and surface roughness of the grown films were investigated using XRD (Model D/max-RC, Rigaku Co.) and atomic force spectroscopy (AFM). In this talk, we report on magnetic and transport properties of the epitaxial MnP thin films using solid source MBE (molecular beam epitaxy).

**Dp-116** **B2 구조를 갖는 FeX(X=Al, Si, Ni, Ga, Ge, In, Sn) 이중합금의 자기변형** 이 선철, 윤 원석, 홍 순철(*울산대학교, 물리학과.*) 자기변형이란 자성체에 자기장을 걸었을 때 그 방향에 따라서 자성체의 외형이 변하는 현상으로서 여러 분야에서 연구되어지고 있고 엑추에이터, 센서, 선형모터 등에 널리 응용되고 있다. 몇몇 희토류 금속합금은 상온에서 높은 자기 변형을 가지는 데 이 합금들은 가격이 비싸고 높은 포화 자기장을 요구할 뿐만 아니라 깨짐성도 크다. 희토류 금속 합금의 이런 문제를 해결하기 위한 방안의 하나로 최근에는 bcc 철에 Ga, Al, Be 등의 비자성체를치환한 합금을 사용하려 하고 있다. 최근의 R. Wu의 논문에 의하면 FeGa 합금의 경우 $L1_0$ 나 $D0_3$ 구조에서 음의 자기변형 값을 가지나 B2 유사구조의 경우에는 양의 강한 자기변형 값을 가졌다 [1]. 본 연구에서는 자기변형에서 중요한 의미를 지니고 있는 B2 구조를 기반으로 하여 대표적 자성물질인 Fe에 비자성물질인 Al, Si, Ga, Ge, In, Sn 와 자성물질인 Ni 이 치환된 합금에 대해 제일원리계산을 수행하여 B2 구조에서 합금의 자기변형을 연구하였다. 계산방법으로는 full-potential linearized augmented plane-wave (FLAPW)을 사용하였으며 교환 상관 포텐셜에 대해서 general gradient approximation(GGA)를 사용하였다. 계산 결과 평형상태일 때의 FeX(X=Al, Si, Ni, Ga, Ge, In, Sn)의 격자상수 값은 각각 2.882, 2.770, 2.861, 2.913, 2.924, 3.216, 3.222 Å을 가졌다. Si, Ge을 화합한 합금의 경우 자성이 나타나지 않았으며 Al, Ni, Ga, In, Sn을 화합된 합금에서는 자성이 Fe 당 각각 0.655, 2.812, 0.770, 2.370, 1.803 $\mu_B$의 자기모멘트 값을 가졌다. 단일 전자 에너지 스펙트럼과 자기변형과의 관계를 상세하게 논의할 예정이다.
참고문헌 [1] R. Wu, J. Appl. Phys. 91, 7358 (2002).

**Dp-117** **Paramagnetic Properties of Ti-Zr-Ni Quasicrystals** LEE yun man, SHIN hyemin, JEON jae-kyun, KIM jae-yong (*Hanyang University, Department of Physics.*) Quasicrystal (QC) is a new structure which contains atoms with a quasi-periodic order rather than a periodic arrangement. Most of QCs are obtained by rapid quenching from molten ingots, suggesting that they are meta-stable. Since their first discovery in 1982, more than 300 QCs are found in Al-based and Ti-based alloys. Among the QCs, alloys made with Ti-Zr-Ni are good materials studying the magnetic properties of quasicrystals due to their interesting electronic properties including similar electronic structure and atomic size of Ti and Zr atoms, while the role of Ni for the stabilization of the QC structure is not clearly understood. We have prepared $Ti_{55-x}Zr_{33}Ni_{12+x}$ ($0 \le x \le 10$) alloys by rapid quenching method. X-ray diffraction (XRD) investigations revealed that a pure quasicrystal phase is formed in a broad range of $5 \le x \le 10$. The magnetization was measured by using a vibrating sample magnetometer (VSM). The results were analyzed by plotting the magnetization (M) as a function of applied magnetic field (H) at different temperatures and also as a function of temperature (T) at different applied magnetic fields. No measurable magnetic hysteresis was obtained. The magnetization values measured at Zero-Field-Cooling (ZFC) and Field-Cooling (FC) process showed no hint of significant difference. M(H) and M(T) data demonstrated that the Ti-Zr-Ni quasicrystals exhibit classical Curie paramagnetic property.

**Dp-118** **Room-temperature ferromagnetism in tetragonal $Mn_{2-x}Cr_xAs$ film grown by molecular-beam epitaxy** HWANG younghun, CHOI Jeongyong, CHO Sunglae(*Univeristy of Ulsan, Physics.*) Epitaxial ferromagnetic(FM) or ferrimagnetic(FIM) thin films on semiconductor have recently attracted much interests for hybrid spintronic devices. Arsenide (As) of transition metals with formula $M_2As$ (M= Mn, Fe, Cr) usually crystallize in three different crystal structures such as hexagonal (P-62m), tetragonal (P4/nmm) or orthorhombic (Pnma) structures. The most stable crystal structure of $M_2As$ (M= Mn, Fe, Cr) is tetragonal, which exhibited antiferromagnetic(AFM) ordering at 573, 325, and 393 K, respectively. The ternary $Mn_{2-x}Cr_xAs$ has complete solid solubility in the tetragonal (P4/nmm) crystal structure with antiferromagnets in the whole range of composition. Generally, in epitaxial thin films on crystalline substrates, various new crystallographic and magnetic phases different from those observed in bulk have been predicted. Here we report the ferromagnetism of epitaxial $Mn_{2-x}Cr_xAs$ film different from the previously antiferromagnetism in bulk based on the magnetization and magneto-transport measurements. The $Mn_{2-x}Cr_xAs$ thin films were grown on GaAs(001) by a molecular beam epitaxy (MBE). The possible reasons for the ferromagnetism in $Mn_{2-x}Cr_xAs$ thin film on GaAs(001) will be discussed in detail.

**Dp-119** **Superparamagnetic Behavier in Ultrathin Pt/CoFe/Pt Multilayer Nanowires** LEE Jae-Chul, KIM Kab-Jin, SHIN Kyung-Ho[1], LEE Chang-Won[2], CHO Young Jin[2], SEO Sunae[2], CHOE Sug-Bong(*Seoul National University. [1]Korea Institue of Science &Technology. [2]Samsung Advanced Institute of Technology.*) For future advance in high-density magnetic recording and non-volatile memory, it is essential to confirm superparamagnetic limit in magnetic nanostructure. We focus on a simplified sample geometry: long nanowires with the length (50 mm) and various width (100 nm – 2 mm). Nanostructures are fabricated on Pt/CoFe(0.3 nm)/Pt with perpendicular anisotropy using electron beam lithography and ion-milling. Hysteresis measurements are made using a magneto-optical Kerr effect measurement system. In this sample, the coercivity drops sharply at the transition point (~200 nm width). The decrement of the coercivity is ascribed to the decrement of the activation volume down to the superparamagnetic limit, which is analyzed within the context of the Arrhenius-Neél model with the consideration of the activation volume. The effect of the nucleation sites at edge roughness is also discussed as another possible origin of

the transition.

**Dp-120** **Asymmetric planar Hall resistance of Fe films grown on vicinal GaAs substrates** YOO Taehee, YEA Sun-Young, CHUNG Sunjae, CHOI Ilsoo, LEE Sanghoon, LIU X.[1], FURDYNA J. K.[1](*Physics Department, Korea University, Seoul 136-701, KOREA. [1]Physics Department, University of Notre Dame, Notre Dame, IN 46556, USA.*) Magnetization reversal process of Fe films grown on vicinal GaAs substrates has been investigated by using magneto-transport experiments. The surface of GaAs substrates in the series were tilted from [001] toward [111] direction by 2°, 5°, and 13°, respectively. The planar Hall effect (PHE) measurements was carried out at room temperature under the identical experimental conditions (i.e. current, field direction, and sample geometry). In the Fe film grown on standard substrate, a typical two-step planar Hall resistance (PHR) hysteresis, which cause by strong cubic anisotropy, was observed. However, asymmetric behavior of PHR has been observed in the Fe films grown on vicinal GaAs substrate. The asymmetry of PHR systematically increases with increasing tilted angle of the GaAS substrate. We have understood such asymmetric PHR behavior observed in the sample grown on the vicinal GaAs substrates in terms of the combined effect from the anomalous Hall effect (AHE) and PHE.[1] The asymmetric PHR of Fe layer grown on vicinal substrate provide four stable states at zero magnetic field, which can be used for the four states memory devices.

[1] W. L. Lim, X. Liu, K. Dziatkowski, Z. Ge, S. Shen, J. K. Furdyna, and M. Dobrowolska, Phys. Rev. B 74, 045303 (2006).



**Dp-121** **MBE 법으로 증착된 MnSb의 강자성 특성 연구** 박 일진, 김 삼진, 김 우철, 김 광주[1], 김 철성(*국민대학교 물리학과. [1]건국대학교 물리학과.*) Mn이 치환된 III-V 혼합물질은 비교적 높은 온도에서 강자성을 발현하기 때문에 가장 기대되는 스핀트로닉스 소자중 하나이다. 본 연구에서는 MnSb 박막의 결정학적 및 자기적 특성에 대하여 연구하였다. Molecular Beam Epitaxy (MBE) 법을 이용하여 단일상의 MnSb을 Si (100): B 기판에 증착하였다. MnSb 박막은 고순도의 Mn과 Sb을 1 X $10^{-8}$ torr 이하의 고진공 하에서 effusion cell을 이용하여 codeposition 하여 단일상의 MnSb/Si(100):B 박막을 제조하였다. MnSb/Si(100):B 의 XRD pattern의 분석결과 단일상의 Ni-As-hexagonal 구조를 가짐을 확인할 수 있었다. Vibrating sample magnetometer (VSM)의 측정결과 MnSb/Si(100):B 는 상온에서 명확한 강자성을 보였으며, 온도에 따른 자화값을 50 K 에서 700 K 까지 측정한 결과 Curie 온도 (TC)는 620 K으로 결정되었다. 50 K에서 300 K까지 저항측정 결과, 온도의 증가에 따라 박막시료의 저항값이 증가하였고 이는 MnSb/Si(100):B 박막이 금속의 특성을 보인다고 할 수 있다. 또한 1T 의 외부자기장 하에서 자기저항을 측정한 결과 자기저항현상은 관측되지 않았다.

**Dp-122** **고립된 Co 단층과 Ag(001) 표면 위의 Co 단층의 자성과 궤도질서** 김 태은, 윤 원석, 윤 석주[1], 홍 순철(*울산대학교 물리학과. [1]경상대학교 물리교육과.*) 최근의 이론 연구 결과에 의하면 W(001) 표면 위에 흡착된 Co 단층은 반강자성 상태가 에너지적으로 안정한 것으로 나타난 반면 고립된 코발트 단층은 강자성 상태가 에너지적으로 안정한 것으로 계산되어졌다. 고립된 Co 단층의 자성을 격자상수의 함수로 계산한 결과, 특정한 격자 상수에서는 스핀 질서 뿐만 아니라 궤도 질서도 보여주는 것으로 계산되어졌다. 일반적으로 궤도 질서는 궤도 구별이 명확한 부도체에서 나타나는 것으로 알려져 있고 금속에서는 알려진 바가 없다.본 연구에서는 Co 단층과 기판 사이의 작용을 최소화하여 고립된 Co 단층의 특성을 유지하여 금속에서의 궤도 질서를 실험적으로 관찰 가능한지를 예측하기 위해 Ag(001) 표면 위의 Co 단층에 대한 제일원리계산을 수행하였다. 계산방법으로는 FLAPW (full potential linearized augmented plane wave) 방법을 사용하였고, 교환 상관 포텐셜에 대해서는 GGA(Generlized Gradient Approximation)을 사용하였다. Ag(001) 표면 위의 Co 단층을 시늉내기 위해 Co 단층이 양면에 있는 7층의 Ag로 구성된 단일판을 사용하였고, 반강자성에 대한 계산을 위해 2차원 격자는 c(2 x 2)로 하였다. 그리고 표면 이완 효과를 고려하기 위해 Co와 기판인 Ag 사이의 간격을 달리 하면서 총에너지 계산을 수행하였다. 단일 전자 에너지 스펙트럼, 스핀 질서, 궤도 질서 사이의 관계에 대해 발표할 예정이다.

**Dp-123** **Electronic structures and magnetic properties of metastable bcc Ni and doped Ni with other bcc elements** KIM Bongjae, CHOI Hong Chul, MIN B.I.(*POSTECH, PHYSICS.*) Ni has a stable fcc phase with magnetism. Recently, the bcc phase of Ni, which is unstable in nature, can be achieved as a thin film on a GaAs using molecular beam epitaxy technique. Since the bcc Ni film on a GaAs substrate is known to experience strain due to the lattice mismatch, the experimental results, however, will not be the same as the bulk properties of bcc Ni. In this presentation, we report the electronic and magnetic properties of bcc Ni and doped Ni with other bcc elements using the first principles band calculation. The stable bcc elements are chosen for doping materials to reinforce the bcc character of bulk Ni. The effects of the pressure upon the electronic, magnetic, and structural properties of Ni are also investigated.

**Dp-124** **Superexchange Interaction in Orthorhombic Perovskite $RMnO_3$ : the Correlation with the Orbital ordering and Structural Distortion** 김 범현, 민 병일(*포항공과대학교, 물리학과.*) The manganese perovskite oxides ($RMnO_3$, R: rare-earth element) show the strong interplay between the orbital, lattice, and spin degrees of freedom. Due to the Jahn-Teller effect, the doubly degenerate $e_g$ orbitals are split and the C-type orbital ordering occurs. Different hopping nature of the orbital ordered system induces the A-type antiferromagnetism (A-AFM) in $RMnO_3$ [1]. The mismatch of R-O and Mn-O bond lengths causes the oxides to have the $GdFeO_3$ type distortion in which the $MnO_6$ octahedra are tilted cooperatively. Decreasing the rare-earth size, the Mn-O-Mn angle decreases from 180° and the transition temperature ($T_N$) of the A-AFM is reduced. Moreover, the magnetic transition occurs from the A-type to E-type through the spiral ordering in the large tilting cases [2]. We have studied the superexchange interaction between neighboring manganese ions with respect to the octahedron tilting

and cooperative Jahn-Teller distortion. For this purpose, we have solved an electronic model for the cluster in which the transition-metal 3d and the oxygen 2p orbitals are included and determine the ground state magnetic configuration.
[1] Hakim Meskine, Haral Konig, and Sashi Satpathy, Phys. Rev. B, 64 094433 (2000). [2] T. Kimura, S. Ishihara, H. Shintani, T. Arima, K. T. Takahashi, K. Ishizaka, and Y. Tokura, Phys. Rev. B, 68 060403 (2003).

**Dp-125** **다결정 $MnCr_2O_4$의 스핀 기저 상태에 관한 연구** 윤 동영, 이 순칠, 오 윤석[1], 김 기훈[1](*한국 과학 기술원, 물리학과. [1]서울대학교, 물리학과.*) 최근 산업적 응용 가능성이 클 것으로 예상하는 multiferroic에 대해 많은 사람들이 관심을 갖고 있다. 우리는 multiferroic의 후보 물질인 스피넬 계열의 다결정 $MnCr_2O_4$를 Zero field $Cr^{53}$ NMR과 SQUID를 이용하여 연구하였다. SQUID로 측정한 자화-온도 곡선에서는 40K 와 20K에서 뚜렷한 상전이를 갖고 있으며, 20K 이하에서의 자성 구조는 원뿔 정렬(conical ordering)로 알려져 있다. 그러나 최근 20 K 이하에서 스핀 유리의 특성과 전자 스핀 요동 등 스핀 기저 상태에 대한 의문은 여전히 남아있다. 우리는 원뿔 정렬 상태의 전자 스핀의 요동을 관찰하기 위하여 $T_2$ relaxation time을 6.9K 에서 15K 까지 측정하였다. 그 결과 전자 스핀 요동은 12K를 전 후로 느린 영역과 빠른 영역의 두 영역으로 나뉘어져 있다는 것이 관찰되었다. 또한 NMR 신호 크기-온도 곡선으로부터 원뿔 정렬의 자구 크기는 온도가 낮아짐에 따라 증가하며, 온도에 따른 히스테리시스도 갖고 있음을 확인하였다. 이러한 자구 크기의 온도 의존성은 원뿔 정렬의 1차 상전이의 특징으로부터 나온 것이라고 예상이 된다. 한편, 20 K 이하에서 스핀 유리 특성이 나타나는 지를 확인하기 위하여 시간에 따른 자화 완화를 여러 온도에서 측정하였다. 그 결과, 9K 이상에서는 자화 완화가 관찰이 되지 않은 반면 그 이하에서는 자화 완화가 관찰이 되었다. 이를 통해 9K 이하의 자성 구조는 스핀 유리 상태라는 것을 확인하였다.

**Dp-126** **Magnetostriction of Fe-Ge Alloy from first-principles calculations** YUN Won Seok, HONG Soon Cheol (*Department of Physics, University of Ulsan.*) High magnetostrictive materials are important in applications such as sensors and actuators. It was recently found that the magnetostriction of Fe-based alloys with some nonmagnetic elements such as Al, Be, and Ga, are significantly enhanced compared with that ($\lambda_{001}$ ~20 ppm) of bcc-Fe. For example, a Fe-Ga alloy greatly enhances the magnetostriction ($\lambda_{001}$ ~260 ppm) at near 19 at. % Ga [1]. The mechanism of this extraordinary enhancement of Fe-Ga alloy still remains as an open problem in spite of extensive efforts. Very recently, D. Wu *et al.* investigated the possibility of the enhancement of magnetostriction for Fe-Ge alloys. The value of $\lambda_{001}$ increases with Ge additions, reaching a maximum of 94 ppm [2]. In this work, we investigated magnetostriction and elastic properties of $Fe_{1-x}Ge_x$ alloys with different Ge concentrations by using the full potential linerized augmented plane wave method within generalized gradient approximation. The optimized lattice constants of $Fe_{0.875}Ge_{0.125}$, $Fe_{0.8125}Ge_{0.1875}$, $Fe_{0.75}Ge_{0.25}$, and $Fe_{0.6875}Ge_{0.3125}$ alloys were determined from the total energies calculation to be 5.779, 5.765, 5.778 and 5.765 Å in ferromagnetic state, respectively. We will discuss our calculation results in detail by comparing with the experimental values and the theoretical results for FeGa alloys.
Reference [1] A. E. Clark *et al.*, J. Appl. Phys. 93, 8621 (2003). [2] D. Wu *et al.*, J. Appl. Phys. 103, 07B307 (2008).

**Dp-127** **Reentrant Weak-ferromagnetic Phase in Haematite Crystal at Low Temperature** LEE Seong-Joo, JUNG Hyunok, LEE Soonchil, DHO Joonghoe[1](*Department of Physics, Korea Advanced Institute of Science and Technology. [1]Department of Physics, Kyungpook National University.*) We investigated the magnetic properties of the natural haematite ($\alpha$-$Fe_2O_3$) crystal at liquid helium temperature by using a SQUID and $^{57}$Fe NMR. The M(T) curve shows that the net magnetization in the (111) plane vanishes at the Morin temperature (260 K) but reappears as temperature decreases below 40 K. Comparison of magnetization and NMR results indicates that the spin state, the spin directions and canting angle, at low temperature is the same with that in the weak-ferromagnetic state above the Morin temperature, but its volume occupies only 3 % of the whole sample. The relaxation of magnetization with time, the difference of the ZFC and FC magnetizations, and the rise of the NMR echo intensity with increasing field exhibit the superparamagnetic behavior of the reentrant weak-ferromagnetic phase. The cluster size of the weak-ferromagnetic phase is smaller than $10^2$ nm and the blocking temperature is higher than 40 K. Comparison of the experimental results for the natural crystal and pure powder seems to imply that the reentrant weak-ferromagnet phase at low temperature is due to an intrinsic magnetic instability.

**Dp-128** **Electronic and Magnetic Properties of the $Fe_3Si$ on Si(001) and GaAs(001) surfaces** HONG Soon Cheol, DORJ Odkhuu(*Univ. of Ulsan, Dept. of Physics.*) Metal-semiconductor heterojunctions have received much attention in the context of spintronics because they could open up the possibility to inject a spin polarized current from a ferromagnetic (FM) metal into a semiconductor. This is a prerequisite for anticipated future electronic devices making use of spin-polarized carriers. From the viewpoint of applications, it is highly desirable to grow well-defined FM metallic films on the most common semiconductors, in particular on the technologically relevant Si and GaAs (001) surfaces. As well-defined $Fe_3Si$ can be synthesized on them because of the similar crystal structure and the small lattice mismatch (-3.89 and 0.05 % for Si and GaAs) of $Fe_3Si$ to Si and GaAs. In this work, we will present theoretical results on the electronic and magnetic properties of the $Fe_3Si$ on Si(001) and GaAs(001) by using the full potential linearized augmented plane wave (FLAPW) method where the exchange-correlation interaction is expressed with general gradient approxiamtion. Magnetic crystalline anisotropy, magnetic circular dichroism spectra, and magnetostriction of the system will be also presented.

**Dp-129** **NiFe/FeMn/CoFe 3층막 구조에서의 열처리 온도에 따른 교환바이어스의 영향** 최 혁철, 김 기연[1], 유 천열, 이

정수[1](*인하대학교, 물리학과. [1]한국원자력연구소, 하나로이용기술개발부.*) 강자성 (F: ferromagnet)과 반강자성 (AF: antiferromagnet)사이의 교환 결합에 의해서 교환 바이어스 현상이 나타는데 이는 F/AF의 계면을 포함하는 자기적 이종접합 구조를 AF의 blocking temperature($T_B$) 이상의 온도에서 field-cooling 시키거나 기판에 일정 자기장이 인가된 상태에서 증착할 때 관측 된다. 교환 바이어스를 이해하기 위한 근본적인 연구로 F/AF/F 구조의 다층막에서 F층의 자화가 역전할 때 AF 자구벽을 가진 AF층에서 나선의 스핀 구조가 형성됨을 관측하는 실험들이 이루어지고 있다. 하지만 F/AF로 교환 결합된 NiFe/IrMn/CoFe의 3중 막에서는 $T_B$ 이상의 온도에서 field-cooling이 진행될 때 Mn 원자들의 내부 확산으로 교환 바이어스가 변하는 현상을 보인다. 본 연구에서는 NiFe(20 nm)/FeMn(15 nm)/CoFe(20 nm)의 3중 막을 증착한 후 열처리 온도에 따른 계면에서의 교환 바이어스의 변화를 조사하였다. VSM (vibrating sample magnetometer)로 자기 이력 곡선을 확인한 결과 NiFe/FeMn와 FeMn/CoFe 계면에서의 교환 바이어스 변화가 서로 상반됨을 보였다. 이에 대해 XRD (x-ray diffraction)를 사용하여 시료의 결정학적 구조와 XPS (X-ray photoelectron spectroscopy)로 depth profile을 조사하였으며 그 결과 FeMn 층에서 Fe과 Mn원자의 구성비가 일정하지 않음을 확인하였다.

**Dp-130** **Formation enthalpy and distribution behaviors of B, C, and N impurities in bcc iron** BAIK SEUNG SU, MIN Byung Il, KWON SE KYUN[1], KOO YANG MO[1](*POSTECH, Dept. of Physics. [1]GIFT.*) To model the microstructure of B, C, and N distributions in bcc iron, we employed the spin-polarized density functional theory (SDFT) using the full-potential linearized augmented plane wave (FLAPW) band method. For the treatment of exchange-correlation energy, we used the generalized gradient approximation (GGA96). The formation enthalpies for both interstitial and substitutional B, C, and N impurities in the Fe bulk supercell and the 2x2x7 Fe slab-supercell were calculated. We found that both the substitutional and the interstitial positioning of boron impurities are energetically comparable each other in the Fe bulk supercell, whereas the interstitial positioning of C and N impurities are more stable than the substitutional positioning in the same bulk supercell. We also found that B, C, and N impurities on the surface are most stable as compared to the impurities in the sub-surface positions in the Fe slab-supercell matrices, which is in good agreement with the experiments.

**Dp-131** **Ferroelectric Properties of $Bi_4Ti_3O_{12}$-$SrBi_4Ti_4O_{15}$ Bi-layered Thin Films Prepared by Chemical Solution Deposition** KIM Sang Su, KIM Jin Won, JO Hyun Kyung, DO Dalhyun, YI Seung Woo, KIM Young Min, KIM Tae Gyu(*Changwon National University, Department of Physics.*) The bismuth layer-structured ferroelectric materials (BLSFs) are considered as the excellent candidates for the ferroelectric random access memories. The BLSFs belong to family of Aurivillius phases which has a general formula $(Bi_2O_2)^{2+}(A_{m-1}B_mO_{3m+1})^{2-}$. In this notation, A-site represents a mono-, bi- or trivalent ion and B-site denotes a tetra-, penta- or hexavalent ion and m is the number of $BO_6$ octahedra in each pseudo-perovskite block. Among the encouraging BLSFs, $Bi_4T_{i3}O_{12}$ (BIT, m = 3), $SrBi_4Ti_4O_{15}$ (SBTi, m = 4) have emerged to be most promising candidates due to their respective merits. Recently, the BIT-SBTi ceramic has been reported with a large remanent polarization. In this work, the BIT-SBTi, and SBTi-BIT bi-layered thin films were prepared on the Pt(111)/Ti/$SiO_2$/Si substrates by a chemical solution deposition method followed by the rapid thermal annealing at 700°C for 3 min in oxygen atmosphere. The crystalline structures of the thin films were analyzed by X-ray diffraction (XRD, Philips APD system) analysis, and the surface morphologies and cross-sectional micrographs were investigated by a scanning electron microscope (SEM, Hitachi S-2400). The ferroelectric properties and leakage current density of the bi-layered thin film capacitors were measured using a ferroelectric tester (Radiant Precision LC 100-K) and an electrometer (Keithely, 6517A).

**Dp-132** **Fabrication and Multiferroic Properties of Thin Films of $x$BiFeO$_3$-($1-x$)$Bi_4Ti_3O_{12}$ System** KIM Sang Su, JO Hyun Kyung, DO Dalhyun, KIM Jin Won, YI Seung Woo, KIM Young Min, KIM Tae Gyu(*Changwon National University, Department of Physics.*) The thin films of mixture of $x$BiFeO$_3$-($1-x$)$Bi_4Ti_3O_{12}$ ($x$=0.4, 0.5, and 0.6) system were prepared by a chemical solution deposition method. The crystal structure of the thin films was analyzed by X-ray diffraction. It was found that thin films (x=0.4 and 0.5) mainly consist of a $Bi_4Ti_3O_{12}$ phase while $Bi_5Ti_3FeO_{15}$ was the major phase of thin film ($x$=0.6). $Bi_5Ti_3FeO_{15}$ showed better ferroelectric properties in remnant polarization and polarization fatigue than those observed in $Bi_4Ti_3O_{12}$. The values of remnant polarization $2P_r$ and coercive field $2E_c$ of thin film ($x$=0.6) were 36 μC/cm$^2$ and 192 kV/cm at an applied electric field of 260 kV/cm, respectively. There was almost no polarization fatigue up to $10^{10}$ switching cycles. Also weak ferromagnetism was observed in $Bi_5Ti_3FeO_{15}$. The results indicate that $Bi_5Ti_3FeO_{15}$ thin films that show the multiferroic property can be an attractive material for application in new type of devices.

**Dp-133** **Frequency-Control of MIT-Induced Electrical Oscillation in $VO_2$ Thin Film** LEE Yong Wook, KIM Bong-Jun[1], CHOI Sungyoul[1], LIM Jung-Wook[1], YUN Sun-Jin[1], CHAE Byung-Gyu[1], KIM Hyun-Tak[1](*ETRI (MIT device team), Pukyong National University (School of electrical and control engineering). [1]ETRI (MIT device team).*) In order to simply generate an electrical oscillation with no inductive components at room temperature, lots of electrical materials with a negative differential resistance have been incorporated for the oscillation generation including perovskite and organic materials. With those materials, however, the oscillation was realizable only at very low temperature, and the oscillation frequency was at most tens of kHz and even fixed as ~40 Hz in case of organic materials. In this paper, we demonstrated a frequency-controllable room-temperature electrical oscillation, whose frequency could be tuned simply by adjusting one of circuit components and increased up to more than 1 MHz, by using $VO_2$ thin film.

**Dp-134** **Effects of Next-nearest Hopping in the Half-filled Ionic Hubbard Model** GO Ara, JEON Gun Sang(*Department of Physics and Astronomy, Seoul National University.*) We study the one-dimensional half-filled Hubbard model with a staggered ionic potential at zero temperature. In the absence of next-nearest-neighbor hopping, it is well known that the system undergoes transitions from a band insulating phase for weak interaction to a Mott insulating phase for strong interaction. We use the cellular dynamical mean-field theory combined with the exact diagonalization technique to investigate the effects of next-nearest hopping on the transition nature of the system. As the next nearest neighbor hopping grows up, the system have a tendency to favor a metallic phase. The phase diagram is obtained and detailed behaviors at the phase boundary are discussed.

**Dp-135** **Optical properties of the charge-density-wave compound $CeTe_2$** OH H. J., LEE K. E.[1], SONG Y. Y.[2], JUNG M. A.[1], MIN B. H.[1], LEE Y. S.[3], KWON Y. S.[1](*Department of Physics, Sungkyunkwan university and Department of Opthalmic Optics, Masan College. [1]Department of Physics, Sungkyunkwan university. [2]Department of Physics, Sungkyunkwan university and Department of Opthalmic Optics, Jeju Tourism College. [3]Department of Physics, Soongsil university.*) The temperature dependence of the optical conductivity of $CeTe_2$ was obtained for the *E//ab*-plane and *E//c*-axis at photon energies ranging from terahertz to visible light. Two gap states are found in the optical conductivity spectra. The magnitudes of the gaps are estimated to be 0.448 and 0.109 *eV* in the *E//ab*-plane. The former is due to perfect nesting, while the latter is due to imperfect nesting. The magnitude of the gap due to perfect nesting on the *c*-axis is evaluated to be 0.854 *eV*. The Drude resonance caused by the ungapped Fermi surface is found only on the *E//ab*-plane since $CeTe_2$ is a quasi-2D material. The portion of the ungapped Fermi surface across all Fermi surfaces is about 3 %.

**Dp-136** **Hybridization gap-open in $CeIn_3$** SONG Y. Y., JUNG M. A.[1], OH H. J.[2], KWON Y. S.[1](*Department of Physics, Sungkyunkwan university and Department of Opthalmic Optics, Jeju Tourism College. [1]Department of Physics, Sungkyunkwan university. [2]Department of Physics, Sungkyunkwan university and Department of Opthalmic Optics, Masan College.*) Reflectivity spectra of $CeIn_3$ are measured at 7, 30, 50, 100, 150, 200 and 300 K in wild energy regions from 6 *meV* to 30 *eV*. Optical conductivity spectra are obtained from a Kramers–Kronig' relation. A hump in the optical conductivity $\sigma_1$ is observed at about 500 $cm^{-1}$ below 100 K, resulting from strong hybridization between conduction electrons and Ce *4f* electronic states. The low frequency Plasmon indicating the existence of heavy particles is also observed below coherence temperature $T^* \sim 100$ K.

**Dp-137** **Optical evidence for a change in the heavy electron Fermi surface at a magnetic quantum critical point of $CeNi_{1-x}Co_xGe_2$** JUNG M. A., OH H. J.[1], SONG Y. Y.[2], HONG J. B., KWON Y. S.(*Department of Physics, Sungkyunkwan university. [1]Department of Physics, Sungkyunkwan university and Department of Opthalmic Optics, Masan College. [2]Department of Physics, Sungkyunkwan university and Department of Opthalmic Optics, Jeju tourism College.*) We have studied optical properties of $CeNi_{1-x}Co_xGe_2$ ($0 \le x \le 1$) via an infrared spectroscopy. Tuning the Co-doping concentration reveals clear demarcation in the optical properties at $x = 0.3$, where a non-Fermi liquid behavior appears. For $x>0.3$, a hump in the optical conductivity $\sigma_1$ is observed at about 0.2 *eV*, resulting from strong hybridization between conduction electrons and Ce *4f* electronic states. For $x \le 0.3$, in contrast, no such hump is observed. The low frequency plasmon observed below the coherence temperature $T^*$ for $x>0.3$ is also consistent with the existence of heavy quasiparticles. These dramatic changes in the optical response at $x = 0.3$ indicate that the heavy electron Fermi surface of $CeNi_{1-x}Co_xGe_2$ ($x>0.3$) ceases to exist at this magnetic quantum critical point.

**Dp-138** **Path-integral Monte Carlo Study of Orientational Ordering of Solid Hydrogen Deuteride** 권 용경, 신 현덕(*건국대학교 물리학과.*) Due to competition between large rotational kinetic energy and anisotropic intermolecular interaction which can be explained by electric quadrupole-quadrupole interaction, quantum solids of molecular hydrogen, $H_2$, $D_2$ and HD exhibit complex orientational order-disorder phase diagrams. Solids of asymmetric HD molecules show orientational ordering at high pressures, where higher rotational levels are mixed into the ground state. At intermediate pressures, significant occupation of the nonzero rotational levels of HD occurs only when temperature is higher than a certain value. This results in peculiar reentrant shape in the pressure-temperature phase diagram of HD. In order to study this ordering of HD, we here consider a system of asymmetric quadrupolar rotors localized at face-centered cubic lattice sites. Using the path-integral Monte Carlo, we find a reentrant shape in their orientational order-disorder phase transition as observed experimentally in solid HD. In our PIMC results, the reentrant behavior is shown at pressures 10~15 GPa with primitive approximation. The large discrepancy between this and experimental value of 50~60 GPa might be due to weakening of the anisotropic interaction at high pressures. Another reason for this discrepancy is time step error in the primitive approximation. For quantitative agreement with the experiments, we incorporate the fourth-order terms into high-temperature density matrices in the path-integral formalism.

**Dp-139** **Rare earth element dependent pseudo gap effects in electron doped cuprates.** 김 창영, 송 동준, 최 규진, 박 승룡, 최 성균, 임 춘식, 김 철, 김 용관, 홍 태윤, EISAKI Hiroshi[1], 김 재훈(*연세대학교, 물리학과. [1]AIST.*) High temperature superconductors (HTSC) have not only the superconducting gap but also pseudo gap (PG), a gap that exists above the transition temperature. While the superconducting gap is directly related to the superconductivity, it is unclear in what role PG plays in HTSC not to mention the origin of it. To pursuit the issue, we performed angle resolved photoemission (ARPES) and Infra-Red (IR) spectroscopy

on electron doped HTSCs. IR showed a PG evolution as a function of temperature which is consistent with our earlier results. Moreover, PG showed a rare earth element ($R_{1.95}Ce_{0.15}CuO_{4,}$, R=Nd, Sm, Eu, Gd) of the PG evolution. The IR results are consistent with our recent ARPES data, and we find a relationship between doping and rare earth exchange.

**Dp-140** **The growth of superconducting $YBa_2Cu_4O_8$ single crystals with Tc=81K at ambient pressure** 김 창영, 허 남정[1], 최 성균, 송 동준, 박 승룡, 임 춘식, 김 철, 김 용관, 정 원식, 고 윤영 (*연세대학교 물리학과. [1]인하대학교 물리학과.*) We performed the flux method in order to synthesize $YBa_2Cu_4O_8$ (Y124), using KOH. This material is the high temperature superconductivity, which shows approximately Tc=80K. Y124 is more intriguing than the well-known $YBa_2Cu_3O_7$ (Y123, YBCO) since the role of the double CuO chain in high temperature superconductivity is still debating. However, the vigorous study cannot be performed up to now due to the difficulty of synthesizing the single crystal: typically, it needs high oxygen pressure up to 3000 bar. However, last year, one interesting paper published at Single Crystal Growth, which about growing Y124 single crystal. This recent method is differentiating in the sense that the extremely high pressure is no longer necessary. Paying attention to this advantage, we have tried to reproduce the single crystal growth. Then, here we present the result. Under 1 atm, that is, at the ambient pressure, black and shiny Y124 single crystal is synthesized from $YBa_2Cu_3O_7$ (Y123) polycrystalline powder with both CuO and KOH. Then we did X-Ray Diffraction in order to check the quality of samples. Based on the good quality, we have been performing angle-resolved photoemission spectroscopy (ARPES). At near future, if we can obtain the relatively larger single crystals (eg, more than 1mm) we may try infrared spectroscopy (IR) or neutron experiments.

**Dp-141** **High resolution angle resolved photoemission studies on quasi-particle dynamics in graphite** 김 창영, 김 범준[1], 김 철, 박 승룡, OHTA Taisuke[2], BOSTWICK Aaron[2], ROTENBERG Eli[2], 김 형도[3], 최 형준, 임 춘식(*연세대학교, 물리 및 응용물리학과. [1]서울대학교, 물리학과. [2]Advanced Light Source, Lawrence Berkeley National Laboratory. [3]포항 가속기 연구소.*) We obtained the spectral function of graphite H point using high resolution angle resolved photoelectron spectroscopy (ARPES). The extracted width of the spectral function (inverse of the photohole life time) near the H point is approximately proportional to the energy as expected from the linearly increasing density of states(DOS) near the Fermi energy. This is well accounted by our electron-phonon coupling theory considering the peculiar electronic density of states near the Fermi level. And we also investigated the temperature dependence of the peak widths by experimentally and theoretically. The upper bound for the electron-phonon coupling parameter is about 0.23, a nearly same value with the previously reported our work at K point.

**Dp-142** **Investigation of $VO^{2+}$Ions in $GeO_2$-$B_2O_3$-$V_2O_5$ Glasses** 김 영훈, 강 재필, 홍 성덕, 차 유정[1], 서 용문, 최 덕, 송 승기(*명지대학교, 물리학과. [1]영남대학교, 물리학과.*) The structures of $VO^{2+}$ions in $GeO_2$-$B_2O_3$-$V_2O_5$ glasses have been studied by EPR.Glass samples of composition K$GeO_2$-$B_2O_3$-R$V_2O_5$ (K=$GeO_2$ mole%/$B_2O_3$ mole%, R=$V_2O_5$ mole% / $B_2O_3$ mole%) were prepared in the range K=0.25~2.0 with R=0.5 and K=0.25~1.0 with R=1.0. Spin Hamiltonian parameters, Fermi contact interaction parameter and dipolar hyperfine coupling parameter have been calculated and analysed. It is found that $V^{4+}$ions in these samples exist as $VO^{2+}$ions in octahedral coordination with a tetragonal symmetry. Information concerning the valence state of transition metal(TM) ions, their concentration, local environment and the nature of interaction between them are reported.

**Dp-143** **Determination of the scaling behaviour of the octahedral rotation in $K_2SnCl_6$ around the structural phase transition temperatures** 김 영훈, 서 용문, 최 덕, 송 승기(*명지대학교, 물리학과.*) $K_2SnCl_6$ has been the prototype crystal for the investigation of lattice dynamics and their critical behaviour in association with phase transitions using the scattering and resonance methods[1]. This crystal undergoes structural phase transitions with a collective rotation of the $SnCl_6$-octahedra as a result of subtle interplay between the rotary lattice mode and the hindered rotation of the $SnCl_6$-octahedra[2]. During this process the surrounding $K^+$-ion cage remains undistorted. This implies that the temperature dependence of the NQR frequency is determined almost completely by the temperature dependence of the rotation angle of the $SnCl_6$-octahedra. We have calculated the NQR frequency in the intermediate phase between the first and the second phase transition temperatures in $K_2SnCl_6$ on the basis of the simple point charge model. Fitting NQR data to the calculated function allows the determination of the scaling behaviour of the rotation angles of the $SnCl_6$-octahedra in the intermediate phase. The excellent agreement between the data and calculation confirms again that the phase transition in $K_2SnCl_6$ is a purely rotative type.

References 1. R. L. Armstrong Phys. Rep. 57 343 (1980), 2. Y. M. Seo, B. S. Kim, S. K. Song, J. Pelzl Hyperfein Inter. DOI 10.1007 (2005)

**Dp-144** **A LDA+U Study of ortho-II $YBa_2Cu_3O_{6.5}$** OH Hyungju, CHOI Hyoung Joon(*Yonsei University.*) The exhibition of clear quantum oscillations in the magnetization (de Haas-van Alphen) and conductivity (Shubnikov-de Haas) were recently reported in ortho-II $YBa_2Cu_3O_{6.5}$. The observations of quantum oscillations in ortho-II $YBa_2Cu_3O_{6.5}$ (YBCO) proved the existence of a closed Fermi surface in the normal state of the underdoped cuprates. The observed orbits have frequencies of ~530 T and ~1650T. In the present work, we study the electronic structures of $YBa_2Cu_3O_{6.5}$ using the so-called LDA+U method which can reproduce the correct magnetic ground state and forbidden gap in correlated antiferromagnetic insulators by adding the on-site Coulomb repulsion *U* to the local density approximation (LDA) in a mean-field-like way. The Fermi surface of $YBa_2Cu_3O_{6.5}$ is analyzed to understand the effects of the on-site Coulomb repulsion *U* on the

quantum oscillation frequencies.

* This work was supported by the KRF (KRF-2007-314-C00075) and by the KOSEF Grant No. R01-2007-000-20922-0. Computational resources have been provided by KISTI Supercomputing Center (KSC-2008-S02-0004).

**Dp-145** **Single Crystal Growth by Chemical Vapor Transport Method** 김 창영, 김 용관, 고 윤영(*연세대학교 물리및 응용물리학과 첨단전자구조 연구실.*) For its interesing physical phenomenon, Charge Density Wave(CDW) phase, transition metal dichalcogenides(MX2) were rapidly studied since 70's. We investigated the self-assembled growth of μm-scale topological crystals of $NbSe_3$, $NbSe_2$, and $TiSe_2$ based on the chemical vapor transportation method. We got large enough and lots of samples upto several mm. The crystal structure was invesgated by X-ray diffraction and Laue experiment.

**Dp-146** **Angle Resolved Photoemission (ARPES) of $Eu_{1-x}La_xB_6$ (x = 0.1, 0.2, 0.3)** MIN Chul-Hee, OH S.-J.[1], KIM J. Y.[2], SUNG N. H.[2], CHO B. K.[2], KIM H.-D.[3](*CSCMR and Department of Physics and Astronomy, Seoul National University, Seoul 151-141, Korea2. [1]CSCMR and Department of Physics and Astronomy, Seoul National University, Seoul 151-141, Korea. [2]Center of Frontier Materials and Department of Materials Science and Engineering, K-JIST, Gwangju 500-712, Korea. [3]Pohang Accelerator Laboratory, Pohang Universtity of Science and Technology, Pohang 790-784, Korea.*) EuB6 is known as a divalent hexaboride that semimetalic band overlap between boron valence band (hole pockets) and Eu 5d conduction band (electron pockets) at X point of the cubic Brillioun zone is predicted by first principle calculation [1], However, it had been also known as a semiconductor by ARPES measurements with 30 eV photon energy [2]. The ARPES data support that EuB6 is an insulator that has an energy gap, and surface defects may dope electrons into the system, so the electron pocket is observed as time elapsed from cleavage of the sample. However, the hole pocket is found without electron pocket with photon energy of 130 eV [3]. Therefore, the electron pocket is from surface.Eu1-xLaxB6 is initially thought to be an electron doped system by a La atom that donates an electron, so the electron pocket can be observed apparently. But, as increasing doping rate the lattice constant is decreasing from 4.19 Angstrom to 4.17 Angstrom (0.5%) [4]. Moreover, the boron octahedrons are tilted or rotated that is supported by a Raman scattering study [5]. These changes may cause various intriguing transport and magnetic properties according to the La concentration. For example, all the compounds show negative Hall coefficients except for x = 0.2 in which the sign changes anomalously around T = 25 K. .Here, we have carried out ARPES of Eu1-xLaxB6 (x=0.1,0.2,0.3) with photon energy of 130 eV and found electron pockets.

[1] J. Kunes &W. E. Pickett, Phys. Rev. B 69, 165111 (2004). [2] J.D. Denlinger et al., Phys. Rev. Lett. 89, 157601 (2002). [3] J.D. Denlinger et al., Abstract for the March 07 meeting of APS [4] Jong-Soo Rhyee et al., Phys. Rev. B 74, 235114 (2006). [5] M. Song et al. J. Magn. Magn. Mater. 310, 1019 (2007)

**Dp-147** **Effects of Bi-based Peroskite Doping on the Ferroeletric Transition in $Pb(Zr,Ti)O_3$ Ceramics** 송 태권, 왕 림, 이 성찬, 조 종호[1], 김 명호(*창원대학교, 나노신소재공학부. [1]창원대학교, 기초과학연구소.*) For the high temperature application of $Pb(Zr,Ti)O_3$ (PZT) piezoceramics, it is asked to develop PZT ceramics of high ferroeletric transition temperature ($T_C$). In the case of $PbTiO_3$, $T_C$ was reported to increase with doping of Bi-based perovskites such as $Bi(Zn_{0.5}Ti_{0.5})O_3$ or $BiFeO_3$. In this work, the doping effects of Bi-based perovskites on PZT ceramics were studied. In Ti-rich composition, $T_C$ increased with doping but $T_C$ decreased at around MPB region. The effects of doping on $T_C$ and piezoelectric properties were compared for different Bi-based perovskites, $Bi(Zn_{0.5}Ti_{0.5})O_3$, $BiFeO_3$, $BiAlO_3$.

**Dp-148** **Orientational Ordering in the Ortho-Para Mixtures of Solid $H_2$** 권 용경, 박 성진, 송 재호, 신 현덕(*건국대학교 물리학과.*) Since a hydrogen molecule has light mass and very large rotational constant, a solid of molecular hydrogen is a translational and rotational quantum solid. Due to requirements on the symmetry of its wave function, this molecule has two species: para-$H_2$ and ortho-$H_2$. One of the interesting features of this molecular solid is that it shows the orientational order-disorder phase transition and this property depends on rotational quantum number J. This ordering is mainly due to the anisotropic interaction between $H_2$ molecules. Odd-J species of ortho-$H_2$ are orientationally ordered at low temperatures to Pa3 structures and they remain ordered as pressure increases. On the other hand, even-J species of para-$H_2$ do not show this orientational ordering at low pressures. However, with increasing pressures, solid para-$H_2$ also experiences a transition to an orientationally-ordered phase. It was reported that a mixed solid of ortho-/para-$H_2$ experiences an orientational ordering and it occurs at higher pressures as the ortho concentration decreases. Furthermore, it was found to be no long-range orientational order below the crtitical ortho concentration of ~ 0.56. In order to investigate the ordering of the ortho-para mixtures, we here consider a system of rigid rotors with electric quadrupole (EQ) moments of either q or zero, localized at FCC lattice sites, because most of the anisotropic intermolecular interactions can be explained by an electric quadrupole-quadrupole interaction. Zero EQ moment is assigned to para-$H_2$ molecules since they are in spherically symmetric J=0 rotational state. We perform the Monte Carlo simulation to compute the order parameter as a function of temperature at various ortho-para ratios. We also calculate the correlation function of the local order parameter to investigate the onset of the long-range order as the ortho concentration increases.

**Dp-149** **Electronic Structure, Spin States, and Thermoelectric Power of Low Dimensional Cobaltates $Ca_3Co_4O_9$ and $Ca_3Co_2O_6$** NOH H-J, SUNG HJ, PARK KJ, JEONG Jinwon, JEONG Jinhwan, KIM Sung Baek[1], CHO B K[2], KIM J Y[2], KIM J-Y[3], KIM

H-D[3](*전남대학교 물리학과. [1]포항공과대학교 물리학과. [2]광주과학기술원 신소재공학과. [3]포항공과대학 포항가속기.*) Recently, cobalt oxides with a low dimensional structure such as $Na_xCoO_2$, $Ca_3Co_4O_9$, $Ca_3Co_2O_6$, etc. have attracted much attention due to the discovery of their large thermoelectric power of ~100 mV/K. Interestingly, these cobaltates show several common features such as low dimensional structure, low electric conductivity, and the suspected mixed-valency of the cobalt ions. To understand the origin of the large thermoelectric power, roughly two approaches have been tried. One is the entropy approach that applies the Heikes formula to the spin-degeneracy of the cobalt ions in the Hubbard model for the strongly correlated electron systems, and the other is the traditional approach in which the thermoelectric power is calculated from the density of the states near the Fermi level under the relaxation time approximation. Many experimental studies have reported that the application of the Heikes formula is not appropriate for the cobaltates, though the spin degeneracy may play a role in part. In order to investigate the origin of the large thermoelectric power of the cobaltates and clarify this issue, we have performed x-ray absorption spectroscopy and photoelectron spectroscopy on the quasi-1 dimensional $Ca_3Co_2O_6$ and quasi-2 dimensional misfit-layered $Ca_3Co_4O_9$ using synchrotron radiation facilities. By combining the Co 2*p* photoelectron spectra, Co 2*p* absorption spectra, and O 1*s* absorption spectra, we obtained valence states and spin states of the Co ions. Additionally we extracted the several important parameters for the electronic structure of the cobaltates using configuration interaction cluster model calculation, and checked the pre-requisites for the Heikes formula.

**Dp-150** **Physical Properties of $Eu_xBa_{1-x}TiO_3$ (x=0 - 0.30) Ceramics** 최 병춘, 전 병억, 김 샛별, 문 병기, 정 중현(*부경대학교.*) We studied the rare earth modification on $BaTiO_3$. In this study, the $Eu_xBa_{1-x}TiO_3$ (x=0 - 0.3; EBT) ceramics were prepared by the wet chemical synthesis. The physical characterization of EBT ceramics were performed by the X-ray diffraction and the scanning electron microscopy. The EBT ceramics displayed the ferroelectric D-E hysteresis at room temperature. We examined the dielectric behaviors during the ferroelectric phase transitions. The dielectric properties of EBT ceramics were observed in the temperature range from RT to 600 °C. The Eu substitution lowered the ferroelectric phase transition temperature. It is considered that Eu ions substitute Ba site rather than Ti site because the ionic radii of $Ba^{2+}$ is larger than that of $Eu^{2+}$ and/or $Eu^{3+}$. Nevertheless, the probability of Eu ion substitute Ti sites was not excluded when Eu was replaced for Ba with higher concentrations in the EBT fine ceramics. In this regards, the electrical properties of intrinsic EBT phase separating from the grain boundary were elucidated by using the dielectric spectroscopy with the Maxwell-Wagner type composite model.

**Dp-151** **New approach to electronic structure studies by ARPES** 김 창영, 정 원식, 임 춘식, 박 승룡, 김 철, 송 동준, 최 성균, 김 용관, 고 윤영(*연세대학교 물리및응용물리학과 첨단전자구조연구실.*) ARPES has traditionally considered as a tool of electronic structural studies in the momentum space. One may speculate that the spectroscopic data obtained in the real and momentum spaces can be converted from one to the other as wave functions in real and momentum spaces are converted from one to the other through the fourier transform. In scanning tunneling spectroscopy(STS), the spectroscopic data obtain in the real space is fourier transformed to produced electronic structure in real space. But there is no exact analogy between the STS and ARPES cases. We try to transform the Graphene ARPES spectra to real space by using atomic orbital of tight binding calculation.

**Dp-152** **Ferroelectric Properties of $LiNbO_3$ Doped $Na_{0.5}K_{0.5}NbO_3$ Lead-free Thin Films Fabricated by RF-Magnetron Sputtering** 김 일원, 이 해준, 박 정민, 배 세환[1], 진 병문[2], 이 정식[3] (*울산대학교, 물리학과. [1]동아대학교, 물리학과. [2]동의대학교, 물리학과. [3]경성대학교, 물리학과.*) The $(Na,K)NbO_3$ ceramics have been studied extensively, because of their good piezoelectric and ferroelectric properties. Recently, $(Na,K)NbO_3$ ferroelectric thin films have been studied for applications in memory devices, due to their high remanent polarization and good fatigue endurance. However, it is difficult to fabricate stabilized NKN films because of the volatility of Na and K ion. In our previous study, $LiNbO_3$ doped NKN ceramics shows a high sinterbility, low leakage current, and enhanced ferroelectric properties.In this study, we have deposited the ferroelectric $(Na,K,Li)NbO_3$ (NKLN) thin films on $Pt(111)/Ti/SiO_2/Si$ substrates by using a RF - magnetron sputtering method and investigated the ferroelectric properties with different annealing conditions such as ambient gas, annealing temperature, and annealing time. The NKLN film annealed at $O_2$ ambient exhibited ferroelectric P-E hysteresis loops and low leakage current properties. The frequency dependant dielectric and impedance properties of NKLN films have been investigated as functions of temperatures. We also have studied the characteristics of leakage current density – applied electric field (J-E) and time (J-t) in order to search the conduction mechanism for the NKLN films.

**Dp-153** **Impedance and dielectric properties of lead-free $0.95(Na,K)NbO_3$-$0.05LiNbO_3$ ferroelectric thin films grown by chemical solution deposition** 김 일원, 이 선영, 원 성식, 안 창원[1], 정 의덕[1], 김 진수[2](*울산대학교, 물리학과. [1]한국기초과학지원연구원 하이테크부품소재연구지원센터. [2]부경대학교, 물리학과.*) Much attention has been paid to obtain excellent lead-free ferroelectrics in alkaline-niobate system, which is environmental friendly and alternate system based on heavy metals. Among the several lead-free ferroelectric materials, $(1-x)(Na,K)NbO_3$-$xLiNbO_3$ (NKN-LN) ceramic offer enhanced ferroelectric and piezoelectric properties with composition around the morphotropic phase boundary (MPB) ($0.05<x<0.07$). Therefore, we have deposited three kinds of different thin films such as $(Na,K)NbO_3$, $(Na,K)NbO_3$-10mol%, and $0.95(Na,K)NbO_3$-$0.05LiNbO_3$-10mol% on the $Pt/Ti/SiO_2/Si$ substrate by chemical solution deposition. We found that $0.95(Na,K)NbO_3$-$0.05LiNbO_3$-10mol% precursor solution is suitable to compensate the Na and K volatility during thermal process. The

$(Na,K)NbO_3$ thin film displayed a secondary phase of $K_4Nb_6O_{17}$, high leakage current and leaky P-E hysteresis loop due to high volatility of both sodium and potassium. While $0.95(Na,K)NbO_3$-$0.05LiNbO_3$-10mol% thin film exhibit a saturated P-E hysteresis loop with remanent polarization ($P_r$) of 10.1 mC/cm$^2$ and low coercive field ($E_c$) of 50 kV/cm, respectively. In this study, we will discuss about impedance and dielectric properties of $0.95(Na,K)NbO_3$-$0.05LiNbO_3$-10mol% thin film.

**Dp-154** **Large strain behavior in lead-free $Bi_{0.5}(Na_{0.78}K_{0.22})_{0.5}$-$TiO_3$-$Na_{0.5}K_{0.5}NbO_3$ ceramics** 안 창원, 정 의덕, ALI Hussain[1], 이 재신[1], 이 해준[2], 김 일원[2](*한국기초과학지원연구원, 하이테크부품소재연구지원센터. [1]울산대학교, 첨단소재공학부. [2]울산대학교, 물리학과.*) The development of lead-free piezoelectric materials has been required from the viewpoint of environmental preservation. We describe the development of lead-free $(1-x)Bi_{0.5}(Na_{0.78}K_{0.22})_{0.5}$-$TiO_3$-$xNa_{0.5}K_{0.5}NbO_3$ [(1-x)BNKT-xNKN] ceramics system and their large strain properties. (1-x)BNKT-xNKN ceramics were synthesized by conventional solid state reaction. A large electric field induced strain of 0.21% is observed in lead-free 0.97BNKT-0.03NKN ceramics under unipolar electric field of 50 kV/cm, which is comparable to that of $PbZr_{0.52}Ti_{0.48}O_3$ ceramics. This large strain is attributed to the lattice change by field induced antiferroelectric-ferroelectric transition. This result indicate that the 0.97BNKT-0.03NKN ceramics can be used a new environmentally friendly candidate piezoelectric material for application in electromechanical devices.

**Dp-155** **Chiral Spin States in the Pyrochlore Heisenberg Magnet** 김 정훈, 한 정훈(*성균관대학교 물리학과.*) Fermionic mean-field theory and variational Monte Carlo calculations are employed to understand the nature of the possible ground states of the Heisenberg model on the pyrochlore lattice. We find the chiral spin states to be the most stable, both within the mean-field theory and the projected wave function studies. Properties of the spin-spin correlation function and the chirality order parameter are calculated for the projected wavefunctions.

**Dp-156** **Quantum Wave-function Localization at Quantum Point Contact** SONG Taegeun, AHN Kang-Hun(*충남대학교, 물리학과.*) We investigate the single particle structure in a two-dimensional quantum ring which has a quantum point contact(QPC). Using numerical calculation, we find localized states on top of the QPC around an eigen-energy of the potential for describing QPC in our model. The states has a property which is robust against system parameter like a ring radius. From the property we can argue that these states strongly support that the quantum point contact physically play a role a quantum dot.

**Dp-157** **In situ x-ray reflectivity studies of the formation of membrane proteins in lipid multilayers on a substrate** LEE Hyunwon, CHA Wonsuk, SONG Sanghoon, CHOI Ahreum[1], JUNG Kwanghwan[1], KIM Hyunjung(*서강대학교 물리학과 &바이오융합기술협동과정. [1]서강대학교 생명과학과.*) Membrane protein과 lipid 간의 상호 작용에 의한 layer 형성 및 구조의 메커니즘에 관한 연구는 바이오 칩과 바이오 센서의 응용에 있어 매우 중요하다. 본 연구에서는 in-situ, 실시간으로, 수용액 속에서 자기조립 방법으로 형성되는 lipid layer의 적층 구조를 X-ray reflectivity를 이용하여 측정하고, membrane protein과의 상호 작용을 관찰하였다. 본 실험에서는 20KeV의 X-ray를 사용하여 수용액을 통과하는 X-ray beam의 흡수를 최소화하였으며, 포항가속기의 5A beamline에서 수행되어졌다. 사용된 DOPC lipid는 친수성을 띠는 머리 부분과 소수성을 띠는 꼬리 부분으로 구성되어 있는데, 이 때문에 수용액 상태에서 자기조립방법을 통해 이중층으로 형성된다. Lipid의 농도와 buffer 종류, 시간에 따라 lipid의 bilayer와 multilayer의 형성 조건을 확인하였다. 농도를 달리한 membrane protein을 형성된 lipid의 적층 구조에 첨가한 후 구조적 변화를 측정하였으며 각 층의 층간 거칠기, 두께와 전자 밀도 등을 측정함으로써 membrane protein의 lipid 내의 침투 메커니즘을 설명하였다.

**Dp-158** **Effective Pathway of Charge Transfer in DNA Duplex** KIM Seongjin, HWANG Sun-Yong[1], YI Juyeon(*Pusan National University, Physics. [1]Korea University, Physics.*) We study the charge transfer rate in a DNA molecule. Especially, we explore poly(dG)-poly(dC) that is in contact with two leads. We find that the effective route for charge transfer is determined by the competition between the direct path along one strand and the detour path via the other. Interestingly, for short length molecule, the direct path takes precedence over the detour path. Moreover, the route depends on both the charge carrier energy and the molecule length. The length dependence of the charge transfer rate in given carrier energy has various decay types; (i)exponential decay, (ii)constant decay, and (iii)algebraic decay. Also, it shows even a crossover between the various decay types.

**Dp-159** **Study of the phase transitions by observation of the A and $^1$H nuclear magnetic resonance in $ANH_4SO_4$ (A=$^7$Li, $^{39}$K, and $^{87}$Rb) single crystals with excellent optical quality** 임 애란, 김 선하[1](*전주대학교, 과학교육과. [1]한국기초과학지원연구원.*) $ANH_4SO_4$ (A=Li, K, and Rb) single crystals were grown using the slow evaporation method. We studied the spectra, spin-lattice relaxation times, $T_1$, and spin-spin relaxation times, $T_2$, of the $^1$H, $^7$Li, $^{39}$K, and $^{87}$Rb nuclei in these three types of single crystals. The nuclear magnetic resonance observations provided a consistent description of the dynamics of the studied nuclei in these materials. The $T_1$ values for the $^1$H nuclei are similar in all three crystals, and the $^1$H spin-lattice relaxation times increase with increasing temperature. However, as the radii of the metal ions increase, a corresponding decrease in the spin-lattice relaxation times of the A nuclei is observed. The differences observed in the spin-lattice relaxation times of the A nuclei upon changing the alkali-metal ion may be related to the ionic radius and the lengths of the A–O bonds. Therefore, the occurrence of phase transitions in these materials seems to be essentially dependent on the presence of the metal ions.

**Dp-160** **$^1$H and $^{87}$Rb nuclear magnetic resonance study of the order-disorder phase transition of $RbHSeO_4$ single crystals** 유

송희, 임 애란(*전주대학교, 과학교육과.*) The ferroelectric phase transition at $T_{C2}$ (=370 K) in $RbHSeO_4$ have been studied by $^1H$ and $^{87}Rb$ solid state NMR. Although not large, the spin-lattice relaxation time, $T_1$, and the spin-spin relaxation time, $T_2$, of rubidium and of the α- and β-type protons show distinct change near the phase transition. The intensity of the signal due to the α–type protons decreases with increasing temperature, and the intensity of α-type protons is quite weak above 330 K: at a temperature which is about 40 K lower than the phase transition temperature, the ordering of the α -type protons occurs. The α-type protons in the ferroelectric phase lead to a noticeable change in the proton magnetic resonance spectra. Our study of the $^1H$ spectra shows that the ferroelectric phase transition in $RbHSeO_4$ is of order-disorder type and is due to the ordering of protons in hydrogen-bonds.

**Dp-161** **Nuclear magnetic resonance study of the thermodynamic properties and phase transitions of α-type $RbAl(SO_4)_2 \cdot 12H_2O$ and β-type $CsAl(SO_4)_2 \cdot 12H_2O$ single crystals** 임 애란, 정 희정(*전주대학교, 과학교육과.*) The thermodynamic properties, spin-lattice relaxation times, $T_1$, and spin-spin relaxation times, $T_2$, of the $^{27}Al$, $^{87}Rb$, and $^{133}Cs$ nuclei in $MAl(SO_4)_2 \cdot 12H_2O$ (M=Rb and Cs) crystals were investigated, and the two crystals were found to lose $H_2O$ with increases in temperature. From our results for $T_1$ and $T_2$, we conclude that the discontinuities near $T_d$ in the $T_1$ curves of the two crystals correspond to structural changes. The splittings of the resonance lines for the $^{27}Al$ nuclei in $MAl(SO_4)_2 \cdot 12H_2O$ increase with increasing temperature, whereas the splittings for the $M^+$ nuclei decrease with increasing temperature. In both crystals, below $T_d$ the water molecules surrounding the $Al^{3+}$ and $M^+$ nuclei form distorted octahedra, whereas above $T_d$ the water molecules around the $Al^{3+}$ and $M^+$ nuclei form regular octahedra and the environment of the $Al^{3+}$ and $M^+$ nuclei has cubic symmetry. This difference is related to the loss of $H_2O$: the octahedra of water molecules surrounding $Al^{3+}$ and $M^+$ are probably disrupted by the loss of $H_2O$. Further, the $T_1$ for the $^{27}Al$ and $^{87}Rb$ nuclei in $RbAl(SO_4)_2 \cdot 12H_2O$ were found to increase below $T_d$ with increasing temperature, whereas the $T_1$ for the $^{27}Al$ and $^{133}Cs$ nuclei in $CsAl(SO_4)_2 \cdot 12H_2O$ were found to decrease. It is possible that this difference is due to the different characteristics of α-type and β-type crystals, so differentiating between α- and β-alums is possible.

**Dp-162** **Anomalous Microwave Absorptions Observed in Various Polystyrene-based Ionomers** 이 창훈, 김 준섭(*조선대학교, 응용화학소재공학과.*) 폴리스타이렌은 스티로폼으로 불리우는 고분자 일반 재료의 원천물질로 잘 알려져 있다. 스타이렌 반복 단위에 acid group을 도입한 후 중화시키게 되면 폴리스타이렌 이오노머라는 이온기를 갖는 고분자로 가공할 수 있다. 본 연구에서는 폴리스타이렌이나 그 이오노머 가공 시 발생할 수 있는 스핀 결함을 사용하여 고분자의 동력학적 정보를 얻고자 전자기공명(electron magnetic resonance; EMR)을 수행하였다. 예상치 않게 매우 크고 넓은 전자기공명 신호를 분광학적 g-인자 10 근처에서 관측하게 되었다. 물리적 연원을 파악하고자 전이금속 원소 분석 및 SQUID 자화 측정, 그리고 X-ray 회절 분석 등이 이루어 졌다. 결과적으로 고분자의 플라스틱 특성이 자기장 내에서의 변한다는 가정하에 설명될 수 있음을 알았으며, 투명 전자기파 차폐 용도로 사용될 수 있음을 논하였다.

**Dp-163** **Study on the Adsorption of the Cationic Molecules at the Air-Sodium Halide Solution Interface** SONG Jinsuk, KIM Mahn Won(*한국과학기술원 물리학과.*) The surface density and adsorption angle of the cationic molecule, Malachite Green(MG) adsorbed at the air-sodium halide solution interface were investigated by the second harmonic generation. It seems that the adsorption number density of MG increases with the increasing concentration of the sodium halide ions. However, the angle of adsorption stays relatively the same. And the more MG molecules adsorb at the interface as the size of the anions is getting larger. It may be due to the charge double layer induced at the air-sodium halide interface, in which the negative surface charge density increases with the size of the halide ions so that it attracts the cationic MG molecules. After the first layer is filled, the next layer appears to have the opposite orientation so that the output second harmonic intensity decreases. Proper molecular model for the cationic molecular adsorption to the surface charge double layer will give the information to quantify the surface charge density

**Dp-164** **Structural and Phase Changes of the Nonionic Cylindrical Micellar Solution by Mixing a Small Amount of Different Surfactants** 김 상현, 김 만원(*KAIST 물리학과.*) In order to observe the effect of the additional amphiphilicmolecules on the structure and phase behaviorof the $C_{12}E_5$ cylindrical micellar solution, we observed the micellar size, cloud temperature and micelle-to-lamellar transition temperature when various amphiphilic molecules added; the spherical micelle forming surfactant LysoPC(neutral), bilayer-forming lipid DMPC(neutral) and spherical micelle-forming surfactant DTAB(charged). DTAB induces length shortening of the cylindrical micelle as *C* increases at constant surfactant mole ratio, and gives dramatic change to phase behavior of $C_{12}E_5$. In contrast to DTAB, DMPC and LysoPC maintained a similar phase behavior and only the transition temperatures were moved to higher temperature for LysoPC, lower temperature for DMPC. It is related to the length growth enhances for DMPC and a length growth suppress for LysoPC. This study gives a systematical observation of the overall phenomenological feature of cylindrical micellar solutions to develop the thermodynamics theory for the surfactant self assembly.

**Dp-165** **X-ray Scattering Study of Organic Films Grown by Organic Molecular Beam Deposition** KO Changhyun, CHA Wonsuk, SONG Sanghoon, KIM Hyunjung(*서강대학교 물리학과.*) 본 연구에서는 저분자 유기 박막의 단원자층 제조에 용이한 Organic Molecular Beam Deposition(OMBD) 방법을 이용하여 Alq3에 대한 초기 성장 조건을 최적화하여 박막의 특성을 연구하였다. 초기성장과정에서 유기 박막의 나노스케일 구조 및 표면특성을 측정하고자 표면의 거칠기, 박막의 두께, 박막의 전자밀도를 확인할 수 있는 x-ray reflectivity와 inplane domain의 구조적 특성

을 확인할 수 있는 transverse diffuse scattering을 이용하였다. 본 연구에서는Effusion cell의 방향을 위쪽에 배치하여, 중력에 의해 시료(Alq3)가 떨어지면서 증착되도록 함으로써 초기 성장의 속도를 조정하는 것이 용이하였다. 특히 증착시 기판의 온도와 증착 후 후열처리 조건을 달리하여 성장조건에 따른 유기박막표면의 morphology를 관찰하였다.

**Dp-166** **요오드 도핑이 유기반도체 tetramethyltetraselenafulvalene(TMTSF)의 구조적, 전기적 특성에 미치는 영향** 윤미라, 이 하진[1], 이 인재(*전북대학교 물리학과. [1]한국기초과학지원연구원.*) Tetramethyltetraselenafulvalene (TMTSF)는 전해결정화 방법을 통해 처음 합성된 저 차원 유기 금속 초전도 물질인 $(TMTSF)_2PF_6$의 주축이 되는 분자로서 전자공여체로서 작용한다. 반면 기상증착(PVD) 방법으로 성장된 단 결정 TMTSF는 p형 반도체의 특성을 보인다. 이 실험은 단 결정 TMTSF 유기 반도체에 요오드를 도핑 하고, 도핑된 TMTSF의 결정 구조를 단 결정 TMTSF, 그리고 $(TMTSF)_2PF_6$ 와 함께 비교 하였다. PVD 방법을 사용하여 성장시킨 정질의 단 결정 TMTSF 유기 반도체를 상온에서 기상상태의 요오드에 노출시켜 자연적으로 확산 도핑이 되도록 하였다. 이후 50 mtorr의 압력과 40~50℃의 온도로 1시간 동안 열처리를 하였다. 이렇게 도핑된 TMTSF는 수 Giga옴에서 수 Kilo옴으로 저항이 감소하는 것을 볼 수가 있었다. X-ray Diffraction (XRD)을 이용하여 결정구조 분석, Electron Probe Microanalyser (EPMA), Photoluminescence(PL), Absorption Spectroscopy을 통한 전자 밴드 구조 분석 결과를 논의하겠다.

**Dp-167** **폴리이미드 박막내 산포된 다층 복합구조 금속산화물 나노입자의 광학적 특성연구** 김 선필, 이 동욱, 김 은규, 김 영호[1](*한양대학교 물리학과. [1]한양대학교 신소재공학과.*) 금속박막과 폴리아믹산 (polyamic acid)의 금속산화반응을 이용하여 자발형성된 금속산화물 나노입자를 제작하는 방법은 수 nm 크기의 구형 금속산화물 나노입자를 폴리이미드 박막내에 균일하게 제작할 수 있어서, 그 동안 많은 연구가 진행되어 왔다. 본 연구에서는 두 가지 이상의 금속을 증착하여 다층 복합구조 금속산화물 나노입자를 제작하여 광학적 특성을 연구하였다. 실험에 사용한 폴리이미드 물질은 BPDA-PDA (biphenly dianhydride - paraphenylene diamine) 계열의 PI-2610D이다. 먼저 진공증착기 (thermal evaporator)를 이용하여 유리 기판위에 금속박막을 증착시킨 후 폴리아믹산과 NMP (N-methyl-2-pyrrolidone) 를 혼합한 용액을 스핀 코팅하였다. 그리고, 폴리아믹산과 금속박막이 반응하도록 실온에서 24시간 동안 유지시킨 후 폴리아믹산을 혼합하는 과정에서 사용된 용매인 NMP를 제거하기 위해 질소 분위기에서 (rapid thermal annealing) 방식을 사용하여 135 °C soft baking 후에 1 ~ 2 시간동안 300 °C ~ 500 °C로 양생하였다. 형성된 금속산화물 나노입자는 고 분해능 투과현미경 (HR-TEM)을 이용하여 형태 및 분포상태를 측정하였으며, 광학적 특성은 UV-Vis spectrophotometer를 이용하여 분석하였다.

■ SESSION: P2
10월 24일(금), 11:00 - 12:45
장 소: 제3전시장

**Ep-001** **Au 나노입자의 자성특성 연구** 조 환웅, 현 영훈, 엄 태운, 서 민수, 이 성재, 이 영백(*한양대학교 물리학과.*) Au 나노입자는 특이한 전기적 특성 및 광학특성을 갖고 있어 바이오센서로서의 응용가능성이 높은 소재로 각광을 받고 있다. 최근에는 나노입자의 강자성 특성으로 인해 자성 특성에 대한 연구 또한 활발하다. 기본적으로 덩어리 상태의 Au는 반자성특성을 갖고 있으나, 나노입자 상태에서는 자성특성이 변화되는 것으로 보고되고 있다. 본 연구에서는 Au 나노입자의 자성특성을 알아보기 위해 티올로 둘러싸인 Au 나노입자를 이용하여 용액상태의 시료와 건조된 시료를 각각 준비하였으며, 건조된 시료의 경우 정량적인 분석을 위해 건조 전 용액의 Au 나노입자 농도를 달리하여 시료를 제작하였다. 시료의 자성특성은 SQUID magnetometer를 이용하여 측정하였으며, 자화곡선을 통해 상온에서 강자성 특성을 보이고 있음을 확인할 수 있었다. 티올로 둘러싸인 Au 나노입자의 농도증가에 따라 포화자화 값이 선형으로 증가하는 것을 확인 할 수 있었으며, 모든 시료가 강자성 특성을 보이는 것을 정량적으로 확인할 수 있었다. 또한, 투과전자현미경 분석을 통해 입자의 분포 및 크기의 균일함도 확인할 수 있었다.

**Ep-002** **수질정보 자동 센싱을 위한 능동형 RFID 시스템 개발** 강 준희, 김 진영[1], 정 용섭(*인천대학교 물리학과. [1]I.H.S.*) 본 연구를 통하여 수질정보를 센싱하고 실시간으로 모니터링 할수 있는 능동형 RFID 시스템을 개발하고자 하였다. 이를위해 Active RFID 송/수신 모듈을 설계하였다. 저전력 설계를 바탕으로 수질정보 수집 및 컨트롤을 위한 무선송수신기(2.45GHz 능동형 송수신 시스템)를 개발하였다. 수질정보는 온도, PH, DO 값을 측정하여 무선 송수신시스템을 통해 모니터링 하도록 구성하였다. 실제 응용하기 위해서는 시스템의 구성비용을 낮추는 것이 중요하기 때문에 본 연구에서는 저가의 RF 트랜시버 CC2510 칩셋을 사용하였다. CC2510 칩셋은 능동형 태그와 능동형 리더(수신기)사이의 거리를 측정하기 위한 수신신호 세기(Received Signal Strength Indicator ; RSSI)를 제공하며, 고유아이디와 수질정보 측정 데이터를 송수신 하는 기능을 담당한다. 물은 우리의 삶에서 필수적이며, 수질오염은 생명과 직결되는 매우 중요한 문제이기 때문에 본 연구의 결과는 매우 중요하게 응용될 수 있다.

**Ep-003** **강자성 펌얼로이 나노선에서 노치형상에 따른 디피닝 자기장의 이론적 유도** 김 갑진, 유 천열[1], 최 석봉(*서울대학교, 물리 천문학부. [1]인하대학교, 물리학과.*) 최근 기존 메모리 소자의 한계를 극복하기 위하여 자구벽을 이용한 차세대 자구벽 메모리가 각광받고 있다. 이러한 자구벽 메모리 소자에서는 자구벽의 위치를 정확히 통제하는 것이 필요하다. 자구벽의 위치를 통제하기 위한 방법으로 나노선에 노치를 형상화하여 열적 들뜸에 의해서 움직이지 않도록 함으로써 자구벽의 안정성을 높이는 방법이 제안되고 있다. 이에 본 연구진은 다양한 노치 형상에 따른 자구벽의 디피닝 자기장을 시뮬레이션(OOMMF)을 통하여 구하였고, 이를 통하여 디피닝 자기장이 노치의 몇 가지 변수에 의한 특정 함수로 구해짐을 발견하였다. 이렇게 구해진 수식과 시뮬레이션 결과는 ±0.5mT 이내에서 일치함을 확인하였다.

**Ep-004** **Effect of Metal-Molecule Contact, Molecular Structure, and Molecular Configuration on Molecular Electronic Conduction** 왕 건욱, 김 태욱, 이 탁희(*Department of Materials Science and Engineering, Gwangju Institute of Science and Technology.*) The idea of utilizing functional molecules as the electronic components in future ultrahigh-density electronic devices has generated tremendous attention. Before such device applications, understanding the charge transport mechanisms through molecular systems is important. The role of the "metal-molecule contact" and "molecular structure" in the electronic transport through organic molecules sandwiched between metallic electrodes is currently an important issue in the field of molecular electronics. First, we performed current-voltage characterization on different-length alkyl (alkanemonothiol and alkanedithiol) self-assembled monolayers (SAMs) contained in microscale via-hole structures in metal-molecule-metal (M-M-M) junctions. Based on the statistical analysis of a large number of molecular devices, we studied charge transport mechanisms, especially the metal-molecule contact effects using a multi-barrier tunneling (MBT) model.[1] Using the MBT model, we could easily determine and compare key transport parameters, such as decay coefficients, resistance-area product, and specific contact resistance for alkyl versus conjugated molecules [2].
We will also discuss recent results about the effect of the molecular configuration on the electronic transport in molecular junctions where the molecular configuration is controlled by conducting atomic force microscopy (CAFM). Our results indicate that the degree of tilting of alkanemonothiol molecules enhances chain-to-chain intermolecular charge transfer, so called through-space tunneling.[3]
[1] Gunuk Wang, Tae-Wook Kim, Hyoyoung Lee, and Takhee Lee, *Phys. Rev. B,* 76, 205320 (**2007**).
[2] Gunuk Wang, Tae-Wook Kim, Yun Hee Jang, and Takhee Lee, *J. Phys. Chem C* 112, 13010 (**2008**).
[3] Hyunwook Song, Hyoyoung Lee, and Takhee Lee, *J. Am. Chem. Soc.* 129, 3806 (**2007**).
* Acknowledgement: National Research Laboratory (NRL) Program of the Korea Science and Engineering Foundation (KOSEF) and the Program for Integrated Molecular System (PIMS) at GIST.

**Ep-005** **Effective Low-temperature Magnetic Resonance Force Microscopy** WON Soonho, SAUN Seung-Bo, KIM Changsoo, LEE SangGap, LEE Soonchil(*Korea Advanced Institute of Science and Technology, Department of Physics.*) Magnetic resonance force microscopy (MRFM) is invented in the early 1990s and it is proven to be a capable tool to detecting magnetic resonance by monitoring the excitation of a mechanical oscillator. In MRFM, low-temperature improves the signal-to-noise ratio by reducing thermal noise of a mechanical oscillator. Recently, we successfully have built low-temperature MRFM. We report effective tuning method with our MRFM equipment operated at 77K and in vacuum ~$10^{-4}$Pa. Homemade MRFM insert, magnet support assembly and additional electronic instrument are properly tunned to magnetic

resonance of sample. MRFM signal was measured on a <76ng paramagnetic sample of diphenylpicrylhydrazil. Although the tuning frequency of the tank circuit was 804MHz at room temperature and changed to 814MHz at 77K, we measured ESR signal of sample using anharmonic modulation technique.

**Ep-006** **Magnetic Domains Of Two Interacting Magnetic Nanowires** 이 한석, 김 택수, 김 승호, 장 영욱, 유 경화, 이 재용 (*연세대학교 물리 및 응용물리 사업단.*) 최근 강자성에 대한 연구는 단일 나노선과 나노선 배열을 중심으로 응용성에 대한 연구로 이루어지고 있다. 특히 단일 나노선에서의 자화반전, 자구벽 이동을 이용한 메모리 및 소자에 대한 연구가 발표되고 있다. 우리는 강자선 나노선의 제작과 이에 따른 자성특성 및 자구의 변화에 대한 연구를 시도하였다. E-beam lithography를 이용하여 0.4 μm와 0.8 μm의 폭을 갖는 100 μm 길이의 나노선을 제작하였다. 두 나노선을 한 묶음으로 6개의 강자선 나노선 묶음을 제작하였다. 6개의 묶음 사이의 간격은 10 μm 로 하였고 나노선 사이의 간격(separation)을 2 μm - 0.07 μm로 조절하였다. E-beam evaporator를 이용하여 Cu(10 nm), $Ni_{80}Fe_{20}$(20 nm), Cu(3 nm)를 차례대로 증착하였다. 자성측정시 자기장을 나노선과 평행한 방향으로 가해 주면서 longitudinal MOKE(magneto-optic Kerr effect)를 이용하여 자기이력곡선을 측정하였다. 한 묶음의 나노선에 대한 자기이력곡선은 각각의 나노선의 스위칭필드(Hsw)에 따라 double-step 자기이력곡선을 보였다. 나노선의 간격은 0.5 μm 보다 큰 경우 일정한 Hsw를 확인하였다. 나노선의 간격이 0.5 μm 이하일 때 Hsw는 급격한 변화를 보였다. 간격이 가까워질수록 나노선 간에 정자기 상호작용이 작용하여 0.4 μm 폭의 나노선의 Hsw가 급격하게 증가하는 것을 관찰하였다. 특히 0.4 μm 폭의 나노선의 Hsw가 급격히 증가하면서 두개의 나노선의 자화상태가 반평행상태에 있는 영역이 넓어지게 되는 것을 자기이력곡선을 통하여 관찰하였다.이러한 상태에 대하여 magnetic force microscope(MFM)을 이용하여 자구를 측정하였다. 나노선을 따라 한 방향으로 자기장을 주어 포화자화상태를 만들어 측정하였다. 예상대로 각각의 나노선은 한쪽 끝에서 어두운 부분을 나타내었고 다른 쪽 끝은 밝은 부분을 보였다. 끝부분에서만 자구가 나타난 것은 모든 나노선이 단일자구를 갖는다는 것을 말해준다. 현재 반평행 상태의 자화에 대해서 MFM을 이용하여 측정 중에 있으며, 추후 학회에서 MFM측정결과를 중심으로 연구결과를 발표할 예정이다.

**Ep-007** **Investigation of Energy band alignments in $HfO_2$/GaAs(100) films as a function of post-annealing temperatures** LEE S. Y., KIM C. Y., CHO M. -H.(*Institute of Physics and Applied Physics, Yonsei University.*) The effects of post-annealing temperatures on the energy band alignments for $HfO_2$/GaAs films was investigated by combining a high resolution x-ray photoemission spectroscopy (HR-XPS) and a high resolution transmission electron microscopy (HR-TEM). The $HfO_2$ film was deposited on oxidized *n*-GaAs (100) substrates by using an atomic layer deposition (ALD) process and then annealed via a rapid thermal process at 600 ℃ and 700 ℃ under an $N_2$ ambient, respectively. The valence band spectra in HR-XPS shows that the values in the valence band offsets were increased from 2.4 eV up to 2.9 eV as increasing post-annealing temperatures, which indicates that this increment is significantly associated with interfacial reactions between $HfO_2$ films and oxidized GaAs substrates. The HR-TEM observation has sustained the formation of Ga oxides in the films and shows the increment of thicknesses in $HfO_2$ films as a function of post-annealing temperatures. In addition, from XPS results, the intensity of Ga 2*p* spectra within the $HfO_2$ films was gradually increased during post-annealing processes, which is consistent with the HR-TEM results.

**Ep-008** **Nanoparticles for Photothermally Controlled Drug Delivery and MRI Enhancement.** 박 희열, 양 재문, 서 성백, 김 규정, 서 진석[1], 김 동현[2], 함 승주[3], 유 경화[4](*연세대학교 나노메디컬 국가핵심 연구센터. [1]연세대학교 진단 방사선 의학과. [2]연세대학교 공과대학. [3]연세대학교 화공학과. [4]연세대학교 물리학과.*) Polymer-metallic multilayer half-shell nanoparticles (H-S NPs) are developed as multifunctional nanoplatforms for photothermally controlled drug delivery and magnetic resonance imaging (MRI) enhancement. These nanoparticles are fabricated by depositing Mn and Au films onto rhodamine-loaded poly(lactic-co-glycolic) (PLGA) nanoparticles; their surface plasmon-resonance frequency is found to be in the near infrared (NIR) range. Drug release from PLGA nanoparticles is enhanced in response to NIR light which is converted into thermal energy. Additionally, the magnetic properties of the Mn layer allow these nanoparticles to act as MRI contrast agents

**Ep-009** **Critical field for domain wall injection in a two layered nanowire** 김 승호, 이 한석, 김 택수, 이 승현, 이 재용, 이 우영(*연세대학교, 물리학과.*) 자성 단일 나노선에 대해서는 최근 많은 연구가 진행되고 있다. 단일 나노선은 그 모양에 의하여 잘 정의된 자기이방성을 가진 단일 자구를 가진 구조라는 점에서 그 기반을 두고 있기 때문에 그 응용성은 메모리 및 논리 소자로서 큰 연구 가능성이 있다. 일반적으로 자성 단일 나노선은 선폭이 좁을수록 형태에 의한 자기이방성이 강해지기 때문에 보자력이 증가한다. 이는 실질적인 응용을 어렵게 한다. 우리는 좁은 나노선에 넓은 나노선을 연결했고, 좁은 나노선에서의 보자력을 작게 만드는 연구를 했다. 최근에 nucleation pad를 이용하여 좁은 나노선에서의 보자력을 감소 시킬수 있다는 보고가 있었다. 또한 서로 다른 자기이방성을 가진 두 구조를 연결할 경우 보자력은 두 자기이방성의 차이에 비례한다는 보고도 있었다.E-beam lithography와 lift-off 방법을 이용해서 넓은 폭을 가진 나노선과 좁은 폭을 가진 나노선을 연결한 구조를 제작했다. 넓은 폭의 나노선은 2000nm에서 700nm까지 크기를 변화시켜주었고, 좁은 폭의 나노선은 500nm에서 100nm까지 크기를 변화 시켜주었다. 나노선의 자성은 micro magneto optic Kerr effect(MOKE)와 magnetic force microscope(MFM)을 이용해서 실온에서 측정하였다.우선 좁은 폭의 나노선이 300nm 이고, 넓은 폭의 나노선이 200nm에서 700nm까지 변화를 시킨 구조에서 측정을 했다. 넓은 폭의 나노선을 연결한 300nm 단일 나노선에서의 보자력이 넓은 폭의 나노선을 연결하지 않은 300nm 나노선에서의 보자력에 비해서 약 1/3정도 감소했다. 이는 이론적으로 계산한 결과와도 거의 같은 값을 나타내주고 있다. 현재 더 좁은 선폭을 가진 나노선에 대한 연구와 함께 이들 구조의 domain에 대한 연구를 진행하고 있으며, 이에 대한 결과를 발표할 예정이다.

**Ep-010** **Photoluminescence Properties of $Eu^{3+}$-doped $YPO_4$ Phosphors** KIM DONG WOO, SEO SEONG JI, R. Balakrishnaiah[1], YI Soung Soo, JANG Kiwan[2], LEE Ho Sueb[2], JEONG Jung Hyun[3](*Department of Electronic Materials Engineering, Silla University, Busan 617-736, Republic of Korea. [1]Department of Electronic Materials Engineering, Silla University, Busan 617-736, Republic of Korea and Department of Physics, Changwon National University, Changwon, 641–773, Republic of Korea. [2]Department of Physics, Changwon National University, Changwon, 641–773, Republic of Korea. [3]Department of Physics, Pukyong National University, Busan 608-737, Republic of Korea.*) Lanthanide-doped materials find potential applications in the fields of lasers, optical amplifiers, phosphors, display devices, etc., due to their characteristic energy level schemes. These materials found wide useful in the development of plasma display panels (PDP), field emission displays (FED) and electro-luminescent panels. Recently, $LnPO_4$ (Ln = Y, La, Gd, Lu) materials have attracted much attention in PDP applications due to their high thermal and chemical stability and high luminescence efficiency under VUV excitation. Therefore, $LnPO_4$-based phosphors have proven as promised materials for PDP applications. Among lanthanide ions, $Eu^{3+}$ ion is one of the most interesting ions due to its simple lower energy levels scheme as well as applications in the fields such as red emitting phosphor by its intense, narrow and monochromatic red emission around 610 nm as a result of $^5D_0 \rightarrow {}^7F_2$ transition. Therefore, in our present work, we have prepared $Eu^{3+}$-doped $YPO_4$ phosphors by solid state reaction method for 0.05 0.1, 0.15 and 0.2 mole concentrations of $Eu^{3+}$ ions. The synthesized materials were characterized by X-ray diffraction (XRD), scanning electron microscopy (SEM), excitation, emission and lifetime measurements. The dependence of various optical and morphological properties of the prepared materials on $Eu^{3+}$ ion concentration has been discussed and the results are compared with those reported in earlier literature.

* Acknowledgements: This work was supported by Korea Research Foundation grant funded by the Korean Government (KRF-J00902).

**Ep-011** **Fabrication and Characterization of Polymer Photovoltaic Devices with Triplet Dopants** SUH Duk-Il, BYEON Clare C., KIM Bok Hyeon, LEE Jongmin, LEE Chang-Lyoul(*Advanced Photonics Research Institute, Gwangju Institute of Science and Technology.*) Organic (polymer) Photovoltaic (PV) devices have some advantages compared to the inorganic PV cells in the aspect of low price, flexibility and large area. Until now, most researches were focused on PV devices using singlet excitons. However, the study of triplet states in PV devices has been much less studied because triplet excitons do not undergo charge transfer. The most commonly used materials for the fabrication of bulk-heterojunctions are poly(3-hexylthiophene) (P3HT) and fullerene derivative [6,6]-phenyl-$C_{61}$-butyric acid methyl ester (PCBM). In this study, we have fabricated and characterized polymer PV devices consisted of polymer (p-type) : PCBM (n-type) with different kinds of phosphorescent materials.

**Ep-012** **Photoluminescence and Raman study of Single-Walled Carbon Nanotubes Dispersed in Aqueous Surfactant Solutions** 유 율리아, 박 준, 성 맹제(*중앙대학교 물리학과.*) Dispersion of single-walled carbon nanotubes (SWCNTs) in aqueous surfactant solution has recently become an important method of isolating SWCNTs. In this work, using photoluminescence and Raman spectroscopy, we studied material property change of HiPCO and CoMoCAT SWCNTs dispersed in 1wt% aqueous surfactant (sodium dodecyl sulfate or deoxycholate sodium salts). CoMoCAT CNTs showed stronger PL intensity than HiPCO CNTs dispersed in the same aqueous surfactant solution. Different PL peak positions, for the same CoMoCAT CNTs, were observed when dispersed in different aqueous surfactant solutions. And similar result was also observed for HipCO CNTs.

**Ep-013** **Unconventional method to form a high conductive transparent electrode using carbon nanotube** PARK Jaehyun, SONG Yoojin[1], HA Jeong Sook[2], LEE Youn-Seoung[3], KANG Seong Jun[4](*Nanometrology Center, Korea Research Institute of Standards and Science, Department of Chemical and Biological Engineering, Korea University. [1]Nanometrology Center, Korea Research Institute of Standards and Science, Department of of Information Communication Engineering, Hanbat National University. [2]Department of Chemical and Biological Engineering, Korea University. [3]Department of of Information Communication Engineering, Hanbat National University. [4]Nanometrology Center, Korea Research Institute of Standards and Science.*) A new method to form a high conductive transparent electrode has been developed using large collections of single walled carbon nanotubes (SWNTs). The approach involves CVD growth of SWNTs using methane or ethanol, followed by sequential nano surface transfer of the collections of CVD grown nanotubes from a silicon dioxide wafer to target substrates, such as high-k thin dielectrics, transparent plates of glass and flexible sheets of plastics. Electrical measurements, such as a sheet resistance, reveal that our SWNTs films are compatible with indium tin oxide (ITO) layers for a transparent electrode. We believe that our approaches are low cost and easy method to form a high conductive transparent electrode, and might be used in electronics, optoelectronics, sensors, nanomechanical systems and microfluidics.

**Ep-014** **Thermal evolution of defects in as-grown and proton-irradiated ZnO** LEE Cheol Eui, LEE EunMo, LEE Su Cheol, PARK Jun Kue(*Department of Physics, Korea University.*) Due to its direct wide bandgap of 3.37eV, zinc oxide (ZnO) has become the focus of many studies. Devices such as detectors, lasers and diodes operating in the ultra-violet (UV) and blue regions of the spectrum have been reported. The study of defects is one of the most important subjects because of the strong influence of these defects on the electrical and optical properties.The undoped ZnO single crystals grown by the hydrothermal method were purchased from Tokyo Denpa Co. (Tokyo, Japan). The samples were irradiated ($Ep$= 0.5 MeV, fluence $10^{15}cm^{-2}$) at room temperature and annealed in an air atmosphere from 100 to 1000 °C in order to follow

the evolution of irradiation defects and their effect on the emission properties. Raman spectra for the implanted sample show the enhancement of vibration modes at about 575 $cm^{-1}$, which indicates introduction of oxygen vacancies. These oxygen vacancies disappear at temperatures of 600–700 °C. Cathodoluminescence measurements reveal that hydrogen ions also passivate deep level emission centers before their release from the sample, leading to the improvement of the UV emission.

**Ep-015** **Photoelectrochemical Behavior of $TiO_2$ Electrode and $TiO_2$ Electrode mixed Metal-Decorated Carbon Nanotubes (CNTs).** 김 창호, 황 성식, 유 경화(*연세대학교 나노메디컬국가핵심연구센터.*) We investigated the photoassisted electrolysis of water using n-type $TiO_2$ and $TiO_2$ mixed metal-decorated carbon nanotubes(CNTs) as electrodes. Compared with conventional $TiO_2$ electrode, larger photocurrent and lower applied potential($E_{bias}$) were found for $TiO_2$ mixed metal-decorated CNTs. Moreover, Pt decoration on CNTs improved the efficiency further. The increase in electron mobility of $TiO_2$ electrode because of the presence of CNTs and the decrease in overpotential for $H_2$ and $O_2$ production are considered as the possible origins of improved efficiency for heterogeneous photocatalysts such as $TiO_2$:CNT-Pt and $TiO_2$:CNT-Pd.

**Ep-016** **Local structural and optical properties of nitrogen-implanted ZnO nanorods** 한 상욱, 박 창인[1], 김 병혁[1], 이 용병[2], 곽 창하[2], 서 수영[2], 김 선효[2], 박 순홍[3](*전북대학교, 과학교육학부. [1]전북대학교, 물리학과. [2]포항공과대학교, 신소재공학과. [3]포항산업과학연구원.*) We investigated the structural and the optical properties of nitrogen-ion implanted ZnO nanorods. Vertically aligned ZnO nanorods were synthesized on $Al_2O_3$ substrates with and without buffer layers by catalyst-free metal organic chemical vapor deposition (MOCVD). Nitrogen ions with energies of 50 - 120 keV and beam flux of $1\times10^{16}$ $cm^{-2}$ were implanted on the vertically aligned ZnO nanorods. Field-emission scanning electron microscopy (FE-SEM) measurements revealed that the ZnO nanorods maintained good shapes for the nitrogen-ion implantation. X-ray diffraction measurements demonstrated that the both nanorods had an ordered wurtzite structure, and that no detectable disorder was observed from the nanorods exposed for the nitrogen-ion beam, compared with untouched ZnO nanorods. Field-emission transmission tunneling microscopy (FE-TEM) measurements on the nitrogen-implanted nanorods showed dark spots spreading over entire nanorod. Extended x-ray absorption fine structure analysis revealed that there was a substantial amount of structural deformation due to the ion implantation. We found that the band gap peak intensity of photoluminescence (PL) was significantly reduced. This also suggests the local structural defects due to the ion-implantation.

**Ep-017** **In-situ X-ray absorption fine structure study of $TiO_2$ under ultraviolet light** 한 상욱, 김 병혁[1], 전 종술, 박 창인[1](*전북대학교, 과학교육학부. [1]전북대학교, 물리학과.*) The local structural properties of $TiO_2$ particles with mean particle size of 100 nm were investigated with and without ultraviolet light (UV) by using in-situ x-ray absorption fine structure. X-ray absorption near edge structure (XANES) revealed that $TiO_2$ particles with anatase and rutile structures, $A_1$, $A_2$, $A_3$ pre-edge peaks were observed clearly from both structures meanwhile the only $A_1$ peak was sharp in Ti metal. We observed that the $A_2$ peak was slightly changed in S-added $TiO_2$. These results imply that the *d*-electrons in the $A_2$ level are more sensitive to the environment than the electrons in the $A_1$ and $A_3$ levels. Under a UV light, we did not observed any change of the XANES signals. Extended x-ray absorption fine structure (EXAFS) measurements showed somewhat change of structural properties due to the UV light. We will discuss the results of the in-situ XANES and EXAFS studies from the $TiO_2$ particles in detail.

**Ep-018** **Local Surface Modification of Organic Self-Assembled Monolayer/Silicon Systems with and without an Interfacial Oxide Layer by an Atomic Force Microscope Tip** HAN Jiwon, SANO Hikaru[1], KIM Young-Jong[1], ICHII Takashi[1], MURASE Kuniaki[1], SUGIMURA Hiroyuki[1](*Kyoto university, Materials Science and Engineering. [1]Kyoto University, Materials Science and Engineering.*) Much attention has been paid to nanoscale patterning of Si substrates covered with a self-assembled monolayer (SAM), because a wide variety of functionalities can be provided to the Si substrate with a nanoscale spatial resolution using the patterned SAMs as etching masks and chemical templates. Scanning probe microscopy (SPM) is one of powerful tools for observation and characterization in minute scales as well as modification of SAM/Si samples. We have conducted patterning SAM/Si samples by locally injecting current from a conductive AFM probe. In this presentation, we report on the SPM-characterization results for two types of SAM samples formed on Si substrates, that is, an alkylsilane SAM formed on an oxide-covered Si substrate and an alkyl SAM formed directly on a Si substrate without surface oxide. Into these SAM samples, current was locally injected from a conductive AFM probe tip at various substrate bias voltages. The current-injected samples were characterized by Kelvin-probe force microscopy (KFM) and scanning capacitance microscopy (SCM) in addition to topographic imaging. Two types of SAM-covered samples were prepared. One was a hexadecyl SAM (HD-SAM) formed on a n-type (resistivity of 1 - 10 Ω cm) Si(111) substrate via its hydrogen-termination. The other was octadecylsilyl SAM (ODS-SAM) grafted on the similar Si substrate with a native oxide layer of approximately 2 nm thick. The SAM/Si samples were modified by applying a sample bias in the range of 1 – 9 V using a Pt-Ir-coated Si cantilever. Nine areas of $0.8\times0.8$ $\mu m^2$ were scanned at a rate of 0.5 μm/s in air (24 °C, 40% RH) on each of the samples by applying a bias voltage. In the case of the HD-SAM/Si which had no interfacial oxide layer, regions fabricated with the sample bias of 6 - 9 V were detectable by SCM and KFM. However, in the case of the ODS-SAM/oxide/Si which had the interfacial oxide layer, distinct SCM and KFM contrasts have been observed at all the regions where were current-injected with applying the sample bias of 1 - 9 V. The origin of the SCM and KFM contrasts of the regions modified at the high voltage range is most likely anodic degradation of

the SAMs and subsequent anodization of the Si substrates, while the contrasts observed only on the ODS-SAM/Si sample at the low bias range of 1 - 5 V for surface modification is considered probably due to charge trapping in the oxide layer and/or at the SAM/oxide interface.

**Ep-019** **Electrical transport of Ni nanowire** KOO Ae-young, CHO M.K.[1], CHO J.W.[2], KIM Y.K.[2], KANG C.J.(*Department of Nano Science and Engineering, Myongji University. [1]Program in Micro/Nano Systems, Korea University. [2]Department of Materials Science and Engineering, Korea University.*) Nanowires were widely pursued one-dimensional nanosystems and provide diverse opportunities in nanotechnology, ranging from nanoelectronic devices to cell-separation and magnetic labeling in biomedicine. We are interested in fabrication, electrical conductivity, optical and magnetic properties of various nanowires by electrodeposition [1]. In this work, Ni nanowires were synthesized in anodized aluminum oxide (AAO) nanotemplates. Their structure and properties were characterized by scanning electron microscopy (SEM), transmission electron microscopy (TEM)/selected-area electron diffraction (SAED), X-ray diffractometry (XRD), vibrating sample magnetometry (VSM), atomic force microscopy (AFM) and electrically conductive AFM (c-AFM). As Ni has very small magnetocrystalline anisotropy, the magnetic properties of the nanowires were investigated as a function of shape anisotropy tailored by the nanowire diameter and length-diameter aspect ratio [2]. The topological study by AFM was performed on individual nanowires in-situ and electrical measurements were completed by c-AFM on both single nanowire and ensemble specimens after chemical mechanical polishing (CMP) [3]. The results reveal that the I-V characteristic of single Ni nanowire is quite different from that of an ensemble. The corresponding transport mechanism is addressed.

**Ep-020** **Density-functional Calculations for Pt Cluster Adsorption on Graphene and Adsorption of Hydrogen Atom** PARK Sora, AHN Jeung Sun, CHI Dam Hieu[1](*Dept. of Physics, Kyung Hee Univ. [1]School of Materials Science, Japan Advanced Institute of Science and Technology.*) Density-functional calculations of the adsorption of Pt clusters on graphene surface were performed for study about support effect of carbon support on catalytic activity of the system consists of Pt cluster and graphene surface. We suggested several possible adsorption sites of Pt cluster on graphene surface which have local energy minimum, and investigated the transition energy between different adsorption sites of Pt cluster. We also calculated the binding energy between hydrogen atom and Pt cluster in each adsorption sites of Pt cluster on graphene surface. The support effect of graphene surface on catalytic activity of the system was found to be related with the change of adsorption sites of Pt cluster on graphene surface for making the binding energy of hydrogen atom and Pt cluster weak due to the change of electronic structure of whole system.

* This work was supported by the Seoul Research and Business Development Program (Grant No. 10583)

**Ep-021** **Influence of titanium and oxidized silicon in amorphous silicon oxide nanowire growth on Au coated substrate by solid state transformation** SONG jin ho, OH E.S., WHANG C.N., CHO M.-H., ANN J.P.[1](*Institute of Physics and Applied Physics, Yonsei University. [1]Korea Institute of Science and Technology.*) Amorphous silicon oxide nanowires (a-SiONWs) were synthesized by direct solid state transformation from silicon substrate. The a-SiONWs were grown on Au/Si Substrates with provided titanium vapor during the annealing in mixture gas of $O_2$ and Ar at 900℃. Without any silicon vapor during the process, a-SiONWs can be grown on the Au/Si substrate resulting from the transformation of Solid-Liquid-Solid rather than the conventional Vapor-Liquid-Solid. In order to investigate the role of silicon oxide grown Si substrate before the growth of nanowire, two alternative samples were prepared: Direct stack structure of Au(4nm)/Ti(1nm)/Si sub without any $SiO_2$ layer (S1) and indirect stack structure of Ai(4nm)/Ti(1nm)/$SiO_2$(100nm)/Si sub with thick $SiO_2$ layer (S2). The significance is that the a-SiONW was only grown on the S2, not on the S1. No growth of the a-SiONW can be associated with the removal of the native oxide layer by the formation of Ti-silicide. As a result, it is revealed that silicon oxide layer is essentially needed to synthesize a-SiONWs.

**Ep-022** **Field Emission Properties of Screen Printed Carbon Nanotube Field Emitter** KANG Jun-Tae, JEONG Jin-Woo, KIM Dong-Il, KIM Ji-Seon, KIM dae-jun[1], LEE Hyeong-Rag[2], SONG Yoon-Ho(*Convergence Component &Materials Research Laboratory, Electronics and Telecommunications Research Institute. [1]Kumho Electics, INC. [2]Kyungpook National University.*) The carbon nanotube (CNT) field emitters based on the paste-printing technology have advantages of cost-effective and large area process for field emission display (FED) and lamp (FEL). The CNT paste was prepared by mixing of multiwalled carbon nanotubes (MWNTs), nano-scale metal filler, organic binding materials. We measured its field emission characteristics including stability and uniformity. It is noted that field emission properties greatly depend on the CNT paste composition and emitter process as well as CNT itself.

**Ep-023** **금 나노입자를 흡착시킨 발광고분자 나노선의 광학적 특성 연구** 이 용백, 박 동혁, 주 진수(*고려대학교 물리학과 하이브리드 나노구조체 연구실.*) 200 nm의 나노 직경을 갖고 있는 Al2O3 (다공성 무기 배경물질)를 이용하여 polythiophene (PTh) 및 그 유도체 나노선을 전기중합방법으로 합성하였다. HF를 이용하여 배경물질을 제거한 후 전자주사 현미경 (SEM) 실험을 통해서 길이가 약 40 μm 이고, 직경이 200~250 nm 인 나노선으로 중합되었음을 확인하였다. 여기에 직경이 5 nm인 금 나노입자를 나노선에 흡착시킨 후 전자투과 현미경 (TEM) 실험을 통해 금 나노입자가 나노선 표면에 흡착되었음을 확인하였다. 이렇게 제작된 하이브리드구조 나노선의 광학적 특성을 확인하기 위해 laser confocal microscope PL 측정하였다.

**Ep-024** **Optical and Electrical Characteristics of Copper**

**Phthalocyanine (CuPc) Nanowires** 정 진선, 이 진우, 김 기현, 주 진수(*고려대학교.*) 나노 직경의 다공성 무기 배경물질 ($Al_2O_3$)을 기반으로 electrophoretic deposition 방법을 이용하여 유기 반도체 copper phthalocyanine (CuPc) 나노선을 제작하였다. Electrophoretic deposition 방법은 $CF_3COOH$와 $10^{-4}$ M의 CuPc를 혼합한 $CHCl_3$ 용액 속에서 직류전압을 가하여 나노선을 성장시켰다. 전자주사현미경 (SEM)을 이용하여 측정된 CuPc 나노선의 반지름이 약 200nm이었고, 길이는 수 십μm임을 확인하였다. 투과전자현미경(TEM)과 Raman, XRD 실험을 통해 나노선의 구조를 확인하였고, UV/Vis 흡수실험과 PL 실험, laser confocal microscope (LCM) PL을 이용하여 CuPc 나노선의 광학적 특성을 측정하였다. CuPc 나노선의 전기적 특성을 파악하기 위하여 4-단자 접촉 방법을 이용하여 구한 전류-전압 (*I-V*) 곡선으로부터 CuPc 나노선 한 가닥의 전기 전도도를 측정하였고, 온도에 따른 CuPc 나노선의 전기 전도도의 변화를 관찰하였다. 또한 CuPc 나노선 한 가닥의 광 전류 변화도 측정하였다.

**Ep-025** **질소이온 주입을 이용한 가시광반응 $TiO_2$계열 광촉매 제조 및 물분해** 허 성환, 조 성오(*한국과학기술원, 원자력 및 양자공학과.*) 입자 크기가 5 nm인 $TiO_2$ 나노입자에 고온 질소도핑 및 200 keV 질소이온 주입을 이용하여 자외선/가시광하에서 물분해가 가능한 광촉매를 제조하였다. $TiO_2$ 나노입자를 $H_2$:$N_2$=1:1의 고온 퍼니스에서 860도씨와 1530도씨로 가열하여 질소가 도핑된 $TiO_{1-x}N_x$를 제조하였고, 200 keV 질소이온을 $TiO_2$/PMMA 혼합필름에 주입(5E16 N-ions/$cm^2$)한 후 아세톤으로 PMMA필름을 여과하여 N-implanted $TiO_2$를 제조하였다. Diffuse reflectance UV-Vis 분광계를 이용하여 흡광특성을 측정하였고, 투과전자현미경(TEM)과 X-선 원소분석(EDX)으로 각 시료의 특성을 확인하였다. 제조된 $TiO_2$ 광촉매와 15% 메탄올 수용액에 150W Xe 램프, 200W Hg-Xe 램프 빛을 조사하여 약 430 μmol/g/h 수소가 생산됨을 확인하였다.

**Ep-026** **Poly (3-hexylthiophene) (P3HT)의 나노입자 제작 및 특성** 주 진수, 이 석호, 박 동혁(*고려대학교 물리학과.*) Poly (3-hexylthiophene) (P3HT)는 유기 전계효과 트랜지스터, 유기 태양전지등의 다양한 분야에서 사용되는 물질이다. 많은 분야에서 이용되고 있는P3HT를 재침전법(reprecipitation)으로 나노입자 형태로 제작하였다. 또한 Au 나노입자가 포함된P3HT나노입자를 같은 방법으로 합성하였다. 나노입자의 형성은 주사 전자현미경(SEM), 투과 전자현미경(TEM), 및 원자력 현미경(AFM)으로 확인했으며, 크기가 대략 100~150 nm임을 확인했다. 두 종류의 나노입자를 균일하게 분산시켜서 필름형태로 제작한 후 자외선-가시광선 흡수 분광법, 광발광 분광법으로 광학적 특성을 관찰했으며, 나노입자 하나의 광발광 특성을 살펴보기 위해 laser confocal microscope으로 광발광 실험을 수행하였다. 또한 제작된 나노입자와 [6,6]-phenyl C61 butyric acid methyl ester (PCBM)를 잘 분산시켜 유기 태양전지 소자를 만들어 광전소자로서의 응용성을 연구하였다.

**Ep-027** **이온주입에 의한 poly(3-methylthiophene) (P3MT) 나노선의 특성변화 연구** 주 진수, 박 성규, 홍 영기, 이 용백(*고려대학교, 물리학과.*) 직경 약 200 nm의 $Al_2O_3$ 나노 다공물질 속에서 P3MT-$TBAPF_6$ 나노선을 합성하였다. 나노선의 길이는 약 10 μm로 조절하였다. P3MT 나노선의 제작을 위해 사용된 용액은 0.05 M의 단량체 3MT와 0.01 M의 도펀트 $TBAPF_6$를 acetonitrile에 섞어 구성하였다. P3MT 나노선을 제작하는데 사용된 $Al_2O_3$는 2 M NaOH 용액을 사용하여 제거하였다. 이온주입은 3 MeV $Cl^{2+}$ 이온을 $3X10^{13}$ ~ $3X10^{15}$ ions/$cm^2$의 dose로 나노선에 주입하였다. 표면변화를 관측하기 위해 SEM을 측정하였다. 구조적 변화를 측정하기 위해 합성된 P3MT 나노선의 UV/Vis, Raman 스펙트럼과 결합에너지를 XPS를 사용하여 측정하였다. Laser confocal microscopy를 사용하여 한 가닥의 P3MT 나노선에 이온주입 전과 후의 PL과 Raman 스펙트럼을 비교, 연구하였다.

**Ep-028** **DBSA(doecylbenzenesulfonic acid)를 도펀트로 사용한 P3HT(Poly 3-hexylthiophene)나노선 합성과 물성연구** 한 윤덕, 박 동혁, 이 석호, 주 진수(*고려대학교 물리학과 하이브리드 나노구조체 연구실.*) DBSA(dodecylbenzenesulfonic acid)를 도펀트로, 3HT(3-hexylthiophene)를 유기 단량체로 이용하고. 용매로는 acetonitrile($CH_3CN$)을 이용하였고, 벽면이 OTS처리된 다공성 템플레이트와 처리되지 않은 다공성 템플레이트를 이용하여 전기화학적 중합방법으로 π-공액 고분자인 P3HT(Poly 3-hexylthiophene) 나노 튜브를 합성하였다. 합성 후 주사전자 현미경(SEM), 투과전자 현미경(TEM)을 이용하여 합성된 P3HT를 확인하였다. 적외선 분광법 (FT-IR), 라만분광법을 이용하여 합성된 P3HT나노선의 구조적인 특성을 확인할 수 있었다. 또한 UV/Vis 흡수, PL 스펙트럼을 비교하였을 때 다공성 템플레이트 벽면을 OTS처리한 P3HT 나노 튜브는 그렇지 않은것에 비해서 천이 현상을 관찰 하였다.

**Ep-029** **귀금속 기반 표면 증강 라만 산란 활성 기판 제조** 조 성오, 유 승화(*한국과학기술원, 원자력 및 양자공학과.*) 표면 증강 라만 산란(SERS, Surface Enhanced Raman Scattering)은 단분자 계측이 가능해진 이후로 매우 민감도가 높은 화학센서로의 응용가능성과 더불어 밝혀지지 않은 메커니즘으로 인해 화학, 물리학, 생물학, 공학 분야에서 많은 관심을 받기 시작했다. 메커니즘을 밝히기 위해서 많은 표면 증강 라만 산란 활성 기판이 제조되고 있으며 여러 실험적인 검증이 이루어지고 있다. 본 연구에서는 실리카 콜로이드 입자로 구성된 육방조밀단일층에 금과 은을 열층작, 플라즈마 스퍼터링 방법으로 코팅을 하여 다양한 morphology의 표면 증강 라만 산란 활성 기판을 제조하였다. 귀금속의 종류, 코팅의 두께 등을 달리하고 벤젠싸이올($C_6H_6S$)을 Probe 분자로 사용하여 SERS 강도를 측정, 비교하였다. 최대 ~$10^6$의 EF(Enhancement Factor)에 도달하였다.

**Ep-030** **증진된 전류구동능력과 작은 문턱전압의 분포를 가진 다중 비트 비휘발성 메모리 소자** 박 상수, 오 세웅, 김 현주[1], 김 경록[2], 김 태환, 곽 계달(*한양대학교 전자통신컴퓨터공학부. [1]한양대학교 정보디스플레이공학과. [2]한양대학교 나노반도체공학과.*) 비휘발성 메모리 소자의 고집적화의 필요성에 의하여 소자 크기를 줄이려는 연구가 많은 관심을 끌고 있다. 그러나, 플래너 형태의 비휘발성 메모리 셀의 크기를 줄일 경우, 단채널 효과와 좁은 폭 효과를 일으키는 문제점을 가지고 있다. 이 문제점을 해결하기 위하여, 비휘발성 메모리의 하나의 셀에 다수의 비트를 저장할 수 있는 다중 비트 셀과 다중 준위 셀에 대한 연구가 활발하게 진행되고 있다. 다중 준위 셀에서 다수의 전하 상태를 구별할

수 있게 센싱하는 것이 대단히 어렵고 또한 다중 비트를 가진 비휘발성 메모리 소자를 구동시키기 위해서는 고성능의 주변 회로 설계가 필요하다. 본 연구에서는 다중 비트 비휘발성 메모리 소자에 대한 전류 구동 능력과 문턱 전압의 분포를 조사하기 위하여 새로운 비휘발성 메모리 소자에 대한 구조를 제안하고 제안한 소자에 대한 특성 조사를 하였다. 비휘발성 메모리 소자는 반도체 기판 위에 돌출된 활성 핀을 갖는다. 활성 핀은 소오스/드레인 영역들과 상기 소오스/드레인 영역들 사이에 채널 영역으로 구성된다. 제안된 비휘발성 메모리 소자에 대하여 TCAD 도구를 사용하여 시뮬레이션을 한 결과 본 연구에서 제안된 구조는 전류구동능력이 기존의 비휘발성 메모리 소자에 비하여 증진되었으며 문턱전압의 분포가 작아졌다. 전하 저장 패턴들 및 제어 게이트들은 채널 영역의 측벽들 뿐 아니라 채널 영역의 상부 영역으로 각각 연장되므로, 기존의 플랫 트랜지스터에 비해 채널 폭이 증대되어 좁은 폭 효과를 억제할 수 있었다. 이러한 결과는 전류구동능력을 향상시킬 수 있고, 문턱전압의 산포를 줄일 수 있다고 생각된다. 이와 같은 결과는 본 연구에서 제안하는 메모리 소자 구조가 저소비 전력에서 작동하는 신뢰성을 가진 비휘발성 메모리 소자로 적용될 수 있음을 제시하고 있다.

* ACKNOWLEDGEMENT - This work was supported by the Korea Science and Engineering Foundation (KOSEF) grant funded by the Korea government (MEST) (No. R0A-2007-000-20044-0).

**Ep-031** **FinFET 구조를 가진 대용량 전하포획 플래시 기억 소자** 오 세웅, 박 상수, 유 주형, 김 동훈, 김 현우[1], 김 태환 (*한양대학교 전자컴퓨터통신공학부. [1]한양대학교 나노반도체공학과.*) 기억소자의 고집적화를 위한 소형화는 기억 소자가 비례 축소되는 경향으로 연구되어 왔다. 이러한 비례 축소에 의한 고집적화를 위한 소자의 소형화가 소자의 절연층 두께의 감소에 따른 누설전류, 단채널 효과 및 협폭효과와 복잡한 공정상의 이유로 한계에 다다를 것으로 예상된다. 이러한 문제를 구조적으로 해결하고, 비례 축소에 의한 고집적화를 이루기 위해 FinFET구조의 소자에 SONOS구조의 메모리층을 올려 전자를 저장 및 소거하는 트랩 막으로 사용하고, 각각의 제어게이트와 플로팅케이트를 분리한 새로운 구조에 대해 연구하였다. NAND형으로 대용량 전하포획 플래시 기억소자의 회로를 구현하기 위해 Fowler-Nordheim tunneling을 기본적인 읽기/쓰기 동작의 주요 메커니즘으로 사용하였고, 각각의 분리된 제어게이트에 인가된 전압 조건에 따라 한 셀당 2-bit의 기억 동작을 시뮬레이션 하였다. 이와 같은 기억 소자구조는 동일한 셀의 면적을 가진 하나의 기억소자에 더 많은 비트를 저장 할 수 있어 대용량 플래시 기억소자 제작에 좋은 동기를 부여할 것으로 생각된다.

* ACKNOWLEDGEMENT - This work was supported by the Korea Science and Engineering Foundation (KOSEF) grant funded by the Korea government (MEST) (No. R0A-2007-000-20044-0).

**Ep-032** **Effect of Mesh Grid Gate and Spacer on the Focal Spot Size for the X-ray Sources** KIM Hyun Suk, DUY Dao Quang, LEE Kang Jea, KIM Jae Hoon, YOON Dang Mo, HA Jung Woong, LIM Jung Ran, HWANG Yong Gyoo, LEE Choong Hun(*Wonkwang University.*) We reported the effects of mesh grid gate and spacer on triode - type X – ray source simulated by Opera 3D. By changing the geometrical parameters of mesh grid gate, the divergence angle of electron beam and therefore focal spot size on the anode has been controlled. The voltage of the gate played an important role in convergence the focal spot size. The spacer which attached between the emitter and mesh grid gate was also investigated. It is exhibited that the time of flight (TOF) of electron beam trajectories has been effected by the spacer, which controls the distance between emitter and the gate. Finally, we have applied those results to verify the effects of mesh grid gate and spacer on the X – ray image.

**Ep-033** **탄소나노튜브의 결점 상태에 따른 암모니아 분자의 흡착 특성변화** 박 선미, 김 상훈, 김 홍정, 이 성엽[1], 신 병욱, 강 준태, 김 제한, 김 창득[2], 이 의완, 이 형락[3](*경북대학교 물리학과. [1]경북대학교 나노과학기술학과. [2]영남대학교 화학공학과. [3]경북대학교 물리학과, 경북대학교 나노과학기술학과, 나노부품실용화센터.*) 빗살형 전극형태(Interdigitaed Electrode)의 기판 위에 교류이중전기영동(AC dielectrophoresis) 방법을 이용하여 탄소나노튜브를 배열한 소자를 제작하여 암모니아에 대한 민감도를 측정해 보았다. 암모니아는 탄소나노튜브에 전자를 주기 때문에 전도도가 감소하는 경향을 보인다. 저농도에서 보이는 급격한 전도도의 변화는 탄소나노튜브의 결점영역(defect site)에 의한 영향으로 추측된다. 이를 검증하기 위해 산소 플라즈마를 이용하여 탄소나노튜브의 표면에 결점을 형성한 후 암모니아에 대한 전도도의 변화를 측정하였다. 그 결과 산소 플라즈마 처리를 하지 않은 소자에 비하여 민감도는 더 커졌으며, 급격한 전도도의 변화를 보이는 영역이 더 넓어졌다. 이를 바탕으로 저농도에서 보이는 민감한 변화는 결점에 의한 현상으로 판단될 수 있다.

**Ep-034** **Improvement of singlewalled carbon nanotubes growth efficiency using catalyst thickness and surface oxidation** KIM Hong Jeong, KIM Chang-Duk[1], KANG Juntae, LEE Sung-Youp[2], SHIN Byong-Wook, PARK Sunmi, KIM Sanghun, KIM Jae-Bum, LEE Eui-Wan, LEE Hyeong-Rag[3](*Department of Physics, Kyungpook National University, Daegu 702-701, South Korea. [1]School of Display and Chemical Engineering, College of Engineering, Yeungnam University, Gyongsan 712-749, Republic of Korea. [2]Department of Nano-science and Technology, Kyungpook National University, Daegu 702-701, South Korea. [3]Department of Physics, Kyungpook National University, Daegu 702-701, South Korea, Department of Nano-science and Technology, Kyungpook National University, Daegu 702-701, South Korea, Nano Practical Application Center, Daegu 704-230, Korea.*) We found that catalyst surface oxidation method was influenced wall control and synthesis of Singlewalled carbon nanotubes (SWNTs) in previous study. Catalyst surface oxidation was effective method for wall control. However the sample and the growth condition in this lab. were synthesised several SWNTs. Therefore, we carried out two method for improvement of SWNTs growth than that. One method is thickness control of Fe catalyst. Fe catalyst thickness was changed from 1 nm to 0.6 nm by electron beam evaporation system. The other method was surface oxidation of Fe catalyst. Former oxidation was treated in air atmosphere. In this time, oxidation was treated in $O_2$ atmosphere (100 sccm). It is fixed quantity and facilitate control oxidation. To results of catalyst surface oxidation is ef-

fective methode for growth improvement of SWNTs, we measured it by FE-SEM, Raman spectroscopy, TEM, XPS.

**Ep-035** **$Er^{3+}$와 $Yb^{3+}$이온이 첨가된 $Gd_3Al_5O_{12}$ 나노형광체의 upconversion 형광특성연구** 김 중환, 최 혜영, 김 진영[1], 노 현미, 정 홍채[1], 문 병기[1], 정 중현[1](*동의대 물리학과. [1]부경대 물리학과.*) $Er^{3+}$과 $Yb^{3+}$이온을 첨가한 구조의 $Y_3Al_5O_{12}$(YAG), $Gd_3Al_5O_{12}$(GAG), $Tb_3Al_5O_{12}$ (TAG) 나노형광제가 solvothermal 방법으로 합성하였다. X선 회절패턴과 scanning electron microscopy(SEM)상을 측정하여 나노분말의 결정구조와 morphology를 확인하였다. $Er^{3+}$의 형광효율은 GAG가 YAG와 TAG에 비하여 상대적으로 우수하였다. Er3+을 첨가한 GAG 나노형광체를 980nm LD로 여기하여 강한 녹색과 적색의 형광을 확인하였으며 $Er^{3+}$-$Yb^{3+}$ 이온을 동시에 첨가하여 upconversion 형광의 세기가 크게 향상되는 것을 확인하였다. 980nm 여기에너지는 $Yb^{3+}$ 이온의 바닥상태에서($^2F_{7/2}$) $^2F_{5/2}$준위로의 흡수에 해당되므로 $Yb^{3+}$이온이 감광제로 작용하며 $Yb^{3+}$ 이온에서 $Er^{3+}$이온으로의 에너지 전달과정에 의한 것으로 알려져 있다. 이상의 과정은 4준위 에너지 모형을 가정하여 설명하였으며 에너지 준위의 비율방정식으로부터 시료의 시간적 거동을 계산하여 $Yb^{3+}$이온의 기여도를 계산하였다.

**Ep-036** **Hydrogen of Ti-Zr-Ni Quasicrystals** LEE Sang-hwa, JEON Jae-kyun, LEE Yunmman, SHIN Hyemin, KIM Euikwoun, LEE jeonggil, CHOI Soo-bin(*Hanyang univesity, Department of physics.*) Qasicrystals(QCs) made with Ti-Zr-Ni are known to excellent materials for hydrogen storage applications because of their high number of tetragonal and octagonal interstitial sites and chemical attraction with hydrogen. QCs were prepared by adding Pd in the Ti-Zr-Ni alloys ($Ti_{53}Zr_{27-x}Ni_{20}Pd_x$, where $0 \le x \le 10$). Hydrogen absorption data and pressure-composition-temperature(P-c-T) curves were obtained by using a lab-built computer-controlled-absorption apparatus. Structure of the samples was analyzed by using X-ray diffraction (XRD) and transmission electron microscope (TEM). By adding a Pd, the vapor pressure of hydrogen in the QCs was increased from 8000 torr to 9000 torr at 300℃. The activation energy of hydrogen was lowered by etching the oxygen layer using plasma and immediate Pd coating.

**Ep-037** **A new system designed to obtain Fullerene($C_{60}$) cluster by using vapor of solution** YEO Seung Jun, CHO Dae Hee, PODE Ramchandra, KIM Hwa Min[1], AHN Jeung Sun(*Kyung Hee University. [1]Catholic University of Daegu.*) From the in-depth investigation of temperature dependence of the luminescence of $C_{60}$ in toluene, benzene and CS2 solutions, we reported that the $C_{60}$ aggregates are formed during cooling at the freezing temperature of these solvents. Furthermore, the $C_{60}$ aggregates were found to be weakly bound clusters which are unstable, upon warming, in liquid solutions above ca.210 K. It was also founded that the $C_{60}$ aggregates can be changed to stable structures by irradiating with UV plulse-laser (Nd:YAG laser, 355nm). As a consequence, we could obtain new-type of nanoscale $C_{60}$ clusters, which appear as round-shaped nanoscale particles in high resolution transmission electron-microscopy (HRTEM) images. However, the yield of the new-type $C_{60}$ clusters obtained by this mehod is too small. So we designed and developed a new system to obtain $C_{60}$ cluster of macroscopic quantity. In this system, $C_{60}$ solution was vaporized to droplet in vacuum, resulting in formation of $C_{60}$ aggregates by evaporating solvent. The system was invented to produce new nanoscale carbon clusters by the irradiation of UV light upon $C_{60}$ aggregates in vacuum. We have characterized the products formed from the new system by using HPLC. Before 60min (peak by fullerene molecules), peaks of 33min~53min mean existence of some materials, bigger than fullerene molecules in the HPLC trace of photo-polymerized $C_{60}$ cluster formed by using the new system. So we can assume that some of these materials are the photo-polymerized $C_{60}$ clusters obtained by this new system. In the presentation, the details of the new system and the results of characterization will be reported

* This work was supported by the Seoul Research and Business Development Program (Grant No. 10583)).

**Ep-038** **선택적 전자선 조사에 의한 표면증강 라만산란 활성 금 나노입자 패턴 제조** 김 용남, 조 성오(*KAIST.*) 금 전구체 필름에 선택적 전자빔 조사와 열처리를 가하여 패턴화된 표면증강 라만산란 (SERS) 활성 금 나노입자 필름을 제조하였다. 금 전구체 필름은 20 keV의 에너지로 $8.29\times10^{16}$ $cm^{-2}$ 의 fluence 만큼 진공에서 전자빔 조사된 후, 600℃에서 30분간 가열되었다. 또한, 패턴화된 필름 내부 금 나노입자의 크기는 금 전구체 필름의 두께를 변화시킴으로써 ~27nm에서 ~112nm 로 조절 가능함을 SEM을 이용하여 확인하였고, 입자의 크기에 따른 독특한 광학적 특성을 나타냄을 UV-Vis 측정을 이용하여 확인하였다. 또한, 생성된 금 나노입자가 기능성 물질로 둘러싸이지 않은 순수한 상태라는 것을 XPS 분석을 통해 확인하였다. 패턴화된 금 나노입자 필름의 SERS 효과를 측정하기 위해 thiophenol (TP)을 이용하였으며, 632.8nm 파장을 가지는 He-Ne 레이저를 여기 파장으로 사용하였다. TP의 1573 $cm^{-1}$ 피크를 기준으로 한 SERS 증강 강도는 약 $10^6$로 측정되었다.

**Ep-039** **Pentacene nanowires array** 조 성기, 이 진우, 김 기현, 정 진선, 주 진수(*고려대학교 물리학과 하이브리드 나노구조체 연구실.*) 유기단분자 pentacene 나노선 배열을 나노 직경의 다공성 무기 배경 물질($Al_2O_3$)을 기반으로 organic vapor transport (OVT) 방법을 이용하여 성장시켰다. HF를 이용하여 배경물질을 제거한 후 전자주사현미경(SEM) 및 투과전자현미경(TEM)을 이용하여 나노선의 길이 및 구조를 확인하였다. 측정된 나노선의 길이는 약 10 μm 이었으며, 직경은 약 200 nm 임을 확인하였다. 성장된 pentacene 나노선 들을 UV/Vis 흡수 실험과 PL 실험을 통해서 광학적 특성을 조사하였다. FT-IR 실험과 Raman 실험을 통해서 분자 구조를 확인하였다. 그리고 laser confocal microscope (LCM) PL 실험을 이용하여 pentacene 나노선 한 가닥에 대한 발광 특성을 관찰하였다.

**Ep-040** **Slow drying of active layers for enhanced performance of the organic photovoltaic cells** LEE Cheol Eui, KIM namkyoon, OH In Hwan, LEE Eunmo(*Department of Physics, Korea University.*) Control of thin film morphology at the nano scale is

critical for optimizing the power conversion efficiency of organic photovoltaic cells based on blends of conjugated polymer with fullerene derivatives. In the case of bulk heterojunctions of regioregular poly(3-hexylthiophene) (P3HT) and a soluble fullerene derivative ([6,6]-phenyl C61-butyric acid methyl ester, PCBM), both thin film morphology and photovoltaics performance are influenced by the rate of drying. Controlling the active layer growth rate results in an increased hole mobility and balanced charge transport. With the increased hole mobility, the regioregular P3HT chains spent a longer time to self-organize themselves. As a result, the morphology evolution of the laterally phase-separated blends of crystalline P3HT and PCBM led to a lower series resistance, thereby increasing the performance of the photovoltaic devices.

**Ep-041** **Electrical Properties of Iodine Doped Single-Walled Carbon Nanotubes: Magnetoresistance and Magneto-thermopower** 안 세정, 남 영우[1], 유 호남[1], 김 유경, 박 지현[1], 유 재승[1], SHI Z[2], JIN Z. X.[3], 박 영우[1](*서울대학교 나노과학기술협동과정, NSI-NCRC. [1]서울대학교 물리천문학부, NSI-NCRC. [2]Beijing National Laboratory for Molecular Science, Peking University. [3]Department of Chemistry, Renmin University.*) Electrical properties of iodine doped single-walled carbon nanotube (SWNT) have been investigated in terms of temperature and magnetic field dependence. The temperature dependence of resistivity shows a crossover from metallic to non-metallic as temperature decreases, which is consistent with the heterogeneous model involving the metallic resistivity and tunneling through the small electrical barriers. At low temperature, the conductivity shows the three-dimensional weak localization behavior. The magnetoresistance (MR) is negative and flattened at high magnetic field. This result is analyzed as weak localization with spin dependent scattering effect at high magnetic field. At high temperature, the MR is positive due to two band model involving the concentration difference between the hole carriers and electron carriers. The thermoelectric power (TEP) is positive in the entire temperature range. The positive TEP indicates that the majority carrier is hole. Also, the nonlinear temperature dependence of TEP can be explained by the effect of density of states peaks. The magneto-thermopower becomes smaller than the zero-field TEP as the magnetic field is applied, The reduction of TEP under magnetic field at low temperature can be due to the reduction of entropy per carrier since the magnetic field induces more ordered state of spins in the system. Also, as a result of the delocalization of he electron wave functions under the magnetic field, the magneto TEP becomes smaller. Because the increased number of delocalized carriers contribute to the smaller entropy.

**Ep-042** **Transport Property Of The Iodine Doped Poly(vinyl Alcohol)-$Cu^{2+}$ Chelate** 유 호남, 박 지현, 남 영우, 김 유경[1], 안 세정[1], 추 승완, 유 미경[2], 조 종수[2], 박 영우(*서울대학교 물리천문학부 NSI-NCRC. [1]서울대학교 나노협동과정 NSI-NCRC. [2]서울대학교 농생명공학부.*) It is reported that conductivity of Poly(vinyl Alcohol)-$Cu^{2+}$ chelate increases as iodine doping [1]. In order to investigate transport property of iodine doped Poly(vinyl Alcohol)-$Cu^{2+}$ Chelate(PVA/$Cu^{2+}$/$I_2$) , we measured temperature dependence of conductivity from room temperature to T=1.7K. Four-probe pressure contact using platinum electrodes is applied for the conductivity measurement and the room temperature conductivity is $\sigma_{RT}=10^{-2}$ ~$10^{-3}$ S/cm and it shows a broad maximum peak at around T=60K {$\sigma$(60K)/ $\sigma_{RT}$=1.4}. We explain temperature dependence of conductivity by heterogeneous model. The magnetoresistance (MR, $\Delta\rho/\rho$) is positive and increased linearly as magnetic field increases up to 7 tesla. In view of strong localization, we considered variable range hopping type conduction at low temperature. In barrier region of heterogeneous model, 2 dimensional hopping process is dominant and has positive magnetoresistance at low temperature. Thermoelectric power (TEP) has been measured from room temperature down to 1.8K to identify charge of carrier. At room temperature, the TEP is +110μV/K and it decreases linearly upon cooling to T=1.8K. The positive TEP and high room temperature value indicate that the (PVA/$Cu^{2+}$/$I_2$) is p-type semiconducting. And yet, the linear temperature dependence of TEP suggests metallic characteristics of the sample. Then, the magneto-TEP has been measured at H=7 tesla for T<28K. The magneto TEP shows a slight reduction compared to the zero-field results indicating little influence of the magnetic field on the TEP.

Reference [1] F. Higashi, C. S. Cho, H. Kakinoki, O. Sumita, *J. Polym. Sci., Polym. Chem. Ed. 17, 313* (1979)

**Ep-043** **Electrical Properties of Carbonized Polyacetylene Film** 남 영우, 최 아정, 김 영수, 유 호남, 백 승재, MATSUSHITA Satoshi[1], AKAGI Kazuo[1], 박 영우(*서울대학교, 물리천문학부. [1]교토대학교, 화학과.*) Pyrolysis treatment on organic polymers is a well-known method to make carbon materials. Polyacetylene, one of representative organic polymers, is synthesized from acetylene gas with nematic liquid crystal and is doped with iodine resulting in macroscopically aligned thin film structures. Afterward, it is carbonized at 800°C and further graphitized at 2600°C. This allows us to attain carbonized polyacetylene film containing aggregated carbon nanofibers about 50nm width and graphitic morphology. Therefore we investigated its electrical properties such as resistivity, magnetoresistance(MR), and magneto thermoelectric power(TEP). The negative MR is observed in whole range of temperature from 1.7K to 300K with magnetic field up to 35 tesla. The obtained MR results are analyzed with weak localization model. TEP shows overall metallic behavior with clear peak at 10K due to magnon-drag and the peak is suppressed in the presence of magnetic field.

**Ep-044** **Temperature dependence of the PL spectra for gamma ray irradiated poly(3-hexylthiophene) thin films** LEE Cheol Eui, KIM Minseok, KIM Namkyoon, LEE Eunmo, PARK Jun Kue[1](*Department of Physics, Korea university. [1]Department of Physics, Korea University.*) The regioregular poly(3-hexylthiophene) (RR-P3HT) is normally used as organic solar cells and was prepared by spin-coating on the quartz glass. All the P3HT films were irradiated in a Cesium-137 source with doses varying from 0 to 150 Gy. After the gamma ray irradiation, the Photoluminescence

(PL) spectra was measured to investigate optical property with temperature varying from 30 to 290 K. At lower temperature, the PL spectra become more intense and red-shifted due to the change of conjugation length with decreasing temperature.

**Ep-045** **Ambipolar Characteristics of Organic Light-Emitting Transistors: Composition Effects** 황 혜민, 김 화정, 김 영규(*경북대학교 화학공학과.*) In the past two decades organic light-emitting devices (OLEDs) have been significantly studied due to their advantages including low-cost manufacturing, low driving voltages, ultrathin and light weight features, and natural color images. Although small size OLED displays are now in market, the way toward large area OLED displays needs further research and development. One of the hardest hurdles to overcome is to achieve low-cost thin film transistors (TFT) which are suitable to operate each OLED pixel with sufficient currents. To date, low temperature polysilicon (LTPS) TFTs are considered one of best candidates but they are too expensive to afford the cost competition. In this regard organic TFTs have been developed but are being a challenging topic owing to their low charge carrier mobility. In this work, as a more futuristic trial, we attempt to make organic light-emitting transistors (OLETs) that integrate both OLED and TFT in a single device fixture. Here, in particular, ambipolar characteristics of OLETs with compositions of p-type and n-type conjugated polymers will be discussed.

**Ep-046** **분무열분해법으로 성장된 $In_2O_3$:Cd 박막의 구조와 광학적 전기적 특성** 서 동주, 오 상미, 임 수경, 김 고은, 최 성휴, 김 건호[1](*조선대학교. [1]경상대학교.*) $In_2O_3$:Cd 박막을 분무열분해법으로 유리기판 위에 성장시켰다. $In_2O_3$:Cd 박막을 성장시키기 위해 사용한 시약은 indium chloride, cadmium chloride 이며, 이차증류수에 이들 시약을 녹여 0.02 mole 수용액을 만든 후 증류수를 혼합하여 분무용액을 만들어 사용하였다. 성장온도와 Cd 농도 변화에 따른 $In_2O_3$:Cd 박막의 결정구조를 규명하기 위하여 X-선 회절분광기(XRD)를 이용하였으며, $In_2O_3$:Cd 박막의 표면과 미세구조는 주사전자현미경(SEM)을 이용하여 관찰하였다. $In_2O_3$:Cd 박막에 입사한 빛의 파장을 변화시키면서 광투과율과 광흡수 스펙트럼을 측정하여 광학적인 특성과 에너지 간격을 구하였다. 시료에 대한 Hall의 효과를 van der Pauw법으로 실온에서 측정하여 비저항, 운반자 농도 등의 전기적 특성을 규명하였다.

**Ep-047** **Oxidation of Fe Ultrathin Films on Pt(111) Surface at Room Temperature** PARK K.-H., CHO S.-G., HAN K.-H., NAHM T.-U.(*Dept. of Phys., Hanyang Univ.*) We have investigated the oxidation of Fe ultrathin layers deposited on Pt(111) substrates by using X-ray photoelectron spectroscopy. It was found that the oxygen atoms were only chemisorbed when the oxygen exposure was below 200 Langmuir, and that the Fe ultrathin layers were partially oxidized with the oxygen exposure of 300 Langmuir at room temperature. The partial oxidation as $Fe_3O_4$ or FeO was observed depending on the thickness of the Fe layers. Upon post-annealing, the oxidized Fe layers were started to decompose into Fe and oxygen gas at a temperature range 700 - 800 K, after which the intermixing between Fe and Pt atoms occurs.

**Ep-048** **Study Of Iinterfacial Electronic Structures In P-I-N Heterostructural-Organic-Photovoltaic Cells By X-ray And Ultraviolet Photoelectron Spectroscopies** PARK Sang Han, JEONG Jin Geol, CHO Sang Wan[1], CHO M. –H.(*Institute of Physics and Applied Physics, Yonsei University. [1]Department of Physics, Boston University.*) The electrical characteristics of the photovoltaic cells can be enhanced by the insertion of a buffer layer. In order to investigate the reasons of the enhancement, the electronic structure of the organic photovoltaic cell was investigated by the *in-situ* x-ray photoelectron spectroscopy combined with ultraviolet photoelectron spectroscopy. The co-depositied zinc phthalocyanine (ZnPc):fullerene ($C_{60}$) layer was employed as an intrinsic buffer layer for high efficiency organic solar cell constructed with the heterostructure of ZnPc/co-depositied ZnPc:$C_{60}$/$C_{60}$ layers. In this study, we report the role of an intrinsic buffer layer(i-) as active layer between transport layers in the *p-i-n* heterostructureal-organic-photovoltaic cell.

**Ep-049** **XRR 측정/결과 신뢰성 향상을 위한 비교시험** 김 창수, 박 재환[1], 신 대근[1], 오 병성[1], 최 용대[2](*한국표준과학연구원. [1]충남대학교 물리학과. [2]목원대학교 기술마케팅학과.*) XRR (X-ray reflectometry)은 나노 두께의 박막의 두께를 측정하는 유망한 도구로 인식되고 있고 나노박막에 대한 XRR 측정 결과의 신뢰성을 향상시키기 위하여 많은 연구가 이루어지고 있다. 반도체 소자의 고직접화를 위하여 고유전율의 박막이 필요로 되고 고유전율 산화막은 두께가 수nm로 얇아지고 정확한 두께 측정을 필요로 하고 있다. 따라서 반도체 소자용 나노 두께의 박막에 대하여 높은 신뢰성으로 측정하고자 많은 노력이 이루어지고 있다. 본 연구에서는 고유전율 HfO2 박막을 이용하여 XRR 비교시험을 진행하였다. HfO2 박막의 두께는 약 10nm이었고 국내 약 10여곳의 기관이 비교시험에 참여하였다. 본 연구에서는 비교시험의 목적, 방법 및 결과 등에 관하여 살펴보았고 나아가 XRR 결과의 신뢰성을 향상시키기 위한 방법들을 살펴보았다.

**Ep-050** **Band bending characterization of magnesium fluoride ($MgF_2$) : *N,N'*-bis(1-naphthyl)-*N,N'*-diphenyl-1,1'-biphenyl-4,4'-diamine (NPB) composite layer / indium tin oxide (ITO) anode interfaces** KIM hyunsung, JEON Pyungeun, LEE Hyunbok, WHANG Chung-Nam, JEONG Kwangho, YI Yeonjin[1], HAN Kyul(*연세대학교. [1]한국표준과학연구원.*) We have investigated both the *N,N'*-bis(1-naphthyl)-*N,N'*-diphenyl-1,1'-biphenyl-4,4'-diamine (NPB) / indium tin oxide (ITO) anode and magnesium fluoride ($MgF_2$) : NPB composite / ITO anode interfaces using *in situ* photoelectron spectroscopy (PES) method including the ultraviolet PES (UPS) and x-ray PES (XPS). The spectroscopic data of the NPB / ITO interface show a band bending with hole accumulation (positive band bending, ohmic) near ITO anode, whereas those of the $MgF_2$:NPB (1:3 and 1:1 volume ratio) / ITO interface show a band bending of electron accumulation (negative band bending, blocking). In accordance with the PES data, the current density-voltage (J-V) characteristics of the Al / NPB (600 Å) / ITO and

Al / NPB (600 Å) / $MgF_2$:NPB (50 Å) / ITO hole only devices indicate the role of the $MgF_2$ to be an insulating buffer layer injection. The Al / NPB / $MgF_2$:NPB (1:1) / ITO device shows around a three times current density increase at 5 V forward bias compared to the Al / NPB / ITO device. PACS number: 73.20-r, 73.40.Sx; 79.60.Jv; 85.60.Jb

**Ep-051** **Deposition Sequence Dependent Chemical Reaction at the Interface Between 8-hydroxyquinolatolithium and Al** LEE Youung Mi, PARK Yongsup, YI Yeonjin[1], KIM Jeong Won[1](*경희대학교 물리학과. [1]한국표준과학연구원.*) One of organic electron injection layer materials, Liq (8-hydroxyquinolatolithium) shows a few advantages over other inorganic materials for organic light emitting device (OLEDs). The interface chemical reaction at the Liq/Al interfaces was investigated by using high resolution synchrotron radiation photoelectron spectroscopy. The different deposition sequence [Liq (0.4, 1 nm) / Al (50 nm) and Al (0.1, 0.3 nm) / Liq (30 nm)] gives different reactions. The Li 1s shows a peak at high binding energy side upon the Al deposition on Liq, which can be attributed to ionic Li atoms throughout the Liq film. However, the reversed stack does not show any changes in Li 1s core levels. Either sequence of film stacks, Liq/Al and Al/Liq produce an interface gap state respectively at 2.1 eV and 2.8 eV below the Fermi level. The valence and N 1s core levels are shifted to the high binding energy side by 0.35 eV on Al/Liq whereas it is not the case on Liq/Al. This can be related to the doping induced band bending with ionic Li. The enhancement of the electron injection with Liq layer on the Al can be explained by the work function reduction of Al surface. We propose that Liq/Al be used as an efficient electron injection layer for inverted OLED.

**Ep-052** **Copper(II) Phthalocyanine Thin Films Structure and Surface Characteristics Induced by Thickness and Temperature Conditions** KANG Sangbaek, YOON Chang-Sun, OH Donghoon, CHAE Youngan, LEE Kiejin[1], KIM Mijung[2], KIM Jin-Tae[2], HONG Seung-Soo[2], LIM In-Tea[1], LEE Keuchan[2], HONG Ki Sung[2], CHA Deokjoon(*(Kunsan Nat'l Univ., Physics). [1](Sogang Univ., Physics). [2](Korea Research Institute of Standarde and Science, Vacuum center ).*) Copper(II) Phthalocyanine thin films were prepared on glass and ITO/glass substrates by using a thermal evaporation system. Different kinds of samples depended on thickness and temperature condition were investigated with near-field scanning microwave microscope(NSMM), XRD, AFM, and UV-VIS spectroscope. Optimum condition of the thinckness and temperature was adapted to fabricate an organic light emitting diode(OLED) with a thickness range below 10 nm scales contacted with Alq3 organic compound.

**Ep-053** **Study of Dielectric Titanium Dioxide Thin Films Grown by Plasma-Enhanced Atomic Layer Deposition** YIM ChanJung, CHO Mann-Ho[1], KWON HakYoung[2], PARK HyungSang[2], KO Dae-Hong(*Yonsei University, Department of Ceramics Engineering. [1]Yonsei University, Institute of Physics and Applied Physics. [2]ASM Genitech Korea Ltd.*) Titanium dioxide ($TiO_2$) thin films were deposited by plasma-enhanced atomic layer deposition (PE-ALD) method with alternating supply of reactant source, $Ti(O\text{-}i\text{-}C_3H_7)_4$ (TTIP), and oxygen plasma as oxidant at different condition. To optimize of $TiO_2$ films deposition, we controlled ALD process conditions such as substrate temperature, source dosing time, RF plasma generating power, RF plasma generating time and reactant $O_2$ gas flow rate. X-ray diffraction (XRD) was used to investigate the structural properties of $TiO_2$ films. It is found that, Ti anatase phase appear at the substrate temperature above 250°C and 500 cycles. Surface analysis of as-grown $TiO_2$ films was investigated by x-ray photoelectron spectroscopy (XPS). The electrical properties of Pt/$TiO_2$/Si and Pt/$TiO_2$/Pt/Si structured films were investigated by I-V, C-V measurements.

**Ep-054** **Study of Electrical Stress Induced Morphology in Organic Light Emitting Device** LEE Young Joo, LEE Jong kyoon[1], YANG Joong hwan[1], KIM Hyunjung(*Department of Physics and Interdisciplinary Program of Integrated Biotechnology, Sogang University, Seoul 121-742, Korea. [1]LG Display (R&D Center), 1007, Deogeun-ri, Wollong-myeon, Paju-si, Gyeonggi-do, Korea.*) We studied the structural degradation induced by electrical stress of the organic light emitting devices (OLEDs) by synchrotron X-ray scattering. The OLED has a multilayered structure of organic layers on indium tin oxide (ITO) coated glass. The constant current (100mA/$cm^2$) was applied between Al cathode and ITO anode of the OLEDs till the maximum luminescence of the electrically non-stressed OLED (sample A) decreased to 80% (sample B) and to 60% (sample C). We measured X-ray reflectivity and diffuse scattering of the OLED samples A, B, and C at room temperature at beamline 5C2 in Pohang Light Source. Certain degradation of the morphology of organic-organic interface was observed in the sample B and the degradation was enhanced in the sample C, i.e., along the increase of the electrical stress. The detailed electrical stress induced interface morphology of the OLED and its resultant luminescence will be discussed.

**Ep-055** **Cat-CVD법을 이용한 초소수성 PTFE(polytetrafluoroethylene) 박막의 제조** 조 정연, 차 정옥, 조 대희, 안 정선, TAKACHI Michihisa[1], OHDAIRA Keisuke[1], MATSUMURA Hideki[1](*경희대학교, 물리학과. [1]Japan Advanced Institute of Science and Technology.*) 초소수성(superhydrophobic) 특성을 갖는 PTFE(polytetrafluoroethylene) 박막을 hexafluoropropylene-oxide (HFPO) gas를 원료가스로 하여 Cat-CVD(catalytic chemical vapor deposition) 방법을 이용하여 증착하였다. Cat-CVD법은 높은 증착 효율을 가지며 대면적 증착이 가능하고 상대적으로 기판온도가 낮은 조건에서 증착이 가능한 장점을 가지고 있다. 본 실험에서는 촉매체(catalyzer)로 텅스텐(W) 와이어를 이용하였고 기판은 유리 기판과 Si(100) 기판을 사용하였다. FT-IR을 측정하여 촉매체 온도, 제막 압력 등의 제막조건을 변화시키면서 증착한 PTFE 박막의 증착여부를 확인하였고, 접촉각을 측정(Kyowa, Drop master DM300)하여 PTFE 막의 발수성을 조사하였다. 촉매체 온도를 변화시키며 증착된 막의 접촉각을 측정한 결과, 촉매체 온도가 85

0℃ 이상일 때 160°이상의 높은 접촉각을 얻을 수 있음을 확인하였다. 또한 제막압력을 변화시켜 증착한 경우, 400mTorr 이상에서 제작된 박이 초소수성 특성을 나타냄을 알 수 있었다.
* 본 연구는 서울시 산학연 협력사업의 지원으로 수행되었습니다.(과제번호 10583)

**Ep-056** **마그네슘합금 AZ91D 에서의 Arc-anodizing 표면처리에 대한 광학적 특성 연구** 유 재인, 김 진희, 유 재용, 박 창훈, 한 병하, 고 병수[1], 김 기홍[2](*(주)태양기전 제2기업부설연구소. [1]영남대학교 물리학과. [2]경운대학교 안경광학과.*) 마그네슘합금은 타금속에 비해 초경량성을 가지며, 전자 차폐성, 진동 감쇄성이 우수한 비철금속이다. 현재는 항공기 엔진부품, 자동차 부품등에 널리 쓰이고 있으며, 또한 휴대폰 케이스로서도 각광을 받고 있다. 그러나 마그네슘합금은 이러한 기능성을 가지면서도 큰 단점을 가지고 있다. 즉 산화가 잘 되는 금속이기 때문에 부식이 빨리 진행된다. 따라서 필수적으로 표면처리가 선행되어져야 한다. 본 연구에서는 표면처리중에서 Arc anodizing에 의해 형성 된 산화막의 광학적 특성을 연구하고자 한다.

**Ep-057** **마그네슘합금 표면처리에 대한 연구** 유 재용, 박 창훈, 유 재인, 김 정화[1], 김 기홍[2](*(주)태양기전 제2기업부설연구소. [1]영남대학교 물리학과. [2]경운대학교 안경광학과.*) 보통 마그네슘합금은 다이캐스트용과 판재용으로 나눌 수 있다. 현재는 판재 보다도 다이캐스트용 마그네슘합금이 많이 사용되어진다. 그 이유는 복잡한 형상의 제품을 만들기에는 마그네슘합금 판재보다 다이캐스트용 합금이 용이하기 때문이다. 현재 판재는 AZ31B 형태를 가지며 제품화를 위해 많은 연구중이다. 본 연구에서는 이러한 제품화를 위해 필수적인 마그네슘합금 표면처리방법에 대해서 기술하고자 한다.

**Ep-058** **Development of the DAS for both Transmission and Backscattered X-ray** HWANG inho, JUNG jinseok, YUK sunwoo, CHOI giwon, BAE taesoo, AHN yoonho, MUN museong(*Korea Orthopedics &Rehabilitation Engineering Center.*) Considerable attention has been focused on digital X-ray systems with transmission. However, only a few attempts have been made using X-ray backscatter systems. This study developed a Data Acquisition System (DAS) for both transmission and backscattered X-rays. The imaging system used X-ray at contineous low energy levels of below 100kvp for backscatter image, which has unique advantages in terms of acquiring information that cannot be obtained using the transmission system. And, we used a variety of X-ray energy level for transmission image. Such systems are of potential benefit in the medical, industrial, security and military fields because of its practical benefits and the low doses used. Due to its large X-ray absorption efficiency and low afterglow, we used PIN photodiode coupled to scintillator. And, the Data Acquisition System(DAS) can be classified into three main groups: an amplifying part, a digital control part, and a back-plane board. To realize the data from DAS, we performed image processing such as histogram equalization, to help visualization, contrast, brightness control, and post-processing blur, image sharpness. Experiments were carried out using a several metal materials and a fish, which produces results similar to those obtained using the human body during X-ray testing.

**Ep-059** **Position Controlled Doping Of Ionic Adsorbates By Induced Bias On Single-walled Carbon Nanotube Thin Film Transistor.** YU Woo Jong, JEONG Seung Yol, KIM Ki Kang, KANG Bo Ram, BAE Dong Jae, LEE Min Baek[1], HONG Seung Hun[1], GAUNKAR Sunanda Prabhu[2], PRIBAT Didier[2], PERELLO David[3], YUN Minhee[3], CHOI Jae-Young[3], LEE Young Hee[3](*Sungkyunkwan University. [1]Seoul National University. [2]Ecole Polytechnique. [3]University of Pittsburgh.*) Doping control on carbon nanotubes (CNTs) is a crucial step for implementation in future nanodevices. Chemical doping of CNT is typically done via functionalization or encapsulation using various molecular adsorbates. Controlling the dopant types and position on the CNT-based thin film transistors (TFTs) and their stability has been a considerable challenge. Here, we report a CNT doping strategy utilizing ionic adsorbates controlled via gate and drain bias. Dopant type was controlled by the polarity of gate bias, and positioning of the adsorbates was expedited by applying drain and gate bias. This enabled us to control n- or p-type doping that leads to forward or reverse Schottky diodes. The combined adsorbates-associated biasing method also allowed a selective dissociation of metallic channels to improve TFT on/off performance. Our approach demonstrates a practical means of fabricating CNT-based random network TFTs with deliberate doping and high stability under ambient conditions.

**Ep-060** **The high resistive poly-CdZnTe thick film utilized in the linear radiation detector** HWANG inho, JUNG jinseok, YUK sunwoo, BAE taesoo, CHOI giwon, AHN yoonho, MUN museong(*Korea Orthopedics &Rehabilitation Engineering Center.*) The linear x-ray detector was fabricated from the high resistive poly-crystalline CdZnTe thick film. The resistivity of the CdZnTe is about $1.2\times10\Omega\cdot cm$ and its thickness is about $150\mu m$. The mobility-lifetime product of poly-crystalline CdZnTe sample is in the range of $8.7\times10^{-7}$~$5.6\times10^{-6} cm^2/V$. For the blocking layer, Schottky barriers were formed by indium. Gold was used for the Ohmic electrode. The detectors were realized by the 16 linearly $1\times1mm^2$ spaced electrodes. Moreover, we have built a multi-channel data acquisition system(DAS) for many applications. The developed DAS system is composed of a 16 channel linear array photodetector, a dual integrator, A/D(Analog to Digital) converter, a digital logic interface and a user interface. The phantom image was acquired by the preliminary x-ray test using this DAS. The Result, we have shown a high resistive polycrystalline CZT can be a good X-ray detector. It has shown promising results which can be used as a linear and area detectors. Also, we expect further utilization as a X-ray detector in industry as well as in medicine, particularly as a intra-oral sensor, a panoramic sensor and mammography sensor.

**Ep-061** **Inhomogeneous barrier and resistive switching of $Pt/SrTiO_3$ junctions** 김 희섭, 박 찬우, 이 성주, 권 민지[1], 김 동욱[1](*한양대학교, 응용물리학과. [1]이화여자대학교, 물리학과.*) We investigated the temperature dependent electrical properties of

Pt/Nb-doped $SrTiO_3$ junctions, exhibiting rectifying and hysteretic transport behaviors. Conventional Schottky diode model failed to explain the current-voltage characteristics, since the estimated Richardson constant was too small. The temperature-dependence of the barrier height and the ideality factor indicated that the fluctuation of the interfacial potential should be included. The model assuming the barrier inhomogeneity was in good agreement with the experimental data, which yielded reasonable value of the Richardson constant. The barrier inhomogeneity dominated the transport properties and affected the resistive switching of our junctions.

**Ep-062** **Conduction Mechanism and Resistive Switching Behaviors of Cu/$TaO_x$/Pt Structures** 차 동재, 이 성주, 정 재욱, 문 봉진, 안 일신, 연 혜성[1], 김 동욱[1](*한양대학교, 응용물리학과. [1]이화여자대학교, 물리학과.*) Resistance-based memories are potential candidates for future nonvolatile memory devices. Especially, resistive switching phenomena in metal-insulator-metal (MIM) structures have attracted great attention due to their compatibility to conventional semiconductor fabrication processes. We describe electrical properties and bipolar resistive switching behaviors of Cu/$TaO_x$/Pt structures. Cu top electrodes and $TaO_x$ insulating layers were sputter-deposited on platinized Si substrates at room temperature. Amorphous $TaO_x$ thin films were grown by varying $O_2$/Ar gas ratio (from 0 to 20 %) at room temperature. The results of X-ray photoelectron spectroscopy (XPS) showed systematic oxidation state change of the $TaO_x$ layers depending on the oxygen partial pressures. The conduction mechanism in the high-resistance state and resistive switching behaviors depended on the oxygen gas ratio during the deposition of the $TaO_x$ thin films. Detailed switching characteristics and the relationship of the conduction mechanism will be discussed.

**Ep-063** **휘발성 유기물 기체에 대한 다조건 다공질규소의 PL 강도와 스펙트럼의 변화 조사** 박 선화, 류 성주, 최 선혜, 김 영유, 송 정훈, 이 기원(*공주대학교, 물리학과.*) 본 연구에서는 단일 기판위에 다양한 제작조건을 갖는 다조건 다공질규소를 제작하고 휘발성 유기화합물 기체에 노출시켰을 때의 PL의 변화를 분석하였다. 다조건 다공질규소는 일정한 전류밀도 하에서 층의 두께 기울기를 갖도록 제작된 시료와 서로 다른 전류밀도하에서 1차원적인 다공의 크기 기울기를 갖는 시료가 실험에 이용되었다. 시료는 수정판(quartz plate)이 사용된 반응셀 내에 설치되었고, 질소기체를 운반기체로 하여 ethanol, methanol 등의 휘발성 유기화합물을 노출시켰다. 여기광으로는 자외선 램프의 254 nm 빛을 사용하였다. 노출 전후의 PL 강도 변화 패턴을 분석하기 위해 CCD 카메라로 시료 전체에서 나오는 발광 이미지를 촬영 하였다. 촬영된 영상은 컴퓨터 프로그램을 통해 시료의 두께와 양극산화 전류밀도의 함수로서 강도 패턴이 분석되었다. 아울러 PL 스펙트럼의 변화를 분석하기 위해 분광기를 이용하여 시료의 위치에 따른 스펙트럼을 측정하고 해석하였다. 이를 통해 다조건 다공질규소의 PL이 휘발성 유기화합물에 의해 그 특성이 변화됨을 알 수 있었다. 본 연구에서 사용된 실험 방법은 종래의 실험방법이 특정 조건으로 제작된 수많은 시료들을 대상으로 최적 감지 특성을 찾던 것에 비해, 단일 기판위에 제작된 다조건 다공질규소를 통해 최적 감지 조건을 손쉽게 찾아 낼 수 있어 다양한 연구 분야에 유용하게 사용할 수 있다.

**Ep-064** **Graphite Oxide를 이용한 다층 Graphene 생성 및 연구** 유 병선, E.S. Kannan[1], 김 길호(*성균관대학교 정보통신공학부. [1]성균관대학교 성균나노과학기술원.*) 최근 Graphene으로 구성된 물체이며 얇은 막으로 형성된 Graphite oxide가 주요한 과학적 연구의 대상이 되고 있다. 이러한 이유는 Graphene의 합성이 중요한 특징을 나타내기 때문이다. 먼저, 이 연구를 위해서 Gaphite 박막으로부터 화학적으로 합성된 Graphite Oxide가 필요했다. Graphite Oxide는 다양한 방법에 의하여 Graphene을 만들 수 있었는데, 그 중의 하나인 Hummer의 방법을 이용하였다. Hummer의 방법은 제조과정이 비교적 쉽고 산출량이 많아 그 중에서 신뢰할 수 있는 Graphene를 얻을 수 있었다. Hummer의 방법을 통해 Graphite Oxide의 얇은 막으로 형성된 입자들을 물에서 분산시키고 30분 동안 초음파에서 쬐어 분해하였다. 결과로 생기는 시료는 실리콘 substrate에 두었고, 그 후 습기를 제거하기 위해서 10분 동안 가열했다. 이렇게 생성된 각각의 얇은 Graphene(단층을 다층으로)을 이용하여 광학현미경을 통해 관측 후, 소스와 드레인 접촉을 하였다. 그리고 이 sample을 폐쇄된 회전식 저온 유지 장치에 의해 적재하고, 250 K에서 6 K의 연속적인 온도에서 전류-전압 측정을 통하여 전계 효과 현상에 관한 특성을 관측하였다.

**Ep-065** **Graphite Oxide 박막의 전계 효과 특성** 안 준용, 이 시영, E.S. Kannan[1], 김 길호[1](*성균관대학교 정보통신공학부. [1]성균관대학교 성균나노과학기술원.*) 고도로 산화된 Graphite Oxide는 흑연과 같이 AB Stacking의 완벽한 육각형의 구조를 가지고 있다. 두 원자층 사이의 격자 공간을 갖는 결정질적인 특성을 갖기 때문에 Graphite Oxide가 전지나 수퍼 커패시터에서의 전극으로써 촉망되는 물질이다. 산소가 탄소보다 더 큰 전기음성도를 가지므로, Graphite Oxide에서의 전자들은 산소에 더 쉽게 가까워진다. 그러므로 산소가 Graphite Oxide에서 trap level로 작용하기 때문에 전자는 전기 전도가 가능하기 위해서는 이 산소 장벽을 넘어서야만 한다. 산소 trap level과 전도대 사이의 에너지 장벽이 외부 바이어스 인가로 조절할 수 있으므로, Graphite Oxide 박막에서의 전기 전도도를 조절할 수 있게 된다. Hummer's method 에 따라 제작한 Graphite Oxide 박막 입자를 증류수에 섞어 $SiO_2$ 층을 표면으로 가지고 있는 p-type 실리콘 기판 위에 떨어뜨린 후 대류식 오븐에서 섭씨 30도에서 30분간 건조시켰다. 그 후 박막 표면에 있는 수분을 제거하기 위해 섭씨 200도로 10분간 annealing을 하였다. 샘플의 표면은 은 에폭시를 이용해 칩에 부착하고, 후면 게이트 바이어스를 Graphite Oxide에 통하도록 가해주었다. 소스와 드레인 전압을 가해주며 게이트 바이어스의 값에 따른 컨덕턴스의 변화를 관찰하였다. 게이트 바이어스가 0에서 5V 사이에서 스위칭될 때 박막 저항은 $10^3$ 배 수준의 크기 변화를 겪는 것이 발견됐다. 양의 값의 게이트 바이어스일 때 trap level과 전도대 바닥 사이의 간격이 전계로 인해 줄어들었다. 이로 인해 전도대에서의 전자의 수가 증가할 수가 있게 되고 Conductance는 증가하게 된다. 소스와 드레인 접촉면에 Graphite Oxide 박막에 직렬로 LED를 연결하여 스위치 동작에 따라 "ON"과 "OFF"를 나타냈다. 샘플은 스위칭에 거의 동시에 반응하는 좋은 과도 특성을 보여주었다. 그러나 "ON"상태에서 적은 전류의 변동이 관찰되었다.

Graphite Oxide 박막을 더 오랜 시간 annealing 했을 때, 전계 효과 특성이 없는 저항 특성을 보여주었다.

**Ep-066** **얇은 박막 Graphite Oxide의 합성과 특성 조사** 이 시영, 안 준용, E.S. Kannan[1], 김 길호[1](*성균관대학교 정보통신 공학부. [1]성균관대학교 성균나노과학기술원.*) 천연 흑연의 산화물인 얇은 박막 Graphite Oxide는 많은 $sp^3$와 그보다 적은 $sp^2$ 탄소 원자를 가진 잘 알려진 층 구조의 화합물이다. 이 박막이 물 안에서 퍼지게 되면 개별적인 그라핀(Graphene) Oxide Sheet로 분리되어 나오게 된다. 얇은 박막 Graphite Oxide는 흑연을 Hummer의 방법에 의해 합성함으로써 얻을 수 있다. 0.5 g의 흑연을 $NaNO_3$ (99%순도) 0.35 g과 혼합한다. 약 30.7 g의 $H_2SO_4$ (96%순도)을 얼음물 내에서 지속적으로 저으며 혼합물에 서서히 첨가한다. $KMnO_4$ 1.95 g을 첨가하면서 그 혼합물을 한 시간 동안 냉각시킨다. 이 혼합물을 20 ℃에서 5일 동안 젓는다. 5%의 $H_2SO_4$ 수용액 50 ml가 희석액으로써, 그리고 산화제를 제거하기 위해 30%의 $H_2O_2$ 1.5 g을 사용한다. 그리고 순수한 물을 이용해 매우 정화된 얇은 박막 Graphite Oxide를 얻는다. 이렇게 얻은 입자들은 건조되고 XRD측정을 하면 흑연이 완전히 산화됐음을 확인할 수 있다. 산화된 흑연은 천연흑연과 상당히 다르다. 흑연은 2θ=26 ° 에서 강한 002 Peak를 확인할 수 있지만 Graphite Oxide의 경우 2θ=12 ° 로 Peak가 이동하게 된다. Sherrer 공식에 의해 계산된 내부 층간 거리는 흑연과 Graphite Oxide가 각각 3.33 Å 과 7.3 Å 으로 나타난다. 반도체 분석 시스템을 사용해 온도변화에 따른 전류(I)-전압(V)을 측정한다. 그러면 샘플은 반도체적인 성질을 나타내며 그것의 저항은 온도가 낮아짐에 따라 증가함을 알 수 있다. 20 K 과 150 K 사이에서 저항은 Arrhenius 행동을 따르고, Arrhenius Plot에 의해 결정된 Trap의 활성화 에너지는 18 meV임을 알 수 있다. 낮은 활성화 에너지는 좁은 Trap을 나타내며 Graphite Oxide의 전자전송 메커니즘은 전장에 의해 증가된 가두어진 전자의 열 이온 방출에 의해 통제된다.

**Ep-067** **Monte Carlo Simulations for Radioactivity in the Atmosphere and in the Airplane** LEE J.H., SHIN J.W., PARK T.-S., HONG S.W.(*Department of Physics, Sungkyunkwan University, Suwon 440-746.*) Geant4 simulation 을 이용하여 두 가지 시뮬레이션을 하였다. 첫 번째로 cosmic-ray에 의해 대기 중에 발생하는 이차 방사선이 대기 중의 중금속에 의해 어떻게 영향을 받는지 시뮬레이션 하였다. 대기 중에 중금속이 존재할 때와 그렇지 않을 때의 방사선 발생 정도를 각각 시뮬레이션 한 뒤 지상에서 받게 되는 환경 방사선 양이 어떻게 변화하는가에 대해 연구하였다. 두번째로 비행기 탑승 시 받게 되는 흡수방사선량이 좌석에 따라 어떤 차이를 보이는 가에 대한 연구를 하였다. 비행고도에서는 대기에 의한 cosmic-ray의 차단효과가 지상에 비해 적으므로 더 많은 방사선을 받게 된다. 좌석에 따른 방사선 피폭 차이가 발생하는지에 대해 알아보기 위하여 Geant4 시뮬레이션을 수행하였다.

**Ep-068** **Sample Heating Device with an Integrated Blackbody for Measuring Directional Spectral Emissivity** 전 상호, 박 승남[1], 이 근우[1](*한남대학교 물리학과. [1]한국표준과학연구원.*) Uncertainty of emissivity using Fourier transformation-infrared (FT-IR) spectrometer results from many sources, that is, temperature measurement in sample and blackbody, difference of optical paths between sample and blackbody, different environment and reflection near sample and blackbody, and so on. Those sources significantly affect the emissivity in particular at low temperature where sample signal is weak. One of the ways to reduce the uncertainty sources is to place sample and blackbody at same position. For this purpose, we have developed a new device so that sample is located in blackbody under vacuum. Results of emissivity will be shown with ceramic and some metals, covered from -20 $^oC$ to 200 $^oC$ with oil or water, and from 2.5 um to 20 um range. Effect of oxidation and surface roughness on emissivity is also studied as a function of temperature and angle.

**Ep-069** **The effect of applied electric field annealing on structure and dielectric properties of $Ba_{1-x}Sr_xTiO_3$ thin films** CHO Kwang-Hwan, KANG Chong-Yun, LEE YoungPak[1], YOON Seok-Jin(*Thin Film Materials Research Center, KIST. [1]q-psi and Dept. of Physics, Hanyang Univ..*) The effect of heat treatment in electric field on the structure and dielectric properties at microwave range of RF magnetron sputtering derived $Ba_{1-x}Sr_xTiO_3$ thin films have been studied. It has been demonstrated that post-annealing in the proper electric field can increase the dielectric constant and the tunability. The increased out-of-plane lattice constant in the electric-annealed films indicated the formation of small polar regions with tetragonal structure, which are responsible for the increased dielectric constant and tunability. It was proposed that the segregation of $Ti^{3+}$ ions caused by electric annealing could induce the formation of $BaTiO_3$-like regions, which are ferroelectric at room temperature. And in dielectric loss, as the Ti-O bonding lengths increase, the energy scattering on the ferroelectric mode also increases.

**Ep-070** **Origin of Electrically Active and Inactive Defects Associated with F Impurtiy in $SiO_2$** 이 은철, 주 형규(*경원대학교 바이오나노학부.*) As MOS devices shrink down to the nanometer scale, it becomes more important to understand defects in $SiO_2$ on an atomic level for fabricating the high-performance device. In this work, we present an atomic model for electrically active and inactive F-related defects, based on a first-principles theoretical method. We find that fluorine plays the dual role in determining electrically properties of $SiO_2$; F interstitial acts as a fixed charge or a charge trap, while its complex with O-deficient centers are electrically inactive. The detailed analyses on the atomic and electronic structures of these defects will be given, and the key process parameters for obtaining the high-quaility $SiO_2$ will be discussed.

**Ep-071** **Effect of Post Gaussian Smoothing on PET/CT Image in Radioactivity Estimation Using Various Scanners** 김 종국, 김 경민, 김 진수, 우 상근, 천 기정(*한국원자력의학원 분자영상연구부.*) The different characteristics of commercial PET/CT scanners make it difficult to compare the intra-subject data acquired from various scanners. We investigate the effect of post-smoothing filter on reconstructed image in the evaluation of mean and/or maximal value of SUV. Both Jaszczak ECT phantom and NEMA IEC

body phantom having hot-sphere insert were used for the acquisition of PET images at two whole-body PET/CT scanners (Siemens Biograph6 and GE Discovery LS). All PET images were acquired with same routine whole-body protocol, and reconstructed using OSEM with post-Gaussian filter (kernel size = 5mm). On the reconstructed images, additional post Gaussian filters with various kernel sizes were applied. VOIs were placed on the regions of hot-sphere inserts to get the mean and maximal values of SUV. The factor values were also estimated in order to compensate partial volume effect (PVE). The kernel size of 8mm was the maximum value making no significant difference of mean SUV values. Post Gaussian smoothing resulted in a bigger decrease in the maximal SUV values (14.9%) than in the mean SUV values (8.3%). With additional post Gaussian smoothing, the variance of maximal SUV values from both scanners were improved from ~ 10.2 % to 4.6 % for 8mm kernel, and that of mean SUVs values were improved to (2.6%). The difference of PVE correction factors was also reduced by 64% with applying smoothing. Maximum SUV value showed significant dependency on spatial resolution and pixel noise comparing to mean SUV. The use of mean SUV with incorporation of PVE correction and post-smoothing could contribute to quantitative diagnosis of tumoral disease, with improved precision and reproducibility.

**Ep-072** **후막형 무기 electroluminescence의 top-emission 구조 특성** 김 진영, 유 세기[1](*성균관대학교, 물리학과.* [1]*한국외국어대학교, 전자물리학과.*) 후막형 무기 electroluminescence (EL) device의 top-emission 구조 특성을 연구하였다. 기존의 bottom-emission 구조와 달리 강유전체인 BaTiO3와 유기바인더의 혼합물로 이루어진 유전층을 Al층이 증착되어진 glass 위에 도포하고, 유전층 위에 평균 직경이 약 28 um인 녹색발광 EL용 형광체와 유기바인더의 혼합물로 이루어진 발광층을 스크린 프린팅 방법으로 도포하였다. 기존의 bottom-emission 구조보다 top-emission 구조가 더 높은 휘도를 얻었다. 구조적인 차이에서 기인하는 전기장의 세기와 빛의 투과 경로를 분석하였다. 이 포스터에서 이 구조적인 차이에 대한 자세한 부석에 대하여 다룰 예정이다.
* 이 연구는 2007년 정부(교육인적자원부)의 재원으로 한국학술진흥재단의 지원을 받아 수행된 연구임(KRF-2007-313-C00299).

**Ep-073** **Multiparametric sensor based on DBR porous silicon for detection of ethanol gas** KIM Hanjung, JANG Jaehyeong, CHENG Horchhong, LEE Ki-Won, KIM Youngyou (*Department of Physics, Kongju National University, Chungnam 314-701, Republic of Korea.*) We made the DBR(distributed Bragg reflector) porous silicon onto silicon wafer and monitored the change of three parameters during exposure of DBR porous silicon to ethanol gas. The sensing parameters were the shift of reflectance peak, the photoluminescence spectrum, and the electrical conductivity. As a result, the spectra of reflectance and photoluminescence shifted toward longer wavelength. And the electrical conductivity increases rapidly. After removing the gas, all parameters return exactly to the initial value. These experimental results are very useful in order to develop renewable gas sensor based on DBR porous silicon.

**Ep-074** **Current-Voltage Characteristic of Porous Silicon of Albumin Absorption** CHENG Horchhong, KIM Hanjung, LEE Ki-Won, KIM Youngyou(*Department of Physics, Kongju National University.*) Porous silicon is a sponge like, which has quite high resistivity. It is very sensitive to the biomaterials that were absorbed. So, it is suitable for the field of sensing. This work is to study the current-voltage characteristic from different thickness and porosity of porous silicon after Albumin was absorbed. The current-voltage was performed both transversal and longitudinal of the sample. The result of the current-voltage measurements have shown that it is a huge difference as a function of present and absence of Albumin on the porous silicon surface. Moreover, it is found that the current-voltages strongly different between the samples that etched in different HF concentration, and the samples that have different thickness.

**Ep-075** **Structual, ferroelectric and magnetic properties of $BiFeO_3/Pb(Zr_{0.52}Ti_{0.48})O_3$ multilayer films fabricated by chemical solution deposition.** 차 정옥, 안 정선, 이 광배[1](*경희대학교 물리학과.* [1]*상지대학교 응용물리전자학과.*) Multiferroic materials, which combine the properties of ferromagnetism, ferroelectricity, and ferroelasticity, have attracted intensively attention owing to their physical mechanisms and potential for the design of multifunctional device applications. For instance, several papers about the ferroelectric properties and magnetoelectric effect in ferroelectric/manganite heterostructures were reported. BiFeO3 (BFO) is one of the few known multiferroic which has the ferroelectric behavior with a high Curie temperature(TC=863°C) and antiferromagnetic behavior with a relatively high Neel temperature (TN=397°C). And it has been shown to possess a rhombohedrally distorted perovskite structure with space group R3c at room temperature. However, it is difficult to observe the ferroelectric hysteresis loops in the bulk BFO ceramic, as well as in the BFO films, prepared by common solid state reactions. In order to improve ferroelectric properties of BFO, a large number of works have been done to prepare BFO films by different methods. Several techniques have been used for fabrication of BFO films, such as pulsed-laser deposition (PLD), chemical solution deposition (CSD), and rf-sputtering. In recent years, some groups researched magnetoelectric composite, which is constructed by ferroelectric layer and ferromagnetic or magnetoelastic layer. This multilayer film can provide a bigger remnant polarization and retain the magnetic properties of BFO. As a familiar ferroelectric materials Pb(ZrxTi1-x)O3 (PZT) has been studied extensively. The fabrication technique of PZT thin film has been reported by many groups. The adjustable Zr/Ti ratio offers more applicability for the multilayer film. In this paper, multilayer multiferroic thin films of BFO/PbZr0.52Ti0.48O3 (PZT) were fabricated on Pt/Ti/SiO2/Si substrate by chemical solution deposition (CSD). In order to obtain the high resistivity of multilayer thin films, we investigate the conditions of the optimized deposition and the annealing process. The structural, electrical and magnetic properties of BFO films have been studied.
* This work was supported by the Soeul Research and Business

Development Program (Grant No. 10583)

**Ep-076** **Radiometric standards for conversion efficiency measurement of photovoltaic cell** 박 승남, 이 동훈, 신 동주, 박 철웅, 박 성종, ZAID Gufron[1](*KRISS. [1]KRISS/UST.*) Solar cell test requires an I-V characteristic measurement under an irradiance level of about 1 solar constant. At KRISS, the spectral irradiance scale can be realized indirectly by the spectral responsivity standard and directly by the blackbody with a well defined aperture. The spectral responsivity has been realized based on a cryogenic radiometer with an uncertainty of 0.01 %. The blackbody temperature is measured traceable to International Temperature Scale -1990. We review the uncertainties of the radiometric quantities which affect the uncertainty of solar cell test.

**Ep-077** **Measurement Capability of Normal Spectral Emissivity at KRISS** 이 근우, 전 상호[1], 박 승남, 이 상현, 권 수용(*한국표준과학연구원. [1]한남대학교 물리학과.*) Infrared emissivity is an important physical quantity to measure radiometric temperature measurements for industrial and medical purposes. We have built a normal spectral measurement system using a Fourier transformation-infrared spectrometer (FT-IRS). Uncertainty of the system mainly results from the reference blackbody, temperature measurement of sample and the FT-IRS. We will show the measurement capability of normal spectral emissivity by evaluating the uncertainty of samples from various materials.

**Ep-078** **감마선영향 완화 중성자계수기** 박 광준, 주 준식, 강 희영, 신 희성, 김 호동(*한국원자력연구원.*) 특수핵물질 계량에 사용되는 중성자계수기(neutron counter)는 감마선을 방출하는 핵분열 생성물이 함께 존재하는 사용후핵연료를 측정하는 경우, 감마선의 영향을 받아 원래의 기능이 저하된다. 중성자계수기 기능저하의 주요 원인은 구성품 중 고속중성자(fast neutron)를 감속시켜 낮은 에너지의 중성자(thermal neutron)로 변화시켜주는 역할을 하는 중성자 감속재(neutron moderator)가 감마선의 영향을 받아 열화(radiation-induced degradation)되기 때문이다. 대부분의 경우 중성자계수기의 중성자 감속재로서 고밀도 폴리에틸렌이 사용되고 있는데, 이는 감속능이 비교적 큰 장점이 있는 반면 감마선에 의한 영향을 받아 원래의 분자구조가 변화되는 단점도 갖고 있다. 그래서 본 연구에서는 중성자 감속능도 어느 정도 크고, 감마선에 의한 영향을 감소시키거나 또는 영향을 받아도 감속재 교체가 용이한 순수한 물(pure water: PW)의 사용을 고려하게 되었다. 똑 같은 크기의 중성자계수기를 갖는 경우, 중성자 감속재로 HDPE를 사용할 때와 PW를 사용할 때의 중성자 측정 효율변화를 확인하기 위하여 MCNP 코드 계산을 수행하였으며, 그 결과 10.73%와 10.32%로 나타났다. 따라서 중성자계수기의 중성자 감속재로서 PW를 사용하게 되면, 감마선에 의한 영향을 줄이면서 측정효율도 어느 정도 유지시킬 수 있다는 것을 확인하게 되었다.

**Ep-079** **Scaling Law and Predictable Resistance Switching of NiO Thin Films** LEE Shin Buhm, CHAE S. C., CHANG S. H., LEE J. S.[1], PARK S.[2], JO Y.[2], SEO S.[3], KAHNG B.[1], NOH T. W.(*ReCOE &FPRD, Department of Physics and Astronomy, Seoul National University, Seoul 151-747. [1]Department of Physics and Astronomy, Seoul National University, Seoul 151-747. [2]Quantum Materials Research Team, Korea Basic Science Institute, Daejeon 305-333. [3]Samsung Advanced Institute of Technology, Suwon, Gyeonggi-do 440-600.*) The semiconductor industry has long searched for a next-generation nonvolatile memory device, which can retain its data even when the power is interrupted. A new concept called resistance random access memory, in which its resistance can be repeatedly switched between a high and a low value by applying electric field, has recently attracted lots of scientific and technological interests. Especially for the unipolar resistance switching, which shows the low-/high-resistance switching along the single bias voltage, switching mechanism are largely classified into formation and rupture of conducting path based on a thermal effect or electronic charge injection effects. All models, however, leave unanswered questions.In this works, normalized third harmonic $B_{3f}$, which is thermal response to an external ac voltage, is measured for low resistance state of Pt/NiO/Pt thin films. $B_{3f}$ is theoretically based on Joule heating effects of local conducting path, and provides a direct measurement of the microscopic current distribution. The scaling of $B_{3f}$ as a function of resistance suggests that nonlinear current-voltage curve is due to Joule heating effects. $B_{3f}$ versus maximum current at the moment of conducing path rupture has a scaling relation. Therefore, $B_{3f}$ can be a new nondestructive parameter to predict rupture of conducting path. All experimental results can be explained by computer simulation based on bond percolation model with Joule heating effects.Our results support that the switching mechanism can be understood by formation and rupture of the conducting path, which can be governed by the percolation nature. Especially, rupture of conducting path is driven by Joule heating effects. Furthermore, these results suggest that broad switching voltage distribution can be reduced by nanoscale-confined conducting paths.

**Ep-080** **Electrical characterization of nonvolatile memory with $SnO_2$ nano-particles in BPDA-PDA polyimide** LEE Dong Uk, HAN Seung Jong, KIM Seon Pil, KIM Eun Kyu, SHIN Jin-Wook[1], CHO Won-Ju[1], KIM Young-Ho[2](*Quantum-Function Spinics Lab. and Department of Physics, Hanyang University. [1]Department of Electronic Materials Engineering, Kwangwoon University. [2]Devision of Advanced Materials Science and Engineering, Hanyang University.*) The nano-floating gate memory (NFGM) devices with $SnO_2$ nano-particles and polyimide gate insulator were fabricated on the *p*-type (100) UNIBOND silicon-on-insulator (SOI) wafers, which have a 100-nm-top silicon layer and a 200-nm-buried oxide layer. Phosphorus doped poly-Si layer with 100-nm-thickness was deposited for source and drain regions on the top Si by low pressure chemical vapor deposition (LPCVD) method at 650 °C. After the formation of active region, the phosphorus doped poly-Si layer was partially removed out to define channel region and then remained phosphorus doped poly-Si layer at the channel edge serves as source/drain of NFGM devices. Then the growth of tunnel oxide with 4.5-nm-thick by dry oxidation and the deposition of Sn layer with 5-nm-thick by using thermal evaporator. The polyamic acid

(PAA) layer with a thickness of 50 nm was spin coated on the thin Sn layer. The PAA is commercial biphenyltertracarboxylic dianhydride-phenylen diamin (BPDA-PDA) type. The curing process was carried out at 400 °C for 1 hour after a soft baking of 135 °C for 30 min in the rapid thermal process system in $N_2$ ambient. The Al gate electrode with a thickness of 200 nm was formed by thermal evaporation, photolithography and aluminum etching processes. The fabricated SOI-NFGM with $SnO_2$ nano-particles were characterized the electrical properties such as capacitance-voltage, current-voltage, flat-band voltage shift, endurance and retention properties.

**Ep-081** **NH3 and CO detection Using Single-walled Carbon nanotubes/Polyaniline** BANG Doyeon, CHOI Hyanghee[1], KIM Seongdong[2], PARK Joonshik[2], YOO Kyunghwa[1](*Yonsei University, Graduate Program for Nanomedical Science. [1]Yonsei University, National Core Research Center for Nanomedical Technology. [2]KETI, Semiconductor &Display Research Center.*) We have fabricated gas sensors using single-walled carbon nanotubes(SWNTs)/polyaniline(PAni) composite by drop coating method on a silicon substrate. The sensor conductance decreases under NH3 atmosphere, whereas it increases under CO atmosphere at room temperature. Compared with the sensors made of SWNTs without PAni, SWNTs/PANI sensors exhibit faster response and better sensitivity over a variety range of concentrations. We have also investigated structure and morphology of SWNTs/PAni composites to study the relation between their structural properties and electrical properties.

**Ep-082** **Optimization of Carbon Nanotube (CNT) Field Emitter for X-ray Generation by Computer Modelling** SHON Chae-Hwa, KIM Jong-Uk, CHOI Hae-Young(*Korea Electrotechnology Research Institute (KERI), Advanced X-ray Medical System Research Group.*) We have developed an X-ray source based on a field-emission electron source using carbon nanotubes (CNTs) for applications to biological, medical and material technologies. In the design of the X-ray sources, it is important to ensure that fine beam focus and efficient electron emission can be simultaneously obtained. The geometrical parameters, such as electrode shape and grid mesh design, including mesh wire thickness and mesh opening area, focusing electrode design, and the gaps between parts (for example, CNT cathode and grid mesh) must be optimized to obtain high quality X-ray source. In this study, for different types of structures, the beam focusing performances with respect to grid mesh and focusing electrode geometry were simulated. The opening area and shapes are controlled and various size of gird thickness is used in the simulation. The distribution of electric field near CNT cathode that is crucial for the emission of electrons from the CNT tips is analyzed with respect to different grid mesh openings.

**Ep-083** **Monitoring of Apoptosis and Necrosis by Capacitance Measurements** 이 리미, 유 경화, 신 전수[1], 김 건홍[2](*연세대학교 나노메디컬 국가핵심연구센터. [1]연세대학교 의과대학 미생물학 교실. [2]연세대학교 의과대학 생화학-분자생물학 교실.*) Apoptosis and necrosis are two different paths for cell death. One of differences between apoptosis and necrosis is the cell morphology. Apoptotic cells shrink without loosing the integrity of their plasma membrane and break into smaller pieces called apoptotic bodies that other body cells recognize and eat. In contrast, necrotic cells swell and their plasma membrane eventually ruptures. Since the cell membrane is closely related to the capacitance (or dielectric constant), we have fabricated a capacitance sensor, which can measure the capacitance of 1~4 cells, and investigated its time dependence during apoptosis and necrosis for TE2 cells induced by TNF related apoptosis inducing ligand (TRAIL) and ethanol. The capacitance decreases monotonically during apoptosis. For necrosis, however, step-like behaviors are observed and dips are found in the dC/dt-t curves. The time-lapse images of TE2 cells, which have been taken simultaneously with the capacitance measurements, show that dips in the dC/dt-t curves are probably due to the rupture of cell membrane. These results suggest that apoptosis and necrosis may be differentiated by the capacitance measurements.

**Ep-084** **Gas Sensor Using Pd-decorated Carbon nanotubes** 최 향희, 김 창호, 김 성동[1], 박 준식[1], 유 경화[2](*연세대학교 나노메디컬 국가핵심연구센터. [1]전자부품연구원. [2]연세대학교 물리학과.*) We have fabricated gas sensors using carbon nanotubes(CNTs) and Pd-decorated CNT on a silicon substrate and detected $NH_3$ and CO gases. The resistance increases under $NH_3$ for both CNT and Pd-decorated CNT sensors. Under CO, however, CNT and Pd-decorated CNT sensors exhibit different behaviors. The resistance decreases for CNT sensors, whereas it increases for Pd-decorated CNT sensors. In addition, a higher sensitivity and a fast response are found in Pd-decorated CNT sensors. Possible origins of enhanced sensitivity for Pd-decorated CNT sensors are discussed.

**Ep-085** **Rubrene polycrystalline transistor channel achieved through in-situ vacuum annealing** IM SEONGIL, KIM JAEHOON, PARK SEWOUNG, JEONG SUNGHOON, CHOI JEONGMIN, HWANG JUNGMIN(*연세대학교 물리학과.*) We report on the rubrene polycrystalline film growth for its thin-film transistor (TFT) applications. Amorphous rubrene thin film was initially obtained on 200 nm-thick $SiO_2$/Si substrate at 40 ℃ in a vacuum chamber by thermal evaporation but in-situ long time post-annealing at the elevated temperatures of 60 ~ 80 ℃ transformed the amorphous phase into crystalline. Based on an optimum condition to cover whole channel area with polycrystalline film, we have fabricated a rubrene-TFT with a relatively high field effect mobility of 0.002 $cm^2$/V s, on/off ratio of ~ $10^4$ and a low threshold voltage of -9 V.

**Ep-086** **Carbon Nanotube - Based Biosensor for Detection Hepatitis B** 유 경화, 오 제승[1], 유 승환, 장 영욱, 임 국진[2](*연세대학교,물리학과. [1]연세대학교,나노메디컬협동과정. [2]LG Life Sciences.*) We have fabricated carbon nanotube based biosensor with a field-effect transistor structure. To minimize the contact effect, the metal contacts were passivated using $SiO_2$ or $SiN_x$ and the microfluidic channels were mounted on the device. Hepatitis B antibodies were

immobilized on the surface of carbon nanotube using a chemical linker. And then, binding of hepatitis B antigens to antibodies were detected by measuring the conductance change in real time. The conductance increased and became nearly constant within 10 min. and an antigen concentration of 100 pg/ml was possibly measured.

**Ep-087** **독특한 발광 호스트 층을 사용하여 제작된 고효율 및 고색순도를 가진 청색 유기발광소자** 방 현성, 추 동철[1], 김 태환[2], 이 석재[3], 서 지현[3], 김 영관[3](*한양대학교 전자컴퓨터통신공학과. [1]한양대학교 디스플레이공학연구소. [2]한양대학교 전자컴퓨터통신공학과, 디스플레이공학연구소. [3]홍익대학교 정보디스플레이공학과.*) 유기발광소자는 차세대 디스플레이 소자와 조명 광원으로서 많은 가능성과 응용성을 가지고 있다. 그러나 유기발광소자의 적색과 녹색 및 청색의 3원색의 소자 중에서 청색 유기발광소자는 적색 및 녹색의 효율을 달성하기 어렵고 재료의 특성상 인광 소자 제작에 어려움이 있으며, 색 순도가 상대적으로 낮은 관계로 전색 디스플레이 패널을 구현하는데 어려움이 있다. 청색 유기발광 소자의 발광 효율을 증가시키고 색 순도를 높이기 위하여 3-tert-butyl-9,10-si(naphtha-2-yl)anthracene (TBADN) 형광 호스트 물질과 1,3-Bis(carbazole-9-yl)benzene (mCP) 인광 호스트 물질을 혼합한 발광층의 구조를 갖는 유기발광 소자를 제작하고 전기적 및 광학적 성질을 조사하였다. 형광 호스트에서의 발광은 적절한 색 순도와 발광 특성을 가지지만 상대적으로 낮은 에너지 밴드갭을 가지고 있고, 최대 25%의 발광 효율을 가지기 때문에 인광에 비해 상대적으로 낮은 효율을 보인다. mCP인광 호스트 물질에 TBADN 형광 호스트 물질을 5, 20 및 50%로 혼합하여 mCP에서 형성된 엑시톤을 TBADN으로 전달되는 에너지 전달 과정을 통하여 효율적인 에너지 전달 과정을 관찰하였고 mCP 또는 TBADN의 단일 물질 구조로 형성된 소자보다 색 순도를 개선하였고 구동 전류 및 구동 전압의 변화에도 불구하고 색좌표가 일정한 소자를 제작할 수 있었다. 이 결과는 혼합된 발광층을 사용한 유기발광소자의 구조가 효율적으로 색 순도를 증가시키고 효율을 증가시킬 수 있음을 제시하고 있다.

* This work supported by the Korea Science and Engineering Foundation (KOSEF) grant funded by the Korea government (MEST) (No. R0A-2007-000-20044-0).

**Ep-088** **녹색 유기발광소자에서 엑시플렉스의 형성과 색좌표의 영향** 이 광섭, 추 동철[1], 김 태환, 김 구영[2], 김 영관[2](*한양대학교 전자통신컴퓨터공학부. [1]한양대학교 디스플레이공학연구소. [2]홍익대학교 정보디스플레이공학과.*) 유기발광소자가 다른 디스플레이 소자에 비하여 많은 장점이 있기 때문에 연구의 관심이 되고 있다. 유기발광소자는 고휘도, 빠른 응답속도, 고효율, 얇은 두께 등 장점을 가지고 지닌 디스플레이로 알려져 있다. 그러나 유기물질간의 계면에서의 전하수송 및 발광현상에 대한 연구는 아직 미흡하다. 엑시플렉스는 서로 다른 분자에 걸쳐 형성되는 엑시톤으로서 유기발광소자의 발광특성에 중대한 영향을 주고 있으며 주로 낮은 이온화 에너지를 가진 정공 수송층과 높은 전자 친화도를 가지는 발광층 계면에서 나타나 발광에 기여를 한다. 발광층의 lowest unoccupied molecular orbital 준위에서의 정공수송층의 highest occupied molecular orbital 준위에서의 정공이 결합을 하여 발광층의 엑시톤에 비해 작은 결합에너지를 갖는 엑시플렉스를 형성하여 발광스펙트럼을 변화하게 한다. 이러한 현상으로 색순도가 나빠지며, 효율도 낮아지는 현상이 나타난다. 본 연구에서는 엑시플렉스를 잘 형성하는 구조를 제작하여 엑시플렉스의 형성에 의한 발광특성의 변화를 관찰하였다. 정공 수송층으로 이온화 에너지가 낮은 m-MTDATA를 사용하여 기존의 발광층의 파장보다 단파장에서 빛이 나타나며, 전압이 증가 할수록 발광지역의 이동으로 인하여 발광층의 순수한 파장의 빛이 나타나는 현상을 전계발광분광 측정으로 관측하였다. 전압의 변화에 대한 CIE 색좌표의 변화로부터 엑시플렉스에 발광스펙트럼의 영향을 관찰하였다. 본 연구를 통해 유기발광소자에서 엑시플렉스의 발생 및 그로 인한 발광특성의 변화를 이해할 수 있게 되었다.

* This work was supported by the Korea Science and Engineering Foundation (KOSEF) grant funded by the Korea government (MEST) (No. R0A-2007-000-20044-0).

**Ep-089** **Magnetic Separation of Colloidal Materials** 김 동락, 권 선희, 이 병섭, 양 형석, 최 연석, 엄 태규[1](*한국기초과학지원연구원 고자기장연구팀. [1]경성대학교 환경공학과.*) 자기장을 이용하여 물질을 분리하는 방법은 이미 오래 전부터 알고 있다. 자기분리방법은 물리적 방법이므로 화학물질 배출의 염려가 없으므로 친환경적 기술이다. 자성을 띠지 않는 물질을 담자화(magnetic seeding)하여 자기분리방법으로 효과적으로 분리할 수 있다. 용액 속의 colloid를 자기장을 이용하여 분리하는 방법에 대하여 발표하고자 한다.

**Ep-090** **Polarization Current from a Capacitor Structure with Poly-4-vinyl phenol (PVP) Dielectrics** HAMZA Ammar, LEE J.-K.(*전북대 물리학과.*) ITO/PVP(poly-4-vinyl-phenol)/ electrode capacitor structures were fabricated and transient time-dependent currents were measured.PVP and PMCF (poly-melamine-co-formaldehyde) as a cross-linker were mixed in PGMEA (propylene glycol 1-monomethyl ether 2-acetate) at different concentrations of PMCF (0, 10, 20, 30, 40 wt. %).After spin coating of a PVP solution mixed with PMCF, the PVP was cross-linked by thermal curing. The samples were cured at varying temperatures between 20 °C and 200 °C.The effects of aging, temperature, and applied voltage have been investigated.After specimens were prepared, with aging time in air, moisture and oxygen affected, the conduction current showed change from high leakage currents (maybe ionic current) to insulated-polarization current. The charge transport in the early first stage was attributed to an ionic process. The second stage after ~60 days showed a polarization current properties from a capacitor structure with PVP (poly-vinyl-phenol) as dielectric.The electrical characteristics seems to be intimately related to the presence of OH groups in the polymer dielectrics. The influence of hydroxyl groups will be discussed.

**Ep-091** **독특한 발광층과 정공수송층을 사용한 청색 유기발광소자의 효율 증진** 안 성대, 이 광섭, 추 동철[1], 김 태환[1], 서 지현[2], 김 영관[2](*한양대학교 전자통신컴퓨터공학과. [1]한양대학교 디스플레이공학연구소. [2]홍익대학교 정보디스플레이공학과.*) 유기발광소자는 차세대 디스플레이소자와 조명소자로 가장 각광받고 있고 액정 디스플레이에 비해 높은 에너지 효율, 고휘도, 빠른 스위칭타임, 저생산비용등의 장점을 가지고 있다. 유기발광소

자의 발광효율을 향상하기 위하여 다양한 구조에 대한 연구가 진행되었으며 이러한 구조들은 발광층에서 전자와 정공의 균형을 조절하여 발광효율을 향상하였다. 본 연구에서는 나노크기의 장벽층이 삽입된 정공수송층과 트랩층이 삽입된 발광층을 사용하여 발광효율의 변화를 조사하였다. 장벽층 및 트랩층으로 5,6,11,12-tetraphenylnaphthacene (rubrene) 층과 1,3,5-tris(N-phenylbenzimidazol-2-yl)benzene (TPBi) 층이 사용되었다. 제작된 유기발광소자에 대하여 전류-전압, 발광세기-전압, 전계분광스펙트럼 측정을 통해 전기적 및 광학적 성질의 변화를 조사하였다. Rubrene 트랩층이 삽입된 정공수송층을 사용한 유기발광소자의 동작전압은 정공수송층의 정공이동도의 감소로 인해 증가하였지만 발광층에 트랩층을 삽입한 유기발광소자는 트랩된 전자 및 정공의 증가로 인해 동작전압이 감소하였다. 두 개의 Gauss 함수로 구성된 rubrene 층과 관련된 EL 피크는 정공수송층과 발광층에 rubrene 층의 삽입에 의해 발생되었으나 DPVBi 발광층의 EL 피크는 TPBi 장벽층에 의해 영향을 받았다. DPVBi 피크는 세개의 Gauss 함수로 분해되었고 세개의 피크의 상대적인 비는 장벽층에 의해 변하였다. DPVBi 와 관련된 EL 피크의 크기 변화는 TPBi 장벽층과 근접한 유기물층의 헤테로계면에서의 발광에 의해 영향을 변화하였다. 본 연구의 결과는 트랩층과 장벽층을 포함하고 있는 발광층과 정공수송층을 사용한 유기발광소자의 발광메카니즘을 이해하는데 도움을 준다.
* 이 논문은 2006년도 정부재원(교육인적자원부 학술연구보성사업비)으로 한국학술진흥재단의 지원을 받아 연구되었음 (KRF-2006-005-J04102)

**Ep-092** **Pantacene organic thin-film transistors inserting the wide bandgap organic material layer** 정 성호, 정 인승, 김 종수[1], 남 윤성, 장 수경, 정 광호(*연세대학교, 물리학과. [1]부경대학교, 화상정보공학부.*) 본 연구는 pentacene을 이용한 Top-contact 유기 박막 트랜지스터에 밴드갭이 큰 유기물질을 전극과 활성층 사이에 삽입하여 소자 특성을 연구하였다.wet oxidation방법으로 산화실리콘막을 100nm성장시킨 p-Si 기판에 effusion cell을 이용하여 pentacene 500nm을 증착시키고, 마스크를 이용 채널길이가 0.1mm가 되는 Au전극을 성장시켜 기본소자를 제작하였다. 유기물질이 적용된 소자는 pentacene 증착후 마스크를 이용하여 유기물질을 증착하고, Au전극을 성장시켰다. 적용된 유기물은 큰 에너지 갭을 갖는 물질로써 PL(Photoluminescence)측정결과 380nm (~3.2eV)에서 최대 intensity peak을 보였다. 전류-전압측정 결과, pentacene/Au 구조의 유기 박막 트랜지스터에 비해 동일 게이트 전압에서 드레인 전류가 50%증가하였다. 유기물이 삽입된 소자의 포화영역에서의 홀 이동도는 0.14cm^2/Vs, on/off은 10E3였다. in-situ UPS(ultraviolet photoemission spectroscopy) 실험을 통해 I.P(Ionization potential energy)는 약 6.0eV이며, hole injection barrier height는 0.95eV에서 0.74eV로 낮아져 HOMO level 위치가 페르미 준위 쪽으로 더 가까이 있게 되었다. 이러한 결과 기존의 유기박막 트랜지스터의 소자 특성을 향상시켰으며 새로운 유기물의 기능적인 특성을 바탕으로 응용소자까지 기대된다.

**Ep-093** **ZnO-based Nonvolatile Memory Thin-film Transistors With Polymer Ferroelectric Single Gate Insulator** IM Seongil, LEE Gyubaek, OH Min Suk, PARK Chan-ho, LEE Kimoon, LEE Kwang-Hyun(*연세대학교 물리및응용물리학과.*) Field effect transistors with ferroelectric gate insulators (FeFETs) have been extensively researched because of their nonvolatile memory retention and nondestructive readout. Their memory effect originates from the ferroelectric polarization of the gate insulator which leads to modulation of the channel conductance. Very recently, researchers study organic thin-film materials for the nonvolatile memory (NVM) applications, desiring the memory to be realized on plastic or glass substrates. Poly(vinylidene fluoride/trifluoroethylene) (P(VDF/TrFE)) copolymer is one of the attractive ferroelectric polymers for the NVM applications since it has a high remnant polarization (~11.9 $\mu C/cm^2$), short switching time (~1ms), and ease of fabrication in thin-film form by the solution process at a low temperature. However, the P(VDF/TrFE) film usually shows large gate leakage current which deteriorates the performance of the FeFETs because TrFE in the middle of the chain can act as a leakage path. In the present study, we have fabricated ZnO-based top-gate FeFETs with a polymer ferroelectric single-layer gate insulator that was formed on patterned ZnO through sequential spin-casting, baking and quenching process of 240-nm-thick poly_vinylidene fluoride/trifluoroethylene P(VDF/TrFE). A capacitor with P(VDF/TrFE) exhibits the remnant polarization and coercive voltage of 3.5μC/cm² and 14V respectively. Our ferroelectrics gate insulator obtained by the quenching process showed remarkably reduced leakage current of $10^{-9}$A. Although its remnant polarization was only 3.5μC/cm², TFT with the P(VDF/TrFE) single layer exhibits a field effect mobility of 0.026 $cm^2/V$ and quit a good memory hysteresis in the transfer characteristics due to the ferroelectric P(VDF/TrFE). The on/off current ratio is about 10 and the retention time of on current is about 2 hours.

**Ep-094** **Photo-Response From P-Organic/N-ZnO Hybrid Semiconductor Diode** IM Seongil, PARK aaron, LEE kimoon, LEE kwanghyun(*연세대학교 물리 및 응용물리학과.*) We report on the fabrication of p-type organic/n-type ZnO hetero-junction diode and its applications. To construct the organic/inorganic hetero-junction, 100 nm-ZnO is deposited on ITO glass by r.f. magnetron sputtering then pentacene or tetracene as a p-type organic semiconductor are evaporated on ZnO layer. Not only to make an ohmic contact with p-organic layer but also to investigate the photo-response properties of the junction, we adopt the semi-transparent $NiO_x$ electrode with large work-function value of ~5.1 eV and transmittance of ~30 %.Both hetero-junction of p-pentacene/n-ZnO and p-tetracene/n-ZnO show rectifying behavior with current-voltage (I-V) characteristic. Both diodes exhibit high current density but p-tetracene/n-ZnO structure has superior photo-response properties to p-pentacene/n-ZnO. These are because pentacene has a higher mobility value but poorer absorption property than that of tetracene.As a result, we can conclude that our p-pentacene/n-ZnO diode has advantages as an electrical device due to high current density, but p-tetracene/n-ZnO diode has superior potentials as a photodetector in the visible and ultraviolet range.

**Ep-095** **Quantification of Channel Thickness Induced Resistance in Pentacene Thin Film Transistors** IM Seongil,

MUN Sungjin, CHOI jeongmin, LEE Kwanghyun(*연세대학교, 물리 및 응용물리학과.*) We report the influence of active layer thickness on the resistance of pentacene-based thin-film transistors (TFTs). Indium-Tin-Oxide (ITO) gate electrodes were patterned by wet etching. Polymer dielectric with a thickness of 230 nm was then deposited by spin casting of poly-4-vinylphenol (PVP). Our pentacene active layers were deposited in the thickness range of 15 – 200 nm by thermal evaporation on dielectric films. The Au source/drain electrodes were finally deposited by thermal evaporation. Another sample was used different gate electrode and dielectric materials. Heavily doped p-type Si and thermally grown $SiO_2$ was used as a gate electrode and dielectric, respectively. Pentacene active layers were deposited in the thickness range of 15 – 100 nm by thermal evaporation on 200 nm $SiO_2$.In the case of $SiO_2$ dielectric, thinner pentacene layers displayed higher drain current ($I_D$). $I_D$ decreased with the channel thickness from -5.3 to -0.41 mA at $V_G$ and $V_D$ of -20 V. And, the field effect mobility (μ) was reduced from 0.65 to 0.41 $cm^2$/Vs. As well, channel thickness induced resistance increased from 0.16 to 0.65 MΩ.However, in the case of PVP dielectric, $I_D$ increased to -4.6 mA until pentacene active thickness increase up to 50 nm-thick, but over the 50 nm, it decreased from -4.6 mA to -2.5 mA as pentacene active thickness increased from 50 to 200 nm. Also, Resistance of active layer thickness decreased from 35 to 15 MΩ until pentacene active thickness increase up to 50 nm, but over the 50 nm it increased. We thus regard the 50 nm as an optimum channel thicknessWe assume that the difference between above two cases may arise from the different crystalline growth of pentacene layer on PVP and $SiO_2$ dielectrics. More quantitative details on the channel thickness will be discussed in the conference.

**Ep-096** **A biofuel cell with enhanced performance by enzymes immobilized on polypyrrole nanowire array** 김 지헌, 양 정도, 오 세재, 유 경화[1](*연세대학교 물리학과. [1]연세대학교 물리학과, 연세대학교 나노메디컬 국가핵심연구센터.*) We developed one-compartment glucose/$O_2$ biofuel cells using enzymes immobilized polypyrrole (PPy) nanowires as electrodes and micro-fluidic channels. The PPy nanowires modified with enzymes such as glucose oxidase and laccase were synthesized through electrochemical polymerization of pyrrole with enzymes and mediators inside the pores of anodized alumina oxide (AAO) membranes. The biofuel cells were characterized in phosphate buffered saline (PBS), pH 7 solution containing 15 mM of glucose. The maximum power density of the cell with the nanowires was found to be higher than the biofuel cells with the flat electrodes by at least 10 times under the same condition probably due to the increase in surface area of electrodes.

**Ep-097** **Reversible Resistive Switching Behaviors in NiO Nanowires** 김 성인, 이 재학, 장 영욱, 황 성식[1], 유 경화[2], 여 운진(*연세대학교 물리학과. [1]연세대학교 나노메디칼 국가핵심연구센터. [2]연세대학교 물리학과, 연세대학교 나노메디칼 국가핵심연구센터.*) Recently, resistive switching phenomena in binary transition metal oxides such as NiO, $TiO_2$, etc. have received considerable attention because of their potential application in non-volatile memory devices. However, these resistive switching behaviors have been reported only in metal oxide thin films, but not in metal oxide nanowires. Here, we have investigated for the first time the reversible and bistable resistive switching behaviors in NiO nanowires. NiO nanowires were fabricated by electrodepositing Ni inside an anodized aluminum oxide (AAO) membrane and oxidizing the Ni nanowires. As in NiO films, unipolar and bistable resistive switching phenomena were observed for both individual NiO nanowires and vertically aligned nanowire arrays. However, compared with NiO films, the forming process took place at much lower electric fields in NiO nanowires, probably due to the grain boundaries being nearly connected through the entire length of the nanowires and metallic Ni defect in the grain boundaries. As a result, the 1 um-long individual NiO nanowire operated successfully under 2.5 V and 0.23 mA. In addition, we have measured the resistive switching properties of the NiO nanowires vertically aligned inside an AAO membrane by using a W tip as the top electrode. Reproducible resistive switching behaviors were clearly seen below 20 V even for 25 um-long NiO nanowires. Therefore, these results demonstrate the feasibility of the development of high-density nanowire-based resistance memory device arrays.

**Ep-098** **Surface plasmon resonance enhanced photoconductivity of gold nanoparticles embedded mesoporous $TiO_2$ nanofibers** YOO Kyung-Hwa, SON Min Soo, IM Ji Eun[1], WANG Kang-Kyun[1], OH Seung-Lim[1], KIM Yong-Rok[1](*Yonsei University, Department of physics. [1]Yonsei University, Department of chemistry.*) We have studied the influence of surface plasmon resonance (SPR) on the photoconductivity in the Au nanoparticle embedded $TiO_2$ nanofibers. Approximately 10 nm – diameter Au nanoparticles were immobilized in mesoporous nanofiber matrix by means of wet chemistry. Clear Coulomb oscillations were observed at 4.2 K, suggesting that Au nanoparticles embedded inside the pores of $TiO_2$ act as metal islands and $TiO_2$ as tunneling barriers. In addition, the absorption spectra exhibited the SPR peak in the visible light range because of the presence of Au nanoparticles. More remarkably, fabricated single nanofiber device shows direct current enhancement by the plasmon excitation. A strong wavelength dependence of current is also measured. These results show the potential of using gold filling mesoporous nanofibers as wavelength-controlled optical nanoswitches.

**Ep-099** **암모니아 분자의 흡착에 의한 탄소나노튜브 전계트랜지스터의 전기이력 강화** 김 상훈, 윤 용주, 이 형락[1], 이 삼녕[2], 하 동한(*한국표준과학연구원. [1]경북대학교. [2]한국해양대학교.*) 탄소나노튜브 전계트랜지스터(CNT-FET)는 게이트전압을 인가할 때 전기이력(hysteresis)을 나타낸다. 본 발표에서는 암모니아 분자의 흡착에 의하여 CNT-FET의 전기이력특성이 증가하는 것을 보이고, 그 원인에 대해서 논의한다. 암모니아는 탄소나노튜브에 전자를 주는 분자로서 탄소나노튜브에 흡착되면 전류-게이트전압 곡선 상의 문턱전압(threshold voltage)을 좌측(즉, 음전위 방향)으로 이동시킨다고 알려져 있다. 그러나 게이트전압을 양의

전압에서 음의 전압으로 변화시킬 경우, 암모니아 가스의 농도가 증가함에 따라 CNT-FET의 전류-게이트전압 곡선의 전기이력의 크기는 증가하며 문턱전압은 예상과는 달리 우측으로 이동하였다. 반면에 일반적으로 탄소나노튜브로부터 전자를 빼앗는 분자로 알려진 산소의 경우는 문턱전압 이동의 역전현상은 나타나지 않았다. 암모니아에 의한 문턱전압 이동의 역전현상은 탄소나노튜브와 절연층 사이 및 그 주위에 흡착된 암모니아 분자가 인가된 양의 게이트 전압으로 인하여 전자를 포획할 수 있음(charge trapping)을 의미한다. 흡착된 분자의 전자포획에 의한 전기이력특성의 변화를 이용하면 CNT-FET를 메모리 소자로서 응용할 수 있을 것으로 기대된다.

**Ep-100** **온도에 따른 네마틱 액정셀의 잔류전압 측정** 장 태석, 오 유미, 김 종현(*충남대학교, 물리학과.*) 액정 디스플레이는 생산공정 과정에서 불순물이 포함되거나 구동 중에 불순물이 생겨나게 된다. 이러한 이온들은 외부전압에 의해 액정셀의 액정층과 배향막 사이에 흡착되고, 흡착된 이온에 의해 액정층에 전압이 가해지는데 이를 잔류전압이라 한다. 본 연구는 온도에 따른 네마틱 액정셀의 잔류전압을 측정하여 그 변화를 관찰하는 것이다. 잔류전압 측정방법은 액정셀에 교류전압을 인가한 상태에서 액정셀의 투과율을 측정하고, 직류전압을 특정시간 동안 인가한 후 교류전압을 인가하여 투과율을 측정한다. 이 두 경우의 투과율 차이를 이용하여 액정셀의 잔류전압을 측정하였다.

**Ep-102** **n-ZnO/p-CNTs heterojunction photodiode** 장 영욱, 강 봉근, 손 민수, 박 민지, 유 경화(*연세대학교, 물리학과.*) We have fabricated n-ZnO/p-CNTs heterojunction photodiode. Aligned p-CNTs were grown on $SiO_2$/Si substrate by thermal CVD. And then, n-ZnO thin film was deposited to make the exhibited clear diode behaviors. Under illuminating of UV light, however, photoswitching was observed at reverse bias voltage.

**Ep-103** **Passivation Effects on ZnO Nanowire Field Effect Transistors under Ambient, Oxygen, and Vacuum Environments** SONG Sunghoon, HONG Woong-Ki, KWON Soon-Shin, LEE Takhee(*Gwangju Institute of Science and Technology, Department of Materials Science and Engineering.*) ZnO nanowires are important materials for nanodevices such as ultraviolet lasers, light-emitting diodes, photodetectors, chemical sensors, and solar cells, due to their direct wide bandgap (3.4 eV) semiconducting properties and large exciton binding energy (60 meV). The electronic properties of ZnO surfaces are strongly affected by the chemical adsorption of ambient gases, primarily oxygen.[1,2] This is due to the change of conductivity caused by surface energy band bending, induced by $O_2$ molecule adsorption.[2] Therefore it is desirable to study their electrical properties as required for wider device applications. In this presentation, we report on a study of the before and after passivation effects on the ZnO nanowire field effect transistors (FETs) under different oxygen environments of ambient air, dry $O_2$, and a vacuum. The FET devices were fabricated with ZnO nanowires, and were protected with a polymethyl methacrylate (PMMA) layer. The electrical properties of the ZnO nanowire FETs were investigated and compared before and after the PMMA passivation under various environments.

References

[1] J. Lagowski, E. S. Sproles Jr, and H. C. Gatos, *J. Appl. Phys.* **48**, 3566 (1977).

[2] Z. Y. Fan, D. W. Wang, P. C. Chang, W. Y. Tseng, and J. G. Lu, *Appl. Phys. Lett.* **85**, 5923 (2004).

**Ep-104** **The Design of Conduction Cooled Superconducting Magnet for Magnetic Separation** 이 병섭, 김 동락, 양 형석, 최 연석, 정 원묵(*기초과학지원연구원.*) 초전도 자석을 이용한 자기분리에 대한 연구가 진행됨에 따라 보다 전문적으로 자기분리에 적합한 초전도 자석의 개발이 요구되고 있다. 이러한 자기 분리용 초전도 자석의 개발을 위해서는 자성 입자의 자기장내에서의 거동 해석과 연계된 설계 방법이 필요하다. 본 연구에서는 자성 입자의 거동 인자를 포함하는 초전도 자석 설계 방법을 제시하고, 자성 입자의 자화율과 입자 크기를 변수로 자기장내 거동 해석을 수행하여 그 유효성에 대한 검토를 수행한다.

**Ep-105** **The Design of Prototype Main Magnets for K120 Superconducting Cyclotron** 이 병섭, 김 동락, 최 연석, 양 형석, 강 준선[1], 김 유석[1](*기초과학지원연구원. [1]원자력의학원.*) 국내의 싸이클로트론에 관한 연구는 방사선 의학을 이용한 암 치료를 목적으로 시작되었다. 싸이클로트론에 관련된 국내 연구 개발 역량이 커짐에 따라, 초전도 자석을 이용한 보다 높은 에너지의 싸이클로트론의 개발이 가능하게 되어 2007년 이후로 현재까지 진행중이다. 개발중인 K120 싸이클로트론은 다양한 탄소 이온을 가속하는 것을 목적으로 하며, 이 논문에서는 현재까지 진행된 싸이클로트론용 초전도 자석의 설계에 대한 결과와 관련된 토의 사항을 기술한다.

**Ep-106** **Carbon Nanotube - Based Biosensor for Detection of Matrix metallopeptidase 9(MMP9)** 이 형섭, 오 제승[1], 유 승환, 장 영욱, 유 경화, 박 윤정(*연세대학교, 물리학과. [1]연세대학교, 나노메디컬협동과정.*) We have fabricated carbon nanotube-based biosensors with the field-effect transistor structure and detected matrix metallopeptidase 9. To minimize the contact effects, the metal contacts were passivated using $SiO_x$ films and the chemical linker, 1-Pyrenebutyric acid N-hydroxy-succinimide ester, was used for immobilization of anti-MMP9 on the carbon nanotube surface. After binding MMP9 to anti-MMP9, the gate voltage was found to shift to negative gate voltages and the conductance at zero gate voltage decreased. We have also detected MMP9 in real time using the microfluidic channels.

**Ep-107** **전자빔에 조사된 고분자의 광학적 특성변화** 이 혁무, 조 성오(*KAIST, 원자력 및 양자공학과.*) 전자빔 조사에 의하여 다양한 폴리머에서 광흡수도, 발광특성 및 광학적 밴드갭의 변화가 관찰되었다. 전자빔은 $2\times10^{-5}$ torr 이하의 고진공 조건하에서 열전자 방출법으로 생성된 전자를 35 kV로 가속하였으며, 열에 의한 추가적인 변화요인을 제거하고자 빔 전류 밀도는 5 μA $cm^{-2}$로 고정하였다. 전구체 폴리머로서는 Poly(1-vinylnaphthalene), Poly(9,9-dioctyl-2,7-divnylenefluorenylene)-alt-co-(9,10-anthracene), poly[2-methoxy-5-(2'-ethyl-hexyloxy)-1,4-phenylene vinylene], poly

(9,9-dioetylfluoreny-2,7-diyl), poly(3-hexyl thiophene), (poly N-vinyl carbazole) 을 사용하였다. 전자빔 조사에 의한 발광특성의 변화는 형광 분광법을 이용하여 측정하였으며, 흡수도 및 광학적 밴드갭의 변화를 위하여 UV/Vis 분광법을 이용하였다. 특히, 전자빔 조사에 의해 야기되는 폴리머의 광학적 밴드갭의 변화는 전자빔 조사방법이 반도체 폴리머를 기반으로 하는 electro-optic 분야에 유용하게 사용될 수 있음을 제시한다.

**Ep-108** **분광타원편광분석법으로 측정된 InP 광특성의 온도의존성에 관한 연구** 강 유진, 김 태중, 공 태호, 정 용우, 변 준석, 김 영동(*경희대학교 물리학과.*) InP 는 광통신 소자 등에 폭넓게 이용되는 $In_xGa_{1-x}As_yP_{1-y}$ 화합물의 endpoint 이며 다양한 소자의 기판으로 이용되는 중요한 물질이다. 최적화된 특수 소자 적용과 개발을 위해서 정확한 유전함수의 값과 밴드갭 분석이 필요하다. InP 의 광특성은 크라머스-크로니히 관계를 사용하지 않고 유전율 함수를 측정하는데 탁월한 분광타원편광분석법에 의해 정확히 알려져 있다. 그러나 상온에서는 $E_2$ 밴드갭 영역에 많은 밴드갭들이 중첩되어있어, 정확한 밴드갭분석을 할 수 없기 때문에 저온에서의 유전율 함수가 필요하다. 저온에서의 연구는 제한된 에너지 영역인 1.3 ~ 5.5 eV 에서만 보고된바 있다. 따라서 본 연구에서는 더 넓은 스펙트럼 에너지 영역인 0.73 ~ 6.48 eV 와 온도범위 25 ~ 700 K 에서 분광타원편광분석법으로 연구를 하였다. 온도가 감소함에 따라, 열 수축으로 인하여 임계점이 청색이동을 하고 전자-광자 상호작용의 감소로 인하여 중첩된 밴드갭의 분리를 관찰 할 수 있었다. 그 결과 저온 측정에서는 상온에서 불가능한 $E_2$ 밴드갭 영역에서 중첩된 4개의 임계점 ($E_0$'(Γ), $E_0$'(Δ), $E_2$, $E_0$'+$\Delta_0$') 을 명확히 분석 할 수 있었다. 또한, 우리는 처음으로 광자 에너지 5.5 eV 이상에서 $E_2$' 과 $E_1$' 두 임계점의 온도의존성을 얻을 수 있었다. 우리는 이 결과들이 InP 를 기반으로 한 광전자 소자의 개발과 밴드계산, 그리고 실시간 모니터링에 유용하게 사용될 것이라고 생각된다.

**Ep-109** **분광타원편광분석법을 이용한 $BaSm_2Ti_4O_{12}$ 박막의 광특성 연구** 황 순용, 윤 재진, 차 영훈, 김 승, 김 영동, 정 영훈[1], 남 산[2](*경희대학교 물리학과. [1]한국요업기술원. [2]고려대학교 신소재공학과.*) 반도체 소자의 고직접화를 위해서는 metal-insulator-metal (MIM) capacitor 의 크기도 작아져야 한다. Insulator 물질로 기존에 사용 되어 왔던 $SiO_2$나 $Si_3N_4$ 등의 물질은 한계가 있어, 더 좋은 효율을 위해서 microwave dielectric materrials 의 연구가 주목 받고 있다. 하지만 고유전율을 가지는 microwave dielectric materrials 들의 정확한 광특성은 거의 보고되지 않고 있어, 본 연구에서는 좋은 microwave dielectric 특성을 가지는 $BaSm_2Ti_4O_{12}$ (BST) 박막을 분광타원편광분석법을 이용하여 분석해 보고자 한다. 분석에 사용될 BST 박막은 rf-magnetron sputtering 을 이용하여 증착하였고, 두 가지 thermal annealing 조건에 대하여 세가지 deposition 온도 조건으로, 각각 6 개의 BST 박막을 비교 분석하였다. BST 박막의 광특성 측정에는 분광타원편광분석기를 사용하여 1.5 에서 6.5 eV 의 에너지영역을 50, 55, 60, 65, 70 도의 입사각으로 측정하였다. 측정된 박막의 유전율 함수 분석은 Tauc-Lorentz 모델로 분석하였으며, 분석된 Tauc-Lorentz 모델의 변수들의 해석으로 BST 박막에 있어서 deposition 온도 조건 보다는 thermal annealing의 과정이 결정화에 더 중요한 영향을 미친다는 것을 알 수 있었다

**Ep-110** **Study for Gadolinium Extraction using Metal Ion Implanter** TRINH Tu Anh, HONG In Seok, LEE Hwa Ryun, CHO Yong Sub(*PEFP, KAERI.*) In Gadolinium, a rare earth element, the partially filled 4f electron orbital is located relatively close to the nucleus and is shielded very efficiently by the outer electrons. Due to this shielding, the intra 4f shell transitions result in very sharp optical emissions. As silicon is implanted by $Gd^+$ ions, it can emit photoluminescence, which is widely applied in optical communication. In this study, the $Gd^+$ extraction condition by metal ion implanter, beam shape and depth profile were studied. The authors find that extraction current is 2μA and beam size is 1cm x 1cm. We irradiated 50 keV $Gd^+$ beam into silicon wafer with dose of $1x10^{17}$ ion/$cm^3$. The depth profile was determined by Rutherford Back Scattering (RBS). Photoluminescence spectra of Gd-doped Si nanocrystal is also study. Detail of our work will be discussed in this report.
* This work is supported by Ministry of Education, Science and Technology of Korea

**Ep-111** **Metal-Insulator Transition (MIT) device application with Transistors** 서 기완, 김 봉준[1], 이 용욱[2], 윤 선진, 김 현탁(*한국전자통신연구원, MIT 소자팀 - 과학기술연합대학원대학교, 차세대소자공학과. [1]한국전자통신연구원, MIT 소자팀. [2]한국전자통신연구원, MIT 소자팀 - 부경대학교, 전기제어공학부.*) Metal-Insulator Transition (MIT) devices switched by the external voltage are fabricated by a pulsed laser deposition (PLD). The current jump of these devices in I-V curves occurs around 10 V. For several applications of the MIT, we have observed the changes of MIT jump voltages ($V_{MIT}$) and the voltage (or current) oscillation on a composite device of the MIT device and a typical transistor such as BJT and FET. $V_{MIT}$ is increased when the external resistor is serially connected. For the composite devices, whereas, $V_{MIT}$ shows an interesting behavior. These devices can be used for potential applications of temperature sensors and frequency-controllable electrical devices.

**Ep-112** **Electrical Characterization of ZnO Nanowire Field Effect Transistors with High-k $Al_2O_3$ Gate Dielectric Layers** SEO Jaeduck, JO Gunho, MAENG Jongsun, KWON Soon-Shin, HONG Woong-Ki, JO Minseok, HWANG Hyunsang, LEE Takhee(*Gwangju Institute Science and Technology, Department of Materials Science and Engineering.*) One-dimensional nanostructures including carbon nanotubes and semiconductor nanowires are promising materials for future nanoelectronic applications. Among these, the ZnO nanowire with a wide bandgap (~3.4 eV) and large exciton binding energy (~60 meV) has attractive attention for diverse nanoscale devics such as field effects transistors (FETs), chemical sensors, light-emitting devices, and photodetectors [1-3]. In particular, the nanowire FETs with $SiO_2$ dielectric layer have been intensively investigated as the fundamental element for integrated circuits. In contrast, high-k gate dielectric materials such as $HfO_2$, $Al_2O_3$, and silicates have been integrated with Si CMOS technology to overcome the gate leakage current and to improve device

performance.[4] In this study, we have investigated the electrical characteristics of the ZnO nanowire FETs with high-k $Al_2O_3$ gate dielectric layer. The controlled-thickness $Al_2O_3$ films were deposited by atomic layer deposition. The equivalent oxide thickness (EOT) to confirm the gate leakage current is obtained by taking the capacitance value measured for dielectric $Al_2O_3$ layers. As the thickness of the gate dielectric $Al_2O_3$ layer was reduced, the source-drain current, the transconductance and mobility increased due to the large capacitance and the threshold voltage shifted toward the negative gate bias direction.

[1] W.-K. Hong, J. I. Sohn, D.-K. Hwang, S.-S. Kwon, G. Jo, S. Song, S.-M. Kim, H.-J. Ko, S.-J. Park, M. E. Welland, and T. Lee, Nano let. 8, 950 (2008) [2] W.I Park, G. C. Yi, M. Kim, and S. J. Pennycook, Adv. Mater. 15, 526 (2003) [3] J. Goldberger, D. J. Sirbuly, M. law, and P. Yang, J. Phys. Chem. B. 109, 9 (2005) [4] M. L Green, E. P Gusev, R. Degrave and E. Garfunkel, J. Appl. Phys. 90, 2057 (2001)

**Ep-113** **Complementary Logic Circuits Based on Hybrid Nanodevices of SWNT and ZnO Nanowire FETs** JO GUNHO, HONG WOONG-KI, SOHN JUNG INN[1], JO MINSEOK, SHIN JIYONG, WELLAND MARK E.[1], HWANG HYUNSANG, GECKELER KURT E., LEE TAKHEE(*Department of Materials Science and Engineering, Gwangju Institute of Science and Technology, Gwangju 500-712, Korea. [1]Nanoscience Centre, University of Cambridge, Cambridge CB3 0FF, UK.*) Recently, we demonstrated that SWNT FETs show a high tolerance against proton radiation [1], while the electrical characteristics of ZnO nanowire FETs are sensitively influenced by the surface trap states at the interface between the ZnO nanowires and dielectric layer [2]. In this presentation, we report predictable and controllable complementary logic circuits based on hybrid nanodevices comprising p-channel SWNT and n-channel ZnO nanowire transistors. Using this hybrid approach, we demonstrated a complementary inverter, NOR and NAND logic gates, and a static random-access memory (SRAM) cell with an operation superior to devices and circuits based on a single carrier type and/or diodes [3-5].

[1] Woong-Ki Hong et al, *Nanotechnology* 17, 5675-5680 (2006). [2] Woong-Ki Hong et al, *Nano Lett.* 8, 950-956 (2008). [3] Yi Cui et al, *Science* 291, 851-853 (2001). [4] Adrian Bachtold et al, *Science* 294, 1317-1319 (2001). [5] Won Il Park et al, *Adv. Mater.* 17, 1393-1397 (2005).

**Ep-114** **Performance of Pd-Pt/WO3 as a hydrogen sensor material in various environments** 심 재영, 이 재동, 진 정모, 정 현식(*서강대학교 물리학과.*) 신재생 에너지의 수요가 급증하고 있는 가운데, 유력한 대체 에너지원인 수소 에너지에 대한 관심 역시 높아져 가고 있다. 하지만 공기 중에서 4% 이상의 농도에서 폭발의 우려가 있는 수소를 안전하게 사용하기 위해서 수소 누출을 조기에 검지할 수 있는 센서기술이 매우 중요한 요소이다. 지금까지 학계와 업계에 소개된 많은 센서 중 특히 광학식 수소 안전센서는 수소 누출이 의심되는 지역에서 오랜 기간 속에서도 수소 누출을 감지할 수 있어야 하기 때문에 높은 신뢰성과 안정성이 요구된다. 이것은 수소 센서 박막으로 사용되는 WO3 기반의 가스채색 물질이 주변의 환경에 대하여 얼마나 안정한 가운데 수소 검지가 가능한지의 여부에 달려있다고 할 수 있다. 그러므로 본 연구에서는 주변 환경의 조건에 따라 수소 센서에 사용되는 박막물질인 Pd-Pt/WO3의 특성이 어떻게 변화하는지를 연구하였다. 스퍼터링으로 Pd-Pt/WO3 수소센서 박막을 제작한 후, 박막의 수소 가스에 대한 선택성을 연구하기 위하여 수소가스 및 유기용매를 포함한 각종 기체들에 노출시켰을 때 박막의 투과도 변화를 측정하였다. 또한 in-situ Raman 분광법을 사용하여 각종 기체에 노출되었을 때 수소센서 박막이 어떤 반응을 보이는지 연구하였다. 뿐만 아니라 주위 온도를 변화시켰을 때 센서 반응이 적절하게 일어나는지 역시 in-situ Raman 분광법을 사용하여 확인하였다. 그 결과 Pd-Pt/WO3 박막은 수소 기체를 제외한 다른 기체에서 특별한 광투과도 변화를 보이지 않았으며 Raman 분광 결과 역시 수소기체의 경우를 제외하고는 특별한 변화를 보이지 않았다. 또한 온도를 -20도 내외에서 50도 내외의 주위 온도 변화에서도 수소 센서 박막의 반응이 적절하게 일어나는 것을 확인할 수 있었다.

**Ep-115** **켈빈 재정의와 음향기체온도계를 이용한 열역학적 온도 측정** 양 인석, 김 용규, 강 기훈(*한국표준과학연구원.*) 현재 열역학적 온도의 단위인 켈빈(kelvin)은 물의 삼중점의 열역학적 온도의 1/273.15 로 정의되어 있다. 이를 포함하여 다수의 기본단위를 물리학의 기본 상수를 이용하여 재정의하려는 노력이 국제적으로 진행되고 있다. 열역학적 온도 정의와 관련되는 기본 상수는 볼쯔만 상수이며, 볼쯔만 상수에 약속된 값을 지정함으로써 켈빈을 재정의할 수 있다. 현재의 온도 정의와 연속성을 갖도록 정의하기 위해서 볼쯔만 상수를 물의 삼중점 부근에서 정밀하게 측정하여야며, 그 방법으로는 음향기체온도계, 유전상수 온도계, 잡음온도계 등을 이용한 것이 있다. 또한 열역학적 온도 측정을 위한 다양한 실험 방법과 연구 진행 상황을 알아보고, 현재 한국표준과학연구원에서 진행하고 있는 음향기체온도계를 이용한 열역학적 온도 측정의 원리와 진행 상황을 정리해본다.

**Ep-116** **Luminescence Properties and Upconversion Dynamics of CNGG:$Tm^{3+}$ Crystal** 김 은식, 장 경혁, 시 량, 서 효진(*Department of Physics, Pukyong National University.*) Luminescence properties of $Tm^{3+}$ ions doped in Calcium Niobium Gallium Garnet $Ca_3Nb_{1.6875}Ga_{3.1875}O_{12}$ (CNGG) crystal are investigated by laser excitation spectroscopy in the temperature region 15 K – room temperature. Luminescence spectra in a spectral region of 400-850 nm are investigated under excitation into various excited states of $Tm^{3+}$ and conduction band of CNGG crystal. The emission band of $Tm^{3+}$ doped CNGG are observed to be broader than those observed in other $Tm^{3+}$ doped crystals. This is due to the disordered structure of CNGG. CNGG crystal has a disordered structure due to enormous variety of different types of ions and cationic vacancies in the regular sites of host lattice. The emissions spectra observed the upconversion by the excitation with 786 nm. The 786 nm light irradiations correspond to excitation into the $^3H_4$ state of $Tm^{3+}$. It is describe the mechanism and dynamics of the upconversion emission in $Tm^{3+}$ doped CNGG.

**Ep-117** **Luminescent Properties and Crystallographic sites**

**of the $Eu^{3+}$ doped in $BaY_2O_4$** 시 량, 장 경혁, 김 은식, QIAO Xuebin, 서 효진(*부경대학교.*) The $Eu^{3+}$ doped $BaY_2O_4$ samples were prepared by High-temperature solid-state reaction and sol-gel methods. X-ray powder diffraction (XRD) analyses confirmed the pure phase of $BaY_2O_4$. Scanning electron microscopy (SEM) measurements indicated the crystalline and size distribution of $BaY_2O_4$:$Eu^{3+}$. The excitation and emission spectra were measured. The site-selective excitation, emission spectroscopy, and luminescence decay have been investigated in the $^5D_0$-$^7F_0$ region under a pulsed, tunable, narrowband dye laser, which shows three different $Eu^{3+}$ sites in $BaY_2O_4$.

**Ep-118** **Vacuum ultraviolet and ultraviolet spectroscopy of $Eu^{3+}$ activated buchwaldite $NaCaPO_4$** HUANG Yanlin, 시 량[1], QIAO Xuebin[1], 장 경혁[1], 김 은식[1], 서 효진[1](*College of Chemistry, Chemical Engineering and Materials Science, Soochow University, China. [1]Department of Physics, Pukyong National University.*) A red emitting phosphor, $Eu^{3+}$-doped buchwaldite $NaCaPO_4$, has been prepared using sol–gel method. X-ray powder diffraction (XRD) analyses confirm the pure crystalline phase of $NaCaPO_4$. The morphologies of the phosphor were investigated by scanning electron-microscopy (SEM), which indicated that the phosphor had a good-quality of surface crystallization. This phosphor had the grain sizes of around 500 nm with fairly narrow size distribution. The vacuum ultraviolet (VUV) synchrotron radiation spectroscopy technique was applied to study the luminescence properties of this phosphor. The excitation spectra revealed that there is an efficient energy transfer from the host to $Eu^{3+}$ ions. Upon excitation with VUV and UV radiation, the phosphor show strong red-emission at around 611 nm corresponding to the forced electric dipole $^5D_0 \rightarrow {}^7F_2$ transition of $Eu^{3+}$ ions.

**Ep-119** **Extreme Ultraviolet 광원을 이용한 Mask의 반사도 측정 및 AIMS, EUV-IL 장비 구축에 대한 연구** 박 찬훈, 정 윤하, 김 성규[1], 정 성우[1], 전 영권[1], 김 동수[2](*포항공과대학교 전자전기공학과. [1]나노기술집적센터. [2]VMT.*) EUVL(Extreme Ultraviolet Lithography)은 13.5nm의 파장을 이용한 기존의 반도체 집적화 한계를 극복할 수 있는 차세대 반도체 리소그래피 기술로서 32nm급 이하의 DRAM, FLASH 메모리 등에 적용될 것으로 예상된다. 본 연구에서는 Extreme ultraviolet (EUV) 을 이용하여 EUV blank mask의 반사도 측정을 수행하였으며, mask의 결함검사를 위한 AIMS와 간섭광을 이용하여 주기적인 패턴을 구현하기 위한 EUV interference lithography (IL) 장치를 구축하였다. 광원으로는 포항가속기연구소의 11B 빔라인의 EUV 광원을 사용하였고 기존 설치된 reflectometer를 이용하여 mask의 반사율 측정을 통하여 mask의 성능 평가를 실시하였다. 마스크의 반사도는 입사각이 84도 일 때 파장 13.5 nm 에서 약 57%를 얻을 수 있었으며 이론적으로 계산한 70%에 근접함을 확인하였다. 또한 AIMS의 image mode와 scanning mode를 이용한 mask 패턴 관측과 mask의 결함 분석을 확인하는 설비를 구축하였다. EUV-IL 장치는 간섭현상을 이용한 장치로 투과형 grating mask를 이용하며 사용되는 grating의 배치에 따라 간섭에 의한 주기적인 패턴을 형성한다. 본 연구에서는 grating mask의 디자인을 이론적으로 접근해 선폭과 간격을 달리한 grating을 제작하였다. EUV-IL은 기존의 EUVL에서 요구되는 복잡한 광학계를 이용하지 않고 간단한 설계를 통한 주기적인 패턴을 만드는 것으로 포항가속기연구소의 3A undulator 빔라인에 구축하였고 향후 여러 연구 분야에 사용될 것으로 기대한다.

* 본 연구는 지식경제부 지원 나노기술집적센터 구축사업과 나노급 반도체용 EUV 리소그래피 핵심기술 개발사업의 일환으로 수행되었음.

**Ep-120** **TEI 이론에 의한 자동차 브레이크 디스크의 열적 특성 평가** 김 석원, 최 병민, 김 진복[1], 이 봉현[2](*울산대학교, 물리학과. [1]명화공업(주). [2]자동차부품연구원.*) 자동차의 안정성을 위하여 중요한 역할을 수행하는 제동장치는 브레이크 디스크, 패드, 캘리퍼 등으로 이루어져 있다. 캘리퍼는 패드를 잡아주는 역할을 하며, 브레이크 디스크와 패드의 접촉에 의한 마찰을 통해 자동차는 멈추게 된다. 디스크와 패드의 접촉에 의해 발생된 열은 디스크 표면에 큰 영향을 미치며 자동차 성능저하의 주된 원인이 된다. 그래서 자동차 제동장치의 설계에 있어서 반드시 열에 의한 현상을 고려해야 한다. TEI(ThermoElastic Instablities) 이론은 디스크 표면에 발생된 열에 의한 현상을 나타내는 대표적인 이론 중의 하나로서, 디스크 표면에 발생된 열이 극소부분에 응집하여 핫스팟(Hot Spot)이 나타나며, 디스크에 열탄성 불안정성(TEI)을 일으킨다는 것이다. 핫스팟에 의한 열탄성 불안정성은 디스크의 성능을 저하시키는 Judder를 발생시킨다. 본 연구에서는 알루미늄과 주철로 각각 이루어진 브레이크 디스크에 TEI 이론을 적용시켜 임계속도와 디스크 표면의 온도 변화를 나타내는 지수 σ를 측정하여 브레이크 디스크의 안정성을 비교 • 분석하였다. 임계속도는 브레이크 디스크가 열적 안정성을 가지는 최대속도이며, σ는 브레이크 디스크의 열적 안정성과 불안정성을 확인할 수 있는 중요한 지표이다.

**Ep-121** **Near-field EMI Shielding Characteristics Of Multi-walled Carbon Nanotube/poly(methyl-methacrylate) Composites Using Micro-strip Line** 주 진수, 김 성환, 이 진우, 이 정엽, 배 상원(*물리학과.*) 다양한 질량비의 다중벽 탄소 나노 튜브(MWCNT)와 poly(methyl-methacrylate) (PMMA)를 혼합하여 두께가 100 ~ 200 μm인 복합체 필름을 제조하였고, 근역장과 원역장에서의 전자기파 차폐 특성을 측정하였다. 복합체를 고르게 분산시키기 위해 high power sonosmasher로 초음파 처리하였다. 원역장에서 EM-2107A와 2 ports flanged coaxial line holder를 사용하여 50MHz에서 13.51GHz 영역에서 전자기파 차폐 효율을 측정하였고, 근역장에서는 micro strip line (MSL)과 MSL 위에 loop 와 rod 안테나를 사용하여 주파수 50 MHz부터 1.5 GHz 대역에서 전자기파 차폐 특성을 측정 및 분석하였다. MWCNT의 질량비가 높아질수록 전기 전도도와 근접장 및 원역장 영역에서 전자기파 차폐 효율은 증가하였다.

**Ep-122** **극미량 수분 발생 기술** 최 병일, 우 상봉, 김 종철(*한국표준과학연구원.*) 극미세 수분의 조절은 첨단산업의 진보에 있어 매우 중요한 문제이다. 반도체 공정이나 디스플레이 산업 등과 같이 첨단기술을 필요로 하는 많은 공정에서는 오염물질 특히 수분은 재품의 물성에 크게 영향을 미쳐 제품의 품질을 좌우하게 된다. 실제로 반도체 공정에서 미세한 수분의 양은 실리콘 기

관 위의 박막의 성장이나 질에 상당한 영향을 미치는데, 첨단 반도체 공정의 발달은 지난 20년 동안 최대허용 불순물의 양을 $10^{-4}$ 배 줄임으로서 가능하였고, 현제 공정에서는 수 ppb 이하의 수분이 포함된 고순도 가스를 요구하고 있다. 본 연구는 이러한 산업계의 요구에 부응하여 ~ppb 정도의 정밀 습도 발생장치를 개발하여 10 nmole/mol ~ 130 μmol/mol 영역의 습도 표준을 확립하였다. 이는 반도체 등 첨단산업의 기술개발에 크게 기여할 것으로 기대된다.

**Ep-123** **Measurement of Extra-Low Water Vapor Permeation Rate for OLED Displays** 최 병일, 우 상봉, 김 종철 (*한국표준과학연구원.*) Flexible organic light emitting devices (OLEDs) are considered to be a next-generation display technology. However, since the materials currently used in OLEDs are highly sensitive to water vapor, a low-water vapor permeation measurement technology is essential to the development of flexible barrier substrates for the encapsulation of the OLEDs.This study developed a testing device for water vapor permeation in the range of ($10^{-3}$~$10^{-6}$) [g/m$^2$ day], which is necessary for the display industry, by using water that included tritium, a radioactive isotope. This method enabled an absolute quantitative measurement of water vapor permeation.Uncertainty of the established apparatus was about 1.88 x $10^{-6}$ [g/m$^2$ day] with respect to a specimen having a water vapor permeation of $10^{-5}$ [g/m$^2$ day], but it is expected that this testing range could be expanded if the temperature of the test chamber were increased.

**Ep-124** **고온고습 습도발생 기술** 최 병일, 김 종철, 우 상봉(*한국표준과학연구원.*) 최근 산업의 발달과 기술은 보다 더 넓은 영역에서의 습도표준의 확립을 요구하고 있고, 요구되는 영역도 산업체에 따라 다양하다. 특히 고온 고습영역에 대한 습도표준의 필요성은 첨단산업과 더불어 전통산업에서도 꾸준히 증대하고 있다. 이는 산업의 고도화 및 효율화에 따른 고온고습과 같은 극한 상황에서의 공정을 관리해야 할 분야가 많아 졌기 때문이다. 이에 표준원에서는 고온고노점 영역의 습도표준을 확립하고자 고노점 습도 발생장치를 개발하게 되었다. 고온고습 영역에서의 습도 발생은 중습 영역에 비해 많은 수분과 열을 필요로 하므로 제작된 고노점 습도발생장치는 기존의 중습 습도발생장치와는 다른 개념으로 제작되었는데, 이의 으며, 습도발생능력은 (-10 ~ +95) $^{o}$C D.P. 이었다.

**Ep-125** **나노분말 비표면적 인증표준물질 개발** 최 병일, 김 종철, 우 상봉(*한국표준과학연구원.*) 최근 NT 등 첨단기술의 발달로 많은 기능성 나노 소재들이 개발되고 있고 이들에 대한 특성의 파악은 매우 중요한데, 특히 비표면적은 이런 기능성 소재의 특성평가에 있어 매우 중요한 지표가 되고 있다. 하지만 비표면적을 측정하는 상용장비와 측정방법들은 그 결과의 해석에 매우 제한적인 요소들이 많으며 이러한 측정방법 및 해석 방법에 따라 결과에서 많은 차이가 있어왔다. 특히 BET 분석방법이 제작회사에 의해 제공되므로 산업현장에서의 다양한 시료들에 대한 특성의 반영을 못하고 있다. 본 연구는 상용 비표면적 측정장비의 신뢰성 검증을 위하여 2 종의 비표면적 인증표준물질을 개발하였다. 이런 검증된 인증물질의 보급은 산업계에 신뢰성 있는 비표면적 측정결과를 줌으로서, 일관성 있는 공정운용에 의한 품질관리, 생산성 향상, 안정성 판단 및 신제품 개발 등에 기여할 것이다

**Ep-126** **Spectral analysis of single celled green algae Chlamydomonas using micro-Raman imaging system** 박 도영, 정 현식, 정 광환[1], 이 건아[1](*서강대학교 물리학과. [1]서강대학교 생명과학과.*) Chlamydomonas reinhardtii는 두 개의 flagella를 이용해 움직이는 녹색의 단세포 생물이다. 약 10 μm의 크기를 가진 이 단세포 생물은 내부에 큰 컵 모양의 chloroplast(엽록체)와 pyrenoid, nucleus 그리고 빛을 지각 할 수 있는 1 μm 크기의 eyespot으로 이루어져 있다. Chlamydomonas는 세포와 분자 생물학에서 근본적인 물음에 대한 연구(다양한 생화적 반응과 광합성, 단백질 합성)의 기본 모델로 사용되어 왔다. 또한, 최근 차세대 에너지원의 하나인 수소 제조에도 이용되고 있다. 본 연구에서는 라만 분광 이미징을 이용하여 clamydomonas의 구성 요소와 광합성 반응에 연관이 있는 eyespot의 세포 내 정확한 위치 추정을 하고자 한다. 생체 세포는 구성에 따라 생화학적 화합물의 분포가 다르다. 이 분포에 따라 각각 화합물에 해당하는 진동모드가 결정된다. 라만 분광법은 이런 생체 세포나 조직의 화합물과 관련한 진동모드 정보를 다른 과정을 거치지 않고 조직 손상이 적으면서 쉽게 측정할 수 있다. 공초점 라만 분광은 514.5nm의 파장을 가진 아르곤 이온 레이저를 여기 광으로 이용 하였으며, 대물렌즈를 통과한 빛은 약 1 ㎛의 크기로 초점을 형성한다. Edge-filter와 전하 결합소자(CCD)를 이용하여 단일세포의 라만 신호를 검출 하였다. 녹색 단세포 생물, Chlamydomonas의 carotenoid와 관련한 진동모드는 각각 1159cm$^{-1}$, 1524cm$^{-1}$이다. 또한, 이 진동모드를 기준으로 chlamydomonas의 라만 이미지를 측정하였다. 이 결과를 보면 광학 현미경 이미지와 차이점을 발견할 수 있다. 광학 현미경으로 확인할 수 없는 세포의 구성요소(핵, 엽록체)를 파악할 수 있다.

**Ep-127** **Simulation of lateral diffusion model of transmembrane protein** 이 상욱, 김 태곤, 김 수용, 김 석원[1](*KAIST, 물리학과. [1]울산대학교, 물리학과.*) P. G. Saffman and M. Delbruck suggested a theoretical model about diffusion in a highly anisotropic environment in 1975. They predict diffusion coefficient D is proportional to ln(1/R), where R is the radius of the diffusing cylinder. However, in 2005, Y. Gambin found experimentally D has 1/R dependence on the radius of the protein using FRAP method. Theoretical support was successively reported by A. Naji in 2007. They show protein-lipid interaction can suppress the mobility of the protein. We perform computer simulation in various situations in order to find realistic diffusion model.

**Ep-128** **Thermoluminescence Spectrum of X-ray Irradiated Diamond Film** KIM Taekyu(*Jeonju National University of Education, Department of Science Education.*) Diamond films were synthesized by a chemical vapor deposition (CVD) and were characterized by the measurement of SEM, XRD, Raman spectrum, and 3-D thermoluminescence(TL). From SEM analysis, the CVD diamond film is grown to be unepitaxial crystallites with pyramidal hillocks. XRD exhibits the strong (111) peak and the weak (220) and (311) peaks of diamond besides the (222) peak of β-SiC. Raman spectrum of synthetic CVD diamond film shows the dia-

mond line at 1332 $cm^{-1}$ and two broad bands around 1350 and 1500 $cm^{-1}$. The three-dimensional TL spectrum of CVD diamond film irradiated with x-ray has one peak located at 560 K and 430 nm. The form factor of 560 K glow peak is calculated to be 0.44 and the kinetic order is found to be first. The activation energy and the escape frequency factor of 560 K glow peak are calculated to be 1.02 eV and $3.4\times10^{7}$ $s^{-1}$, respectively. From the result of curve fitting method. the activation energy and kinetics of the 560 K glow curve are fitted to be 1.04 eV and first order, respectively. The emission spectrum at 560 K is split into 1.63 eV, 2.60 eV, and 3.07 eV emission bands. The 1.63 eV emission band is found to be related to an optical center corresponding to a silicon-vacancy. The 2.60 eV emission band ascribed to an H3 center associated with a point defect consisting of nitrogen-vacancy pairs. The 3.07 eV emission band is associated with the A center related to extended defects and two nearest neighbor nitrogen atoms on C sites.

**Ep-129** **Thermoluminescence of Neutron and X-ray Irradiated $MgAl_2O_4$ Spinel** KIM Taekyu(*Jeonju National University of Education, Department of Science Education.*) The thermoluminescence (TL) of $MgAl_2O_4$ spinel irradiated with neutron and x-ray were measured. Glow curve of irradiated $MgAl_2O_4$ spinel shows single dominant peak at 415 K with large width. Form factor of 415 K glow peak is calculated to be 0.52 and depends on the second kinetic order. TL intensity of $MgAl_2O_4$ spinel irradiated with x-ray after neutron is smaller than that with neutron only due to the optical bleaching of x-ray. Based on the peak shape method, the activation energy for τ, δ and ω are calculated to be 0.79 eV, 0.80 eV and 0.79 eV, respectively. Also, the activation energy of 0.745 ± 0.01 eV is computed from the initial rise method. The emission spectrum of 415 K glow peak is splitted into 518 nm and 683 nm emission bands, which are related with the hole captured at $V^{2+}$ and $Cr^{2+}$ impurities, respectively. Due to the hole capture cross-section of $Cr^{2+}$ being larger than that of $V^{2+}$, the TL peak temperature of the 683 nm emission band is lower than that of 518 nm emission band. The wide width of 415 K glow peak is caused by the overlap of glow curves with different emission wavelengths and peak temperatures.

**Ep-130** **Carbon Nanotube Resonator-Based Biosensors** LEE Hyun-Seok, LEE Hee-Jo[1], CHOI Hyang Hee[2], YOOK Jong-Gwan[1], YOO Kyung-Hwa(*Department of Physics, Yonsei University, Seoul 120-749, KOREA. [1]Department of Electrical and Electronic Engineering, Yonsei University, Seoul 120-749, KOREA. [2]National Core Research Center for Nanomedical Technology, Yonsei University, Seoul 120-749, KOREA.*) We demonstrate microwave resonant carbon nanotube-based biosensors using a streptavidin-biotin system. A clear resonance is observed at 10~13 GHz for the carbon nanotube resonator. After binding the streptavidin to the biotinylated nanotube, the electrical resonant frequency of the sensor exhibits a dramatic shift to a lower frequency by 0.7 ~ 1.3 GHz. The simulation results suggest that the resonance frequency shift can be ascribed to the capacitance change of the nanotube.

■ SESSION: P2
10월 24일(금), 11:00 - 12:45
장 소: 제3전시장

**Fp-001** **Thermal Exponents from Specific Heat: 2-D Triangular-lattice Ising Antiferromagnets in an External Magnetic Field** HWANG Chi-Ok, SEUNG-YEON Kim[1](*국가수리과학연구소. [1]충주대학교.*) We evaluate the density of states g(M,E) as a function of energy E and magnetization Mof the Ising models on square and triangular lattices, using the exact enumeration method for small systems and Wang-Landau method for larger systems.From the density of states the average specific per spin has been obtained and from the peak positions and finite-size scaling the thermal exponents were obtained. The results agree with those from Fisher zero approach.

**Fp-002** **Optimization of consensus time by mixing the voter and the majority voter models on scale-free networks** YANG Jae-Suk, KWAK Wooseop[1], KIM In-mook(*Korea Univ. [1]Chosun Univ.*) We introduce a spin model mixed the majority voter model withprobability p and the voter model with probability 1-p andthen we measure the consensus time of it on the scale-freenetworks with various degree exponents. We find that theconsensus time depends on both p and degree exponents. When all spinsare following either the voter model or the majority voter model,the average consensus time takes too long. On the other hand, whenspins are following the majority voter model and sometimes theyare following the voter model, the average consensus time isshortened. We find that the optimized ratio to minimize theconsensus time is p=0.88(1) from numerical calculation.

**Fp-003** **Critical behavior of the XY model on uncorrelated and correlated random networks** KWAK Wooseop, YANG Jae-Suk[1], GOH Kwang-Il[1], KIM In-mook[1](*Dept. of Physics, Chosun University. [1]Dept. of Physics, Korea University.*) We study numerically the critical behavior of the XY model on the Erdos-Renyi random graphand a growing random network model, representing the uncorrelated and the correlated randomnetworks, respectively. We also checked the dependence of the critical behaviors on the choice oforder parameters; the ordinary unweighted and the degree-weighted magnetizations. On the Erdos-Renyi random network, the critical behavior of the XY model is found to be of the second-order withthe estimated exponents consistent with the standard mean-field theory for both order parameters.On the growing random network, on the contrary, we found that the critical behavior is not of thestandard mean-field type. Rather, it exhibits behaviors reminiscent of those in the infinite-orderphase transition for both order parameters, such as the lack of discontinuity in specific heat andthe non-divergent susceptibility at the critical point, as observed in the percolation and the Pottsmodels on some growing network models.

**Fp-004** **Partition Function Zeros of the Superantiferromagnetic Ising Model on Square Lattice** 송 현석, 이 재환, 김 진민, 김 승연[1](*숭실대학교, 물리학과. [1]충주대학교, 교양학부.*) We study the square lattice ising model with nearest neighbor and next-nearest neighbor interactions by using Wang-Landau Monte Carlo algorithm. It is believed that four different phases appear in this model : paramagnet, ferromagnet, antiferromagnet, and superantiferromagnet. The properties of phase transition into superantiferromagnet are almost unknown even though extensive studies have been performed. We obtain the distribution of the partition function zeros in the complex temperature plane from the density of states which is calculated by Wang-Landau algorithm. Controlling the coupling ratio between two interactions, we investigate the properties of phase transition into superantiferromagnet.

**Fp-005** **Self-organized criticality in Axelrod model** 김 홍주, 육 순형, 김 엽(*경희대학교 물리학과.*) 우리는 문화의 형성과 파급에 관한 Axelrod 모형의 SOC(self-organized criticality) 현상에 대하여 연구하였다. Axelrod 모형은 문화계의 무질서도($q$)에 따라서 전체 문화계가 단일문화에 속하는 질서상태(ordered phase)와 문화계가 다수의 문화로 세분화되는 무질서상태(disordered phase)인 두 가지의 흡수상태(absorbing state)로 나뉘게 된다. 모든 위치의 문화적 특성이 완벽하게 동일한 질서 흡수상태는 안정된 상태이며 다른 경우는 준안정된 상태라 할 수 있다. 문화계가 준안정된 흡수상태에 들어갔을 때 한 위치의 문화적 특성을 바꾸어 흡수상태를 교란시키는 single feature perturbation을 수행하게 되면 계는 점점 안정된 흡수상태로 변화한다[1]. 우리는 정규격자와 네트워크 위에서 single feature perturbation 수행 후 다시 흡수상태에 들어갈 때까지의 시간($t$)와 그때 문화적 특성이 변화한 노드의 수($s$)를 각각 측정하였다. Numerical simulation 으로부터 $t$와 $s$의 분포가, $P(t){sim}t^{-\alpha}$, $P(s){sim}s^{-\tau}$와 같이 멱법칙(power-law)을 만족함을 알아냈다. 이러한 멱법칙 거동과 관련된 SOC 현상에 관하여 논의한다.
[1] K. Klemm, V. M. Eguiluz, R. Toral, and M. San Miguel, Phys. Rev. E 67, 045101 (2003).

**Fp-006** **자유 축적 그물망 위에서의 Axelrod 모델** 조 민수, 김 홍주, 육 순형, 김 엽(*경희대학교.*) 우리는 다리수 분포(degree distribution)가 $P(k){sim}k^{-gamma}$를 만족하는 자유축척 그물망 위에서 문화의 형성과 파급에 관한 Axelrod모형에 대하여 연구하였다. Axelrod 모형의 무질서도를 $q$라 하면임계값 $q_c$가 존재한다. $qq_c$일 때는 구성원소들이 서로 다른 문화를 갖게 되는 무질서상태가 된다. 이런 질서-무질서 상전이 현상의 특성이 자유 축척 그물망의 다리수 지수$gamma$에 의존하여 어떻게 변화하는지를 연구하였다.$gammale3$에서는 $q_c$가 유한 그물망의 크기 $N$에 대하여$q_{c}(N){sim}N^{eta}(eta>0)$와 같은 멱법칙을 만족함을 유한크기 축척(finite size scaling)이론을 사용하여 알아내었다. 이는 $N ightarrowinfty$일 때 또는 무한크기의 그물망위에서는 상전이는 존재하지 않고 문화계는 어떤 $q$에서도 항상 질서상태에 있음을 의미한다. 반면 $gamma>3$에서는 $N ightarrowinfty$일 때 유한한$q_{c}$에서 상전이가 나타남을 보였다.

**Fp-007** **Continuum percolation of nanotubes** 윤 여광,

육 순형, 김 엽(*경희대학교.*) The connectedness and conductivity of a nanotube-based system has been two of the most important physical quantities to understand the nanostructure and designing a nanoscale device. In this study, we apply the continuum percolation theory to nanotube-based systems. Using the Monte Carlo simulations, we find that there exists a certain concentration of nonotubes (percolation threshold), $n_c$ above which the macroscopically connected cluster of nanotubes is formed. In particular, we show that $n_c$ decreases as the isotropy of the nanotube orientation increases. Furthermore, we also measure the conductivity near $n_c$ for various nanotube orientations. We expect that our study provides routes to manipulate the percolation threshold and the level of conductivity in designing nanodevices.

**Fp-008** **이차원 엑스와이 모형(two-dimensional XY model)에서의 정보전달 동역학** KIM Minsu, CHOI M. Y.(*Seoul National University, Department of Physics and Astronomy.*) 계와 주변 환경 사이의 정보 교환에 초점을 맞춘 정보전달 동역학(information transfer dynamics)을 엑스와이 모형에 적용하여 그 거동을 조사하고, 엔트로피 추출 풀이법(Entropic sampling algorithm)을 이용하여 시늉내기한다. 기존의 정보전달 동역학 연구에서 다루었던 이징 모형(Ising model)은 비연속적인 대칭성을 가지는 반면 엑스와이 모형은 연속적인 대칭성을 가지므로 질서맺음변수(order parameter)의 확률밀도함수를 계산하고 그를 통하여 연속적인 형태의 정보 엔트로피를 구하고, 그 변화에 따라 엔트로피 추출 시늉내기를 수행한다. 덧붙여 U(1) 대칭성을 깨는 자기마당의 영향을 조사하고 이징 모형과 비교한다. 특히 시간에 따라 변화하는 자기마당에서 계의 응답을 분석하는데 질서맺음변수의 상관함수(correlation function)의 거동을 기술하는 시간눈금을 얻어서 외부 자기마당의 변화 시간눈금과 비교하고, 그 사이의 결맞음(coherence) 효과를 이징 모형의 경우와 비교하여 논의한다.

**Fp-009** **Conserved mass aggregation with mass-dependent fragmentation and diffusion rate** KIM Yup, LEE Dong-jin, KWON Sungchul(*경희대학교 물리학과.*) We study the condensation phenomena of the conserved-mass aggregation withmass-dependent diffusion rate and fragmentation on scale-free network (SFN) with$P(k)\sim k^{-\gamma}$. In the model, the whole mass $m$ of a node isotropically diffusewith rate $D(m)=m^{-\alpha}$. With rate $\omega$, a mass $m^{\lambda}$ is fragmentedfrom the node and moves to the randomly selected nearest neighboring node. The modelexhibits various phases by the competition of diffusion and fragmentation. First, weconsider SFNs of $\gamma>3$. For $\alpha>0$, there is a crossover $\alpha_c$ over which the fragmentation characterizes thecondensation phenomena. For $\alpha<\alpha_c$, the phenomena is determined by the diffusion. Examining the stability condition of an aggregate, we find $\alpha_c=(\gamma-2)/(\gamma-1)$. For $\alpha \geq \alpha_c$, the system undergoes the same typeof the condensation transitions as those of the zero-range process. For$\alpha<\alpha_c$, the system is in fluid phase characterized by diffusion. $\alpha_c$changes from $(\gamma-2)/(\gamma-1)$ to $1-\lambda$ at $\lambda=1/(\gamma-1)$. For$\alpha <0$, $\alpha_c$ is given as $\alpha_c = -\lambda$ over which the system is inthe fluid phase characterized by fragmentation. At $\alpha=\alpha_c$, since thediffusion and fragmentation are equivalent, the condensation transitions occurs. For$\alpha <\alpha_c$, the complete condensation takes place by diffusion. On the otherhand, for $\gamma \leq 3$, the structure of the phase diagram is not changed except$\alpha_c$ is terminated at $\lambda=1/(\gamma-1)$ over which the system is in the fluidphase by fragmentation. Incomplete condensed phase replaces the fluid phase by diffusionof $\gamma>3$.

**Fp-010** **Phase Response Curves of Coupled Oscillators** KO Tae-Wook, ERMENTROUT Bard[1](*Department of Physics, Korea University. [1]Department of Mathematics, University of Pittsburgh.*) Many real oscillators are coupled to other oscillators and the coupling can affect the response of the oscillators to stimuli. We investigate phase response curves (PRCs) of coupled oscillators. The PRCs for two weakly coupled phase-locked oscillators are analytically obtained in terms of the PRC for uncoupled oscillators and the coupling function of the system. Through simulation and analytic methods, the PRCs for globally coupled oscillators are also discussed.

**Fp-011** **Structure of correlations with partially surrogated price fluctuations** 임 규창, 김 수용, 김 경식[1](*한국과학기술원. [1]부경대학교.*) The well-known facts of financial markets supports that the pricefluctuation contains the information about the complexity ofinteractions among market participants. In this work, we present anew surrogate method in order to find the dependency of higher-ordercorrelations on the magnitude of price fluctuations. By sorting thereturns into several groups with respect to the level offluctuations, we show that the large fluctuations characterize thestructure of temporal correlations of a financial time series. Inparticular, by investigating the positive and the negative partsseparately, we confirm that the risk-averse behavior of traders is explicitly observed in financial markets.

**Fp-012** **Return Intervals Analysis of the Korean Stock Market** 전 웅, 정 우성[1], 문 희태(*한국과학기술원. [1]포항공과대학교.*) We investigate scaling and memory effects in return intervals between price volatilities above a certain threshold for the Korean stock market. We find that the distribution of return intervals can be approximated by a scaling function that depends only on the ratio between the return interval and its mean. We also find memory ffects such that a large (or small) return interval follows a large (or small) interval by investigating the conditional distribution and mean return interval.

**Fp-013** **Negative Feedback Loop for Post-transcriptional Regulation in Circadian Expression of mouse Period3** KIM Sung-Hoon, WOO Kyung-Chul[1], LEE Kyung-Ha[1], KIM Do-Yeon[1], KIM Kyong-Tai[1], KIM Seunghwan[2](*School of Interdisciplinary Bioscience and Bioengineering, Pohang University of Science and Technology. [1]Laboratory of Molecular Neurophysiology, Department of*

*Life Science, Division of Molecular and Life Science, Pohang University of Science and Technology. [2]Asia Pacific Center for Theoretical Physics, National Core Research Center for Systems Biodynamics, Non-linear and Complex System Laboratory, Department of Physics, Pohang University of Science and Technology.*) A circadian rhythm of physiological processes is generated by the transcriptional and translational control of clock genes. In addition to both regulatory mechanisms, it is identified that some of clock genes are modulated by a post-transcriptional way – UTR-mediated mRNA decay, cap-independent translation, and so forth. Recently, it is reported that UTR-mediated mRNA decay is important in circadian oscillations of mouse period3 (mPer3), one of the clock genes. We propose here a simple model for describing the post-transcriptional regulation in circadian mPer3 expression. First, we experimentally identified the post-transcriptional regulatory factors and their roles in circadian oscillations. Then, based on a negative feedback loop, we created a mathematical model consisting of components for mPer3 (mRNA, cytosolic and nuclear proteins) and post-transcriptional regulatory factors. Numerical simulation shows that our model is consistent with biological experiments and illustrates how the oscillation profile of mPer3 is changed by post-transcriptional regulatory factors.

**Fp-014** **Spam Source Clustering With Similarity Measure And A Potential Landscape** SHIN Jeongkyu, KIM Seunghwan (*APCTP, NCSL, Department of Physics, POSTECH, Pohang, Korea 790-784.*) The spam detection is one of the most challenging problems in electric communication networks. The IP spoofing, which falsifies the referrer, is a well-known method to disturb the depender in specifying where and whom spam sources are from.We suggest a method to specify the spam source. We speculate that each spam source that either has the same victim list or uses the same spam hosting program. We construct the spam source - target relationship as a bipartite network and construct a weighted network by projecting it using similarity measure.We define potential energy of nodes as the total flow at each node, that is, a summation of weights of all links, which is used to cluster spammers into a few spam source groups. This method is tested with the weblog spam data.Our proposed method can be extended to diverse categorization problems, such as the multiple text categorization, time-series analysis and the network subunit clustering.

**Fp-015** **Betweenness centrality of network skeleton** 고영진, 육 순형, 김 엽(*경희대학교 물리학과.*) 우리는 network에서 degree correlation과 network의 기본 골격(skeleton)이 transport 현상에 미치는 영향에 대하여 연구하였다. 이를 위해 다양한 degree correlation을 가지는 network의 minimum spanning tree(MST)와 infinite incipient percolation cluster (IIC)의 node betweenness centrality, $C$를 측정하였다. Erd\"{o}s-R\'{e}nyinetwork (ERN)의 MST에서 $C$의 분포 $P_{MST}(C)$는 $P_{MST}(C) \simC^{-\delta_{MST}}$의 멱법칙이 만족함을 보였으며 $\delta_{MST}$는 degree correlation과 관계없이 일정함을 발견하였다. ERN의 IIC에서 $P_{IIC}(C)$의분포 역시 $P_{IIC}(C) \sim C^{-\delta_{IIC}}$의 멱법칙을 만족하고$\delta_{IIC}$는 degree correlation에 관계없음을 보였다. 반면 scale-free network (SFN)의 $\delta_{MST}$는 network이 degree correlation에 영향을 받음을 발견하였으며, neutral한 degree correlation을 갖는 경우 $\delta_{IIC}\simeq1.5$임을 보였다.

**Fp-016** **Characterizing noise in genetic oscillatory systems** 민 병준, 고 광일, 김 인묵(*고려대학교, 물리학과.*) Noise is inherent in cellular networks involving many genes, RNAs, and proteins, and affects deeply living systems. Therefore, we need stochastic method to fully understand the genetic circuits, not only the deterministic method. Here we present a framework for studying the noise characteristics and their propagation property of systems with oscillatory activity. Using an exact stochastic simulation of three-component genetic circuit constituting a negative feedback loop, we quantify the fluctuations and correlations in the periods and amplitudes of oscillations as well as the strength of local fluctuations.

**Fp-017** **Betweenness centrality of correlated networks** LEE Sungmin, YOOK Soon-Hyung, KIM Yup(*경희대학교 물리학과.*) 우리는 network의 degree correlation이 betweenness cetrality (BC)에 미치는 영향에 대한 연구를 하였다. BC는 network의 수송현상 (transport) 등의 동역학적 특성을 결정짓는 중요한 양이다. Network의 correlation은 Peason's coefficient $r$에 의해서 측정되는데 우리는 이 $r$값을 변화시키는 방법으로 link rewiring (LR) 방법을 사용하였다. LR를 통해서 생성된 network들의 BC 분포 $P(b)$ 과 BC의 degree 의존성 $b(k)$ 등을 측정함으로써 degree correlation이 동역학적 특성에 미치는 영향을 연구하였다. Scale-free network (SFN) 은 degree 분포가 $P(k) \sim k^{-\gamma}$ 와 같은 power-law 를 만족시키는 network이다. $r=0$인 SFN에서는 $P(b)$와 $b(k)$가 power-law를 가짐이 잘 알려져 있는데 $r>0$인 SFN에서 BC를 측정한 결과 $\2< gamma \leq 3$인 SFN에서는 $P(b)$와 $b(k)$가 power-law에서 벗어나는 것을 발견하였다. 반면에 $\gamma > 3$인 SFN에서는 $P(b)$와 $b(k)$가 $r=0$인 경우와 동일한 power-law를 만족한다.

**Fp-018** **Mathematial model for glucose regulation** 강 혁, 최 무영[1], 한 경림[2], 김 진웅[2](*고등과학원 물리학부. [1]서울대학교 자연과학대학 물리천문학부. [2]서울대학교 약학대학 약학과.*) We describe the development of a whole feedback model for interactions between insulin secreting beta cells and other organs such as liver, muscle, and fat cells. First, we construct a mathematical model for glucose regulation in the presence of mutations in the glucokinase gene, which phosphorylates glucose to glucose-6-phosphate. The resulting defects lead to a rise in the threshold of blood glucose that triggers insulin secretion in beta cells. The model consists of enzymatic reactions of glycolysis, mitochondrial ATP production, and mathematical descriptions of molecular mechanism of glucose induced insulin secretion. With the reduced glucokinase activity taken into consideration, the model displays oscillations of key components of blood glucose regulation, including insulin secretion, calcium oscillation, and membrane action potential bursting. Finally, we construct a whole feedback model for glucose regulation

and devise means to compensate for the defects in glucokinase, considering fast dynamics of bursts and slow dynamics of glucose-insulin feedback. From the whole feedback model, critical regulatory points are found.

**Fp-019** **Dynamics of Stomatal Conductance in Response to Humidity under Osmo-regulation and Drawdown Hypotheses** KWON Hyunwoong, CHOI M. Y.(*Seoul National University, Department of Physics and Astronomy.*) The size of a stomatal aperture is determined by epidermal and guard cell turgor pressure. If, during transpiration, water potentials of the guard cell and of the epidermal cell reduce by the same amount, with the osmotic pressure of the cells unchanged, the mechanical advantage of the epidermal cell over the guard cell would cause the stoma to close when humidity increases. This accounts just for transient wrong-way responses of stomata. In the steady-state responses, on the other hand, a number of experimental evidences indicate that the guard cell turgor pressure should overcome the epidermal mechanical advantage; this may be achieved through active regulation of the guard cell osmotic pressure and/or drawdown of guard cells compared with epidermal cells. To probe the validity of these two hypotheses, we carry out extensive numerical simulations with either hypothesis and obtain results in general agreement with the experimental ones.

**Fp-020** **A Mesoscopic Model for a Double-stranded DNA** 전 재형, 성 우경(*포항공과대학교.*) Two single-stranded DNAs (ssDNA) are self-assembled into a double-stranded DNA (dsDNA) via hydrogen bondings and stacking interactions. While the ssDNA is a flexible linear polymer, interestingly, the dsDNA is a helical polymer which exhibits large bending and twist stiffnesses. In this work, we present a mesoscopic mechanical model for DNA conformation and elasticity, and study how the helix with a large bending stiifness forms from two ssDNAs. We show that stacking interactions, modelled by next-nearest-neighbor interactions between apposing bases, can explain these unique features of dsDNA. Geometrical constants for B-DNA such as helicity, diameter, and pitch are quantitatively explained well. Also it shows that the DNA undergoes a helix-ladder conformational transition under high extensional forces in an agreement with over-stretching transition observed in force-extension experiments. Most importantly, this mesoscopic model can derive a twistable wormlike chain Hamiltonian, along with the stacking-induced bending and twisting stiffnesses. We find their magnitudes are in a good agreement with measured values, their relative ratio being determined solely by the geometrical constants.

**Fp-021** **Kineitcs of a DNA confined by Bio-adhesive Vesicles: Photo Image Analysis** 남 기문, 이 남경(*세종대학교 물리학과.*) We studied kinetics of the confined DNAs due to the spreading of a vesicle on the glass substrate. The phospholipids membrane decorated with biotins binds on the streptavidin coated substrate upon spreading. The end grafted mono-disperse DNAs on the substrate spreads under the vesicle pushed by the vesicle front. After the vesicle adhesion, the stretched segment under the vesicle remains straight while the remaining part fluctuates. In order to investigate the relaxation kinetics of the DNA under that circumstance, we analyzed DNA's photo images obtained by the experiments carried by C.M. Marques group (ICS, Strasbourg). We evaluated the mass distribution along the contour of each DNA molecule and calculated the tension profiles. The tension mainly depends on the distances from the vesicle center and the grafted position. For each segment, the uniform tension is found ( <0.5 pN) inside of the patch where the molecule is confined. Our study indicates that the kinetics of a confined DNA is frozen due to the suppression of longer modes.

**Fp-022** **문학작품 속 단어배열에 관한 Self-Organized Criticality 연구** 서 병훈, 심 경무, 박 병윤, 이 호현, 이 해심, 임 헌만[1], 김 학진[1], 김 종현(*충남대학교 물리학과. [1]충남대학교.*) 문서작성 프로그램을 사용하다 보면 한 단어(혹은 그 이상)의 유무로 인해 문장 또는 문단 전체가 이동하는 현상을 볼 수 있다. 이것은 한 단어의 영향으로 인해 뒤에 위치하는 단어들이 순차적으로 영향을 받고 그것이 반복되어 어느 임계점 이상이 되면 문단 전체가 영향을 받는 Self-Organized Criticality현상의 하나로 볼 수 있다. 각 단어의 알파벳수와 영향 받는 줄 수의 분포로 이것이 Self-Organized Criticality 현상임을 알고 다각도의 분석을 하였다. 특히 이 연구에서는 널리 알려져 있는 문학작품들을 통해 언어별, 작가별 성향에 따라 특징이 어떻게 나타나는지 알아보았다.

**Fp-023** **The Mechanism of High Flexibility of DNA on Short Length Scales: The Role of Thermal Bubbles** 이 오철, 전 재형, 성 우경(*포항공과대학교, 물리학과.*) Recently, it has been revealed that, at length scale of several tens nano meters, double-stranded DNA (dsDNA) has a persistence length less than 50 nm (i.e., its well-known typical value), exhibiting high flexibility. In this work, we study the flexibility of short dsDNAs via numerical simulations and analytical theory, and show that the observed high flexibility is attributed to thermal bubbles. Using our breathing DNA model, we obtain the end-to-end distances and force-extension curves of dsDNAs, from which we examine how their persistence lengths are influenced by the thermally-induced bubbles and forks. We find that the persistence length is about 20 nm at contour length 1.7 nm and approaches to 50 nm as the contour length increases to about 34 nm. This behavior can be quantitatively explained well by our theoretical prediction which includes a single bubble in the middle of DNA. This implies that, although bubble occurrences are rare at a physiological temperature, they can lead to a persistence length much shorter than 50 nm on short length scales, as shown in the experiments. We also find that, due to forks, dsDNAs denature at a critical length 6.8 nm (20 base pairs) at a physiological temperature and its critical length increases with temperature.

**Fp-024** **콜로이드에 속박된 리간드-리셉터의 결합 반응 연구** 신 익철, 이 남경(*세종대학교.*) 생물학적 진단방법의 개발이 요구되면서 콜로이드에 속박된 리간드-리셉터의 특정기 반

응 동역학적 제어 기술이 크게 발전하였다. 새로운 실험 기술은 리간드-리셉터를 포함하는 자기 콜로이드와 연결자(spacer)의 분자구조 디자인을 통하여 반응률의 시간에 대한 변화를 통해 반응에 필요한 시간을 직접 측정할 수 있도록 하였다. 콜로이드상에서의 반응-확산 현상을 정량적으로 이해하기 위하여 이 연구과제에서는 자성을 띤 콜로이드가 자기장에 의해 한 줄로 늘어서게 되는 실험적 상황을 고려, 서로 접촉한 상태에서 회전확산 운동하는 구로 모델링하고 이들 구면상에 속박된 리간드-리셉터의 반응률을 전산모사실험으로 조사하였다. 리간드가 결합된 연결자의 내부 자유도가 있을 경우에 연결자의 길이와 유연성에 대한 의존성을 조사하였다. 특히 다중시간간격 알고리듬을 사용하여 계산 시간의 대부분이 반응영역근처에서 이루어지도록 하여 전산모사실험의 효율을 높였다.

**Fp-025** **대칭성에 따른 최적 광자띠틈 구조** 정 형채 (*세종대학교, 물리학과.*) 두 종류의 다른 광학적 성질을 가지는 물질을 배열하는 구조 중 TM-편극 광자띠틈이 최대인 구조를 전산 역학적 방법으로 구하였다. 특히, 이차원 배열의 경우 주어진 회전 대칭성의 최적 구조를 고려하였는데, 대칭성에 따른 밀도파의 합을 계산하여, 그 합이 특정 문턱값을 넘는지 여부에 따라 서로 다른 물질을 배열하는 방법으로 최적 구조를 구하였다. 이 결과, 결정구조 대칭성의 경우는 주기적 구조를 (결정구조에) 금지된 대칭성의 경우는 준결정 구조를 얻었다. 두 무질의 유전 상수 비가 큰 경우는 결정체 구조가, 비가 작은 경우에는 준결정 구조가 상대적 최적 구조가 되었다.

**Fp-026** **입자간 순수 반발상호작용에 의해 일어나는 2차원에서의 자발적 구조형성** 권 희영, 홍 상신, 장 병권, 원 창연(*경희대학교 이과대학 물리학과.*) 나노기술의 발전과 함께 소재와 도구의 나노화가 이루어지면서, 나노체간 상호작용에 의한 자발적 구조형성과, 구조의 상(phase)에 관한 연구가 활발히 진행중이다. 지금까지의 연구에서는 주로 근거리 인력과 원거리 척력을 가지는 상호작용이 있는 경우에 생기는 줄무늬나 방울무늬 등의 미세상(microphase)에 관한 연구가 있어 왔다. 우리는 순수 척력만을 가지는 에너지 모델을 가지고 입자의 밀도와 계의 온도에 따른 자발적 상들의 형성과 그 상들 간의 상전이를 연구하였다. 순수한 반발 상호작용을 강한 척력의 근거리 상호작용과 약한 척력의 원거리 상호작용의 두 가지 구간으로 나누어 주었을 때, 그 거리간의 비율, 입자의 밀도, 온도 등의 영향에 따라 크게 줄무늬와 방울무늬 상태의 두 가지 자발적 상을 형성한다. 고정된 온도에서는 밀도에 변화에 따라서 낮은 밀도에서는 육각형의 격자구조를 가지는 방울무늬 상태를 형성하고 밀도가 커짐에 따라 임계 밀도 이상이 되면 줄무늬의 상태로 변환이 되었다. 그리고 고정된 밀도에 의해서는 온도가 증가함에 따라 방울무늬가 줄무늬 상태로 변환이 되는 현상이 관찰되었다. 우리는 이런 밀도와 온도를 변수로 하는 상전이의 특성을 고정온도-개수 분자동역학 Monte Carlo 시뮬레이션을 통해 정량화 하였고, 이론적인 모델을 통한 수치적 계산과 비교하였다.

**Fp-027** **Numerical study of morphology and ion channel distribution of a bipolar neuron** KIM Seunghwan, LEE Dongmyeong(*APCTP, Brain Research Center &NCSL, Dept. Physics, POSTECH, Pohang, Korea 790-784.*) Neurons have diverse morphological and physiological properties, which determine their function. Neurons are commonly classified according to the number of processes; e.g. unipolar, bipolar or multipolar neurons. We study simple bipolar and unipolar neuron models based on the cable theory. To understand information processing of the neuron, we study how morphology influences the propagation of action potentials (AP) along the axon. We measure the inter-spike interval (ISI) as a function of the radius and ion channel density of the soma. We find that there exists a critical ion channel density, which depends on the soma radius, below which the propagation failure occurs and the ISI increases sharply. The implications of these findings are discussed in the contect of the information processing in bipolar neurons.

**Fp-028** **FOLDFINDER: Protein Fold Recognition based on profile-profile alignment usingpredicted secondary structure** JOO Keehyoung, LEE Jinwoo[1], LEE Sung Jong[2], LEE Jooyoung (*Korea Institute for Advanced Study, School of computational scineces. [1]Kwangwoon University, Department of Mathematics. [2]University of Suwon, Department of Physics.*) The first step of template based protein structure modeling is fold recognition, where one seeks for proteins whose structures can be used as templates for modeling a protein of unknown structure. In this work, we propose a new fold recognition method called FOLDFINDER which is based on a profile-profile alignment method that also incorporates predicted secondary structure information. In order to generate the optimal alignment, the method utilizes global-local dynamic programing based on a score function defined by the correlations between profiles together with affine gap penalty. Parameters of FOLDFINDER are optimized using the reference alignment of HOMSTRAD. We have applied the FOLDFINDER in our blind prediction of CASP8 targets. Examples of successful fold recognitions as well as some of its limitations will be discussed. Detecting remote homologs remains as a challenge for our future work, where one needs to incorporate additional terms such as the predicted solvent accessibility.

**Fp-029** **Optical Angular Trapping of Micro-size Biological Objects Using Form Birefringence** HA Chungil, PAK Hyuk Kyu, KIM Kipom[1](*Pusan National University, Dept. of Physics. [1]Univ. of California Santa Barbara, Materials Dept., USA*) We use micro-size biological objects, liposomes of several tens of μm, which are synthesized from soybean asolectin by using a gentle hydration protocols. The optical properties of the liposomes used in this experiment do not include chemically anisotropic birefringence. In trapping a liposome using optical tweezers, we find that the liposome rotates around the focusing spot of the trap in response to the elliptically polarized incident light. We explain the rotation of the chemically isotropic micro-size biological object in connection with the angular-momentum conservation of the polarized beam and the form birefringence characterized by the geometrical anisotropy of the object. One can make practical application of this study in investigating the dynamic properties of micro-size biological objects with similar characterization, such as red blood cells.